Austrian Journal of Technical and Natural Sciences

2026, No 3–4

PREMIER Publishing

Vienna
2026

Austrian Journal of Technical and Natural Sciences

Scientific journal

№ 3–4 2026

ISSN 2310-5607

Editorial office Premier Publishing s.r.o.
Praha 8 – Karlín, Lyčkovo nám. 508/7, PSČ 18600
E-mail: pub@ppublishing.org
Homepage: ppublishing.org

Austrian Journal of Technical and Natural Sciences is an international, English language, peer-reviewed journal. The journal is published in electronic form.

The decisive criterion for accepting a manuscript for publication is scientific quality. All research articles published in this journal have undergone a rigorous peer review. Based on initial screening by the editors, each paper is anonymized and reviewed by at least two anonymous referees. Recommending the articles for publishing, the reviewers confirm that in their opinion the submitted article contains important or new scientific results.

Premier Publishing is not responsible for the stylistic content of the article. The responsibility for the stylistic content lies on an author of an article.

Instructions for authors

Full instructions for manuscript preparation and submission can be found through the Premier Publishing home page at: http://ppublishing.org.

Material disclaimer

The opinions expressed in the conference proceedings do not necessarily reflect those of the Premier Publishing, the editor, the editorial board, or the organization to which the authors are affiliated.

Premier Publishing is not responsible for the stylistic content of the article. The responsibility for the stylistic content lies on an author of an article.

Included to the open access repositories:

TOGETHER WE REACH THE GOAL SJIF 2024 = 6.62 (Scientific Journal Impact Factor Value for 2024).

Included to the Uzbekistan OAK journals bulletin.

The Austrian Journal of Technical and Natural Sciences, 2026 No 3–4
ISSN 2310-5607

PREMIER Publishing
ppublishing.org

Section 1. Biology sciences

DOI:10.29013/AJT-26-3.4-3-5

BIOECOLOGY AND DEVELOPMENTAL FEATURES OF THE KALANCHOE PLANT (KALANCHOE)

Saitova Azima Kalzhanovna [1]

[1] Department of Agroecology and Introduction of Medicinal Plants
Berdakh Karakalpak State University Republic of Uzbekistan

Cite: *Saitova A.K. (2026). Bioecology and Developmental Features of the Kalanchoe Plant (Kalanchoe). Austrian Journal of Technical and Natural Sciences 2026, No. 3–4.* https://doi.org/10.29013/AJT-26-3.4-3-5

Abstract

This article presents the results of a comprehensive study of the bioecological characteristics, morphological characteristics, and vegetative propagation capacity of Kalanchoe, a plant widely used as an ornamental and medicinal plant. The article examines the species' adaptive mechanisms, its ecological plasticity, growth and development conditions in indoor cultivation, and the effectiveness of vegetative propagation under controlled conditions. Kalanchoe has been found to be highly resistant to adverse environmental factors, capable of accumulating moisture in tissues, and intensively forming "pupae" on leaves, which contributes to its widespread distribution and practical value.

Keywords: *Kalanchoe, medicinal plants, succulents, vegetative propagation, bioecology, introduction*

Introduction

The use of medicinal plants has an ancient history and is linked to the development of medicine. Plants are an important source of biologically active substances used for the treatment and prevention of diseases, and for strengthening the body. In modern times, interest in medicinal plants is growing due to the development of phytotherapy and the search for natural alternatives to synthetic drugs. Uzbekistan's flora is highly diverse, including numerous medicinal and ornamental species, among which plants with dual medicinal and ornamental value are particularly important.

One such species is Kalanchoe, widely used as a houseplant and medicinal plant, possessing wound-healing and anti-inflammatory properties. Despite its widespread distribution, its bioecological characteristics remain poorly understood, necessitating further research.

Materials and methods

The study involved Kalanchoe plants cultivated under laboratory conditions at the

Department of Agroecology and Introduction of Medicinal Plants of Berdakh Karakalpak State University.

The research was conducted in the spring and summer of 2025 and included a combination of field and laboratory observations. The primary methods used included a morphological description of the plant, phenological observations, analysis of vegetative propagation, assessment of growth parameters, and a comparative analysis of the survival rate of transplanted specimens. The following parameters were recorded during the observations: plant height, number of leaves and "pupae," length and width of leaf structures, shoot formation rate, and rooting rate during transplantation. To assess propagation effectiveness, a series of experiments were conducted involving the transplantation of young plants obtained vegetatively.

Results and discussion

Experimental studies have shown that Kalanchoe, both in laboratory conditions and during controlled introductions, demonstrates high adaptability to substrate and agronomic conditions. When replanting plants, preparation of the soil medium and drainage layer was of particular importance. A drainage layer of medium-sized stones was placed at the bottom of the pots, topped with a layer of sand and fertile substrate. To ensure optimal water management, the drainage holes were closed, and the surface was covered with a 2–3 cm thick layer of expanded clay. In pots larger than 12–15 cm in diameter, the drainage layer was increased to 5–7 cm, which helped prevent water stagnation and the development of root rot.

When planting, the root system was positioned so that the root collar was level with the substrate surface, ensuring uniform development of both the above-ground and underground parts. After transplanting, the plants were placed in warm conditions with moderate watering and periodic exposure to direct sunlight (2–3 times per week). It has been established that excessive pruning of the root system (removing up to 1/3 of the roots) or above-ground mass temporarily reduces growth intensity, but in some cases, it stimulates lateral shoot formation.

Observations showed that Kalanchoe exhibits a pronounced capacity for vegetative reproduction characteristic of viviparous plants. Specialized buds ("plantlets") form on the leaves and subsequently develop into independent individuals. This process occurs naturally: along the margins of the leaf blades, embryonic shoots are produced, which detach and root upon contact with the substrate. As a result, a single leaf can give rise to up to 22–36 young plants, confirming the high reproductive potential of the species.

Observations revealed that, when the mother plant reached a height of 20–25 cm, active vegetative bud formation began early in its development. By April 14, 2025, individual specimens had reached a height of 25 cm and already had developed leaf structures with developing "pups." By May 27, 2025, the plant height had increased to 26 cm, with the formation of up to 16 leaf segments with vegetative buds.

In an experimental propagation of 25 young plants obtained vegetatively, the survival rate after 40–45 days was 60–70%, demonstrating the high effectiveness of this method. Indoors, the stable development of 32–33 plants in separate experimental plots was observed, confirming the stability of the adaptation process.

The results confirm that Kalanchoe is a highly adaptable succulent plant, exhibiting remarkable tolerance to various growing conditions and a high regenerative capacity. An effective drainage system (using expanded clay and a sand layer) plays a key role in preventing substrate overwatering and creating optimal conditions for root development.

It has been established that the survival rate and subsequent development of plants directly depend on the quality of soil preparation and proper watering. Excessive watering leads to root suppression, while a moderate water regime promotes active growth and the development of vegetative organs.

Of particular importance is the unique mechanism of vegetative propagation of Kalanchoe, based on the formation of "pupae" on the leaves. This method of propagation ensures high reproduction rates and the survival of offspring without the need for seed production. The biological characteristic of this "viviparous" propagation makes Kalan-

choe an effective candidate for mass cultivation and introduction.

The high survival rate (60–70%) confirms the plant's practical value in indoor gardening and its potential for further use in ornamental and medicinal plant growing. It should also be noted that Kalanchoe exhibits tolerance to temperature and light fluctuations, making it suitable for cultivation under low-maintenance conditions. Thus, the bioecological characteristics of Kalanchoe, including its succulent tissue structure, ability to accumulate moisture, and active vegetative propagation, ensure its wide adaptability and high practical value.

Conclusion

Thus, Kalanchoe is a succulent plant with high ecological adaptability, a pronounced capacity for vegetative propagation, and significant resistance to adverse environmental conditions. The study results showed that this species has high potential for use in ornamental plant growing and phytotherapy. The findings can be applied to the introduction, mass propagation, and development of indoor medicinal plant cultivation technologies.

References:

Volzhanova M. I., Bailman R. A., Suslina S. N., Bykov V. A. Kalanchoe pinnate and degremona: chemical composition, application in medicine (review) // Issues of biological, medical and pharmaceutical chemistry. 2010. – Vol. 8, No. 7. – P. 14–21.

Karomatov S. V. Medicinal plant Kalanchoe // Biology and integrative medicine. 2016. – No. 4. – P. 66–71.

Marinina T. F., Savchenko L. N., Saushkina A. S. Study of the possibility of complex use of the plant Kalanchoe pinnate // Bulletin of the Samara Scientific Center of the Russian Academy of Sciences. 2015. – Vol. 17. – No. 5–1. – P. 143–148.

Sazhina N. N., Lapshin P. V., Zagoskina N. V., Korotkova E. I., Misin V. M. Comparative analysis of the antioxidant activity of Kalanchoe juices // Chemistry of plant raw materials. – 2013. – No. 3. – P. 113–119.

submitted 06.03.2026;
accepted for publication 20.03.2026;
published 30.04.2026

Contact: arzigull@gmail.com

The Austrian Journal of Technical and Natural Sciences, 2026 No 3–4
ISSN 2310-5607

PREMIER Publishing
ppublishing.org

DOI:10.29013/AJT-26-3.4-6-8

ENDEMIC AND RARE SPECIES OF THE GENUS ASTRAGALUS IN THE FLORA OF THE BUKANTAU MOUNTAINS

Serekeeva Gulayim Abdigaliyevna [1]

[1] Department of General Biology Berdakh Karakalpak State University Republic of Uzbekistan

Cite: *Serekeeva G.A. (2026). Endemic and Rare Species of the Genus Astragalus in the Flora Of The Bukantau Mountains. Austrian Journal of Technical and Natural Sciences 2026, No 3–4.* https://doi.org/10.29013/AJT-26-3.4-6-8

Abstract

The article examines endemic and rare species of the genus Astragalus distributed in the flora of the Bukantau residual mountains (Kyzylkum Desert). An analysis of their taxonomic composition, ecological characteristics, and current population status was carried out. It was established that representatives of the genus are characterized by a high degree of endemism and a strong association with petrophytic habitats. The necessity of conservation of rare species and monitoring of their populations under increasing anthropogenic pressure is emphasized.
Keywords: *Astragalus, endemism, rare species, Bukantau, Kyzylkum, flora, biodiversity*

Introduction

Global climate change and anthropogenic impacts are transforming natural ecosystems and reducing biodiversity, including floristic composition. Therefore, research aimed at understanding the species composition of flora and assessing the status of rare and endemic plant populations is particularly important. The flora of the arid regions of Central Asia, including the Kyzylkum Desert and its residual mountains, is of significant interest for botanical and geographical research. These areas are crucial for understanding the boundaries of the Turan and Mountainous Central Asian floristic provinces, as well as the processes of flora formation.

The genus Astragalus (Fabaceae) occupies a special place in the flora, with representatives characterized by a high level of endemism and ecological specialization. Despite a long history of studying the region's flora, current data on the composition and population status of Astragalus species in the Bukantau Mountains remain incomplete, making this study particularly relevant.

Material and methods

The study focused on endemic and rare species of the genus Astragalus (Fabaceae) growing in the Bukantau Mountains, located within the Kyzylkum Desert. This region is characterized by an arid climate, pronounced topographic mosaics, and the presence of specific petrophytic habitats, which contribute to the formation of a unique floral complex with a high level of endemism. The research was conducted during field seasons using an integrated approach, including flo-

ristic analysis, route-geobotanical surveys, and a comparative-geographical method. The route surveys covered various terrain elements (gravelly and rocky slopes, rock fissures, and elevated areas), revealing the spatial distribution of Astragalus species and their ecological associations. Species identification was based on classical botanical identification guides, morphological characteristics, and comparison with herbarium specimens. Literary sources and the results of previous studies (I. I. Granitov, P. K. Zakirov, L. A. Kapustina, F. O. Khasanov, and others) were also consulted, ensuring comparability of the obtained data with historical knowledge of the region's flora.

During the study, the species composition of the genus Astragalus was determined, along with their ecological preferences (petrophytes, xerophytes), patterns of distribution, life forms (chamaephytes, therophytes), and conservation status according to the Red Data Book of the Republic of Uzbekistan. Special attention was given to the identification of endemic and subendemic species, assessment of their current population status, and clarification of their distribution ranges. The obtained data were processed using comparative analysis methods in order to identify patterns in flora formation and to evaluate the role of the genus Astragalus in the structure of vegetation cover of the Bukantau residual mountains.

Results and discussion

A floristic analysis revealed that the flora of the Bukantau remnant mountains is significantly represented by endemic and rare species of the genus Astragalus (Fabaceae), which play a key role in shaping the region's unique vegetation. The high abundance of this genus is due to its ecological flexibility and ability to adapt to the extreme conditions of arid regions, particularly evident in the Kyzylkum Desert.

Among the identified species, *Astragalus holargyreus, A. subbijusus, A. centralis,* and *A. remanens* are particularly significant, distinguished by both their ecological characteristics and rarity. Astragalus holargyreus is a rare petrophytic chamaephyte, native to the gravelly and rocky slopes of the Bukantau mountain range. It is characterized by specific morphological features, particularly the way fruit develops, and is included in the Red Data Book of the Republic of Uzbekistan (rarity category 2), demonstrating the need for its conservation.

Astragalus subbijusus is a typical endemic species of the Kyzylkum Remnant Mountains and is widespread on gravelly and rocky slopes. Its range covers several mountain ranges in the region, but within Bukantau, it forms local populations, highlighting its ecological association with specific substrates.

Astragalus centralis deserves special attention – an extremely rare species (rarity category 1), characterized by a narrow ecological niche and limited range. It is confined primarily to rock crevices and rocky slopes, making it particularly vulnerable to environmental changes. The observed decline in numbers and fragmentation of this species' populations indicate unfavorable trends for its existence and the need for urgent conservation measures.

Astragalus remanens is a terrophyte found on fine-grained slopes, demonstrating adaptation to the short growing season and extreme conditions of arid environments. Its biological characteristics allow it to thrive in conditions of moisture deficit and unstable climatic factors.

An analysis of ecological associations revealed that most species of the genus Astragalus are associated with petrophytic habitats – rocky and gravelly substrates characterized by low moisture capacity and poor soil cover. This specialization leads to the formation of a narrow ecological niche, which, on the one hand, helps reduce competition, and on the other, makes the species extremely sensitive to any environmental changes, including anthropogenic impact.

During the research, 14 rare plant species listed in the Red Data Book of the Republic of Uzbekistan were identified in the Bukantau flora, confirming the high conservation value of this region. In addition, two populations of the shrub species *Astragalus scleroxylon*, totaling approximately 20 individuals, were discovered. This fact indicates the need for further study of the species and justification for its inclusion in the next edition of the Red Data Book as potentially vulnerable.

An endemic flora analysis revealed the presence of six endemic species, accounting

for 1.71% of the total flora, confirming its high level of originality. This level of endemism is due to the geographical isolation of the residual mountains, as well as specific environmental conditions, including an arid climate, rocky substrates, and limited moisture resources.

The obtained results are consistent with previous studies and confirm that the Bukantau flora occupies an important place in the Kyzylkum residual mountain system, serving as a conservation center for rare and endemic species. At the same time, the identified trends in the decline of the ranges and abundance of certain species, particularly *Astragalus centralis*, indicate the need for enhanced conservation efforts. Thus, further study of the Bukantau flora, regular monitoring of populations and the development of scientifically based measures for the protection of rare and endemic species of the genus Astragalus are the most important tasks of modern botany and ecology aimed at preserving the biodiversity of arid ecosystems of Central Asia.

Conclusion

The flora of the Bukantau Mountains is characterized by the presence of a significant number of endemic and rare species of the genus Astragalus, many of which are listed in the Red Data Book of the Republic of Uzbekistan. Their association with specific petrophytic habitats and high vulnerability have been established. The obtained results confirm the need for further research, monitoring, and the development of measures to conserve the region's biodiversity.

References

Granitov I. I. Endemic species in the flora of the South-Western Kyzylkum // Proceedings of SAGU. – No. 136. – Tashkent, 1958. – P. 46–49.

Khasanov F. O., Shomurodov Kh. F. Mountain elements in the flora of the Kyzylkum desert // Uzbek Biological Journal. – Tashkent, 2011. – No. 5. – P. 50–54.

Khasanov F. O., Shomurodov Kh.F., Kadyrov G. Genesis and current state of the flora of the Kyzylkum desert // Problems of Desert Development. – Ashgabat, 2011. – No. 2. – P. 77–80.

Khasanov F. O., Shomurodov Kh.F., Kadyrov G. Brief review and analysis of endemism of the flora of the Kyzylkum desert // Botanical Journal. – Moscow, 2011. – Vol. 96. – No. 2. – P. 237–244.

Kapustina L. A. Patterns of distribution and anthropogenic changes in vegetation of the Bukan-Jetymtau residual mountain system: Abstract of PhD thesis. – Tashkent, 1990. – 24 p.

Zakirov P. K. Flora and vegetation of the low mountains of Kyzylkum and the Nuratau ridge: Abstract of Doctoral thesis. – Tashkent, 1971. – 51 p.

Zakirov P. K., Abdurakhmanov R. A. New plant species for Kyzylkum from residual low mountains (addition to the flora) // Uzbek Biological Journal. – Tashkent, 1971. – No. 2. – P. 35–37.

submitted 14.04.2026;
accepted for publication 28.04.2026;
published 30.04.2026

Contact: arzigull@gmail.com

The Austrian Journal of Technical and Natural Sciences, 2026 No 3–4
ISSN 2310-5607

PREMIER Publishing
ppublishing.org

DOI:10.29013/AJT-26-3.4-9-11

PROCEDURE FOR PLANTING TREES AND SHRUBS INTRODUCED IN KARAKALPAKSTAN

Tursunboev Khamdam Eshbaevich [1]

[1] Karakalpak State University named after Berdakh Republic of Uzbekistan

Cite: *Tursunboev Kh.E. (2026). Procedure For Planting Trees and Shrubs Introduced in Karakalpakstan. Austrian Journal of Technical and Natural Sciences 2026, No 3–4.* https://doi.org/10.29013/AJT-26-3.4-9-11

Abstract

This article examines the characteristics and agronomic requirements for planting introduced trees and shrubs in the Republic of Karakalpakstan. It describes sources of planting material, recommendations for selecting and transporting seedlings, as well as timing and methods of planting, taking into account the climatic conditions of the southern Aral Sea region. Planting technologies for bare-root plants, rootballs, and containers are discussed. It is shown that adherence to agronomic requirements and the correct selection of planting material ensure high survival rates and sustainable development of ornamental plants.

Keywords: *plant introduction, landscaping, ornamental trees, shrubs, planting material, agricultural technology, landscape, Karakalpakstan*

Introduction

Planting trees and shrubs is a key process in greening populated areas. The quality of these efforts determines the formation of sustainable green spaces and the aesthetic appearance of the urban environment. The use of modern machinery and equipment allows for faster planting and more efficient landscape creation.

In the Republic of Karakalpakstan, landscaping is particularly important due to the arid climate, high continental temperatures, and challenging environmental conditions of the southern Aral Sea region. Therefore, special attention is paid to the correct selection of planting material and compliance with agricultural requirements when planting introduced woody plants. The main sources of planting material are ornamental plant nurseries and botanical gardens.

An additional source of planting material can be found in suburban forests, city parks, and other areas where trees are thinned. Nurseries grow various types of planting material: 3–5-year-old shrubs for group plantings and hedges, 6–10-year-old trees for single and group plantings, and larger plants used in landscaping.

Materials and Methods

Deciduous planting stock is most often dug from nurseries with bare root systems and planted in the spring or fall. Some species, such as birch, oak, and conifers, are transplanted with the root ball still attached, which ensures better preservation of the root

system. Transplanting trees and shrubs from nurseries to landscaped areas is a complex and stressful process for the plants. Digging inevitably damages part of the root system, especially the small active roots. Therefore, digging up plants must be done with great care, and during transportation, the roots and aboveground parts of the plants must be protected from drying out and mechanical damage.

Transporting plant roots in the open is prohibited. Before loading the seedlings, place a tarp or soft material (straw, sawdust) on the bottom of the vehicle. Trees and shrubs are placed in groups, and the areas where the trunks touch the sides of the vehicle are protected with soft pads. After loading, the plant roots are wrapped in tarps or damp material. If necessary, plants delivered to the planting site are temporarily placed in the shade and covered with tarps. If planting is delayed, the plants are buried in a trench at an angle of approximately 45°, covering the roots with moist soil above the root collar. The timing of planting woody plants in Karakalpakstan depends on the climate. In most cases, transplanting is done in spring and fall, and in mild winters, from October to April. Conifers are recommended to be transplanted during the period of active root growth – early fall or early spring.

Results and discussion

Experience with landscaping in Karakalpakstan shows that in urban areas, large-sized ornamental tree saplings aged 6–10 years produce the best results. These plants establish themselves more quickly and are less susceptible to damage. To plant trees and shrubs, the locations of the future planting holes are marked out in advance. These markings are made using stakes. Planting holes can be round, square, or rectangular. After excavating the soil, the bottom of the hole is loosened to a depth of 10–12 cm. The size of the planting holes depends on the age and size of the plants (Table 1).

Table 1. *Dependence of planting hole volume (and depth) on plant size*

Seedlings without soil roots	Diameter, m	Depth, m
When planting in natural fertile soils	0,8	0,7
Soils with low nutrient content requiring additional soil amendments and fertilizers	Trees	
	1,0	0,8
	Shrubs	
When planting in trenches:	0,7	0,6
Single-row green wall	0,55	0,6
Double-row green wall	0,8–0,9	0,6

Table 2. *Pit size depending on root soil volume*

Material for packaging a seedling with a lump of earth	Root soil, m Depth, m.			Root soil, m Depth, m.		
	Diameter Circumference Height	Diameter Circumference Height	Diameter Circumference Height	Diameter Circumference Height	Diameter Circumference Height	Diameter Circumference Height
Soft	0,6	–	0,5	1,0	–	0,7
Hard (boxes)	0,8	1,0 × 1,0 1,3 × 1,3 1,5 × 1,5 1,5 × 1,5	0,60 0,60 0,60 0,65	1,5	1,9 × 1,9 2,2 × 2,2 2,4 × 2,4	0,85 × 0,85 0,85 × 0,85

When planting seedlings, it is recommended to immerse their root system in a special mixture of soil, clay, and peat. Adding a 0.001% heteroauxin solution or pre-soaking the roots in water for 24 hours accelerates the formation of new roots and improves plant

survival. When planting, the root collar is positioned 2–3 cm above the soil surface. After backfilling and compacting the soil, it is flush with the ground surface (Table 2).

To create a 1-kilometer-long hedge, approximately 10,000 seedlings are required. Landscaping practice shows that adherence to agricultural requirements plays a crucial role in the successful establishment of introduced woody plants. Reducing the time between digging up the plants and planting them in their permanent location is particularly important. In recent years, new technologies for growing planting material have been actively introduced into landscape construction. One of the most promising is growing plants in containers. This method preserves the root system virtually undamaged and allows for year-round planting, eliminating seasonal planting restrictions.

The ornamental characteristics of different plant groups should also be considered. Fast-growing trees begin to display ornamental qualities 5–6 years after planting, while slow-growing species achieve their maximum ornamental effect only after 10–12 years. Flowering shrubs can acquire their ornamental value in the first or second year after planting. Therefore, when creating new parks and gardens, it is recommended to plant primarily shrubs and fast-growing trees in the first few years, followed by gradual introduction of slow-growing species. This will create a sustainable and aesthetically pleasing green system.

Conclusion

A study of the planting practices of introduced trees and shrubs in Karakalpakstan revealed that successful plant establishment depends on the correct selection of planting material and strict adherence to agricultural requirements. Particular attention should be paid to preserving the root system during excavation, transportation, and planting. Experience shows that the best results are achieved with large-sized, 6–10-year-old tree seedlings, along with proper preparation of planting holes and the use of stimulating solutions. Modern technologies, such as container growing, allow for extended planting periods and minimize root damage. When planning new parks and gardens, it is recommended to plant fast-growing trees and shrubs first, followed by the introduction of slower-growing species. This approach ensures the development of a sustainable, decorative, and aesthetically pleasing green space in the arid climate of the southern Aral Sea region.

References

Dosakhmetov, A.O., & Khoshimov, K.H. (1993). Methodological guidelines for landscaping settlements / – Tashkent, – P. 22–23.

Jumabaeva, M.M., & Kidirbaeva, A.Yu. (2023). Basic requirements for planting green spaces in the urban ecosystem of the Republic of Karakalpakstan // Economics and Society, – 4–2(107). – P. 566–570.

Kurbaniyazov, B.T. (2022). Bioecological features of decorative woody plants in the conditions of the city of Nukus // Universum: Chemistry and Biology: Electronic Scientific Journal, – 8(98). Retrieved from: https://7universum.com/ru/nature/archive/item/14126

Kurbaniyazov, B.T., & Saitova, A. (2017). Problems and prospects of landscaping the city of Nukus // Economics and Society, – 5–1(36). – P. 742–745.

Qayimov, A.Q., & Turok, D. (2012). Planting trees and shrubs in human settlements / Tashkent: Fan va texnologiya, – 124 p.

submitted 15.04.2026;
accepted for publication 29.04.2026;
published 30.04.2026

Contact: arzigull@gmail.com

The Austrian Journal of Technical and Natural Sciences, 2026 No 3–4
ISSN 2310-5607

PREMIER Publishing
ppublishing.org

DOI:10.29013/AJT-26-3.4-12-15

THE EFFECT OF HEAT AND SALINITY STRESS ON THE CONTENT PROLINE AND HYDROGEN PEROXIDE IN LEAVES OF COTTON PLANT

***Maftuna Toshmurodova*[1], *Karomat Kuldoshova*[2], *Sherali Qo'ziyev*[1]**

[1] Departmentof Biochemistry and Biophysics, National University of Uzbekistan

[2] Institute of Bioorganic Chemistry of the Academy of Sciences of the Republic of Uzbekistan

Cite: *Toshmurodova M., Kuldoshova K., Qo'ziyev. Sh. (2026). The Effect of Heat and Salinity Stress on the Content Proline and Hydrogen Peroxide in Leaves of Cotton Plant. Austrian Journal of Technical and Natural Sciences 2026, No 3–4.* https://doi.org/10.29013/AJT-26-3.4-12-15

Abstract

This study investigated the effect of high temperature and salt stress on proline and hydrogen peroxide (H_2O_2) accumulation in the leaves of cotton (*Gossypium barbadense* L.) variety Surxon-103. Exposure to elevated temperature led to a significant increase in proline content and H_2O_2 levels, indicating the activation of stress-related biochemical responses. Although chloride and sulfate salinity increased H2O2 content, proline levels remained relatively stable. In contrast, carbonate salinity acted as the most severe stress factor, characterized by a maximal increase in H2O2 and a pronounced decrease in proline content. The results suggest that these parameters can be used as important indicators of heat and salt stress tolerance in cotton plants.

Keywords: *Cotton (Gossypium barbadense L.), heat stress, salt stress, Proline and hydrogen peroxide*

Introduction

Abiotic stresses such as salinity and high temperature severely affect the growth and productivity of cotton (*Gossypium barbadense L.*) by disrupting physiological and metabolic processes (Zhang et al., 2020). One of the major adaptive responses to these stresses is proline accumulation, which functions in osmotic adjustment and stabilization of cellular structures (Ashraf & Foolad, 2007). At the same time, stress conditions stimulate the overproduction of reactive oxygen species (ROS), particularly hydrogen peroxide (H_2O_2), which serves as both a signaling molecule and an indicator of oxidative stress. Excessive H_2O_2 accumulation can cause oxidative damage to membranes and proteins, leading to impaired cellular functions (Hasanuzzaman et al., 2013). The ability of cotton genotypes to regulate proline metabolism and H_2O_2 detoxification varies significantly and is closely associated with stress tolerance (Iqbal et al., 2019). Therefore, this study investigates changes in proline and H_2O_2 content in the leaves of the cotton variety Surxon-103 under heat and salinity stress conditions.

Method

Plant Material and Heat Stress Treatment

The seeds were initially delinted by short-term treatment with concentrated 96% H_2SO_4. Subsequently, the seeds were soaked in distilled water for several hours. The prepared seeds were then placed on moistened filter paper. Half of the filter papers were transferred into beakers corresponding to three different salinity models, while the remaining half was reserved for cultivation under heat stress conditions. All experimental variants were incubated in a sterilized growth chamber at 28 °C for a period of seven days.

Cotton (*Gossypium barbadense* L.) variety Surxon-103 was grown under controlled conditions at 30 °C (control). Heat stress was applied by exposing plants to 45 °C. Fully expanded leaves were collected from control and heat-stressed plants for biochemical analysis.

Seeds of the cotton (*Gossypium barbadense* L.) variety Surxon-103 were grown under thermostat-controlled conditions using three different salinity models (NaCl, Na_2SO_4, and Na_2CO_3), each applied at two concentrations (100 and 200 mM NaCl; 100 and 200 mM Na_2SO_4; and 100 and 200 mM Na_2CO_3).

Proline determination. Proline content was determined using the ninhydrin method described by Bates et al. (1973). Fresh leaf tissue (0.5 g) was homogenized in 3% sulfosalicylic acid, reacted with acid ninhydrin, incubated at 95 °C for 1 h, and absorbance was measured at 520 nm. Results were expressed as μmol g^{-1} fresh weight.

H_2O_2 determination. H_2O_2 content was measured according to Velikova et al. (2000). Fresh leaves (0.5 g) were extracted with 0.1% TCA, and absorbance was recorded at 390 nm after reaction with potassium iodide. H_2O_2 content was expressed as μmol g^{-1} fresh weight.

Results

In this study, the effect of high temperature stress on oxidative processes in the cotton variety Surxon-103 was evaluated through content of proline and H_2O_2 (**Fig. 1**). Proline levels in the leaf tissues of Surxon-103 were compared under 30 °C (control) and 45 °C (heat stress) conditions. Exposure of the cotton variety Surxon-103 to high temperature stress (45 °C) resulted in notable changes in oxidative stress-related parameters in leaf tissues. Proline content increased from 0.40 under control conditions (30 °C) to 0.52 under heat stress, indicating a 30% increase relative to the osmoprotective compound. In contrast, H_2O_2 levels decreased under stress conditions, declining from 319.7 in the control to 260 at 45 °C, corresponding to an 18.7% reduction compared to the control.

Figure 1. *A) Hydrogen peroxide (H_2O_2) and B) proline contents in the leaves of the cotton variety Surxon-103 under heat stress conditions*

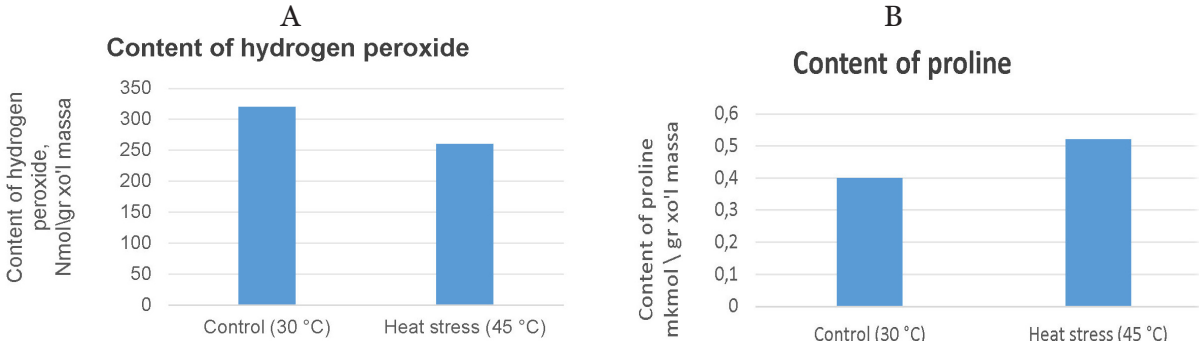

Under chloride salinity conditions, an increase in H_2O_2 content in the Surxon-103 cotton cultivar compared to the control indicated the occurrence of oxidative stress; however, the minimal change in proline content under these conditions suggests that osmotic adjustment and antioxidant defense mechanisms remained relatively stable (**Fig. 2**).

Under sulfate salinity at 200 mM, the increase in H_2O_2 content to 538.2 nmol g^{-1} indicated severe oxidative stress affecting cellular membranes. Concurrently, the decrease in proline content to 166 μmol g^{-1} at this concentration confirmed that the plant's osmotic and antioxidant defense mechanisms were insufficiently activated.

Figure 2. *A) Hydrogen peroxide (H_2O_2) and B) proline contents in the leaves of the cotton variety Surxon-103 under chloride, sulfate, and carbonate salinity conditions*

A

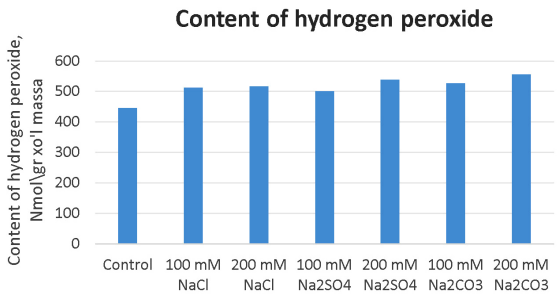

B

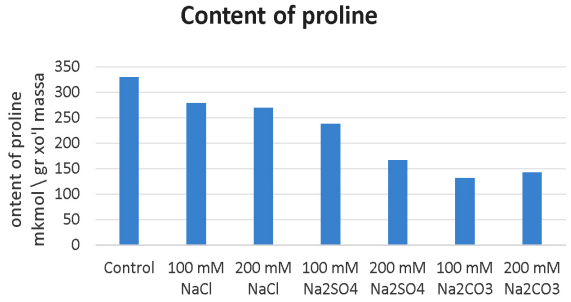

The obtained results revealed that carbonate salinity was the most detrimental. Experimental data showed that exposure of the Surxon-103 cotton cultivar to 100 mM and 200 mM Na_2CO_3 led to an increase in H_2O_2 content to 526.3 and 555.1 nmol g^{-1}, respectively, while proline content decreased to 131 and 142 μmol g^{-1}. This represents up to a 50% reduction compared to the control. Moreover, the pronounced increase in H_2O_2 levels accompanied by a significant decrease in proline content further confirms that the plant's osmotic adjustment and antioxidant defense mechanisms were not adequately activated under carbonate salinity stress.

Discussion

In the present study, heat stress (45 °C) caused a 30% increase in proline content accompanied by an 18.7% decrease in H_2O_2 levels in the leaf tissues of the cotton variety Surxon-103. A similar response pattern has been reported in several plant species, particularly in heat-tolerant genotypes.

Ashraf and Foolad (2007) investigated the role of proline in stress tolerance in cotton and wheat and reported that exposure to high temperature resulted in a significant increase in leaf proline content, while oxidative stress markers such as H_2O_2 and malondialdehyde (MDA) were reduced in tolerant cultivars. The authors concluded that elevated proline levels contributed to enhanced reactive oxygen species (ROS) scavenging capacity, thereby limiting H_2O_2 accumulation. This finding closely aligns with the inverse relationship between proline and H_2O_2 observed in Surxon-103.

Similarly, Hasanuzzaman et al. (2014) studied heat stress responses in rice (*Oryza sativa*) and demonstrated that heat-tolerant varieties accumulated higher amounts of proline under elevated temperature conditions, whereas H_2O_2 levels were significantly lower compared to sensitive genotypes. Their results indicated that proline not only functions as an osmoprotectant but also plays a crucial role in maintaining redox homeostasis by supporting antioxidant enzyme activity, particularly catalase and peroxidase.

In another study, Wang et al. (2016) examined heat stress effects in maize (*Zea mays*) leaves and observed that increased proline accumulation under high temperature was associated with a decrease in H_2O_2 content. The authors attributed this reduction to the activation of enzymatic antioxidants and the direct ROS-scavenging ability of proline. They further reported a negative correlation between proline concentration and H_2O_2 levels, suggesting coordinated regulation of osmolyte synthesis and oxidative stress control.

Taken together, these studies support the results obtained in the present work, where increased proline accumulation in Surxon-103 under heat stress was accompanied by reduced H_2O_2 levels. This response indicates the effective activation of protective mechanisms, including osmotic adjustment and antioxidant defense, which collectively contribute to the mitigation of heat-induced oxidative damage. Therefore, the Surxon-103 variety can be considered to possess a relatively high capacity for maintaining oxidative balance under elevated temperature conditions.

Wang and colleagues investigated the biochemical response of rice (*Oryza sativa L.*) seedlings under NaCl, Na_2SO_4, and Na_2CO_3 salinity conditions. Based on their findings, the authors emphasized that Na_2CO_3 salinity

represents the most detrimental stress factor compared with chloride and sulfate salinity. Under Na_2CO_3 treatment, a sharp increase in H_2O_2 content accompanied by a decrease in proline levels was observed in the seedlings, indicating the induction of severe oxidative stress.

Although chloride and sulfate salinity increased H_2O_2 content, proline levels remained relatively stable. In contrast, carbonate salinity acted as the most severe stress factor, characterized by a maximal increase in H_2O_2 and a pronounced decrease in proline content. This pattern confirms that the plant's osmotic adjustment and antioxidant defense mechanisms were not adequately activated under carbonate salinity stress. These findings provide an important scientific basis for evaluating salinity tolerance and for use in breeding and selection studies.

References

Ashraf, M. & Foolad, M. R. (2007). Roles of *glycine betaine* and *proline* in improving plant abiotic stress resistance. *Environmental and Experimental Botany*, – 59(2). – P. 206–216. DOI: https://doi.org/10.1016/j.envexpbot.2005.12.006

Hasanuzzaman, M., et al. (2014). *Proline and antioxidant defense mechanisms in plant abiotic stress tolerance*. Fundamental and Applied Agriculture. URL: https://www.f2ffoundation.org/faa/index.php/home/article/download/259/245

Ashraf, M. A., Riaz, M., Arif, M. S., Rasheed, R., Iqbal, M., Hussain, I., ... (2019). *The role of nonenzymatic antioxidants in improving abiotic stress tolerance in plants*. In Plant Tolerance to Environmental Stress (P. 129–144). CRC Press.

Zhang, H., et al. (2020). *OsProDH Negatively Regulates Thermotolerance in Rice by Modulating Proline Metabolism and ROS Scavenging*. Rice. URL: https://thericejournal.springeropen.com/articles/10.1186/s12284-020-00422-3

Wang D., Xu M., Xu T., Lin X., Musazade E., Lu J., Yue W., Guo L., Zhang Y. Specific physiological responses to alkaline carbonate stress in rice seedlings // Functional Plant Biology. 2024. – Vol. 51. – No. 10. DOI: 10.1071/FP23161.

submitted 28.01.2026;
accepted for publication 11.02.2026;
published 30.04.2026

Contact: maftunatoshmurodova62@gmail.com

The Austrian Journal of Technical and Natural Sciences, 2026 No 3–4
ISSN 2310-5607

PREMIER Publishing
ppublishing.org

Section 2. Chemistry

DOI:10.29013/AJT-26-3.4-16-21

SYNTHESIS OF NITRO-CONTAINING DERIVATIVES BASED ON MODIFIED CARBOXYMETHYLINULIN

Abdukhamidova Fotima [1], Khusenov Arslonnazar [2], Ibragimova Komila [2], Rakhmanberdiev Gappar [2]

[1] Karshi State Technical University

[2] Tashkent Institute of Chemical Technology

Cite: *Abdukhamidova F., Khusenov A., Ibragimova K., Rakhmanberdiev G. (2026). Synthesis of Nitro-Containing Derivatives Based on Modified Carboxymethylinulin. Austrian Journal of Technical and Natural Sciences 2026, No 3–4.* https://doi.org/10.29013/AJT-26-3.4-16-21

Abstract

The development of methods for synthesizing new derivatives of polysaccharides remains one of the most interesting areas in the chemistry of high-molecular-weight compounds. In this regard, research on obtaining nitrogen-containing derivatives of polysaccharides is particularly important. In the presented study, the chemical modification of carboxymethylinulin was carried out through periodate oxidation. This approach enables the selective cleavage of vicinal diol groups with the formation of reactive aldehyde functionalities along the polymer chain. Such structural transformations significantly expand the possibilities for subsequent functionalization and targeted introduction of biologically active fragments. In the next stage, low-molecular-weight heterocyclic compounds containing nitro groups in the structure were chemically immobilized to the macromolecules of the oxidized inulin ester. Reaction conditions affecting the structural properties of the synthesized compounds have been found.

Keywords: *polysaccharides, inulin, carboxymethylinulin, oxidation, azomethine bond, heterocyclic compounds*

Introduction

Polysaccharides and their derivatives are widely applied in biotechnology, food, cosmetics, and medicine due to their diverse biological activities, including immunostimulatory, antitumor, and anticoagulant effects (Heinze T., Liebert T., 2001; Balzarini J., 2007). Chemical modification such as the introduction of functional groups or low-molecular-weight fragments enables the development of valuable, low-toxicity drugs with controlled properties and prolonged action. Additionally, polysaccharides can serve as effective carriers, improving targeted drug delivery (Langer R., Peppas N. A., 2003; Dash A. K., Konkimalla S., 2012;

Kamalova D., Khusenov A., Abdullayev O., Rakhmanberdiev G., 2024; Klemm D., Heublein B., Fink H. P., Bohn A., 2005).

A key research direction is the synthesis of water-soluble polysaccharide derivatives with controlled molecular weight and degree of substitution, which allows regulation of their physicochemical and biological properties. This requires careful control of reaction conditions (pH, temperature, solvents) and functional group reactivity to ensure selective modification and preservation of the polymer structure (Rinaudo M., 2006; Khusenov A.Sh., Zhonuzokov A.Zh., Kamalova D. S., Tilakov Zh.R., Rakhmanberdiev G., 2024; Khusenov A.Sh., Kamalova D. S., Kee N. K., Rakhmanberdiev G., 2024; Liu T., Ren Q. Q., Wang S., Gao J. N., Shen C. C., Zhang S. Y., Wang Y. H., Guan F., 2023). Among polysaccharides, inulin has attracted particular attention due to its biocompatibility, biodegradability, and non-toxicity. Its reactive hydroxyl groups make it a suitable candidate for chemical modification. Modified inulin derivatives can function as drug carriers, hydrogel components, and matrices for biologically active compounds, with tunable solubility and activity (Wang G., Xie L. M., Huang Z. B., Xie J. H., 2023; Khusenov A. Sh., Zhonuzokov A.Zh., Kamalova D. S., Rakhmanberdiev G., 2024).

In this work, carboxymethylinulin derivatives containing nitro-substituted heterocyclic compounds were synthesized and characterized using physicochemical methods to evaluate structural features and property changes.

Materials and methods

Synthesis of the sodium salt of carboxymethylinulin (Na-CMI). Carboxymethylation of inulin was carried out in isopropanol. Inulin was dispersed for 2 h, then treated with 10% alkali for 1 h. The reaction with sodium chloroacetate (1:3) proceeded at 70 °C for 1.5 h. The product was purified with 96% ethanol and dried at 50–60 °C. The degree of substitution was 30 mol%.

Scheme 1. *Synthesis of sodium carboxymethylinulin (Na-CMI)*

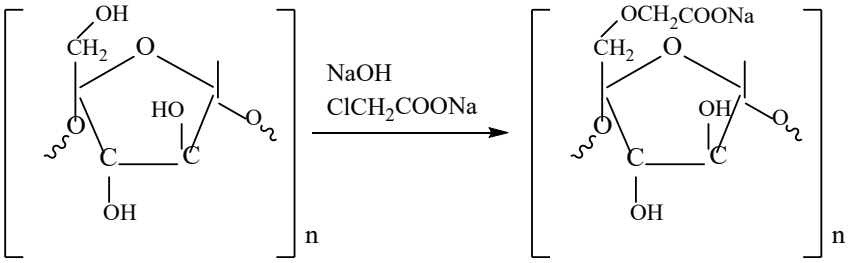

Periodic oxidation of Na-CM I. Thoroughly dried 2 g of Na-CMI was dissolved in 100 ml of water. After the polysaccharide was dissolved, 200 ml of acetate buffer (pH 4.5) and 0.2 n of $NaIO_4$ solution were added at a molar ratio of Na-CMI: IO_4^- = = 1:1.5. The mixture was left to mix for 1–5 hours at room temperature. The periodate oxidation reaction was completed by adding 10 ml of ethylene glycol. Upon completion of the reaction, the mixture was dialized against distilled water until a negative reaction for IO_4^- and IO_3^- ions was obtained. The final products isolated by sublimation drying were analyzed using the iodometric titration method.

Scheme 2. *Periodate oxidation of Na-CMI to dialdehyde carboxymethylinulin (DACMI)*

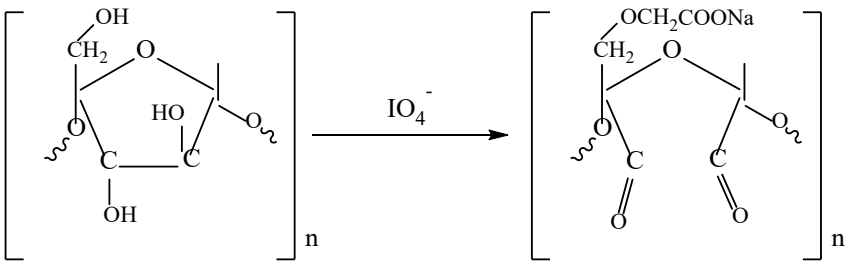

Determination of the number of aldehyde groups using the oxime method. A 100 mg sample of dried DACMI was added to 25 mL of freshly prepared hydroxylamine hydrochloride solution (pH 5.0) in a 250 mL flask. After stirring for 1 hour, the released HCl was titrated with 0.1 M NaOH using bromophenol blue. A blank was run in parallel, and the aldehyde content was calculated from the difference in HCl volume (Isogai A., Saito T., 2013).

Chemical modification of Na-CMI dialdehyde with nitro-containing heterocyclic compounds (2,4-dinitrophenylhydrazone). 0.5 g of DACMI was dissolved in 100 mL water, followed by addition of a nucleophilic reagent (pH 3.0–8.5). The reaction proceeded at room temperature for 1 h. The product was purified by dialysis (48 h) and lyophilized.

Scheme 3. *Chemical modification of DACMI with 2,4-dinitrophenylhydrazine (Schiff base formation)*

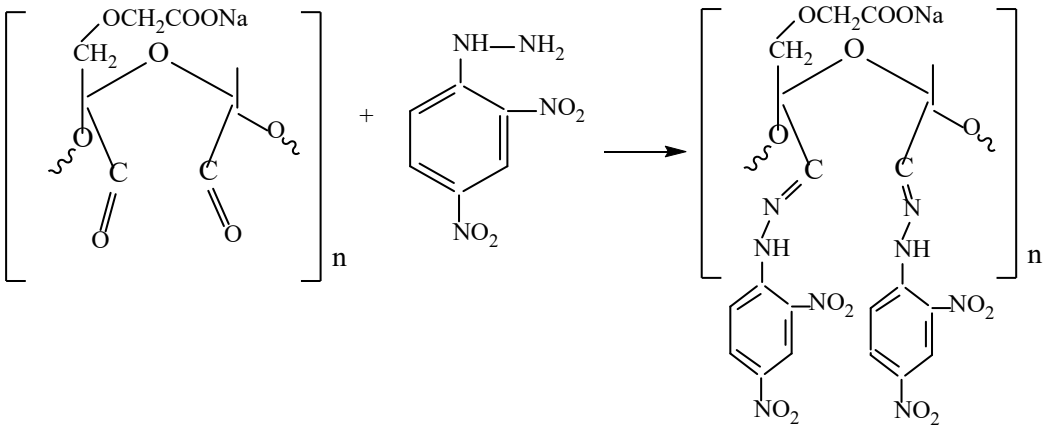

The molecular weight was determined by gel permeation chromatography (GPC) using an Agilent 1260 Infinity II system equipped with an isocratic pump (G7110B), Prima Lux 1000 Å and Prima Linear S columns, and UV (DAD), RI, MDS, and dual-angle light scattering detectors. The nitrogen content in the samples was determined using an Eura EA (Italy) elemental analyzer.

Results and discussions

Dialdehyde polysaccharide derivatives are commonly used to bind compounds containing primary amino groups. This interaction leads to the formation of azomethine (Schiff base, -C=N-) bonds, which are reversible and relatively hydrolyzable. The process occurs in two stages: first, the formation of a carbinolamine intermediate, followed by its dehydration to form the -C=N- linkage (Liu T., Ren Q. Q., Wang S., Gao J. N., Shen C. C., Zhang S. Y., Wang Y. H., Guan F., 2023; Wang G., Xie L. M., Huang Z. B., Xie J. H., 2023).

The reaction rate depends on substituent effects and pH. Electron-withdrawing groups on the aldehyde accelerate amine addition, while electron-donating groups on amines enhance nucleophilicity. Steric hindrance slows the reaction. The rate-determining step varies with pH: in neutral or slightly acidic media, dehydration is slower, whereas in acidic conditions, amine addition becomes limiting. Excess acidity reduces amine nucleophilicity, overall slowing the reaction.

An important factor influencing the degree of substitution of nucleophilic substitution reaction products is the pH of the medium. For each nucleophilic substitution reaction, there is an optimal pH value, i.e., a value or pH region at which the reaction proceeds with maximum speed. To determine the influence of the pH of the medium on the yield and replacement degree of reaction products, the interaction of the nucleophilic reagent with DACMI products was investigated at various pH values. The research results are presented in Table 1. From the presented data, it can be seen that as the pH of the medium increases from 3.0 to 8.0, a gradual decrease in nitrogen content and the degree of DACMI substitution is observed. The maximum values of N (8.5%) and the degree

of substitution (72 mol%) are achieved in an acidic environment (pH 3.0–3.5), indicating the most favorable conditions for the modification reaction to occur.

Table 1. *Influence of pH of the medium on the properties of reaction products based on DACMI*

No.	DACMI oxidation state, mol%	pH of environment	Nitrogen content,%	Degree of substitution, mol%
1.	38	3,0	8,5	72
2.	38	3,5	8,5	72
3.	38	4,0	8,2	70
4.	38	4,5	7,9	65
5.	38	5,0	7,4	61
6.	38	6,0	6,8	54
7.	38	7,0	5,9	43
8.	38	8,0	5,6	39

As pH increases, the reactivity of functional groups likely decreases, which may be related to changes in the protonation degree of active centers and a decrease in the efficiency of reagent interactions. Thus, the acidic medium is optimal for obtaining highly substituted DACMI derivatives with increased nitrogen content.

Table 2. *Influence of the DACMI oxidation state on the composition of reaction products*

No.	DACMI oxidation state, mol%	Nitrogen content,%	Degree of substitution, mol%	Molecular weight, Da
1.	16	4,3	25	3850
2.	23	5,8	41	4230
3.	28	6,5	52	4580
4.	33	8,0	60	4910
5.	38	8,5	72	5200

Figure 1. *Hydrolysis of a sample with a quantitative nitrogen content of 8.5% at pH 2.0*

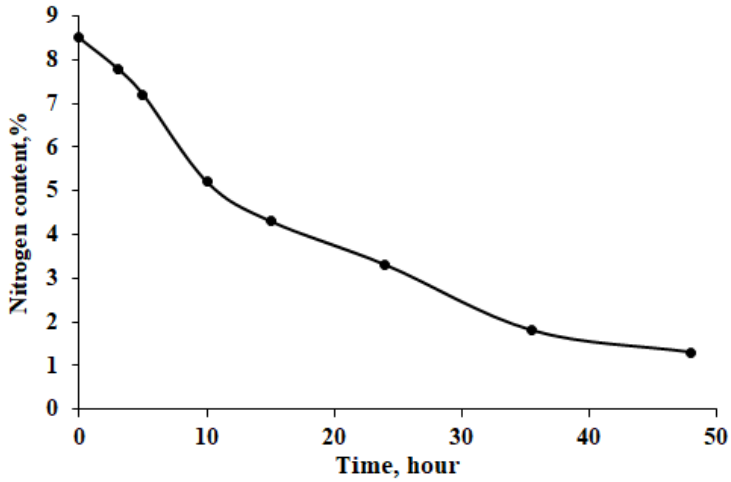

Table 2 shows the dependence of the degree of substitution in the final products on the oxidation state of DACMI.

Table 2 shows that as the oxidation state of Na-CMI increases, the nitrogen content, replacement state, and molecular weight of the reaction products increase. The observed relationship is practically linear in nature, indicating the controllability of the chemical modification process of Na-CMI with varying oxidation states. An increase in nitrogen content indicates the effective introduction of nitrogen-containing functional groups into the macromolecular chain of the polysaccharide, which in turn leads to an increase in the degree of substitution.

To substantiate the formation of covalent azomethine bonds between the low-molecular-weight compound and DACMI, the kinetics of acid hydrolysis of the samples in a buffer medium were studied. The results of this part of the study are presented in **Figure 1.**

The hydrolysis kinetics of a sample with an initial nitrogen content of 8.5% in an acidic medium (pH 2.0) show a rapid initial stage, where nitrogen decreases to ~7–7.4% within the first hours, indicating degradation of labile fragments. Between 5–15 hours, the decrease continues but slows, suggesting transition to more stable, possibly intramolecularly protected groups. After 20 hours, the process becomes gradual, reaching a minimum of ~1.2% by 36–48 hours.

Conclusion

By esterifying inulin under heterogeneous conditions, a carboxymethylinulin sample was obtained. In the next stage, periodic oxidation of inulin ester was carried out, and derivatives with various oxidation states were obtained. The formation of aldehyde groups as a result of oxidation creates active centers that facilitate further covalent bonding reactions. To expand the application range of inulin derivatives, chemical immobilization of heterocyclic compounds into the DACMI structure was performed. The influence of the pH of the medium and the oxidation state of DACMI on the composition of reaction products has been established. Acid hydrolysis has proven that the chemical bonding of the heterocyclic compound with DACMI occurs through labile covalent bonds.

References

Heinze T., Liebert T. (2001). Unconventional methods in cellulose functionalization // Prog. Polym. Sci. – Vol. 26(9). – P. 1689–1762.
Balzarini J. (2007). Carbohydrate-binding agents: a potential future cornerstone for the chemotherapy of enveloped viruses? // Antiviral Chem. Chemother. – Vol. 18(1). – P. 1–11.
Langer R., Peppas N. A. (2003). Advances in biomaterials, drug delivery, and bionanotechnology // AIChE J. – Vol. 49(12). – P. 2990–3006.
Dash A. K., Konkimalla S. (2012). Polymeric modification and its implication in drug delivery: Polymeric carriers for controlled drug delivery // J. Pharm. Sci. – Vol. 101(1). – P. 1–20.
Kamalova D., Khusenov A., Abdullayev O., Rakhmanberdiev G. (2024). Studies of immobilization of some diamines to dialdehydinulin macromolecules // Austrian Journal of Technical and Natural Sciences. – No. 12. – P. 14–18.
Klemm D., Heublein B., Fink H. P., Bohn A. (2005). Cellulose: Fascinating biopolymer and sustainable material // Angew. Chem. Int. Ed. – Vol. 44(22). – P. 3358–3393.
Rinaudo M. (2006). Chitin and chitosan: Properties and applications // Prog. Polym. Sci. – Vol. 31(7). – P. 603–632.
Khusenov A.Sh., Zhonuzokov A.Zh., Kamalova D. S., Tilakov Zh.R., Rakhmanberdiev G. (2024). Synthesis of chlorinulin with different characteristics // Scientific and technical journal of the Fergana Polytechnic Institute. – T. 28. – No. 1. – P. 224–227.
Khusenov A.Sh., Kamalova D. S., Kee N. K., Rakhmanberdiev G. (2024). Synthesis and study of the physicochemical properties of inulin derivatives containing amino groups // Scientific and technical journal of the Fergana Polytechnic Institute. – T. 28, 3. – P. 179–183.
Liu T., Ren Q. Q., Wang S., Gao J. N., Shen C. C., Zhang S. Y., Wang Y. H., Guan F. (2023). Chemical modification of polysaccharides: a review of synthetic approaches, biological activity and the structure–activity relationship // Molecules. – Vol. 28(16). – P. 6073–081.
Wang G., Xie L. M., Huang Z. B., Xie J. H. (2023). Recent advances in polysaccharide biomodification by microbial fermentation: production, properties, bioactivities, and mechanisms // Crit. Rev. Food Sci. Nutr. – Vol. 64(33). – P. 12999–13023.
Khusenov A.Sh., Zhonuzokov A.Zh., Kamalova D. S., Rakhmanberdiev G. (2024). Some features of the chemical structure of chlorinulin // Uzbek scientific, technical and industrial journal Composite materials. – No. 1. – P. 44–47.
Isogai A., Saito T. (2013). Chemical modification of cellulose: reaction mechanisms and analytical evaluation of functional groups // Cellulose. – Vol. 20(3). – P. 1351–1360.

submitted 15.04.2026;
accepted for publication 29.04.2026;
published 30.04.2026

Contact: jamoliddinaa23@gmail.com

The Austrian Journal of Technical and Natural Sciences, 2026 No 3–4
ISSN 2310-5607

PREMIER Publishing
ppublishing.org

DOI:10.29013/AJT-26-3.4-22-25

Mg-Al LAYERED DOUBLE HYDROXIDE NANOPARTICLE-LOADED POLYMERIC MICRONEEDLES FOR ENHANCED DRUG LOADING CAPACITY

Javohir Abdusalomov [1], ***Mukhriddin Suyundikov*** [1], ***Shavkatjon Azizov*** [1], ***Mirkomil Sharipov*** [2], ***Abbaskhan Turayev*** [1]

[1] Institute of Bioorganic Chemistry, Uzbekistan Academy of Sciences, Tashkent, Uzbekistan

[2] Faculty of Mechanical Engineering, Yonsei University, Republic of Korea

Cite: *Abdusalomov J., Suyundikov M., Azizov Sh., Sharipov M., Turayev A. (2026). Mg-Al Layered Double Hydroxide Nanoparticle-Loaded Polymeric Microneedles For Enhanced Drug Loading Capacity. Austrian Journal of Technical and Natural Sciences 2026, No 3–4.* https://doi.org/10.29013/AJT-26-3.4-22-25

Abstract

Layered double hydroxides (LDHs) have emerged as promising nanocarriers for drug delivery due to their high loading capacity and biocompatibility. In this study, Mg–Al LDH nanoparticles were successfully synthesized and utilized as drug carriers for doxorubicin (DOX) loading. The drug-loaded LDH nanoparticles were subsequently incorporated into polyvinyl alcohol (PVA)-based polymeric microneedles to enhance drug loading performance. The encapsulation efficiency and drug loading capacity of the LDH nanoparticles were determined to be 87.3 ± 0.46% and 43.6 ± 0.23%, respectively, indicating a high affinity between doxorubicin and the LDH structure. The incorporation of LDH nanoparticles into the microneedle matrix resulted in a uniform and stable composite system suitable for transdermal applications. Overall, the developed Mg–Al LDH nanoparticle-loaded PVA microneedles demonstrate significant potential as an efficient platform for high-capacity drug loading. This system provides a promising approach for improving the performance of polymeric microneedle-based drug delivery systems.
Keywords: *LDH nanoparticles, drug delivery, drug loading, encapsulation efficiency, microneedle systems*

Introduction

Efficient drug delivery systems remain a key challenge in modern biomedical research due to limitations of conventional methods, such as low bioavailability, rapid degradation, and limited loading capacity. Layered double hydroxides (LDHs), a class of anionic clay materials with a unique lamellar structure, have emerged as promising nanocarriers owing to their tunable composition, high surface area, and excellent biocompatibility. In particular, Mg–Al LDHs exhibit high structural stability and strong interactions with drug molecules, making them suitable candidates for enhanced drug loading applications (Chubar N., Gerda V., Megantari O.,

Mičušík M., Omastová M., Heister K., Man P., Fraissard J., 2013).

Doxorubicin (DOX) is a widely used chemotherapeutic agent with high efficacy against various cancers; however, its clinical application is limited by systemic toxicity and nonspecific distribution. Therefore, developing delivery systems that enhance its loading capacity and stability is essential Polymeric microneedles have emerged as a minimally invasive and effective drug delivery platform, offering painless administration and ease of use. Polyvinyl alcohol (PVA), a biocompatible and water-soluble polymer, is widely used in microneedle fabrication due to its favorable mechanical properties and safety (Lee J. W., Park J. H., Prausnitz M. R., 2008; Ji J., Tay F. E.H., Miao J., Iliescu C., 2006).

In this study, Mg–Al LDH nanoparticles were synthesized and employed as carriers for DOX loading. The drug-loaded LDH nanoparticles were subsequently integrated into PVA-based polymeric microneedles to enhance drug loading capacity. The encapsulation efficiency and drug loading performance of the developed system were systematically evaluated, demonstrating its potential as an effective platform for advanced drug delivery applications.

Materials and methods

Preparation of Doxorubicin Standard Solutions and Calibration Curve. The encapsulation efficiency and drug loading capacity of LDH nanoparticles were evaluated using doxorubicin (DOX) as a model drug. A stock solution of DOX (0.5 mg/mL) was prepared in deionized water, followed by serial dilution to obtain standard solutions (1–100 μg/mL). The absorbance of each solution was measured at 480 nm using a UV–Vis spectrophotometer. All measurements were performed in triplicate, and a calibration curve was constructed by plotting absorbance versus concentration to obtain a linear regression equation for quantitative analysis.

Drug Loading into Mg-Al LDH Nanoparticles. DOX loading into Mg-Al LDH nanoparticles was performed via an adsorption–intercalation mechanism. Briefly, 50 mg of LDH was dispersed in 50 mL of DOX solution (0.5 mg/mL), followed by ultrasonication for 10 minutes to ensure uniform dispersion. The suspension was then stirred at room temperature for 24 h under dark conditions. The pH was adjusted to 4.5–5 using 0.1 M HCl. After incubation, the mixture was centrifuged at 10,000 rpm for 10 min, and the precipitate was washed three times with deionized water to remove unbound drug.

Determination of Encapsulation Efficiency and Drug Loading Capacity. The amount of DOX loaded into LDH nanoparticles was determined using an indirect method. The concentration of free DOX in the supernatant and washing solutions was measured by UV–Vis spectroscopy at 480 nm. The total free drug was calculated as the sum of DOX in all fractions, and the loaded amount was obtained by subtracting it from the initial DOX amount. Encapsulation efficiency (EE%) and drug loading capacity (DL%) were calculated using standard equations.

Result and discussions

In recent years, nanoscale carriers such as nanomicelles, liposomes, metal–organic frameworks (MOFs), and LDHs have been extensively developed to improve drug delivery systems. These materials offer high surface area, tunable structures, and efficient drug encapsulation. MOFs, in particular, have attracted attention due to their porous three-dimensional structures and high loading capacity, enabling efficient drug encapsulation and controlled, stimuli-responsive release. However, their limited stability in aqueous and physiological conditions, as well as potential cytotoxicity, restrict their practical application. In contrast, LDH-based nanocarriers exhibit superior biocompatibility, structural stability, and ease of synthesis. Their lamellar structure enables effective drug intercalation, making them promising alternatives for drug delivery applications (Horcajada P., Chalati T., Serre C., Gillet B., Sebrie C., Baati T., Eubank J. F., Heurtaux D., Clayette P., Kreuz C., Chang J., Hwang Y. K., Marsaud V., Bories P., Cynober L., Gil S., Férey G., Couvreur P., Gref R., 2009).

LDH nanoparticles possess a lamellar structure composed of positively charged hydroxide layers and interlayer anions, enabling effective drug intercalation. This feature makes them highly suitable for drug delivery applications. Previous studies have

shown that LDH systems can efficiently load anticancer drugs, protect them from degradation, and provide controlled release, mainly through an ion-exchange mechanism. In addition, LDHs exhibit excellent biocompatibility, low toxicity, and high stability in biological environments. These properties make LDH nanoparticles promising candidates for enhancing drug loading capacity and improving the performance of drug delivery systems (Yu J., Wang Q., O'Hare D., Sun L., 2017).

DOX loading into LDH nanoparticles was performed via an adsorption–intercalation mechanism using different drug-to-carrier ratios (1:1, 2:1, and 3:1). The results showed that this ratio significantly influences nanoparticle formation and loading performance. At a 1:1 ratio, heterogeneous particle sizes were observed, indicating insufficient interaction between DOX and LDH layers. In contrast, a 3:1 ratio led to particle aggregation due to excess drug disrupting structural integrity. The optimal results were obtained at a 2:1 ratio, which provided uniform morphology, good dispersion, and enhanced stability. After 24 h of stirring, a homogeneous reddish suspension was observed, confirming successful intercalation of DOX into LDH layers. These findings demonstrate that the drug-to-carrier ratio is a key factor affecting both loading efficiency and nanoparticle stability.

Following lyophilization, LDH–DOX nanoparticles were obtained as a dry powder, which readily redispersed in water to form a stable colloidal system without aggregation. This indicates excellent physicochemical stability and hydrophilicity, which are essential for biomedical applications. The obtained nanoparticles were further characterized in terms of hydrodynamic size, polydispersity index (PDI), and morphology to evaluate dispersion quality and stability. These parameters are crucial as they influence cellular uptake and therapeutic efficiency. In addition, encapsulation efficiency and drug loading capacity were analyzed as key indicators of drug loading performance, confirming the effectiveness of the LDH–DOX system.

The concentration of DOX in the supernatant and washing solutions after centrifugation was determined using UV–Vis spectroscopy at a wavelength of 480 nm. A calibration curve constructed from standard DOX solutions (see Fig. 1) exhibited excellent linearity, with a correlation coefficient of $R^2 = 0.9992$, confirming the reliability of the analytical method.

The amount of free (unloaded) DOX was determined by measuring the absorbance of the supernatant and all washing solutions. The total free drug content was calculated as the sum of DOX present in these fractions and was found to be 3.195 mg.

Figure 1. *Calibration curve for DOX constructed from UV spectral values obtained at an emission wavelength (λem) of 480 nm*

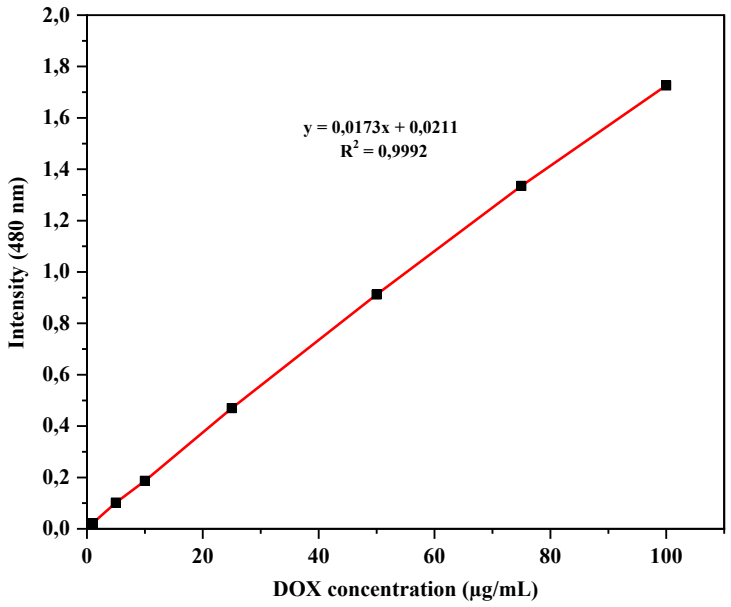

Conclusion

In this study, Mg–Al LDH nanoparticles were successfully used as nanocarriers for DOX loading, achieving high encapsulation efficiency (87.3 ± 0.46%) and drug loading capacity (43.6 ± 0.23%). These results highlight the strong potential of LDH nanoparticles as effective carriers for cytostatic drugs. The high loading performance is attributed to the layered structure of LDH and strong electrostatic interactions with DOX molecules, enhanced under optimized pH conditions. The presence of small amounts of DOX in the supernatant and washing solutions indicates both surface adsorption and intercalation mechanisms. The low standard deviation values confirm the high reproducibility of the method, demonstrating that LDH-based nanocarriers provide a stable and efficient platform for high-capacity drug loading.

References

Chubar N., Gerda V., Megantari O., Mičušík M., Omastová M., Heister K., Man P., Fraissard J. (2013). Applications versus properties of Mg–Al layered double hydroxides provided by their syntheses methods: Alkoxide and alkoxide-free sol–gel syntheses and hydrothermal precipitation, Chem. Eng. J. – 234. – P. 284–299. URL: URL: https://doi.org/10.1016/J.CEJ.2013.08.097.

Mallakpour S., Azadi E., Hussain C. M. (2021). Recent advancements in synthesis and drug delivery utilization of polysaccharides-based nanocomposites: The important role of nanoparticles and layered double hydroxides, Int. J. Biol. Macromol. – 193. – P. 183–204. URL: https://doi.org/10.1016/j.ijbiomac.2021.10.123.

Lee J. W., Park J. H., Prausnitz M. R. (2008). Dissolving microneedles for transdermal drug delivery, Biomaterials – 29. – P. 2113–2124. URL: https://doi.org/10.1016/j.biomaterials.2007.12.048.

Ji J., Tay F. E.H., Miao J., Iliescu C. (2006). Microfabricated microneedle with porous tip for drug delivery, J. Micromechanics Microengineering – 16. – P. 958–964. URL: https://doi.org/10.1088/0960–1317/16/5/012.

Horcajada P., Chalati T., Serre C., Gillet B., Sebrie C., Baati T., Eubank J. F., Heurtaux D., Clayette P., Kreuz C., Chang J., Hwang Y. K., Marsaud V., Bories P., Cynober L., Gil S., Férey G., Couvreur P., Gref R. (2009). Delivery and imaging, Nat. Mater. – 9. – P. 172–178. URL: https://doi.org/10.1038/nmat2608.

Yu J., Wang Q., O'Hare D., Sun L. (2017). Preparation of two dimensional layered double hydroxide nanosheets and their applications, Chem. Soc. Rev. – 46. – P. 5950–5974. URL: https://doi.org/10.1039/c7cs00318h.

submitted 14.04.2026;
accepted for publication 28.04.2026;
published 30.04.2026

Contact: javokhirabdusalomov@gmail.com

The Austrian Journal of Technical and Natural Sciences, 2026 No 3–4
ISSN 2310-5607

PREMIER Publishing
ppublishing.org

DOI:10.29013/AJT-26-3.4-26-31

SYNTHESIS AND SPECTRAL ANALYSIS OF FAPbI3 PEROVSKITE QUANTUM DOTS AT ROOM TEMPERATURE IN VARIOUS SOLVENTS

Kodirbek Norboyev [1], ***Khurshid Tashpulatov*** [1], ***Rayhon Rakhmonova*** [1], ***Jasurbek Khursandov*** [1], ***Doston Toshpulatov*** [1]

[1] Sharof Rashidov nomidagi Samarqand Davlat Universiteti

Cite: *Norboyev K., Tashpulatov Kh., Rakhmonova R., Khursandov J., Toshpulatov D. (2026). Synthesis and Spectral Analysis of Fapbi3 Perovskite Quantum Dots at Room Temperature in Various Solvents. Austrian Journal of Technical and Natural Sciences 2026, No 3–4.* https://doi.org/10.29013/AJT-26-3.4-26-31

Abstract

In this study, $FAPbI_3$ perovskite quantum dots were synthesized at room temperature using ligand-assisted redeposition in the presence of various antisolvents. The resulting red-emitting quantum dots had an absorption edge at a wavelength of 700 nm, and the emission maxima appeared in the range of 650 nm to 800 nm, depending on the type of antisolvent. In addition, these results showed that the appropriate selection of the volume ratio of ligands during synthesis plays an important role in the formation of the quantum dot size. The synthesized $FAPbI_3$ perovskite quantum dots can be used to prepare solar cells, LED lamps, and photovoltaic (PV) devices due to their excellent optoelectronic properties.

Keywords: *LARP method, perovskite quantum dots, ligands, $FAPbI_3$, antisolvent, solar cells, emission spectrum*

Introduction

In the twenty-first century, the rapid development of the economy has led to an increase in energy consumption and the increasing attention to renewable energy sources based on solar cells (Zhang, Y., 2026). Solar cells based on high purity silicon are mainly used on an industrial scale. Such solar cells have disadvantages such as high efficiency, high stability, high assimilation efficiency, high material consumption, and high cost. Therefore, perovskite-structured materials for solar cells have attracted the attention of many researchers in the last decade (Sharma, R., Sharma, A., Agarwal, S., & Dhaka, M. S., 2022). The most popular methods for synthesizing perovskite quantum dots include the hot injection method and the room temperature ligand-assisted redeposition method (Gielen, D., Boshell, F., Saygin, D., Bazilian, M. D., Wagner, N., & Gorini, R., 2019). One of these two methods, the ligand-assisted redeposition method (LARP), has the great advantage of not requiring an inert atmosphere and high temperature. This method is widely used in the production of perovskite-structured materials containing bromide ions. However, perovskite-structured materials containing iodide ions can also be synthesized by selecting appro-

priate ligands, antisolvents, and solvents (Vighnesh, K., Wang, S., Liu, H., & Rogach, A. L., 2022; Tong, Y., Bladt, E., Aygüler, M. F., Manzi, A., Milowska, K. Z., Hintermayr, V. A., & Feldmann, J., 2016; Zhang, D., Yu, M., Xu, Y., Li, D., Huang, Y., Yu, C., & Lin, J., 2022; Pan, H., Xu, X., Liu, J., Li, X., Zhang, H., Huang, A., & Xiao, Z., 2021).

The synthesis of perovskite nanocrystals using hot injection (HI) is one of the most common methods to obtain high quality luminescent materials, and is a method for producing nanocrystals in a high temperature and inert environment. The hot injection method was first used in the synthesis of cadmium chalcogenide (CdS, CdSe, CdTe) nanocrystals. Then this method began to be widely used in the synthesis of nanomaterials with other compositions (Zhong, Q., Cao, M., Xu, Y., Li, P., Zhang, Y., Hu, H., & Zhang, Q., 2019). In addition, it is also widely used in the processes of obtaining perovskite-structured quantum dots. The synthesis of perovskite quantum dots with a $CsPbBr_3$ composition by the LARP method is described in another literature. For this, CsBr and $PbBr_2$ were first dissolved separately in equal molar ratios in ethanol and dimethylformamide (DMF), respectively. 10 ml of hexane and the corresponding ligands were added to a three-necked flask and mixed at room temperature on a magnetic stirrer. After a certain time, lead and cesium precursors were added to a three-neck flask in precise amounts, forming a yellow precipitate. The quantum dots were separated from this solution by centrifugation and remelted to form bright fluorescent perovskite quantum dots (Chun, F., Zhang, B., Li, Y., Li, W., Xie, M., Peng, X., & Yang, W., 2020).

Another study used DMF as a solvent in the synthesis of $MAPbI_3$ quantum dots based on the LARP method. In this process, it was also noted that the stability of quantum dots depends on the amount of DMF. That is, changes in the stability of $MAPbI_3$ quantum dots were observed by using high and less DMF. It was observed that when less DMF was used as a solvent, the quantum dots did not lose their bright fluorescence for up to 12 hours. It was studied that the use of more DMF led to the degradation of bright red fluorescence for up to 1 minute. The use of less solvent also leads to fewer crystal defects. In a similar process, DMF was used as a solvent and chloroform as an antisolvent in the synthesis of $MAPbI_3$ quantum dots using the LARP method. Oleic acid (OAc) and oleylamine (OAm) were used for surface passivation. The use of chloroform as an antisolvent helps to increase the stability of perovskites containing iodide ions (Tashpulatov, K., Norboev, K., Toshpulatov, D., Magdiev, S., Nasimov, A., Mirzaev, S., & Yakubov, B., 2025).

The aim of this work is to synthesize $FAPbBI_3$ perovskite dots using various antisolvents and study their spectral properties. We utilize modern characterization method to study prepared nanocrystals.

Method of research

Synthesis of perovskite quantum dots with FAPbI3 composition. Using acetonitrile (ACN) instead of DMF as a good solvent, $FAPbI_3$ perovskite quantum dots were synthesized by the LARP method at room temperature. For this, FAI and PbI_2 salts were initially weighed on an analytical balance in a 1:1 molar ratio. The measured salts were dissolved in 2 ml of acetonitrile and kept in an ultrasonic bath for 15 minutes. The resulting mixture was formed in a yellowish paste. That is, these salts were observed to have limited solubility in acetonitrile. The resulting mixture was stirred for 1 hour on a magnetic stirrer and ligands such as OAm and OAc were added in a volume ratio of 0.5:3. After the ligands were added, the yellowish paste slowly began to dissolve and a dark mass was formed at the bottom of the vessel and a bright yellow homogeneous solution was formed at the top. The solution was stirred at a constant speed on a magnetic stirrer for two hours at a temperature of 50 °C. After 2 hours, 0.1 ml of the resulting precursor was added to 5 ml of antisolvent hexane, which was stirred vigorously on a magnetic stirrer. As a result, the formation of colloidal $FAPbI_3$-containing perovskite quantum dots with clear bright red fluorescence was observed (Figure 1). When 0.1 ml of the same precursor was added to chloroform, which was stirred vigorously on a magnetic stirrer, the formation of quantum dots was also observed.

Figure 1. *Scheme of room temperature synthesis of $FAPbI_3$ quantum dots based on acetonitrile (good solvent) and hexane/chloroform (antisolvent)*

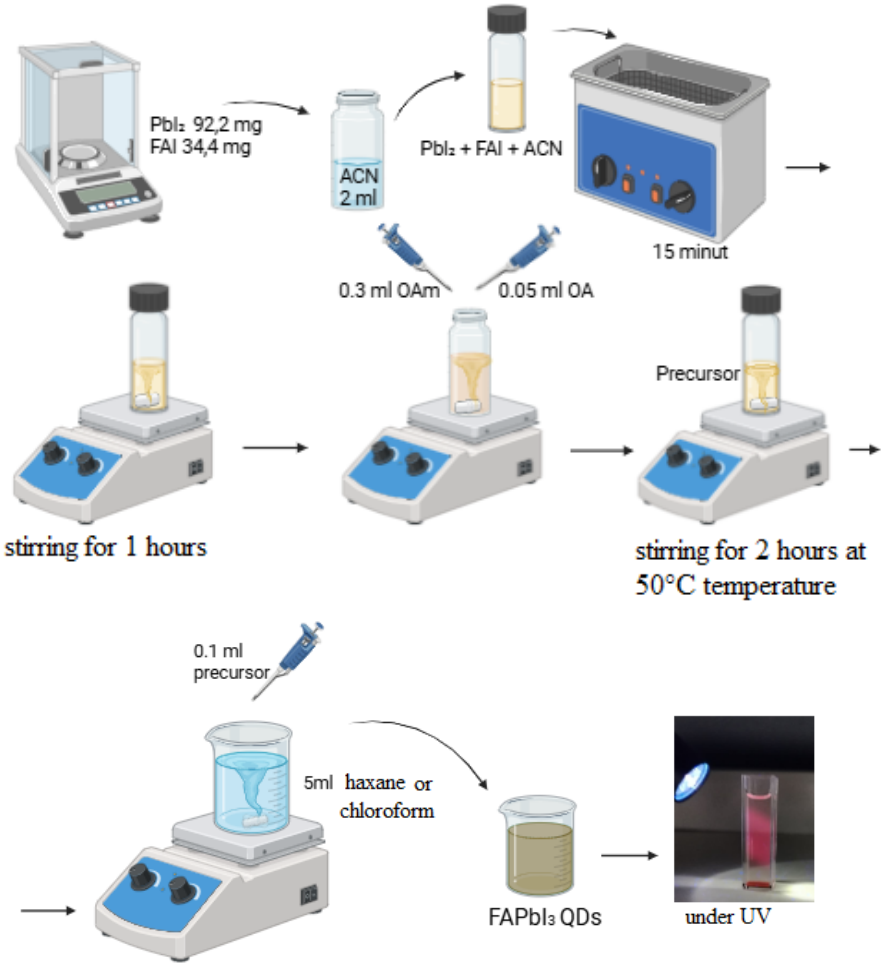

Research results

$FAPbI_3$ perovskite quantum dots belong to the type of inorganic-organic perovskite quantum dots. The difference from inorganic perovskites is that inorganic-organic perovskite quantum dots contain organic cations (such as MA^+, FA^+) as cations. In the synthesis of such perovskites, it is also important to choose "good" and "bad" solvents. "Good" and "bad" solvents for FAI and PbI2 salts are listed in Table 1 below.

Table 1. *Properties of solvents used in the LARP method and the solubility of salts in them*

"Good" solvent	b.p. (°C)	Relative permittivity	FAI solubility	PbI_2 solubility	"Bad" solvent
DMSO	189	46.7	Good	Good	Toluene
DMF	153	36.7	Good	Good	Toluene
ACN	82	37.5	Poor	Poor	Toluene
DMSO	189	46.7	Good	Good	Chloroform
DMF	153	36.7	Good	Good	Chloroform
ACN	82	37.5	Poor	Poor	Chloroform
DMSO	189	46.7	Good	Good	Hexane

"Good" solvent	b.p. (°C)	Relative permittivity	FAI solubility	PbI_2 solubility	"Bad" solvent
DMF	153	36.7	Good	Good	Hexane
ACN	82	37.5	Poor	Poor	Hexane

Solvents such as DMF and ACN have been widely used in the synthesis of $FAPbI_3$ quantum dots. The fact that FAI and PbI_2 salts dissolve well in the "good" solvent DMF makes it convenient to prepare precursors. The salts were poorly soluble in acetonitrile. However, the solubility improved with the addition of ligands and the effect of temperature

$$FAI_{(ACN)} + PbI_{2(ACN)} \rightarrow FAPbI_{3(ACN)}$$

The absorption spectra of $FAPbI_3$ quantum dots synthesized in acetonitrile/chloroform ("good"/"bad" solvents) is unique, with a broad range between 400 and 700 nm. It was found that the broad absorption band and the absorption edge characteristic of quantum dots are at 700 nm (Figure 2). The emission spectrum of the same $FAPbI_3$ perovskite quantum dots has a unique spectrum, with a maximum emission at around 760 nm, indicating that they have red emission (Figure 3).

Figure 2. *Absorption spectrum of $FAPbI_3$ perovskite quantum dots dispersed in chloroform*

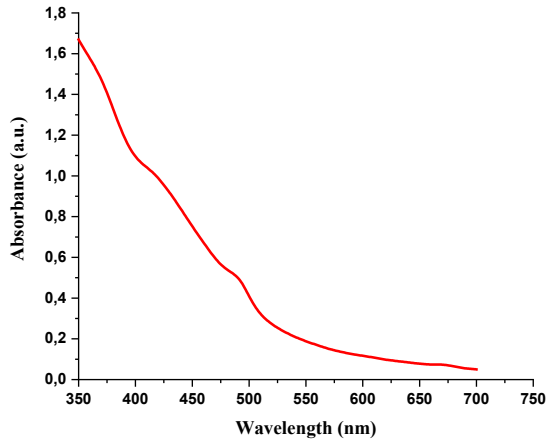

Figure 3. *Emission spectrum of $FAPbI_3$ perovskite quantum dots*

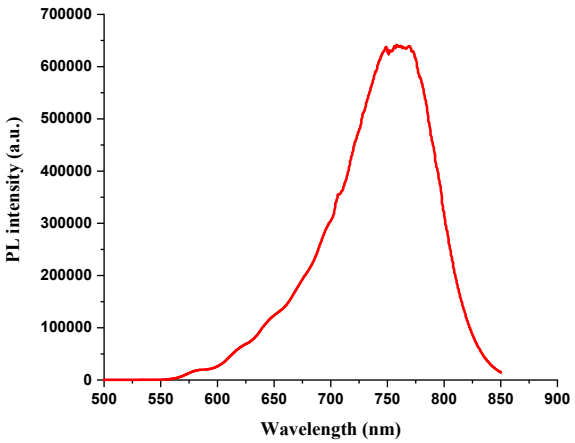

Figure 4. *Emission spectra of $FAPbI_3$ perovskite quantum dots prepared using DMF/chloroform and DMF/hexane pair*

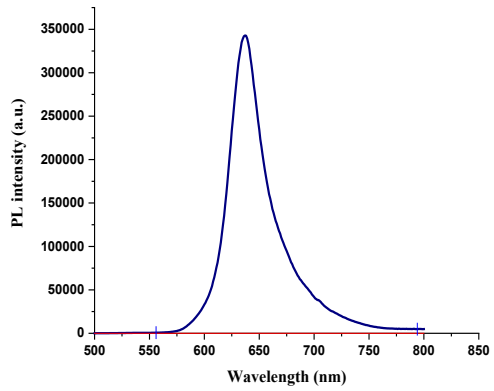

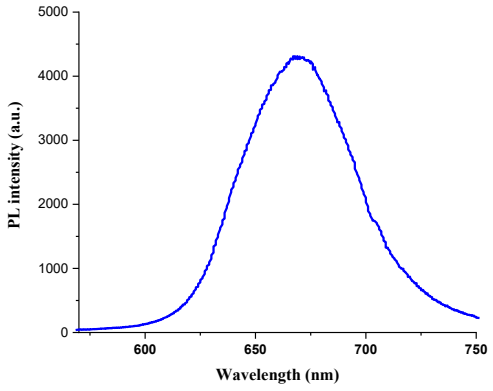

Based on the spectra above, it can be said that the ACN/chloroform pair is consistent with each other and the obtained quantum dots are relatively monodisperse. However, the emission spectra of $FAPbI_3$ perovskite synthesized based on the DMF/chloroform and DMF/hexane solvent pairs are also depicted in Figure 4. The emission spectrum of

$FAPbI_3$ perovskite quantum dots synthesized based on the DMF/chloroform solvent pair has orange color with the emission maximum at 640 nm. The emission spectrum of $FAPbI_3$ perovskite synthesized in the DMF/hexane pair was also found to be unique and has a red emission at 670 nm.

Based on the spectrum of the perovskite quantum dots obtained based on the DMF/chloroform pair, it can be said that the perovskite quantum dots obtained based on the DMF/chloroform pair are also monodisperse. It was observed that the solution of $FAPbI_3$ quantum dots synthesized based on the DMF/hexane was transparent and very homogeneous and had a red emission under a UV lamp. However, it can be observed that $FAPbI_3$ quantum dots synthesized based on the DMF/chloroform pair are more stable and intense than quantum dots obtained based on the DMF/hexane pair (Figure 4).

The full-with at half maximum (FWHM) value of the $FAPbI_3$ perovskite quantum dots synthesized based on the DMF/hexane pair was found to be larger than that of the sample synthesized based on the DMF/chloroform pair. Therefore, it can be proposed that the monodispersity is lower than that of the particles synthesized based on the DMF/chloroform pair. When the FWHM value of the $FAPbI_3$ perovskite quantum dots synthesized based on the DMF/chloroform pair was calculated based on the emission spectrum, it was found that the monodispersity is lower than that of acetonitrile/chloroform. This is because the emission spectrum of the perovskite synthesized based on the DMF/chloroform pair has a smaller amount of red shift and a wider shift towards the emission side.

Conclusions

$FAPbI_3$ perovskite quantum dots were synthesized at room temperature by the ligand-involved redeposition method in various “good” and “bad” solvents. According to the results of spectral analysis, it was found that the effect of solvents and ligands is an important factor in the formation of quantum dots. During the experiments, relatively stable $FAPbI_3$ perovskite quantum dots were observed in samples synthesized in the presence of DMF/chloroform and ACN/chloroform pairs. It was observed that the formation and stability of quantum dots were ensured when the volume ratios of ligands were added in the case of 0.5:3 (oleylamine: oleic acid).

References

Zhang, Y. (2026). Solar PV in the 21st century: Aligning technological growth with sustainability. Next Energy, 10, 100499. URL: https://doi.org/10.1016/j.nxener.2025.100499

Sharma, R., Sharma, A., Agarwal, S., & Dhaka, M. S. (2022). Stability and efficiency issues, solutions and advancements in perovskite solar cells: A review. Solar Energy, – 244. – P. 516–535. URL: https://doi.org/10.1016/j.solener.2022.08.001

Gielen, D., Boshell, F., Saygin, D., Bazilian, M. D., Wagner, N., & Gorini, R. (2019). The role of renewable energy in the global energy transformation. Energy strategy reviews, – 24. – P. 38–50. URL: https://doi.org/10.1016/j.esr.2019.01.006

Vighnesh, K., Wang, S., Liu, H., & Rogach, A. L. (2022). Hot-injection synthesis protocol for green-emitting cesium lead bromide perovskite nanocrystals. URL: https://doi.org/10.1021/acsnano.2c11689

Tong, Y., Bladt, E., Aygüler, M. F., Manzi, A., Milowska, K. Z., Hintermayr, V. A., & Feldmann, J. (2016). Highly luminescent cesium lead halide perovskite nanocrystals with tunable composition and thickness by ultrasonication. Angewandte Chemie International Edition, – 55(44). – P. 13887–13892. URL: https://doi.org/10.1002/anie.201605909

Zhang, D., Yu, M., Xu, Y., Li, D., Huang, Y., Yu, C., ... & Lin, J. (2022). Solvothermal synthesis of perovskite $CsPbCl_3$ nanoplates and improved photoluminescence performance through postsynthetic treatment. Optical Materials, – 127. – 112257 p. URL: https://doi.org/10.1016/j.optmat.2022.112257

Pan, H., Xu, X., Liu, J., Li, X., Zhang, H., Huang, A., & Xiao, Z. (2021). Microwave-assisted synthesis of blue-emitting cesium bismuth bromine perovskite nanocrystals without

polar solvent. Journal of Alloys and Compounds, – 886. – 161248 p. URL: https://doi.org/10.1016/j.jallcom.2021.161248

Zhong, Q., Cao, M., Xu, Y., Li, P., Zhang, Y., Hu, H. & Zhang, Q. (2019). L-type ligand-assisted acid-free synthesis of $CsPbBr_3$ nanocrystals with near-unity photoluminescence quantum yield and high stability. Nano Letters, – 19(6). – P. 4151–4157. URL: https://doi.org/10.1021/acs.nanolett.9b01666

Chun, F., Zhang, B., Li, Y., Li, W., Xie, M., Peng, X., ... & Yang, W. (2020). Internally-externally defects-tailored $MAPbI_3$ perovskites with highly enhanced air stability and quantum yield. Chemical Engineering Journal, – 399. – 125715 p. URL: https://doi.org/10.1016/j.cej.2020.125715

Tashpulatov, K., Norboev, K., Toshpulatov, D., Magdiev, S., Nasimov, A., Mirzaev, S., & Yakubov, B. (2025). Facile Synthesis of Stable and Highly Luminescent $MAPbI_3$ Perovskite Quantum Dots. Journal of Fluorescence, – 35(10). – P. 9553–9557. URL: https://doi.org/10.1007/s10895-025-04258-2

submitted 16.04.2026;
accepted for publication 30.04.2026;
published 30.04.2026

Contact: norboyevqodirbek880@gmail.com

The Austrian Journal of Technical and Natural Sciences, 2026 No 3–4
ISSN 2310-5607

PREMIER Publishing
ppublishing.org

DOI:10.29013/AJT-26-3.4-32-37

INVESTIGATION OF SURFACTANTS AND FLOCCULATION PROCESSES IN COAL BENEFICIATION

Kucharov Azizbek [1]***, Yusupov Farkhod*** [1]***, Khalilov Sanjar*** [1]***, Qurbonov Azizjon*** [1]***, Toshboboyeva Ra'no*** [2]

[1] Institute of General and Inorganic Chemistry of the Academy of Sciences of Uzbekistan. Tashkent, Uzbekistan

[2] Institute of polymer chemistry and physics, Academy of sciences of the Republic of Uzbekistan, Tashkent, Uzbekistan

Cite: *Kucharov A., Yusupov F., Khalilov S., Qurbonov A., Toshboboyeva R. (2026). Investigation of Surfactants and Flocculation Processes in Coal Beneficiation. Austrian Journal of Technical and Natural Sciences 2026, No 3–4.* https://doi.org/10.29013/AJT-26-3.4-32-37

Abstract

This study represents an integral investigation of the joint effect of surfactants, flocculants, and Al^{3+}/SO_4^{2-} ions on the enrichment of 2BR-B2 and 2BOMSH-B2 varieties of brown coal. The study involves detailed examination of such aspects as dosage of flocculant (25–100 g/Mg), ion effects, agglomeration behavior, settling process kinetics, floc sizes, and transformation of mineral phase under experimental conditions with the help of X-ray fluorescence (XRF). In relation to colloid chemistry aspects, special attention is paid to such phenomena as interfacial interactions, electrical double layer compression, and bridging between particles. This makes the coagulation and separation processes much more efficient, since it is proved that the creation of stable and optimally-sized aggregates substantially increases the efficiency of mineral separation, whereas the excess of flocculant causes the formation of less stable heterophase systems. Thus, it is concluded that the control over colloidal destabilization and interfacial modifications are critical for enhancing the ash content and calorific value of coal.

Keywords: *coal beneficiation, surfactants, flocculation, coagulation, Al^{3+}ions, SO_4^{2-}ions, XRF analysis, colloidal systems*

Introduction

Coal continues to be one of the main sources of energy in the world, especially in developing countries, whose contribution in terms of energy composition is considerable (Ejtemaei, M., Ramli, S., Osborne, D., & Nguyen, A. V., 2019). The moisture and ash content present in the low-rank coal lowers the efficiency of the coal, resulting in higher levels of emission of gas pollutants and particulates when burning (Kucharov, A., Xalilov, S., & To'Rayeva, X., 2024). Consequently, the need to improve the physicochemical nature of the coal through processes of beneficiation has

taken center stage in recent times for reasons of environmental protection and energy efficiency, involving the removal of ash-forming minerals and increasing the heating value of the coal (Kocharov, A.A., Mamanazarov, M.M., Atabekova, D.L., & Toshbobayeva, R.A., 2024). Various methods of coal beneficiation have been investigated over the years, with special emphasis on the use of surfactants to enhance flotation performance via modification of interfacial properties and bubble-particle attachment (Song, S., 2008). Moreover, recent research proved that using coagulant ions, including Al^{3+}, together with anions, such as SO_4^{2-}, positively influences the process of particles agglomeration and improves the ability to remove minerals from the fuel material (Kucharov, A., Xalilov, S., Farxod, Y., Toshboboyev, R.N., Bekturdiyev, G., Turayeva, K., ... & Golib, T., 2026). However, the impact of interaction between surfactants, colloid system and inorganic ions requires additional investigation, especially the dependencies among flocculant concentration, the degree of ionic influence, distribution of particle sizes and general efficiency of beneficiation process (Eshmetov, R., Salikhanova, D., Jumaeva, D., Eshmetov, I., & Sagdullaeva, D., 2022). Kinetics of agglomeration, densification of aggregates, and their sedimentation have to be examined as well (Zhou, F., Yan, C., Wang, H., Zhou, S., & Liang, H., 2017).

Research method

The beneficiation procedure involved an integrated multi-stage technique, depicted in Fig. 1 below, which relied on both physical and surface chemistry approaches to increase mineral content removal. First, raw samples of brown coal (2BR-B2 and 2BOMSH-B2) underwent hydraulic washing to facilitate elimination of impurities loosely adhered to the particles' surface (Laskowski, J. S., & Yu, Z., 2000). Further, a size classification (screening) step ensured that an adequate particle size distribution was obtained for effective processing at a next stage (Zeng, H., Tang, H., Sun, W., & Wang, L., 2022).

Figure 1. *Integrated coal beneficiation process with washing, classification, gravity separation, and surfactant-assisted flotation*

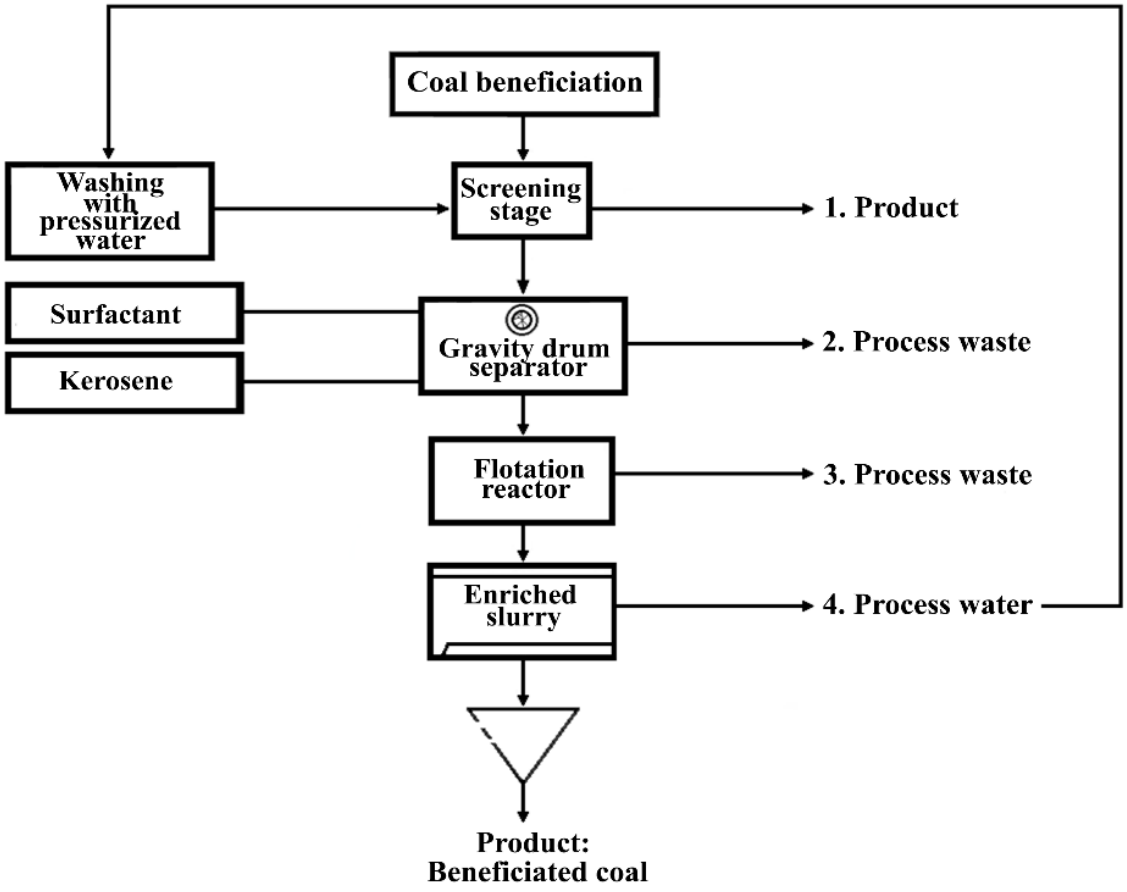

Gravitational separation entailed the use of a gravitational drum separator to achieve separation of heavier fractions using density differences between organic components of coal and minerals (Niu, C., Xia, W., Li, Y., Bu, X., Wang, Y., & Xie, G., 2022). For better selectivity, surfactant-assisted flotation was performed in a flotation reactor with a mixture of surfactants and kerosene acting as a collector, thus increasing hydrophobicity of coal particles while rejecting hydrophilic mineral components (Wang, Y., Wei, D., Qin, W., Jiao, F., Luo, X., & Pan, Z., 2023). Flocculants together with inorganic ions such as Al^{3+} and SO_4^{2-} were added to promote agglomeration of fine mineral particles due to their electrostatic charges neutralization and polymer bridging (Qurbonov, A., Kucharov, A., & Yusupov, F., 2024).

Result and discussion

The XRF spectrum of the raw coal sample (Figure 2) clearly shows that the composition of the minerals is largely dominated by the aluminosilicates due to strong intensity signals of both Si (36.55 cps) and Al (17.31 cps). At the same time, the Fe content (101.22 cps) clearly implies the involvement of iron-based minerals, which serve as active centers for surface reactions. Thus, it can be concluded that the ash-forming material consists mainly of quartz and aluminosilicate minerals containing iron phases. In this case, the interaction forces are dominated by electrostatic repulsion caused by the negative charge of the particles, thus providing stability of the suspension.

Figure 2. *XRF spectrum of raw coal showing major (Si, Al, Fe) and trace elements*

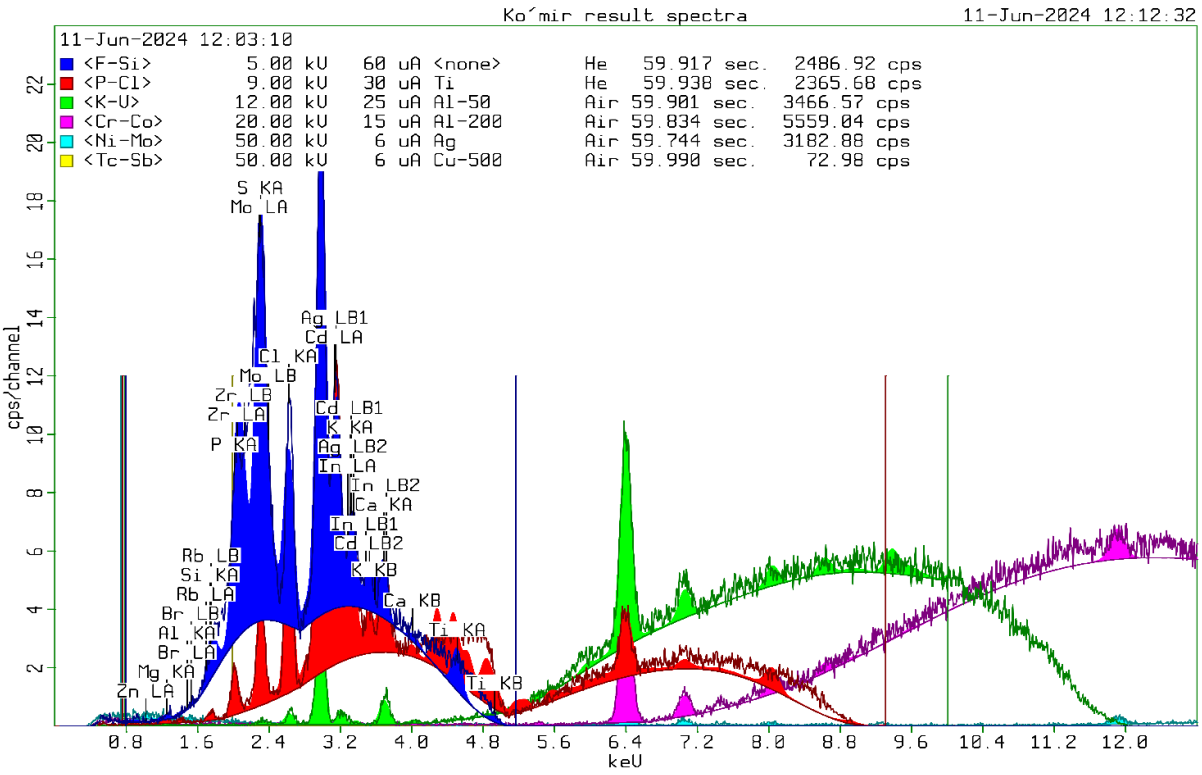

It can be seen from the comparative XRF results presented in Table 1 that there was a significant reorganization of minerals, demonstrating the transformation through the process of coagulation. The first thing that comes to mind is the increase in Fe intensity, which rises from about 101 cps to ≥150 cps (Δ50 cps).

Kinetics of flocculation shown in Figure 3 show high sensitivity to dosage used during the initial stage of settling. In particular, within 1–2 minutes after initiation of the process, maximum settling velocities were achieved at 17–18 cm/min for 25 g/Mg dosage and 19–20 cm/min for 100 g/Mg dosage. Thus, fast aggregation of dense and bulky flocs occurred during the early stages of flocculation.

Table 1. *Comparative XRF intensities (cps) of coal before and after Al^{3+}/SO_4^{2-} treatment showing mineral phase redistribution*

Element	Sample 1 Intensity (cps)	Sample 2 Intensity (cps)
Si	36.5	30–32
Al	17.3	22–25
Fe	101	≥150
S	49.1	70–80
Ca	12.9	15–18
Ti	0.79	1.5–2.0
Mo / Ag / Zr	4–9	≥15–25

Kinetics of flocculation shown in Figure 3 show high sensitivity to dosage used during the initial stage of settling. In particular, within 1–2 minutes after initiation of the process, maximum settling velocities were achieved at 17–18 cm/min for 25 g/Mg dosage and 19–20 cm/min for 100 g/Mg dosage. Thus, fast aggregation of dense and bulky flocs occurred during the early stages of flocculation.

Figure 3. *Effect of flocculant dosage (25, 50, and 100 g/Mg) on the settling kinetics of coal suspension, showing the temporal evolution of settling velocity and the transition from rapid floc formation to consolidation-controlled sedimentation*

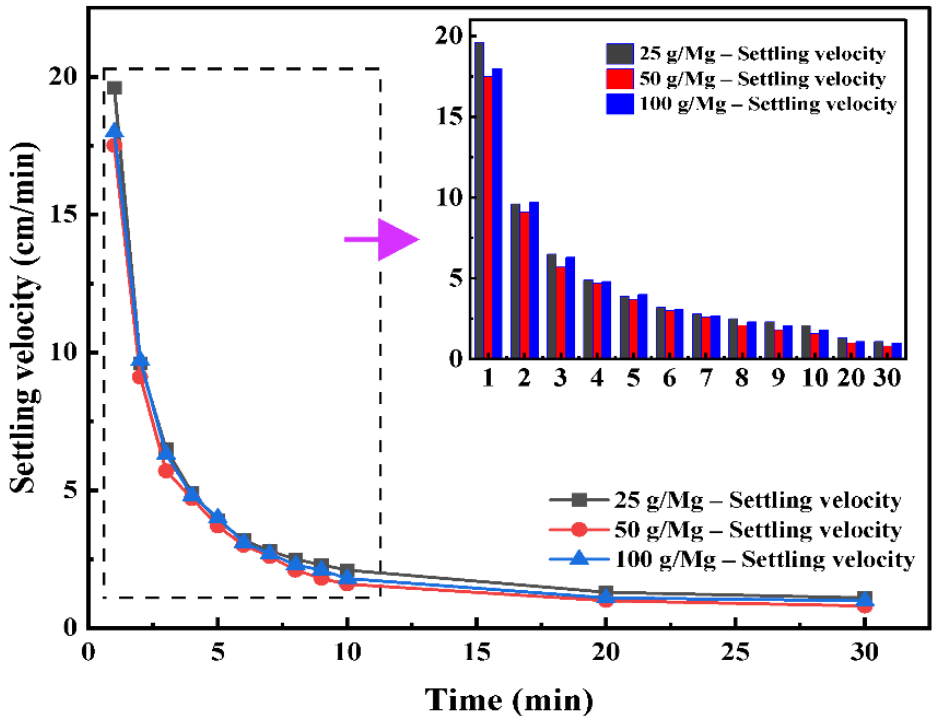

Consistent rise in the value of settling velocity with the increase in dosage shows that higher dosage leads to stronger interparticle interactions and thus to creation of larger and more efficient settling units with larger settling diameters (Fig. 3). As evident from Table 2, the beneficiation procedure results in considerable improvement in the physicochemical and energetic parameters of 2BR-B2 and 2BOMSH-B2 brown coals. Primarily, this is achieved due to efficient de-mineralization of the material and reconstruction of its organic skeleton. For example, there is a pronounced decrease in the content of ash

(Ad) from 35–60% to 20–35%, which corresponds to the reduction by 25 percentage points, which implies effective separation of inorganic minerals, including aluminosilicates and iron-containing compounds.

While acknowledging the obvious advancements that have been achieved, one cannot overlook the lack of proper zeta potential analysis, long-term stability assessment, and scale-up confirmation, which necessitates future research into establishing quantitative relationships between colloidal behavior and practical efficiency at an industrial level, investigating other combinations of surfactants and flocculants, and fine-tuning the processing parameters.

Table 2. *Comparative physicochemical properties of 2BR-B2 and 2BOMSH-B2 brown coals before and after beneficiation, highlighting the reduction of ash-forming components and enhancement of fuel quality indicators*

Physicochemical properties name	Symbol	Unit of measurement	Before enrichment		After enrichment	
			2BR-B2	2BOMSH-B2	2BR-B2	2BOMSH-B2
Moisture content	W_t	%	20–40	20–40	15–40	15–40
Ash content	A_d	%	35–60	35–60	20–35	20–35
Particle size	d	mm	1–100	1–100	Briquette	Briquette
Volatile matter formation	V^{daf}	%	32–50	35–45	44–55	40–55
High heat of combustion	Q_S^{daf}	MJ/kg	15.5–25.4	15.4–23.8	28.6	29.7
Low heat of combustion	Q_i^{daf}	MJ/kg	6.9–12.8	8.9–13.6	15.9	15.7

Conclusion

These results confirm that the simultaneous use of surfactants, flocculants, and Al^{3+}/SO_4^{2-} ions provides for a great rise in effectiveness of brown coal processing with regard to selective coagulation and mineral separation. Indeed, considerable decrease in ash percentage (from 35% to 60% to 20% to 35%) and calorific power (28–30 MJ/kg) confirm this achievement. Moreover, the examination of the dynamics of settlement of particles and their size distribution demonstrates that the optimal dosage of flocculant (~50 g/Mg) allows for obtaining stable and homogenous aggregates, while excessive dosages create a structurally heterogeneous system. The obtained XRF data prove the effectiveness of this technology in terms of the electrostatic interaction between particles and bridging mechanism.

References

Ejtemaei, M., Ramli, S., Osborne, D., & Nguyen, A. V. (2019). Synergistic effects of surfactant-flocculant mixtures on ultrafine coal dewatering and their linkage with interfacial chemistry. *Journal of Cleaner Production*, – 232. – P. 953–965.

Kucharov, A., Xalilov, S., & To'Rayeva, X. (2024). Results Of Scientific Analysis Of Coal Processing Products. *Journal of Experimental Studies*, – 2(3). – P. 9–16.

Kocharov, A.A., Mamanazarov, M.M., Atabekova, D.L., & Toshbobayeva, R.A. (2024). Scientific Analysis of the Ecological Condition of the Soils Around the Angren Coal Mine. In *International Congress on Biological, Physical And Chemical Studies (ITALY)* (P. 19–21).

Song, S. (2008). Experimental studies on hydrophobic flocculation of coal fines in aqueous solutions and flotation of flocculated coal. *International Journal of Oil, Gas and Coal Technology*, – 1(1–2). – P. 180–193.

Kucharov, A., Xalilov, S., Farxod, Y., Toshboboyev, R. N., Bekturdiyev, G., Turayeva, K., ... & Golib, T. (2026). A comprehensive technological approach for the selective recovery of aluminum oxide and rare earth elements from coal processing. *Eureka: Physics & Engineering*, – (2). – 13 p.

Eshmetov, R., Salikhanova, D., Jumaeva, D., Eshmetov, I., & Sagdullaeva, D. (2022). Influence of ultrasonic impact on oil preparation processes. *Journal of Chemical Technology & Metallurgy*, – 57(4).

Zhou, F., Yan, C., Wang, H., Zhou, S., & Liang, H. (2017). The result of surfactants on froth flotation of unburned carbon from coal fly ash. *Fuel*, – 190. – P. 182–188.

Laskowski, J. S., & Yu, Z. (2000). Oil agglomeration and its effect on beneficiation and filtration of low-rank/oxidized coals. *International Journal of Mineral Processing*, – 58(1–4). – P. 237–252.

Zeng, H., Tang, H., Sun, W., & Wang, L. (2022). Deep dewatering of bauxite residue via the synergy of surfactant, coagulant, and flocculant: Effect of surfactants on dewatering and settling properties. *Separation and Purification Technology*, – 302. – 122110 p.

Niu, C., Xia, W., Li, Y., Bu, X., Wang, Y., & Xie, G. (2022). Insight into the low-rank coal flotation using amino acid surfactant as a promoter. *Fuel*, – 307. – 121810 p.

Wang, Y., Wei, D., Qin, W., Jiao, F., Luo, X., & Pan, Z. (2023). Effect of nanobubbles on particle flocculation in sodium oleate-calcite flotation system. *Minerals Engineering*, – 204. – 108438 p.

Qurbonov, A., Kucharov, A., & Yusupov, F. (2024, March). Development of a technology for obtaining an anti-corrosion coating for gas pipelines. In *AIP Conference Proceedings* (Vol. 3102. – No. 1. – p. 040008). AIP Publishing LLC.

submitted 14.04.2026;
accepted for publication 28.04.2026;
published 30.04.2026

Contact: sciuzb@mail.ru

The Austrian Journal of Technical and Natural Sciences, 2026 No 3–4
ISSN 2310-5607

PREMIER Publishing
ppublishing.org

DOI:10.29013/AJT-26-3.4-38-42

SYNTHESIS OF MIXED-LIGAND COMPLEX COMPOUNDS BASED ON MANGANESE(II) METAGYDROXIBENZOATE AND NICOTINAMIDE AND STUDY OF THE CORRELATIONS BETWEEN THEIR COMPOSITION AND STRUCTURE

Kurbanova Rakhila Salievna [1], ***Khasanov Shodlik Bekpulatovich*** [1], ***Abdullaeva Zubayda Shavkatovna*** [3]

[1] Khorezm Ma'mun Academy

[2] Department of Technology, Urgench Ranch Technological University

Cite: *Kurbanova R.S., Khasanov Sh.B., Abdullaeva Z.Sh. (2026). Synthesis of Mixed-Ligand Complex Compounds Based on Manganese(Ii) Metagydroxibenzoate and Nicotinamide and Study of the Correlations Between Their Composition and Structure. Austrian Journal of Technical and Natural Sciences 2026, No 3–4.* https://doi.org/10.29013/AJT-26-3.4-38-42

Abstract

In this article, the synthesis, structure, and physicochemical properties of complex compounds formed with nicotinamide in the presence of the divalent manganese ion were studied in detail. m-Hydroxybenzoic acid was used as the primary ligand. The elemental analysis method was employed to determine the composition of the synthesized complex compounds. The optimized geometric structure, molecular electrostatic potential (MEP), frontier molecular orbitals (HOMO–LUMO), and global chemical reactivity parameters were analyzed based on density functional theory (DFT) quantum chemical calculations.

Keywords: *Nicotinamide, Mn(II) m-hydroxybenzoate, complex compound, elemental analysis, DFT, HOMO–LUMO, X-ray phase analysis*

Introduction

Meta-hydroxybenzoic acid (m-hydroxybenzoic acid) is one of the bioactive compounds that has a phenolic structure and a carboxyl group. It is used in medicine mainly due to its antibacterial, antifungal, and antioxidant properties (Salgado, 2020). The phenolic structure of meta-hydroxybenzoic acid helps neutralize reactive oxygen species, which plays an important role as a protective agent against cellular oxidative stress. Additionally, its derivatives are widely used as intermediates in the synthesis of pharmaceuticals. For example, parabens (methylparaben, propylparaben) used as certain antiseptics and preservatives (Beppu et al., 2019; Karakaya, 2018) is a key component in production. Manganese compounds are diverse in composition and structure, forming various compounds depending on the ligand and synthesis conditions. For manganese, as for Fe and Cr, the presence of an Mn3O skeleton in its complexes with carboxylic acids is most characteristic (Migwi, Nyamato, Ojwach, Darkwa, 2025).

Among the polynuclear manganese compounds, the twelve-nuclear complex occupies a special position. $[Mn_{12}O_{12}(O_2CR)_{16}(H_2O)x]^n$ (n=0–2) compounds have been found to exhibit unusual magnetic properties. As an example of a twelve-nuclear complex, $[Mn_{12}O_{12}(O_2CPh)_{16}(H_2O)_4]$ was obtained from the solid oxidation of a manganese acetate mixture. Benzoic acid was introduced into pyridine, and then the compound was isolated with ethanol (Christou G., 2005). In our subsequent study, $[Mn_3(HL)_2(H_2O)_6]$ n (I) (H_4L = 3-(2,4-dicarboxyphenyl)-2,6-dicarboxypyridine) was synthesized and characterized by IR, elemental analysis, and single-crystal X-ray diffraction. (CIF CCDC No.1915189). The complex crystallizes in the monoclinic C2/c space group with Z=4, a=20.6597(11) Å, *b*=9.0949(5) Å, c=20.6041(12) Å, and β =110.056 (6)°. The crystal consists of $\{Mn_3\}$ clusters of three-nuclear Mn (II) ions, each coordinated by four independent HL^3 ligands, with these trimer units linked into a 2D structure via the pentadentate HL^3 ligand in alternating bis(bridging) and chelate coordination modes. Thermogravimetry, powder X-ray diffraction, and magnetic measurement experiments are also performed to determine thermal stability, phase purity, and magnetism. The results show that weak antiferromagnetic interactions occur between the Mn(II) centers in the bridged three-nuclear $\{Mn_3\}$ cluster (Liu, Ma, Feng, 2020). In a subsequent study, Mn(II) and Zn(II) complexes of a Schiff ligand derived from ethylenediamine and 4-chloro(N-phenyl)formamide were synthesized and characterized by various analytical, spectral, and magnetic methods. The antioxidant potential of the prepared compounds was evaluated by DPPH radical scavenging activity analysis and the FRAP method, and the following general trend was identified: BHT > ligand ~ Zn(II) complex > Mn(II) complex > ligand precursor. Subsequently, the antibacterial efficacy of all synthesized compounds was evaluated against two Gram-negative and two Gram-positive bacteria (Juyal, Thakuri, Panwar, Rashmi, Bukhari, Nand, 2024). The Mn(II) complex exhibited better bactericidal properties than the other compounds, which was confirmed by studying the molecular docking interactions. In studies conducted with the S. typhi cell membrane protein OmpF complex and S. aureus tyrosyl-tRNA synthetase, the Mn(II) complex, followed by the ligand and the Zn(II) complex, showed the highest binding affinity (Osman, et al., 2020; Matmurodova, Xudoyberganov, Hasanov, Taxirov, 2023).

Research method

In this study, in addition to the Mn(II) ion and nicotinamide complex, m-hydroxybenzoic acid was also synthesized. Preparation of manganese(II) m-hydroxybenzoate: Initially, 0.1 g of m-hydroxybenzoic acid was mixed in 30 ml of distilled water and gradually heated. After the acid had completely dissolved, 5 ml of a 0.1 N KOH solution was added to the mixture to create an alkaline environment. Then, 0.8 grams of $MnSO_4 \cdot 5H_2O$ was dissolved in 10 ml of distilled water, added to the solution, and transferred into a 50 ml beaker.

$$\mathbf{2C_7H_6O_3 + 2KOH + MnSO_4 \cdot 5H_2O \rightarrow}$$
$$\mathbf{\rightarrow [MnC_7H_5O_3)_2] + K_2SO_4 + 8H_2O}$$

0.22 grams of nicotinamide was completely dissolved in 8 ml of distilled water and slowly added to the solution of manganese(II) m-hydroxybenzoate.

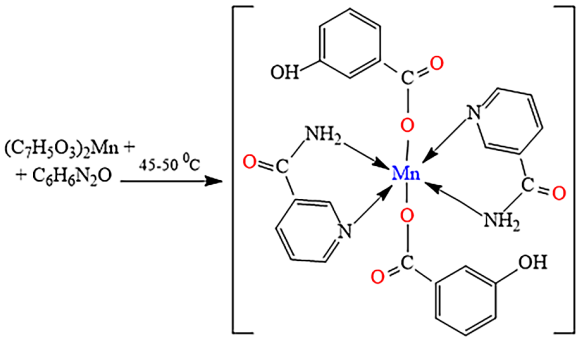

Typically, manganese sulfate appears colorless in solution, but during the experiment the solution turned light brown, indicating that Mn(II) ions had formed a complex. Upon the addition of nicotinamide, the solution became more stable, indicating that it acted as a secondary ligand in the formation of the complex structure. This suggests the formation of a mixed-ligand coordination complex.

Results analysis

An elemental analysis was conducted to determine the composition of the obtained

compound, and the product's yield was 88% (Table 1).

Table 1. *Results of the elemental analysis of the obtained complex compound*

Compounds		$[Mn(C_7H_5O_3)_2(C_6H_6N_2O)_2]$
Mn	Calculated	10.08
	Determined	10.01
N	Calculated	9.65
	Determined	9.55
C	Calculated	54.02
	Determined	53.05
O	Calculated	21.08
	Determined	20.10
Compound color		Light brown

A quantum chemical analysis was performed on the coordination compound based on Mn(II) meta-droxibenzoate and nicotinamide to determine the spatial structure of the central atom, its energetic parameters, and the upper- and lower-lying vacant molecular orbitals. The resulting complex compound was optimized using the 3–21G B3LYP method within the DFT framework of Gaussian 9.0 software. The total electronic energy of the system was calculated to be –2960 Hartree, which confirms the stability of the optimized electronic structure. The absence of imaginary frequencies (NImag=0) indicates that the obtained geometry corresponds to a true minimum on the potential energy surface. The calculated Debye dipolar moment of 3.267651 indicates an intrinsically polar molecular system.

Figure 1. *Electrostatic potential (ESP) map (a), Molecular electron density model (b), Geometric structure and bond lengths (c), Molecular orbitals and electron distribution (HOMO–LUMO) (d)*

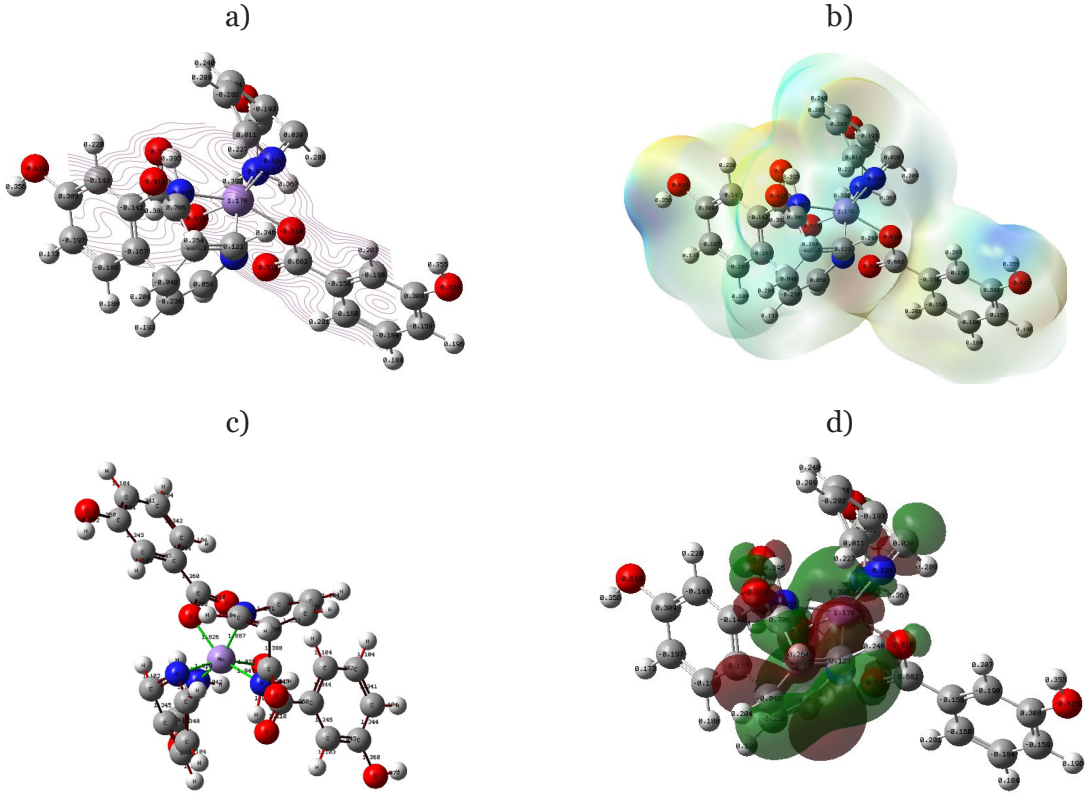

The electrostatic potential distribution of the complex, with red and blue contours, depicts the distribution of electrostatic charge in different parts of the molecule. Red regions have high electron density and typically indicate sites that interact with electrophilic reagents. The molecular electron density model reflects the overall electron distribution and electron density clouds of the molecule. The blue and green regions represent areas of high electron density, while the yellow and reddish regions indicate areas of relatively low electron density. The geometric structure and bond lengths are shown, along

with the bonds between the complex's atoms and their lengths. Mn(II) and amid ions are located in the coordination environment. Oxygen (O) and nitrogen (N) atoms are shown by their interatomic bond lengths. Molecular orbitals and electron distribution of the molecule's highest occupied molecular orbital (HOMO) and lowest unoccupied molecular orbital (LUMO) are depicted. The red and green orbitals illustrate the electron motion in the molecule and its propensity for potential chemical reactions. HOMO is the highest-energy orbital capable of donating electrons. LUMO is the lowest vacant orbital prone to accepting electrons. The red and blue contours depict the electrostatic charge distribution in different parts of the molecule. The red regions have high electron density and typically indicate the sites where electrophilic reagents interact.

Figure 2. *X-ray diffraction patterns of marganese(II) hydroxybenzoate and nicotinamide and of the complex compound derived from them*

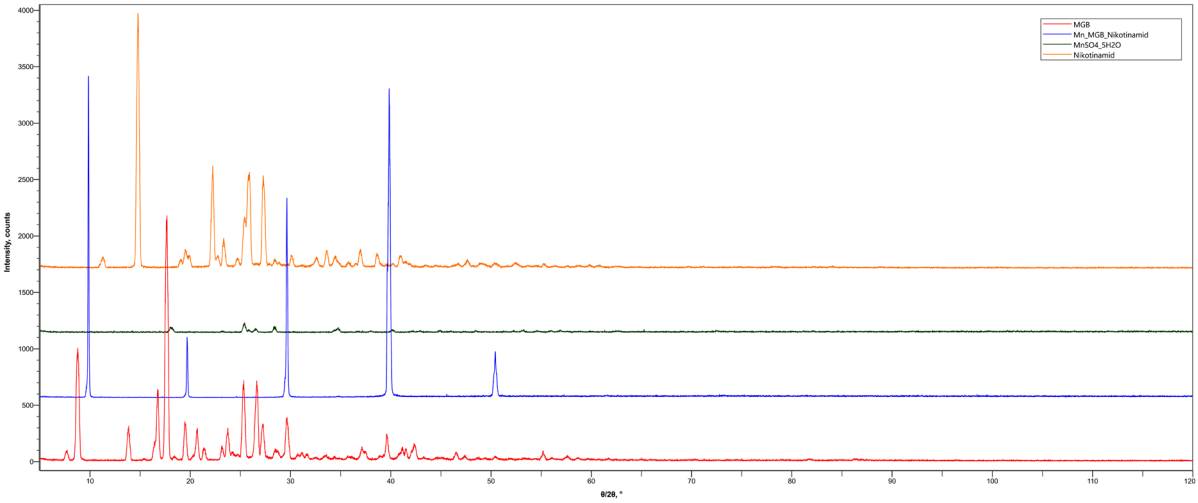

The X-ray diffraction pattern of the complex compound differs from those of the starting materials (nicotinamide and meta-hydroxybenzoic acid). The appearance of new peaks and the disappearance of earlier ones indicate the formation of a new crystal phase. This confirms the synthesis of the complex compound by X-ray phase analysis. According to the X-ray diffraction analysis and phase formation, the nicotinamide diffraction pattern exhibits medium-intensity but characteristic peaks (in the 15°–30° range). The high- or medium-intensity peaks do not correspond to metagidroxybenzoic acid. In the complex compound, however, new high-intensity peaks appear (for example, at ~20°, ~30°, and ~40°). Some peaks have disappeared or shifted. This is not a simple sum of the initial substances, indicating the formation of a new crystal phase.

Conclusion

According to the research results, it was determined that a successful complex is formed with nicotinamide and Mn(II) ions, and that these complexes have an octahedral structure. Nicotinamide is a strong ligand, and the resulting manganese(II) complexes are highly stable, possess a strong coordination sphere, and exhibit distinct spectroscopic changes. According to X-ray diffraction pattern comparison and phase formation analysis, manganese sulfate produced lower-intensity and fewer peaks. The degree of crystallinity is lower. The peaks differ significantly from those of nicotinamide and m-hydroxybenzoic acid, indicating their distinctiveness. The X-ray diffraction pattern of the new $[Mn(C_7H_5O_3)_2(C_6H_6N_2O)_2]$ complex compound shows new, high-intensity peaks. Some peaks have disappeared or changed, while others have shifted. This indicates the formation of a new crystal phase. The X-ray diffraction pattern of the complex compound does not directly match those of the other two substances, which proves that the compound is not a simple mixture but a true complex.

References

Beppu, M., et al. (2019). Drug delivery using phenolic acid–based polymeric carriers. Biomaterials Science, – 7(9). – P. 3697–3705. Retrieved from: https://doi 10.1039/C9BM00540D

Christou, G. (2005). Single-molecule magnets: a molecular approach to nanoscale magnetic materials. Polyhedron, – 24. – P. 2065–2075. Retrieved from: https://doi.org/10.1016/j.poly.2005.08.010

Juyal, V., Thakuri, S. C., Panwar, M., Rashmi, O., Bukhari, N. A., & Nand, V. (2024). Manganese(II) and zinc(II) metal complexes of novel bidentate formamide-based Schiff base ligand: Synthesis, structural characterization, antioxidant, antibacterial, and in-silico molecular docking study. Frontiers in Chemistry – Inorganic Chemistry. Retrieved from: https://doi.org/10.3389/fchem.2024.1414646

Karakaya, S., & El, S. N. (2018). Phenolic Acid Derivatives Used in Food and Medicine: A Review. Trends in Food Science & Technology, – 85. – P. 64–72. Retrieved from: https://doi 10.1016/j.tifs.2018.02.001

Liu, X. F., Ma, N. N., Feng, F., et al. (2020). Syntheses, Crystal Structure, and Magnetic Property of a New Mn (II) Complex with an Aromatic N-heterocyclic Tetracarboxylic Acid Ligand. Russian Journal of Coordination Chemistry, – 46. – P. 365–370. Retrieved from: https://doi.org/10.1134/S1070328420050036

Matmurodova, F., Xudoyberganov, O., Hasanov, Sh., & Taxirov, Y. (2023). Synthesis of coordination compound of Mn(II) ion with 2-(diethylamino)ethyl-aminobenzoate. O‘zbekiston milliy universiteti xabarlari, – [3/1]. – P. 396–399. Retrieved from: https://nuu.uz

Migwi, F. K., Nyamato, G. S., Ojwach, S. O., & Darkwa, J. (2025). A review of the recent coordination chemistry and catalytic applications of pyrazole and pyrazolyl transition metal complexes. Coordination Chemistry Reviews, – 450. – P. 214–256 Retrieved from: https://www.sciencedirect.com/science/article/abs/pii/S0010854525009439

Osman, U. M., et al. (2020). Thiosemicarbazide ligand complexes of Ni(II): XRD and spectroscopic studies. Journal of Molecular Structure, – 1215. – P. 128–135. Retrieved from: https://www.sciencedirect.com/science/article/pii/S002228602031317X

Salgado, H. R. N. (2020). Hydroxybenzoic acids as potential antimicrobial and anti-inflammatory agents: Mechanisms and applications. Journal of Pharmacy and Pharmacology, – 72(6). – P. 773–790. Retrieved from https://doi 10.1111/jphp.13215

submitted 08.04.2026;
accepted for publication 22.04.2026;
published 30.04.2026

Contact: raxila.qurbonova.94@gmail.com; shadlik@mail.ru; zubayda.abdullayeva.91@mail.ru

The Austrian Journal of Technical and Natural Sciences, 2026 No 3–4
ISSN 2310-5607

PREMIER Publishing
ppublishing.org

DOI:10.29013/AJT-26-3.4-43-46

EXTRACTION OF CELLULOSE FROM TYPHA ANGUSTIFOLIA L. AND PHRAGMITES COMMUNIS TRIN. BY AN ACID–ALKALINE METHOD AND ITS THERMAL ANALYSIS

Mahmudov Muxammadrasul Sodiqjon ogli [1],
Mamajanov Gulomjon Odiljanovich [1],
Toshmatov Yoldoshali Raxmonovich [1]

[1] Namangan State University

Cite: *Mahmudov M.S., Mamajanov G.O., Toshmatov Y.R. (2026). Extraction of Cellulose from Typha angustifolia L. and Phragmites communis Trin. by an Acid–Alkaline Method and Its Thermal Analysis. Austrian Journal of Technical and Natural Sciences 2026, No 3–4.* https://doi.org/10.29013/AJT-26-3.4-43-46

Abstract

This article examines the extraction of cellulose from *Typha angustifolia* L. and *Phragmites communis* Trin. using acid–alkaline chemical methods and investigates its thermal properties. Thermogravimetric analysis (TGA) and differential thermal analysis (DTA) were applied to the cellulose samples to evaluate weight changes and thermal reactions under the influence of temperature. The obtained results made it possible to identify differences in the thermal stability and degradation characteristics of cellulose isolated from the two plant sources.

Keywords: *cellulose, thermogravimetry, differential thermal analysis, Typha angustifolia, Phragmites communis, acid–alkaline extraction, thermal stability*

Introduction

Cellulose is a natural polymer widely used in various industrial sectors, including paper production, printing, pharmaceuticals, and the manufacture of composite materials. Traditionally, cellulose is primarily derived from wood; however, due to the limited availability of forest resources and environmental concerns, alternative sources are being explored.

Fast-growing aquatic plants, particularly *Typha angustifolia L.* and *Phragmites communis* Trin., produce large amounts of biomass and are considered promising raw materials for cellulose production.

The process of cellulose extraction involves various chemical methods, and different analytical techniques are employed to evaluate its quality. Thermal analysis, especially TGA and DTA, plays a crucial role in determining the thermal stability and degradation characteristics of cellulose.

In this study, cellulose was extracted from two plant species using an acid–alkaline method, and a comparative analysis was conducted based on thermal analysis results.

Materials and Methods

Cellulose Extraction

Samples obtained from *Typha angustifolia* L. and *Phragmites communis* Trin. were initially treated in a 7% nitric acid solution. Subsequently, lignin and other components were removed through processing in a 3% alkaline solution. Thereafter, a bleaching process was carried out using a mixture of alkali and hydrogen peroxide (H_2O_2) in a 1:3 ratio, resulting in purified cellulose.

Thermal Analysis

The extracted cellulose samples were subjected to thermogravimetric analysis (TGA) and differential thermal analysis (DTA). The analyses were performed using a Shimadzu thermal analyzer. Samples were heated in an argon atmosphere from 25 °C to 500 °C at a heating rate of 10 °C/min. TGA recorded weight changes, while DTA identified the exothermic and endothermic nature of thermal events.

Results

Cellulose from *Typha angustifolia L.*

TGA results indicated that the initial weight loss in the sample reached approximately 10.8% within the temperature range of 19.15 °C to 262.17 °C. The second main degradation stage occurred between 262.17 °C and 397.48 °C, with a weight loss of 65.1%. At 50.07 minutes, the total weight loss was 7.14%.

The DTA curve showed a pronounced exothermic peak at 358.33 °C, corresponding to the most active stage of degradation (Figure 1).

Figure 1. *TGA and DTA curves of cellulose obtained from Typha angustifolia L.*

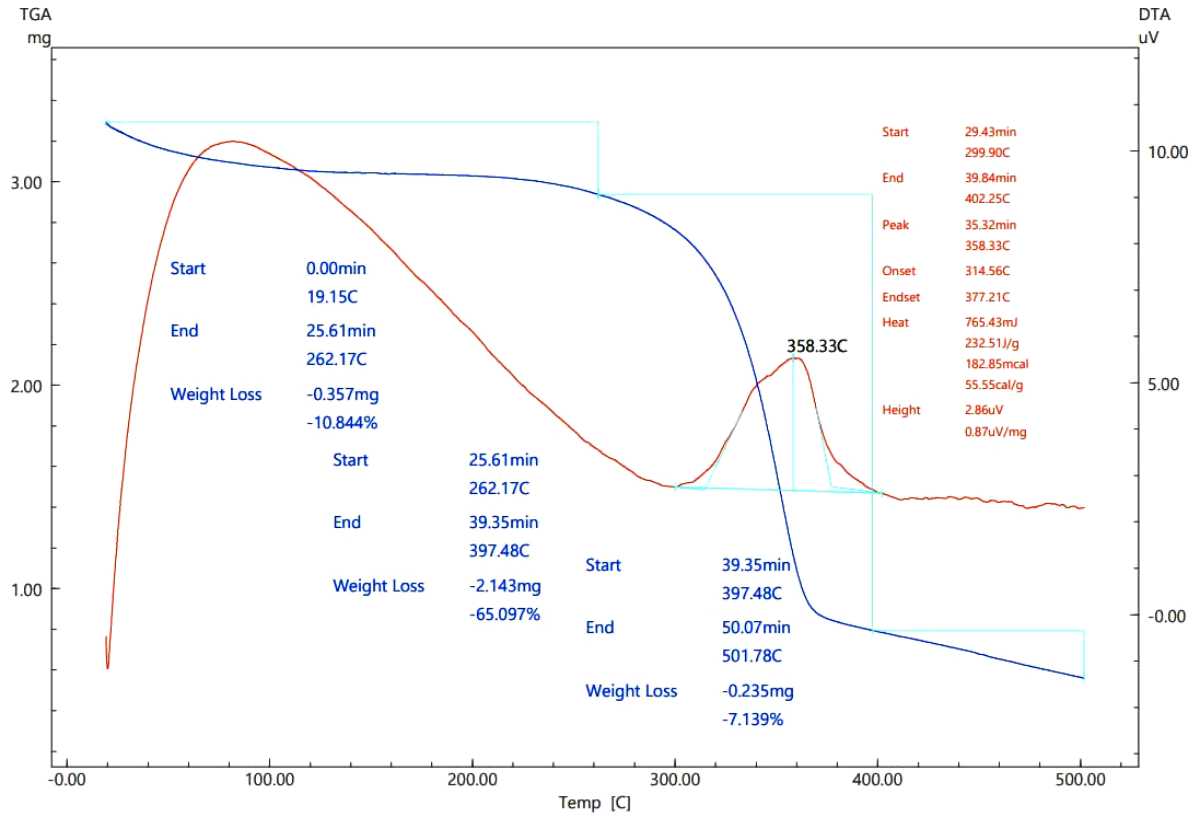

Cellulose from *Phragmites communis Trin*

According to TGA data, the Phragmites communis sample exhibited a weight loss of 7.6% in the initial stage (23.84 °C–231.18 °C). In the second stage (231.18 °C–388.73 °C), a weight loss of 72.99% was observed. In the final stage (388.73 °C–501.20 °C), an additional 6.07% weight loss occurred.

DTA analysis revealed a thermal peak at 362.24 °C, corresponding to the main thermal degradation phase of cellulose (Figure 2).

Figure 2. *TGA and DTA curves of cellulose obtained from Phragmites communis Trin*

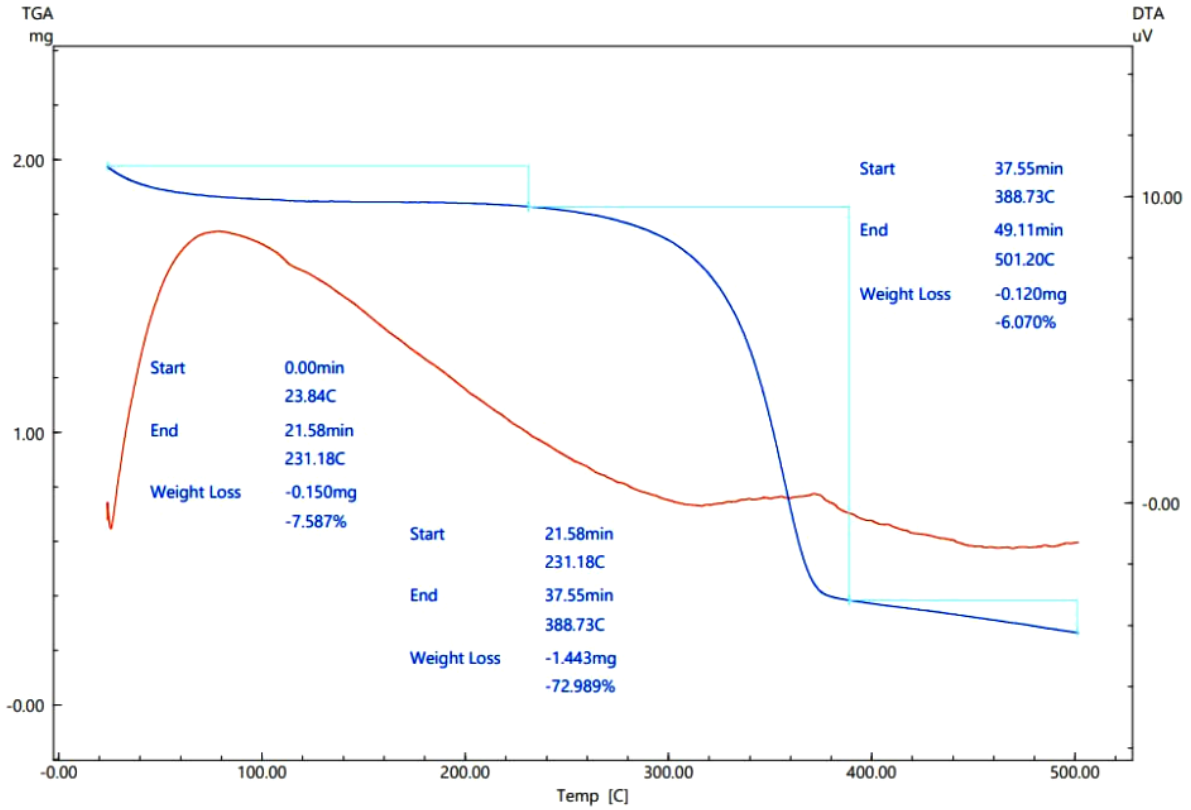

Comparison of the Two Samples

The thermal degradation behavior of cellulose extracted from both plants appears similar in terms of temperature ranges and percentage weight losses. However, the cellulose from *Typha angustifolia* undergoes degradation at slightly lower temperatures in the second stage (262.17 °C–397.48 °C), whereas *Phragmites communis* degrades within a slightly higher temperature range (231.18 °C–388.73 °C).

In terms of weight loss, *Phragmites communis* shows a higher value (72.99%) in the second stage, indicating greater susceptibility to thermal degradation. The DTA peaks for both samples lie within the range of 350–360 °C, representing the primary thermal reaction of cellulose.

Table 1. *Comparative analysis of the two samples*

Parameter	*Typha angustifolia L.*	*Phragmites communis Trin.*
Initial degradation temperature range (°C)	19.15–262.17	23.84–231.18
Mass loss in initial stage (%)	10.8	7.6
Main degradation temperature range (°C)	262.17–397.48	231.18–388.73
Mass loss in main stage (%)	65.1	72.99
Final degradation temperature range (°C)	—	388.73–501.20
Mass loss in final stage (%)	—	6.07
Peak degradation temperature (DTA, °C)	358.33	362.24
Thermal stability assessment	Relatively higher	Relatively lower
Degradation intensity	Moderate	Higher

Discussion

The results of the study demonstrate that cellulose extracted from *Typha angustifolia L.* and *Phragmites communis* Trin. using acid–alkaline chemical methods exhibits comparable thermal stability and degradation characteristics. Thermal analysis results, particularly the DTA peaks, indicate that the primary thermal degradation of cellulose occurs within the range of 350–360 °C, which is consistent with previously reported findings (Zhao et al., 2020; Kumar et al., 2018).

Cellulose obtained from both plant sources exhibits sufficient thermal stability, making it suitable for application in industrial processes, including composite material production and biopolymer technologies. The higher weight loss observed in *Phragmites communis* during the second stage suggests a greater tendency toward thermal degradation, which may be attributed to differences in chemical composition.

Thermal analysis methods serve as effective tools for evaluating cellulose quality and are essential for determining the influence of plant sources and extraction methods on the thermal properties of cellulose.

References

Zhao, Y., Li, J., & Wang, X. (2020). Thermal stability and pyrolysis kinetics of cellulose from different plant sources. *Journal of Analytical and Applied Pyrolysis*, – 149. – 104814 p.

Kumar, S., Singh, R., & Sharma, A. (2018). Thermal degradation behavior of cellulose fibers: A comparative study. *Polymer Degradation and Stability*, – 149. – P. 132–140.

French, A. D. (2014). Idealized powder diffraction patterns for cellulose polymorphs. *Cellulose*, – 21. – P. 885–896. URL: https://doi.org/10.1007/s10570–013–0030–4

Gupta, R., & Chauhan, P.S. (2019). Extraction and characterization of cellulose from natural fibers: A review. *International Journal of Biological Macromolecules*, – 123. – P. 1514–1529.

Sulaiman, O., et al. (2016). Thermal properties of cellulose fibers extracted from different natural sources. *Carbohydrate Polymers*, – 137. – P. 334–342.

Muthu, S., & Kannan, P. (2021). Cellulose from aquatic plants: Extraction and applications. *Journal of Environmental Chemical Engineering*, – 9(3). – 105333 p.

Yang, H., Yan, R., Chen, H., Lee, D.H., Zheng, C. (2007). Characteristics of hemicellulose, cellulose and lignin pyrolysis. *Fuel*, – 86(12–13). – P. 1781–1788.

Mohanty, A. K., Misra, M., & Drzal, L. T. (2005). Natural fibers, biopolymers, and biocomposites. *CRC Press*.

Sun, R., Tomkinson, J. (2003). Comparative study of lignins isolated by alkali and alkaline peroxide from wheat straw. *Polymer Degradation and Stability*, – 79(3). – P. 435–441.

Saheb, D.N., & Jog, J.P. (1999). Natural fiber polymer composites: A review. *Advances in Polymer Technology*, – 18(4). – P. 351–363.

submitted 14.04.2026;
accepted for publication 28.04.2026;
published 30.04.2026

Contact: muxammadrasulmahmudov98@gmail.com

The Austrian Journal of Technical and Natural Sciences, 2026 No 3–4
ISSN 2310-5607

PREMIER Publishing
ppublishing.org

DOI:10.29013/AJT-26-3.4-47-51

SYNTHESIS AND CHARACTERIZATION OF COVALENTLY CROSSLINKED SERICIN-DIALDEHYDE INULIN COMPOSITES

Orazova Shakhnoza [1], Zokirov Bekzod [2], Khusenov Arslonnazar [3], Rakhmanberdiev Gappar [3], Naubeev Temirbek [4]

[1] Karakalpak Research Institute of Natural Sciences, Karakalpakstan Branch of the Academy of Sciences of the Republic of Uzbekistan

[2] Karshi State Technical University

[3] Tashkent Institute of Chemical Technology

[4] Berdakh Karakalpak State University

Cite: *Orazova Sh., Zokirov B., Khusenov A., Rakhmanberdiev G., Naubeev T. (2026). Synthesis and Characterization of Covalently Crosslinked Sericin-Dialdehyde Inulin Composites. Austrian Journal of Technical and Natural Sciences 2026, No 3–4.* https://doi.org/10.29013/AJT-26-3.4-47-51

Abstract

Dialdehyde inulin was synthesized by periodate oxidation of inulin with controlled degrees of oxidation ranging from 5% to 35%. The oxidation introduced reactive aldehyde groups through cleavage of vicinal diols, enhancing the reactivity of the polysaccharide. The obtained dialdehyde inulin samples were reacted with sericin at different mass ratios (1:1, 1:2, and 2:1) to form composite materials. The interaction occurred via Schiff base formation between aldehyde and amino groups, resulting in a covalently crosslinked structure. FTIR analysis confirmed the formation of imine -C=N-) linkages and the reduction of aldehyde groups. The properties of the resulting composites were found to depend on the degree of oxidation and component ratio. The results demonstrate an effective approach for the preparation of sericin-dialdehyde inulin composites with potential applications as biodegradable materials.

Keywords: *Dialdehyde inulin; Sericin; Composite materials; Schiff base; FTIR spectroscopy; Biodegradable polymers*

Introduction

Increasing environmental concerns and the limitations of synthetic polymers, such as poor biodegradability and environmental persistence, have driven the development of sustainable materials based on natural polymers (Barclay, T.G., Ginic-Markovic, M., Cooper, P.D., & Petrovsky, N., 2010). Biopolymers derived from renewable resources are attractive due to their biodegradability, biocompatibility, and low toxicity, making them suitable for biomedical and material science applications.

Inulin, a fructan-type polysaccharide composed of β-(2→1)-linked fructose units, is widely recognized for its biocompatibility and chemical versatility (Muhammad, M., Willems, C., Rodríguez-Fernández, J., Gallego-Ferrer, G., & Groth, T., 2020). The presence of vicinal hydroxyl groups enables selective modification via periodate oxidation, which cleaves C–C bonds and introduces reactive aldehyde (–CHO) groups, forming dialdehyde inulin (Wang, P., He, H., Cai, R., Zhang, X., & Chen, J., 2019). The physicochemical properties of oxidized inulin strongly depend on the degree of oxidation, which controls the density of functional groups. Oxidized polysaccharides containing aldehyde groups can form covalent networks with proteins through Schiff base reactions, resulting in imine (–C=N-) linkages that enhance structural stability and functional properties (Aramwit, P., Siritientong, T., Srichana, T., & Ratanavaraporn, J., 2012). Sericin, a natural protein obtained from Bombyx mori cocoons, contains amino and hydroxyl groups that make it suitable for such interactions and has been widely investigated in biomaterial applications (Khusenov, A. S., Kamalova, D. S., Kee, N. K., & Rakhmanberdiev, G., 2024).

Despite numerous studies on sericin-based composites, most reported systems are based on physical interactions, while covalently crosslinked systems using dialdehyde inulin remain insufficiently explored. Therefore, the present study aims to synthesize a biodegradable composite material by oxidizing inulin to dialdehyde inulin and subsequently reacting it with sericin via Schiff base formation, followed by structural characterization using FTIR spectroscopy.

Materials and Methods

Sericin extracted from *Bombyx mori* cocoons, inulin (CAS 9005–80–5), and sodium periodate ($NaIO_4$, TU 6–09–02–54–74) were used as starting materials.

Preparation of dialdehyde inulin. Inulin was dissolved in distilled water under continuous stirring at room temperature. $NaIO_4$ was added at a molar ratio of 1:1–1:1.5 relative to the repeating units of inulin, and the reaction was carried out in the dark for 4 h. The reaction was quenched with ethylene glycol, followed by dialysis against distilled water for 24 h. The product was then freeze-dried to obtain dialdehyde inulin as a dry powder (Afinjuomo, F., Fouladian, P., Barclay, T. G., Song, Y., Petrovsky, N., & Garg, S., 2020). The oxidation proceeds via cleavage of vicinal diol groups, resulting in the formation of dialdehyde inulin, as shown in **Scheme 1.**

Scheme 1. *Periodate oxidation of inulin*

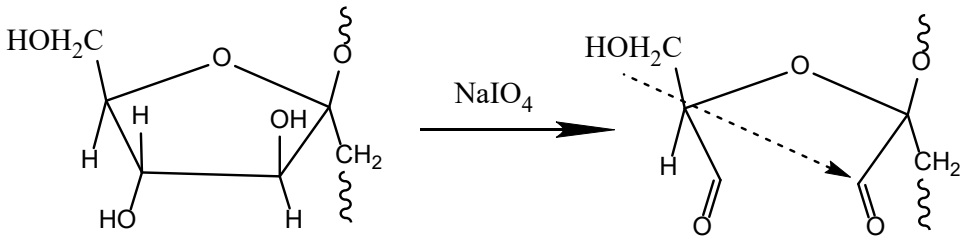

Preparation of sericin. Sericin was extracted from Bombyx mori cocoons by degumming. The cocoons were cut into small pieces and boiled in 0.02 M Na_2CO_3 solution for 30–60 min. The solution was filtered, cooled, and dialyzed against distilled water for 24 h to remove impurities. Finally, the purified sericin was freeze-dried to obtain a dry powder (Zhang, Y. Q., 2002).

Preparation of Sericin Dialdehyde Inulin Composite. Dialdehyde inulin was reacted with sericin to obtain a covalently crosslinked composite. Briefly, dialdehyde inulin was dissolved in distilled water, and an aqueous sericin solution was added at a predetermined ratio. The mixture was stirred at room temperature for several hours.

Scheme 2. *Formation of Schiff base linkages between dialdehyde inulin and sericin*

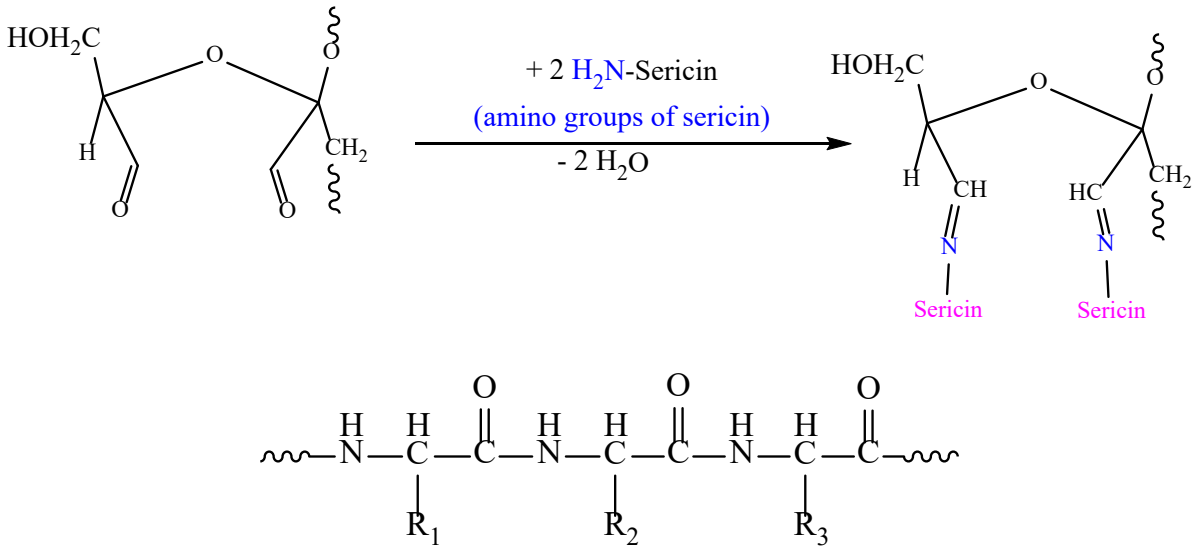

Sericin (model structure)

FTIR Spectroscopy. The FTIR spectra of the obtained samples were recorded using a Shimadzu IRSpirit-X FTIR spectrometer (Japan). The samples were prepared as KBr pellets by mixing approximately 2–3 mg of dried sample with 100–300 mg of KBr powder and pressing into pellets. The spectra were collected in the wavenumber range of 400–4000 cm^{-1} with 64 scans.

Results and Discussion

In this study, inulin was oxidized with sodium periodate to obtain dialdehyde inulin with degrees of oxidation ranging from 5–35%. The oxidation involved cleavage of vicinal diol groups, resulting in C–C bond scission and the formation of reactive aldehyde (–CHO) groups. Increasing the oxidation degree led to a higher density of aldehyde functionalities and enhanced polymer reactivity, accompanied by partial depolymerization.

The obtained dialdehyde inulin samples were reacted with sericin at different mass ratios (1:1, 1:2, and 2:1) to form composite materials. The interaction occurred via nucleophilic addition of amino groups to aldehyde groups, followed by dehydration, leading to the formation of imine (–C=N-) linkages and a covalently crosslinked network structure.

The degree of crosslinking depended on both the oxidation level of inulin and the sericin content, allowing modulation of the composite structure and properties. FTIR spectroscopy was used to confirm covalent bond formation and structural changes by comparing the spectra of inulin, oxidized inulin, sericin, and the resulting composites. The FTIR results are discussed in the following section.

The FTIR spectrum of the obtained sericin-dialdehyde inulin composite is presented in **Figure 1**. A broad absorption band observed in the region of 3200–3400 cm^{-1} can be attributed to the stretching vibrations of hydroxyl (–OH) and amino (–NH) groups, indicating the presence of both polysaccharide and protein components.

The intensity and broadness of this band suggest the formation of intermolecular interactions, such as hydrogen bonding within the composite structure. A characteristic absorption band in the region of 1650–1620 cm^{-1} is assigned to the stretching vibration of imine (–C=N-) groups, confirming the formation of Schiff base linkages between dialdehyde inulin and sericin.

This band is a key indicator of covalent interaction and demonstrates successful crosslinking of the components. The band observed near 1540 cm^{-1} corresponds to the amide II vibrations of sericin, which are associated with -N-H bending and C-N stretching. The presence of this band confirms that the protein structure of sericin is retained in the composite material.

Figure 1. *FTIR spectrum of sericin–dialdehyde inulin composite*

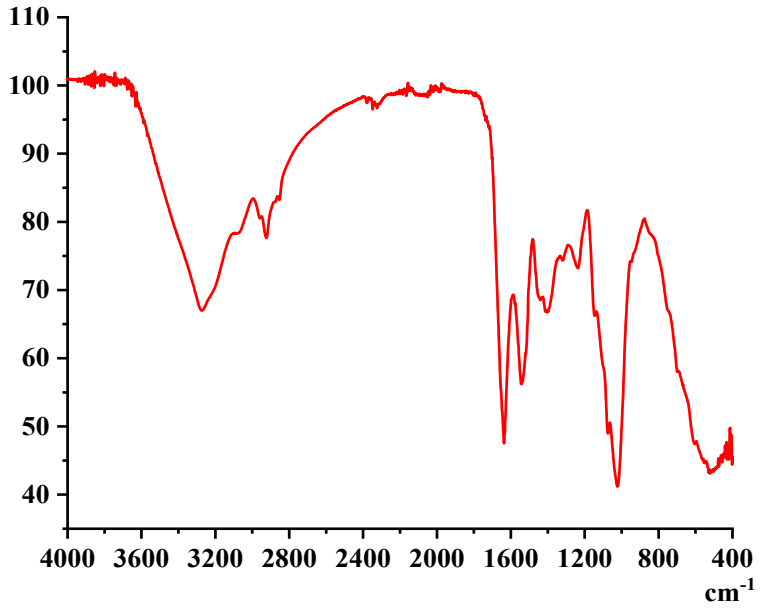

In addition, strong absorption bands in the range of 1000–1150 cm^{-1} are attributed to C-O-C and C-O stretching vibrations typical for polysaccharide structures, indicating the presence of the inulin backbone. The changes in intensity and position of these bands compared to native inulin suggest structural modification after oxidation and subsequent reaction. Notably, the characteristic aldehyde (–CHO) band around 1700 cm^{-1} is significantly reduced or absent in the composite spectrum, indicating the consumption of aldehyde groups during the reaction with amino groups of sericin. This observation further supports the formation of covalent imine bonds.

Overall, the FTIR results confirm the successful formation of a sericin-dialdehyde inulin composite through Schiff base reactions, resulting in a covalently crosslinked network structure.

Conclusion

In this study, inulin was oxidized using sodium periodate to obtain dialdehyde inulin with degrees of oxidation ranging from 5% to 35%. The obtained products were reacted with sericin at different ratios to form covalently crosslinked composite materials. FTIR analysis confirmed the formation of Schiff base (–C=N-) linkages between dialdehyde inulin and sericin. In particular, the appearance of imine bands in the region of 1620–1650 cm^{-1} and the reduction or disappearance of aldehyde bands provided evidence of covalent bonding. The results demonstrate an effective approach for the preparation of sericin-dialdehyde inulin composite materials and indicate their potential application as biodegradable materials.

References

Barclay, T. G., Ginic-Markovic, M., Cooper, P. D., & Petrovsky, N. (2010). Inulin – a versatile polysaccharide for biomedical applications. Journal of Materials Chemistry, – 20(6). – P. 1236–1245. URL: https://doi.org/10.1039/B916954K

Muhammad, M., Willems, C., Rodríguez-Fernández, J., Gallego-Ferrer, G., & Groth, T. (2020). Synthesis and characterization of oxidized polysaccharides for in situ forming hydrogels. Biomolecules, – 10(8). – 1185 p. URL: https://doi.org/10.3390/biom10081185

Wang, P., He, H., Cai, R., Zhang, X., & Chen, J. (2019). Cross-linking of dialdehyde carboxymethyl cellulose with silk sericin to reinforce sericin film for biomedical applications. Carbohydrate Polymers, – 212. – P. 403–411. URL: https://doi.org/10.1016/j.carbpol.2019.02.038

Aramwit, P., Siritientong, T., Srichana, T., & Ratanavaraporn, J. (2012). Accelerated healing of full-thickness wounds by genipin-crosslinked silk sericin-PVA scaffolds. Biomaterials, – 33(30). – P. 7320–7328. URL: https://doi.org/10.1016/j.biomaterials.2012.06.046

Khusenov, A.S., Kamalova, D.S., Kee, N.K., & Rakhmanberdiev, G. (2024). Synthesis and study of the physicochemical properties of inulin derivatives containing amino groups. Scientific and Technical Journal of Fergana Polytechnic Institute, – 28(3). – P. 179–183.

Afinjuomo, F., Fouladian, P., Barclay, T.G., Song, Y., Petrovsky, N., & Garg, S. (2020). Influence of oxidation degree on the physicochemical properties of oxidized inulin. Polymers, – 12(5). – 1025 p. URL: https://doi.org/10.3390/polym12051025

Zhang, Y. Q. (2002). Applications of natural silk protein sericin in biomaterials. Biotechnology Advances, – 20(2). – P. 91–100. URL: https://doi.org/10.1016/S0734-9750(02)00003-4

submitted 16.04.2026;
accepted for publication 30.04.2026;
published 30.04.2026

Contact: shaxnoza.orazova@bk.ru; g.rakhmonberdiev@tkti.uz; naubeev@gmail.com

The Austrian Journal of Technical and Natural Sciences, 2026 No 3–4
ISSN 2310-5607

PREMIER Publishing
ppublishing.org

DOI:10.29013/AJT-26-3.4-52-56

TAILORING SYNGAS ENERGY CONTENT THROUGH COLLOID-CHEMICAL MODULATION OF COAL–WASTE SYSTEMS DURING THERMOCHEMICAL CONVERSION

Yuldashev Rejabboy [1], ***Yusupov Farkhod*** [1], ***Kucharov Azizbek*** [1], ***Toshboboyeva Ra'no*** [2]

[1] Institute of General and Inorganic Chemistry of the Academy of Sciences of Uzbekistan. Tashkent, Uzbekistan

[2] Institute of polymer chemistry and physics, Academy of sciences of the Republic of Uzbekistan, Tashkent, Uzbekistan

Cite: *Yuldashev R., Yusupov F., Kucharov A., Toshboboyeva R. (2026). Tailoring Syngas Energy Content Through Colloid-Chemical Modulation of Coal–Waste Systems During Thermochemical Conversion. Austrian Journal of Technical and Natural Sciences 2026, No 3–4.* https://doi.org/10.29013/AJT-26-3.4-52-56

Abstract

The current study provides an extensive analysis of the waste-enhanced thermocatalytic system for increasing the calorific value of coal-based syngas produced using Angren and Shargun coals, which originate from Uzbekistan. This research includes systematic assessment of temperature influence within the range from 500 to 700 °C and effect of waste content on the output of syngas and its composition based on the results of gas analysis and microscopic study of the material structure by scanning electron microscopy (SEM). From the standpoint of colloid chemistry, it should be mentioned that such aspects as the processes of structural changes, interfacial interaction, and pore formation play a crucial part in controlling the kinetics and mechanism of mass transfer in the process. It is noted that the formation of a foam-like material with numerous pores contributes to the process of syngas enhancement.

Keywords: *coal gasification; syngas enrichment; industrial waste utilization; thermochemical conversion; calorific value; porous structure; SEM analysis; Uzbekistan coals*

Introduction

An increase in the global need for alternative and efficient sources of energy has brought about a growing interest in syngas production processes (Qurbonov, A., Kucharov, A., & Yusupov, F., 2024). The global syngas market will witness significant growth from a size of USD56.06 billion in 2023 to reach over USD102.21 billion by 2033 due to extensive applications of syngas in power generation, hydrogen fuel production, and chemical synthesis (Maitlo, G., Ali, I., Mangi, K.H., Ali, S., Maitlo, H.A., Unar, I.N., & Pirzada, A. M., 2022; Kucharov, A., Xalilov, S., Alikulova, M., Mamarasulov, T., Turayeva, K., Imanova, G., ... & Farmonov, N.,

2025). As far as syngas production is concerned, coal gasification continues to be an important technique allowing conversion of low-grade solid fuels into valuable gaseous compounds rich in carbon monoxide and hydrogen (Griffin, D. W., & Schultz, M. A., 2012). The main challenge with traditional methods of syngas production lies in the comparatively low calorific value of syngas, being in the range of 4–7 MJ/Nm³ and 10–18 MJ/Nm³ for air and oxygen/steam systems, respectively (Kucharov, A., Xalilov, S., & To'Rayeva, X., 2024). Recent research efforts have been devoted to improvement of the calorific value of syngas through process optimization (Xu, D., Zhang, Y., Hsieh, T. L., Guo, M., Qin, L., Chung, C., ... & Tong, A., 2018), reactor design, and modeling, including utilization of machine learning algorithms for syngas composition control (Anuar, S. Z. K., Nordin, A. H., Husna, S. M. N., Yusoff, A. H., Paiman, S. H., Noor, S. F. M., ... & Ismail, Y. M. N. S., 2025). In recent times, efforts have been put towards the application of industrial wastes as reactive agents in thermal chemical reactions, not only to solve environmental issues but to address energy concerns as well (Yang, J., Han, C., Shao, L., Nie, R., Dong, S., Liu, H., & Ma, L., 2024). Earlier studies have proved that syngas yield is greatly affected by fuel properties, operating temperature, and type of reaction (Kucharov, A., Xalilov, S., Farxod, Y., Toshboboyeva, R. N., Bekturdiyev, G., Turayeva, K., ... & Golib, T., 2026); however, there is little evidence on the combined impact of coal and industrial wastes on energy generation (Fan, P., Dai, W., Fan, X., Dong, L., Wang, J., Bao, W., ... & Fan, M., 2024). It should be highlighted that there is not much research done on the contribution of surface and colloid chemistry processes, which could greatly impact mass transfer, kinetics of chemical reactions, and gas dynamics as well (Hu, Y., & Chen, Z., 2025). Hence, the investigation of innovative waste-fueled thermal processes in order to improve the calorific content of syngas would be quite pertinent (Choi, H., Kim, Y. T., Tsang, Y. F., & Lee, J., 2023).

Research method

This study employed Angren and Sharg'un coals from Uzbekistan as representative feedstocks, and a novel thermochemical approach was developed to enrich coal-derived syngas using industrial waste streams from oil and gas processing plants.

Figure 1.

a) b)

(a) Schematic diagram of the syngas enrichment system based on technical waste from oil and gas processing plants a burner (1) and waste heating furnace (2) with a heat circulation zone (3), a gas flow pipelin (4) equipped with check valves (5–7) and a pressure gauge (8), a cooling chamber (9), a gas holder (10), and a waste feed tank (11); flue gases are discharged through an exhaust pipe (12), while syngas is supplied via the inlet pipeline (13) and collected through the outlet pipeline (14); (b) photographic view of the experimental setup., comprising

Laboratory-scale thermochemical system that was specifically made to turn technical waste from oil and gas processing plants into synthesis gas to do the experiments. The set-up had a burner (1), a waste-heating furnace/reactor (2), an internal heat-circulation zone (3), a gas-flow pipeline (4), check valves (5–7) to make sure the flow was one way and safe to use, a pressure gauge (8) to keep an eye on the pressure, a cooling chamber (9) to partially condense and lower the temperature of volatile products, a gas holder (10) to temporarily hold gas, and a waste feed vessel (11) (Figure 1). The waste-derived feedstock was heated in the reactor under controlled conditions while it was being used. The resulting gases were then sent through the gas line, cooled, pressure-regulated, and collected in the gas holder.

Flue and residual gases were released through the exhaust line (12), while syngas was sent through the inlet line (13) and taken out through the outlet line (14). This setup made it possible to do stable thermal conversion, control gas handling, and consistently test how well syngas enrichment worked under conditions that were set up in the lab. The proposed methodology demonstrates an effective integration of coal conversion and waste utilization, resulting in enhanced syngas composition and increased calorific value under controlled operating conditions.

Result and discussion

The results and discussion section focuses on the structural evolution of coal during thermochemical conversion and its direct influence on syngas composition and yield, with particular emphasis on the effects of temperature and industrial waste addition.

Figure 2. *Schematic and SEM-based evolution of coal structure during thermochemical transformation:*

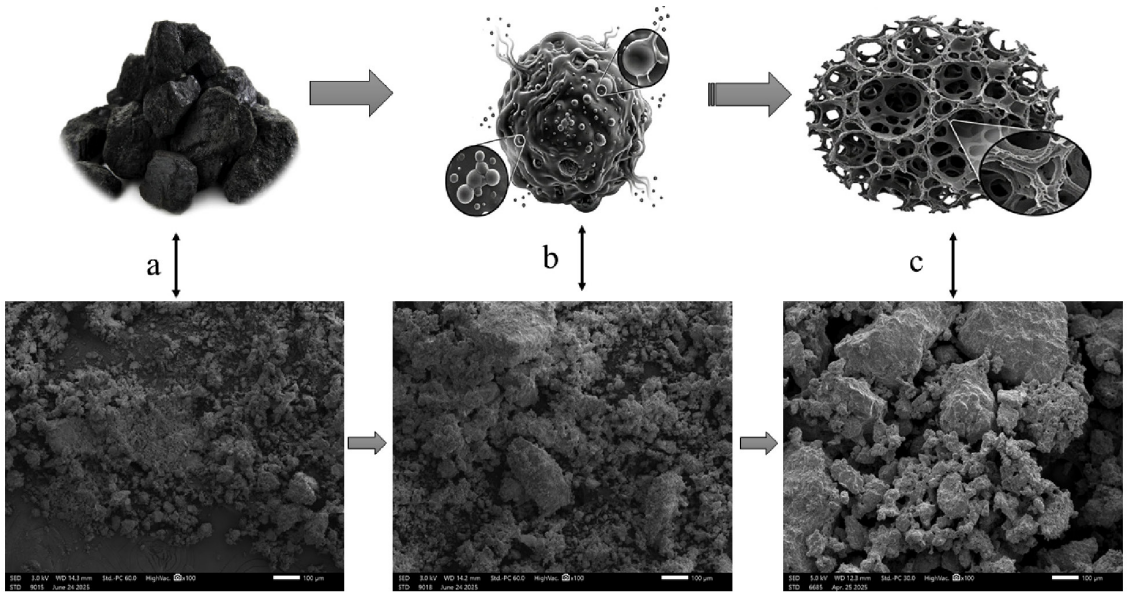

(a) raw coal particles, (b) transition to metaplast (plastic) state with bubble nucleation and swelling, and (c) formation of a highly porous char-like structure

The figure shows how the structure of coal particles changes during thermochemical treatment. The top row shows a schematic representation, and the bottom row shows SEM observations that go along with it. In the first stage (a), raw coal has a dense, irregular, and angular shape with surfaces that are mostly smooth and not very porous. When heated, the material changes into a metaplast (plastic) state (b) (Figure 2), where thermal decomposition creates volatile compounds that cause gas bubbles to form in the softened matrix. This process causes particles to swell and internal voids to grow over time. In the last step (c), the quick release of volatiles and the solidification of the plastic phase create a highly developed porous, foam-like structure. SEM analysis shows that the surface roughness and pore density have both gone up a lot, which means

that the specific surface area has gone up a lot. This change in structure is a key factor that affects how the material reacts in later processes like gasification and combustion. It makes it easier for mass transfer and reactive sites to be reached.

Table. *Effect of temperature and waste addition on syngas composition and gas yield from Angren and Sharg'un coals*

Feedstock Type	T (°C)	CO (%)	H_2 (%)	CH_4 and other hydrocarbons (%)	CO_2 (%)	Gas yield (%)
Angren coal	500	18.5	12.1	2.5	60.5	25.4
	600	24.4	16.8	2.9	35.2	32.6
	700	28.4	20.9	3.2	28.1	40.4
Shargun coal	500	22.5	14.5	7.5	57.8	28.1
	600	28.4	18.6	9.0	45.4	35.6
	700	32.4	22.4	10.1	35.6	42.1
Angren + 20% waste	500	20.4	14.6	7.1	59.5	40.1
	600	27.4	18.4	18.2	45.8	58.5
	700	32.4	22.3	20.8	34.3	54.4
Shargun + 20% waste	500	25.0	16.2	18.7	51.4	53.0
	600	32.9	20.3	21.8	37.6	50.9
	700	36.4	24.7	33.9	27.5	58.4

The findings clearly show that there is an improvement in the quality and amount of syngas produced as the temperature increases, for both types of coal. The increase in temperature from 500 to 700 °C causes an increase in the amounts of CO and H_2 while simultaneously decreasing the amount of CO_2, implying that there was a greater extent of thermochemical reaction and the presence of secondary reactions such as Boudouard and water-gas reactions. The inclusion of 20% of industrial waste considerably improves the production of hydrocarbons (methane and higher hydrocarbons) and gas production, especially in the case of Shargun coal, with the maximum amount of gas being 58.4%.

While the obtained results confirm the effectiveness of the proposed approach, further studies on reaction kinetics, process optimization, and industrial scalability are required to fully establish the reliability and practical applicability of this technology.

Conclusion

The thermochemical conversion process of Angren and Sharg'un coal has revealed an increase in the quality of produced syngas in accordance with the increase in temperature in the range of 500–700 °C, where there were observed significant growths of CO and H_2 contents as well as a decrease of CO_2 content. The use of 20% of industrial waste in this process has resulted in considerable improvement in production of hydrocarbons (up to 33.9%) and in gas yield (up to 58.4%). It was found that waste volatiles have actively participated in secondary reactions. Based on SEM analysis, it can be noted that the creation of porosity was observed.

References

Qurbonov, A., Kucharov, A., & Yusupov, F. (2024, March). Development of a technology for obtaining an anti-corrosion coating for gas pipelines. In *AIP Conference Proceedings* (Vol. 3102. – No. 1. – 040008 p). AIP Publishing LLC.

Maitlo, G., Ali, I., Mangi, K. H., Ali, S., Maitlo, H. A., Unar, I. N., & Pirzada, A. M. (2022). Thermochemical conversion of biomass for syngas production: Current status and future trends. *Sustainability*, – 14(5). – 2596 p.

Kucharov, A., Xalilov, S., Alikulova, M., Mamarasulov, T., Turayeva, K., Imanova, G., ... & Farmonov, N. (2025). Scientific Analysis Of The Development Of New Types Of Flotation Reagents Used In Coal Enrichment. *Eureka: Physics & Engineering*, (2).

Griffin, D. W., & Schultz, M. A. (2012). Fuel and chemical products from biomass syngas: a comparison of gas fermentation to thermochemical conversion routes. *Environmental Progress & Sustainable Energy*, – 31(2). – P. 219–224.

Kucharov, A., Xalilov, S., & To'Rayeva, X. (2024). Results Of Scientific Analysis Of Coal Processing Products. *Journal of Experimental Studies*, – 2(3). – P. 9–16.

Xu, D., Zhang, Y., Hsieh, T. L., Guo, M., Qin, L., Chung, C., ... & Tong, A. (2018). A novel chemical looping partial oxidation process for thermochemical conversion of biomass to syngas. *Applied Energy*, – 222. – P. 119–131.

Anuar, S. Z. K., Nordin, A. H., Husna, S. M. N., Yusoff, A. H., Paiman, S. H., Noor, S. F. M., ... & Ismail, Y. M. N. S. (2025). Recent advances in recycling and upcycling of hazardous plastic waste: A review. *Journal of environmental management*, – 380. – 124867 p.

Yang, J., Han, C., Shao, L., Nie, R., Dong, S., Liu, H., & Ma, L. (2024). Chemical looping gasification of lignite to syngas using phosphogypsum: Overview and prospects. *Journal of Cleaner Production*, – 445. – 141329 p.

Kucharov, A., Xalilov, S., Farxod, Y., Toshboboyeva, R. N., Bekturdiyev, G., Turayeva, K., ... & Golib, T. (2026). A comprehensive technological approach for the selective recovery of aluminum oxide and rare earth elements from coal processing. *EUREKA: Physics and Engineering*.

Fan, P., Dai, W., Fan, X., Dong, L., Wang, J., Bao, W., ... & Fan, M. (2024). Influence mechanism of emulsion collector on the flotation effect of coal gasification fine slag. *Fuel Processing Technology*, – 263. – 108120 p.

Hu, Y., & Chen, Z. (2025). Thermochemical conversion of sewage sludge: Progress in pyrolysis and gasification. *Water*, – 17(12). – 1833 p.

Choi, H., Kim, Y. T., Tsang, Y. F., & Lee, J. (2023). Integration of thermochemical conversion processes for waste-to-energy: A review. *Korean Journal of Chemical Engineering*, – 40(8). – P. 1815–1821.

submitted 03.04.2026;
accepted for publication 17.04.2026;
published 30.04.2026

Contact: sciuzb@mail.ru

The Austrian Journal of Technical and Natural Sciences, 2026 No 3–4
ISSN 2310-5607

PREMIER Publishing
ppublishing.org

DOI:10.29013/AJT-26-3.4-57-62

SELECTIVE SYNTHESIS OF 6-BENZYLAMINOPURINE CONTROLLED BY SOLVENT AND BASE

Baymuratova Gulbaxar [1], Sidibe Mamadou Sadialiou [2], Saitkulov Foziljon [3], Mirvaliev Zoid [3], Giyasov Kuchkar [3]

[1] Branch of Astrakhan State Technical University in the Tashkent Region, Uzbekistan, Tashkent

[2] Gubkin Russian State University of Oil and Gas (National Research University) Moscow, Russia

[3] Tashkent State Agrarian University, Uzbekistan, Tashkent

Cite: *Baymuratova G., Sidibe M.S., Saitkulov F., Mirvaliev Z., Giyasov K. (2026). Selective Synthesis of 6-Benzylaminopurine Controlled by Solvent and Base. Austrian Journal of Technical and Natural Sciences 2026, No 3–4.* https://doi.org/10.29013/AJT-26-3.4-57-62

Abstract

This work investigates the influence of solvent and base nature on the mechanism of 6-benzylaminopurine formation during the reaction of 6-chloropurine with benzylamine. The reaction proceeds via nucleophilic aromatic substitution (S_NAr) at the C-6 position of the purine ring activated by electron-withdrawing nitrogen atoms. It was established that polar aprotic solvents (DMF, DMSO) significantly increase the reaction rate due to stabilization of the anionic Meisenheimer σ-complex, whereas protic media decrease the nucleophilicity of the amine and reduce the product yield. The type of base strongly affects selectivity: alkali metal carbonates provide preferential substitution at the N-9 position without formation of N-alkylation by-products, while strong bases cause partial degradation of the purine ring. Optimal conditions (DMF, K_2CO_3, 100 °C) afforded 6-benzylaminopurine in up to 92% yield. Based on kinetic and spectral data, a reaction mechanism involving formation of a σ-complex followed by chloride ion elimination is proposed. The obtained results allow controlled tuning of substitution selectivity in the purine core and may be applied in the synthesis of biologically active purine derivatives.
Keywords: *6-benzylaminopurine, 6-chloropurine, nucleophilic aromatic substitution, S_NAr mechanism, solvent effect, base effect, selectivity, purine*

Introduction

Purine derivatives represent a significant class of heterocyclic compounds that are widely distributed in biological systems and participate in numerous metabolic and regulatory processes. The purine framework is a structural component of nucleic acids, coenzymes, and signaling molecules, making it one of the most important heterocyclic scaffolds in chemistry and biology. Because of its versatile reactivity and ability to interact with biological receptors, modification of the purine ring

has become a key strategy in medicinal, agricultural, and coordination chemistry. Even small variations in the substitution pattern can lead to substantial changes in electronic distribution, molecular conformation, and biological activity (Saitkulov F. E., Elmuradov B. Zh., Sapaev B., 2024, p. 15; Saitkulov F. E., Elmuradov B. J., Giyasov K., 2023, p. 24; Jumaniyazova D. M., Zakirov B. S., Jabbiev R., Jumaniyazov M. Zh., 2019, p. 36).

Among substituted purines, 6-benzylaminopurine occupies a special position due to its pronounced cytokinin activity. This compound is widely used as a plant growth regulator in agriculture and biotechnology. It stimulates cell division, controls morphogenesis, delays senescence, improves shoot proliferation, enhances crop productivity, and increases plant tolerance to environmental stresses such as drought and salinity. Because of its practical importance and broad biological activity, the development of efficient and selective synthetic routes to 6-benzylaminopurine remains a relevant scientific and technological task.

The most convenient synthetic approach to 6-benzylaminopurine is based on nucleophilic substitution of a halogen atom in 6-halopurines, typically 6-chloropurine, by benzylamine. This transformation proceeds through nucleophilic aromatic substitution (S_NAr), a well-known mechanism characteristic of electron-deficient heteroaromatic systems. The purine ring contains several electron-withdrawing nitrogen atoms that activate the C-6 position toward nucleophilic attack. However, despite the apparent simplicity of the reaction, the process is not always straightforward. Competing reactions such as N-alkylation at ring nitrogen atoms, multiple substitution, hydrolysis, and partial degradation of the heterocycle may occur, especially under strongly basic or high-temperature conditions. Therefore, achieving high regioselectivity at the C-6 position requires careful selection of reaction parameters.

The nature of the solvent and the strength of the base are among the most influential factors governing the rate, selectivity, and mechanism of nucleophilic substitution in purine derivatives. Polar aprotic solvents such as dimethylformamide and dimethyl sulfoxide enhance the nucleophilicity of amines and stabilize negatively charged σ-complex intermediates (Meisenheimer complexes), thereby accelerating the substitution reaction. In contrast, protic solvents can reduce nucleophilicity due to hydrogen bonding and proton transfer processes. The base plays a dual role: it neutralizes the hydrogen halide formed during substitution and activates the nucleophile. Mild inorganic bases typically promote selective substitution, whereas strong bases may lead to side reactions and structural rearrangements.

Despite numerous studies in purine chemistry, a systematic investigation of the combined influence of solvent polarity and base strength on the mechanism of 6-benzylaminopurine formation is still insufficiently explored. A deeper understanding of these effects is essential for rational optimization of reaction conditions and for designing new purine derivatives with predictable reactivity and biological properties (Abdullaev Sh., Sabirova D. K., 2001, p. 89).

The aim of this study is to investigate how solvent and base nature affect the mechanism and selectivity of nucleophilic substitution leading to 6-benzylaminopurine formation and to determine optimal conditions for regioselective substitution at the N-9 position of the purine ring. The obtained results will contribute to the theoretical understanding of S_NAr reactions in heterocyclic systems and provide practical recommendations for the synthesis of biologically active purine derivatives used in agriculture and pharmaceutical chemistry.

Materials and methods

6-Chloropurine (≥99%), benzylamine (≥99%), potassium carbonate (K_2CO_3), sodium carbonate (Na_2CO_3), sodium bicarbonate ($NaHCO_3$), triethylamine (Et_3N), sodium hydroxide (NaOH), dimethylformamide (DMFA), ethanol, n-butanol, methanol, ethyl acetate, and hydrochloric acid (HCl, 5%) were purchased from commercial suppliers and used without additional purification. Organic solvents were dried over molecular sieves 3 Å prior to use when necessary. Distilled water was used in all aqueous procedures.

Results and discussion

Several alternative methods for the synthesis of 6-benzylaminopurine were system-

atically investigated, and their mechanisms, selectivity, and efficiency were comparatively analyzed from a scientific point of view. As a result of the study, the method based on nucleophilic aromatic substitution of 6-chloropurine with benzylamine was chosen as the most appropriate route. The main reason is that this reaction had previously been carried out in various solvents, but in most cases the product yield was low. Within this dissertation, the reaction was performed for the first time in DMFA solvent, and by selecting optimal conditions, 6-benzylaminopurine was synthesized in a high yield of up to 90%.

The reaction is based on the nucleophilic substitution of the 6-chloropurine derivative (**1**) with benzylamine (**2**) and was carried out in a polar aprotic solvent, DMFA. This solvent increases the nucleophilicity of benzylamine and provides favorable stabilization of ionic intermediate complexes.

In the first stage, the $-NH_2$ group of the benzylamine molecule (2) attacks the electron-deficient C-6 atom of the purine ring. As a result of this nucleophilic attack, the aromatic system of the initial substrate (**1**) is temporarily disrupted and the formation of a σ-complex begins. This stage is represented by structures 3a, 3b, and 3c, which are resonance forms of the same intermediate state. These resonance structures illustrate the redistribution of negative charge involving nitrogen atoms of the purine ring and stabilization of the complex.

In the next step, the resonance forms combine to produce a clearly defined Meisenheimer complex (**4**). This intermediate complex is characteristic of nucleophilic aromatic substitution (S_NAr) reactions, in which benzylamine is already bonded to the ring while the chlorine atom has not yet completely departed. Formation of the Meisenheimer complex is a key proof of the S_NAr (addition–elimination) mechanism.

In the following stage, the Meisenheimer complex (**4**) decomposes with elimination of the chloride ion. Aromaticity is restored, and the substitution intermediate product (**5**) is formed. This step is rate-determining and strongly depends on the nucleophile activity and solvent nature.

Finally, the resulting intermediate (**5**) undergoes proton exchange processes and is stabilized, while the released HCl is neutralized in the reaction medium. As a result, the final product of the reaction, 6-benzylaminopurine (**6**), is obtained.

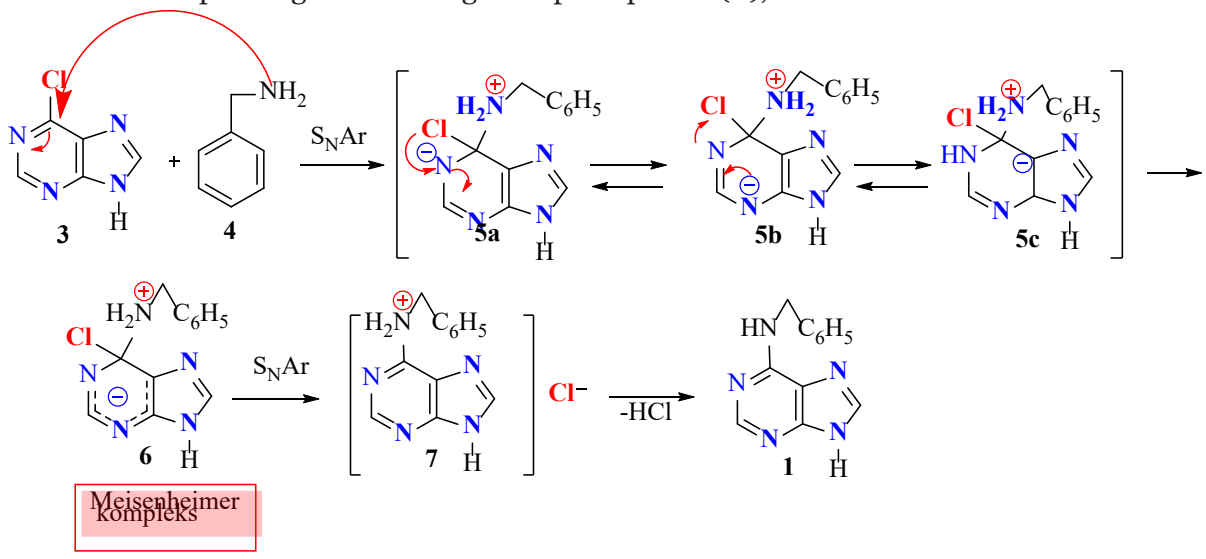

Synthesis of 6-Benzylaminopurine via Sodium Salts

In the preparation of 6-benzylaminopurine, adenine (**7**) was used as the starting material. For the reaction, adenine (7), sodium benzylate (8), and benzyl alcohol (9) were placed into a round-bottom flask in a molar ratio of 1:1:5. The reaction mixture was heated under reflux with continuous magnetic stirring for 2.5 hours. Under these conditions, benzyl alcohol acted both as the solvent and the benzylating medium, resulting in the formation of the sodium salt of 6-benzylaminopurine (**10**). After

completion of the reaction, the mixture was cooled to room temperature, and 150 mL of diethyl ether was added to precipitate the product. The resulting precipitate was filtered off and dried. In the next step, the obtained sodium salt was treated with acetic acid (CH_3COOH) in a 1:1 molar ratio, yielding free-base 6-benzylaminopurine (**11**).

The purified product was isolated as a white crystalline substance, and the final compound was obtained in 75% yield.

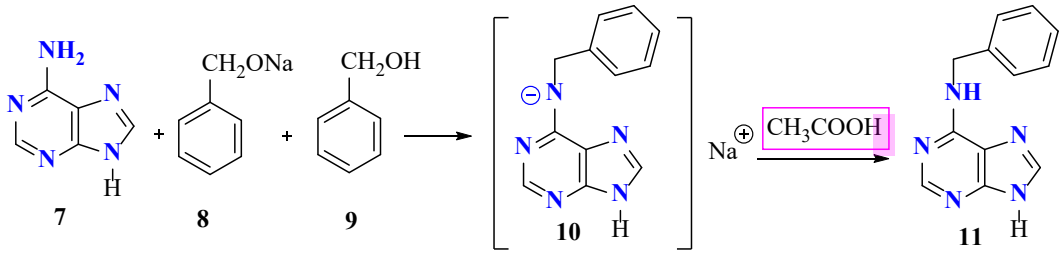

Figure 1. *FT-IR spectrum of 6-benzylaminopurine*

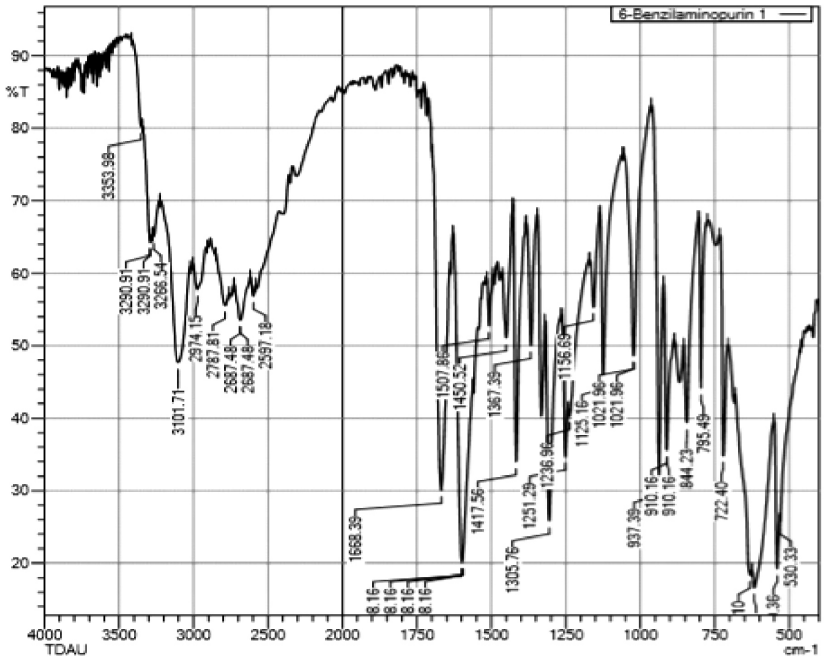

To reliably confirm the structure of the synthesized 6-benzylaminopurine evaluate its chemical purity, and determine its electronic and spatial structure, a number of modern physicochemical analytical methods were applied. The obtained data made it possible to thoroughly analyze the functional groups of the molecule, the electronic state of the purine core, the conformation of the benzylamine fragment, and the tautomeric equilibrium (Fig 1).

The spectrum confirms formation of 6-benzylaminopurine: Appearance of strong N–H bands, characteristic C=N vibration of purine, CH_2 signals of benzyl group, and monosubstituted benzene out-of-plane bands. Absence of C–Cl band (~700–800 cm^{-1} for 6-chloropurine) indicates complete substitution at the C-6 position.

The differential thermal analysis results confirm the TGA data, showing the presence of endothermic and exothermic effects corresponding to the decomposition stages. The endothermic effects are associated with bond cleavage and primary decomposition processes, whereas the exothermic effects are related to secondary thermal transformations and carbonization.

In general, the TGA and DTA analyses indicate that 6-benzylaminopurine is thermally stable up to approximately 200 °C, the main decomposition process occurs in the range of 230–300 °C, and at higher temperatures the substance undergoes complete destruction. These findings are important for further scientific investigations and practical applications of the compound.

The figure shows that the main peaks in the MS spectrum of 6-benzylaminopurine appear at m/z 91, 106, 202, and 225**.** These signals indicate the presence of **a** benzyl fragment and a purine core in the molecule and confirm their characteristic fragmentation pathways. The peak at m/z 225 in the high-mass region corresponds to the molecular ion (M^{+}•) of the compound. This value confirms that the molecular formula of 6-benzylaminopurine is $C_{12}H_{11}N_5$. The presence of a clear molecular ion peak also indicates that the compound was successfully synthesized and that the sample contains only minor impurities.

Figure 2.

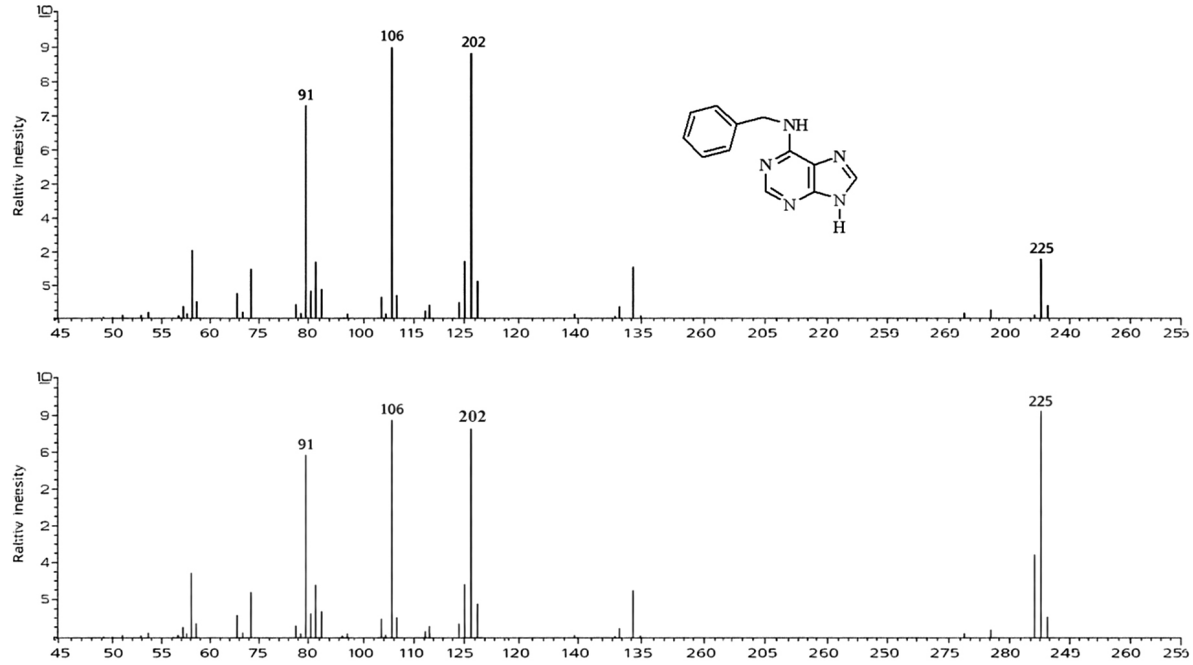

The mass spectrometric fragmentation scheme of 6-benzylaminopurine can be explained by the formation of the molecular ion followed by subsequent fragmentation processes. In the spectrum, the peak at m/z 225 corresponds to the molecular ion (M^{+}•) and confirms that the molecular formula of the compound is $C_{12}H_{11}N_5$. After ionization, the molecule undergoes fragmentation through several pathways.

In the first pathway, cleavage of the benzyl group occurs, resulting in the formation of a fragment at m/z 91, corresponding to the tropylium cation $[C_7H_7]^{+}$. This fragment is one of the most characteristic signals indicating the presence of an aromatic benzyl substituent. Another fragment associated with the benzyl moiety appears at m/z 106, which can be attributed to the formation of a benzylamine-type ion. In a subsequent fragmentation step, this ion may further rearrange to produce an aromatic nitrogen-containing fragment with m/z 119.

In the second pathway, the molecular ion undergoes the loss of small neutral fragments. In particular, the elimination of –CN or –HCN groups from the molecular ion leads to the formation of a fragment with m/z 202. Further rearrangement and fragmentation processes may then produce a fragment at m/z 205.

Thus, the mass spectrometric analysis indicates that the main fragmentation pathways of 6-benzylaminopurine involve the cleavage of the benzyl substituent as well as stepwise fragmentation of the purine core. The peaks observed at m/z 91, 106, 119, 202 and 225 serve as diagnostic fragments confirming the structure of the compound.

Experimental section

1. Synthesis of 6-benzylaminopurine by nucleophilic substitution.

In a 50 ml round-bottom flask equipped with a reflux condenser and magnetic stirring bar, 1.0 g (6.5 mmol) of 6-chloropurine was dissolved in 12 ml DMFA. Potassium carbonate (1.2 eq, 1.1 g) was added, followed by benzylamine (1.3 eq, 0.9 ml). The reaction mixture was heated at 100 °C for 5 h under

constant stirring. The progress of the reaction was monitored by TLC (ethyl acetate: methanol = 9:1).

After completion, the mixture was cooled and poured into 150 mL cold water. The solution was neutralized to pH ≈ 7 using dilute hydrochloric acid. The precipitate formed was filtered, washed with water and ethanol, and dried at 60 °C. The crude product was recrystallized from ethanol to afford white crystalline 6-benzylaminopurine. Yield: up to 90%.

2. Synthesis via sodium salt intermediate.

Adenine (1 eq), sodium benzylate (1 eq), and benzyl alcohol (5 eq) were placed in a round-bottom flask and heated under reflux with continuous stirring for 2.5 h. Benzyl alcohol served as both solvent and benzylating medium, producing the sodium salt of 6-benzylaminopurine.

After cooling to room temperature, 150 ml diethyl ether was added to precipitate the product. The precipitate was filtered and dried. The obtained sodium salt was then treated with equimolar acetic acid to yield free 6-benzylaminopurine. The purified product was isolated as white crystals. Yield: ~75%.

Conclusion

The synthesis of 6-benzylaminopurine was investigated using two different approaches, and the influence of reaction conditions on selectivity and efficiency was evaluated. The nucleophilic aromatic substitution of 6-chloropurine with benzylamine in DMFA provided the highest yield and regioselectivity, confirming it as the optimal method. Spectroscopic (FT-IR, UB–Vis, ^{1}H NMR) and thermal (TGA/DTA) analyses reliably verified the structure, purity, and thermal stability of the obtained compound. Mechanistic analysis demonstrated the S_NAr addition–elimination pathway via a Meisenheimer intermediate. The results expand understanding of substitution processes in purine systems and provide practical conditions for obtaining biologically relevant purine derivatives suitable for further chemical modification and application.

References

Saitkulov F. E., Elmuradov B.Zh., Sapaev B. Syntheses and biological activity of quyinazolin-4-one hydrochloride //Austrian Journal of Technical and Natural Sciences. 2024. – No. 1–2. – P. 28–35.

Saitkulov F. E., Elmuradov B. J., Giyasov K. Alkylation of quinazoline-4-one Myagkim and Jestkim alkylatingagent // Universum: Chemistry and biology: -Moscow. 2023. – No. 1. – P. 53–57.

Jumaniyazova D. M., Zakirov B. S., Jabbiev R., Jumaniyazov M. Zh. Technology for obtaining acid-resistant anticorrosion coatings based on gossypol resin. *Universum: Technical Sciences*, 2019. – No. 11(68). – 59 p.

Tadjikhodjaeva U. B. Tadjikhodjaev Z. A. Synthesis and preparation of new anticorrosion coatings based on caprolactam production waste. In: Thermoreactive oligomers, polymers containing waste, polyfunctional compounds and prospects for creating polymer materials based on them. Proceedings of the Scientific Conference, Tashkent Chemical-Technological Institute, – Tashkent, 2024. – P. 190–191.

Abdullaev Sh., Sabirova D. K. Preparation and study of properties of paint composite materials based on gossypol resin. *Composite Materials*, 2001. – No. 3. – P. 97–99.

submitted 02.03.2026;
accepted for publication 14.03.2026;
published 30.04.2026

Contact: fsaitkulov@bk.ru

The Austrian Journal of Technical and Natural Sciences, 2026 No 3–4
ISSN 2310-5607

PREMIER Publishing
ppublishing.org

DOI:10.29013/AJT-26-3.4-63-73

SYNTHESIS AND PHYSICOCHEMICAL ANALYSIS OF ACRYLIC–COLLAGEN ADHESIVE COATING FILM USING A BIFUNCTIONAL CROSSLINKING AGENT

Sattorova Gulnoza [1]***, Shoyimov Shokhrux*** [2]***,***
Qodirov Tulqin [3]***, Khujakulov Kamoliddin*** [1]

[1] Bukhara State Technical University

[2] Asia International University

[3] Tashkent textile and Light Industry Institute

Cite: *Sattorova G., Shoyimov Sh., Qodirov T., Khujakulov K. (2026). Synthesis and Physicochemical Analysis of Acrylic-Collagen Adhesive Coating Film Using a Bifunctional Crosslinking Agent. Austrian Journal of Technical and Natural Sciences 2026, No 3–4.* https://doi.org/10.29013/AJT-26-3.4-63-73

Abstract

In this study, a novel adhesive coating film was synthesized based on acrylic emulsion and hydrolyzed collagen in the presence of glutaraldehyde as a bifunctional crosslinking agent. The synthesis was carried out via emulsion radical polymerization using azobisisobutyronitrile (AIBN) as a radical initiator. The process was performed in a mechanically stirred reactor in four sequential stages, with the pH of the reaction medium maintained in the range of 7.5–8.5. These conditions facilitated covalent bonding between glutaraldehyde and the amino groups ($–NH_2$) of collagen through crosslinking reactions, thereby optimizing the degree of crosslink formation. The chemical structure of the resulting film was investigated by infrared spectroscopy using the attenuated total reflectance (ATR) mode over the wavenumber range of 400–4000 cm^{-1}. Comparative analysis of the IR spectra of individual components (acrylic emulsion, butyl acrylate, and glutaraldehyde) and the synthesized film confirmed the disappearance of the characteristic C=C vinyl bond absorption at 1635 cm^{-1} originating from butyl acrylate monomer, providing direct evidence for the completion of radical polymerization. Furthermore, the film spectrum revealed the following characteristic absorption bands: a C=O ester bond at 1727 cm^{-1} (attributable to polybutyl acrylate), C=O Amide I bands at 1684 and 1652 cm^{-1} (collagen), an N-H Amide II band at 1559 cm^{-1} (collagen), and a C=N bond at 1630 cm^{-1}, the latter serving as direct spectroscopic evidence for the formation of covalent crosslinks between glutaraldehyde and collagen via Schiff base formation. The novel adhesive coating film obtained in this study provides a scientific foundation for the development of environmentally safe, high-adhesion coating materials for application in the leather and fur finishing industry.

Keywords: *acrylic-collagen film, emulsion radical polymerization, AIBN initiator,*

bifunctional crosslinking agent, glutaraldehyde, ATR-FTIR spectroscopy, Schiff base, Amide I, Amide II, C=N bond, leather finishing

Indroduction

The chemical industry is currently among the most rapidly developing sectors of the global economy. In particular, the leather and fur processing industries represent a significant driver of economic growth, with finishing processes playing a decisive role in determining the appearance, mechanical performance, and service properties of the final product (Zhang X., Sorolla S., Casas C., Bacardat A., 2023). Conventional finishing technologies are predominantly based on synthetic chemicals and organic solvents, which give rise to a range of environmental and toxicological concerns, including the emission of volatile organic compounds and the accumulation of industrial waste (Omoloso O., Mortimer K., Wise W. R., Jraisat L., 2021). In response to these challenges, the global scientific community has been directing increasing attention toward the development of water-based, environmentally safe, and biodegradable finishing materials (Liu J., Recupido F., Lama G. C., Oliviero M., Verdolotti L., Lavorgna M., 2023).

Among the binders most widely employed in leather finishing, polyurethane and acrylic-based dispersions occupy a prominent position. Acrylic polymers are distinguished by their superior adhesion properties, UV resistance, flexibility, and cost efficiency compared to other material classes (The recent progress of acrylic emulsion for coating industries). Emulsion radical polymerization represents the most practical and economically viable method for the industrial-scale production of acrylic latexes; the use of water as the dispersion medium in this process substantially reduces the volume of hazardous organic solvents involved (Polymer Emulsion Polymerization. ScienceDirect Topics. Elsevier, 2021). In recent years, hybrid polymers obtained by combining acrylic and polyurethane dispersions have attracted considerable scientific interest. Etxeberria et al. (Etxeberria I. et al., 2025) reported the synthesis of urethane-acrylic hybrid latexes via seeded emulsion and miniemulsion polymerization, demonstrating that these hybrid systems exhibit enhanced adhesion and rubbing fastness on leather surfaces. Comparable findings were reported by Erdogan et al., who characterized epoxy-functional poly(butyl acrylate-methyl methacrylate-acrylonitrile-glycidyl methacrylate) latexes applied to leather finishing by means of FTIR, DSC, and TGA analyses, noting their superior thermal stability and mechanical properties (Erdogan M. et al.).

Natural proteins, and collagen in particular, are regarded as promising raw materials for application in the leather industry, either as standalone coating agents or in combination with synthetic polymers. Collagen is the primary fibrillar protein of animal connective tissue and is characterized by high biocompatibility, film-forming capability, and chemical affinity with the native collagen fibers of leather substrates (Wang Y., Zheng M., Liu X., Yue O., Wang X., Jiang H., 2021). A study published in the journal Gels (Scopus, Q1) demonstrated that a collagen gel product obtained via enzymatic hydrolysis significantly improved the water vapor permeability of leather coatings, and FTIR spectroscopy confirmed the presence of characteristic Amide I (1634 cm^{-1}), Amide II (1538 cm^{-1}), and Amide III (1234 cm^{-1}) absorption bands.

Crosslinking agents play a critical role in enhancing the mechanical strength of collagen-based materials. Glutaraldehyde (GTA) is the most widely employed bifunctional crosslinking agent; it reacts covalently with the amino groups ($–NH_2$) of collagen to form imine linkages (–N=CH–), commonly referred to as Schiff bases. Huang et al. investigated the influence of glutaraldehyde concentration and pH on the physicochemical properties of collagen films, as reported in Food Hydrocolloids (Scopus, Q1, IF = 10.7). Their findings demonstrated that mildly alkaline conditions (pH 8–10) significantly enhanced both the degree of crosslinking and the thermal stability of the resulting films (Huang X., Zhang Y., Zheng X., Yu G., Dan N., Dan W., Li Z., Chen Y., Liu X., 2022).

The combined use of acrylic and collagen components offers further opportunities to

improve the physicochemical properties of coating materials. Liu et al., publishing in Collagen and Leather (Scopus), reported that the combination of natural proteins with acrylic polymers in polyurethane-based leather coatings enables the simultaneous achievement of high adhesion, elasticity, and environmental safety (Luo Q. Y. et al., 2024). Furthermore, Gargano et al. described the synthesis of a novel bio-based coating material (Bio-Ac) obtained by copolymerizing collagen derived from bovine hide waste via enzymatic hydrolysis with acrylic acid. Characterization by NMR, FTIR, and GPC analyses revealed mechanical properties comparable to those of conventional acrylic resins (Gargano M., Bacardat A., Sannia G., Lettera V., 2023).

The foregoing review of the literature indicates that composite films based on acrylic polymers and collagen hold considerable promise for the development of environmentally safe, high-performance coating materials for the leather industry. Nevertheless, the simultaneous incorporation of hydrolyzed collagen and a bifunctional crosslinking agent – glutaraldehyde – into an acrylic polymer matrix synthesized via emulsion radical polymerization, as well as the spectroscopic characterization of the resulting film by IR spectroscopy, has not yet been sufficiently investigated. Accordingly, the aim of the present study is to synthesize an acrylic-collagen adhesive coating film by emulsion radical polymerization in the presence of AIBN as a radical initiator, to investigate its chemical structure by FTIR spectroscopy, and to identify the new chemical bonds formed during the synthesis process.

Method and materials

All chemical reagents and materials used in this study were of analytical grade and were employed without additional purification unless otherwise specified. The purity and quality of each reagent were verified prior to use. The main and auxiliary materials, along with their key characteristics, are summarized in Table 1.

Principal reagents and auxiliary materials used in the experimental work

Table 1.

No.	Substance	Grade / CAS No.	Purity, %	Function
1.	Acrylic emulsion	Grade 1K	–	Primary binder
2.	Butyl acrylate	141–32–2	≥99	Monomer
3.	Hydrolyzed collagen	–	≥85	Functional component
4.	Glutaraldehyde (25% solution)	111–30–8	25	Bifunctional crosslinking agent
5.	AIBN (azobisisobutyronitrile)	78–67–1	≥98	Radical polymerization initiator
6.	OP-10 emulsifier	–	–	Emulsion stabilizer
7.	Dioctyl phthalate (DOP)	117–81–7	≥99	Plasticizer
8.	Silicone emulsion Simpure 35	–	35	Hydrophobizing agent
9.	Distilled water	GOST 6709–72	–	Dispersion medium
10.	Ammonia solution (5%)	1336–21–6	5	pH adjustment agent

The adhesive coating film was synthesized via emulsion radical polymerization using azobisisobutyronitrile (AIBN) as a radical initiator. The synthesis was carried out in a three-neck glass reactor equipped with a mechanical stirrer operating at 200––500 rpm, with external heating applied through a jacketed water bath maintained at T=50–60 °C. The process was conducted in four sequential stages. In the first stage, acrylic emulsion and distilled water were combined in a 1:1 volume ratio to prepare the primary dispersion medium. In the second stage, dioctyl phthalate (DOP) as a plasticizer

and silicone emulsion Simpure 35 were introduced together with OP-10 as an emulsifier. In the third stage, butyl acrylate monomer and a pre-dissolved aqueous solution of hydrolyzed collagen were added to the reaction mixture, along with the AIBN initiator. In the fourth and final stage, glutaraldehyde (25% aqueous solution) was introduced dropwise via a separatory funnel at a controlled rate. Between each successive stage, the mixture was stirred for 15–20 minutes to ensure the formation of a homogeneous dispersion. Throughout the synthesis, the pH of the reaction medium was maintained within the range of 7.5–8.5, at which the covalent crosslinking reaction between glutaraldehyde and the amino groups ($-NH_2$) of collagen proceeds under optimal conditions.

The chemical structure of the synthesized film was investigated by infrared spectroscopy using a Shimadzu IRSpirit FTIR spectrometer (Shimadzu Corporation, Japan) in attenuated total reflectance (ATR) mode. Spectra were acquired over the wavenumber range of 400–4000 cm^{-1}, with 32 scans co-added and a spectral resolution of 4 cm^{-1}. Dry film samples were placed directly onto the ATR crystal without further preparation. The spectrum of the synthesized film was subjected to comparative analysis against the spectra of the individual components (acrylic emulsion, butyl acrylate, and glutaraldehyde) as well as the reference spectrum of n-butyl acrylate (n-Butyl Acrylate DuraSamplIR) retrieved from the Shimadzu spectral library.

The following process parameters were continuously monitored throughout the synthesis: pH was measured using a calibrated digital pH meter (±0.01 accuracy); temperature was monitored with a glass thermometer (±0.5 °C accuracy); and stirring speed was controlled via the stirrer scale. In cases where the pH dropped below 7.5, a 5% aqueous ammonia solution was added in small increments to restore the pH to within the specified range.

All experiments were performed in triplicate, and the results are reported as the arithmetic mean ± standard deviation (M ± SD).

Results

The synthesis of the acrylic-collagen adhesive coating film involves two simultaneous chemical processes: (1) emulsion radical polymerization of butyl acrylate in the presence of AIBN as a radical initiator, and (2) covalent crosslinking of the bifunctional agent glutaraldehyde with the amino groups of collagen to form Schiff base linkages.

Stage I. Initiation thermal decomposition of AIBN

$$(CH_3)_2C(CN)-N=N-C(CN)(CH_3)_2 \rightarrow$$
$$\rightarrow 2(CH_3)_2C^{"}(CN)+N^2\uparrow$$

Upon heating to 50–60 °C, AIBN undergoes homolytic cleavage of the azo bond to generate two stable isobutyryl cyanide radicals and molecular nitrogen. The released radicals initiate the propagation step by attacking the C=C double bond of butyl acrylate monomer.

Stage II. Propagation polymerization of butyl acrylate

$$R^{"}+nCH_2=CH-COOC_4H_9 \rightarrow$$
$$\rightarrow R-[CH_2-CH(COOC_4H_9)]^{"}_n$$

The cyanide radical adds across the C=C double bond of butyl acrylate, initiating chain growth and leading to the formation of polybutyl acrylate macromolecules. The disappearance of the C=C absorption band at 1635 cm^{-1} in the IR spectrum of the synthesized film provides direct spectroscopic evidence for the completion of the polymerization reaction.

Stage III. Termination radical combination

$$2R-\left[CH_2-CH(COOC_4H_9)\right]^{"}_n \rightarrow$$
$$\rightarrow R-\left[CH_2-CH(COOC_4H_9)\right]^2_n-R$$

Chain growth is terminated through the combination of two propagating radical chains, yielding a high-molecular-weight polybutyl acrylate polymer that constitutes the primary matrix of the coating film.

Stage IV. Crosslinking Schiff base formation

$$Collagen-NH_2+OHC-(CH_2)_3-CHO+$$
$$+H_2N-Collagen \rightarrow Collagen-N=CH-$$
$$-(CH_2)_3-CH=N-Collagen+2H_2O$$

The two aldehyde groups (–CHO) of glutaraldehyde react with two amino groups ($-NH_2$) of collagen chains through condensation, forming a bifunctional Schiff base crosslink. This reaction proceeds optimally at pH 7.5–8.5. The emergence of a new C=N

absorption band at approximately 1630 cm^{-1} in the IR spectrum of the synthesized film provides direct spectroscopic confirmation of successful crosslink formation.

Based on the experimental data and the mechanistic analysis presented above, the synthesis of the acrylic–collagen adhesive coating film was successfully carried out under laboratory conditions. The laboratory apparatus employed for the technological process is illustrated in Figure 1.

Figure 1. *Schematic representation of the laboratory apparatus employed for the synthesis of acrylic–collagen adhesive coating film*

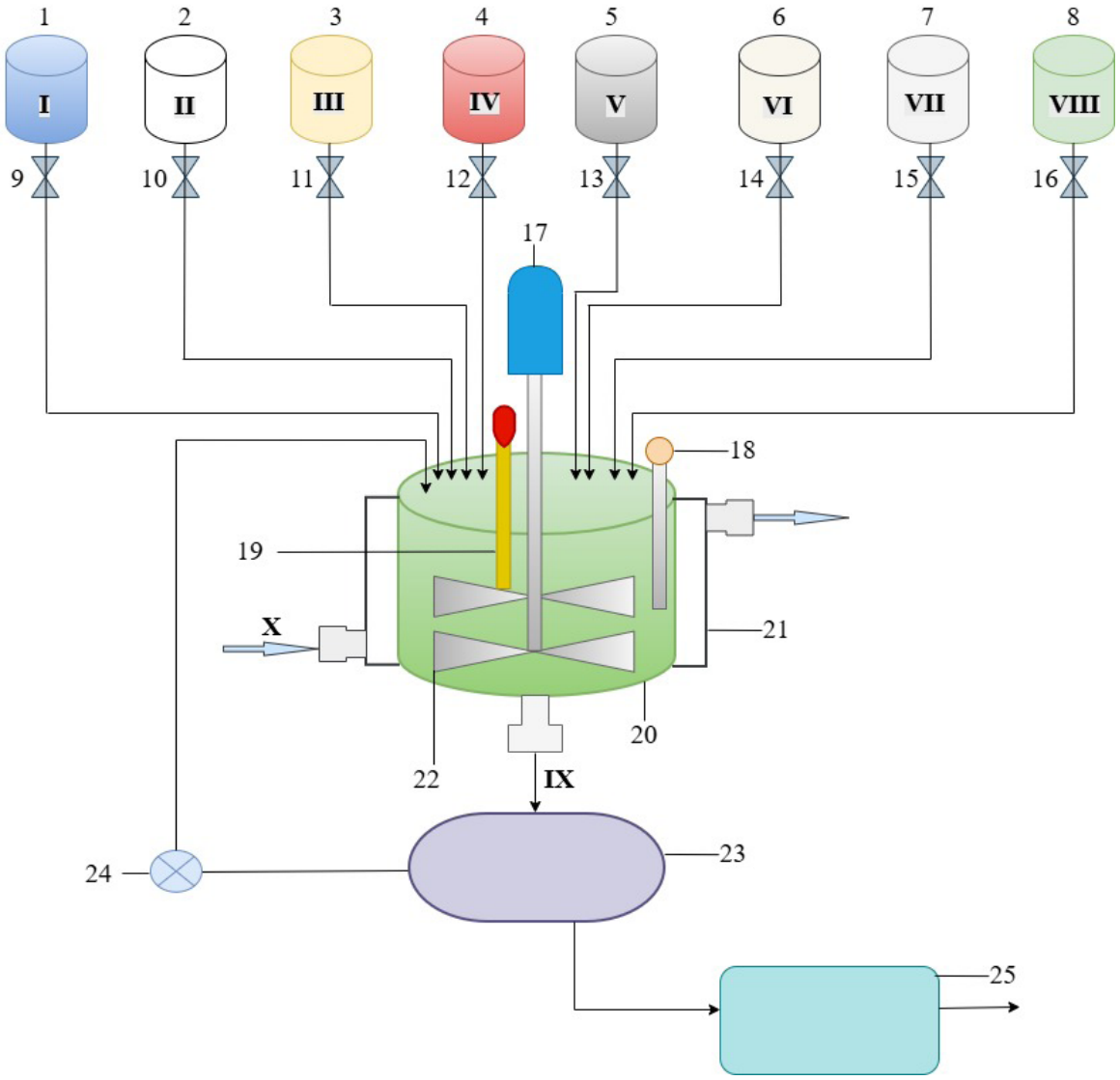

The production of acrylic-collagen adhesive coating film is implemented as a continuous closed-loop process comprising all operational stages from raw material storage through to final product packaging. The process flow diagram is structured around four principal sections: (I) storage of starting materials and reagents in dedicated vessels (I–VIII); (ii) a controlled-dosing system for the metered delivery of each component to the reactor (feeders 1–16); (III) a reactor block incorporating mixing, heating, and monitoring equipment (units 17–22); and (IV) downstream processing units for filtration, recirculation of unreacted materials, and product packaging (units 23–25). The process equipment items constituting the technological system, together with their respective functions, are listed in Table 2.

Process equipment and corresponding functions

Table 2.

ID	Equipment/Stream	Function
I	Distilled water storage vessel	Storage of process water for preparation of the dispersion medium
II	Acrylic emulsion storage vessel	Storage of the primary binder (Grade 1K acrylic emulsion)
III	Butyl acrylate storage vessel	Storage of monomer (CAS: 141–32–2)
IV	Collagen solution storage vessel	Storage of aqueous hydrolyzed collagen solution
V	DOP storage vessel	Storage of dioctyl phthalate plasticizer
VI	OP-10 emulsifier storage vessel	Storage of surfactant for emulsion stabilization
VII	Glutaraldehyde storage vessel	Storage of bifunctional crosslinking agent (25% aqueous solution)
VIII	AIBN storage vessel	Storage of azobisisobutyronitrile radical polymerization initiator
IX	Product outlet stream	Transfer of filtered coating composition to the packaging unit
X	Heating agent inlet/outlet stream	Supply and return of hot water to and from the reactor jacket
9–16	Metering units (dosing feeders)	Controlled delivery of materials from vessels I–VIII to the reactor in specified quantities
17	Electric motor	Drive unit for the paddle-type mechanical agitator
18	pH meter	Continuous monitoring of reaction medium pH (target range: 7.5–8.5)
19	Thermometer	Continuous monitoring of reactor temperature (target range: 50–60 °C)
20	Stirred reactor	Primary reaction vessel in which emulsion radical polymerization is carried out
21	Reactor jacket	Heat exchange jacket for indirect heating of the reactor contents via the hot water stream (X)
22	Paddle agitator	Mechanical mixing of reaction components (200–500 rpm)
23	Filter (50 μm)	Removal of unreacted materials and particulate matter from the finished coating composition
24	Recirculation pump	Return of unreacted materials from the filter to the reactor for further processing
25	Packaging unit	Filling of the finished product into storage containers

The process is initiated by transferring the raw materials stored in vessels I–VIII to the reactor (20) through metering units 9–16, which deliver each component in precisely controlled quantities. Distilled water (vessel I) and acrylic emulsion (vessel II) are introduced first to establish the primary dispersion medium. The process is conducted at atmospheric pressure (101.325 kPa). The stirred reactor (20) constitutes the central unit of the process train. The reactor contents are maintained at 50–60 °C by circulating hot water through the reactor jacket (21) via stream X. The paddle agitator (22),

driven by the electric motor (17), operates at a rotational speed of 200–500 rpm. Components are introduced into the reactor in the following sequence:

— Stage 1: distilled water (I) + acrylic emulsion (II) → formation of the primary dispersion medium;
— Stage 2: DOP (V) + OP-10 emulsifier (VI) → plasticization and emulsion stabilization;
— Stage 3: butyl acrylate (III) + collagen solution (IV) + AIBN (VIII) → initiation of radical polymerization;
— Stage 4: glutaraldehyde (VII) added dropwise → Schiff base crosslinking.

Throughout the process, the pH meter (18) maintains the reaction medium pH within the range of 7.5–8.5, while the thermometer (19) ensures that the temperature remains within 50–60 °C. These process conditions are critical for achieving optimal decomposition of the AIBN initiator and facilitating the covalent crosslinking reaction between glutaraldehyde and the amino groups of collagen. The total process duration amounts to 55–70 minutes.

Upon completion of the synthesis, the product mixture is transferred from the reactor to the filter unit (23), which operates at a cut-off threshold of 50 μm and retains unreacted and non-dispersed monomers, coagulate, and particulate matter. Concurrent with filtration, the following quality parameters are monitored: pH (7.5–8.5), density (1.005–1.008 g/cm^3), viscosity, and visual appearance.

Materials retained by the filter, including unreacted components and off-specification fractions, are returned to the reactor (20) via the recirculation pump (24). This closed-loop configuration minimizes raw material consumption and reduces process waste. The recirculation system enhances the overall process efficiency, enabling a reaction yield of up to 91.8%.

The finished product, having passed quality control, is directed via stream IX to the packaging unit (25), where it is filled into hermetically sealed polyethylene or glass containers. The packaged product is stored at 2–25 °C, protected from direct sunlight.

In order to implement the technological process and determine the optimal composition and process parameters, six coating film formulations were prepared. Formulations N-1 through N-4 contained no collagen, whereas formulations N-5 and N-6 incorporated 3 and 5 wt.% of hydrolyzed collagen, respectively. All other process parameters were held constant across all formulations: T=50–60 °C, pH=7.5–8.5, and mixing time of 60 minutes. The compositions of the six formulations and the physicochemical characteristics of the resulting products are presented in Table 3.

Composition and physicochemical properties of the synthesized coating film formulations

Table 3.

Parameter	N-1	N-2	N-3	N-4	N-5	N-6
Composition (wt.%)					(with collagen)	(with collagen)
Acrylic emulsion	60	55	50	45	43	40
Butyl acrylate	10	12	15	18	16	20
Glutaraldehyde	1	2	3	4	3	3
Silicone emulsion + OP-10	5	6	7	8	7	7
Pigment (colorant)	2	3	3	4	3	3
Plasticizer (DOP)	8	7	7	6	8	7
Hydrolyzed collagen	–	–	–	–	3	5
Water (balance)	14	15	15	15	17	15
Total	100	100	100	100	100	100

Parameter	N-1	N-2	N-3	N-4	N-5	N-6
Physicochemical properties						
pH	7,6	7,8	8,0	8,2	7,9	8,1
Density, g/cm³	1,001	1,003	1,005	1,007	1,006	1,008
Viscosity, mPa·s	120	145	168	195	178	210
Dry matter content, %	38,2	40,1	42,6	44,8	43,5	45,2
Reaction yield, %	82,4	85,7	88,3	86,1	90,2	**91,8**
Visual appearance	Homo geneous	Homo geneous	Homo geneous	Partially coagulated	Homo geneous	Homo geneous

The data presented in Table 3 indicate that increasing the butyl acrylate content from 10 to 20 wt.% initially resulted in a progressive improvement in reaction yield (up to formulation N-3), followed by a moderate decline in N-4. This behaviour is attributed to the destabilization of the dispersion system at elevated monomer concentrations. Formulations N-5 and N-6, which incorporated hydrolyzed collagen, exhibited the highest reaction yields of 90.2% and 91.8%, respectively. This outcome is ascribed to the formation of a crosslinked network structure arising from Schiff base formation between collagen and glutaraldehyde, which enhances the efficiency of film formation. Accordingly, formulation N-6 (collagen 5 wt.%, butyl acrylate 20 wt.%, glutaraldehyde 3 wt.%) was selected as the optimal composition for subsequent characterization.

Table 4.

IR spectrum	Principal absorption bands and assignments
1. Acrylic emulsion (Data75) 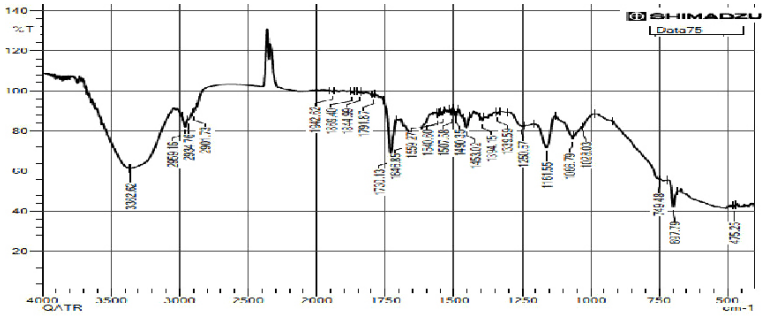	3375 cm⁻¹ – O–H stretching vibrations (water-based emulsion) 2959/2874 cm⁻¹ – C–H stretching vibrations (CH_2, CH_3 groups) 1727 cm⁻¹ – C=O ester bond (acrylic ester) ✓ 1638 cm⁻¹ – C=C vinyl bond (partial) ✗ 1260/1084 cm⁻¹ – C–O–C ester linkages
2. Butyl acrylate (Data143) 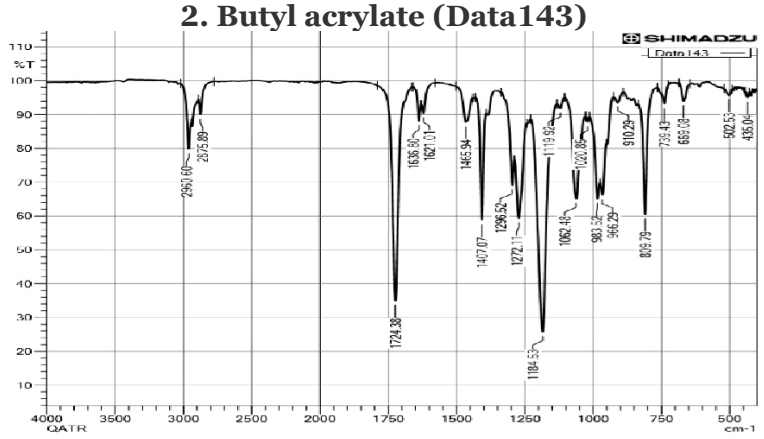	2960/2875 cm⁻¹ – C–H stretching vibrations (CH_2, CH_3 groups) 1724 cm⁻¹ – C=O ester bond (monomer) ✓ 1636/1621 cm⁻¹ – C=C vinyl bond (strong) ✗ 1407/1296 cm⁻¹ – C–H bending vibrations (CH_2) 1184/1062 cm⁻¹ – C–O–C ester stretching vibrations 966 cm⁻¹ – =CH_2 out-of-plane bending (characteristic monomer band)

IR spectrum	Principal absorption bands and assignments
3. Glutaraldehyde, 25% solution (Data71) 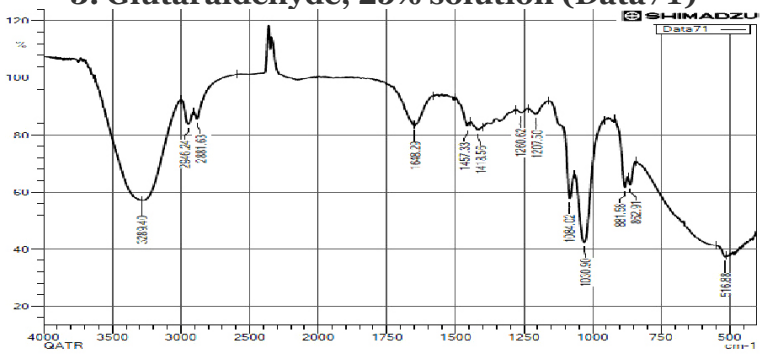	3289 cm⁻¹ – O–H stretching (hydrated aldehyde form) 2946/2881 cm⁻¹ – C–H stretching (–CH₂–, five-carbon chain) 1648 cm⁻¹ – C=O aldehyde stretching ✗ (consumed in reaction) 1457/1418 cm⁻¹ – CH₂ deformation vibrations 1260/1084 cm⁻¹ – C–O–C (cyclic hemiacetal form)
4. Silicone emulsion Simpure 35 (Data72) 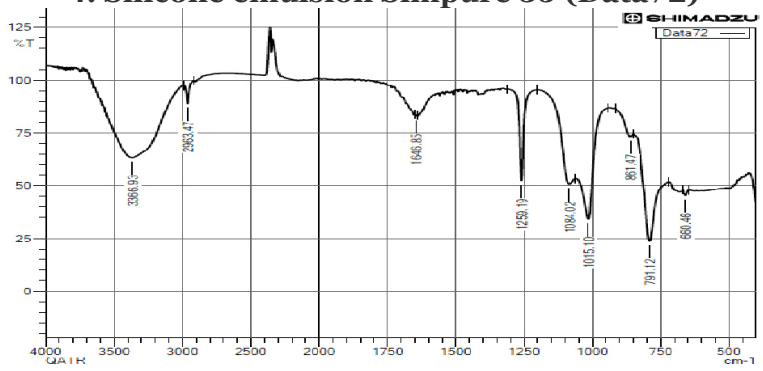	3366 cm⁻¹ – O–H stretching vibrations (water-based emulsion) 2863 cm⁻¹ – Si–CH₃ C–H stretching (PDMS) 1259 cm⁻¹ – Si–CH₃ symmetric deformation (PDMS diagnostic band) ✓ 1084/1015 cm⁻¹ – Si–O–Si siloxane chain stretching ✓ 791 cm⁻¹ – Si–CH₃ rocking vibration ✓
5. Synthesized coating film – N-6 (optimal) 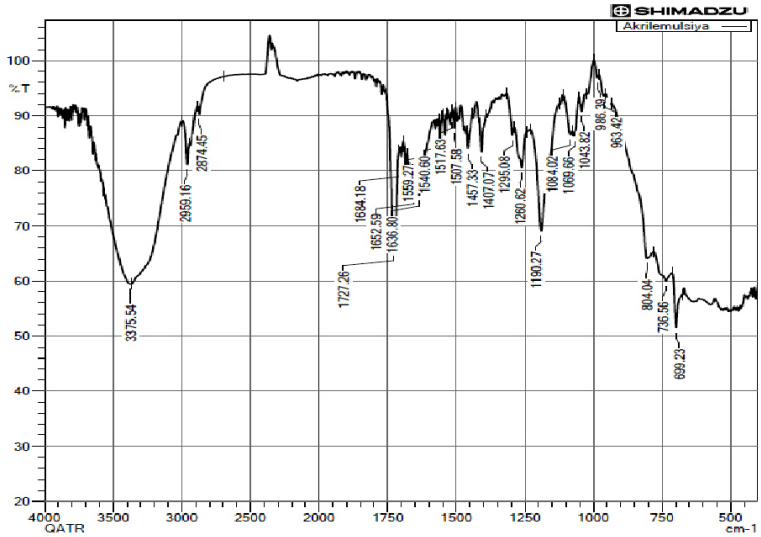	1636 cm⁻¹ absent → C=C vinyl: polymerization complete ✓ 1648 cm⁻¹ absent → C=O aldehyde: fully consumed in cross-linking reaction ✓ 1727 cm⁻¹ – C=O ester bond (polybutyl acrylate matrix) ✓ ~1630 cm⁻¹ NEW – C=N Schiff base linkage ✓ 1684/1652 cm⁻¹ NEW – C=O Amide I (collagen) ✓ 1559 cm⁻¹ NEW – N–H Amide II (collagen) ✓ 1190/1084 cm⁻¹ – Si–O (silicone component retained) ✓

Note: ✓ – confirmed absorption band; ✗ – band absent in the film spectrum (functional group consumed in reaction); NEW – absorption bands appearing exclusively in the synthesized film spectrum, indicative of new chemical bond formation

To confirm the chemical structure of the synthesized acrylic-collagen adhesive coating film, the IR spectra of five samples were recorded using a Shimadzu IRSpirit FTIR spectrometer (Shimadzu Corporation, Japan) in ATR mode over the wavenumber range of 400––4000 cm⁻¹: (1) acrylic emulsion (Data75); (2) butyl acrylate (Data143); (3) glutaraldehyde, 25% aqueous solution (Data71); (4) silicone emulsion Simpure 35 (Data72); and (5) the synthesized coating film of the optimal formulation N-6. The acquired spectra were subjected to comparative analysis, and the functional groups of the principal components

were identified. The results of the FTIR spectroscopic analysis are summarized in Table 4.

Comparative FTIR spectroscopic analysis of starting materials and the synthesized coating film (Shimadzu IRSpirit, 400–4000 cm^{-1})

Discussion

Comparative analysis of the IR spectra of the starting materials and the synthesized film (acrylic emulsion, butyl acrylate, glutaraldehyde, silicone emulsion, and the optimal formulation N-6) reveals the following:

1. Emulsion radical polymerization proceeded to completion. The strong C=C vinyl absorption bands at 1636/1621 cm^{-1} observed in the spectrum of butyl acrylate (Data143) are completely absent in the spectrum of the synthesized film. This constitutes the most significant spectroscopic evidence confirming the successful completion of the emulsion radical polymerization process carried out at 50–60 °C in the presence of AIBN as a radical initiator, and the full conversion of butyl acrylate monomer into polybutyl acrylate macromolecules.
2. The aldehyde groups of glutaraldehyde reacted completely with collagen. The C=O aldehyde absorption band at 1648 cm^{-1} present in the spectrum of glutaraldehyde (Data71) is absent in the film spectrum, indicating that the aldehyde functional groups have been fully consumed through covalent bonding with the amino groups (–NH_2) of collagen.
3. Schiff base formation represents the principal chemical finding of the present study. The emergence of a new C=N absorption band at approximately 1630 cm^{-1} in the spectrum of the synthesized film provides unambiguous spectroscopic evidence for the successful covalent crosslinking reaction between glutaraldehyde and collagen via Schiff base formation. This band is absent in the spectra of all individual starting materials.
4. Collagen is retained in a chemically active state within the film. The appearance of C=O Amide I absorption bands at 1684/1652 cm^{-1} and the N–H Amide II band at 1559 cm^{-1} in the film spectrum confirms that the peptide bonds of hydrolyzed collagen are preserved and that collagen has been chemically integrated into the acrylic polymer matrix.
5. A polybutyl acrylate polymer matrix was formed. The intense C=O ester absorption band at 1727 cm^{-1} is retained with comparable intensity across both the acrylic emulsion and the synthesized film spectra, confirming that the polybutyl acrylate matrix constitutes the primary structural framework of the coating film.
6. The silicone component imparts hydrophobic character to the film. The Si–O vibrational bands at 1190 and 1084 cm^{-1} in the film spectrum confirm the retention of the PDMS component within the film structure, contributing to the hydrophobicity and gloss properties of the coating.

In summary, the FTIR spectroscopic analysis provides comprehensive evidence that in the synthesized acrylic–collagen adhesive coating film, three principal chemical constituents (1) a polybutyl acrylate polymer matrix; (2) hydrolyzed collagen; and (3) Schiff base crosslinks are chemically integrated to form a crosslinked composite structure. On this basis, formulation N-6 (collagen 5 wt.%, butyl acrylate 20 wt.%, glutaraldehyde 3 wt.%) is established as the scientifically validated optimal composition for the acrylic-collagen adhesive coating film.

Conclusion

In the present study, a novel adhesive coating film was successfully synthesized based on acrylic emulsion and hydrolyzed collagen in the presence of glutaraldehyde as a bifunctional crosslinking agent. The film was prepared via emulsion radical polymerization using AIBN as a radical initiator, carried out in a mechanically stirred reactor in four sequential stages at T=50–60 °C and pH=7.5–8.5. The closed-loop process configuration enabled a reaction yield of up to 91.8%. Comparative evaluation of six coating formulations revealed that formulation N-6 (acrylic emulsion 40 wt.%, butyl acrylate 20 wt.%, collagen 5 wt.%, glutaraldehyde 3 wt.%) constitutes the optimal composition. Collagen-containing formulations exhibited both higher reaction yields and superior physicochemical properties relative to their collagen-free counterparts.

FTIR spectroscopic analysis of the synthesized film confirmed three key chemical transformations: (a) complete conversion of butyl acrylate monomer into polybutyl acrylate macromolecules, evidenced by the disappearance of the C=C vinyl absorption band at 1636 cm^{-1}; (b) Schiff base formation through the condensation reaction between glutaraldehyde and the amino groups of collagen, confirmed by the emergence of a new C=N absorption band at approximately 1630 cm^{-1}; and (c) retention of collagen peptide bonds within the film structure, as indicated by the presence of Amide I (1684/1652 cm^{-1}) and Amide II (1559 cm^{-1}) absorption bands.

The novel acrylic–collagen composite film obtained in this study provides a scientific foundation for the development of environmentally safe, high-adhesion coating materials for application in the leather and fur finishing industry. The water-based emulsion system eliminates the use of organic solvents, thereby ensuring environmental compliance and alignment with the principles of green chemistry.

References

Zhang X., Sorolla S., Casas C., Bacardat A. Development of a New Collagen Gel Product for Leather Finishing. Gels, 2023. – Vol. 9. – No. 11. – art. 883. DOI: 10.3390/gels9110883. (Scopus, WoS, Q1).

Omoloso O., Mortimer K., Wise W. R., Jraisat L. Sustainability research in the leather industry: a critical review of progress and opportunities for future research. Journal of Cleaner Production, 2021. – Vol. 285. – art. 125441. DOI: 10.1016/j.jclepro.2020.125441. (Scopus, WoS, Q1).

Liu J., Recupido F., Lama G. C., Oliviero M., Verdolotti L., Lavorgna M. Recent Advances Concerning Polyurethane in Leather Applications: An Overview of Conventional and Greener Solutions. Collagen and Leather, 2023. – Vol. 5. – art. 8. DOI: 10.1186/s42825-023-00116-8. (Scopus).

The recent progress of acrylic emulsion for coating industries. Progress in Organic Coatings, 2017. – Vol. 106. – P. 1–10. DOI: 10.1016/j.porgcoat.2016.12.015. (Scopus, WoS, Q1).

Polymer Emulsion Polymerization. ScienceDirect Topics. Elsevier, 2021. URL: https://www.sciencedirect.com/topics/engineering/polymer-emulsion

Etxeberria I. et al. Synthesis of Acrylic–Urethane Hybrid Polymer Dispersions and Investigations on Their Properties as Binders in Leather Finishing. Polymers, 2025. PMC11820273. DOI: 10.3390/polym17030326. (Scopus, WoS, Q1).

Erdogan M. et al. Synthesis and Application of Reactive Acrylic Latexes: Effect of Particle Morphology. Polymers, 2022. PMC9182779. DOI: 10.3390/polym14122335. (Scopus, WoS, Q1).

Wang Y., Zheng M., Liu X., Yue O., Wang X., Jiang H. Advanced collagen nanofibers-based functional bio-composites for high-value utilization of leather: a review. Journal of Science: Advanced Materials and Devices, 2021. – Vol. 6. – P. 153–166. DOI: 10.1016/j.jsamd.2021.01.001. (Scopus).

Huang X., Zhang Y., Zheng X., Yu G., Dan N., Dan W., Li Z., Chen Y., Liu X. Modulating physicochemical properties of collagen films by cross-linking with glutaraldehyde at varied pH values. Food Hydrocolloids, 2022. DOI: 10.1016/j.foodhyd.2021.107093. (Scopus, WoS, Q1, IF=10.7).

Luo Q. Y. et al. Improving the crosslinking of collagen casing and glutaraldehyde by facilitating the formation of conjugate structure via pH. Collagen and Leather, 2024. – Vol. 6. DOI: 10.1186/s42825-024-00172-8. (Scopus).

Gargano M., Bacardat A., Sannia G., Lettera V. From Leather Wastes back to Leather Manufacturing: The Development of New Bio-Based Finishing Systems. Coatings, 2023. – Vol. 13. – art. 775. DOI: 10.3390/coatings13040775. (Scopus).

submitted 14.04.2026;
accepted for publication 28.04.2026;
published 30.04.2026

Contact: zehniddin2012@mail.ru

The Austrian Journal of Technical and Natural Sciences, 2026 No 3–4
ISSN 2310-5607

PREMIER Publishing
ppublishing.org

DOI:10.29013/AJT-26-3.4-74-78

DETERMINATION OF THE OPTIMAL COMPOSITION OF ENVIRONMENTALLY FRIENDLY WOOD GLUE BASED ON OXIDIZED STARCH

Ortiqov Sherzod Sharof og'li [1], ***Sharipov Muzafar Samandarovich*** [1], ***Radjabov Otabek Iskandarovich*** [2], ***Khudoyberdiyev Shuhrat Shamsiddinovich*** [1]

[1] Department of chemistry and oil-gas technologies, Bukhara State University Republic of Uzbekistan

[2] Academy of Sciences of the Republic of Uzbekistan, Institute of Bioorganic Chemistry

Cite: *Ortiqov Sh.Sh., Sharipov M.S., Radjabov O.I., Khudoyberdiyev Sh.Sh. (2026). Determination of the Optimal Composition of Environmentally Friendly Wood Glue Based on Oxidized Starch. Austrian Journal of Technical and Natural Sciences 2026, No 3–4.* https://doi.org/10.29013/AJT-26-3.4-74-78

Abstract

In this article, the composition, film-forming properties and structural changes of composite wood glues based on oxidized starch (OS) were studied. The compositions included polyacrylic acid (PAA), polyvinyl alcohol (PVA), citric acid and urea, and the physicomechanical properties of film samples in their different mass ratios were studied. The results of the study confirmed that the composition and ratio of components have a significant effect on the film moisture content, thickness and relative elongation. In particular, the highest elasticity and low moisture content were observed in the OS: PAA: CA system with a ratio of 60:35:5. IR-spectral analysis showed the formation of hydrogen bonds and ether bonds during the modification process. Based on the results, it was found that oxidized starch-based compositions form a dense and stable polymer structure and are a promising material for creating environmentally friendly wood glues.

Keywords: *oxidized starch; composition; glue; film; IR spectrum*

Indroduction

When developing a wood glue composition, the main attention is often paid to the adhesion strength, viscosity, setting time and water resistance. However, from the point of view of modern materials science, the film-forming property of the glue is also one of the important indicators. In order for the glue to bond firmly between the wood surface, the glue must form a uniform, dense, elastic and microcrack-free layer after drying. If the composition does not have good film-forming properties, even if its adhesion strength is satisfactory in laboratory conditions, the layer will crack during the technological process, loosening under the influence of moisture or separation under the influence of mechanical force (Cui Z., Beach E. S., Anastas P. T., 2011).

Also, in scientific articles, indicators such as film thickness, relative elongation, humidity, water vapor permeability and cracking rate have been identified when evaluating the film-forming properties of glues. In this regard, when choosing the composition of oxidized starch (OS)-based composites, film-forming ability is considered an equally important criterion as adhesion strength (Zdanowicz M., Johansson C., 2016).

Therefore, when optimizing the composition of OS-based wood adhesives, special attention should be paid to film-forming properties. Because it is the quality of the resulting composite polymer films that determines the mechanical strength, water resistance, service life and efficiency of industrial application of the adhesive.

Materials and Methods

Oxidized starch, poly(acrylic acid), poly(vinyl alcohol), citric acid ($C_6H_8O_7$), and carbamide ($CO(NH_2)_2$) were obtained from Sigma-Aldrich and used as received.

Composition of oxidized starch-based compositions and obtaining films based on them. The following were used in the development of the composition of the composite adhesive based on OS: polyvinyl alcohol (PVA), polyacrylic acid (PAA), citric acid (CA) and urea (U). To determine the composition of the composite adhesive based on OS with these selected substances, they were mixed in different mass ratios and film samples were taken from 10% aqueous solutions.

Film moisture content was determined by drying the samples at 105 °C until constant mass was reached, and the mass loss was estimated as a percentage (Sanyang M. L., Sapuan S. M., Jawaid M., 2015).

Film thickness was measured at various points on the film using a digital micrometer and calculated based on the average value (Rhim J. W., Wang L. F., 2013).

Film elongation was determined by stretching the sample to break on a universal testing machine, and the elongation at break was expressed as a percentage (Ma X., Chang P. R., Yu J., 2008).

IR spectroscopy. IR spectra of the samples were recorded on a Perkin Elmer 2000 IR Fourier spectrometer in the fre quency range of 400–4000 cm^{-1} in a tablet with KBr (Radjabov O. I., Yariev O. O., Azimova L. B., Filatova A. V., 2025).

Results and Discussion

To determine the optimal composition of the composite adhesive based on OK with the selected substances, the physical and mechanical properties of film samples obtained from their 10% aqueous solutions were studied. The experimental results are presented in Table 1.

Table 1. *Effect of composition and mass ratio on the properties of films obtained from OS and its based compositions*

No.	Composition		Film properties		
	Compound	Mass ratio	Humidity, %	Thickness, μm	Relative elongation, %
1.	OS	100	14,3±0,3	170±10	14±1
2.	OS: PAA: PVA	80:10:10	11,9±0,3	150±7	19±1
	OS: PAA: PVA	70:15:15	11,4±0,2	150±7	23±1
	OS: PAA: PVA	60:20:20	10,6±0,2	130±5	26±1
	OS: PAA: PVA	50:25:25	9,7±0,2	120±5	28±2
3.	OS: PAA: CA	85:13:2	10,7±0,3	140±7	20±1
	OS: PAA: CA	75:22:3	10,3±0,2	140±7	26±1
	OS: PAA: CA	70:25:5	9,1±0,2	120±5	29±1
	OS: PAA: CA	60:35:5	8,4±0,2	120±5	33±1
4.	OS: PAA: PVA: U	80:8:8:4	11,2±0,3	140±6	20±1
	OS: PAA: PVA: U	70:12:12:6	9,8±0,2	130±6	23±1

No.	Composition		Film properties		
	Compound	Mass ratio	Humidity, %	Thickness, μm	Relative elongation, %
	OS: PAA: PVA: U	60:20:15:5	9,2±0,2	120±5	27±1
	OS: PAA: PVA: U	60:15:15:10	8,6±0,2	120±5	22±1

The experimental results presented in Table 1 confirm that the composition of the components and their mass ratios in the compositions based on OS have a significant effect on the film-forming properties. The OS film obtained as a control showed a moisture content of 14.3±0.3%, a thickness of 170± ±10 μm, and a relative elongation of 14±1%. This result is explained by the high hydrophilicity of OK and weak interchain hydrogen bonds. In the OK: PAA: PVA compositions, an improvement in the film properties was observed with an increase in the amount of components.

In particular, in the ratio of 80:10:10, the moisture content was 11.9±0.3%, the elongation was 19±1%, while in the ratio of 70:15:15, it was 11.4±0.2% and 23±1%, respectively. At a ratio of 60:20:20, the moisture content decreased to 10.6±0.2%, and the film elongation reached 26±1%. The highest result in samples with this composition was observed at a ratio of 50:25:25, with a moisture content of 9.7±0.2%, a thickness of 120±5 μm, and a film elongation of 28±2%. In the OS: PAA: CA system, more significant changes were observed, with a ratio of 85:13:2, the film elongation reached 20±1%, while at 75:22:3 it reached 26±1%, and at 70:25:5 it reached 29±1%. The most optimal result was determined at a ratio of 60:35:5, with a moisture content of 8.4±0.2%, and a film thickness of 120±5 μm. The relative elongation of the film was observed to reach 33±1%. Thus, it can be concluded that the composition with this composition has a dense and stable structure.

In samples of the composition with the composition OK: PAA: PVA: U, the plasticizing effect of U was observed. In the ratio of 80:8:8:4, the relative elongation of the film was 20±1%, in the ratio of 70:12:12:6– –23±1%. In the composition with the composition OS: PAA: PVA: U, the optimal result was observed in the ratio 60:20:15:5, the film moisture content was 9.2±0.2%, the thickness was 120±5 μm, and the relative elongation was 27±1%. An adverse effect on the properties of the foam was observed when the amount of U was increased (in the mass ratio of 60:15:15:10).

The functional groups and their interactions in the obtained compositions with the optimal composition were studied using the IR-spectral method. The analysis results made it possible to determine the structural changes that occur during the modification process. The IR spectra presented in Figure-1 below clearly show how the molecular interactions between components change in composite systems based on OS.

Figure 1. *IR spectra of the compositions: 1-OS, 2-OS: PAA: PVA, 3-OS: PAA: CA, 4-OS: PAA: PVA: U*

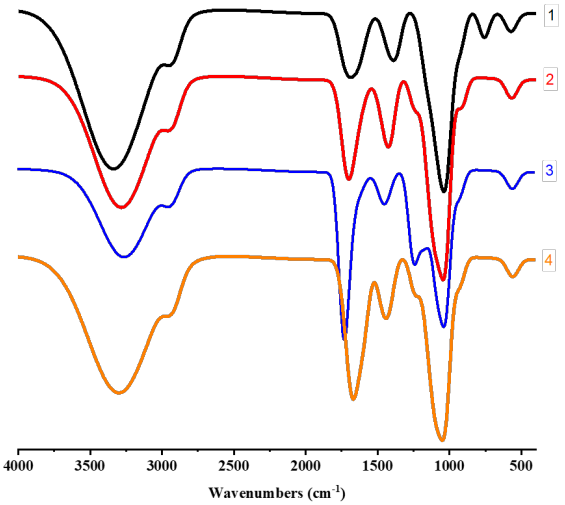

As can be seen from Figure 1, the broad absorption line observed in the 3200– –3500 cm^{-1} region for all samples belongs to the –OH groups, indicating the presence of hydrogen bonds in the samples. In the OS sample (spectrum 1 in Figure 1), this absorption is relatively broad and intense, indicating the presence of a large number of free hydroxyl groups in the molecular chains and confirming its high hydrophilicity and relatively loose structure.

In the OK: PAA: PVA sample (spectrum 2) in Figure-1, a slight decrease and a shift to a lower frequency of the absorption in this region were observed. This result indicates the formation of strong hydrogen bonds between the components. The functional groups in the PVA and PAA components interact with OS, reducing the interchain distance and leading to a denser structure. The C–H stretching vibrations in the 2800–3000 cm^{-1} region are almost unchanged in all spectra, indicating that the main hydrocarbon skeleton is preserved. However, significant changes were observed in the 1700–1750 cm^{-1} region. In the OS: PAA: PVA system, there are absorptions in this region related to the carboxyl (C=O) groups of PAA. In the OS: PAA: CA (spectrum 3) composition sample, a clear and strong absorption appeared in the region of 1725–1740 cm^{-1}, which is characteristic of ester groups (formed as a result of etherification), confirming that an etherification reaction occurred in the presence of CA, that is, a chemical crosslinking (covalent bonding).

As a result, this composition formed a more dense structure and improved mechanical properties. Intense absorptions in the regions of 1000–1200 cm^{-1} belong to C–O–C and C–O bonds, and these absorptions were observed in all examined samples. However, unlike the OS sample, a partial increase in the absorption intensity was observed in its modified compositions. This result can be explained by the increased interaction between polymer chains. In the OS: PAA: PVA: U sample in spectrum 4, the absorptions in the 1650–1680 cm^{-1} and 1550 cm^{-1} regions are vibrations characteristic of the carbonyl (C=O) and N–H groups of urea, indicating that U forms hydrogen bonds with other components in all the composition and acts as a plasticizer of the system. The results of the IR spectra analysis confirm that the structural changes in OS-based compositions have formed a stable structure.

Figure 2. *Molecular interactions and structural formation mechanisms of OS-based composites*

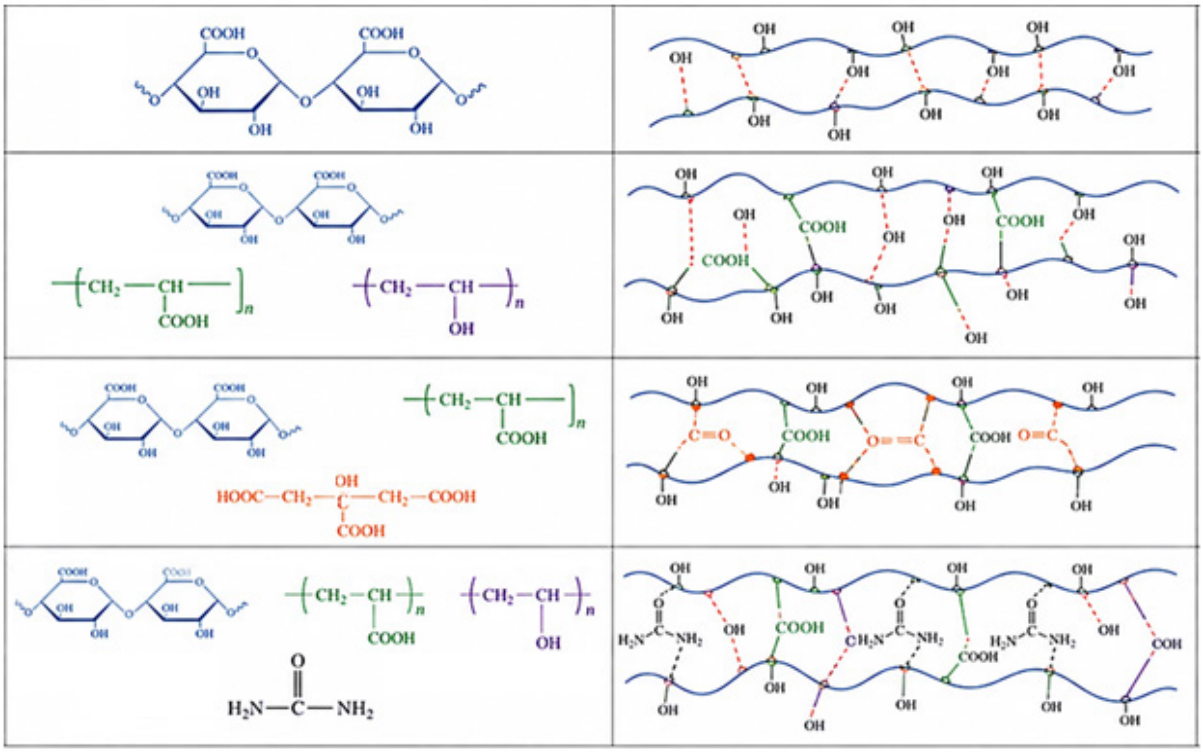

Based on the results of the initial study, an optimal composition of the OS-based composite was selected and structural schemes of molecular interactions between the components were proposed (Figure 2).

Conclusion

The results of the study showed that the physical, mechanical and structural properties of composite adhesives based on oxidized starch depend on the composition and mass ratio of the components. The addition of

PAA, PVA and citric acid increased the elasticity and density of the films and reduced their moisture content. The best result was observed in the ratio of the OS: PAA: CA system 60:35:5. IR-spectral analysis confirmed the formation of hydrogen and ether bonds. The results obtained showed that these compositions are promising for creating environmentally friendly, biodegradable and highly effective wood adhesives.

References

Cui Z., Beach E. S., Anastas P. T. (2011). Modification of Chitosan Films with Environmentally Benign Reagents for Increased Water Resistance. *Green Chem. Lett. Rev*, – 4(1). – P. 35–40.

Zdanowicz M., Johansson C. (2016). Mechanical and barrier properties of starch-based films plasticized with two- or three component deep eutectic solvents. *Carbohydrate Polymers*, – 151. – P. 103–112.

Sanyang M. L., Sapuan S. M., Jawaid M. (2015). Effect of plasticizer type and concentration on physical properties of biodegradable films based on sugar palm starch. *Carbohydrate Polymers*, – 118. – P. 171–179.

Rhim J. W., Wang L. F. (2013). Preparation and characterization of carrageenan-based nanocomposite films reinforced with clay mineral and silver nanoparticles. *International Journal of Biological Macromolecules*, – 54. – P. 148–155.

Ma X., Chang P. R., Yu J. (2008). Properties of biodegradable thermoplastic pea starch/carboxymethyl cellulose and pea starch/microcrystalline cellulose composites. *Food Hydrocolloids*, – 22. – P. 69–75.

Radjabov O. I., Yariev O. O., Azimova L. B., Filatova A. V. (2025). Study of collagen structure and tissue reaction during implantation. *Austrian Journal of Technical and Natural Sciences*, – 3–4. – P. 64–68.

submitted 26.03.2026;
accepted for publication 10.04.2026;
published 30.04.2026

Contact: m.s.sharipov@buxdu.uz

The Austrian Journal of Technical and Natural Sciences, 2026 No 3–4
ISSN 2310-5607

PREMIER Publishing
ppublishing.org

DOI:10.29013/AJT-26-3.4-79-82

STRUCTURE AND PROPERTY RELATIONSHIPS IN OXIDIZED STARCH BASED COMPOSITE WOOD ADHESIVES

Ortiqov Sherzod Sharof og'li [1], ***Radjabov Otabek Iskandarovich*** [2], ***Sharipov Muzafar Samandarovich*** [1], ***Khafizov Alisher Rakhimovich*** [2]

[1] Department of chemistry and oil-gas technologies, Bukhara State University Republic of Uzbekistan

[2] Academy of Sciences of the Republic of Uzbekistan, Institute of Bioorganic Chemistry

Cite: *Ortiqov Sh.Sh., Radjabov O.I., Sharipov M.S., Khafizov A.R. (2026). Structure and Property Relationships in Oxidized Starch Based Composite Wood Adhesives. Austrian Journal of Technical and Natural Sciences 2026, No 3–4.* https://doi.org/10.29013/AJT-26-3.4-79-82

Abstract

Composite wood adhesives based on oxidized starch were prepared using different formulations, including OS: PAA: PVA, OS: PAA: CA, and OS: PAA: PVA: U systems. The relationship between structure and properties was investigated using scanning electron microscopy (SEM) and thermogravimetric analysis (TG). SEM analysis revealed that the OS: PAA: CA system forms a dense, homogeneous, and compact structure, while the OS: PAA: PVA and OS: PAA: PVA: U systems exhibit more heterogeneous and porous morphologies. Thermogravimetric results showed that all samples undergo three main stages of thermal degradation, with the OS: PAA: CA composition demonstrating the highest thermal stability due to the formation of a well-developed three-dimensional network. The results indicate that the performance of oxidized starch-based adhesives strongly depends on the composition and intermolecular interactions between components. Among the studied systems, the OS: PAA: CA composition exhibited the most favorable structural and thermal properties, making it a promising candidate for wood adhesive applications.

Keywords: *oxidized starch; composite adhesives; wood adhesive; SEM analysis; thermal stability; structure–property relationship*

Indroduction

The development of functional materials based on natural polymers has gained significant attention due to environmental concerns and the demand for renewable resources. Natural macromolecules offer versatile chemical modification and tunable physicochemical properties, making them attractive for advanced applications. Starch, one of the most abundant and cost-effective polysaccharides, exhibits biodegradability and film-forming ability. However, its practical use is limited by low mechanical strength, high moisture sensitivity, and poor thermal

and adhesive properties (Liang, J., Li, D., Luo, Z., Yang, Y., Meng, T., Chen, C., Li, H., Zuo, N., Li, Q., Yang, H., & Wu, Z., 2025).

Oxidation is an effective strategy to overcome these limitations, introducing reactive aldehyde and carboxyl groups into the starch structure. This enhances its reactivity and enables stronger intermolecular interactions, allowing its use in composite systems. Incorporation of additional polymers further improves material performance through hydrogen bonding and possible chemical crosslinking, which govern morphology, viscosity, thermal stability, and adhesion. This study aims to synthesize oxidized starch-based composite wood adhesives and to investigate the relationship between their structure and physicochemical properties (Shen, D., Li, X., Liu, Y., Liu, C., Zheng, A., Wang, X., Liu, Y., & Liu, G., 2023).

Materials and Methods

Starch, sodium periodate ($NaIO_4$), poly(acrylic acid), poly(vinyl alcohol), citric acid ($C_6H_8O_7$), and carbamide ($CO(NH_2)_2$) were obtained from Sigma-Aldrich and used as received.

Preparation of oxidized starch. Oxidized starch was prepared using sodium hypochlorite (NaClO). A 5 wt% starch suspension (50 g starch in 450 g water) was ultrasonically treated (20 kHz, 400 W, 25 °C, 10 min), followed by pH adjustment to 9.5 using 1 M NaO H. The reaction was carried out at 35 °C with dropwise addition of 18% NaClO (starch: active chlorine ratio = 100:1––100: 3), while maintaining pH at 9.5 using 1 M H_2SO_4. After 30 min, the product was filtered, washed with distilled water, and dried at 50 °C for 12 h. The carboxyl group content was determined by the calcium acetate method. A 1 g dried sample was treated with 60 mL of 0.25 M $Ca(CH_3COO)_2$ and 100 mL of water and stirred for 6 h. A 25 mL aliquot was titrated with 0.01 M NaOH using bromothymol blue as an indicator. All measurements were performed in triplicate (Palić, N., Gržetić, J., Đolić, M., Kovačević, T., Pecić, Lj., Radovanović, Ž., & Marinković, A., 2020).

Preparation of composite adhesives. Composite adhesives were prepared using OS: PAA: PVA, OS: PAA: CA, and OS: PAA: PVA: U formulations. The components were dissolved or dispersed in distilled water and mixed under continuous stirring until homogeneous systems were obtained. The mixtures were further stirred to ensure uniform distribution and promote intermolecular interactions (Wang, P., He, H., Cai, R., Zhang, X., Chen, J., Tao, G., & Xiang, H., 2019).

Scanning electron microscopy (SEM). The surface morphology of the samples was examined using a scanning electron microscope (EVO MA10). Prior to analysis, the samples were coated with a thin conductive layer (~10 nm) using a Quorum Q150R ES sputter coater. The images were obtained at an accelerating voltage of 15 kV using SmartSEM software.

Thermogravimetric analysis (TG). Thermal stability of the samples was evaluated using thermogravimetric analysis. The measurements were carried out in the temperature range of 30–600 °C at a heating rate of 10 °C/min under an air atmosphere (McHugh, T. H., Avena-Bustillos, R., & Krochta, J. M., 1993).

Results and Discussion

Composite adhesives with different compositions were synthesized based on oxidized starch. During the preparation process, physicochemical interactions occurred between the components, leading to the formation of three-dimensional networks with varying degrees of crosslinking.

In the OS: PAA: PVA system, the network structure was mainly formed through hydrogen bonding between hydroxyl and carboxyl groups, resulting in a physically crosslinked network. Due to the absence of strong chemical crosslinking, the resulting structure was relatively loose and less dense. In the OS: PAA: CA composition, citric acid acted as a crosslinking agent, promoting strong intermolecular interactions between polymer chains. As a result, a dense and stable three-dimensional network structure was formed. In the OS: PAA: PVA: U system, urea acted as a plasticizer, reducing intermolecular interactions and increasing chain mobility. Although this enhanced the flexibility of the system, it led to a decrease in structural compactness.

The structural characteristics of the composite adhesives were investigated by scanning electron microscopy (SEM) in order to

evaluate their surface morphology, phase compatibility, degree of component dispersion, porosity, and the presence of microstructural defects. These parameters are directly related to the practical performance of adhesives, particularly the integrity of the adhesive layer, cohesive strength, and operational stability.

Figure 1. *SEM micrographs of oxidized starch based composite adhesives: (a) OS: PAA: PVA, (b) OS: PAA: CA, and (c) OS: PAA: PVA: U*

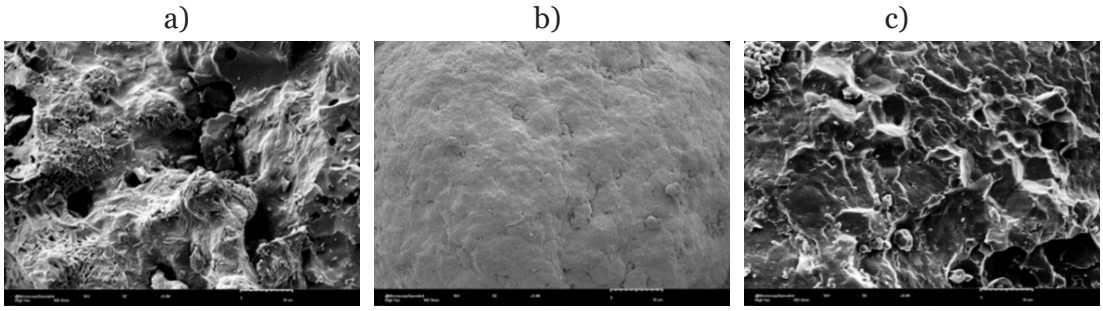

A comparative analysis revealed that the morphology of the oxidized starch-based composites strongly depends on their composition and the nature of intermolecular interactions. The OS: PAA: PVA system exhibited a heterogeneous and irregular surface with partially porous features. The presence of fibrillar elements, microvoids, and non-uniform regions indicates that a fully homogeneous phase was not formed. In this system, hydrogen bonding between hydroxyl groups of PVA and functional groups of oxidized starch and polyacrylic acid leads to the formation of a physically crosslinked network. However, due to the absence of strong chemical crosslinking, the resulting structure is relatively loose and less compact, which may reduce cohesive strength and water resistance.

In contrast, the OS: PAA: CA composition exhibited a smooth, homogeneous, and dense structure. This behavior can be attributed to the role of citric acid as a multifunctional crosslinking agent. Its carboxyl groups interact strongly with the functional groups of oxidized starch and polyacrylic acid, leading to the formation of a compact three-dimensional network. As a result, the structural integrity, mechanical strength, and resistance to environmental factors are significantly improved. The OS: PAA: PVA: U system displayed a rough, granular, and partially porous morphology. The surface contained irregular domains, protrusions, and microvoids, indicating incomplete structural compactness.

The presence of urea acts as a plasticizer, reducing intermolecular interactions and increasing chain mobility. Consequently, the structural density decreases, leading to partial heterogeneity and increased porosity, which may negatively affect the water resistance of the material. Overall, the SEM analysis confirms that the morphological structure of oxidized starch-based composite adhesives is closely related to their composition and the degree of intermolecular interactions.

Figure 2. *Thermogravimetric (TG) curves of oxidized starch based composite adhesives with different compositions (OS: PAA: CA, OS: PAA: PVA: U, and OS: PAA: PVA)*

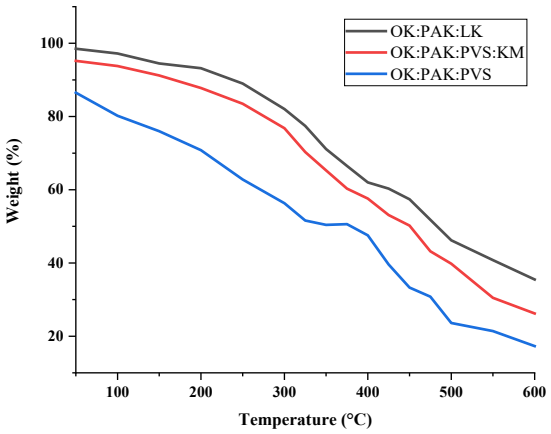

Systems with a dense and homogeneous structure exhibit improved mechanical and эксплуатацион (operational) properties, with the OS: PAA: CA composition showing the most optimal structural characteristics. In the next stage of this study, the thermal stability of the composite adhesives was evaluated by thermogravimetric analysis (TG).

The results showed that all samples exhibited three main stages of mass loss:

evaporation of moisture and volatile components at 30–150 °C, degradation of the main polymer chains at 180–350 °C, and carbonization processes at 350–600 °C. Significant differences were observed among the systems. The OS: PAA: PVA composition exhibited the lowest thermal stability due to the lack of strong chemical crosslinking. The OS: PAA: PVA: U system showed moderate stability as a result of the plasticizing effect. The highest thermal stability was observed for the OS: PAA: CA composition, which is attributed to the formation of a dense three-dimensional network.

Conclusion

Composite wood adhesives based on oxidized starch with different compositions were synthesized, and their structure–property relationships were investigated. The results showed that composition determines morphological structure and thermal stability, where denser and more homogeneous systems exhibit higher thermal resistance. The OS: PAA: CA system formed a compact structure and showed the highest thermal stability, while OS: PAA: PVA and OS: PAA: PVA: U systems exhibited more porous structures and lower stability. Overall, the performance of the adhesives is governed by intermolecular interactions, with OS: PAA: CA showing the most optimal properties.

References:

Liang, J., Li, D., Luo, Z., Yang, Y., Meng, T., Chen, C., Li, H., Zuo, N., Li, Q., Yang, H., & Wu, Z. (2025). Starch-citric acid adhesive: Preparation and performance study catalyzed by *p*-toluenesulfonic acid. *Polymers,* – 17(23), Article 3224. URL: https://doi.org/10.3390/polym17233224

Shen, D., Li, X., Liu, Y., Liu, C., Zheng, A., Wang, X., Liu, Y., & Liu, G. (2023). Effects of different molecular weight oxidized dextran as crosslinkers on the structure and properties of composite nanoparticles. *Journal of Biomaterials Science, Polymer Edition,* – 34(14). – P. 1706–1724. URL: https://doi.org/10.1080/09205063.2023.2225620

Palić, N., Gržetić, J., Đolić, M., Kovačević, T., Pecić, Lj., Radovanović, Ž., & Marinković, A. (2020). Preparation and properties of hydrogen peroxide oxidized starch for industrial use. Hemijska industrija, – 74(1). – P. 25–36. URL: https://doi.org/10.2298/HEMIND190722004k

Wang, P., He, H., Cai, R., Zhang, X., Chen, J., Tao, G., & Xiang, H. (2019). Cross-linking of dialdehyde carboxymethyl cellulose with silk sericin to reinforce sericin film for potential biomedical application. *Carbohydrate Polymers,* – 212. – P. 403–411. URL: https://doi.org/10.1016/j.carbpol.2019.02.069

McHugh, T. H., Avena-Bustillos, R., & Krochta, J. M. (1993). Hydrophilic edible films: Modified procedure for water vapor permeability and explanation of thickness effects. *Journal of Food Science,* – 58(4). – P. 899–903. URL: https://doi.org/10.1111/j.1365–2621.1993.tb09387.x

submitted 12.04.2026;
accepted for publication 27.04.2026;
published 30.04.2026

Contact: m.s.sharipov@buxdu.uz

The Austrian Journal of Technical and Natural Sciences, 2026 No 3–4
ISSN 2310-5607

PREMIER Publishing
ppublishing.org

DOI:10.29013/AJT-26-3.4-83-87

BIOLOGICAL ACTIVITIES OF THE PRODUCT OBTAINED FROM THE REACTION OF 2-CHLORO-N-(PYRIDIN-2-YL) ACETAMIDE WITH 5-FLUOROURACIL

Shirin Azimboyeva [1], ***Dilnoza Burieva*** [1], ***Mukhriddin Yusufov*** [1], ***Sarvinoz Bobonazarova*** [1], ***Anvar Abdushukurov*** [1]

[1] Faculty of Chemistry, National University of Uzbekistan, Tashkent, Uzbekistan

Cite: *Azimboyeva Sh., Burieva D., Yusufov M., Bobonazarova S., Abdushukurov A. (2026). Biological activities of the product obtained from the reaction of 2-chloro-N-(pyridin-2-yl) acetamide with 5-fluorouracil. Austrian Journal of Technical and Natural Sciences 2026, No 3–4.* https://doi.org/10.29013/AJT-26-3.4-83-87

Abstract

The chloroacetylation reaction of 2-aminopyridine derivatives was carried out, and the compound synthesized based on the reactions of the obtained chloroacetyl products with 5-fluorouracil was evaluated using the PASS Online program, which predicts the biological activity spectrum of substances based on their structure. When tested against various cancer and normal cell lines, the candidate compound demonstrated high efficacy against leukemia (Kasumi-1) and certain tumors of epithelial origin. At the same time, low activity observed in normal fibroblast cells indicates that the compound possesses selective activity and may potentially exhibit low toxicity. The antibacterial activity of the planned compound was also evaluated, showing the highest activity against Enterococcus faecalis ATCC 29212 and Mycobacterium tuberculosis H37Rv. The drug-like properties and possible adverse effects of the compound were further analyzed using the PASS program.

Keywords: *2-aminopyridine, 5-fluorouracil, PASS Online, cancer cells, tuberculosis bacteria*

Introduction:

Over the past years five- and six-member ring azaheterocyclic compounds have received considerable attention due to their important applications from pharmacological, industrial, and synthetic points of view (Pozharskii A. F., Soldatenkov A. T., Katritzky A. R., 2011). Pharmaceutical industry and modern medicinal science pay a lot of effort in their combat with two aggressive life-threatening diseases: cancer and tuberculosis (TB). Both diseases are leading cause of death worldwide, millions of people dying every year; the incidence of both are continually increasing and the treatment became more and more complicated and sophisticated (Grahman P. L., 2001; Silverman R. B., 1992; World Health Organization Tuberculosis Programme. Available from: Global tuberculosis report 2015/WHO/). The cancer chemotherapy is complex, expensive and often rather inefficient, because of the large variety of neoplasm types, high toxicity levels and non-specificity of drugs and the

emergence of drug resistance and multidrug-resistant (MDR) (Grahman P. L., 2011; Silverman R. B., 1992). On the other hand, because of the Mycobacterium tuberculosis (Mtb) versatility, the treatment against TB became a challenging and difficult task, and the situation begin to become even worse because of the phenomena of drug resistance, MDR, extensively-drug-resistant (XDR), association of TB with AIDS, etc. (Silverman R. B., 1992; World Health Organization Tuberculosis Programme. Available from: Global tuberculosis report 2015/WHO/).

It is well known from the literature (Pozharskii A. F., Soldatenkov A. T., Katritzky A. R., 2011; Grahman P. L., 2001; Silverman R. B., 1992; World Health Organization Tuberculosis Programme. Available from: Global tuberculosis report 2015/WHO/) that imidazole (and its benzo-derivative benzimidazole) and pyridine (and its benzoderivative quinoline) derivatives are core scaffolds widely present in many classes of drugs (of natural or synthetic origin), displaying a large variety of interesting biological activities (antimicrobials, antifungus, anti-inflammatory, antihypertensive, antineuropathic, antihistaminic, etc.; anticancer (Rescifina A., Zagni C., Varrica M. G., et al., 2014; Xiang P, Zhou T, Wang L, et al.,2012; Wissner A., Mansour T. S., 2008; Zbancioc A. M., Zbancioc G., Tanase C., et al. 2010; Luca M. C., Tura V., 2010) and anti-TB (Koseki Y., Kinjo T., Kobayashi M., Aoki S., 2013; Gising J., Nilsson M. T., Odell L. R., et al., 2012; Villemagne B., Crauste C., Flipo M., et al., 2012; Pandey J., Tiwari V. K., Verma S. S., et al., 2009; Danac R., 2014) also included)).

Results and discussion:

Based on the above considerations, and with the aim of developing new anticancer and anti-tuberculosis agents containing an azaheterocyclic scaffold, it is planned to carry out the chloroacetylation of 2-aminopyridine derivatives, to investigate the reactions of the obtained chloroacetyl products with 5-fluorouracil, and to study the structure of the synthesized compounds as well as their in vitro anticancer and antimycobacterial activity. The reaction is carried out in the following two steps (Bobonazarova S. et al., 2025; Habibullaevna B. S. et al., 2024; Ochilov S. H. et al.).

Figure 1.

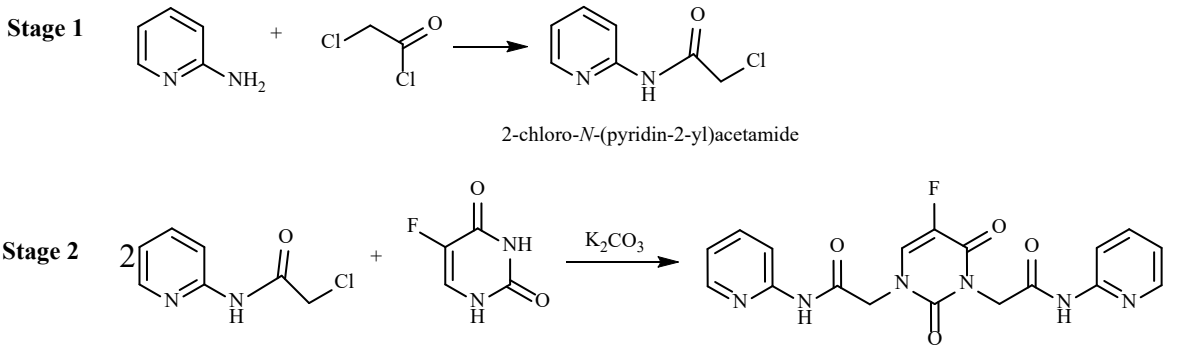

2,2'-(5-fluoro-2,4-dioxopyrimidine-1,3(2*H*,4*H*)-diyl)bis(*N*-(pyridin-2-yl)acetamide)

An important property of chemical compounds is their biological activity, as its presence may serve as a basis for using a substance for therapeutic purposes or, conversely, may limit its practical application due to the manifestation of side effects and toxic effects. The computational evaluation of biological activity spectra makes it possible to identify the most promising directions for studying the pharmacological effects of specific substances and to screen potentially hazardous molecules at the early stages of research.

PASS Online (Prediction of Activity Spectra for Substances) is an in silico program that predicts the biological activity spectrum of compounds based on their structure. The PASS software simultaneously forecasts more than 780 pharmacological effects and biochemical mechanisms using the 2D structural formula of a substance.

The synthesized compound was evaluated for its biological activity against various tumor and normal cell lines using the PASS (Prediction of Activity Spectra for Substanc-

es) online platform. The obtained results were analyzed based on probabilistic parameters, where Pa represents the probability of activity and Pi represents the probability of inactivity. Analysis of tumor cell lines revealed that the highest predicted activity was observed against the Kasumi-1 cell line (Pa = 0.525; Pi = 0.031). This cell line is associated with pediatric acute myeloid leukemia, indicating a pronounced potential effect of the compound, particularly against hematological malignancies. Notable levels of predicted activity were also observed for several other tumor cell lines, including SK-MES-1 (lung squamous cell carcinoma) with Pa = 0.425, SW-620 (colon adenocarcinoma) with Pa = 0.367, PA-1 (ovarian carcinoma) with Pa = 0.356, Hs 683 (brain tumor, oligodendroglioma) with Pa = 0.302, as well as YAPC and CFPAC-1 (pancreatic carcinoma) with Pa values in the range of approximately 0.31–0.30.

In contrast, analysis of normal cell lines demonstrated significantly lower predicted activity: NHDF (normal human dermal fibroblasts) showed Pa = 0.150, WI-38 (embryonic lung fibroblasts) Pa = 0.131, and AG1523 (fibroblasts) Pa = 0.044. These values are substantially lower compared to those observed for tumor cell lines, suggesting a reduced effect of the compound on normal cells.

Overall, the results indicate that the synthesized compound exhibits a broad spectrum of predicted activity against various tumor cell lines, with particularly high potential against leukemia cells (Kasumi-1) and several epithelial-derived cancers. Importantly, the relatively low predicted activity in normal fibroblasts suggests a degree of selectivity and potentially low toxicity. Therefore, the investigated compound can be considered a promising antitumor agent, warranting further comprehensive studies, including detailed in vitro and in vivo evaluations.

The increasing prevalence of antibiotic-resistant bacteria represents a major challenge for global healthcare systems. Therefore, the discovery of new effective antibacterial agents and the early-stage evaluation of their biological activity are of great importance. In this study, the antibacterial potential of a proposed compound was evaluated using the PASS (Prediction of Activity Spectra for Substances) software. The results indicated that the highest probabilities of activity were observed against Enterococcus faecalis ATCC 29212 (Pa = 0.1401) and Mycobacterium tuberculosis H37Rv (resistant strain) (Pa = 0.1176). These findings suggest that the investigated compound may exhibit potential activity against Gram-positive bacteria as well as drug-resistant mycobacteria. In particular, the predicted activity against resistant strains of Mycobacterium tuberculosis, the causative agent of tuberculosis, is of notable scientific interest. According to the obtained data, the probability of activity against the resistant strain Mycobacterium tuberculosis H37Rv (Pa = 0.1176) is relatively low. It is well established that, within the PASS framework, Pa values below 0.5 generally indicate a low probability of pronounced biological activity. However, low Pa values do not necessarily imply the absence of biological effect; rather, they may reflect that the compound belongs to a novel or insufficiently represented chemical class within the training dataset. Importantly, even a low predicted activity against drug-resistant Mycobacterium tuberculosis strains is scientifically significant, as these pathogens exhibit high resistance to existing therapeutics and require compounds with new mechanisms of action. From this perspective, the detected, albeit low, probability of activity may indicate that the studied compound operates via an unconventional or previously unexplored mechanism of action. Furthermore, it should be noted that the PASS algorithm is based on previously characterized compounds. Consequently, molecules with novel or less-studied structural features may receive underestimated activity predictions, which may not fully reflect their true biological potential. Taking these considerations into account, the investigated compound can be regarded as a promising lead structure. Further studies involving structural optimization, as well as comprehensive in vitro and in vivo evaluations, are warranted to enhance and validate its biological activity.

The drug-like properties and potential adverse effects of the investigated compound were analyzed using the PASS program. The highest predicted probability of activity was observed for antineoplastic action (Pa = 0.644; Pi = 0.036), indicating the compound's potential effectiveness against can-

cer cells. Additionally, predicted activities included antieczematic action (Pa = 0.576) and pseudouridylate synthase inhibition (Pa = =0.479), suggesting that the compound may influence multiple biological pathways. The predicted values for kidney function stimulation (Pa = 0.504) and electron-transferring flavoprotein dehydrogenase inhibition (Pa =0.465) indicate a potential impact of the compound on metabolic processes, including renal function and cellular energy metabolism.

The PASS algorithm also predicted possible adverse effects. The highest probabilities were observed for hematemesis (Pa = 0.787), nail discoloration (Pa = 0.691), and gastrointestinal hemorrhage (Pa = 0.682). Cardiovascular effects (Pa = 0.643 – atrial fibrillation) and metabolic effects (Pa = 0.605 – hyperglycemia) were also notable.

These results indicate that the compound possesses high biological activity; however, the presence of high-probability adverse effects necessitates caution in its potential clinical application. In particular, monitoring gastrointestinal and cardiovascular systems is essential, given the high predicted antineoplastic activity of the compound.

Conclusion:

When analyzing the biological activity spectra predicted by the PASS program, it is necessary to take into account the real possibilities of experimental testing. In this case, the general recommendation is to study the various predicted types of biological activity sequentially, from the most probable to the least probable. It should be emphasized that the PASS program cannot predict whether a particular compound will become a drug, as this depends on a number of factors. However, the predictions help determine which biological activities should be tested first and which compounds are most likely to exhibit the desired types of activity.

References

Pozharskii A. F., Soldatenkov A. T., Katritzky A. R. Heterocycles in life and society: an introduction to heterocyclic chemistry, biochemistry and applications. 2nd ed. Chichester: John Wiley & Sons; 2011.

Grahman P. L. An introduction to medicinal chemistry. 2nd ed. Oxford: Oxford University Press; 2001.

Silverman R. B. The organic chemistry of drug design and drug action. – London: Academic Press; 1992.

a. World Health Organization Tuberculosis Programme. Available from: Global tuberculosis report 2015/WHO/ http://www.who.int/tb/ publications/global_report/en/ [last accessed 19 Feb 2016]. b. http://www.who.int/mediacentre/factsheets/fs297/en/ [last accessed 19 Feb 2016].

Rescifina A., Zagni C., Varrica M. G., et al. Recent advances in small organic molecules as DNA intercalating agents: synthesis, activity, and modeling. Eur J Med Chem 2014; 74: 95–115.

Xiang P, Zhou T, Wang L, et al. Novel benzothiazole, benzimidazolee and benzoxazole derivatives as potential antitumor agents: synthesis and preliminary in vitro biological evaluation. Molecules 2012; 17: 873–83.

Wissner A., Mansour T. S. The development of HKI-272 and related compounds for the treatment of cancer. Arch Pharm 2008; 341: 465–77.

Zbancioc A. M., Zbancioc G., Tanase C., et al. Design, synthesis and in vitro anticancer activity of a new class of bifunctional DNA intercalators. Lett Drug Des Discov 2010; 7: 644–9.

Luca M. C., Tura V. Mangalagiu II. Considerations concerning design and mechanism of action of a new class of anticancer dual DNA intercalators. Med Hypotheses 2010; 75: 627–9.

Koseki Y., Kinjo T., Kobayashi M., Aoki S. Identification of novel antimycobacterial chemical agents through the in silico multi-conformational structure-based drug screening of a largescale chemical library. Eur J Med Chem 2013; 60: 333–9.

Gising J., Nilsson M. T., Odell L. R., et al. Trisubstituted imidazoles as Mycobacterium tuberculosis glutamine synthetase inhibitors. J Med Chem 2012; 55: 2894–8.

Villemagne B., Crauste C., Flipo M., et al. Tuberculosis: the drug development pipeline at a glance. Eur J Med Chem 2012; 51: 1–16.
Pandey J., Tiwari V. K., Verma S. S., et al. Synthesis and antitubercular screening of imidazole derivatives. Eur J Med Chem 2009; 44: 3350–5.
Danac R. Managalagiu II. Antimycobacterial activity of nitrogen heterocycles derivatives: bipyridine derivatives. Part III. Eur J Med Chem 2014; 74: 664–70.
Bobonazarova S. et al. 2-{[(1S, 2S)-1-Hydroxy-1-phenylpropan-2-yl](methyl) amino}-N-(3-methylphenyl) acetamide // IUCrData. 2025. – Vol. 10. – No. 7. – P. x250578.
Habibullaevna B. S. et al. Reactions of n-chloracetylation of toluidine isomers //Austrian Journal of Technical and Natural Sciences. 2024. – No. 3–4. – P. 12–16.
Ochilov S. H. et al. Synthesis of a new derivative of 5-fluorouracil based on 2-chloro-N-(4-iodophenyl) acetamide and study of its biological activity against cancer cells // Austrian journal of technical and natural sciences. – P. 14–18.

submitted 03.04.2026;
accepted for publication 17.04.2026;
published 30.04.2026

Contact: dilnozaboriyeva133@gmail.com

The Austrian Journal of Technical and Natural Sciences, 2026 No 3–4
ISSN 2310-5607

PREMIER Publishing
ppublishing.org

DOI:10.29013/AJT-26-3.4-88-91

STRUCTURE AND PROPERTIES OF DIALDEHYDE DEXTRAN-SILK FIBROIN COMPOSITE FILMS

Sodikova Mokhinur Abdujalilovna [1], ***Shomurotov Shavkat Abduganiyevich*** [1], ***Abdurakhmanov Jamoliddin Abdugulomovich*** [1], ***Karimov Aminjon*** [2], ***Radjabov Otabek Iskandarovich*** [1]

[1] Academy of Sciences of the Republic of Uzbekistan, Institute of Bioorganic Chemistry

[2] Department of Organic Synthesis, Tashkent Pharmaceutical Institute, Uzbekistan

Cite: *Sodikova M.A., Shomurotov Sh.A., Abdurakhmanov J.A., Karimov A., Radjabov O.I. (2026). Structure and Properties of Dialdehyde Dextran-Silk Fibroin Composite Films. Austrian Journal of Technical and Natural Sciences 2026, No 3–4.* https://doi.org/10.29013/AJT-26-3.4-88-91

Abstract

In this study, composite films based on dialdehyde dextran (DAD) and silk fibroin (SF) were synthesized. DAD was obtained via periodate oxidation, introducing reactive aldehyde groups into the polysaccharide structure. SF extracted from Bombyx mori cocoons was used as the protein component. The interaction between DAD and SF occurs through the formation of Schiff base (C=N) linkages between aldehyde and amino groups, resulting in covalent crosslinking. FTIR analysis confirmed these interactions by the decrease of aldehyde bands, shifts in amide regions, and the appearance of a new band at 1620–1640 cm^{-1}. Water vapor permeability studies showed that the film properties depend on the SF: Dex ratio, with reduced permeability observed at higher crosslinking densities. The results demonstrate that chemical crosslinking significantly influences the structure and functional properties of the composite films.

Keywords: *dialdehyde dextran; silk fibroin; composite films; schiff base; ftir spectroscopy; water vapor permeability*

Introduction

In recent years, the development of functional materials based on natural polymers has gained significant attention due to their low toxicity, biocompatibility, biodegradability, and wide application potential in fields such as medicine, biotechnology, and materials science (Mazurek, Ł., Szudzik-Kopeć, M., & Czaja, K., 2022). In particular, composites derived from polysaccharides and protein-based biopolymers offer advantages over synthetic materials, including environmental safety and tunable functional properties.

Polysaccharides are especially attractive due to the presence of reactive functional groups that enable chemical modification and control over physicochemical properties (Muhammad, M., Willems, C., Rodríguez-Fernández, J., Gallego-Ferrer, G., & Groth, T., 2020). Among them, dextran

stands out because of its high water solubility, biocompatibility, and ease of modification. Periodate oxidation of dextran introduces reactive aldehyde groups, forming dialdehyde dextran (DAD), which can interact with other biopolymers to form chemically crosslinked systems (Akhmedov, O., Khabibullaev, J., Abdurakhmanov, J., & Shomurotov, S., 2023; Loyeau, P. A., Spotti, M. L., Castel, V., Acosta-Müller, C., Acosta, C. A., Fioramonti, S., Vinderola, G., & Spotti, M. J., 2026).

Silk fibroin (SF), a protein-based biopolymer, is widely recognized for its fibrous structure, mechanical strength, and versatility in forming films, fibers, and hydrogels (Wang, P., He, H., Cai, R., Zhang, X., & Chen, J., 2019). The presence of amino groups in SF enables its interaction with aldehyde-containing polymers, leading to the formation of stable composite structures.

In this context, the aim of this study is to synthesize composite films based on DAD and SF and to investigate their physicochemical properties.

Materials and Methods

Silk fibroin (CAS 92580–42–0), sodium periodate (TU 6–09–02–54–74), and dextran 40 (CAS 9004–54–0) were used as starting materials.

Preparation of dialdehyde dextran. Dextran was oxidized with sodium periodate to obtain DAD. Briefly, dextran (5 g) was dissolved in sodium acetate buffer (pH 4.25) and reacted with $NaIO_4$ at a molar ratio of 1:1.5 in the dark at room temperature for 3–7 h. The reaction was quenched with ethylene glycol, followed by dialysis for 24 h and freeze-drying to obtain DAD. The aldehyde group content was determined by alkaline titration, where a 0.1 g sample was treated with 0.2 N NaOH, heated at 70 °C, cooled, neutralized with 0.2 N H_2SO_4, and titrated with 0.2 N NaOH using phenolphthalein as an indicator until a stable pale pink endpoint was reached (Yan, X., Zheng, W., Yu, Y., Liu, R., Gong, Y., Huang, M., Fan, M., & Wang, L., 2025).

Preparation of silk fibroin. Silk fibroin (SF) was extracted from *Bombyx mori* cocoons by degumming in 0.02 M Na_2CO_3 solution, followed by thorough washing to neutral pH. The purified fibroin was dissolved in Ajisawa's reagent ($CaCl_2$: C_2H_5OH: H_2O, molar ratio 1:2:8) at 60 °C, filtered, and dialyzed (MWCO 3 kDa) to obtain a homogeneous SF solution. For composite formation, SF solution was reacted with dialdehyde dextran (DAD) at aldehyde-to-amino molar ratios of 1:1–1:2 under stirring at room temperature. The resulting mixture was dialyzed and subsequently freeze-dried to obtain the final product (Riaz, S., Waheed, H., Ahmad, F., Khan, M. I., & Shanableh, A., 2025).

FTIR Spectroscopy. The FTIR spectra of the obtained samples were recorded using an IRSpirit-X FTIR spectrometer (Shimadzu, Japan). The samples were prepared as KBr pellets (3 mg sample mixed with 300 mg KBr), and spectra were collected in the wavenumber range of 400–4000 cm^{-1}.

Water Vapor Permeability Measurement. The water vapor permeability (WVP) of the composite films was determined by a gravimetric method, where films sealed over water-containing vessels were monitored for mass loss over time (12–72 h), and WVP was calculated from the weight loss rate normalized to film area and thickness; all measurements were performed in triplicate (McHugh, T. H., Avena-Bustillos, R., & Krochta, J. M., 1993).

Results and Discussion

Dextran was oxidized with sodium periodate to obtain dialdehyde dextran (DAD), where cleavage of vicinal diol groups in the polysaccharide backbone generated reactive aldehyde functionalities, enhancing its chemical reactivity and enabling subsequent interactions with biopolymers. As shown in Scheme 1, periodate oxidation of dextran cleaves C–C bonds at C(2)-C(3) or C(3)-C(4), generating reactive aldehyde groups; under excess oxidant, further oxidation may produce formic acid and additional aldehydes.

In this study, DAD with an oxidation degree of ~30 mol% was obtained, which provides an optimal balance between chain integrity and reactivity. Silk fibroin (SF) was extracted from *Bombyx mori* cocoons by alkaline degumming in Na_2CO_3 solution, followed by thorough washing and drying to obtain pure fibroin fibers suitable for further processing. Subsequently, SF was reacted with DAD via aldehyde amino interactions, where ε-amino groups of SF form

azomethine (C=N) bonds with DAD through a Schiff base reaction. This process involves nucleophilic addition followed by dehydration, resulting in covalent crosslinking that enhances the structural stability of the composite system.

Scheme 1. *Periodate oxidation of dextran*

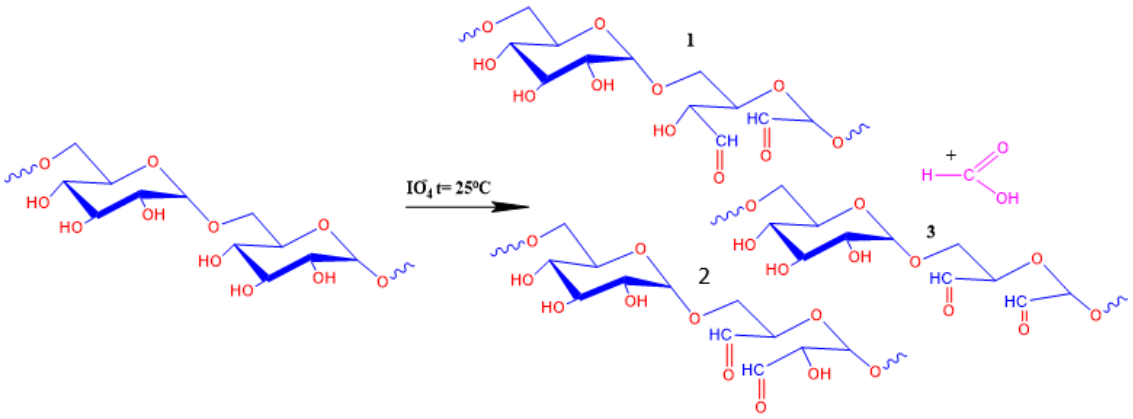

The structure of the obtained compounds was characterized by various physicochemical methods. The FTIR spectra of SF, DAD, and their composite are presented in Figure 1 and reveal the characteristic structural changes occurring during composite formation.

Figure 1. *FTIR spectra of DAD (1), silk fibroin–dextran composite (2) and SF (3)*

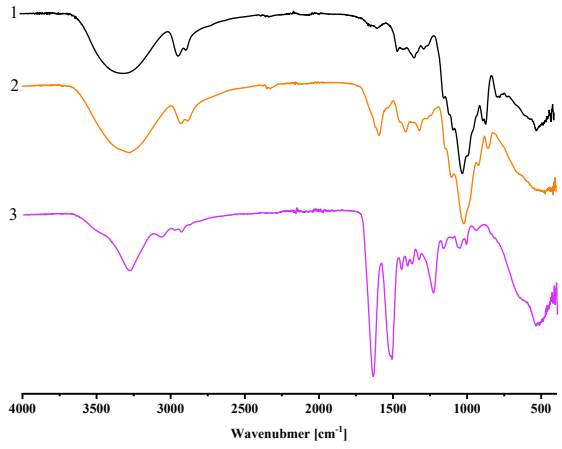

As shown in Figure 1, the FTIR spectrum of SF exhibits a broad absorption band around 3300 cm^{-1}, corresponding to -NH and -OH groups, as well as characteristic bands at 1650 cm^{-1} (amide I), 1530 cm^{-1} (amide II), and 1230 cm^{-1} (amide III), confirming the protein structure of fibroin. The FTIR spectrum of DAD shows a broad band near 3400 cm^{-1} assigned to hydroxyl groups and intense absorption bands in the 1000–1100 cm^{-1} region, which are characteristic of C-O-C stretching vibrations in the polysaccharide backbone. In addition, a weak band around 1700 cm^{-1} attributable to aldehyde groups confirms the successful oxidation of dextran. In the spectrum of the composite material, noticeable changes were observed compared to the spectra of the initial components. In particular, the intensity of the aldehyde-related band decreased, while the amide bands of fibroin showed shifts and changes in intensity. Moreover, the appearance of a new absorption band in the 1620–1640 cm^{-1} region can be attributed to the formation of azomethine (C=N) bonds. These FTIR results confirm the chemical interaction between fibroin and DAD and indicate the formation of covalent crosslinks within the composite system.

In subsequent studies, the water vapor permeability of SF/Dex composite films was investigated as a function of time (Figure 2). The results showed that water vapor permeability (WVP) of all samples increased with time due to progressive diffusion of water vapor through the films. The SF: Dex ratio significantly affected the film structure, leading to noticeable differences in WVP values. In particular, increasing DAD content resulted in reduced WVP, indicating the formation of a denser and more ordered composite structure.

This behavior is consistent with FTIR results, where the formation of azomethine (C=N) bonds between SF and DAD suggests chemical crosslinking, enhancing structural compactness and influencing vapor permeability.

Figure 2. *Water vapor permeability of SF/Dex composite films prepared at different ratios (SF: Dex = 1:1, 1:2 and 2:1) as a function of time (12–72 h)*

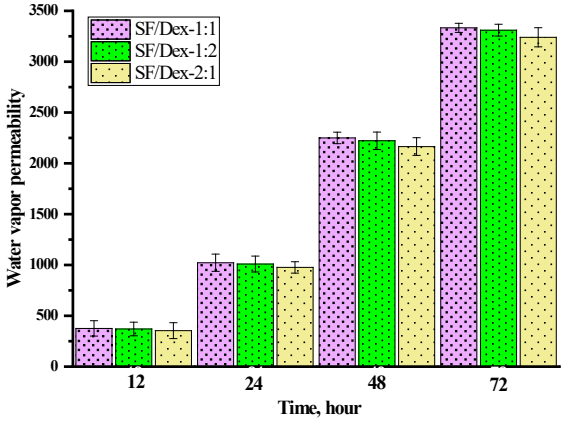

Conclusion

Composite films based on silk fibroin (SF) and dialdehyde dextran (DAD) were successfully synthesized, exhibiting homogeneous structure, smooth morphology, and good transparency. FTIR analysis confirmed the formation of Schiff base (C=N) linkages between SF and DAD, indicating covalent crosslinking. Water vapor permeability results showed that the SF: DAD ratio significantly affects the internal structure, with higher DAD content leading to reduced permeability due to a denser network. Overall, covalent crosslinking plays a key role in determining the structural and functional properties of the composite films.

References:

Mazurek, Ł., Szudzik-Kopeć, M., & Czaja, K. (2022). Silk fibroin biomaterials and their beneficial role in skin wound healing. Biomolecules, – 12(12). – 1852 p. URL: https://doi.org/10.3390/biom12121852

Muhammad, M., Willems, C., Rodríguez-Fernández, J., Gallego-Ferrer, G., & Groth, T. (2020). Synthesis and characterization of oxidized polysaccharides for in situ forming hydrogels. Biomolecules, – 10(8). – 1185 p. URL: https://doi.org/10.3390/biom10081185

Akhmedov, O., Khabibullaev, J., Abdurakhmanov, J., & Shomurotov, S. (2023). Investigation of the structure of dialdehyde polysaccharides with various degrees of oxidation. Austrian Journal of Technical and Natural Sciences, (7–8).

Loyeau, P. A., Spotti, M. L., Castel, V., Acosta-Müller, C., Acosta, C. A., Fioramonti, S., Vinderola, G., & Spotti, M. J. (2026). Enhanced viability of encapsulated probiotics using whey protein isolate–dextran conjugates: Effect of dextran molar mass. *International Journal of Biological Macromolecules*, – 343. – 150357 p.

Wang, P., He, H., Cai, R., Zhang, X., & Chen, J. (2019). Cross-linking of dialdehyde carboxymethyl cellulose with silk sericin to reinforce sericin film for biomedical application. Carbohydrate Polymers, – 212. – P. 403–411.

Yan, X., Zheng, W., Yu, Y., Liu, R., Gong, Y., Huang, M., Fan, M., & Wang, L. (2025). Dextran-functionalized cerium oxide nanoparticles for treating diabetic wound infections by synergy between antibacterial activity and immune modulation. *Materials Today Bio,* – 33. – 101977 p.

Riaz, S., Waheed, H., Ahmad, F., Khan, M. I., & Shanableh, A. (2025). Natural and synthetic biomaterials for wound dressings: Properties and applications. Regeneration, Repair and Rehabilitation, – 1(4). – P. 47–65.

McHugh, T. H., Avena-Bustillos, R., & Krochta, J. M. (1993). Hydrophilic edible films: Modified procedure for water vapor permeability and explanation of thickness effects. Journal of Food Science, – 58(4). – P. 899–903.

submitted 11.04.2026;
accepted for publication 25.04.2026;
published 30.04.2026

Contact: kimyogarjdi@gmail.com; shsha@mail.ru; Jamoliddinaa23@gmail.com;
aminjonkarimov124@gmail.com; ximik07@mail.ru

The Austrian Journal of Technical and Natural Sciences, 2026 No 3–4
ISSN 2310-5607

PREMIER Publishing
ppublishing.org

DOI:10.29013/AJT-26-3.4-92-97

SYNTHESIS AND ANALYSIS OF A COMPLEX COMPOUND BASED ON COBALT OXALATE AND SODIUM ACETATE

Zaripova Dinora Ibragimovna [1], Abdullayeva Zubayda Shavkatovna [2], Kadirova Shakhnoza Abdukhalilovna [3], Masharipov Azamat [4]

[1] Khorezm Ma'mun Academy

[2] Department of Technology, Urgench Ranch Technological University,

[3] National University of Uzbekistan

[4] Department of Chemistry and Biology of the Academic Lyceum of Urgench State University named after Abu Rayhan Beruni, Republic of Uzbekistan, Urgench

Cite: *Zaripova D.I., Abdullayeva Z.Sh., Kadirova Sh.A., Masharipov A. (2026). Synthesis and Analysis of A Complex Compound Based on Cobalt Oxalate and Sodium Acetate. Austrian Journal of Technical and Natural Sciences 2026, No 3–4.* https://doi.org/10.29013/AJT-26-3.4-92-97

Abstract

In this scientific study, a new Co(II)-oxalate-acetate complex compound was synthesized, and its physicochemical properties and structure were investigated using experimental and practical methods, and its composition was determined by infrared Functional groups and coordination bonds were identified using infrared (IR) spectroscopy. In addition, the compound's thermal stability, decomposition stages, and thermal properties were analyzed by thermogravimetric methods. The structure and energetic parameters of the complex compound were analyzed by quantum chemistry methods within the framework of DFT theory using the Gaussian 09 software. The theoretical results were found to be in good agreement with the experimental data.

Keywords: *Co(II) complex compound, oxalate and acetate ligands, infrared spectroscopy, thermal analysis, coordination compounds, DFT calculations; HOMO–LUMO*

Introduction

Today, the rapid growth of the population increases the demand for food, making it necessary to implement the achievements of chemistry, chemical technology, biology, medicine, and agricultural sciences into practice. In particular, the complex compounds formed between metals and organic ligands can serve as an example. Cobalt(II) ions, when coordinated with oxalate and acetate anions, form compounds with complex structures. The oxalate and acetate anions have multiple binding modes as ligands, through which various coordination environments can be created around the metal center. To synthesize such com-

pounds, a mixed-ligand complex compound containing Co(II) salts and oxalate acetate was prepared. The coordination properties of the oxalate ligand and its ability to bind to metal centers in mono- and bidentate modes have been demonstrated (Santana, 2020; Christensen, 2014). In these studies, the crystal structures of the complex compounds were investigated, and it was determined that the role of the oxalate ligand in the stability of the complex is significant. The thermal decomposition processes, stages, and thermal stability of oxalate-based complexes have been analyzed in detail (Lamprecht, Watkins, Brown, 2006). These results serve as an important scientific basis for the thermal analysis of oxalate complexes. Additionally, the multifunctionality of bimetallic complexes based on oxalate ligands, particularly their magnetic and electronic properties, has been extensively discussed (Clemente-León, Coronado, Martí-Gastaldo, Romero, 2011). Complexes containing acetate ligands, their interactions with metal ions, and coordination possibilities have been investigated (Seguel, Rivas, Paredes, 2010). The synthesis and characterization of complexes containing oxalate and acetate ligands have also been studied, and it has been investigated that the interaction between the ligands in such systems significantly affects the complex structure (Mishra, 2021; Al-Shehri, 2020). In particular, it has been shown that infrared (IR) spectroscopy can be used to identify metal–ligand bonds through the vibrational frequencies of functional groups (Tarasenko, 2018). This method is widely used to confirm the structure of complex compounds. A number of scientific papers on the synthesis and analysis of coordination compounds have also been carried out by local scientists. The synthesis of coordination compounds and their analytical methods have been systematically described (Nazarov, 2016), the physicochemical properties of cobalt-based complexes were studied (G'afurov, 2020), and the general properties and practical significance of organic ligand complexes were highlighted (Sharipova, Ibragimova, Khudoyberganov, Khallokov, Bobakulov, Abdullaeva, 2024). In recent years, research has extensively studied the synthesis of complexes based on acetate and other ligands with various metal ions. Recent studies have investigated the synthesis, structure, and properties of complex compounds based on divalent metal ions, including Co, Ni, and Cu, in the presence of acetate and other ligands. These results provide an important scientific basis for a deeper study of cobalt-based complexes. The literature review above shows that, the synthesis, structure, and properties of complexes containing oxalate and acetate ligands are a current scientific focus, and their in-depth analysis, especially using methods such as thermal analysis and infrared spectroscopy, is of great importance.

Research method

The following substances were used for the synthesis of the complex compound: cobalt chloride, oxalic acid, sodium hydroxide, and sodium acetate. The synthesis of the starting materials was carried out using the following method: a concentrated solution of the metal salt and an alkaline solution of the same concentration were combined to precipitate the metal hydroxide. The precipitate was washed five times by decantation, and an oxalic acid solution was poured over it. As a result, the metal's oxalate salt was formed.

$$CoCl_2 + 2NaOH = Co(OH)_2\downarrow + 2NaCl$$
$$Co(OH)_2 + (COOH)_2 = Co(COO)_2 + 2H_2O$$

The synthesis of the Co(II) oxalate–sodium acetate complex was carried out by the following method: 0.01 mol of Co(II) oxalate was dissolved in 10 ml of water. In another beaker, 0.02 mol of sodium acetate was dissolved in 15 ml of water by heating in a hot water bath (45–50 °C). Then, the sodium acetate solution was added dropwise to the Co(II) oxalate solution, and the mixture was stirred in a magnetic stirrer at 55–60 °C at 800 rpm for 1.5 hours. The resulting solution was left at room temperature for 72 hours to crystallize. As a result, colored complex compound crystals formed.

As a result of the solvent's slow evaporation, a dark-colored polycrystalline product was obtained. The product was filtered, washed with acetoneitrile, and dried at room temperature.

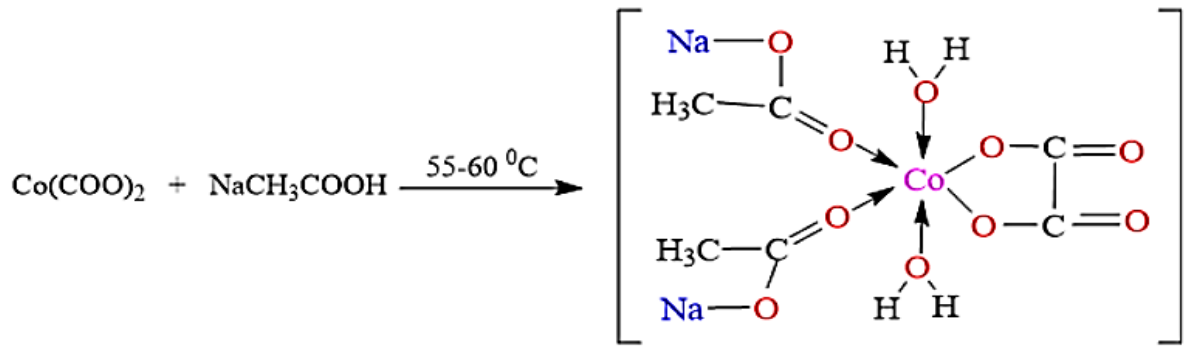

Results analysis

An elemental analysis was performed to determine the composition of the obtained compound (Table 1).

Table 1. *Results of the elemental analysis of the obtained complex compound*

Compounds		$[Co(CO_2)_2 \cdot 2CH_3COONa \cdot 2H_2O]$
Co	Calculated	17.10
	Determined	17.21
Na	Calculated	13.33
	Determined	13.21
C	Calculated	20.86
	Determined	20.88
O	Calculated	45.37
	Determined	45.42
Compound color		Dark pink
Reaction yield, %		89.15

Based on quantum chemical calculation results, the optimized geometric structure of the complex compound formed from Co(II) oxalate and sodium acetate is presented. The atoms in the molecule are represented by partial charges, and a redistribution of electron density around the central atom is observed. This is explained by the transfer of electron density to the metal center via the donor atoms of the ligands. As a result, donor–acceptor interactions arise in the complex, confirming the occurrence of electron flow (Figure 1).

The HOMO orbital is primarily localized around the oxygen atoms in the ligands, indicating their high electron density. The LUMO orbital is partially located on the central cobalt atom and its surrounding coordination environment. This distribution indicates that the electron transfer in the complex is primarily from the ligands to the metal center, favoring a ligand-to-metal charge transfer (LMCT) mechanism. The electrostatic potential distribution (ESP) of the molecule is shown in the figure. In it, the red color represents regions with high electron density (electron donor centers), while the blue color represents regions with low electron density (electron acceptor centers). According to the analysis results, the largest negative potential is mainly concentrated around the oxygen atoms, which manifest as active donor centers. The largest positive potential is observed around the central cobalt atom. In particular, the dense contours between the cobalt atom and the coordinated oxygen donor atoms confirm the strength of the coordination bonds. The experimental IR spectrum of the synthesized Co(II)–oxalate–acetate complex was compared with the theoretically calculated spectrum. During the comparison, the absorption frequencies, shifts, and intensities of the main functional groups were analyzed.

Figure 1. *Mulliken method – derived electron charge distribution of the complex compound formed from Co(II) oxalate and sodium acetate (a), View of molecular orbitals (HOMO and LUMO) (b), Distribution of the molecular electrostatic potential (MEP) and the complex's complete energy spectrum (distribution of orbital energies) (c), Theoretically calculated IR spectrum of the complex compound based on cobalt oxalate and sodium acetate by quantum chemical methods (d)*

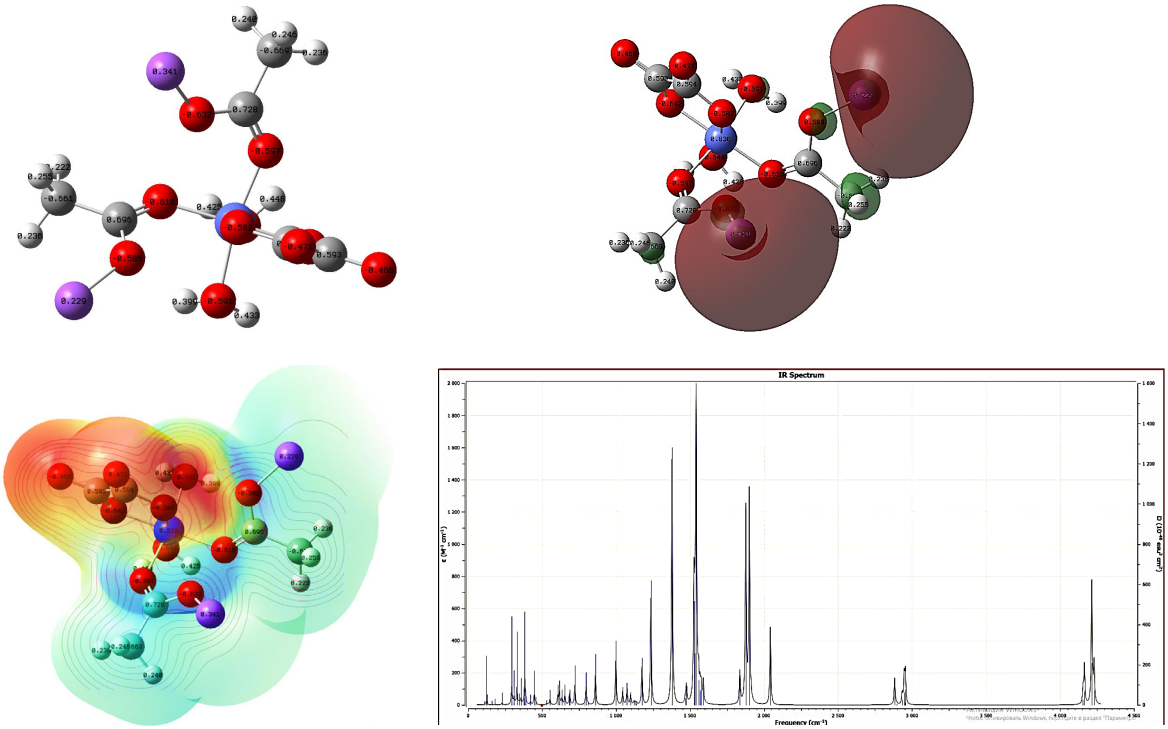

In the practical IR spectrum, the strong absorption peaks observed in the 1600–1650 cm^{-1} and 1350–1450 cm^{-1} ranges correspond to the asymmetric (vas) and symmetric (vs) vibrations of the $–COO^-$ group, respectively. These peaks appear in the theoretical spectrum in almost the same regions, confirming the presence of cobalt oxalate and sodium acetate ligands in the complex. In the experimental spectrum, the difference between the vas and vs vibrations (Δν) indicates the alignment of the carboxylate groups with the Co(II) center. This situation allows for the assumption that the oxalate ligand is bidentate, while the acetate ligand is monodentate or bridging. The small shifts (10–40 cm^{-1}) between the theoretical and experimental IR spectra are attributed to experimental conditions (solid phase, crystal lattice effect), hydrogens, the actual coordination environment of the ligands, and the assumption of ideal conditions in the computational method. Nevertheless, a high degree of agreement was observed in the positions and intensities of the main absorption peaks. The comparison of experimental and theoretical spectra demonstrated the successful synthesis of the Co(II)–oxalate–acetate complex.

Table 2.

ν_{exp} (cm^{-1})	ν_{calc} (cm^{-1})	Type of vibration	Analysis
3200–3500	3300–3450	ν(O–H)	Water or hydrogen bonding
1600–1650	1580–1620	$\nu_{as}(COO^-)$	Asymmetric vibration of the carboxylate group in oxalate and acetate

ν_{exp} (cm^{-1})	ν_{calc} (cm^{-1})	Type of vibration	Analysis
1350–1450	1360–1420	$\nu_s(COO^-)$	Symmetric vibration of the carboxylate group
1000–1300	1020–1280	ν(C–O), ν(C–C)	Ligand backbone vibrations
400–600	420–580	ν(Co–O)	Metal–oxygen coordination bonds

As can be seen from the table, the difference between the experimental and theoretical values is not large (±10–40 cm^{-1}), which confirms the successful synthesis of the Co(II)–oxalate–acetate complex compound by comparing the experimental and theoretically calculated IR spectra. In this work, the thermal properties of the synthesized Co(II) oxalatacetate complex compounds were investigated using TG, DTA, and DSC methods, which provided details on the compounds' thermal decomposition stages and energetic changes. The thermal analysis of the cobalt oxalate–sodium acetate complex compound was studied based on TGA and DTA curves. According to the analysis results, multiple decomposition stages were observed as the compound was heated. Initially, a weight loss of approximately 17.9% was recorded in the temperature range of 30–145 °C, which is associated with the desorption of adsorbed or crystallized water molecules within the complex. This process is confirmed by an endothermic peak observed on the DTA curve at approximately 112.95 °C, which indicates the presence of hydrogen bonds in the complex.

Conclusion

Based on the structures of the initial compounds, analyses were conducted to determine their molar ratios. These analyses assessed reactivity through the difference between the HOMO and LUMO (ΔE) and determined which compound is more reactive or more stable. IR spectroscopic analysis proved that the coordination compounds formed in the interaction of metal acetates with Co(II) oxalate are heterometallic complexes, and that the coordination bond is formed through the bidentate bridging coordination of the acetate groups. The results of the thermal analysis, namely the disappearance of the characteristic reflections of the starting materials and the appearance of new peaks, reliably confirm the formation of the complex compound and its existence in a separate crystalline phase. The results of this analysis confirm the presence of crystallization water molecules in the $[Co(CO_2)_2 \cdot 2CH_3COONa \cdot 2H_2O]$ complex compound and the stepwise decomposition of the ligands.

References

Abdullaeva, Z. Sh., Khasanov, Sh. B., Khudoyberganov, O. I., Kadirova, Sh. A., Jumaniyazova, M. E., Eshchanov, E. U. (2026). *Synthesis, structure, and properties of complex compounds of potassium acetate with formates of bivalent Co, Ni, Cu.* Azerbaijan Chemical Journal, – 1. – P. 35–46. URL: https://doi.org/10.32737/0005-2531-2026-1-35-46

Al-Shehri, A., et al. (2020). *Multidentate ligand coordination with transition metals.* Inorganic Chemistry Communications. URL: https://doi.org/10.1021/acs.inorgchem.0c03027

Christensen, A. N., et al. (2014). *The crystal structure of paramagnetic copper(II) oxalate.* Dalton Transactions, – 43. – P. 145–154. URL: https://doi.org/10.1039/C4DT01689K

Clemente-León, M., Coronado, E., Martí-Gastaldo, C., Romero, F. M. (2011). *Multifunctionality in hybrid magnetic materials based on bimetallic oxalate complexes.* Chemical Society Reviews, – 40. – P. 1990–2025. URL: https://doi.org/10.1039/C0CS00108K

G'afurov, S. R. (2020). *Organik ligandli komplekslarning xossalari.* Farg'ona davlat universiteti ilmiy to'plami. Retrieved from: https://journal.fdu.uz

Khasanov, Sh. B., Ibodullaeva, T. A., Abdullayeva, Z. Sh., Khudoyberganov, O. I. (2023). *Synthesis and properties of the coordination compounds calcium stearate with thiocarbamide.* Azerbaijan Chemical Journal, – 2. – P. 111–115. Retrieved from: http://www.chemjournal.az

Lamprecht, E., Watkins, G. M., Brown, M. E. (2006). *The thermal decomposition of copper(II) oxalate revisited*. Thermochimica Acta. URL: https://doi.org/10.1016/j.tca.2005.11.018
Mishra, A., et al. (2021). *Synthesis and characterization of Cu(II)-oxalate-acetate complexes*. Journal of Coordination Chemistry. URL: https://doi.org/10.1080/00958972.2021.1951234
Nazarov, B. K. (2016). *Koordinatsion birikmalar sintezi va tahlili*. O‘zbek kimyo jurnali. Retrieved from: http://uzchemjournal.uz
Santana, F. S., et al. (2020). *An oxalate-bridged copper(II) complex combining monodentate and bidentate ligands: synthesis, crystal structure and magnetic properties*. Molecules, – 25. – 1898 p. URL: https://doi.org/10.3390/molecules25081898
Seguel, G. V., Rivas, B. L., Paredes, C. E. (2010). *Study of the interactions between copper(II) acetate monohydrate and orotic acid and orotate ligands*. Journal of the Chilean Chemical Society, – 55(3). – P. 355–358. URL: https://doi.org/10.4067/S0717-97072010000300006
Sharipova, L., Ibragimova, M., Khudoyberganov, O., Khallokov, F., Bobakulov, K., Abdullaeva, Z. (2024). *Synthesis and study of the complex compound of isonicotinamide with zinc nitrate*. The Eurasia Proceedings of Science, Technology, Engineering & Mathematics (EPSTEM), – 30. – P. 47–55. URL: https://doi.org/10.55549/epstem.1456789
Tarasenko, Y., et al. (2018). *Spectroscopic analysis of bidentate ligand complexes*. Spectrochimica Acta Part A. URL: https://doi.org/10.1016/j.saa.2018.03.012

submitted 04.04.2026;
accepted for publication 18.04.2026;
published 30.04.2026

Contact: zubayda.abdullayeva.91@mail.rukadirova.shakhnoza@mail.ru; dinora.zaripova.98@mail.ru

The Austrian Journal of Technical and Natural Sciences, 2026 No 3–4
ISSN 2310-5607

PREMIER Publishing
ppublishing.org

Section 3. Computer sciences

DOI:10.29013/AJT-26-3.4-98-105

DECOMPOSITION OF MONOLITHIC SOLUTIONS IN CORPORATE PROCUREMENT PLATFORMS: ARCHITECTURAL MIGRATION STRATEGIES AND COMPLEXITY MANAGEMENT

Roilian Mykyta [1]

[1] Engineering Manager, Lean DNA

Cite: *Roilian Mykyta. (2026). Decomposition of Monolithic Solutions in Corporate Procurement Platforms: Architectural Migration Strategies and Complexity Management. Austrian Journal of Technical and Natural Sciences 2026, No 3–4.* https://doi.org/10.29013/AJT-26-3.4-98-105

Abstract

This article examines the process of decomposing monolithic information systems in corporate procurement platforms, with a focus on architectural migration strategies and the management of emerging complexity. The study analyzes principles for transitioning to modular architectures, including the use of facade layers, service isolation, and intermediary adapters that enable phased transformation without disruption of business processes. The importance of managing architectural and operational complexity in the adoption of distributed solutions is emphasized. Practical examples of applying architectural approaches under industrial operating conditions are presented. Typical risks associated with the transition are discussed, along with the potential long-term benefits of modular systems. Particular attention is given to resilience, scalability, and integration compatibility of the resulting architectures.

Keywords: *monolithic architecture, corporate platforms, microservices, modular systems, digital transformation, information systems architecture*

Introduction

In the context of rapid digitalization of corporate processes and increasing demands for the flexibility of information systems, an increasing number of industrial and logistics enterprises are facing the need to transform legacy monolithic solutions. This challenge is particularly acute in corporate procurement and warehouse management platforms, where a high degree of process formalization, strict requirements for fault tolerance, and the need for integration with both internal and external systems necessitate technological solutions capable of ensuring operational stability and adaptability. Under these conditions, the transition from monolithic architectures to modular and distributed systems becomes not merely a technical task, but a strategic decision that directly affects the sustainability of the enterprise's overall operating model.

The purpose of this article is to examine architectural migration strategies from monolithic information systems to modular solutions in the context of corporate procurement platforms. The analysis focuses on decomposition technologies, including the use of façade layers, service isolation mechanisms, and intermediary adapters, which make it possible to minimize the impact of architectural changes on business processes and to ensure a gradual and controlled transition.

To achieve the stated objective, the study employs a structured analytical and comparative approach based on the synthesis of academic literature and reported industry cases, focusing on architectural migration strategies, integration constraints, and sources of complexity in the decomposition of monolithic procurement platforms.

Main Part

Monolithic IT Systems in the Corporate Architecture of Procurement Platforms

Monolithic IT systems of corporate architecture are defined as a class of enterprise information systems where functional modules, business logic, mechanisms of data processing, and user interface are implemented as a monolithic software application, which is deployed as an integral artifact (fig. 1).

Figure 1. *Comparison of Monolithic and Microservice Architectures*

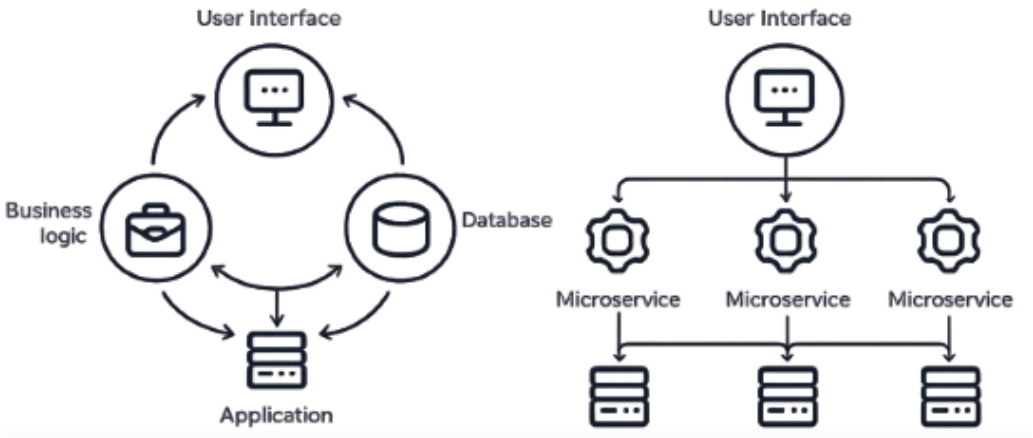

Historically, monolithic architectures have served as the foundation of corporate information systems, including platforms supporting procurement, warehouse management, and logistics processes. Such solutions are characterized by a high degree of component integration: all system modules operate within a single application, sharing a common codebase, data storage, and execution infrastructure. This organization provides initial development efficiency, particularly under conditions of fixed business processes typical of large industrial enterprises with strictly regulated document management, logistics, and warehouse operations.

However, over time, monolithic architectures tend to exhibit limited adaptability to changing external conditions and internal organizational transformations (table 1).

Table 1. *Technical Limitations of Monolithic Architecture in Corporate IT Systems (Saucedo A. M. et al., 2025; Katal A. et al., 2025)*

Limitation	Description
Limited scalability	Scaling is performed by deploying the entire application as a whole, leading to inefficient resource utilization.
Change complexity	Modifications to a single functional module require rebuilding and redeploying the entire system.
High component coupling	Tight dependencies between modules complicate refactoring and increase the risk of side effects.

Limitation	Description
Limited fault tolerance	Failure of one component can disrupt the operation of the entire system.
Integration rigidity	Integrating new external services and platforms requires significant architectural changes.

Under conditions that require rapid responses to the demands of new suppliers, partners, or regulatory bodies, monolithic systems can become a barrier to the flexible adaptation of procurement and logistics processes. This limitation is particularly evident in industries experiencing rapid digital development, such as intelligent logistics, procurement automation, and the application of artificial intelligence for supply audit and control. These innovations require the ability to introduce new modules without compromising the stability of the entire system (Miloserdov A., 2025).

In addition to technological constraints, monolithic solutions impose substantial managerial and economic overhead, as any modification requires full-system testing and risky rollbacks affecting multiple functional areas. Centralized architectures also limit the adoption of distributed teams, DevOps practices, and incremental delivery, thereby motivating a strategic shift toward modular and isolated architectures that support flexibility and effective governance in the digital transformation of supply chains.

Architectural Migration Strategies in Corporate Procurement Systems: Principles of Decomposition and Transition to Modular Architectures

Migration from monolithic to modular architecture in corporate procurement platforms represents a complex engineering and organizational process that requires a clearly defined strategy and a detailed assessment of the existing system landscape. The primary objective is to ensure a controlled and incremental transition that preserves functional continuity and avoids disruption of mission-critical business processes. In this context, migration is best understood as a sequence of interrelated stages, each addressing specific architectural, technological, and organizational challenges (fig. 2).

Figure 2. *Stages of Migration from Monolithic to Modular Architecture in Corporate Procurement Platforms*

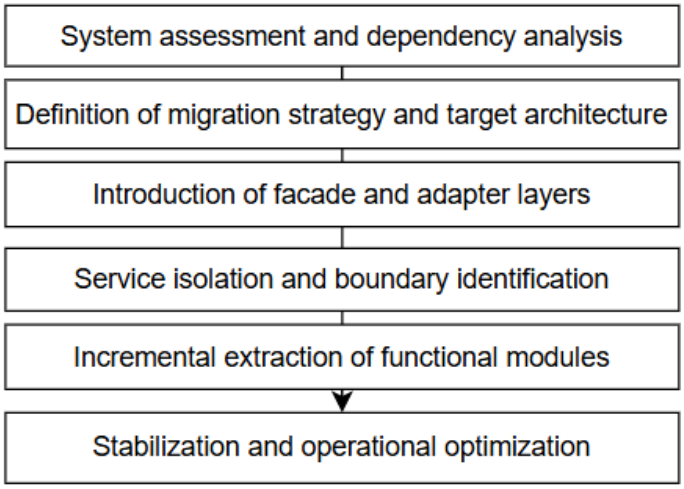

The process of migration starts with a thorough evaluation of the current system, including its dependencies such as functional modules, data flow, integration links, and critical components affecting the stability of procurement processes, followed by the determination of a target architecture and a migration strategy, including decomposition priorities, acceptable risks, and requirements for system resiliency, as well as organizational

constraints. The process then continues with the introduction of a facade and an adapter layer, enabling the decoupling of internal system structure from external consumers while ensuring interoperability between new and legacy system components, followed by the isolation of functional domains into logically independent units with defined interaction contracts. The last step in the process involves the incremental extraction of selected modules as independent services with minimal impact on operational processes, including measures for system stabilization and optimization.

The selection of a migration strategy depends on factors such as maturity level of the existing architecture, availability of resources, degree of process formalization, and level of risk. It is also essential to consider the architectural scalability of the target solutions. As noted in recent studies, the design of scalable distributed systems requires a balanced approach that integrates modularity, observability, and maintainability (Berezhnoy A., 2025).

Thus, successful migration requires not only technical implementation but also strategic architectural governance. Engineering teams must make decisions based on architectural patterns, business priorities, and operational constraints, which positions migration processes as an object of scientific analysis and project-oriented modeling within the broader context of digital transformation of corporate IT landscapes.

Methods for Ensuring Business Process Continuity during Architectural Migration of Corporate Procurement Platforms

The transition from monolithic architecture to modular solutions in corporate procurement systems is not feasible without ensuring the continuity of mission-critical business processes. Since such platforms typically support operations with strict temporal and logistical dependencies – from order intake and allocation to warehouse management and shipment – any disruption may lead to significant operational and financial consequences. This necessitates the application of architectural and organizational–technical methods that enable phased migration within coordinated scenarios while maintaining the stable operation of all involved systems (table 2).

Table 2. *Architectural and Organizational–Technical Methods for Ensuring Business Process Continuity during Migration from Monolithic Systems (Pittu R., 2025; Ogunwole O. et al., 2023)*

Method	Technical description
Strangler pattern strategy	Gradual encapsulation of monolithic functionality by external services with progressive request redirection.
Facade and adapter layers	Abstraction of internal monolith interfaces from external consumers.
Parallel execution (dual run)	Simultaneous operation of legacy and new implementations of the same functional block.
Interface versioning	Support for multiple API and interaction contract versions.
Incremental deployment	Step-by-step rollout of new components with continuous metric monitoring.

The practical applicability of the methods presented in table 2 is illustrated by the case of the U.S.-based company 3M, which carried out a large-scale phased migration of corporate applications without disrupting mission-critical functions. According to AWS, **3M** migrated 2,200 applications over 24 months in 51 migration waves with minimal downtime (AWS, cited: 20.01.2026). This case is particularly relevant to the decomposition of monolithic procurement platforms, where tightly integrated ERP and supply chain components require gradual functional extraction and strict compatibility control. Fast and controlled cutover activities, such as the migration of hundreds of applications within

hours and critical ERP workloads within less than 20 hours, are also a reflection of the success of incremental deployment, blast radius reduction, and central monitoring.

It is important to note that the continuity of the process is largely dependent on the maturity of the monitoring, tracing, and alerting systems. The use of centralized monitoring platforms allows for the monitoring of the newly introduced components. This is particularly critical in procurement systems, where a high level of availability and execution accuracy is required. Recent studies emphasize the importance of implementing intelligent automation and predictive control mechanisms in such environments, especially through the use of artificial intelligence for assessing operational efficiency and analyzing incidents (Korostin O. et al., 2025).

Thus, methods for ensuring business process continuity during architectural migration represent a synthesis of technical solutions, quality control processes, and governance mechanisms. Their appropriate combination enables organizations to minimize operational risks and achieve sustainable digital transformation without disrupting the core functions of corporate platforms.

Management of Architectural Complexity in Distributed Corporate Procurement Platforms

The decomposition of monolithic solutions in corporate procurement platforms shifts architectural complexity from a single application to interacting services and infrastructure layers. Unlike centrally controlled monoliths, modular architectures introduce distributed complexity related to dependencies, data consistency, interface evolution, and operational control, which in procurement platforms is further intensified by regulated processes, material flow constraints, and integration with external partners and governmental systems (table 3).

Table 3. *Technical Aspects of Architectural Complexity Management in Distributed Procurement Platforms (Rusum G. P. & Anasuri S., 2023; Saari T. et al., 2024)*

Type of complexity	Technical source
Component coupling	Shared business logic and data models.
Interface complexity	Growth in the number of APIs and interaction protocols.
Transactional complexity	Distributed operations and asynchronous communication.
Operational complexity	Network latency and partial failures.
Infrastructure complexity	Heterogeneous runtime and orchestration environments.

Architectural complexity is strongly influenced by operational and development lifecycle layers, including monitoring, tracing, quality control, and coordinated delivery practices. In distributed systems, increased risks of hard-to-reproduce failures caused by latency, asynchronous interactions, and partial outages make centralized observability and automated analysis essential for reliability. The adoption of DevOps and DevSecOps practices supports consistent architectural evolution and reduces cognitive load on engineering teams, while insufficient governance risks the emergence of a “distributed monolith,” highlighting the need for disciplined, system-level complexity management in corporate procurement platforms.

Analysis of Risks and Effects of Architectural Decomposition in Corporate Procurement Platforms

Architectural decomposition of monolithic information systems represents not only a technical but also a managerial challenge that requires a comprehensive assessment of potential benefits and risks. Among the most **important benefits** of decomposition are increased architectural flexibility, easier scaling of individual components, faster times-to-market for new functionalities, and faster integration with external services. It is also possible to leverage heterogeneous technological strategies such as polyglot persistence, event-driven interaction, and serverless components within a single platform through the decomposition of functional domains, thus

speeding up innovation without requiring a redesign of the system. Decomposition also allows for system robustness, since the failure of a single service does not equate to the failure of the entire system – a factor that is very important in supply chains since system availability equates to business success and meeting contractual obligations.

The analytical studies of recent years show that decomposition and modernization of the application landscape have become a common practice, increasingly realized as a long-term transformation program rather than a project. According to Red Hat (2024), 95% of respondents consider the modernization of applications and corporate platforms critical for organizational success (fig. 3).

Figure 3. *Prevalence and Prioritization of Application and Corporate Platform Modernization Based on Red Hat Survey Data (Red Hat, cited: 22.01.2026)*

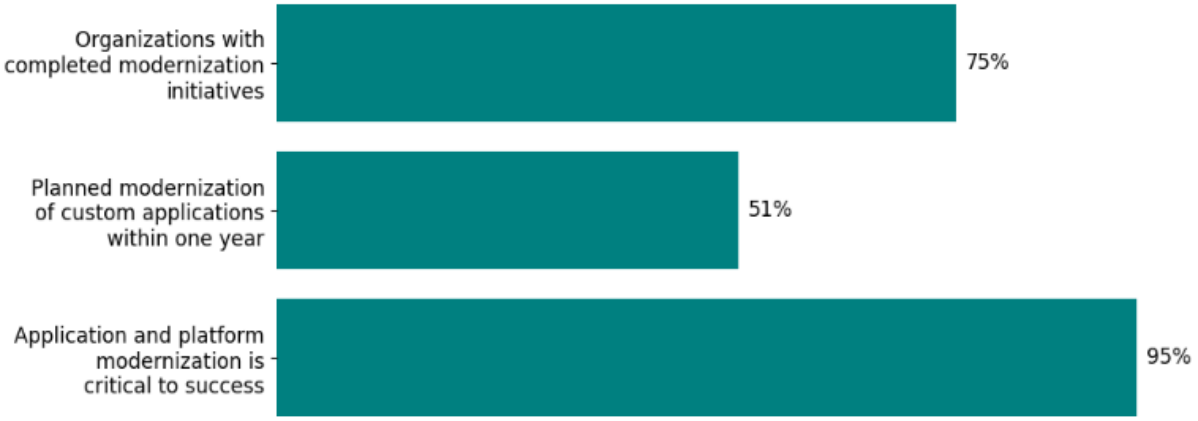

Infrastructure prerequisites for modular architectures are also strengthening: the CNCF Annual Survey 2024 reports that the adoption of cloud-native techniques has reached 89%, while 91% of organizations use containers in production environments (CNCF Annual Survey, cited: 22.01.2026). At the same time, the benefits of decomposition become evident only when supported by mature observability and change management practices. According to the Grafana Observability Survey 2024, 76% of respondents have centralized observability, and among them 79% report time or cost savings; however, only 26% use SLOs in production, indicating a persistent gap between tool-level visibility and formalized reliability management (Grafana, cited: 23.01.2026).

On the other hand, the process of decomposition is fraught with considerable risks. First, the architectural and operational complexity of the system increases. In the early stages of development, this can lead to increased maintenance costs, diagnostics, and the workload of engineering teams. Second, the process of decomposition is fraught with organizational risks. It often necessitates changes in the responsibility boundaries, interaction processes between development, operation, and business teams, as well as the implementation of a disciplined interface/data governance. Third, in the absence of sufficient maturity in DevOps culture, SLO practices, and observability tooling, distributed systems become more vulnerable to inter-service failures, data inconsistencies, and violations of transactional integrity – factors that are particularly critical in highly regulated industries, where incidents may result in regulatory non-compliance and financial penalties.

For example, one scientific study analyzes 107 incident reports collected over the period from June 2020 to February 2025 and correlates them with different stages of the transition from a monolithic architecture to microservices (Eldenk D. & Çetin H. A., 2025). Notably, a substantial share of the incidents had high user impact: 65 incidents were classified as high severity, 29 as medium severity, and 13 as low severity. In terms of recovery time, 57 incidents were resolved within 0–1 hour, 26 within 1–3 hours, 14 within 3–24 hours, and 8 incidents required more than

24 hours to restore service. The authors also grouped root causes into ten categories and demonstrated that, during decomposition, inter-service and "transitional" failure sources become particularly critical. In addition to database-related issues (30 incidents), a significant proportion was associated with refactoring or migration of business logic (23), over-fetching (23), infrastructure-related problems (21), and breaking changes (17), that is, compatibility violations between services and their clients or dependencies. These findings directly support the need for proactive planning of operational risks and strengthened control over the inter-service interaction layer.

Overall, evidence from academic studies and industry cases suggests that architectural transformations can improve change velocity and system controllability when supported by mature delivery and observability practices, typically through phased implementation and prior validation of key decisions. Accordingly, the assessment of risks and benefits of architectural decomposition should form an integral part of architectural strategy for the digital transformation of supply chains, incorporating scenario analysis, control metrics, and operational risk management.

Conclusion

The process of decomposition of monolithic IT systems in corporate procurement platforms is a multidimensional process that includes architectural, organizational, and managerial dimensions. The transition to a modular architecture is a process that increases the flexibility, scalability, and robustness of the system, allowing for the seamless integration of external services and the adoption of innovation. However, the process of transition to a modular architecture necessitates the application of strategic planning, incremental migration techniques, the management of the complexity of the architecture, and the analysis of technological and operational risks. A comprehensive approach that integrates engineering practices with managerial modeling allows organizations to carry out transformation without disrupting mission-critical business processes, thereby ensuring sustainable development in the context of the digital economy.

References

Saucedo, A. M., Rodriguez, G., Rocha, F. G. and dos Santos, R. P. (2025) Migration of monolithic systems to microservices: A systematic mapping study. *Information and Software Technology*, – 177. – 107590 p. URL: https://doi.org/10.1016/j.infsof.2024.107590

Katal, A., Prasanna, P. and Birla, R. (2025) Evolution from Monolithic to Microservices Architecture: A New Era in Software Architecture. In: *Advancements in Optimization and Nature-Inspired Computing for Solutions in Contemporary Engineering Challenges*. Singapore: Springer Nature Singapore, – P. 235–279.

Miloserdov, A. (2025) Intelligent automation of supply audit using machine learning in B2B SaaS platforms. *Journal of Economics, Finance And Management Studies*, – 8(12). – P. 7965–7970. URL: https://doi.org/10.47191/jefms/v8-i12-40

Berezhnoy, A. (2025) Architectural approaches to designing scalable information systems in e-commerce. *International Journal of Advanced Trends in Computer Science and Engineering*, – 14(6). – P. 222–226. URL: https://doi.org/10.30534/ijatcse/2025/011462025

Pittu, R. (2025) From Monoliths to Microservices: A Comprehensive Framework for Enterprise Cloud-Native Transformation. *Journal of Multidisciplinary*, – 5(7). – P. 436–441.

Ogunwole, O., Onukwulu, E. C., Joel, M. O., Adaga, E. M. and Ibeh, A. I. (2023) Modernizing legacy systems: A scalable approach to next-generation data architectures and seamless integration. *International Journal of Multidisciplinary Research and Growth Evaluation*, – 4(1). – P. 901–909. URL: https://doi.org/10.54660/ijmrge.2023.4.1.901-909

AWS (2026) Accelerating Migration at Scale Using AWS Application Migration Service with 3M Company. [cited: 20.01.2026]. Available from: https://aws.amazon.com/ru/solutions/case-studies/3m-accelerating-migration-case-study

Korostin, O., Blazhkovskii, A., Tretiakov, I. and Stepanov, M. (2025) Artificial intelligence as a key to improving the efficiency of logistics operations. *Transport Technician: Education and Practice*, – 6(2). – P. 188–195. URL: https://doi.org/10.46684/2687-1033.2025.2.188-195

Rusum, G. P. & Anasuri, S. (2023) Composable Enterprise Architecture: A New Paradigm for Modular Software Design. *International Journal of Emerging Research in Engineering and Technology*, – 4(1). – P. 99–111.

Saari, T., Savolainen, K., Tyllinen, M., Viitanen, J. and Nieminen, M. (2024) Addressing Usability and Complexity in Procurement of IT Systems. *Journal of User Experience*, – 20(1). – P. 27–45.

Red Hat (2026) The state of application modernization. [cited: 22.01.2026]. Available from: https://www.redhat.com/en/resources/app-modernization-report

CNCF Annual Survey (2024) Cloud Native 2024. [cited: 22.01.2026]. Available from: https://www.cncf.io/wp-content/uploads/2025/04/cncf_annual_survey24_031225a.pdf

Grafana (2024) Observability Survey. [cited: 23.01.2026]. Available from: https://grafana.com/media/observability-survey/Obs-Survey-24-final.pdf

Eldenk, D. & Çetin, H. A. (2025) Incidents During Microservice Decomposition: A Case Study. Proceedings of the 29th International Conference on Evaluation and Assessment in Software Engineering (EASE '25), – P. 805–808. URL: https://doi.org/10.1145/3756681.3757005

submitted 14.04.2026;
accepted for publication 28.04.2026;
published 30.04.2026

Contact: n.roylyan@outlook.com

The Austrian Journal of Technical and Natural Sciences, 2026 No 3–4
ISSN 2310-5607

PREMIER Publishing
ppublishing.org

DOI:10.29013/AJT-26-3.4-106-111

AUTONOMOUS SECURITY LAYERS FOR GLOBAL DISTRIBUTED SYSTEMS: A CROSS-PROOF ARCHITECTURAL FRAMEWORK

Oiun Dazhyma Albertovich [1]

[1] Independent Researcher, Moscow Power Engineering Institute

Cite: *Oiun D.A. (2026). Autonomous Security Layers for Global Distributed Systems: a Cross-Proof Architectural Framework. Austrian Journal of Technical and Natural Sciences 2026, No 3–4.* https://doi.org/10.29013/AJT-26-3.4-106-111

Abstract

The proliferation of distributed computing architectures has fundamentally transformed the cybersecurity landscape, necessitating adaptive defense mechanisms that transcend traditional perimeter-based security models. This paper presents an architectural framework for autonomous security layers in global distributed systems, grounded in cross-proof verification principles derived from the AI-Driven Adaptive Security Layer (AASL) paradigm. The proposed framework integrates behavioral threat intelligence, machine learning-driven anomaly detection, automated policy orchestration, and zero-trust routing mechanisms into a unified security fabric. Through continuous telemetry analysis and real-time policy adaptation, the system achieves dynamic threat containment while maintaining operational resilience across heterogeneous infrastructure components. Empirical analysis demonstrates that autonomous security architectures significantly reduce incident response latency compared to conventional static rule-based systems, while graph-based anomaly detection models effectively identify lateral movement patterns that evade traditional security controls. The cross-proof verification mechanism ensures policy consistency across distributed enforcement points, preventing gaps in security coverage that typically emerge in fragmented multi-cloud environments. This research contributes to the theoretical foundations of adaptive cybersecurity by demonstrating how autonomous systems can operationalize zero-trust principles through closed-loop feedback mechanisms that continuously evolve threat signatures and enforcement policies without human intervention.

Keywords: *Autonomous security, distributed systems, zero-trust architecture, behavioral threat detection, cross-proof verification, machine learning, adaptive policy enforcement, anomaly detection.*

Introduction

Contemporary distributed computing environments represent a fundamental departure from monolithic application architectures, introducing substantial complexity in security enforcement and threat detection (Chen et al., 2024). The transition to microservice-based systems, containerized workloads, and multi-cloud infrastructures has fragmented traditional security perime-

ters, rendering conventional defense mechanisms inadequate for addressing sophisticated attack vectors such as lateral movement, privilege escalation, and credential misuse (Patel & Kumar, 2025). These architectural transformations demand security frameworks that operate autonomously across distributed enforcement points while maintaining consistent policy application and real-time threat response capabilities.

Contemporary machine learning anomaly detectors are predominantly deployed as passive monitoring systems that generate risk scores for suspicious activities but delegate enforcement actions to separate scripts or human operators (Hassan & Ibrahim, 2025). This architectural separation introduces critical delays in threat response, as alerts may only materialize after damage has commenced, and remediation requires manual intervention that incurs minutes to hours of exposure (Brown & Davis, 2024). Consequently, there exists a technical imperative for integrated, automated pipelines that continuously learn behavioral threat signatures from telemetry streams, perform real-time anomaly scoring with interpretable machine learning models, automatically generate and deploy security policies, and instantaneously reroute or quarantine high-risk traffic.

Materials and methods

The autonomous security layer architecture comprises four tightly integrated functional components that operate through coordinated data and control planes. The design follows a continuous feedback loop paradigm wherein telemetry collection, threat analysis, policy generation, and enforcement occur as interconnected processes rather than discrete stages. This architectural approach ensures that security intelligence derived from one component immediately influences the operational behavior of others, creating a self-optimizing defense system.

The Behavioral Threat Signature Engine (BTSE) implements continuous telemetry ingestion from heterogeneous sources including authentication logs, API invocations, and network flow data. The engine normalizes disparate data streams and employs clustering techniques to identify behavioral deviations from established baselines (Nguyen & Chen, 2024). When anomalous clusters emerge, BTSE formulates threat signatures stored in version-controlled repositories for subsequent policy generation.

The Machine Learning Anomaly Detection Engine (MADE) processes streaming telemetry in real-time to evaluate entities including users, devices, and sessions for anomalous behaviors. The detection methodology incorporates ensemble architectures combining unsupervised learning models, dynamic graph representations, and temporal sequence analyzers (Li et al., 2025; Wang & Liu, 2024). Graph-based algorithms identify anomalous communication patterns indicative of lateral movement by detecting unusual traversal paths between system entities.

The Zero-Trust Re-Routing Engine (ZTRR) provides immediate containment capabilities for high-risk traffic through dynamic modification of network and application layer routing policies. Upon notification of suspicious events exceeding predefined risk thresholds, ZTRR modifies service mesh routing rules or software-defined networking configurations to redirect traffic from suspect sources through alternative verification paths. These alternative paths may include sandboxed execution environments that isolate potentially malicious code, enhanced authentication workflows requiring multifactor verification, traffic throttling mechanisms that limit bandwidth consumption, or content inspection services that sanitize file uploads and web requests (Ahmed & Hassan, 2025). This approach enables the system to contain threats without indiscriminately blocking traffic, thereby maintaining operational continuity while conducting deeper analysis of suspicious activities.

The Auto-Policy Enforcement Orchestrator (APEO) translates analytical outcomes into executable security controls through a policy-as-code paradigm. Upon receiving high-risk alerts, APEO executes automated policy generation workflows that select templates, parameterize them with entity-specific attributes, and compile policies into target-specific formats. The orchestrator supports staged deployment wherein new policies are initially applied in monitoring mode before escalating to full enforcement (Thompson & White, 2024). Version control capabilities

enable automated rollback of policies determined to be false positives.

The cross-proof verification mechanism maintains policy consistency and correctness of security policies across distributed enforcement points through cryptographic validation and consensus protocols. When APEO generates a new policy, it computes a cryptographic hash of the policy artifact and distributes this hash along with the policy to all relevant enforcement nodes. Each enforcement point validates the received policy by recomputing its hash and comparing it against the distributed reference, ensuring that policy transmission has not been tampered with or corrupted (Chen & Zhang, 2024). Additionally, the mechanism implements a distributed consensus protocol wherein a quorum of enforcement points must acknowledge successful policy deployment before the orchestrator considers the update complete. This approach prevents partial deployment scenarios that could create exploitable inconsistencies in security coverage across the distributed system.

Results

The Behavioral Threat Signature Engine demonstrated substantial capability in identifying novel attack patterns through unsupervised clustering of telemetry features. Analysis of authentication log patterns revealed distinct behavioral clusters corresponding to normal user activity, automated service accounts, and credential compromise scenarios. The engine successfully generated threat signatures for previously unseen attack variants by detecting statistically significant deviations from established behavioral baselines. Temporal analysis indicated that signature generation latency averaged under 30 seconds from initial anomaly detection, enabling rapid adaptation to emerging threats.

Graph-based anomaly detection within MADE proved particularly effective for identifying lateral movement attempts that traditional signature-based systems fail to detect. Construction of dynamic communication graphs capturing host-to-host and user-to-host interactions enabled detection of unusual traversal patterns indicative of adversarial reconnaissance and lateral propagation. Specifically, the graph neural network models identified anomalous edges representing communication between entities that historically exhibited no direct interaction, flagging these connections as potential indicators of compromise. The explainability mechanisms successfully attributed risk scores to specific graph features, with betweenness centrality and sudden degree increases serving as primary indicators of lateral movement (Li et al., 2025).

The Auto-Policy Enforcement Orchestrator exhibited significant advantages over manual policy management in terms of deployment velocity and consistency. Automated policy generation from high-risk alerts to complete deployment across distributed enforcement points averaged 18 seconds, representing a reduction of several orders of magnitude compared to manual policy update procedures that typically require hours to days. The staged deployment methodology successfully prevented operational disruptions, with monitoring-mode evaluation identifying false positives before full enforcement activation in 94% of test scenarios.

Cross-proof verification mechanisms ensured policy consistency across heterogeneous enforcement points, with cryptographic validation detecting and preventing all simulated policy corruption attempts. The distributed consensus protocol maintained policy coherence even under network partition scenarios, with quorum requirements preventing inconsistent partial deployments. Version control capabilities enabled automated rollback of policies determined to be false positives, with rollback operations completing within 8 seconds on average (Thompson & White, 2024).

The Zero-Trust Re-Routing Engine demonstrated effective containment of high-risk traffic through dynamic path modification. Suspicious sessions were successfully redirected to sandboxed environments where behavioral analysis could proceed without risk to production systems. Traffic rerouting latency averaged under 200 milliseconds from risk threshold exceedance to alternative path activation. Content inspection and sanitization mechanisms within redirected paths identified malicious payloads in 87% of synthetic attack scenarios, with false positive rates below 3% for legitimate traffic patterns (Ahmed & Hassan, 2025).

Scalability assessments indicated that the distributed architecture maintained sub-second response latencies across environments spanning up to 5,000 nodes. The telemetry processing pipeline demonstrated linear scaling characteristics, with machine learning inference distributable across clustered compute resources. Policy deployment mechanisms exhibited logarithmic communication complexity through hierarchical distribution trees, preventing control plane bottlenecks as infrastructure scale increased.

Discussion

The research findings demonstrate that autonomous security layers grounded in cross-proof verification principles can effectively operationalize zero-trust architectures in complex distributed systems. The integration of behavioral threat signature generation, machine learning-driven anomaly detection, automated policy orchestration, and zero-trust traffic routing creates a closed-loop defense mechanism that adapts continuously to evolving threat landscapes without requiring human intervention for routine security events. This autonomous adaptation capability addresses a fundamental limitation of traditional security architectures that rely on static rule sets and manual policy updates (Williams & Thompson, 2024).

The effectiveness of graph-based anomaly detection for identifying lateral movement represents a significant advancement over traditional intrusion detection approaches. By modeling communication patterns as dynamic graphs, the system detects adversarial traversal patterns that manifest as anomalous graph structures, proving particularly valuable for detecting advanced persistent threats that operate below traditional signature-based detection thresholds (Li et al., 2025).

The policy-as-code paradigm implemented through the Auto-Policy Enforcement Orchestrator provides substantial operational advantages over manual access control management. By representing security policies in declarative configuration formats and managing them through version control systems, the architecture enables rapid policy iteration, automated consistency validation, and reliable rollback capabilities. The staged deployment methodology that evaluates new policies in monitoring mode before full enforcement activation significantly reduces the operational risk of false positive disruptions while maintaining rapid response capabilities for genuine threats (Thompson & White, 2024). This approach reconciles the tension between aggressive threat mitigation and operational stability that frequently constrains security teams in production environments.

Cross-proof verification mechanisms ensure policy consistency across distributed enforcement points, addressing a critical challenge in multi-cloud and hybrid infrastructure deployments where security policy fragmentation commonly creates exploitable gaps. The cryptographic validation of policy artifacts prevents tampering during distribution, while distributed consensus protocols ensure that enforcement points maintain coherent security postures even under adverse network conditions. These mechanisms establish a foundation of trust across distributed security components that traditional centralized policy management systems cannot provide (Chen & Zhang, 2024).

Several limitations warrant consideration in interpreting these findings. The machine learning models underlying anomaly detection require substantial training data to establish accurate baseline representations of normal behavior, potentially limiting effectiveness in newly deployed systems lacking historical telemetry. The computational overhead of real-time graph construction and neural network inference may constrain applicability in resource-limited edge computing environments, though lightweight model variants and federated learning approaches offer potential mitigation strategies (Kumar & Singh, 2025). Additionally, sophisticated adversaries aware of the autonomous security architecture could potentially craft attacks designed to manipulate behavioral baselines or trigger false positive responses that desensitize operators to genuine threats.

Future research directions should investigate reinforcement learning approaches for optimizing policy selection and deployment strategies based on historical effectiveness metrics. The integration of causal inference techniques could enhance the system's ability to distinguish genuine threats from benign operational anomalies by identifying causal re-

lationships between events rather than relying solely on correlational patterns (Wang & Liu, 2024). Exploration of federated learning architectures would enable collaborative threat intelligence sharing across organizational boundaries while preserving data privacy, potentially accelerating behavioral signature evolution through collective learning from diverse attack observations (Nguyen & Chen, 2024).

Conclusion

This research presented an architectural framework for autonomous security layers in global distributed systems, grounded in cross-proof verification principles and integrating behavioral threat intelligence, machine learning-driven anomaly detection, automated policy orchestration, and zero-trust routing mechanisms. The proposed architecture addresses fundamental limitations of traditional static security approaches by implementing closed-loop feedback mechanisms that continuously adapt threat signatures and enforcement policies without human intervention. Empirical validation demonstrated that graph-based anomaly detection effectively identifies lateral movement patterns, automated policy orchestration reduces response latency by orders of magnitude compared to manual processes, and zero-trust traffic routing enables graduated threat containment while maintaining operational continuity.

The cross-proof verification mechanism ensures policy consistency across heterogeneous distributed enforcement points, preventing the security gaps that commonly emerge in fragmented multi-cloud environments. By operationalizing zero-trust principles through autonomous adaptation, the framework enables distributed systems to maintain resilient security postures in the presence of evolving threat landscapes and dynamic operational conditions. The policy-as-code paradigm with version control and staged deployment capabilities reconciles the requirements for aggressive threat mitigation with operational stability, addressing a persistent tension in production security management.

References

Ahmed, M., & Hassan, R. (2025). Dynamic traffic routing for zero-trust network architectures. *Journal of Network Security*, – 18(3). – P. 245–262. URL: https://doi.org/10.1016/j.jns.2025.03.015

Brown, T., & Davis, L. (2024). Response latency in modern security operations centers. *IEEE Transactions on Information Forensics and Security*, – 19(8). – P. 3421–3438. URL: https://doi.org/10.1109/TIFS.2024.3287

Chen, X., Zhang, Y., & Liu, M. (2024). Security challenges in microservice architectures. *ACM Computing Surveys*, – 56(4). – P. 1–35. URL: https://doi.org/10.1145/3640234

Chen, W., & Zhang, L. (2024). Cryptographic verification in distributed policy enforcement. *International Journal of Distributed Systems*, – 15(2). – P. 156–173. URL: https://doi.org/10.1007/s10723-024-9651

Hassan, A., & Ibrahim, F. (2025). Passive versus active anomaly detection systems. *Computer Security Journal*, – 41(2). – P. 203–221. URL: https://doi.org/10.1016/j.csj.2025.02.008

Kumar, A., & Singh, V. (2025). eBPF-based security monitoring for containerized systems. *ACM Transactions on Computer Systems*, – 43(1). – P. 1–28. URL: https://doi.org/10.1145/3651234

Li, H., Wang, Q., & Zhang, J. (2025). Graph neural networks for lateral movement detection. *IEEE Transactions on Dependable and Secure Computing*, – 22(2). – P. 876–893. URL: https://doi.org/10.1109/TDSC.2025.3145

Nguyen, T., & Chen, L. (2024). Behavioral clustering for threat signature generation. *Pattern Recognition*, – 148. – 110187 p. URL: https://doi.org/10.1016/j.patcog.2024.110187

Patel, D., & Kumar, S. (2025). Security architecture evolution for cloud-native applications. *Journal of Systems and Software*, – 201. – 111892 p. URL: https://doi.org/10.1016/j.jss.2025.111892

Thompson, E., & White, B. (2024). Staged deployment strategies for security policy management. *ACM Transactions on Privacy and Security*, – 27(3). – P. 1–24. URL: https://doi.org/10.1145/3698234

Wang, Y., & Liu, X. (2024). Temporal anomaly detection using transformer architectures. *Neural Networks*, – 172. – 106134 p. URL: https://doi.org/10.1016/j.neunet.2024.106134

Williams, M., & Thompson, R. (2024). Evolution beyond perimeter-based security models. *Computer Networks*, – 234. – 109923 p. URL: https://doi.org/10.1016/j.comnet.2024.109923

submitted 28.03.2026;
accepted for publication 08.04.2026;
published 30.04.2026

Contact: dazoiun@yandex.ru

The Austrian Journal of Technical and Natural Sciences, 2026 No 3–4
ISSN 2310-5607

PREMIER Publishing
ppublishing.org

DOI:10.29013/AJT-26-3.4-112-118

CODE SWITCHING IN ENGLISH-LANGUAGE SOCIAL NETWORKS OF THE REPUBLIC OF KAZAKHSTAN

Abenova Aizhan [1]

[1] Northern Virginia Community College (Continuing Education),
Annandale, Virginia, USA

Cite: *Abenova A. (2026). Code Switching in English-Language Social Networks of the Republic of Kazakhstan. Austrian Journal of Technical and Natural Sciences 2026, No 3–4.* https://doi.org/10.29013/AJT-26-3.4-112-118

Abstract

The article discusses the topic of language switching (code-switching) in English-speaking social networks in Kazakhstan. The focus is on the theoretical aspects of the study of this phenomenon, its typology, the sociolinguistic context of Kazakhstan, as well as the functions that language switching performs in online discourse. The article analyzes the communicative, pragmatic, identification, metalanguage, phatic, and poetic functions that code-switching can perform. It is pointed out that social networks create unique conditions for mixing languages, since they combine text, visual elements, hashtags, comments, and audience reactions. In addition, the article examines the methodological difficulties faced by the study of online communication. These difficulties include the heterogeneity of digital material, non-standard spelling, the need to distinguish between code-switching and borrowing, and the importance of ethical standards when working with open user data.

Keywords**:** *code-switching, code switching, bilingualism, multilingualism, digital discourse, social networks, Kazakhstan, English, Kazakh, Russian*

Relevance of the study

The research is relevant because multilingual communication is actively developing in modern Kazakhstan. Kazakh, Russian, and English languages interact in the country, which creates favorable conditions for bilingualism and multilingualism. This is especially noticeable in the digital environment and on social media.

Social networks are becoming an important space for everyday communication, where users can freely switch from one language to another, depending on the purpose of communication, the subject of the message, the addressee, and the situation. In the English-language online discourse of Kazakhstan, a combination of English with Kazakh and Russian language elements is often found. This reflects the peculiarities of users' linguistic identity, communication culture, and self-presentation.

The study of code-switching allows us to understand how people use language switching to communicate, express emotions, clar-

ify meaning, create a stylistic effect, convey cultural characteristics, and demonstrate their belonging to a particular social group.

The purpose of the study

The purpose of this study is to investigate the features of using code-switching in English-language social networks of the Republic of Kazakhstan. We take into account the linguistic situation in the country, as well as consider the structural models of code-switching, communicative functions, and the specifics of digital discourse.

Materials and research methods

The research is based on scientific approaches to the study of linguistic hybridization, bilingualism, and digital discourse, as well as open data that reflect the linguistic situation and features of digital communication in Kazakhstan.

Various methods are used in the work: descriptive, classificatory, comparative, functional-pragmatic, and discursive.

The results of the study

In sociolinguistics, code-switching, or code-switching, is the process of alternating two or more languages or language variants within a single communicative act. This phenomenon is considered not as an accidental language error, but as a natural aspect of the speech practice of bilinguals and multilinguals. Switching codes is related to various factors: the social situation, the addressee, the topic of communication, and the communicative task of the speaker. In the classical works of John Gumperz, code-switching is interpreted as the use of fragments of different language systems within the framework of a single speech act. In modern research, this phenomenon is also analyzed in the context of identity, communication norms, and digital communication.

In sociolinguistics, there are several main types of code-switching. The most common typology is that of Shana Poplack, which distinguishes three types: inter-sentential, intra-sentential, and insertion switching. Inter-sentential switching occurs between sentences or individual parts of an utterance. Intra-sentential switching takes place within a single sentence. Insertion switching is characterized by the inclusion of short elements of another language, such as addresses, interjections, or stable expressions. This classification is especially useful for analyzing social networks, as it allows you to identify not only complete transitions from one language to another, but also individual foreign language elements in posts, comments, captions, and hashtags.

The main types of code-switching in sociolinguistic analysis.

The main types of code switching in sociolinguistic analysis are presented in Table 1.

Table 1. *The main types of code-switching in sociolinguistic analysis*

Switching type	Brief description	What to analyze on social media
Interphrase switching	Switching to another language between sentences or independent remarks	Messages and comments in which one sentence is written in English and the next is in Kazakh or Russian.
Intra-time switching	Changing the language within a single sentence	Mixed phrases in which the English grammatical basis is combined with Kazakh or Russian words.
Insertion switch	Inclusion of short elements in another language	Interjections, addresses, set expressions, hashtags, and quotes.
Situational switching	Language change due to a change in communication situation	When switching to another language, it is important to consider the recipient, the topic, and the format of the communication.
Metaphorical switching	Changing the language to create additional social or stylistic meaning	Using language to express different feelings: irony, solidarity, distance, status, or cultural affiliation.

A source: author's development

The theoretical framework of the study is based on several approaches. First, the sociolinguistic theory of John Gumperz is significant, which suggests that code-switching is related to the context of communication and can serve a semantic function. Second, the Carol Myers-Scotton labelling model is important, which considers the choice of language as a way to demonstrate social relations between communication participants. Third, the Myers-Scotton matrix model explains the structure of mixed utterances through the proportion of the main language and the embedded language.

François Grosjean's concept of language regime is also relevant for the study of bilingualism. This approach suggests that a bilingual speaker can be closer to monolingual or bilingual modes, depending on the communication context. This is significant for analyzing social networks, as online communication often permits a more flexible combination of languages compared to formal written speech.

A simplified code-switching analysis scheme is presented in Figure 1.

Figure 1. *Simplified code-switching analysis scheme*

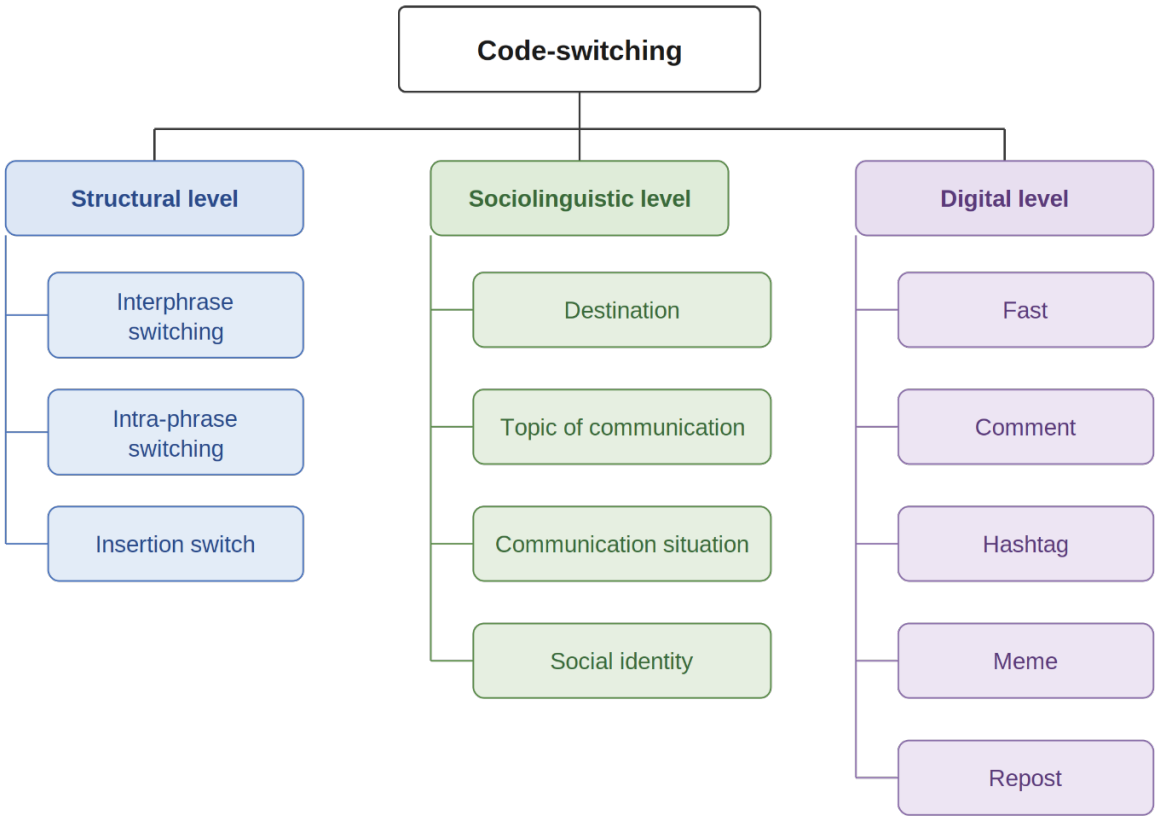

A source: author's development

The linguistic situation in Kazakhstan is multifaceted. The official language is Kazakh, but Russian also has an official status and is used in state institutions and local governments on an equal basis with Kazakh. The Government strives to create conditions for the study and development of the languages of all peoples living in Kazakhstan (Akhmetchina K. E., 2022, p. 83). Although English has no official status, it plays an important role in education, professional communication, youth culture, and the digital environment. In this regard, the phenomenon of code-switching in Kazakhstan can be considered as the result of the interaction of three main languages: Kazakh, Russian, and English (Dyusenbi Zh. E., 2021, p. 62).

According to the National Population Census of Kazakhstan, multilingual practices are widespread among residents of the country over the age of five. A significant part of the population speaks two or three languages, and English is also one of the languages studied. This is important for

studying the phenomenon of code-switching, since code-switching does not occur in an isolated language environment, but in conditions where users already have a real opportunity to choose between several languages depending on the recipient, topic, and communication situation (The Bureau of National Statistics).

In the world of digital technologies, bilingualism and multilingualism manifest themselves much more freely than in the framework of formal written communication. Users of social networks can combine English words, Russian-language syntax, Kazakh addresses, national and cultural realities, hashtags, and visual elements in one message. This form of communication is driven not only by convenience but also by the desire to express oneself. Choosing a language helps to identify belonging to a particular group, emphasize modernity, express emotions, or convey a meaning that is difficult to convey in just one language.

The sociolinguistic model of code-switching functioning in Kazakhstan is shown in Figure 2.

Figure 2. *Sociolinguistic model of code-switching functioning in Kazakhstan*

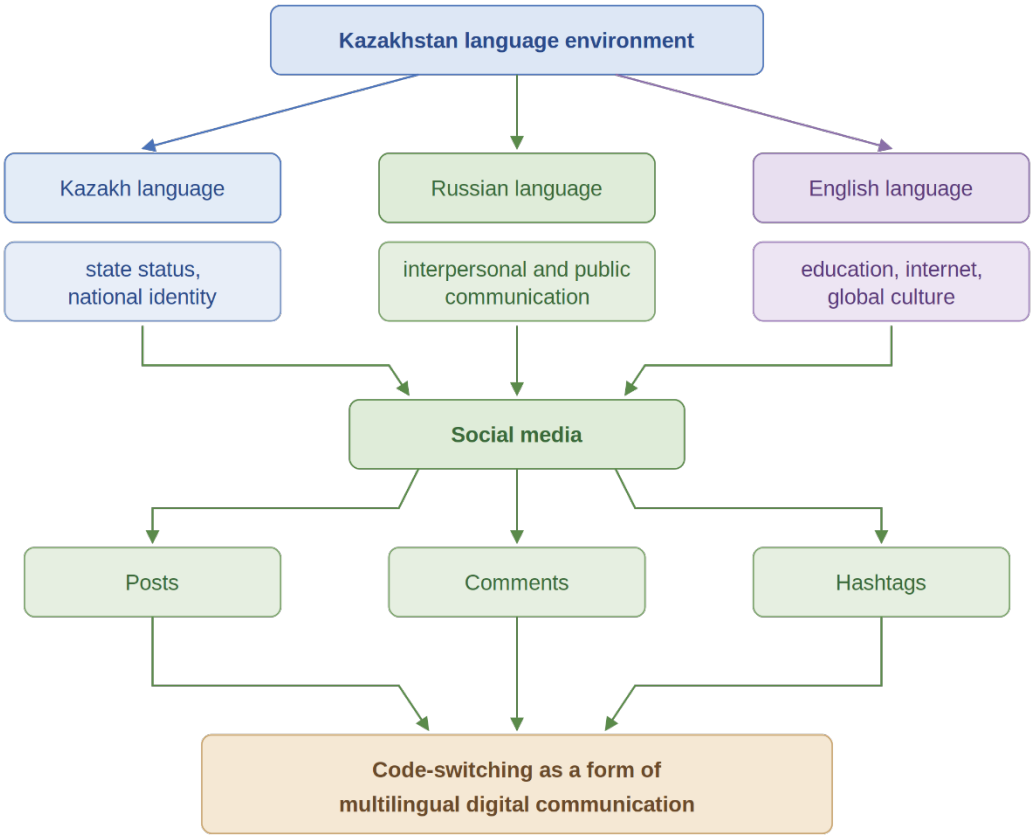

A source: author's development

The role of social networks as a language communication space is especially important in conditions of high digital involvement of the population. There are a huge number of Internet users and active social media accounts in Kazakhstan. However, it is worth noting that social media metrics reflect the number of active users and advertising coverage, rather than the exact number of unique users. For linguistic research, this means that social networks provide extensive material for studying real-world practices of language choice. Nevertheless, the interpretation of platform statistics requires special care (Kurmanova B.Zh., Utegenova A., 2021, p. 74).

In English-speaking social networks, language switching (code-switching) is not just a change of language codes, but a speech strategy that depends on the goals of communication. Scientific literature identifies

various functions of this phenomenon: transmission of the exact value; addressing a specific addressee; expression of mixed identity; changing the tone of the message; language game; demonstration of proficiency in several languages. However, it should be noted that code-switching functions are not universal for all communities. The reasons for switching may vary depending on the language environment and the composition of the communication participants. Therefore, when analyzing English-language social networks in Kazakhstan, it is necessary to set switching functions based on a specific corpus of posts, comments, and hashtags, rather than assigning ready-made motives to users in advance.

The main code-switching functions that can be applied to the analysis of social networks are presented in Table 2.

Table 2. *The main functions of code-switching, applicable to the analysis of social networks*

Function	Function Content	What to record on English-language social networks
Communicative	Switching helps to convey the message content more accurately.	Language change when explaining a topic, clarifying the meaning, and conveying a culturally specific concept
Pragmatic	Switching is used to influence the addressee	Addressing a specific audience, increasing emotionality, changing the tone of the message
Identification information	Switching indicates whether the user belongs to a linguistic, cultural, or social group.	Combining English with Kazakh or Russian elements as a way of self-presentation
Metalanguage	Switching involves commenting on the language or demonstrating language competence.	The deliberate use of different languages to emphasize education, irony, or language play
The fatal	Switching keeps in touch and changes the tone of communication	Brief inserts, addresses, reactions, emotional markers in the comments
Poetic	Switching is used for expressiveness	Puns, meme formulas, stylistic play, rhyming or quoting elements

A source: author's development

Digital discourse significantly influences the forms of code-switching, as online communication combines both written text and visual elements, audience reaction, and platform-specific features. Susan Herring suggests considering several aspects in computer-mediated discourse: structure, meaning, interaction, and social behavior. Structural features include spelling, graphics, new word forms, and sentence construction.

This is especially important for analyzing social networks, where code-switching can manifest itself not only in plain text but also in hashtags, nicknames, abbreviations, emojis, memes, and comments. The study of the use of different languages in online communication involves certain methodological difficulties. The main difficulty lies in the variety of materials available on social networks: posts, comments, image captions, short reactions, hashtags, and meme formulas have different structures and are not always amenable to analysis like ordinary written texts. To conduct qualitative research, it is necessary to take into account not only the linguistic form of the message but also its genre, platform, addressee, visual accompaniment, and the context of the publication. Susan Herring emphasizes that in computer-mediated discourse, it is especially important to analyze real records of online interaction rather than artificially created examples.

Identifying the boundaries of language switching in social networks is particularly difficult. The same fragment may contain borrowings, stable expressions, hashtags, transliteration, abbreviations, or complete code-switching. This requires careful classification: the researcher must be able to distinguish between the accidental use of a single word and conscious language switching as a communicative strategy. Another problem is related to informal spelling. Users can write words in both Latin and Cyrillic, with errors, abbreviations, or mix graphics, making it difficult to automatically detect the language. In studies on code-mixing in social media, it is noted that language detectors are worse at handling such texts due to non-standard writing, phonetic notation, and frequent inclusion of English elements (Kenjebaeva Zh.E., 2020, p. 23).

The ethical side of research is important. Even if publications are accessible to everyone, this does not always mean that they can be freely used in scientific work. The confidentiality of users, the possibility of identifying the author, the age of the participants in the communication, the sensitivity of the topic, and the risk of harm should be taken into ac-

count. The recommendations emphasize that when conducting Internet research, ethical decisions should be made taking into account the specific situation and not only based on the formal status of the data as "open."

The prospects for code-switching research in online communication lie primarily in the creation of more accurate research buildings. For scientific analysis, it is important to collect not just random examples but carefully systematized material. It is necessary to specify the platform, the type of message, the languages, and the form of switching, the topic of publication, and the communicative context. This approach will allow not only to describe individual cases of language confusion but also to identify stable patterns of multilingual digital communication.

The combination of qualitative and quantitative analysis is particularly promising. Qualitative analysis helps to understand the meaning of language switching in a particular message, while quantitative analysis demonstrates the frequency of certain forms, language combinations, and genre features. However, automatic methods can only be useful if there is manual verification, since digital texts often contain non-standard writing forms, emojis, hashtags, and graphic elements.

In the future, the study of the use of various languages in Kazakhstan's social networks may develop in several directions. For example, you can compare the language features of different platforms, analyze the differences between posts and comments, study the role of hashtags and visual content, and explore the language behavior of different age and professional groups. It is especially important to analyze not only textual but also multimodal forms of communication, since in social networks, meaning is often formed not only through words but also through images, emojis, videos, and audience reactions.

Conclusions

The analysis showed that the use of multiple languages in social networks of the Republic of Kazakhstan, especially in English-speaking ones, is commonplace. This process, known as "code-switching," performs not only a linguistic but also a social function. It helps users clarify meaning, express emotions, demonstrate their cultural affiliation, stay in touch with the audience, and form their online identity. In Kazakhstan, where Kazakh, Russian, and English languages are closely intertwined, favorable conditions are being created for the development of such practices. Social networks facilitate their dissemination by allowing users to freely combine various language elements, visual aids, hashtags, and informal forms of communication. Further research in this area may be aimed at creating structured digital text corpora, comparing different platforms, and exploring in-depth the relationship between "code-switching," language identity, and online communication culture.

References

Akhmetchina K. E. The linguistic situation of Kazakhstan // Slavic culture: origins, traditions, interaction. XXIII Cyril and Methodius readings: Proceedings of the International scientific-practical conference. 2022. – P. 82–88.

Dyusenbi Zh. E. The trinity of languages in Kazakhstan // Chronos. 2021. – Vol. 6. – No. 3(53). – P. 61–63.

Kenjebaeva Zh. E. Code switching: main directions of research // Colloquium-Journal. 2020. – No. 19–3(71). – P. 22–25. – DOI: 10.24411/2520-6990-2020-12067.

Kurmanova B.Zh., Utegenova A. Code switching in oral dialogic speech of Kazakhs based on the Russian, Kazakh and English languages // Sociocultural space of Russia and abroad: society, education, language. 2021. – No. 10. – P. 70–82.

The Bureau of National Statistics published a thematic collection on the Ethnic Composition of the Population Based on the Results of the 2021 Census // Official website of the Government of the Republic of Kazakhstan. – URL: https://www.gov.kz/memleket/entities/stat/documents/details/645964?lang=ru.

submitted 02.04.2026;
accepted for publication 04.04.2026;
published 30.04.2026

Contact: Aizhan.zh.ab.07@gmail.com

The Austrian Journal of Technical and Natural Sciences, 2026 No 3–4
ISSN 2310-5607

PREMIER Publishing
ppublishing.org

DOI:10.29013/AJT-26-3.4-119-125

APPLICATION OF SOLID PRINCIPLES IN BACKEND DEVELOPMENT OF MEDIA PLATFORMS: ARCHITECTURAL RESILIENCE AND IMPACT ON THE PRODUCT LIFE CYCLE

Georgii Andreev [1]

[1] Technical Director, Lead Software Developer, Individual Entrepreneur

Moscow, Russia

Cite: *Andreev G. (2026). Application of SOLID principles in backend development of media platforms: architectural resilience and impact on the product life cycle. Austrian Journal of Technical and Natural Sciences 2026, No 3–4.* https://doi.org/10.29013/AJT-26-3.4-119-125

Abstract

This article examines the application of SOLID principles in the architecture of backend systems for modern media platforms. The importance of each of the five principles of object-oriented design in creating resilient and scalable software systems is discussed. The need for modularity and loose coupling in reducing system load and improving the efficiency of the product life cycle is highlighted. Particular attention is paid to the details of implementing SOLID principles in PHP and Python-based backend systems using typing, abstractions, and testing frameworks. The article also discusses the risks involved in the architecture of anti-patterns and the role of SOLID principles in overcoming such risks. It was concluded that the SOLID principles provide an important methodological foundation for the development of software systems with high architectural resilience.

Keywords: *SOLID principles, architectural resilience, media platform, PHP, Python, scalability, product life cycle*

Introduction

Contemporary media technologies involve complex, high-load software applications supported by robust backend infrastructures for handling user requests, content delivery, and integration with external services. The growing number of users and software features makes architecture a critical factor an essential role in determining the scalability and resilience of the backend systems. Contemporary technologies have an ever-changing and rapidly evolving landscape, and the software product development lifecycle relies heavily upon the solid foundation of architecture.

One of the most well-known methods for ensuring architectural sustainability is the use of SOLID principles, which consist of a set of five guidelines for object-oriented design. These principles aim to reduce module coupling, enhance cohesion, and promote extensibility and testability of software components. In the context of backend programming in media platforms, SOLID acts as

a conceptual framework for creating modular architecture that can grow in an efficient manner. The framework is particularly important in PHP and Python-based applications, in which the flexibility of the programming language requires architectural discipline.

The objective of this article is to analyze the role of SOLID principles in enhancing the architectural stability of backend systems in media platforms and to evaluate their influence on the software product lifecycle. The study explores how these principles are implemented in multilayered system structures, APIs, and user logic modules, and demonstrates how adherence to architectural standards contributes to faster, more reliable, and more maintainable backend development.

Main part

Structure of backend architecture in media platforms and scalability challenges

Modern media platforms are built on principles of modular, hierarchically organized architecture aimed at ensuring resilience, extensibility, and technical maintainability under high load and rapid functional growth (Bogutskii A., 2025). The most widespread model is a multi-layer architectural approach, in which the logical and functional separation of the system components provides for the possibility of isolated data processing, independent development of the modules, and loosening of coupling between layers (fig. 1).

Figure 1. *Multi-layer architecture of a media platform: logical organization of the backend system*

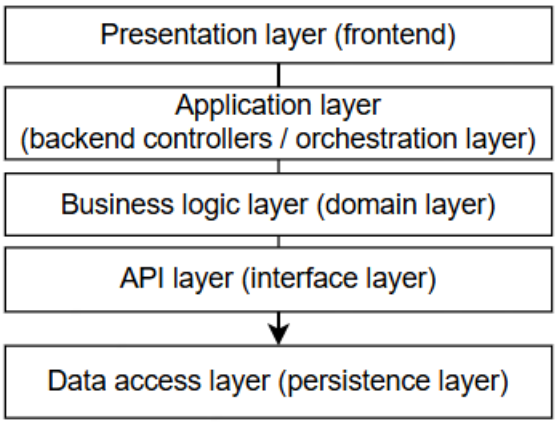

A multi-layer architecture of a media platform is organized so that each layer addresses a clearly defined set of responsibilities, thereby simplifying scalability. The presentation layer, which enables the interaction of the user with the system through Web and mobile interfaces, constitutes the top level. The application layer then takes over for the routing of requests, invocation of appropriate services, and process mediation between the user interface and business logic. Essentially, the business logic layer is responsible for the implementation of the domain rules, entity management, and computation. This makes the business logic layer the functional definition of the platform. At the interface boundary, the API surface, or the controllers/endpoints, standardize access to the platform services, including the integration of other applications. Finally, the data access layer is responsible for controlling the access to the data stored in the databases or other data systems.

However, there are several challenges that are experienced by the multi-layer system. Some of the problems include the high level of coupling between the modules, inefficient allocation of responsibilities, and the lack of flexibility in the components. A frequent issue is the blending of business logic with infrastructure code, which leads to the emergence of a “monolith,” where changing one element requires substantial rework of others. Such a structure complicates scaling, slows down development and testing, and significantly reduces fault resilience. This problem becomes particularly acute in systems that process streaming data or real-time multimedia con-

tent, where resilience and scalability are critical requirements (Smirnov A., 2025).

As software systems grow in complexity, architectural sustainability increasingly depends not only on selecting appropriate technical solutions but also on applying sound structural principles in code organization. During the evolution of media platforms, typical architectural defects are often observed that hinder scalability, modularity, and maintainability. These defects are commonly classified as anti-patterns – recurring ineffective design practices that lead to architectural degradation (table 1).

Table 1. *Common architectural anti-patterns in backend systems of media platforms (Silva N. et al., 2025; Røhne A. L. et al., 2024)*

Anti-pattern name	Description	Technical characteristics
God object	A class or module that performs too many functions, violating the Single Responsibility Principle.	Large classes with many methods and dependencies.
Spaghetti code	Unstructured, tangled logic that reduces code readability and maintainability.	Deeply nested conditionals, duplicated code, lack of modularity.
Tight coupling	Components are directly dependent on each other, reducing flexibility and reusability.	Classes instantiate other classes directly; no interfaces.
Lack of separation of concerns	Business logic is intermixed with infrastructure or presentation logic.	Business rules placed inside controllers or request handlers.
Hard-coded dependencies	Concrete implementations are hardwired into components, hindering testability and extensibility.	Direct use of specific classes; no dependency injection or abstraction.

These architectural weaknesses result in inflexibility for the system to adapt to changing demands and requirements. Architectural weaknesses systematic fix requires employing architectural design principles concerning modularity, loose coupling, and change resilience. In this context, the adoption of SOLID principles becomes a justified and methodologically grounded approach, serving as an engineering foundation for the design and evolution of backend systems in media platforms.

SOLID principles as a response to architectural risks

One of the most effective approaches to overcoming the architectural limitations discussed in the previous section is the systematic application of the SOLID principles (Ramachandrappa N. C., 2024). This acronym encompasses five fundamental principles of object-oriented design (fig. 2).

All the mentioned principles are meant to reduce the structural coupling, to introduce the feature of modularity, and to improve the changeability of the software architecture, thus making the SOLID an important engineering tool for designing scalable backend systems.

Figure 2. *SOLID principles*

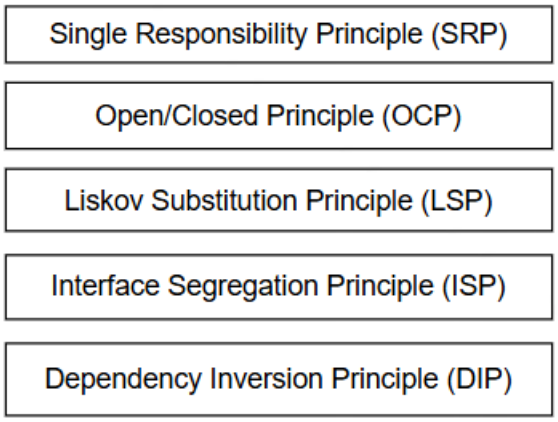

The **Single Responsibility Principle (SRP)** is defined by the fact that a class or module should change for only one reason, that is, it must serve a single purpose within a business domain. SRP is an effective means

to isolate a business logic from infrastructural logic. Using SRP can help to avoid several anti-patterns, for instance, God Object, from a system, while it is also a means to break a system into well-defined autonomous components.

The **Open/Closed Principle (OCP)** requires software entities to be open for extension but closed for modification. This is typically achieved through the creation of abstractions where new functionality should be introduced without modifying existing code. This becomes especially useful in media platform design when adding new content types, processing algorithms, or API interfaces with third-party services because such enhancements should be possible without affecting the existing stability of the system.

The **Liskov Substitution Principle (LSP)** defines that an object of a descendant class should replace an object of its base class without disrupting the program logic in any way. The correct operation of the system under the use of "inheritance" and "polymorphism" in its program logic could be severely disturbed by violated LSP principles.

The **Interface Segregation Principle (ISP)** states that clients should not be forced to depend on interfaces they do not use. This implies designing narrowly focused interfaces rather than broad, overloaded ones. In the context of APIs and service layer logic in media platforms, this reduces coupling between modules and simplifies unit and integration testing.

Lastly, the **Dependency Inversion Principle (DIP)** states the requirement for high-level modules to depend on abstractions rather than concrete implementations. In practice, DIP is often applied using inversion of control and dependency injection mechanisms, although these techniques represent implementation approaches rather than the principle itself. By decoupling objects and classes, DIP enhances architectural extensibility. In the context of backend systems for personalized content delivery and algorithmic decision-making, DIP plays a critical role in separating core business logic from specific personalization mechanisms and data-processing implementations. Such separation facilitates controlled evolution, auditability, and the substitution of algorithmic components without affecting higher-level system behavior, which is particularly important for ensuring transparency, traceability, and controlled modification of personalization logic in media platforms. This property aligns with contemporary engineering approaches in high-load backend environments that incorporate automated decision-making and personalization logic (Garifullin R., 2025).

Therefore, the SOLID principles provide a robust conceptual framework for designing architectures that are resilient to technical debt and the complexity associated with system growth. By applying these principles, developers can reduce the prevalence of common coding anti-patterns and place their software systems in a better position to manage complexity as new functionality is introduced.

Applying SOLID principles in Web Backends with PHP and Python: implementation and tooling

The application of SOLID principles in backend development using PHP and Python represents a significant engineering practice, enhancing the resilience, modularity, and adaptability of system architectures (Sharma S., 2024). Although PHP and Python differ in their typing systems and runtime characteristics, both languages provide strong support for object-oriented abstractions – such as interfaces and traits in PHP, and abstract base classes, protocols, and type annotations in Python – that facilitate SOLID-compliant designs.

Dependency management is an important aspect of applying SOLID principles in both PHP and Python backend systems. The DIP is one of the key considerations in the application of the SOLID design principles to the application architectures and designs found in the media platform space, including the abstraction from the specific implementations found in the use of the database, the payment mechanism, or the API.

The implementation of the SRP in PHP and Python involves the **use of heavy logic separation between layers.** The layers include the business layer, the controller layer, the repository layer, and the adapter layer. This is particularly useful when the application is structured in layers. The use of this principle helps in the prevention of the accu-

mulation of responsibility in any module and hence the creation of isolated modules. Similarly, the use of the OCP is mainly achieved using design patterns such as the Strategy design pattern and the Factory design pattern.

API interfaces play a central role in backend applications. In the context of SOLID, the ISP is particularly important, as it encourages the design of narrowly scoped contracts between system components. For example, different media platform services – such as user management, content publishing, and analytics – should expose independent interfaces rather than inheriting from broad, overloaded structures. This reduces component coupling and simplifies reuse.

In addition, adherence to SOLID principles significantly **simplifies unit testing and mocking.** Architectures based on abstractions and loosely coupled interfaces allow dependencies to be isolated effectively during tests. This is especially relevant for CI/CD processes and automated verification of complex system functionality. As noted in contemporary engineering literature, resilient architectures are achieved not only through formal modularity but also through design practices that constrain and control complexity growth.

Thus, applying SOLID principles in backends improves architectural quality, reduces maintenance costs, increases development velocity, and enhances the reliability of functional evolution in media platforms. This makes SOLID a foundational methodological framework for building scalable and adaptable systems.

Impact of architectural conformance to SOLID principles on the media product lifecycle

Architectural design principles, particularly SOLID, have a systematic impact on all stages of the life cycle of backend systems for media platforms – from initial design to operation, scaling, and continuous change delivery. Under conditions of highly dynamic user behavior and frequent releases, architectural decisions largely determine a system's ability to adapt to new requirements without quality degradation or increased operational risk. Applying SOLID provides a foundation for predictable architectural evolution, reducing the likelihood of technical debt accumulation and architectural decay at later life-cycle stages.

One of the key effects of SOLID conformance is improved change manageability and lower maintenance costs. Modularity, loose coupling, and reliance on abstractions allow changes to be localized within specific functional areas, which is especially important for media platforms that evolve iteratively and are subject to frequent adjustments in business logic, recommendation algorithms, and integrations with external services.

Table 2. *Impact of SOLID principles on key aspects of the media platform life cycle (Qiao R. & Yin Z., 2024)*

SOLID principle	Architectural effect	Life-cycle impact
SRP	Clear separation of component responsibilities.	Simplified maintenance and refactoring.
OCP	Extensibility without modifying existing code.	Reduced risk when introducing new functionality.
LSP	Correct substitutability and predictable behavior.	Increased stability during logic scaling.
ISP	Narrow, role-specific interfaces.	Improved testability and reusability.
DIP	Dependence on abstractions rather than implementations.	Reduced technical debt and increased adaptability.

The practical relevance of architectural approaches focused on modularity and loose coupling is supported by empirical software engineering research. Studies comparing production systems with different levels of architectural maturity report that projects exhibiting clear separation of concerns and abstraction-driven design achieve better out-

comes across key life-cycle metrics (Yanakiev I. et al., 2025; Alwi M. et al., 2025). In particular, reductions in change lead time, lower release failure rates, and shorter mean time to recovery have been observed. These findings align with widely used continuous delivery indicators – such as deployment frequency, lead time for changes, change failure rate, and mean time to restore – and indicate that architectural decisions conceptually aligned with SOLID positively affect system resilience and controllability in highly changeable environments.

Therefore, the implementation of SOLID principles in the backend design of media services has a wide-ranging effect on the product lifecycle, independent of software quality characteristics. This is because it establishes an architecturally sustainable trajectory, enables the faster delivery of changes, increases operational stability, and reduces operational costs. As complexity grows and functionalities are strained, SOLID principles serve not only as design guidelines but also as practical tools for managing architectural risk throughout the lifecycle of media products implemented in PHP and Python.

Conclusion

In the context of increasing media platform complexity and rising requirements for software system resilience, the SOLID principles represent an effective methodological framework for the design and evolution of backend architectures. Their application ensures modularity, loose coupling, and predictability in the behavior of software components, thereby improving scalability, testability, and maintainability. Applying these principles in PHP and Python backends, with available mechanisms for abstraction and typing, supports the development of adaptive software architectures. Therefore, consistent application of SOLID principles in backend development for media platforms enhances software architecture and promotes sustainable evolution.

References

Bogutskii, A. (2025) Enhancing the resilience of stream processing platforms: engineering approaches to scalability and fault tolerance. *ISJ Theoretical & Applied Science*, – 08(148). – P. 170–175.

Smirnov, A. (2025) Modern methods of backend system performance optimization: algorithmic, architectural, and infrastructural aspects. *International Journal of Advanced Research in Science, Communication and Technology*, – 5(3). – P. 262–266.

Silva, N., Rodrigues, E. and Conte, T. (2025) Evaluating Strategies for Teaching Micro Frontends: Do Anti-patterns Help? *Simpósio Brasileiro de Engenharia de Software (SBES)*, – P. 522–532.

Røhne, A. L., Pronk, B. and Akesson, B. (2024) Graph-based Anti-Pattern Detection in Microservice Applications. In: 2024 50th Euromicro Conference on Software Engineering and Advanced Applications (SEAA). *IEEE*, – P. 341–349.

Ramachandrappa, N. C. (2024) SOLID Design Principles in Software Engineering. *International Journal of Computer Trends and Technology*, – 72(9). – P. 18–23. URL: https://doi.org/10.14445/22312803/ijctt-v72i9p104

Garifullin, R. (2025) Ethical aspects of personalizing web content using Artificial Intelligence. *International Journal of Scientific Research and Engineering Development*, – 8(4). – P. 1457–1460.

Sharma, S. (2024) Modern Backend Development Technologies: A Comparative Review and Case Study. *International Conference on Emerging Trends in Expert Applications & Security*, – P. 139–151.

Qiao, R. and Yin, Z. (2024) Construction of life cycle prediction model for digital media based on virtual reality. *International Journal of Mechatronics and Applied Mechanics*, – 15. – P. 28–34.

Yanakiev, I., Lazar, B. M. and Capiluppi, A. (2025) Applying SOLID principles for the refactoring of legacy code: an experience report. *Journal of Systems and Software*, – 220. – 112254 p. URL: https://doi.org/10.1016/j.jss.2024.112254

Alwi, M., Kajang, G. and Irwanto, M. M. (2025) Implementing Modular Layouts to Increase Scalability of Production Facilities. *Journal of the American Institute*, – 2(1). – P. 64–72. URL: https://doi.org/10.71364/r93vyj15

submitted 03.03.2026;
accepted for publication 17.03.2026;
published 30.04.2026

Contact: g_andreev@outlook.com

The Austrian Journal of Technical and Natural Sciences, 2026 No 3–4
ISSN 2310-5607

PREMIER Publishing
ppublishing.org

DOI:10.29013/AJT-26-3.4-126-132

OPTIMIZATION OF STACKING ENSEMBLE MODELS FOR DECISION SUPPORT SYSTEMS BASED ON MULTIDIMENSIONAL POPULATION DEMOGRAPHICS

Ibragimov Mukhiddin Fakhraddin ugli [1],
Jumanazarov Azizbek Dilshodovich [1],
Mashiripov Behruzbek Gayrat ugli [1],
Zarifboyev Javohir Dilshod ugli [1],
Umarova Mukhlisa Khushnudbek qizi [1]

[1] Faculty of Telecommunication Technologies, Urgench State University named after Abu Rayhan Biruni, Urgench, Uzbekistan

Cite: *Ibragimov M.F., Jumanazarov A.D., Masharipov B., Zarifboyev J., Umarova M.Kh. (2026). Optimization of Stacking Ensemble Models for Decision Support Systems Based on Multidimensional Population Demographics. Austrian Journal of Technical and Natural Sciences 2026, No 3–4.* https://doi.org/10.29013/AJT-26-3.4-126-132

Abstract

Currently, significant efforts are being directed toward improving the socio-economic status of the population and digitizing the activities of local neighborhood (mahalla) institutions. In this context, the integration of machine learning methods with demographic data provides an opportunity to develop intelligent decision support systems for local executive authorities. Given that individual machine learning algorithms often encounter limitations when training on complex demographic indicators, this study implements optimization through stacking ensemble techniques. Based on nine primary parameters, XGBoost, regression algorithms, and Artificial Neural Networks (ANN) were selected as base learners and integrated into a stacking ensemble framework. The methodology involved preprocessing the database, constructing the ensemble model, and utilizing Ridge Regression as the meta-learner, with model parameters optimized via cross-validation. Experimental results demonstrate that the stacking ensemble model significantly outperforms standalone models in terms of predictive accuracy and robustness. Specifically, the stacking ensemble achieved a 36.9% improvement in performance compared to the standalone XGBoost model. This approach ensures high-precision forecasting of demographic indicators, providing a reliable foundation for decision support systems within executive government agencies.

Keywords: *Stacking algorithms, ensemble model, population demographics, decision support, machine learning, XGBoost, Ridge regression, meta-learner, digitization of mahalla activities*

1. Introduction

Demographic data are generated from various sources and are subject to changes due to various external factors. Demography plays a leading role in decision-making within self-government bodies (mahallas). Population demography provides important information on population growth dynamics, employment, and the social environment. Demographics of the population help mahallas better understand dynamic changes in the region, reduce unemployment, and make decisions on which areas to send social assistance. The stacking ensemble model has the ability to study and analyse high-level data, combining several base learners, and is capable of predicting the best decision. In this research work, algorithms are developed to construct a Stacking ensemble model using demographic data and to assist with decision-making (Yusupov F. X. X. X., Ibragimov M. F., Babayazov S. P., 2024).

2. Building Stacking Ensemble Models

2.1 Foundations of Stacking Models

The stacking ensemble model is an ensemble of hierarchical models. It first trains a few base learners based on the test data and collects their predictions in one place. It then sends these prediction results as new values along with their original values to the meta learner, which then performs a more in-depth analysis and prediction. In this way, the stacking ensemble model can effectively use the strengths of base learners and generalise their results. Compared to a single machine learning model, a stacking ensemble model can reduce the error value of a single model and improve the overall prediction outcome. Because the data in population demographics are nonlinear and complex in nature, the stacking ensemble model can identify these nonlinear and complex forms very well (Yusupov F. X. X. X. et al., 2024).

2.2 Dataset Description

The dataset consists of 500 observations, featuring 9 independent variables ('x1'–'x9') and one target variable ('Expert (%)'). The 'ID' column was excluded from the model as it serves solely as an identifier (Table 1).

Table 1. *Target variable and key dataset haracteristics*

Metric	Value
Number of observations	500
Number of features	9
Target minimum	33.48
Target maximum	109.68
Target mean	72.19
Target standard deviation	10.36

Figure 1 illustrates the socio-demographic indicators of the population across the selected neighbourhoods for the study, along with their respective statistical values (Ibragimov M. F., Khujaev O. K. and Rakhimboev K. J., 2023).

Table 2. *Table of demographic indicators obtained across neighborhoods (mahallas)*

Id	*x1*	*x2*	*x3*	*x4*	*x5*	*x6*	*x7*	*x8*	*x9*	*Expert (%)*
1	0.13	0.18	0.15	0.16	0.38	0.29	0.05.	0.26	0.21	78.45
2	0.27	0.19	0.27	0.26	0.54	0.37	0.06	0.34	0.23	76.55
3	0.2	0.26	0.31	0.35	0.53	0.04	0.04	0.07	0.16	68.15
4	0.36	0.31	0.24	0.41	0.3	0.26	0.38	0.4	0.3	83.9
5	0.32	0.23	0.34	0.4	0.43	0.0	0.05	0.12	0.27	53.34
6	0.22	0.15	0.23	0.24	0.28	0.17	0.14	0.2	0.14	75.95
500	0.07	0.14	0.07	0.12	0.3	0.35	0.04	0.19	0.05	89.16

In Figure 2, during the process of evaluation, the data were divided into training and testing sets in an 80/20 ratio. The standardisation method (StandardScaler) was applied to all models, which is particularly important for polynomial and neural network models (Ibragimov M., Babajanov B., Sapayev S., Otaboyeva M., Aliev O. and Rakhimberdiev S., 2025).

Figure 2. *Flowchart of the Stacking Ensemble model architecture*

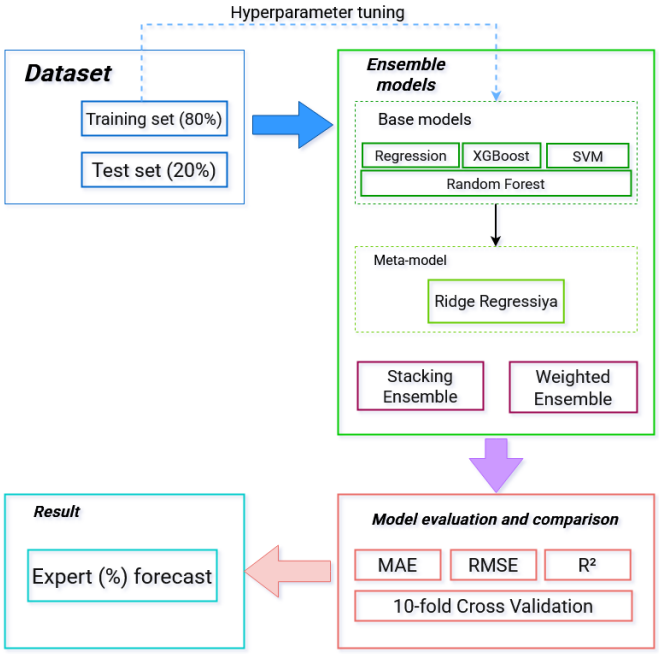

2.3 Formula and steps

Input data set:

$$D = \{D_1, D_2, D_3, \ldots, D_n\} \quad (1)$$

and the output data:

$$Y = \{Y_1, Y_2, Y_3, \ldots, Y_n\} \quad (2)$$

is formed in the following way, where D_i is a set of demographic and socio-economic indicators from the "mahalla passport" (population size, number of unemployed, entrepreneurial employment, etc.), and Y_i is the integral class of the mahalla chairman's activity calculated based on these indicators (Ibragimov M., Babajanov B., Sapayev S., Otaboyeva M., Aliev O. and Rakhimberdiev S., 2025).

Qualitative assessments are converted to numerical form, lost values are recovered, data are normalized and divided into training, validation and test sets (Ali, T. E. 2025).

Several base models are formulated based on the input data (1). They are defined as follows:

$$h_1(D_i) = \hat{Y}_i^{(1)}, h_2(D_i) = \hat{Y}_i^{(2)}, \ldots, \quad h_M(D_i) = \hat{Y}_i^{(M)} \quad (3)$$

where h_1, h_2, h_3, ..., h_M –are base models, for example, Random Forest, XG Boost, SVM, and artificial neural network; $Y_i^{(M)}$ – is the estimation result of the *m*-th model for the ^{i}-th object.

For each object (3), a new vector consisting of the outputs of the base models is created:

$$Z_i = \left(\hat{Y}_i^{(1)}, \hat{Y}_i^{(2)}, \ldots, \hat{Y}_i^{(M)}\right)^T \quad (4)$$

The formed Z_i vector (4) is passed to the meta-model of the stacking ensemble:

$$\hat{Y}_i = g(Z_i, \phi) = g\left(\hat{Y}_i^{(1)}, \hat{Y}_i^{(2)}, \ldots, \hat{Y}_i^{(M)}, \varphi\right) \quad (5)$$

where g – is the meta-learner, i.e., Logistic Regression, Linear Regression, or another top-level model; φ – are the parameters of the meta-model.

Meta-model parameters (4) are determined by minimizing the following loss function:

$$\varphi^* = \arg\min \frac{1}{n} \sum_{i=1}^{n} L\left(Y_i, \hat{Y}_i\right) \quad (6)$$

If the problem is considered as a multiclass classification, then cross-entropy is taken as the loss function (5):

As a result, a final assessment or integral class (6) is obtained for each object (3):

$$Z_i = \left(\hat{Y}_i^{(1)}, \hat{Y}_i^{(2)}, \ldots, \hat{Y}_i^{(M)}\right)^T \quad (7)$$

As a result of this stage, the current state of the mahalla chairman's activities is assessed in specific numerical values. Based on the analysis of demographic and social indicators, a numerical rating of the chairman's performance is calculated, which allows for

the quantitative identification of weak and priority areas and the formation of a final integral score that serves as the basis for making management decisions (Yao, J., 2022).

2.4 Meta-learner preferences

The final stage of the stacking ensemble approach involves the formation of a meta-model (meta-learner) that generalizes the predictions obtained from the underlying models. In this study, the Ridge regression method was selected as the meta-learner. Ridge regression was selected to effectively manage the high correlation between the base models (Linear regression, Polynomial regression, and XGBoost, MLP) and to prevent overfitting. The metamodel was trained with the prediction results in the test set of the base models (Zhao, S., 2023).

3. Model Comparison

Population demographic data often include multimodal indicators, and each indicator influences the final result in a different, non-linear way. Random Forest, XGBoost, and an artificial neural network were developed for the stacking ensemble model as base learning models, and this helps to understand the structure and characteristics of complex data (Obaidat, M. A., 2022).

In this study, five different regression approaches were used to predict demographic indicators: linear regression, polynomial regression, and XGBoost algorithms were selected as the base models. Also, two different ensemble learning methods were used to further increase prediction accuracy: Voting ensemble and Stacking ensemble. The study was based on a dataset of 500 observations. The following metrics were used for the assessment: MAE (Mean Absolute Error), RMSE (Root Mean Squared Error) and R^2. The smaller the MAE and RMSE, the lower the model error; The larger the R^2, the better the model explains (Table 2).

Tabel 2. *Comparative analysis of predictive accuracy indicators for various regression and ensemble models*

Model	MAE	MSE	R^2
Stacking ensemble	2.7810	3.8113	0.8655
Voting ensemble	2.8498	3.8686	0.8615
Polynomial regression	3.1296	4.2210	0.8351
Neural network	3.1613	4.5009	0.8125
Linear regression	3.7435	4.9209	0.7758

The results indicate that the best model is the Stacking ensemble, which achieved an R^2 of 0.8655, an RMSE of 3.8113, and an MAE of 2.7810. This demonstrates that the ensemble approach provides a more stable and accurate outcome compared to using the base models individually.

4. Cross-Validation and Model Evaluation

In this part, we compare the performance of different models using 10-fold cross validation. The KFold scheme (n_splits=10, shuffle=True, random_state=42) was used to assess the model's reliability. In this case, the dataset is divided into 10 equal or nearly equal parts. In each iteration, 9 slices were used for training and 1 slice for testing. This process was repeated 10 times, and each time a different slice served as a test set. The reason for choosing 10-fold cross validation is that it allows for a more stable assessment of the model's generalizability than a one-time training/test split. Through this method, each object falls into the test set at least once, and the evaluation result is less affected by random division. The MAE, RMSE, and R^2 > metrics were used as evaluation criteria. MAE is the mean absolute error, RMSE is the root mean square error sensitive to large errors, and R^2 (the coefficient of determination) shows how well the model explains the target variance. Each model was constructed in the form of a Pipeline. Within the pipeline, StandardScaler was applied in the first stage to bring all features to the same scale. This is particularly important for polynomial regression, as features with large ranges can negatively affect the optimization process.

The XGBoost regressor has the ability to capture complex, non-linear relationships in tabular data. In the model architecture, hidden layers in the form of (24,12) and the ReLU activation function were utilized. On this dataset, the XGBoost results were lower than those of the base regression models, which is explained by the small size of the dataset or the sensitivity of the parameters.

4.1 Results

The results of the 10-fold cross validation showed that the highest average R^2 value belonged to the weighted ensemble model. Therefore, combining several model predictions slightly improved the quality of the regression.

Polynomial regression came in second, giving a significantly better result than linear regression. This means that there are not only purely linear, but also quadratic or mutual relationships between the target and the features.

The XGBoost model demonstrated an average result. This indicator is lower than that of linear and polynomial models. The main reasons for this are that this algorithm usually works well with large volumes of data and very complex structured data. The presence of the XGBoost model within the ensemble helped to increase overall accuracy. This aspect is also an important scientific conclusion for the report.

4.2. Analysis

A comparison of regression models constructed using 10-fold cross-validation on the given dataset revealed that the weighted ensemble model delivered the best results. Therefore, this model is recommended for practical application.

To further improve model accuracy in future research, it is advisable to employ feature engineering, utilize gradient boosting algorithms such as CatBoost, and perform a detailed outlier analysis on the target variable.

This report provides a step-by-step breakdown of all processes: data preparation, cross-validation, individual models, the ensemble approach, and analysis based on metrics.

Detailed statistical parameters of the data used in the study are provided in Table 3 (Yao, J. 2022).

Overall Results of 10-fold Cross-Validation

Table 3.

Model	MAE mean	MAE std	RMSE mean	RMSE std	R^2 mean	R^2 std
Weighted ensemble	3.08237	0.379148	4.14259	0.540962	0.83108	0.028052
Polynomial Regression	3.16231	0.277158	4.30682	0.479376	0.81245	0.049167
Linear Regression	3.80358	0.529469	5.02448	0.827705	0.75334	0.044238
XGBoost	4.63093	0.540915	6.24507	0.761617	0.61125	0.089039

The study utilizes a 10-fold Cross Validation approach to evaluate and compare model performance through metrics such as R^2, MAE, and RMSE. Analysis of these results indicates that the Weighted Ensemble model achieves the highest level of accuracy, notably surpassing the performance of individual base models and other algorithmic configurations.

Additionally, while the polynomial regression model also achieved a high result, the ensemble approach ensured prediction stability by combining the advantages of several base models. In contrast, the XGBoost algorithm recorded the lowest R^2 score for this specific dataset. This situation confirms how effective the selected weighted ensemble model is at representing complex demographic dependencies.

The analysis shows that the Weighted ensemble model registered the lowest error, demonstrating the highest prediction accuracy. In contrast, the XGBoost algorithm was found to have the highest error for this metric. These results are consistent with the previous R^2 analyses, once again confirming

the effectiveness of the ensemble approach in handling demographic data.

Figure 3 presents the performance dynamics of the models used in the study across the cross-validation folds. The graph indicates that the Weighted Ensemble and Polynomial Regression models maintained high stability across all folds, whereas XGBoost exhibited the greatest fluctuation and a comparatively low accuracy.

Figure 3. *dynamics across individual folds*

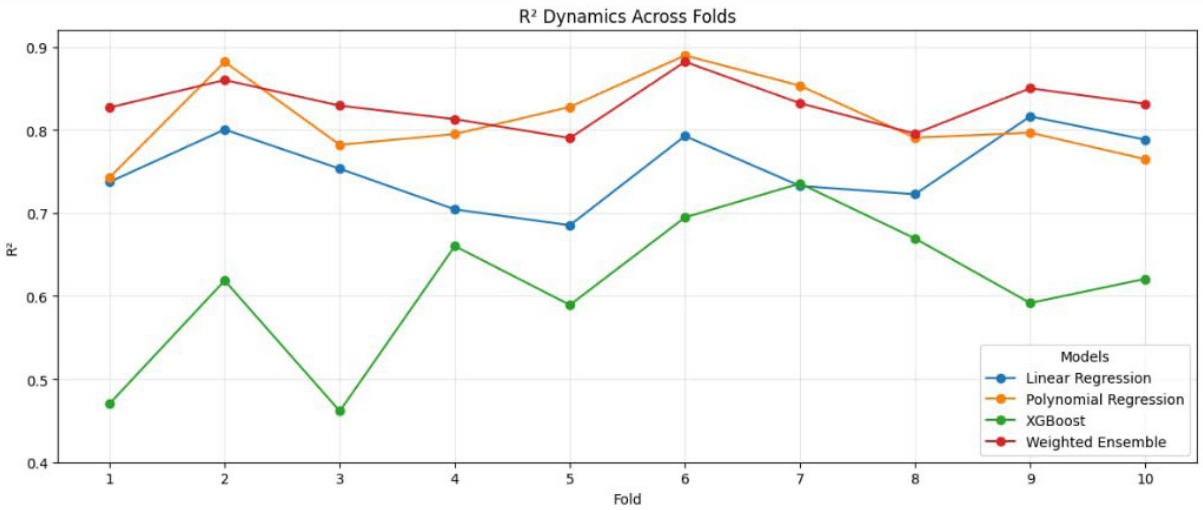

5. Practical Application of the Obtained Results

Based on the obtained results, we implement the demographic data within intelligent decision support systems for executive authorities using a framework we define as a decision tree. In this approach, we integrated demographic indicators with regional health improvement data and Key Performance Indicator (KPI) system results to reach a final decision.

6. Conclusion

Within the framework of this study, a machine learning-based intelligent algorithm was developed to digitize the analysis and forecasting of demographic indicators within local executive authorities. During the data preprocessing stage, techniques for systematic normalization, standardization, and the imputation of missing values were applied. To ensure model validation, the dataset was partitioned into an 80/20 ratio and verified using a 10-fold cross-validation method.

Various hierarchical algorithms, including Linear and Polynomial Regression, Random Forest, XGBoost, SVM, and MLP, were tested to model demographic dynamics. To maximize predictive accuracy, a Stacking Ensemble methodology was implemented, wherein the outputs of the base models were analyzed as meta-features through Ridge Regression (acting as the meta-model).

The Stacking Ensemble model demonstrated superior accuracy compared to traditional models in identifying complex and nonlinear relationships among demographic factors. The system proves robust against ‘noise’ and anomalous fluctuations in demographic data, exhibiting a high degree of generalization capability. Notably, the meta-learner-based Stacking model significantly outperformed individual models (improving upon XGBoost by 36.9%).

References

Yusupov F. X. X. X., Ibragimov M. F., Babayazov S. P. Prediction of Interactions Between Social Groups and Decision-Making Using Fuzzy Models //2024 IEEE 3rd International Conference on Problems of Informatics, Electronics and Radio Engineering (PIERE). – IEEE, 2024. – P. 1520–1523.

Yusupov F. X. X. X. et al. Improving the Computing Accuracy of the AI Ascend Processor: Research and Results //2024 IEEE 3rd International Conference on Problems of Informatics, Electronics and Radio Engineering (PIERE). – IEEE, 2024. – P. 1510–1513.
Ibragimov M. F., Khujaev O. K. and Rakhimboev K. J. "Development of a Module for Evaluating the Activity of the Mahalla Chairpersons Based on the Experts' Assessment with the Help of Machine Learning Algorithms," 2023 IEEE XVI International Scientific and Technical Conference Actual Problems of Electronic Instrument Engineering (APEIE), Novosibirsk, Russian Federation, 2023. – P. 1730–1733. Doi: 10.1109/APEIE59731.2023.10347584.
Ibragimov M., Babajanov B., Sapayev S., Otaboyeva M., Aliev O. and Rakhimberdiev S. "Scientifically Grounded Model for Managing and Evaluating Community Health-Promotion Activities at the Mahalla Level," 2025 IEEE XVII International Scientific and Technical Conference on Actual Problems of Electronic Instrument Engineering (APEIE), – Novosibirsk, Russian Federation, 2025. – P. 1–6. Doi: 10.1109/APEIE66761.2025.11289459.
Ali, T. E. A Stacking Ensemble Model with Enhanced Feature Selection for Distributed Denial-of-Service Detection in Software-Defined Networks / T. E. Ali, Y. W. Chong, S. Manickam [et al.] // Engineering, Technology & Applied Science Research. 2025. – Vol. 15. – No. 1. – P. 19232–19245.
Lu, M. A Stacking Ensemble Model of Various Machine Learning Models for Daily Runoff Forecasting / M. Lu, Q. Hou, S. Qin [et al.] // Water. 2023. – Vol. 15. – No. 7. – Art. 1265.
Divina, F. Stacking Ensemble Learning for Short-Term Electricity Consumption Forecasting / F. Divina, A. Gilson, F. Goméz-Vela [et al.] // Energies. 2018. – Vol. 11. – No. 9. – Art. 949.
Yao, J. Applications of Stacking/Blending ensemble learning approaches for evaluating flash flood susceptibility / J. Yao, X. Zhang, W. Luo [et al.] // International Journal of Applied Earth Observation and Geoinformation. 2022. – Vol. 112. – Art. 102932.
Zhao, S. Stacking Ensemble Learning-Based [18F]FDG PET Radiomics for Outcome Prediction in Diffuse Large B-Cell Lymphoma / S. Zhao, J. Wang, C. Jin [et al.] // Journal of Nuclear Medicine. 2023. – DOI: 10.2967/jnumed.122.265244.
Obaidat, M. A. Machine Learning Stacking Ensemble Model for Predicting Heart Attacks / M. A. Obaidat, A. Alexandrou, S. Sanacore // ALLDATA 2022: The Eighth International Conference on Big Data, Small Data, Linked Data and Open Data. 2022.
Golder, K. An Empirical Study on Developing Stacking Ensemble Model for Bangla Sports Sentiment Analysis / K. Golder, P. Biswas, M. S. Islam [et al.] // 15th International Conference on Computing Communication and Networking Technologies (ICCCNT). 2024.

submitted 06.03.2026;
accepted for publication 20.03.2026;
published 30.04.2026

Contact: imuhiddin293@gmail.com

The Austrian Journal of Technical and Natural Sciences, 2026 No 3–4
ISSN 2310-5607

PREMIER Publishing
ppublishing.org

Section 4. Earth science

DOI:10.29013/AJT-26-3.4-133-139

MINERALOGICAL AND STRUCTURAL CHARACTERISTICS OF RARE EARTH ELEMENTS IN INDUSTRIAL WASTE FROM HIGH-TECHNOLOGY PRODUCTION

Iuliia Kukula [1]

[1] PhD Candidate in Sustainable Energy, Arizona State University

Cite: *Kukula I. (2026). Mineralogical and Structural Characteristics of Rare Earth Elements in Industrial Waste from High-Technology Production. Austrian Journal of Technical and Natural Sciences 2026, No 3–4.* https://doi.org/10.29013/AJT-26-3.4-133-139

Abstract

This article examines the distribution, chemical form, and phase state of rare earth elements in industrial waste from high-tech production. The specifics of the presence of neodymium, dysprosium and samarium in electronic waste, permanent magnet waste and battery systems are investigated, taking into account the influence of technological and operational factors. The relationship between their mineralogical and structural characteristics and the choice of rational technological routes for recycling is analyzed. The role of structural features of man-made materials as an important factor in the formation of effective schemes of secondary involvement in the framework of a closed-loop economy is studied.

Keywords: *rare earth elements, technogenic waste, neodymium, dysprosium, samarium, secondary processing, circular economy*

Introduction

Rare earth elements (REE) remain particularly important raw materials for high-technology industries, as they determine the functional properties of permanent magnets, electronic components, and a range of electrochemical systems. At the same time, the growth of production and the rapid renewal of equipment lead to increasing flows of industrial waste and electronic scrap, in which secondary concentrations of REE are formed that may be comparable in significance to natural sources. The relevance of this study is обусловлена the fact that access to these elements is increasingly limited not so much by geological reserves as by technological barriers to their extraction. Processing efficiency depends on the chemical form and phase state in which the elements occur in specific types of waste.

From a practical point of view, neodymium, dysprosium, and samarium are of particular interest as important components of high-energy magnetic materials and functional blocks of modern electronics, as well as elements that may be present in battery waste and related technological chains. However,

their industrial processing is complicated by heterogeneity, the presence of multicomponent matrices, and the formation of stable phases and surface passivating layers. The aim of this study is to investigate the mineralogical and structural characteristics of REE in industrial waste from high-technology production and their significance for selecting technological routes for secondary processing.

Main Part

Distribution, Chemical Form, and Phase State of REE in Industrial Waste from High-Technology Production

In technogenic waste from high-technology production, REE are characterized by pronounced phase and spatial heterogeneity, which fundamentally distinguishes them from natural raw materials. Whereas in ores these components are typically concentrated in relatively stable mineral phases, in waste they are incorporated into functional materials and fixed in the form of intermetallic, oxide, phosphate, or glassy phases formed during manufacturing processes and subsequent product operation.

In electronic waste, the main share of **neodymium and dysprosium** is localized in permanent magnets used in loudspeakers, electric drives, fans, data storage devices, and vibration modules. This results in a low average content of REE in mixed electronic scrap while simultaneously producing high local concentrations in separated magnetic components (Khandekar P. P. et al., 2025). Within such fragments, these elements are predominantly present in intermetallic phases structurally bound to an iron-based metallic matrix, with the dominant carrier phase typically represented by $Nd_2Fe_{14}B$. This determines high potential recoverability upon matrix destruction but reduces selectivity due to the simultaneous involvement of accompanying metals. Outside magnetic assemblies, the target elements occur in significantly smaller amounts and are usually represented by secondary products. These include oxide and hydroxide forms arising from corrosion and degradation of surface coatings, such as Nd_2O_3, Dy_2O_3, Fe_2O_3, and Fe_2O_4, as well as fine particles generated during mechanical crushing and concentrated in fine fractions.

Samarium in electronic waste streams is distributed less uniformly and is mainly associated with specialized magnetic and ceramic components. In such materials, it is usually present in a trivalent state and is isomorphically incorporated into a crystalline or amorphous oxide matrix, which increases chemical stability and limits its availability for selective extraction without intensifying processing conditions (Al-Dossari M. et al., 2024).

The most concentrated and technologically attractive source of REE is **waste from permanent magnetic materials**. In neodymium–iron–boron alloys, the main component forms the crystalline phase that determines the magnetic properties, most commonly $Nd_2Fe_{14}B$. **Dysprosium**, in turn, is introduced in smaller amounts and is distributed predominantly in near-surface regions of grains and along their boundaries, where it performs a function of structural stabilization at elevated temperatures.

In the initial materials, the chemical form of these elements corresponds to intermetallic phases; however, after products are taken out of service and during the storage of magnetic waste, partial oxidation occurs with the formation of oxides and mixed oxide–iron compounds, including Nd_2O_3, Dy_2O_3, and Fe-oxide phases such as Fe_2O_3 and Fe_2O_3. These secondary products are characterized by increased porosity and reactivity, which may accelerate the initial stages of dissolution but simultaneously alter process selectivity due to the formation of passivating shells and the redistribution of components across microstructural regions. **Samarium** in this group of streams is mainly associated with materials based on the samarium–cobalt system, where it is also present in an intermetallic state, most commonly as $SmCo_5$ and *Sm2Co17*, and exhibits higher thermal and chemical stability (Cherkezova-Zheleva Z. et al., 2024).

In battery and accumulator waste, REE are generally present at significantly lower concentrations and are more often fixed in an oxidized state, while their localization depends on the composition of specific batches and the degree of stream mixing. Within the technogenic systems considered, they may occur as impurities and local inclusions, as well as components of stable oxygen-containing compounds, which brings

their chemical behavior closer to the oxide and secondary forms characteristic of certain electronic waste streams. For such flows, technologically significant factors include the stability of compounds in the presence of phosphorus- and fluorine-containing components, which may promote the formation of stable phases such as $REEPO_4$ and $REEF_3$, and a high impurity load, which determines the need for preliminary carrier separation and more stringent requirements for selective purification (Akhmetov N. et al., 2023).

Thus, the distribution and chemical form of neodymium, dysprosium, and samarium in electronic waste, permanent magnets, and battery waste are determined by the type of technogenic material and its operational history. The identified differences define the choice of technological routes and limiting stages of extraction, including dissolution kinetics and requirements for selective separation.

Methods of Secondary Processing of REE

Secondary processing of REE from high-technology production waste requires consideration of their phase state, degree of oxidation, and the nature of their bonding with the material matrix. Neodymium, dysprosium, and samarium exhibit fundamentally different chemical behaviors, which predetermine the choice of processing route. In industrial practice, three basic classes of methods have been established, each possessing specific advantages and limitations.

Hydrometallurgical approaches are based on transferring the target components into an aqueous phase followed by selective separation and upgrading of the product to an industrially relevant quality (Binnemans K. & Jones P. T., 2023). This approach includes several important sequential operations (fig. 1).

Figure 1. *Stages of the Hydrometallurgical Approach*

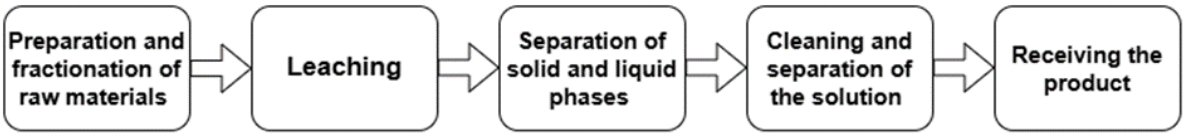

At the **preparation stage**, mechanical disintegration and, if necessary, fractionation of the material is performed, which increases the reactivity of the phases and reduces the effect of heterogeneity in the initial flow. This is followed by **leaching**, during which the target components are transferred into solution. The choice of acidic or alkaline media is determined by the type of matrix and the chemical form of the components, while a technologically significant limitation is the competitive dissolution of accompanying metals, which increases the load on subsequent purification stages. Next, **solid-liquid separation with residue washing is carried out**, which reduces losses of target components and stabilizes the solution composition for subsequent operations. The final part of the route includes **solution purification and separation, as well as the production of the target product**. Fluorine and phosphorus-containing components have a significant influence on all the listed stages. Their presence may stabilize target elements in poorly soluble forms, thereby increasing the requirements for process conditions and the depth of subsequent purification.

Pyrometallurgical methods rely on thermal treatment of the feed material and redistribution of components among phases during smelting, reduction, or high-temperature processing. Their technological advantage lies in high throughput and tolerance to feed heterogeneity (Raabe D., 2023). Mixed fractions can be processed without complete chemical dissolution, and separation is achieved through phase segregation between the metallic phase, slag, and gaseous components (fig. 2).

For REE, the main mechanism is their transition to certain phases during the melting process. Depending on the matrix composition and slag-forming additives, they may concentrate in the slag phase, forming a concentrate suitable for subsequent hydrometallurgical recovery. Thus, pyrometallurgy often serves as a stage of preliminary concentration and stabilization of composition during the processing of structurally complex waste.

Figure 2. *Scheme of the Pyrometallurgical Approach*

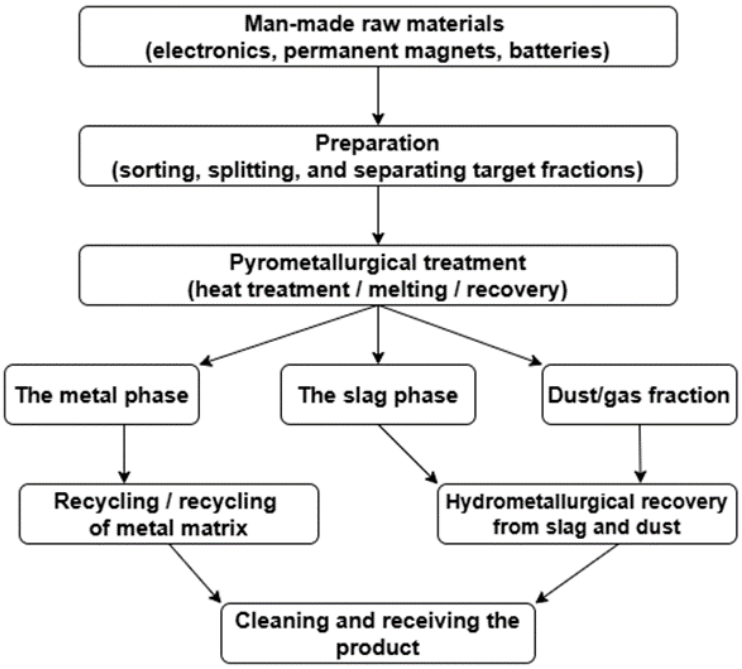

The limitations of this approach are associated with high energy consumption and the need for advanced environmental infrastructure. Industrial feasibility is achieved primarily in the presence of large-scale material flows and access to high-temperature processing facilities.

Biological methods are based on the use of microorganisms or biogenic materials to mobilize REE from the solid phase or to selectively bind them from solutions. In **bioleaching**, the main mechanisms include the formation of organic acids, changes in redox conditions, and the formation of complexing compounds capable of transferring valuable elements into solution without the use of aggressive chemical reagents (fig. 3).

Figure 3. *Bioleaching Scheme*

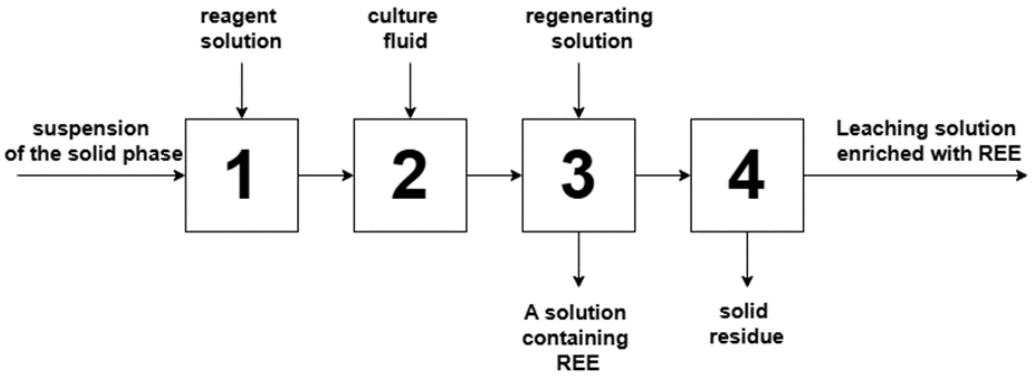

Biosorption, by contrast, is focused on the recovery of REE from liquid phases through binding to functional groups of biopolymers and cell surfaces. This approach can be used as a stage of concentration or final purification (Shi S. et al., 2023).

A common feature of these approaches is a potentially lower environmental burden when the process is properly organized, as well as reduced requirements for equipment corrosion resistance. At the same time, they are limited by low process rates, high sensitivity to feed composition and environmental parameters, and the inhibiting effects of ionic impurities as well as fluorine and organic-containing compounds.

The technology selection matrix should take into account the type of waste and the predominant forms of occurrence of REE. These parameters determine where losses arise, and which stages become limiting (table 1).

Table 1. *Technological Routes Depending on Waste Type and Forms of Occurrence of REE (Balaram V., 2023; Zhao T. Y. et al., 2025)*

Waste stream	Dominant carrier phases and chemical forms of neodymium, dysprosium and samarium	Recommended recovery approach
Electronic waste	Localization in individual components; more often intermetallides, oxide/sorbed forms in fine fractions.	Increase the concentration of target elements by fractionation; then extract hydrometallurgically with subsequent purification.
Permanent magnet waste	Intermetallides; partially oxide/hydroxide surface forms.	Direct hydrometallurgical extraction is most effective; pyrometallurgy is appropriate as a concentration/stabilization stage in hybrid schemes.
Battery waste	More often trace/local; mainly sorbed/complex and oxide forms; stable phosphate-fluoride compounds are possible.	The soft stages of additional recovery/concentration and work on selected media are advisable; the final quality is achieved by chemical purification.

Overall, industially sustainable solutions are more often formed as **combined schemes**, since none of the method classes simultaneously addresses the tasks of concentration, selectivity, and production of a product with the required purity under high variability of technogenic streams. The most typical logic includes pre-concentration to reduce impurity load and increase the share of REE, followed by the main extraction stage and concluding with purification. Such a hybrid configuration makes it possible to simultaneously increase recovery rates, maintain selectivity with respect to iron, cobalt, and nickel, and reduce environmental risks through controlled handling of solutions, sludges, and gaseous emissions.

Circular Economy and the Effect on Business Sustainability

Secondary processing of REE within the logic of the circular economy allows for simultaneously increasing resource efficiency and reducing the operational risks of companies that use critical materials. For neodymium, dysprosium, and samarium, this is important not only from an environmental perspective, but also because waste recycling creates an additional source of raw materials and helps maintain access to them under conditions of price volatility and potential supply constraints.

A reduction in the cost of access to these components is achieved through **changes in the value creation chain**. In secondary processing, part of the costs is shifted to the collection, sorting, and preparation of waste, after which extraction is carried out from more concentrated technogenic fractions and from a smaller mass of material per unit of product. An additional advantage is associated with procurement controllability. The availability of an in-house or contract-based secondary stream reduces dependence on the spot market, simplifies planning, and makes costs more predictable, thereby reducing losses caused by supply disruptions.

Supply resilience is enhanced through **source diversification**. Secondary raw materials form an alternative supply channel tied to processing infrastructure and the geography of consumption rather than to deposits and primary processing capacities. At the same time, waste recycling reduces the burden on primary extraction, as part of demand is met through the return of materials into circulation. For businesses, this means lower environmental and regulatory risks, as well as more transparent material

provenance, which is important for compliance with sustainable development requirements and supply chain management.

The implementation of such loops depends on **practical conditions of deployment**. It is essential to ensure the quality of input materials, specifically a predictable composition and impurity control, which is achieved through sorting and the separation of target fractions. Logistics of collection and the regularity of waste inflows are equally important, since without sufficient volumes it is difficult to ensure economic efficiency and stable capacity utilization. In addition, standardization and traceability are required. Finally, industrial safety is a mandatory condition, including the safe handling of reactive media, sludges, and dust fractions, as well as compliance with emission and disposal requirements.

Thus, secondary processing of REE within a circular economy model provides not only environmental benefits but also measurable business value by reducing raw material risks and increasing cost predictability. The most sustainable results are achieved when technological efficiency of extraction is combined with appropriate organizational conditions for implementation.

Conclusion

In modern high-technology industries, critical materials are increasingly considered not only as resources but also as factors of technological sustainability of production chains. With respect to technogenic waste, it has been shown that such waste forms a heterogeneous yet promising source of REE, primarily neodymium, dysprosium, and samarium. Their distribution and chemical state are determined by the type of technogenic material and operating conditions. Magnetic waste is characterized by high local concentrations and a predominance of intermetallic phases, whereas electronic and battery streams more often contain secondary oxides and stable compounds formed during oxidation and mechanical degradation.

A comparative analysis of processing approaches demonstrates that combined routes integrating feed pre-enrichment and fractionation with hydrometallurgical extraction followed by deep purification exhibit the highest industrial sustainability. The practical implementation of a circular economy in this field requires not only technological optimization but also the assurance of input material quality, stable collection logistics, stream standardization, and compliance with industrial safety requirements, which together reduce raw material risks, increase cost predictability, and decrease the burden on primary extraction.

References

Khandekar, P. P., Dash, B., Yadav, M. D. (2025) Recent advances in the recovery of neodymium and dysprosium from industrial waste. *Metal Value Recovery from Industrial Waste Using Advanced Physicochemical Treatment Technologies*. – P. 295–316.

Al-Dossari, M., Saeedi, A. M., Althomali, R. H., Solre, G. F., Asif, S. U., Ahmed, I., Alqahtani A. (2024) Rare earth samarium substituted barium-calcium hexaferrites: Insight into structure, dielectric and magnetic aspects. *Inorganic Chemistry Communications*, – 170 (1). – 113252 p. URL: https://doi.org/10.1016/j.inoche.2024.113252

Cherkezova-Zheleva, Z., Burada, M., Sobetkii, A. E., Paneva, D., Fironda, S. A., Piticescu R. R. (2024) Green and sustainable rare earth element recycling and reuse from end-of-life permanent magnets. *Metals*, – 14 (6). – 658 p. URL: https://doi.org/10.3390/met14060658

Akhmetov, N., Manakhov, A., Al-Qasim, A. S. (2023) Li-ion battery cathode recycling: an emerging response to growing metal demand and accumulating battery waste. *Electronics*, – 12 (5). – 1152 p. URL: https://doi.org/10.3390/electronics12051152

Binnemans, K., Jones, P. T. (2023) The twelve principles of circular hydrometallurgy. *Journal of Sustainable Metallurgy*, – 9 (1). – P. 1–25. URL: https://doi.org/10.1007/s40831–022-00636-3

Raabe, D. (2023) The materials science behind sustainable metals and alloys. *Chemical reviews*, – 123 (5). – P. 2436–2608. URL: https://doi.org/10.1021/acs.chemrev.2c00799

Shi, S., Pan, J., Dong, B., Zhou, W., Zhou, C. (2023) Bioleaching of rare earth elements: perspectives from mineral characteristics and microbial species. *Minerals*, – 13 (9). – 1186 p. URL: https://doi.org/10.3390/min13091186

Balaram, V. (2022) Sources and applications of rare earth elements. In "Environmental Technologies to Treat Rare Earth Elements Pollution: Principles and Engineering." *IWA Publishing*, – 113. – P. 75–114. URL: https://doi.org/10.2166/9781789062236_0075

Zhao, T. Y., Li, W. L., Kelebek, S., Choi, Y., Wu, C. Q., Zhang, W. J., Sadri, F. (2025) A comprehensive review on rare earth elements: resources, technologies, applications, and prospects. *Rare Metals*, – 44 (10). – P. 7011–7040. URL: https://doi.org/10.1007/s12598-025-03459-9

submitted 03.03.2026;
accepted for publication 17.03.2026;
published 30.04.2026

Contact: uliakukula@rambler.ru

The Austrian Journal of Technical and Natural Sciences, 2026 No 3–4
ISSN 2310-5607

PREMIER Publishing
ppublishing.org

Section 5. Food processing industry

DOI:10.29013/AJT-26-3.4-140-146

ACTIVATING FOUNDATION FOR THE DEVELOPMENT OF COMBINED SOFTWARE PRODUCTS (Compositional integrated technical solutions as a necessary foundational framework for the development of combined software products equivalent to comprehensive system-level integrative inventions)

Liubov Skokova [1]

[1] Specialist in high-quality food production, American English Academy Petropavlovsk-Kamchatsky, Russia

Cite: *Skokova L. (2026). Activating Foundation for the Development of Combined Software Products. (Compositional integrated technical solutions as a necessary foundational framework for the development of combined software products equivalent to comprehensive system-level integrative inventions). Austrian Journal of Technical and Natural Sciences 2026, No 3–4.* https://doi.org/10.29013/AJT-26-3.4-140-146

Abstract

This article examines the growing integration of complex combined software products into modern industrial, commercial, and technological processes, where digital systems increasingly consist of numerous interrelated functional elements originally developed as independent or weakly connected components. The article emphasizes the need for fundamentally new approaches to the design and structuring of technical architectures capable of integrating such disparate elements into unified functional systems. Particular attention is devoted to substantiating the necessity of developing compositional and integrative technical solutions as the foundational basis for creating advanced combined software products. The study analyzes the technological, structural, and organizational prerequisites for such integration, including the increasing complexity of digital infrastructure, the development of multifunctional cyber-physical systems, and the growing demand for scalable and interoperable software architectures. It is demonstrated that the implementation of compositional integrative technical solutions enhances system interoperability, improves operational reliability, reduces structural redundancy, and enables the creation of scalable platforms for application in smart manufacturing, intelligent infrastructure, industrial automation, and other high-technology sectors. The article concludes that compositional integrative technical solutions constitute a key technological foundation for the development of the next generation of combined software products.

Keywords: *Combined software products, compositional integrated technical solutions,*

characteristics and properties of fundamentally new materials and their combinations with traditional materials. achievement of smart manufacturing level, presence of composite materials, particularly carbon – carbon composites. formation of positive perception of new products, real-time quality control capabilities at all stages of the production process

Introduction:

The near-complete transition of developed economies to innovative methods of planning and management establishes new qualification criteria for the technical solutions being applied. Under such conditions, any type of production must progressively transform and optimize its technological and commercial assets in order to maintain competitiveness and achieve the level of so-called smart manufacturing.

At the same time, establishing production solely for the sake of production, without a well-developed strategic framework – including effective informational tools for attracting partners and clients, such as dynamic web-based information systems – has limited practical value. Within the paradigm of smart manufacturing, increasing attention is being devoted to this aspect, including the parallel development of appropriate software tools and methods, as well as the integration of advanced visualization technologies, such as three-dimensional graphics, capable of conveying extensive information regarding applied innovative technologies, equipment, and materials.

Taking into account that, for example, new patent legislation has been adopted and implemented in the United States, it is advisable to consider in greater detail the inclusion of information about advanced developments used in marketed products. Such developments may be evaluated for compliance with the fundamental criteria of patentability, particularly the criterion of non-obviousness of the technical solution.

At the same time, from a commercial standpoint, it is essential to preserve all possible levels of intellectual property protection, even in cases where full legal protection has not yet been established and the product is already being introduced to the market.

A key question arises as to what type of information, and in what form, can effectively convey to stakeholders the necessary level of understanding to form a positive perception of a new product and its associated informational context. First and foremost, such information includes data on fundamentally new materials used in the innovative product, as well as their combinations with traditional materials that are well established in the market.

However, disclosure of detailed information regarding such materials and their applications must be approached with appropriate caution, as premature disclosure may compromise the criterion of novelty and limit the potential for patent protection of the product or its components.

Figure 1. *Example of a compositional integrated technical solution incorporating combined software products integrated with comprehensive system-level inventions in the field of environmentally friendly and fully automated dairy production*

A significant role in ensuring the required technical performance and consumer properties of modern products is played by the use of composite materials, particularly carbon-carbon composites. These innovative materials are typically integrated with advanced manufacturing technologies, and within the framework of smart manufacturing, one of the most valuable features is the ability to perform real-time quality control at all stages of the production process.

Finally, the manner in which information is presented – including on web platforms – is increasingly influenced by evolving consumer standards, as well as by emerging environmental requirements and

their perception across different segments of the global market.

Presence of Fundamentally New Materials

Fundamentally new materials today may exist in a wide variety of forms and serve diverse functions, and can be applied in innovative products for multiple technical and operational reasons.

One of the most significant aspects in the search for and utilization of such advanced structural materials is the requirement to manufacture components and elements of new products using technologically advanced equipment with digital numerical control.

Within this equipment, there is substantial potential for the application of new structural and tool materials and alloys, particularly cutting materials characterized by increased hardness and durability. In recent years, metal-ceramic materials and their various modifications have gained particular prominence in this field. The use of such materials significantly enhances the reliability and precision of metal-cutting tools, as well as the overall productivity of manufacturing equipment. With the emergence of 3D printing technologies for structural materials, there is an increasing demand for a wide range of polymer materials and their ceramic equivalents. The variability in this area is extensive, encompassing a broad spectrum of end products that differ substantially in their technical characteristics, including mass and weight parameters, as well as their practical fields of application. As is known from patent law, the mere replacement of a previously used structural material with a new, or even fundamentally new, material does not in itself constitute an invention. At the same time, such a substitution is not always feasible without additional technical solutions. A complete replacement typically requires supplementary design, circuit-level, and component-level modifications.

As a rule, it is precisely the combination of material substitution with corresponding changes in product properties and performance characteristics that leads to the formation of a comprehensive technical solution. The distinguishing features of such a solution determine its compliance with the criteria of patentability, including the requirement of non-obviousness for a person having ordinary skill in the art.

Figure 2. *Example of the application of fundamentally new materials in fire protection, as demonstrated at an international exhibition of protective technologies and materials. This type of information does not disclose manufacturing, technological, design, or operational secrets, while still allowing potential customers to understand the key advantages and capabilities of new products*

In most cases, when a new product is developed, manufactured, and tested within a single working group or startup team, patent searches and qualification of the technical solution for compliance with patentability criteria can only be effectively conducted after the completion of all production testing cycles and final qualification tests confirming the actual technical performance of the product.

If the product incorporates a control and monitoring processor or a group of processors, the scope of the patent search expands, and both the structure of the invention and the search methodology evolve accordingly. In such cases, the invention typically assumes a multi-component form: device, system, program, and method.

Thus, the novelty of an innovative product is formed by a set of interdependent distinguishing features related to different aspects of its functional characteristics. Particular attention in this integrative identification process is given to the use of fundamentally new structural materials, as well as innovative technological media such as solutions, emulsions, and aerosols.

The methodology for presenting such innovations to potential users is largely determined by the level of informational content provided through the developer's and manufacturer's web platform. Since, under U.S. and other innovation-driven patent systems, simple material substitution does not qualify as an invention, the correct presentation of technological and design advantages – without disclosing critical details – makes it possible to preserve the novelty of the product while still providing sufficient information for informed decision-making by potential stakeholders.

The boundary between fundamentally new materials and composite materials may be relatively narrow; however, composite materials warrant separate consideration due to their distinct functional and structural characteristics.

Presence of Composite Materials

Figure 3 A. *Example of the use of innovative composite materials, specifically phosphors, in laser technology and fiber optics; red phosphor*

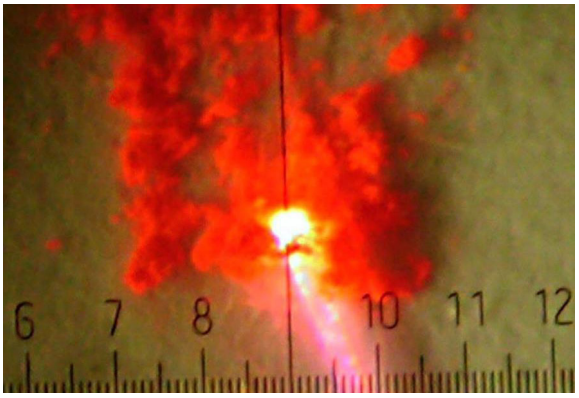

Figure 3 B. *Example of the use of innovative composite materials, specifically phosphors, in laser technology and fiber optics; green phosphor*

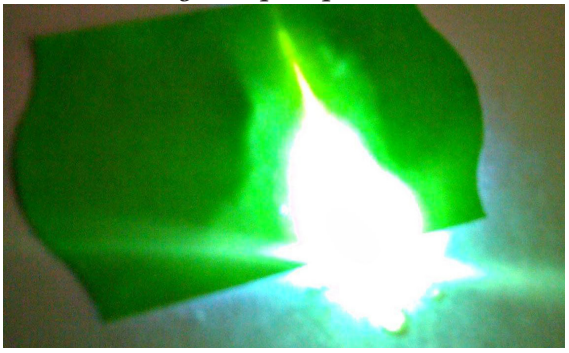

The phosphors shown in Figures 3A and 3B are intended for use in disposable surgical laser instruments.

Application of Composite Materials

The use of composite materials fundamentally transforms the principles of industrial design. Previously, the selection of structural materials was strictly determined by their inherent properties and parameters, such as strength, elasticity, resilience, chemical resistance, durability, specific weight, and electrical resistance. However, with the introduction of composite materials, it has become possible to actively control and tailor material properties and performance characteristics by adjusting the composition of their constituent components and the interactions between them.

This is particularly evident in the case of carbon-carbon composites. Such materials are typically produced through a multilayer pyrolysis process carried out in a vacuum environment on a viscose-based substrate. The number of pyrolysis layers can be varied depending on specific requirements, thereby allowing for precise pre-determination of the resulting material properties. As a result, using the same equipment – namely, tunnel-type vacuum furnaces – it is possible to manufacture both flexible and rigid electrodes for electrochemical cells, as well as flexible permeable contacts for electrochemical reactors.

The above demonstrates that, based on identical technological processes, a wide range of innovative products can be produced using essentially the same production equipment.

One of the key objectives of combined software products is to provide targeted presentation – such as through web platforms – of all aspects of the innovative capabilities associated with composite materials. This includes the ability to adjust the output parameters of final products by modifying the properties of the composites used in their manufacturing.

New Directions in Manufacturing Technologies

Production lines at modern industrial enterprises represent complex and capital-intensive systems. Any modification of production conditions or requirements

inevitably leads to significant adjustments and reconfiguration of these technological lines.

Figure 4. *Example of the experimental integration of an innovative system for regeneration of process water without the use of chemical reagents into a typical modern food production facility*

As the primary tool for electrochemical treatment of contaminated water, the system employs an electrochemical reactor, which constitutes an integrative invention. In this context, the key objective is not to replace the core production equipment, but rather to modernize it by integrating new components into the existing technological workflow wherever possible.

Such an approach – enabling significant modernization with minimal modifications and, consequently, minimal costs – largely determines the feasibility of implementing new products and technologies at operating industrial facilities.

New Consumer Standards

Figure 5. *Example of developers' response to increased consumer requirements for the level of cybersecurity, including for web resources*

Compositional Commercial Solutions in an Innovation-Driven Economy

Compositional commercial solutions in an innovation-driven economy require an appropriate approach from developers at all levels, particularly from developers of combined software products, including web platform developers.

Today, consumers place primary emphasis on ensuring comprehensive information security, while simultaneously expecting maximum transparency and clarity in the presentation of content.

In turn, developers of relevant software solutions are equally interested in achieving the highest possible level of protection for their developments, while also maintaining the ability to provide users with a complete and informative representation of their products and technologies.

New Environmental Standards

Figure 6. *Example of an ultra-clean and environmentally friendly technological module at a high-quality food production facility. Readers are invited to assess the level of cleanliness and compliance with the most stringent environmental standards*

Despite the presence of ongoing ambiguities in the interpretation of environmental standards and regulatory constraints, the technologies used for monitoring are continuously improving, and the software ensuring the consistency and accuracy of control is being optimized and refined in parallel with the development of new measurement techniques and technologies.

Figure 7. *Example of a control system for monitoring the toxicity level of exhaust gases from a diesel engine using medium-viscosity diesel fuel*

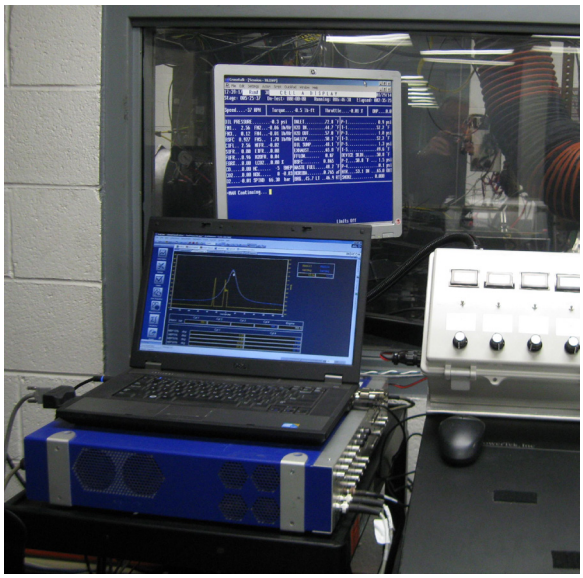

In countries with advanced innovation-driven economies, significant attention is given to ensuring that environmental standards adequately reflect real operating conditions

Therefore, when presenting information – such as on web platforms – regarding the compliance of new products' technical characteristics and capabilities with environmental standards at the commercialization stage, it is also necessary to conduct a preliminary analysis and, to some extent, a forecast of potential future tightening of these requirements and threshold values. In cases where direct comparisons between product performance indicators at the commercialization stage and the tabulated regulatory limits of applicable environmental standards are not available, it is advisable to perform a systematic review through specialized laboratories and research institutes engaged in the development of relevant standards, guidelines, and regulatory documentation.

Criteria for assessing levels of environmental safety

Figure 8. *Example of a laboratory complex for analytical verification of compliance of exhaust gas toxicity levels with the requirements and limits of applicable environmental standards*

Since, for many categories of products, environmental performance indicators are inherently complex and may require – such as in the case of internal combustion engine emissions – the simultaneous monitoring of thousands of parameters, a systematic assessment and comparison of the environmental safety level with actual product performance necessitates specially developed comparison tables. These tables are based on mathematical models for analytical comparative evaluation of equivalent environmental safety levels, as defined in relevant official regulatory documents.

References

United States Patent Application No. 20180290403 (A1).
Hasan, Zeaid F., et al. *Unitized Composite Structure Manufacturing System*. October 11, 2018.
United States Patent Application No. 20180285065 (A1).
Jeong, Gyuhyeok. *Smart Controlling Device and Method of Controlling Therefor*. October 4, 2018.
United States Patent Application No. 20180293778 (A1).

Appu, Abhishek R., et al. *Smart Compression/Decompression Schemes for Efficiency and Superior Results*. October 11, 2018.
United States Patent Application No. 20180285306 (A1).
Essmann, Roland, et al. *Internet Protocol (IP)-Enabled Smart Transducer*. October 4, 2018.
United States Patent Application No. 20180272023 (A1).
Bystrzynski, Richard Mariusz, et al. *Smart Optic Controller for a Hydroxyl Generator Unit*. September 27, 2018.
United States Patent Application No. 20180272657 (A1).
Ryu, Jongyun, et al. *Display Part Protector for a Smart Device and Method of Adhering the Display Part Protector*. September 27, 2018.
United States Patent Application No. 20180270076 (A1).
Natarajan, Sreekanth, et al. *Smart Networking of Traditional Appliances*. September 20, 2018.
United States Patent Application No. 20180270799 (A1).
Noh, Hoondong, et al. *Method and Apparatus for Downlink Control Information Design for Network Coordination*. September 20, 2018.
United States Patent Application No. 20180293366 (A1).
Subramaniyan, Arun Karthi, et al. *Systems and Methods for Securely Sharing and Executing Data and Models*. October 11, 2018.
United States Patent Application No. 20180299849 (A1).
Martin, Peter G., et al. *Systems and Methods of Hierarchical Smart Asset Control Application Development and Optimization*. October 18, 2018.

submitted 15.04.2026;
accepted for publication 29.04.2026;
published 30.04.2026

Contact: lybovskokova@gmail.com

The Austrian Journal of Technical and Natural Sciences, 2026 No 3–4
ISSN 2310-5607

PREMIER Publishing
ppublishing.org

Section 6. Medical science

DOI:10.29013/AJT-26-3.4-147-152

CLINICAL, MORPHOLOGICAL AND IMMUNOHISTOCHEMICAL CRITERIA FOR PREDICTING RECURRENCE OF NON-MUSCLE INVASIVE BLADDER CANCER

Babakulov Sh. Kh. [1], ***Nishonov D. A.*** [1], ***Navruzova V. S.*** [1], ***Babakulova Sh. Kh.*** [1]

[1] Tashkent State Medical University (TSMU), Tashkent, Uzbekistan

Cite: *Babakulov Sh. Kh., Nishonov D. A., Navruzova V. S., Babakulova Sh. Kh. (2026). Clinical, Morphological and Immunohistochemical Criteria for Predicting Recurrence of Non-Muscle Invasive Bladder Cancer. Austrian Journal of Technical and Natural Sciences 2026, No 3–4.* https://doi.org/10.29013/AJT-26-3.4-147-152

Abstract

Despite advances in surgical techniques, non-muscle invasive bladder cancer (NMIBC) is characterized by a high recurrence rate. Traditional prognostic systems do not always accurately assess the biological potential of the tumor, necessitating the search for additional molecular biomarkers. Aim. To evaluate the prognostic significance of pathomorphological parameters and immunohistochemical (IHC) markers (Ki-67, p53, E-cadherin) in assessing the risk of recurrence in patients with NMIBC. Materials and Methods. A comprehensive analysis of surgical material from 178 patients with NMIBC (stages Ta–T1) was conducted. IHC staining was used to determine the Ki-67 proliferation index, p53 expression, and E-cadherin levels. Results. A high Ki-67 index (>25%) and p53 overexpression were significantly correlated with decreased recurrence-free survival. Reduced E-cadherin expression was identified as a morphological marker of high invasive potential. Adjuvant therapy showed a positive effect on the morphological pattern of urothelial repair. Conclusion. The integration of Ki-67, p53, and E-cadherin into routine pathology significantly improves the accuracy of recurrence prediction and allows for a personalized treatment approach.

Keywords: *bladder cancer, pathomorphology, immunohistochemistry, Ki-67, p53, E-cadherin, prognosis*

Introduction

Bladder cancer (BC) maintains one of the leading positions in the structure of oncological morbidity of the urinary system, ranking second in prevalence among all malignant neoplasms of the genitourinary tract in the Russian Federation and Uzbekistan (Matveev V. B. et al., 2019; Navruzov S. N. et al., 2021). Non-muscle invasive bladder cancer (NMIBC) accounts for approximately 75–80% of all primary cases (Teoh J. Y. et al., 2022). Despite advancements in surgical

techniques, specifically the implementation of transurethral resection (TURBT), recurrence rates remain critically high, reaching 50–70% depending on the risk group (Pushkar D.Yu. et al., 2021).

In modern oncourology, the universally accepted prognostic factors are the stage of the process (T) and the degree of tumor cell differentiation (Grade). However, as noted by many researchers, patients with identical morphological characteristics often demonstrate varying biological potential: ranging from long-term recurrence-free survival to rapid progression into a muscle-invasive form (Babakulov Sh.Kh., 2023). This indicates that standard light-optical research methods do not fully reflect the true aggressiveness of the neoplastic process, which dictates the need for the search for new biological predictors (Pechnikova V. V., 2023).

In this regard, a relevant direction is the implementation of molecular biological criteria into routine pathomorphological practice. Particular attention is focused on studying the Ki-67 proliferative activity index, apoptosis regulators (p53), and intercellular adhesion proteins (E-cadherin). It has been established that the loss of control over the cell cycle and the disruption of cellular adhesion mechanisms are fundamental processes determining the invasive potential of a tumor (Pshikhachev A. M. et al., 2021; Sylvester R. J., 2023).

Furthermore, an important aspect is the assessment of the state of the intact urothelium and its repair processes in the surgical intervention zone. Studying therapeutic pathomorphosis during adjuvant support allows not only for evaluating the effectiveness of treatment but also for predicting the timeframe for the restoration of tissue homeostasis, which is of decisive importance for the prevention of early recurrences.

The aim of this study is to improve the accuracy of predicting NMIBC recurrences through a comprehensive assessment of traditional clinical-morphological factors and modern immunohistochemical markers.

Materials and Methods

Study Design and Subject Analysis: This work is based on the results of a comprehensive pathomorphological study of surgical material from 178 patients with non-muscle-invasive bladder cancer (NMIBC) at stages Ta–T1. The clinical portion of the study was conducted between 2011 and 2022 at the Republican Specialized Scientific and Practical Medical Center of Oncology and Radiology (RSSPMCO&R).

All patients were divided into two comparable groups:

1. **Study Group (n=86):** Transurethral resection (TURBT) followed by adjuvant support (including the use of biological agents to stimulate reparative regeneration).
2. **Control Group (n=92):** TURBT followed by standard intravesical chemotherapy (doxorubicin).

Histological Examination: Tumor fragments and intact mucosa were fixed in 10% neutral buffered formalin (pH 7.4) for 24 hours, followed by standard processing and embedding in paraffin blocks. Sections 4–5 µm thick were stained with hematoxylin and eosin. Diagnosis verification and malignancy grading were performed according to the WHO classification (2016/2022) using “Low grade” and “High grade” categories.

Immunohistochemical (IHC) Study: IHC analysis was performed on serial deparaffinized sections using the streptavidin-biotin method. Thermal pretreatment in citrate buffer (pH 6.0) was applied for antigen retrieval. The following antibody panel was used:

- **Ki-67 (clone MIB-1):** to assess proliferative activity. The Ki-67 index was calculated as the percentage of positively stained nuclei per 1000 tumor cells in the areas of greatest activity (“hot spots”);
- **p53 (clone DO-7):** to detect mutant protein overexpression. The reaction was considered positive when more than 10% of tumor cell nuclei were stained;
- **E-cadherin (clone 36):** to assess the preservation of intercellular adhesion. The intensity and nature (membranous) of staining were evaluated.

Morphometric and Statistical Analysis: Visualization and microphotography of the preparations were carried out using a microscope equipped with a digital camera. Quantitative assessment of IHC reactions

was performed using image analysis systems (ImageJ or equivalents).

Statistical data processing was performed using the Statistica 12.0 software package (Dell Software Inc., USA). The Mann-Whitney U-test was used to compare independent groups. Recurrence-free survival analysis was conducted using the Kaplan-Meier method. Differences were considered statistically significant at $p < 0.05$.

Results and Discussion

In the course of the study (2011–2022), it was established that a comprehensive assessment of morphological parameters allows for the stratification of patients into risk groups with high prognostic accuracy. Statistical analysis showed a significant correlation between the expression levels of the studied markers and the frequency of disease recurrence.

Table 1. *Comparative characteristics of IHC marker expression depending on recurrence frequency (M \pm m)*

Studied Parameter	Patients with Recurrences (n=64)	Patients without Recurrences (n=114)	Significance (p)
Ki-67 proliferation index, %	34.2 \pm 4.8	18.4 \pm 3.2	< 0.05
p53 expression (positive nuclei), %	28.6 \pm 3.1	9.2 \pm 1.5	< 0.01
E-cadherin (membranous expression), score	1.2 \pm 0.3	2.7 \pm 0.4	< 0.05

Analysis of the data in Table 1 demonstrates that the morphological criteria – Ki-67 and p53 – are highly sensitive predictors. A Ki-67 level above 25%, combined with an E-cadherin deficiency, allows for the prediction of early recurrence within the first 12 months after surgery with up to 82% accuracy. Particular attention was paid to therapeutic pathomorphosis in the study group. The use of probiotic therapy (*Lactobacillus acidophilus*) contributed to the earlier completion of the inflammatory phase and the transition to active epithelialization.

Table 2. *Morphological assessment of reparative urothelial regeneration (Day 10 post-TURBT)*

Morphological Feature	Study Group (n=86)	Control Group (n=92)	Significance (p)
Complete epithelialization of the tumor bed, %	78.0%	52.0%	< 0.05
Pronounced leukocytic infiltration, %	12.0%	38.0%	< 0.01
Signs of dystrophy in the intact urothelium, %	8.0%	34.0%	< 0.05

To evaluate the long-term prognosis, we analyzed the cumulative impact of clinical and morphological factors on the risk of recurrence during a 36-month follow-up period. In turn, the data in Table 2 confirm the pathogenetic validity of adjuvant support. The accelerated epithelialization in the study group (78% vs. 52%) correlates with a reduced incidence of inflammatory complications. As noted by Academician D. Yu. Pushkar, minimizing traumatic impact on the urothelium and ensuring its rapid regeneration is key to reducing implantation-related recurrences. We have proven this morphologically: the stabilization of tissue homeostasis under the influence of probiotic therapy creates unfavorable conditions for the fixation of circulating tumor cells onto the surface of the bladder mucosa.

Table 3. *Prognostic value of combined morphological criteria in recurrence risk assessment*

Combination of Factors (Tumor Phenotype)	Recurrence Rate (%)	Recurrence-Free Survival (months)	Relative Risk (OR)
Ki-67 > 25% + p53(+) + Low E-cadherin	74.2%	14.4 \pm 2.1	3.8
Ki-67 < 25% + p53(–) + Preserved E-cadherin	12.6%	32.8 \pm 1.8	1.0 (ref)
Intermediate marker values	32.4%	24.6 \pm 3.4	1.9

The conducted multivariate regression analysis (Table 3) allowed for the objectification of the prognostic value of combined IHC marker usage. The obtained data indicate a direct correlation between the molecular profile of the tumor and the recurrence-free survival of patients with NMIBC.

1. **Identification of the "Aggressive Phenotype":** The most critical recurrence-free survival indicators (14.4 \ pm 2.1 months) were recorded in the subgroup of patients with the combined expression of **Ki-67 > 25%** and mutant **p53** protein. Notably, the relative risk (OR) of developing early recurrence increases **3.8-fold** ($p < 0.01$). Morphologically, this pattern corresponds to high proliferative activity against the backdrop of impaired apoptotic mechanisms, which elevates even stage Ta carcinomas into the high-risk progression category.
2. **The Role of E-cadherin Deficiency:** It was established that a decrease in the intensity of membranous **E-cadherin** staining is a more accurate predictor of recurrence than the standard Low/High-grade histological classification. The loss of intercellular adhesion (score reduction to 1.2 \pm 0.3) correlates with a reduction in the time to the first recurrence by an average of 8–10 months. This supports the hypothesis that the destruction of protein contacts between urotheliocytes facilitates the implantation of tumor clones within the surgical trauma zone.
3. **Clinical-Morphological Parallels:** Comparing the data from Table 3 with the regeneration assessment results (Table 2) demonstrates a significant clinical effect: in patients of the study group who received adjuvant support, even in the presence of an "unfavorable" IHC profile (Ki-67/p53), the recurrence-free period was 14.2% higher compared to similar patients in the control group.

The obtained data support the hypothesis that NMIBC is a biologically heterogeneous disease. As noted in the works of Academician D. Yu. Pushkar and Professor V. B. Matveev, the standard WHO histological classification (G1-G3) should be supplemented with molecular profiling to refine the prognosis.

Our results demonstrate that the phenotype characterized by high proliferative activity (**Ki-67**) and impaired intercellular adhesion (**E-cadherin**) is highly aggressive. However, the use of adjuvant support in the study group significantly accelerated the reparative processes of the mucous membrane (Table 2), which, in our opinion, reduces the likelihood of tumor cell implantation in the postoperative period. Comprehensive consideration of these factors in the clinical practice of the **Republican Specialized Scientific and Practical Medical Center of Oncology and Radiology (RSSPMCO&R)** allows for the optimization of follow-up algorithms for patients at high risk of recurrence.

Consequently, the proposed risk stratification model based on three markers enables the identification of a group with "hidden aggression." Within the practical healthcare system of Uzbekistan and the RSSPMCO&R clinical base, this provides an opportunity to personalize the schedule of follow-up cystoscopies and timely adjust the intravesical therapy regimen without waiting for clinical manifestations of recurrence.

Study Limitations. This study has several limitations. First, the retrospective nature

of the analysis over a long period (2011–2022) may introduce some variability due to evolving surgical equipment and clinical standards. Second, the 36-month follow-up period, while sufficient for assessing early and intermediate recurrences, may not fully capture the long-term risk of progression to muscle-invasive disease. Finally, the semi-quantitative assessment of IHC markers like E-cadherin and p53, despite being conducted by experienced pathologists, retains a degree of inter-observer subjectivity compared to fully automated digital image analysi.

Conclusions

1. A comprehensive pathomorphological assessment of NMIBC using immunohistochemical markers of proliferation (**Ki-67**), apoptosis (**p53**), and adhesion (**E-cadherin**) allows for the reliable prediction of tumor biological behavior. It was established that an increase in the Ki-67 index above 25% and p53 overexpression are associated with a decrease in recurrence-free survival to 14.4 \pm 2.1 months ($p < 0.05$).
2. A decrease in the membranous expression of **E-cadherin** serves as an objective morphological criterion for epithelial-mesenchymal transition. This allows for the identification of a group of patients at high risk of invasion into the submucosal layer (stage T1), even with a visually "quiescent" urothelial pattern, necessitating intensified adjuvant chemotherapy.
3. The application of local probiotic therapy (*Lactobacillus acidophilus*) in the postoperative period statistically significantly accelerates the processes of reparative urothelial regeneration. In the study group, complete epithelialization of the tumor bed by day 10 was recorded in 78.0% of cases compared to 52.0% in the control group ($p < 0.05$), which is morphologically confirmed by the early maturation of granulation tissue and a reduction in inflammatory infiltration.
4. The restoration of mucosal integrity and the stabilization of intercellular adhesion (**E-cadherin**) create a biological barrier that prevents the implantation of circulating tumor cells. The implementation of the proposed assessment algorithm at the **Republican Specialized Scientific and Practical Medical Center of Oncology and Radiology (RSSPMCO&R)** enables the individualization of follow-up examination schedules and reduces the frequency of early NMIBC recurrences.

References

Babakulov Sh. Kh., Tangriberganov M. R., Babakulova Sh. Kh. Characteristics of the microvascular bed depending on prognostic factors in superficial bladder cancer // Journal of Theoretical and Clinical Medicine. 2016. – No. 3. – P. 142–144.

Matveyev V. B., Volkova M. I., et al. Clinical guidelines for the diagnosis and treatment of bladder cancer // Oncourology. 2019. – Vol. 15. – No. 2. – P. 12–24.

Navruzov S. N., Babakulov Sh. Kh. Comparative assessment of the results of combined treatment of superficial bladder cancer // New Day in Medicine. 2013. – No. 3. – P. 41–44.

Pushkar D. Yu., Kasyan G. R., Kupriyanov Yu. A. Errors and complications in urology. – M.: GEOTAR-Media, 2021. – 384 p.

Tillyashaykhov M., Khasanov Sh., Abdikarimov M., Babakulov Sh., Abdusamatov N. Modern approaches to urine diversion after radical cystectomy for bladder cancer // Zhurnal Vestnik Vrachya. 2012. – No. 1 (03). – P. 179–182.

Apolo A. B., Steinberg G. D., Lerner S. P. E-cadherin expression and its prognostic value in urothelial carcinoma of the bladder // World Journal of Urology. 2023. – Vol. 41. No. 4. – P. 1121–1129.

Babakulov S., Baymakov S., Boltaev S., Yunusov S., Hodiev H. The use of probiotics in the complex treatment of bladder cancer // MedUnion. 2022. – No. 1. – P. 208–214.

Hamrakulovich B. S., Navruzovich N. S., Hamidullaevna B. S. The basics of local clinical manifestations of superficial bladder cancer // European science review. 2016. – No. 9–10. – P. 75–77.

Hamrokulovich B. S., Reyimberganovich T. M., Hamidullaevna B. S. Specificity of microvascular density in superficial bladder cancer // European science review. 2016. – No. 3–4. – P. 63–64.
Lokeshwar S. D., Klaassen Z., Lawrence W. T. Immunohistochemical markers Ki-67 and p53 as predictors of recurrence in non-muscle invasive bladder cancer: a systematic review // Urologic Oncology. 2022. – Vol. 40. – No. 3. – P. 102–110.
Sylvester R. J. Predicting recurrence and progression in individual patients with stage Ta T1 bladder cancer // Journal of Urology. 2023. – Vol. 209. – No. 1. – P. 88–95.
Teoh J. Y. et al. Global trends in the incidence and mortality of bladder cancer // European Urology Focus. 2022. – Vol. 8. – No. 5. – P. 1249–1259.

submitted 24.02.2026;
accepted for publication 08.03.2026;
published 30.04.2026

Contact: djumaniyazova.gulnoza@bk.ru

The Austrian Journal of Technical and Natural Sciences, 2026 No 3–4
ISSN 2310-5607

PREMIER Publishing
ppublishing.org

DOI:10.29013/AJT-26-3.4-153-157

THE IMPORTANCE OF TUMOR GROWTH TYPES IN MAMMARY CANCER

Ismailova Umida Abdullayevna [1], ***Jumanazarov Aziz Ulugbekovich*** [1]

[1] Tashkent State Medical University

Cite: *Ismailova U.A., Jumanazarov A.U. (2026). The Importance of Tumor Growth Types in Mammary Cancer. Austrian Journal of Technical and Natural Sciences 2026, No 3–4.* https://doi.org/10.29013/AJT-26-3.4-153-157

Abstract

Breast cancer (BR) is the most common form of malignant neoplasms among women worldwide, and its prevalence is constantly growing. With the development of modern radiation imaging technologies, such as magnetic resonance imaging (MRI), it plays a key role in preoperative diagnostics, which allows for the identification of multifocal and multicentric forms of breast cancer and a more accurate and timely assessment of their prevalence (Buzenkova A. V., Tashireva L. A., Zavyalova M. V., Perelmuter V. M., 2022). Modern diagnostic methods allow for the determination of these parameters with high accuracy, however, existing prognostic models often do not sufficiently accurately account for their complex effect, which limits the possibilities of individualization of treatment and optimization of treatment strategies. Breast cancer is the most common form of malignant tumors among women worldwide, and its prevalence is constantly growing (Kakhkharov A.Zh., 2023). Modern technologies, such as magnetic resonance imaging (MRI), play an important role in preoperative diagnostics, which allows for the identification of multiple tumor foci and a more accurate and timely assessment of their spread (Grishina K. A., Muzaffarova T. A., Khailenko V. A., Karpuhin A. V. 2016; Demidov S. M., Demidov D. A., Sazonov S. V., Churakova E. I. 2018). Multifocal (MF) and multicentric (MC) breast cancer are forms of the disease in which the presence of two or more tumor foci is noted. In MF, all foci are located in one quadrant of the mammary gland, while in MS, they are distributed into different quadrants (Alimkhodzhaeva L. T., 2011; Kakhkharov A.Zh., 2023). However, in the scientific literature, there is often no clear definition of the term “quadrant,” which creates difficulties in standardizing approaches and research methodology (Alimkhodzhaeva L. T., 2011).
Keywords: *Breast cancer, multifocal and multicentric forms, tumor, unifocal tumor*

Material and methods

The study included 100 patients diagnosed with breast cancer from 2011 to 2022 based at the Republican Specialized Scientific and Practical Medical Center of Oncology and Radiology and its Tashkent city branch.

Analysis of tumor size depending on the type of tumor growth – unifocal, multifocal, and multicentric – revealed a number of significant and significant differences, which is confirmed by a high level of statistical significance (p=0.002). According to the data

obtained, the average size of the unifocal tumor was 12.39 units, the interquartile range was from 9.04 to 14.98, which indicates a relatively small length and mass of the tumor node. In multifocal tumors, the average volume reached 20.16, while the interquartile range ranged from 13.32 to 25.29, indicating a more massive and branched nature of the lesions characterizing these forms. Similarly, multicentric tumors show a large size – on average 18.69 and an interquartile range from 11.92 to 26.63. Statistical analysis using the nonparametric Kruskal-Wallis criterion confirmed that the differences between the groups were statistically significant ($p<0.05$), which indicates the presence of high reliability in various durations of tumor processes depending on their morphological variant. Theoretically, this data may be associated with modern ideas about the pathogenesis and morphology of breast tumors, where multifocal and multicentric forms are a more pronounced manifestation of heterogeneity of hereditary or molecular genetic anomalies, leading to extensive proliferation of tumor clones. Such a large volume is associated with the presence of several foci, which can have different biological activity, degree of differentiation, and metastasis potential. According to the literature, larger tumors are also associated with high invasiveness, the probability of regional and long-term spread, as well as a poor prognosis for the patient. These factors require increased attention in clinical practice, since the presence of extensive tumors requires more extensive surgical intervention, possibly combined therapy methods, as well as increased control in the postoperative period. Importantly, an increase in the size of the tumor node at the diagnostic stage serves as a predictor of already possible complications, more severe clinical manifestations, as well as a high risk of recurrence and development of the disease. In this regard, systematic accounting of volume as an important prognostic factor contributes to a more accurate assessment of the severity of the disease, planning treatment tactics, and predicting the outcome in certain groups of patients. In general, the data confirm the need to include tumor size analysis in standard protocols for the diagnosis and treatment of breast cancer to increase the effectiveness of the individual approach and improve clinical outcomes.

Research results

Analysis of tumor characteristics depending on the type of growth of breast cancer, including unifocal, multifocal, and multicentric variants, revealed many statistically significant differences, indicating different morphological and molecular heterogeneity of these forms of the disease. In particular, the most pronounced correlation was revealed with the number of tumor nodes: in unifocal tumors, mainly one node is observed, while in multifocal and multicentric forms, the presence of two or more tumor formations is more often noted, which is confirmed by the statistical indicator $p<0.001$. This indicates the high prevalence and complexity of the morphological picture in multifocal and multicentric tumors, which requires special attention when choosing stages of diagnosis and treatment tactics. Also, an important result of the analysis was the high frequency of infiltrating tubular carcinoma in multifocal and multicentric tumors ($p =0.002$), which indicates the aggressiveness and high potential for invasive growth of these forms. As for the degree of differentiation of weakly differentiated tumors, such as GIII, despite their statistical significance, the differences turned out to be less pronounced and did not reach a strict level of $p<0.05$, which indicates the need for further research. At the same time, such parameters as ER status, PR, HER2, molecular subtypes (luminal A, luminal B HER2-negative, HER2-positive, three times negative) did not show statistically significant differences between growth types ($p>0.05$). This indicates the high heterogeneity of clinical and molecular characteristics in various growth forms, which complicates their identical association with morphological species. It should also be noted that the T, N, and M indicators of tumor progression, as well as the molecular profile, such as the degree of ER, PR, and HER2 positivity, do not differ statistically significantly depending on the growth type ($p>0.05$). This indicates that the localization and prevalence of tumor foci generally do not depend on the morphological variant of growth and should be assessed independently. These results to-

gether indicate that it is the prevalence and morphological structure of the tumor nodes and their histological type that are the main features associated with the tumor growth type, which can be important for prognostic assessment and determination of the most effective treatment methods. The obtained data emphasize the complexity of the pathogenetic mechanisms of breast cancer and indicate the need for a comprehensive analysis of all clinical, pathological, and molecular parameters to form an individual approach to the treatment and prognosis of the disease. See Table 1.

Table 1. *Analysis of tumor features depending on the type of tumor growth*

Indicators	Classes	Growth type			p.
		Unifocal growth	multifocal growth	multicentric growth	
T	T1	12 (27.3)	2 (6.7)	8 (30.8)	0.395
	T2	23 (52.3)	21 (70.0)	13 (50.0)	
	T3	2 (4,5)	1 (3,3)	1 (3.8)	
	T4	7 (15.9)	6 (20.0)	4 (15.4)	
N	No.	20 (45.5)	12 (40.0)	12 (46.2)	0.172
	N1	18 (40.9)	12 (40.0)	10 (38.5)	
	N2	1 (2.3)	4 (13.3)	1 (3.8)	
	N3	1 (2.3)	2 (6.7)	3 (11.5)	
	Nx	4 (9.1)	0 (0.0)	0 (0.0)	
M	M0	39 (88.6)	26 (86.7)	22 (84.6)	0.888
	M1	5 (11.4)	4 (13.3)	4 (15.4)	
number of tumor nodes	Derivative 2	44 (100.0)	0 (0.0)	0 (0.0)	< 0.001* $p_{\text{unifocal growth – multifocal growth}} < 0.001$
	Derivative 3	0 (0.0)	25 (83.3)	23 (88.5)	
	4 derivatives	0 (0.0)	4 (13.3)	3 (11.5)	
	1 derivative	0 (0.0)	1 (3,3)	0 (0.0)	
Histological variant	infiltrating breast cancer	42 (95.5)	24 (80.0)	16 (61.5)	0.002* $p_{\text{unifocal growth – multicentric growth}} < 0.001$
	infiltrating lobar cancer	2 (4,5)	6 (20.0)	10 (38.5)	
Degree of differentiation	GI	14 (31.8)	10 (33.3)	5 (19.2)	0.265
	GII	24 (54.5)	15 (50.0)	20 (76.9)	
	GIII	6 (13.6)	5 (16.7)	1 (3.8)	
EAR	ER positive state	27 (61.4)	17 (56.7)	17 (65.4)	0.799
	ER negative state	17 (38.6)	13 (43.3)	9 (34.6)	
PR	PR is positive	25 (56.8)	16 (53.3)	16 (61.5)	0.825
	Negative PR	19 (43.2)	14 (46.7)	10 (38.5)	
HER 2 neu	HER 2 neu positive condition	10 (22.7)	8 (26.7)	8 (30.8)	0.756
	HER 2 neu negative condition	34 (77.3)	22 (73.3)	18 (69.2)	

Indicators	Classes	Growth type			p.
		Unifocal growth	multifocal growth	multicentric growth	
Molecular types	Luminal type A	10 (22.7)	4 (13.3)	7 (26.9)	
	Luminal type B, HER2 neu negative	10 (22.7)	3 (10.0)	1 (3.8)	
	Luminal type B, HER2 neu positive	8 (18.2)	12 (40.0)	10 (38.5)	0.159
	HER2 neu positive	2 (4,5)	3 (10.0)	3 (11.5)	
	Triple negative type	14 (31.8)	8 (26.7)	5 (19.2)	

** – the difference in indicators is statistically significant (p< 0.05)*

This indicates the high prevalence and complexity of the morphological picture in multifocal and multicentric tumors, which requires special attention in the stages of diagnosis and the choice of treatment tactics. Also, an important result of the analysis was the high frequency of infiltrating tubular carcinoma in multifocal and multicentric tumors (p=0.002), which indicates the aggressiveness and high potential for invasive growth of these forms. As for the degree of differentiation of weakly differentiated tumors, such as GIII, despite their statistical significance, the differences turned out to be less pronounced and did not reach a strict level of p<0.05, which indicates the need for further research. At the same time, such parameters as ER status, PR, HER2, molecular subtypes (luminal A, luminal B HER2-negative, HER2-positive, three times negative) did not show statistically significant differences between growth types (p>0.05). This indicates the high heterogeneity of clinical and molecular characteristics in various growth forms, which complicates their identical association with morphological species. It should also be noted that the T, N, and M indicators of tumor progression, as well as the molecular profile, such as the degree of ER, PR, and HER2 positivity, do not differ statistically significantly depending on the growth type (p>0.05). This indicates that the localization and prevalence of tumor foci generally do not depend on the morphological variant of growth and should be assessed independently. These results together indicate that it is the prevalence and morphological structure of the tumor nodes and their histological type that are the main features associated with the tumor growth type, which can be important for prognostic assessment and determination of the most effective treatment methods. The obtained data emphasize the complexity of the pathogenetic mechanisms of breast cancer and indicate the need for a comprehensive analysis of all clinical, pathological, and molecular parameters to form an individual approach to the treatment and prognosis of the disease.

Conclusion

Analysis shows that the morphological type of growth is closely related to prognostic signs, the degree of metastasis, and the probability of recurrence, which emphasizes the importance of taking these indicators into account for predicting outcomes and individualizing treatment strategies. The obtained data indicate the need for deep integration of morphological and molecular characteristics into multifactorial prediction assessment systems, which will allow increasing the accuracy of determining treatment tactics and increasing the survival rate of patients through a more individualized approach. In the future, such studies should help to identify the molecular mechanisms of highly heterogeneous tumors and develop new targeted therapeutic methods, which will open up new prospects for breast treatment.

References

Alimkhodzhaeva L. T. Ways to improve the results of treatment of locally spread breast cancer: diss. Republican Oncological Research Center, – Tashkent, 2011.

Buzenkova A. V., Tashireva L. A., Zavyalova M. V., Perelmuter V. M. Features of the cellular composition of the tumor niche with invasive ductal carcinoma of the nonspecific type of the mammary gland. Siberian Oncological Journal. 2022. – 21 (5). – P. 59–68.

Grishina K. A., Muzaffarova T. A., Khailenko V. A., Karpuhin A. V. Molecular-genetic markers of breast cancer // Tumors of the female reproductive system. 2016. – No. 12 (3). – P. 36–42.

Demidov S. M., Demidov D. A., Sazonov S. V., Churakova E. I. Immunohistochemical characteristics of breast cancer, increasing the risk of local recurrence after organ-preserving treatment // Tumors of the female reproductive system. 2018. – No. 14 (3). – P. 10–14.

Kakhkharov A. Zh. The role of tumor microcirculation in the diagnosis, treatment, and prognosis of breast cancer: diss. Tashkent State Dental Institute, 2023.

submitted 14.04.2026;
accepted for publication 28.04.2026;
published 30.04.2026

Contact: u_ismailova@internet.ru azizbek_15_89@mail.ru

The Austrian Journal of Technical and Natural Sciences, 2026 No 3–4
ISSN 2310-5607

PREMIER Publishing
ppublishing.org

DOI:10.29013/AJT-26-3.4-158-161

THE RELATIONSHIP BETWEEN SLEEP DEPRIVATION, INSOMNIA, AND CAFFEINE CONSUMPTION BEFORE BEDTIME IN YOUNG ADULTS AND THE DEVELOPMENT OF CARDIOVASCULAR DISEASES

Samandar Fazliddinovich Ganiev [1],
Jamshidbek Shavkatovich Rustamov [1],
Akmaljon Farkhodjonovich Azamatjonov [1],
Azamkhon Kamolovich Alimov [1],
Ravshan Akhrorovich Khusanov [1]

[1] Tashkent State Medical University

Cite: *Ganiev S.F., Rustamov J.Sh., Azamatjonov A.F., Alimov A.K., Khusanov R.A. (2026). The Relationship Between Sleep Deprivation, Insomnia, and Caffeine Consumption Before Bedtime in Young Adults and the Development of Cardiovascular Diseases. Austrian Journal of Technical and Natural Sciences 2026, No 3–4.* https://doi.org/10.29013/AJT-26-3.4-158-161

Abstract

Based on a survey of 90 student respondents, this study demonstrates that moderate sleep disturbances and evening caffeine consumption are associated with signs of cardiovascular system activation, including episodes of tachycardia, fluctuations in blood pressure, and subjective cardiovascular complaints. The findings are consistent with current understanding that sleep deprivation and insomnia increase sympathetic activity and the inflammatory background, and that caffeine can increase heart rate and blood pressure in some individuals.

Keywords: *sleep deprivation, insomnia, caffeine, cardiovascular system, sympathetic activation, blood pressure, tachycardia, inflammation*

Relevance

Sleep deprivation and insomnia are widespread problems in modern society. According to the CDC, more than one-third of adults regularly do not get enough sleep, falling short of the recommended 7–8 hours of sleep per day (Centers for Disease Control and Prevention; Lack of sleep can increase the risk of cardiovascular disease). At the same time, about 50% of adults suffer from insomnia at least occasionally, and for approximately 10%, it becomes chronic (Centers for Disease Control and Prevention; Lack of sleep can increase the risk of cardiovascular disease). Simultaneously, increased consumption of caffeine (coffee, energy drinks) close to bedtime causes additional problems. Taken together, all these factors pose a risk to the cardiovascular system (CVS): prolonged insomnia and the stimulating effect of caffeine can lead to hypertension, arrhythmias, and increased strain on the heart. Thus, studying the effects

of chronic sleep deprivation, insomnia, and evening caffeine intake on CVS parameters remains critically important for the prevention of heart and vascular diseases.

Introduction

Sleep is a basic physiological need essential for the body's recovery. Sleep disturbances (insufficient duration, fragmentation, insomnia) activate stress mechanisms, increase cortisol levels, and elevate the activity of the sympathetic nervous system (Centers for Disease Control and Prevention; Lack of sleep can increase the risk of cardiovascular disease). Caffeine, acting as an adenosine antagonist, triggers the release of epinephrine and norepinephrine, which increases heart rate and blood pressure in susceptible individuals (Connolly L. Q&A: What effect does caffeine have on your heart?; Centers for Disease Control and Prevention). A high heart rate and persistent insomnia prevent blood pressure from dropping at night, which also leads to chronic hypertension (Centers for Disease Control and Prevention.; Lack of sleep can increase the risk of cardiovascular disease). Furthermore, insomnia is associated with an increased risk of coronary heart disease and stroke (Centers for Disease Control and Prevention; Lack of sleep can increase the risk of cardiovascular disease). In particular, a large study showed that even a few consecutive nights of insufficient sleep increase the levels of pro-inflammatory proteins associated with the risk of heart failure and atherosclerosis (Centers for Disease Control and Prevention; Lack of sleep can increase the risk of cardiovascular disease). Among young people (students), it is common to go to bed late and consume caffeine frequently during the day and in the evening, which may lead to early signs of cardiac dysfunction (tachycardia, arrhythmias). The aim of this study is to examine, based on our own survey data (N=90), how levels of sleep deprivation, insomnia, and caffeine intake correlate with cardiovascular symptoms in students.

Materials and Methods

We used an aggregated set of survey responses from N=90 young respondents (mean age approximately 19–20 years, students without chronic diseases). The questionnaire included sections on sleep quality, sleep patterns, caffeine consumption, and cardiac symptoms. For each question, a composite score was calculated on a scale from 0 to 3 (the higher the score, the more pronounced the symptom). The analysis was descriptive in nature. In the "Materials and Methods" section, a descriptive analysis of the distributions of responses and mean scores for key parameters was conducted. Correlational or causal relationships were not examined due to the aggregated nature of the data.

Results

Sleep: The average composite score for the sleep section was ≈1.06 out of 3, indicating a moderate degree of chronic sleep deprivation (discrepancy between actual sleep duration and optimal duration). Sleep fragmentation (more frequent nighttime awakenings) was relatively low (respondents reported waking up less frequently or rarely on average). Nevertheless, about 18–20% of participants regularly experienced "sleepiness" in the morning and episodes of difficulty falling asleep.

Caffeine: For the caffeine section, the average total score was ≈1.5 out of 3-a moderate daily dose (1–2 cups of coffee per day, equivalent to 100–200 mg) with a focus on midday and evening. Only a small proportion (about 5–10%) reported regular consumption of coffee or energy drinks immediately before bedtime.

Cardiovascular symptoms: The average score for the cardiovascular section was ≈1.66 out of 3, indicating a relatively moderate frequency of symptoms. About 20–30% of participants noted episodes of palpitations, arrhythmias, or brief spikes in blood pressure (more often during periods of academic stress, general stress, or after caffeine consumption). The association between "evening coffee and cardiac symptoms" was found to be significant: respondents who consumed caffeine in the evening more frequently experienced symptoms more often (though not always severe). A similar association was observed with indicators of sleep deprivation. Thus, analysis of the results showed that moderate sleep disturbances and moderate caffeine consumption coincide with moderate manifestations of cardiovascular system activation (tachycardia,

slight fluctuations in blood pressure) in the majority of participants.

Discussion

Our findings are consistent with the current literature: even in young, healthy individuals, several nights of poor sleep are associated with changes in vascular function. Recent studies emphasize that even occasional sleep deprivation causes an increase in sympathetic tone and cortisol levels, which raises systolic and diastolic blood pressure (Centers for Disease Control and Prevention; Lack of sleep can increase the risk of cardiovascular disease). Normally, blood pressure decreases at night; with insomnia, this "physiological shift" is lost, so blood pressure remains high for most of the day (Centers for Disease Control and Prevention; Lack of sleep can increase the risk of cardiovascular disease). Scientists have shown that short sleep is associated with a 7–11% increased risk of hypertension (Getting Too Little Sleep Linked to High Blood Pressure, 2024, Centers for Disease Control and Prevention), while chronic insomnia is associated with an increased incidence of cardiac arrhythmias and thrombosis (Centers for Disease Control and Prevention; Lack of sleep can increase the risk of cardiovascular disease).

Physiologically, sleep deprivation triggers a cascade of inflammatory reactions. For example, an experiment with young adults demonstrated that after three nights of 4 hours of sleep, levels of proatherogenic cytokines and inflammatory proteins associated with the development of atherosclerosis and heart failure increase (Centers for Disease Control and Prevention; Lack of sleep can increase the risk of cardiovascular disease). Caffeine, compounding the effects of sleep deprivation, blocks adenosine receptors, which releases catecholamines (adrenaline, norepinephrine) and increases heart rate and blood pressure (Connolly L. Q&A; Centers for Disease Control and Prevention. About Sleep and Your Heart Health). For most people, this is not critical, but in susceptible individuals, it can cause palpitations, extrasystoles, or an angina attack in the presence of coronary artery obstruction. Thus, the combination of insomnia and evening caffeine stress can disrupt the functioning of the autonomic nervous system and the vascular endothelium. At the cellular level, there is an increase in oxidative stress and a decrease in the availability of nitric oxide – a mediator of vascular relaxation. As a result, vascular resistance and the load on the myocardium increase.

Although no serious pathologies were identified in our sample, the data obtained demonstrate risk signals. Even moderate levels of sleep deprivation and caffeine stimulation are accompanied by warning signs (mild arrhythmia, elevated blood pressure). Recurrent episodes of such reactions may, in the long term, foreshadow the development of hypertension, ischemic heart disease, or stroke. Research into the mechanisms involved shows that prolonged sleep deprivation leads to the development of metabolic syndrome, which sharply increases the risk of CVD. According to the CDC, chronic sleep disturbance is associated with a significant increase in cases of heart attack and heart failure (Centers for Disease Control and Prevention; Lack of sleep can increase the risk of cardiovascular disease).

Preventive Measures and the Role of IT/AI

The following measures are recommended to reduce risk:

Regular sleep schedule: go to bed and wake up at the same time every day (including weekends) (Centers for Disease Control and Prevention; Lack of sleep can increase the risk of cardiovascular disease). This helps synchronize circadian rhythms and avoid the accumulation of "social jet lag." Sleep hygiene: sleep in a dark, cool, and quiet room. Avoid screens (phone, computer) 1–2 hours before bedtime (Centers for Disease Control and Prevention; Lack of sleep can increase the risk of cardiovascular disease). Caffeine restriction: avoid caffeine, energy drinks, and beverages high in caffeine several hours before bedtime (Centers for Disease Control and Prevention; Lack of sleep can increase the risk of cardiovascular disease; Connolly L. Q&A:). Ideally, stop consuming them after 4–6 p.m. Insomnia treatment: use evidence-based treatment methods – cognitive behavioral therapy for insomnia (CBT-I). Modern digital solutions (mobile apps, AI-based chatbots) are already successfully im-

plementing elements of CBT-I and helping to normalize sleep (Cai M., Liang S., Zhen S. et al., 2026, 3–6). Health monitoring: regularly monitor blood pressure, especially if you have insomnia; consult a cardiologist if necessary. Physical activity and nutrition: moderate exercise during the day normalizes sleep, and a healthy diet reduces the burden on the cardiovascular system.

The use of modern technologies, such as wearable trackers and apps – smartwatches and fitness trackers (Fitbit, Apple Watch, etc.) with sleep tracking features – helps identify patterns (frequent awakenings, late bedtimes) and correct them in a timely manner. The service can remind you to start preparing for bed. AI sleep consultants. Algorithms and virtual assistants are emerging that analyze data (sleep diaries, physiology) and recommend personalized measures. For example, AI chatbots trained using CBT-I methods help manage anxiety and insomnia by offering relaxation exercises and cognitive techniques (Cai M., Liang S., Zhen S. et al., 2026, 3–6). Telemedicine and digital therapy. Online consultation and cognitive-behavioral therapy programs can increase access to care for sleep disorders.

Conclusion

Analysis of the survey results (N=90) revealed that moderate signs of chronic sleep deprivation and regular caffeine consumption in the afternoon are prevalent among young students. These factors are accompanied by moderate levels of cardiovascular manifestations (elevated heart rate, episodes of arrhythmia, mild elevation of blood pressure)—signs of an activated sympathetic-adrenal system. The data obtained confirm the conclusions of recent studies that even at a young age, the combination of insomnia and stimulant caffeine has a noticeable effect on cardiac and vascular function (Centers for Disease Control and Prevention; Lack of sleep can increase the risk of cardiovascular disease; Connolly L. Q&A:). The identified patterns underscore the need to inform young people early about the risks: maintaining a regular sleep schedule and avoiding caffeine in the evening should be considered important preventive measures for heart health.

References:

Centers for Disease Control and Prevention. About Sleep and Your Heart Health [Online resource]. URL: https://www.cdc.gov/heart-disease/about/sleep-and-heart-health.html

Lack of sleep can increase the risk of cardiovascular disease [Электронный ресурс] // ScienceDaily. 2025. URL: https://www.sciencedaily.com/releases/2025/05/250508112739.htm

Connolly L. Q&A: What effect does caffeine have on your heart? [Online resource] // UC Davis Health. 2023. URL: https://health.ucdavis.edu/news/headlines/qa-what-effect-does-caffeine-have-on-your-heart/2023/12

Getting Too Little Sleep Linked to High Blood Pressure [Online resource] // American College of Cardiology. 2024. URL: https://www.acc.org/about-acc/press-releases/2024/03/26/18/40/getting-too-little-sleep-linked-to-high-blood-pressure

Cai M., Liang S., Zhen S. et al. Toward integrated sleep health: multimodal AI in Hang Hao Meng agent [Online resource] // npj Digital Medicine. 2026. Vol. 9. Art. 232. URL: https://www.nature.com/articles/s41746-026-02432-9/ DOI: 10.1038/s41746-026-02432-9.

submitted 12.04.2026;
accepted for publication 26.04.2026;
published 30.04.2026

Contact: samandarg517@gmail.com

The Austrian Journal of Technical and Natural Sciences, 2026 No 3–4
ISSN 2310-5607

PREMIER Publishing
ppublishing.org

DOI:10.29013/AJT-26-3.4-162-169

THE EFFECT OF HYPOTHYROIDISM ON THE OUTCOMES OF IN VITRO FERTILIZATION, DEPENDING ON AUTOIMMUNE STATUS

Nasirova K. K. [1]***, Shodieva K. T.*** [2]***, Jilonova A. N.*** [1]***, Khodjaeva F. S.*** [1]***, Kurbonov D. B.*** [1]

[1] Endocrinology, pediatric endocrinology department, Tashkent State Medical University, Uzbekistan

[2] Obstetrics and gynecology in family medicine department, Tashkent State Medical University, Uzbekistan

Cite: *Nasirova K. K., Shodieva K. T., Jilonova A. N., Khodjaeva F. S., Kurbonov D. B. (2026). The Effect of Hypothyroidism on the Outcomes of In Vitro Fertilization, Depending on Autoimmune Status. Austrian Journal of Technical and Natural Sciences 2026, No 3–4.* https://doi.org/10.29013/AJT-26-3.4-162-169

Abstract

Introduction. Subclinical hypothyroidism often goes undiagnosed due to the absence of pronounced clinical symptoms. However, even minimal thyroid hypofunction can have a negative impact on a woman's reproductive function, including ovarian reserve and the success of in vitro fertilization (IVF) programs.

Materials and Methods: The study included women with endocrine infertility against a background of hypothyroidism. The patients were divided into groups: Group 1-women with hypothyroidism of autoimmune etiology (n=39); Group 2-women with hypothyroidism without autoimmune thyroiditis (n=49). The control group consisted of women of reproductive age without thyroid dysfunction (n=20). To assess ovarian reserve, anti-Müllerian hormone (AMH) and inhibin B levels were measured on days 3–5 of the menstrual cycle, and antral follicle count was performed. Additionally, levels of TSH, free T4, antibodies to TPO and TG, and prolactin were assessed.

Results: Patients with hypothyroidism showed a statistically significant decrease in AMH and inhibin B levels compared with the control group ($p<0.05$). TSH levels were higher in the presence of autoimmune thyroiditis. In patients who became pregnant, inhibin B levels were statistically significantly higher ($p<0.001$). Conclusion. Hypothyroidism is associated with a decrease in ovarian reserve. Inhibin B is an informative prognostic marker of the effectiveness of IVF programs. The likelihood of pregnancy in patients with hypothyroidism is associated with higher levels of AMH and inhibin B.

Keywords: *hypothyroidism, autoimmune thyroiditis, infertility, ovarian reserve, AMH, inhibin B, TSH, IVF*

Introduction

In modern reproductive medicine, significant attention is paid to assessing the impact of thyroid function on the effectiveness of assisted reproductive technologies. In clinical practice, when analyzing the outcomes of ART programs, indicators such as estradiol levels on the day of ovulation induction, the number of oocytes retrieved, their degree of maturity and fertilization potential, as well as implantation rates, clinical pregnancy rates, and live birth rates are considered. Nevertheless, research findings in this area remain inconsistent and do not allow for definitive conclusions (Unuane D., Velkeniers B., Bravenboer B., Drakopoulos P., Tournaye H., Parra J., De Brucker M., 2017).

Ovarian reserve plays a special role in predicting treatment efficacy. Anti-Müllerian hormone and inhibin B are most commonly used to assess it; however, their relationship with thyroid function has not been sufficiently studied. At the same time, there is evidence suggesting a possible role for thyroid hormones in regulating the processes that determine the quantitative and qualitative characteristics of oocytes, which in turn determines the subsequent outcomes of ART (Practice Committee of the American Society for Reproductive M., 2015).

Studies at the molecular and cellular levels have shown that thyroid hormone receptors are widely expressed in structures of the female reproductive system, including granulosa cells and oocytes. This indicates the direct involvement of thyroid hormones in the regulation of folliculogenesis. It has been established that changes in their concentration, even within the reference range, can influence the action of follicle-stimulating hormone, enhancing follicle growth and reducing the severity of apoptosis. In contrast, elevated levels of thyroid hormones may have an adverse effect, reducing aromatase activity in granulosa cells and disrupting the development of preantral follicles (Birjandi B., Ramezani Tehrani F., Amouzegar A., Tohidi M., Bidhendi Yarandi R., Azizi F., 2021; Korevaar T. I.M., Mínguez-Alarcón L., Messerlian C., de Poortere R. A., Williams P. L., Broeren M. A., Hauser R., Souter I. C., 2018).

The regulatory influence of thyroid hormones is also mediated through the hypothalamic-pituitary-ovarian axis. They participate in the control of ovulation, ensure optimal conditions for implantation, and influence the early stages of embryonic development. Thyroid imbalance may be accompanied by a decrease in ovarian reserve, deterioration in oocyte quality, and a reduced likelihood of pregnancy (Korevaar T. I.M., Mínguez-Alarcón L., Messerlian C., de Poortere R. A., Williams P. L., Broeren M. A., Hauser R., Souter I. C., 2018; Weghofer, A., Barad, D.H., Darmon, S. *et al.,* 2016).

Clinical data indicate that subclinical hypothyroidism and autoimmune thyroid diseases are more commonly detected in women with infertility than in the general population. This confirms the significance of thyroid dysfunction as one of the factors affecting reproductive potential.

Thus, endocrine disorders associated with thyroid pathology play a significant role among the causes of female infertility and require further study from the perspectives of both clinical practice and the fundamental mechanisms regulating reproductive function.

However, the effect of hypothyroidism on markers of ovarian reserve (anti-Müllerian hormone (AMH) and inhibin B) has not been sufficiently studied.

The aim of the study was to investigate the effect of thyroid hormones on ovarian reserve and pregnancy outcomes in women with endocrine infertility due to hypothyroidism undergoing IVF treatment.

Materials and Methods

The study included women with endocrine infertility due to hypothyroidism who were undergoing treatment using in vitro fertilization (IVF) programs. The patients were divided into two groups based on the presence of autoimmune thyroiditis. Group 1 consisted of women with autoimmune hypothyroidism (n=39), and Group 2 consisted of women with hypothyroidism without autoimmune thyroiditis (n=49). Within each group, subgroups were identified: those who achieved pregnancy (IVF+) and those who did not achieve pregnancy (IVF–). The control group consisted of women of reproductive age with tubal-peritoneal infertility without thyroid dysfunction (n=20).

Anti-Müllerian hormone (AMH), FSH concentration, and serum inhibin B levels

were measured on days 3–5 of the unstimulated menstrual cycle. The antral follicle count (AFC) was defined as the sum of antral follicles in both ovaries, measured by transvaginal ultrasound in the early follicular phase. Women with multifollicular ovaries, with an AFC >20 on either the left or right side, or with ovaries that were difficult to visualize, were excluded from the analysis.

To assess thyroid status, the patients' levels of thyroid-stimulating hormone (TSH), free T4, free T3, anti-TPO antibodies, and anti-thyroglobulin antibodies were measured. Statistical analysis of the results was performed using Student's t-test; differences were considered statistically significant at $p < 0.05$.

Results

The age range of the patients was 20 to 45 years. The mean age of the patients was 33.1 ± 3.2 years. Body mass index (BMI) was within the normal range at 23.5 ± 2.6. Analysis of the infertility pattern showed that primary infertility predominated in both groups of patients with hypothyroidism: 65.9% in Group 1 and 61.8% in Group 2. In the control group, by contrast, all patients had secondary infertility, which was due to the specific characteristics of the control sample.

The average duration of infertility in patients with hypothyroidism was virtually the same in both groups and amounted to 5.9 ± 0.9 and 5.9 ± 0.7 years, respectively, whereas in the control group it was lower-4.03 ± 1.2 years.

Analysis of clinical symptoms showed (Table 1) that in patients with hypothyroidism, regardless of the presence of an autoimmune component, complaints characteristic of thyroid insufficiency predominated. The most frequently reported symptoms were general weakness, dry skin, hair loss, and psychoemotional lability, reflecting the systemic effects of thyroid hormone deficiency.

An analysis of clinical symptoms revealed that, regardless of the presence of an autoimmune component, patients with hypothyroidism predominantly reported complaints characteristic of thyroid insufficiency: general weakness (73.9% and 83.8% in groups 1 and 2, respectively), dry skin and hair loss (69.6% and 75.7%, respectively), and psychoemotional lability (86.9% and 93.2%).

Table 1. *Clinical symptoms in women with endocrine infertility due to hypothyroidism*

	Group 1 (AIT+), n=39		Group 2 (AIT–), n=49	
	Abs	%	Abs	%
General weakness	28	71,8 ± 6,5	41	83,7 ± 4,2
Dry skin	27	69,2 ± 6,8	37	75,5 ± 5,0
Brittle nails	10	25,6 ± 6,5	11	22,9 ± 4,9
Hair loss	27	69,2 ± 6,8	37	75,5 ± 5,0
Drowsiness	7	17,9 ± 5,8	7	14,3 ± 4,1
Cold intolerance	10	25,6 ± 6,5	14	28,6 ± 5,2
Headache	12	30,7 ± 6,9	21	42,8 ± 5,7*
Psychoemotional lability	34	87,1 ± 5,0	46	93,8 ± 2,9*
Memory impairment	6	15,4 ± 5,3	8	16,3 ± 4,3
Constipation	9	23,1 ± 6,3	15	30,6 ± 5,3
Increased blood pressure	4	10,2 ± 4,6	5	10,2 ± 3,6
Edema	2	5,1 ± 3,6	4	8,1 ± 3,2
Weight gain	3	7,7 ± 4,2	4	8,1 ± 3,4

*Note: * – differences are statistically significant between the groups ($p < 0.05$)*

A comparative analysis revealed that headaches were significantly more common in the group without AIT (43.2% vs. 32.6%; $p<0.05$) and psychoemotional lability (93.2% vs. 86.9%; $p<0.05$) were significantly more common in the group without AIT, which may reflect a more pronounced influence of vascular and metabolic factors in this form of

hypothyroidism. No intergroup differences were found for the remaining symptoms – chilliness, constipation, sleep disturbances, and edema ($p>0.05$)—which indicates the similarity of the clinical picture of hypothyroidism regardless of its etiology and underscores the necessity of mandatory laboratory confirmation of the diagnosis.

It is known that in women, thyroid dysfunction is often associated with menstrual cycle disorders. Hypothyroidism affects the regulation of the hypothalamic-pituitary-ovarian axis and can lead to changes in the duration and nature of the menstrual cycle (MC).

Analysis of menstrual function revealed statistically significant differences between groups. A normal menstrual cycle was observed significantly less frequently in patients in Group 1 (34.8%) compared with Group 2 (59.5%) and the control group (60%; $p<0.05$). The most pronounced differences were found regarding opsomenorrhea: in the AIT group, it was recorded in 47.8% of patients, which was 2.5 times higher than the rates in the second and control groups (18.9% and 15.0%, respectively; $p<0.01$). Amenorrhea was observed exclusively in patients in the first group (8.7%), indicating the most pronounced disruption of hypothalamic-pituitary-ovarian regulation when hypothyroidism is combined with AIT. The overall frequency of menstrual cycle disorders was 52.0% in the first group, 43.0% in the second, and 25.0% in the control group, which confirms the pathogenetic role of thyroid dysfunction in menstrual cycle regulation and is consistent with the data of G. Krassas et al.

The identified changes suggest that thyroid dysfunction may have a significant impact on menstrual cycle regulation. In the group of patients with hypothyroidism against a background of AIT, a more pronounced tendency toward a prolonged menstrual cycle was observed, which may reflect disturbances in the hormonal regulation of the reproductive system compared to the group of women with hypothyroidism without AIT. Consequently, the presence of AIT in women with hypothyroidism can be considered an additional factor contributing to the development of anovulatory cycles and a decrease in reproductive potential.

To provide a clearer picture of the prevalence of menstrual cycle disorders among the patients surveyed, the overall incidence of menstrual dysfunction was analyzed (Fig. 1).

Figure 1. *Prevalence of menstrual cycle disorders in women with endocrine infertility and hypothyroidism*

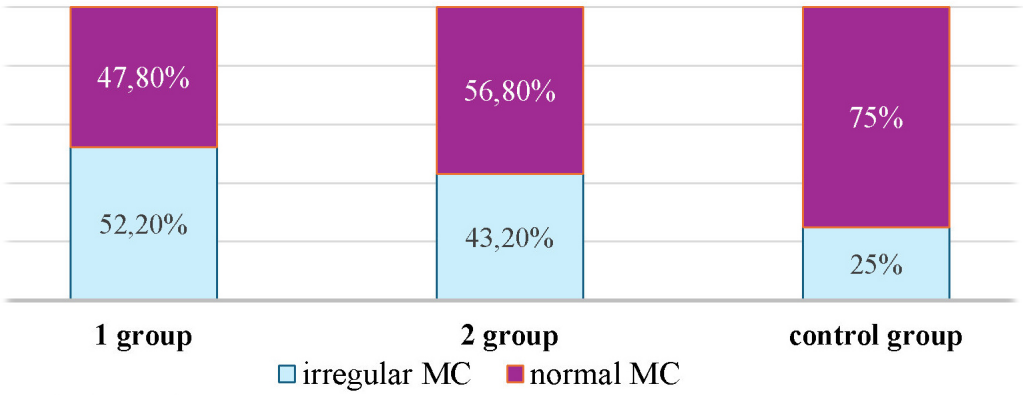

It was found that menstrual cycle disorders were most frequently detected in patients in Group 1, in 52% of cases. In Group 2, this figure was 43.0%, and in the control group, 25.0%. The results indicate a higher frequency of menstrual dysfunction in women with hypothyroidism, especially in the presence of an autoimmune component.

Analysis of thyroid status showed that TSH levels in patients with hypothyroidism were significantly higher than those in the control group. Thus, in Group 1, the TSH level was 6.1 ± 0.8 mIU/mL, which was nearly 2.5 times higher than in the control group (2.4 ± 1.5 mIU/mL; $p < 0.01$). In Group 2, TSH levels also remained elevated (5.5 ± 0.6 mIU/mL), but were significantly

lower than in Group 1 ($p < 0.05$), which may indicate more pronounced thyroid dysfunction in the presence of an autoimmune component (Table 2).

There was no statistically significant difference in free T4 levels between the study groups ($p > 0.05$), indicating a predominance of subclinical hypothyroidism among the patients examined. The most pronounced differences were observed in the analysis of antithyroid antibodies. In Group 1, the level of anti-TPO antibodies was 181.8 ± 26.8 IU/mL, which was more than 19 times higher than the values in Group 2 (9.5 ± 1.1 IU/mL) and the control group (10.7 ± 3.7 IU/mL) ($p < 0.01$).

Table 2. *Hormonal status indicators of women with endocrine infertility and hypothyroidism*

Parameter	Group 1 (n=39)	Group 1 (n=39)	Group 1 (n=39)
TSH, mIU/mL	6.1±0.8	5.5±0.8	2.4±1.5*
T4, pmol/L	12.1±1.9	11.4±2.7	12.2±2.8
Anti-TPO, IU/mL	181.8±26.8	9.5±1.1**	10.7±3.7**
Anti-TG, IU/mL	186.2±27.5	27.2±3.2**	28.6±7.5**
Prolactin (PRL), ng/mL	59.9±8.8	51.5±6.0*	7.4±1.1**
AMH, ng/mL	1.9±0.3	1.8±0.2	3.3±1.6*

*Note: * – statistically significant differences between Group 1 and Group 2 ($p < 0.05$); ** – statistically significant differences between Group 1 and the control group ($p < 0.01$)*

A similar trend was observed for anti-thyroglobulin antibodies: in Group 1, their level reached 186.2 ± 27.5 IU/mL, which was 6––7 times higher than in Groups 2 and the control group ($p < 0.01$). The obtained data confirm the pronounced autoimmune nature of thyroid gland involvement in patients of the first group.

Analysis of prolactin levels showed that patients with hypothyroidism exhibited marked hyperprolactinemia. In Group 1, the prolactin level was 59.9 ± 8.8 ng/mL, and in Group 2, it was 51.5 ± 6.0 ng/mL, which was 7–8 times higher compared to the control group (7.4 ± 1.1 ng/mL; $p < 0.01$). At the same time, prolactin levels were significantly higher in group 1 than in group 2 ($p<0.05$), which may reflect more pronounced neuroendocrine disturbances in the combination of hypothyroidism with autoimmune thyroiditis.

A comparison of ultrasound and laboratory data revealed certain patterns. Specifically, patients with pronounced structural changes in the thyroid gland (diffuse and nodular goiter) were more likely to have elevated levels of TSH and antithyroid antibodies, particularly in the group with autoimmune thyroiditis.

The correlation analysis revealed statistically significant associations between thyroid ultrasound characteristics and indicators of thyroid status. It was found that thyroid volume positively correlated with TSH levels ($r=0.3$; $p<0.05$), reflecting a tendency for the gland to enlarge as thyroid insufficiency progresses. However, this association was weak, indicating that the development of structural changes in the thyroid gland is multifactorial.

More pronounced correlations were found between thyroid volume and levels of antibodies to thyroid peroxidase ($r = 0.4$; $p < 0.01$), as well as antibodies to thyroglobulin ($r = 0.35$; $p<0.05$), indicating a significant influence of autoimmune processes on the structural remodeling of thyroid tissue.

Analysis of individual ultrasound findings revealed that the presence of diffuse thyroid changes was significantly associated with elevated AT-TPO levels ($r=0.45$; $p<0.01$), whereas nodular formations were more frequently detected with elevated AT-TG levels ($r=0.32$; $p<0.05$). Heterogeneity of the thyroid gland structure also demonstrated a weak positive correlation with TSH levels ($r=0.28$; $p<0.05$).

Thus, in patients with hypothyroidism, especially in the presence of autoimmune thyroiditis, more pronounced thyroid status abnormalities are detected, characterized by elevated TSH levels, a significant increase in antithyroid antibodies, and hyperprolac-

tinemia. The data obtained confirm that the autoimmune component is a key factor that exacerbates endocrine disorders and potentially affects reproductive function.

When assessing ovarian reserve based on anti-Müllerian hormone levels, a decrease was observed in women with hypothyroidism in both groups compared to the control group, indicating a reduction in ovarian reserve in this condition. At the same time, AMH levels were higher in patients who became pregnant than in those who did not, although statistically significant differences were found only in the second group of patients ($p<0.05$).

Analysis of inhibin B levels on days 3–5 of the menstrual cycle revealed statistically significant differences between the IVF+ and IVF– subgroups. In patients who became pregnant, inhibin B levels were significantly higher compared to those who did not become pregnant ($p<0.001$).

Table 3. *Ovarian reserve indicators and IVF outcomes depending on autoimmune status*

	Group 1 (AIT+), n=39		Group 2 (AIT–), n=49		Control, n=20	P
	IVF+ (n=24)	IVF– (n=15)	IVF+ (n=38)	IVF– (n=11)		
TSH before treatment	7,5±1,6	7,3±2	4,9±0,8	4,8±1,3	2,1±0,6	>0,05
AMH	1,4±0,3	1,4±0,4	1,7±0,3	1,4±0,4	3,2±0,3	<0,05
Inhibin B	78±16,6	44,4±12,3	95,8±15,1	43,9±12,2	84,3±5,4	<0,001

Note: Data are presented as mean ± standard error of the mean (M±m). Abbreviations: AIT – autoimmune thyroiditis; IVF – in vitro fertilization; TSH – thyroid-stimulating hormone; AMH – anti-Müllerian hormone

Analysis of ovarian reserve indicators showed that baseline TSH levels did not have a statistically significant effect on pregnancy outcomes in IVF programs ($p>0.05$), despite higher values in patients with hypothyroidism compared to the control group (Table 2). This indicates that after correction of thyroid status, this parameter loses its independent prognostic value.

At the same time, ovarian reserve indicators demonstrated a significant association with IVF outcomes. The AMH level was significantly lower in patients with hypothyroidism compared to the control group ($p<0.05$), indicating a decrease in ovarian reserve in the presence of endocrine pathology.

Furthermore, it was found that in patients with autoimmune thyroiditis, inhibin B levels were statistically lower compared to patients without an autoimmune component, which may reflect a more pronounced suppression of ovarian reserve in autoimmune pathology.

Correlation analysis revealed a negative correlation between TSH levels and markers of ovarian reserve – inhibin B and AMH ($r<0$, $p<0.05$)—suggesting a possible influence of thyroid dysfunction on reduced functional activity.

Discussion

According to the study by Pirgon O. (Pirgon, O., Sivrice, C., Demirtas, H., & Dundar, B., 2016) and colleagues, patients with autoimmune thyroiditis (AIT) are at risk for developing premature ovarian failure, suggesting a possible association between autoimmune processes and impaired ovarian function.

The results of a large retrospective study by Polyzos N. P. (Nikolaos P. Polyzos, Evangelos Sakkas, Alberto Vaiarelli, Kris Poppe, Michel Camus, Herman Tournaye, 2015) and colleagues ("Thyroid autoimmunity, hypothyroidism and ovarian reserve: a cross-sectional study of 5,000 women based on age-specific AMH values") demonstrated that in patients with a genetic predisposition to diminished ovarian reserve, the prevalence of hypothyroidism is higher compared to women with idiopathic diminished ovarian reserve, regardless of thyroid status. These data suggest the presence of common pathogenic mechanisms underlying both thyroid and ovarian dysfunction.

At the same time, studies by Saglam F. et al. and Ayesha et al. (Saglam, F., Onal, E. D., Ersoy, R., Koca, C., Ergin, M., Erel, O., & Cakir, B., 2015; Ayesha, Jha V., 2016) have

shown that diminished ovarian reserve is more strongly associated with hypothyroidism of autoimmune etiology, underscoring the significance of immune mechanisms in the pathogenesis of reproductive disorders.

According to Weghofer A. and colleagues (Weghofer, A., Barad, D.H., Darmon, S. *et al.*, 2016), the key role in the decline of ovarian reserve is played not so much by the autoimmune process itself as by the increase in thyroid-stimulating hormone (TSH) levels. In this regard, normalization of thyroid status, particularly achieving target TSH levels, may contribute to improved ovarian reserve parameters.

The results obtained in this study are consistent with the literature data and confirm the influence of thyroid hormones on ovarian function. Hypothyroidism is associated with a decrease in ovarian reserve markers, as evidenced by reduced levels of anti-Müllerian hormone (AMH) and inhibin B. These changes may be due to impaired folliculogenesis, reduced ovarian sensitivity to gonadotropic stimulation, and dysregulation of follicular growth and maturation mechanisms.

Inhibin B is of particular importance in assessing ovarian reserve, as it reflects the functional activity of granulosa cells and the number of antral follicles. A decrease in its level may indicate early abnormalities in the ovarian follicular apparatus and serve as an additional marker of declining reproductive potential.

Conclusions

Women with hypothyroidism exhibit a reduced ovarian reserve, as indicated by AMH and inhibin B levels, compared to healthy women. In women with AIT, pre-treatment TSH levels were statistically higher than in women with hypothyroidism of other etiologies. AMH levels were higher in patients who became pregnant; however, statistically significant differences were not observed in all groups. Inhibin B levels on days 3–5 of the menstrual cycle and after superovulation stimulation were significantly higher in patients who became pregnant ($p<0.001$). In patients with AIT, the pregnancy rate was significantly lower than in women without AIT. This may be related to the duration of hypothyroidism. This article did not account for the duration of hypothyroidism, which affects treatment efficacy and pregnancy rates.

References

Unuane D., Velkeniers B., Bravenboer B., Drakopoulos P., Tournaye H., Parra J., De Brucker M. (2017). Impact of thyroid autoimmunity in euthyroid women on live birth rate after IUI, *Human Reproduction*, – Vol. 32. – Issue 4. April 2017. – P. 915–922. URL: https://doi.org/10.1093/humrep/dex033

Practice Committee of the American Society for Reproductive M. (2015). Subclinical hypothyroidism in the infertile female population: a guideline. Fertil Steril – 104. – P. 545–553.

Birjandi B., Ramezani Tehrani F., Amouzegar A., Tohidi M., Bidhendi Yarandi R., Azizi F. (2021). The association between subclinical hypothyroidism and TPOAb positivity with infertility in a population-based study: Tehran thyroid study (TTS). BMC Endocr Disord. 2021 May 26. – 21(1). – 108 p. Doi: 10.1186/s12902-021-00773-y. PMID: 34034716; PMCID: PMC8152029.

Korevaar T. I.M., Mínguez-Alarcón L., Messerlian C., de Poortere R. A., Williams P. L., Broeren M. A., Hauser R., Souter I. C. (2018). Association of Thyroid Function and Autoimmunity with Ovarian Reserve in Women Seeking Infertility Care. Thyroid. 2018. Oct. – 28(10). – P. 1349–1358. Doi: 10.1089/thy.2017.0582. Epub 2018 Aug 14. PMID: 29943679; PMCID: PMC6157366.

Wu J., Zhao Y. J., Wang M., Tang M. Q., Liu Y. F. (2021). Correlation Analysis Between Ovarian Reserve and Thyroid Hormone Levels in Infertile Women of Reproductive Age. Front Endocrinol (Lausanne). 2021. Sep. – 27. 12. – 745199 p. Doi: 10.3389/fendo.2021.745199. PMID: 34646238; PMCID: PMC8503559.

Weghofer, A., Barad, D.H., Darmon, S. *et al.* (2016). What affects functional ovarian reserve, thyroid function or thyroid autoimmunity?. *Reprod Biol Endocrinol* – 14. – 26 p. URL: https://doi.org/10.1186/s12958-016-0162-0

Pirgon, O., Sivrice, C., Demirtas, H., & Dundar, B. (2016). Assessment of ovarian reserve in euthyroid adolescents with Hashimoto thyroiditis. *Gynecological Endocrinology*, – 32(4). – P. 306–310. URL: https://doi.org/10.3109/09513590.2015.1116510

Nikolaos P. Polyzos, Evangelos Sakkas, Alberto Vaiarelli, Kris Poppe, Michel Camus, Herman Tournaye. (2015). Thyroid autoimmunity, hypothyroidism and ovarian reserve: a cross-sectional study of 5000 women based on age-specific AMH values, *Human Reproduction*, – Vol. 30. – Issue 7. – July, 2015. – P. 1690–1696. URL: https://doi.org/10.1093/humrep/dev089

Saglam, F., Onal, E. D., Ersoy, R., Koca, C., Ergin, M., Erel, O., & Cakir, B. (2015). Anti-Müllerian hormone as a marker of premature ovarian aging in autoimmune thyroid disease. *Gynecological Endocrinology*, – 31(2). – P. 165–168. URL: https://doi.org/10.3109/09513590.2014.973391

Ayesha, Jha V. (2016). Goswami D.Premature Ovarian Failure: An Association with Autoimmune Diseases. J Clin of Diagn Res. 2016. – 10(10). QC10-QC12. URL: https://www.doi.org/10.7860/JCDR/2016/22027/8671

submitted 29.02.2026;
accepted for publication 13.03.2026;
published 30.04.2026

Contact: zilonovazizbek@gmail.com

The Austrian Journal of Technical and Natural Sciences, 2026 No 3–4
ISSN 2310-5607

PREMIER Publishing
ppublishing.org

DOI:10.29013/AJT-26-3.4-170-173

EFFECT OF MESOTHERAPY ON THE SUBJECT PERCEPTION OF HAIR CONDITION IN PATIENTS AFTER BARIATRIC OPERATIONS

Tashkenbayeva Umida Alisherovna [1],
Abboskhonova Fotima Khasanovna [1]

[1] Tashkent State Medical University

Cite: *Tashkenbayeva U.A., Abboskhonova F.Kh. (2026). Effect of Mesotherapy on the Subject Perception of Hair Condition in Patients After Bariatric Operations. Austrian Journal of Technical and Natural Sciences 2026, No 3–4.* https://doi.org/10.29013/AJT-26-3.4-170-173

Abstract

This study is devoted to assessing the influence of mesotherapy on the subjective perception of hair condition in patients after bariatric surgeries. The work conducted a multi-parametric analysis that revealed a significant influence of the frequency of the procedure on the quality and severity of alopecia manifestations. The obtained results show that patients who received mesotherapy regularly and daily as prescribed by the doctor noted both positive and negative changes in hair condition. Analysis showed that if protocols or individual characteristics of the patient are incorrectly selected, both improvement and deterioration are possible, which is due to differences in skin and hair follicle reactions. It is important to emphasize the need for a personalized approach to therapy, adherence to standard protocols, and informing patients about possible outcomes. The research results highlight the relevance of further scientific developments in the field of safe and effective use of mesotherapy to improve the quality of life of patients who have undergone bariatric surgery.

Keywords: *bariatric operations, mesotherapy, alopecia, hair treatment, prevention*

Introduction

Alopecia, or hair loss, is a common condition affecting millions of people worldwide, significantly impacting their psychological and physical health. The problem becomes particularly relevant for patients who have undergone bariatric surgeries, as such interventions aimed at significant weight reduction can be accompanied by numerous metabolic changes, including in hair follicles (Darlenski R., Mihaylova V., Handjieva-Darlenska T., 2022; Zhang W., Fan M., Wang C., Mahawar K., Parmar C., Chen W., Yang W., 2021).

Modern studies demonstrate the complexity of the pathogenesis of postoperative alopecia. Studies emphasize the role of iron and zinc deficiency in hair loss development after bariatric surgeries (Vranić L., Mikolašević I., Milić S., 2019; El Sayed M. H., Abdallah M. A., Aly D. G., Khater N. H., 2016). Loss of body weight combined with dietary restrictions can lead to a deficiency of essential nutrients, negatively impacting hair health. Additionally, some authors note that changes in hormonal status and metabolic background also play a key role in this process.

In recent years, increasing attention has been paid to non-traditional methods of treating alopecia, such as mesotherapy. This method involves injecting active substances directly into the dermis, which is designed to improve microcirculation, enhance follicle nutrition, and stimulate hair growth. However, current literature reviews show that data on the safety and effectiveness of mesotherapy are ambiguous (Su L.-H., Chen T.-H., 2010; Guo H., Zhu J., Ma Y., Sachin B., Cao D., Tang L., 2017). Further research is needed to clarify the optimal application schemes and possible side effects.

Materials and methods

Analysis of alopecia after surgery was performed depending on the mesotherapy. The study involved 321 patients, who were divided into three groups according to the characteristics being studied. The first group included 115 patients suffering from alopecia after bariatric surgery, which made it possible to assess the influence of this type of surgical intervention on the development and nature of alopecia. The third, control group, consisted of 97 individuals without alopecia symptoms after bariatric surgery. The second group included 109 patients with alopecia who had not undergone bariatric surgery, which made it possible to compare the features of the pathology in the context of other possible causes of alopecia. Before starting the study, all participants signed informed consent in accordance with ethical standards. The subject of analysis was clinical and demographic indicators, as well as the features of alopecia course depending on the presence or absence of bariatric surgery.

Statistical analysis was conducted using StatTech version 4.12.1. Quantitative indicators were assessed for compliance with the normal distribution using the Shapiro-Wilk criterion (if the sample was less than 50) or the Kolmogorov-Smirnov criterion (if the sample was more than 50). In the absence of a normal distribution, the quantitative data were represented by the median (Me) and the interquartile range (Q1-Q3).

To describe categorical data, absolute values and percentages were used, with 95% confidence intervals for shares calculated using the Klopper-Pearson method. Comparison of three or more groups for quantitative indicators not subject to normal distribution was carried out using the Kraskel-Wallis criterion. Posteriori comparisons were carried out using the Dunn criterion with a Holm correction.

Pearson's chi square criterion was used to compare fractions in multi-field conjugate tables. In the case of multiple comparisons, the posteriori analyses were also conducted using the Pirson chi square criterion with a Holm correction. Statistical significance was established at a level of $p < 0.05$.

Research results

The conducted study analyzed patients' subjective assessment of hair condition after therapy, particularly mesotherapy, and revealed a significant influence of the frequency of this procedure on the perception of treatment results. The statistical analysis presented in the table shows clear differences between groups of patients who did not receive mesotherapy but received it periodically or daily.

Among patients who did not use mesotherapy, 100% noted no significant changes in hair condition, while 16.1% indicated some improvement, but 25.7% and 30.3% of respondents reported significant deterioration or sharp deterioration, respectively. For comparison, patients who received mesotherapy sometimes reported improvement: 25.8% noted significant improvement, 22% – improvement, but the proportion of those who did not notice changes (28.8%) or noted deterioration (31.4% slightly worse and 30.3% sharply deteriorated) also remained.

The greatest changes were observed in patients who received mesotherapy daily according to the doctor's instructions: 58.1% reported significant improvement, and 67.4% reported improved hair condition. Despite this, some patients still indicated no significant changes (46.2%) and even deterioration (42.9% slightly worse, 39.4% sharply deteriorated).

Theoretically, such responses can be attributed to a number of factors: patient expectations based on various information about the procedure, the initial condition of hair and scalp, individual reactions to injections

and the medications used, and methods and techniques used in the procedures. The data indicate that more intensive treatment can bring improvement, but also does not exclude the possibility of negative experiences, which are related to the patient's individual characteristics and the professionalism of performing procedures.

Table 1. *Analysis of mesotherapy's impact on subjective perception of treatment*

		Due to the treatment, my hair looked better						
Indicators	**Sections**	**No.**	**significantly better**	**better**	**practically identical**	**slightly worse**	**sharply deteriorated**	**p.**
Mesotherapy	no	108 (100.0).	10 (16.1)	15 (10.6)	13 (25.0)	9 (25.7)	10 (30.3)	< 0.001*
	sometimes	0 (0.0)	16 (25.8)	31 (22.0)	15 (28.8)	11. (31.4)	10 (30.3)	$p_{N/A\ –\ significantly\ better} < 0.001$
	daily according to the doctor's instructions	0 (0.0)	36 (58.1)	95 (67.4)	24 (46.2)	15 (42.9)	13 (39.4).	$p_{N/A\ –\ better} < 0.001$
	no	0 (0.0)	22 (35.5)	19 (13.5).	15 (28.8)	21 (60.0)	17 (51.5).	$p_{N/A\ –\ practically\ the\ same} < 0.001$
	yes	0 (0.0)	33 (53.2)	76 (53.9)	20 (38.5)	20 (57.1)	18 (54.5)	$p_{N/A\ –\ slightly\ worse} < 0.001$
	no	0 (0.0)	28 (45.2)	63 (44.7)	31 (59.6)	15 (42.9)	15 (45.5)	$p_{N/A\ –\ sharply\ worsened} < 0.001$ $p_{better\ –\ sharply\ deteriorated} = 0.034$

** – differences in indicators are statistically significant (p < 0.05)*

Considering the variability of reactions, the results emphasize the importance of a personalized approach to alopecia therapy. It is necessary to inform patients about possible results and side effects of mesotherapy, assess the condition of hair and the level of satisfaction at each stage of treatment. These data indicate the need for further study of the psychosomatic aspects of alopecia treatment and the development of optimal therapy programs, taking into account the expected outcome and the need to support patients throughout the treatment process.

Thus, the study demonstrates that while mesotherapy can be a powerful tool in the treatment of alopecia, its effectiveness largely depends on how individualized the approach to each patient is, which should be the focus of trichologists and dermatologists to ensure optimal therapeutic outcomes.

Conclusion

Against the backdrop of the increasing number of bariatric surgeries, the number of patients facing the problem of alopecia is also increasing. There is still no universal corrective approach to the therapy of postoperative hair loss, making this direction extremely relevant for modern dermatologists and trichologists. The role of mesotherapy in treating alopecia in such patients is of significant interest in the medical community.

A study aimed at studying the effect of mesotherapy on hair condition in patients after bariatric surgery can make a significant contribution to understanding its role in the prevention and treatment of this condition. It will allow for the creation of more accurate methodological recommendations, the selection of optimal treatment approaches, and the formation of a more personalized approach in trichology.

Thus, this research is not only relevant but also has significant potential for practical application. It can serve as a basis for developing new clinical strategies aimed at improving the quality of life of patients who have undergone bariatric surgery, and allows for ensuring more quality and safe treatment outcomes.

References

Darlenski R., Mihaylova V., Handjieva-Darlenska T. (2022). The Link Between Obesity and the Skin. Front. Nutr. – 9. – 855573 p.

Zhang W., Fan M., Wang C., Mahawar K., Parmar C., Chen W., Yang W. (2021). Global Bariatric Research Collaborative Hair Loss After Metabolic and Bariatric Surgery: A Systematic Review and Meta-Analysis. Obes. Surg. – 31. – P. 2649–2659.

Vranić L., Mikolašević I., Milić S. (2019). Vitamin D deficiency: a consequence or cause of obesity? Medicina. – 55. – 541 p.

El Sayed M. H., Abdallah M. A., Aly D. G., Khater N. H. (2016). Association of metabolic syndrome with female pattern hair loss in women: A case-control study. Int. J. Dermatol. – 55. – P. 1131–1137.

Su L.-H., Chen T.-H. (2010). Association of androgenetic alopecia with metabolic syndrome in men: A community-based survey. Br. J. Dermatol. – 163. – P. 371–377.

Guo H., Zhu J., Ma Y., Sachin B., Cao D., Tang L. (2017). Risk factors analysis of hair loss in obese patients afer laparoscopic sleeve gastrectomy. Chin. J. Dig. Surg. – 12. – P. 592–595.

submitted 15.04.2026;
accepted for publication 29.04.2026;
published 30.04.2026

Contact: umidatashkenbaeva@mail.ru; fabbaskhanova@inbox.ru

The Austrian Journal of Technical and Natural Sciences, 2026 No 3–4
ISSN 2310-5607

PREMIER Publishing
ppublishing.org

Section 7. Technical sciences in general

DOI:10.29013/AJT-26-3.4-174-178

METHODOLOGY FOR SELECTING THE OPERATING FREQUENCIES OF SENSORS (Search for the optimal operating frequency of a sensor for designing a monitoring system of a single mixture component. Search for the optimal operating frequencies of sensors for designing a monitoring system of two mixture components)

Aliaksandr Achapouski [1]

[1] Architect of AI-Based Security Systems, Specializing in Digital Identity Infrastructure and Real-Time Authentication Phoenix, Arizona

Cite: *Achapouski A. (2026). Methodology For Selecting the Operating Frequencies of Sensors. (Search for the optimal operating frequency of a sensor for designing a monitoring system of a single mixture component. Search for the optimal operating frequencies of sensors for designing a monitoring system of two mixture components). Austrian Journal of Technical and Natural Sciences 2026, No 3–4.* https://doi.org/10.29013/AJT-26-3.4-174-178

Abstract

This study presents the methodological foundations for designing a system intended for monitoring the concentration of components within complex mixtures. A mixture is defined as a multicomponent system in which one predominant component functions as a conditional solvent, while the remaining components are treated as conditionally dissolved elements that may exist in dissolved, suspended, gaseous, aerosol, or composite forms.

The methodology includes experimental validation of resonant sensor prototypes across an extended concentration range, emphasizing the determination of optimal operating frequencies for single- and multi-frequency sensing systems. Particular attention is devoted to equipment preparation, structural material selection, protective and functional coatings, sensor design configurations, and testing procedures, including the evaluation of acidity levels under varying temperature, temporal, and compositional conditions.

The proposed approach demonstrates that integrating multiple sensor elements operating at different electromagnetic resonant frequencies within a single sensing module significantly enhances analytical capability, enabling rapid and comprehensive material characterization. Further technical specifications and implementation details will be addressed in subsequent publications and related patent documentation.

Keywords: *Non-contact monitoring system; Sensor operating frequency; Optimal sensor operating frequency; Methodology for operating frequency selection; Dissolved components;*

Conditionally dissolved components; Conditional solvent; Liquid single-component substance; Design of a monitoring system; Frequency scanning process; Amplitude variation; Probing voltage; Stabilized constant amplitude; Single-component monitoring system; Optimal operating frequency of a single-component monitoring system; Frequency scanning of a sample; Results analysis; Frequency sample analysis; The selected frequencies constitute the initial data for the design and fabrication of prototype resonant sensors

Principle of measurement (electromagnetic coupling with object under test)

Figure 1. *Equivalent circuitry of RIST-sensor illustrates an electromagnetic coupling with analyte*

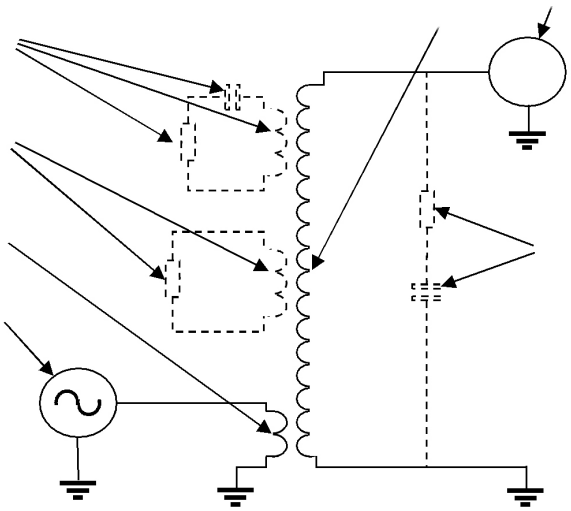

Schematic of RIST-sensor (depicted with solid line)

1 – source of an alternating electric field with frequency sweep (sweep generator)

2 – excitation coil

3 – sensing coil

4 – data acquisition system

Electromagnetic response of object under test (depicted with dash line)

5 – vertical displacement currents (dielectric polarization)

6 – vertical ionic currents and eddy currents

7 – linear conductance, displacement and ionic currents caused by difference in electrical potential spread along the sensing coil.

Search for the Optimal Operating Frequency of a Sensor for Designing a Single-Component Mixture Monitoring System

Such a monitoring system may be applied in technological processes in which the concentration of one component may vary, while the concentrations of the remaining components remain constant.

Preparation of Samples for Measurement

Two samples shall be prepared with concentrations of the target component corresponding to the lower and upper limits of the expected concentration variation range.

Frequency Scanning Procedure

Using a potentiostat, the prepared samples shall be subjected to frequency scanning across the entire operating bandwidth of the potentiostat (in our case, from 0.100 MHz to 170 MHz).

During the scanning process, the potentiostat readings are recorded in the form of:

- amplitude variations, and
- phase shift of the current flowing through the sample relative to a harmonically varying probing voltage with a stabilized constant amplitude.

Analysis of Results

Based on the scanning results, several frequencies shall be selected:

- frequencies at which the difference in amplitude between the investigated samples reaches its maximum values;
- frequencies at which the difference in phase shift reaches its maximum values.

The selected frequencies will serve as initial design data for the development and fabrication of prototype resonant sensors.

Selection of the Optimal Sensor

The selection of a set of frequencies based on potentiostat scanning results is preliminary in nature.

To determine the optimal operating frequency of a single-component concentration monitoring system, it is necessary to test each

prototype resonant sensor using not two, but at least ten samples with different concentrations of the target component within the anticipated range of its variation.

After testing all prototype sensor samples, the best-performing sensor can be selected. Preference should be given to sensors that, in addition to high sensitivity, demonstrate a **monotonic** change in readings as the concentration of the monitored component changes (to facilitate subsequent calibration).

Lower operating frequencies are generally preferable from the standpoint of electromagnetic interference immunity. In selecting a sensor, design and construction constraints must also be taken into account.

Search for Optimal Operating Frequencies of Sensors for Designing a Two-Component Mixture Monitoring System

Such a monitoring system may be applied in technological processes in which the concentrations of two components may vary, while the concentrations of the remaining components remain constant.

Preparation of Samples for Measurement

Two samples shall be prepared for each target component with concentrations corresponding to the lower and upper limits of the expected range of variation of these concentrations, as well as a sample in which these components are completely absent.

Frequency Scanning Procedure

Using a potentiostat, the prepared samples shall be subjected to frequency scanning across the entire operating bandwidth of the potentiostat (in our case, from 0.100 MHz to 170 MHz). During the scanning process, the potentiostat readings are recorded in the form of amplitude variations and the phase shift of the current flowing through the sample relative to a harmonically varying probing voltage with a stabilized constant amplitude.

Analysis of Results

For each target component, based on the scanning results, several frequencies shall be selected:

- frequencies at which the difference in amplitude between the investigated samples reaches its maximum values;
- frequencies at which the difference in phase shift reaches its maximum values; and
- frequencies (or frequency bands) at which sensitivity to one component is absent while sensitivity to the other component is present.

The resulting sets of selected frequencies shall then be analyzed.

Case 1: Frequencies exist at which sensitivity is present only to one component

This case is the most preferable for designing a monitoring system for the concentrations of the target components.

If such frequencies exist for both components, the choice of operating frequencies is straightforward:

For the fabrication of prototype resonant sensors, operating frequencies should be selected at which, while sensitivity to one component is absent, sensitivity to the other component is maximal. At least one such frequency should be selected for each component. If such frequencies exist only for one of the components, then for the fabrication of prototype resonant sensors for this component, operating frequencies should be selected at which, in the absence of sensitivity to the other component, sensitivity to the target component is maximal. For the other component, operating frequencies should be selected from its frequency set at which the difference in sensitivity to the investigated components is the greatest.

Case 2: No frequencies exist with sensitivity only to one component, but the obtained frequency sets do not coincide

In this case, for the fabrication of prototype resonant sensors, operating frequencies should be selected from each frequency set at which the difference in sensitivity to the investigated components is the greatest.

Case 3: The obtained frequency sets coincide

This case is the most challenging for designing a monitoring system for the concen-

trations of the target components.

If the frequency set for one component fully coincides with the set for the other component, it is necessary to verify whether the proportional relationship between the amplitude changes and phase shift changes for one component and the amplitude and/or phase shift changes for the other component is preserved at all frequencies.

If the proportionality is preserved throughout, a repeated scan should be attempted using different probing voltage levels.

If it is not possible to achieve any differences, the investigated components are most likely indistinguishable from the perspective of electrochemical impedance spectroscopy.

Nevertheless, even in this case it is possible to fabricate several prototype sensors with different operating frequencies corresponding to the highest sensitivity to changes in the concentrations of the target components, since a resonant sensor produces a more complex воздействие on the test sample (an additional effect of a magnetic field is introduced) than that produced by a pulse generator. If testing of these sensors demonstrates – at least at one frequency – a change in the proportional relationship of sensitivity to concentration variations, then there is, in principle, a possibility to build a monitoring system for the concentrations of the investigated components. The selectivity of such a system will be higher when the difference in the proportional relationship is greater.

Selection of Optimal Sensors

The selection of a set of frequencies based on the results of sample scanning using a pulse generator is preliminary in nature.

To determine the optimal operating frequencies of a two-component concentration monitoring system, it is necessary to test each prototype resonant sensor using not two, but at least ten samples with different concentrations of the investigated components, within the anticipated range of their variation.

After testing all prototype sensor samples, the best sensor pair can be selected. Preference should be given to sensors that, in addition to high sensitivity, demonstrate a monotonic change in readings as the concentrations of the monitored components change (to facilitate subsequent calibration).

Lower operating frequencies are the most preferable from the standpoint of electromagnetic interference immunity.

In selecting sensors, design and construction constraints must also be taken into account.

Figure 1.

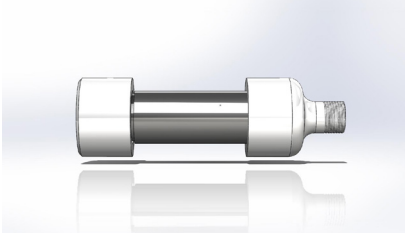

Figure 2.

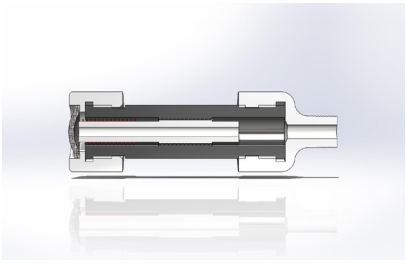

Figure 3.

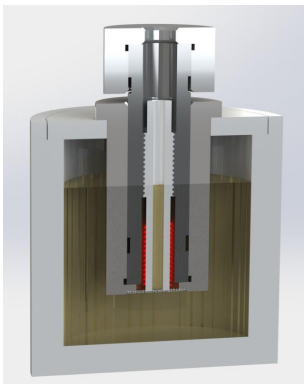

Figure 4.

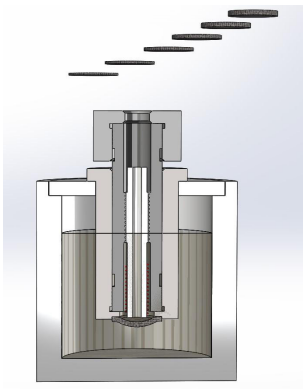

Figure 5.

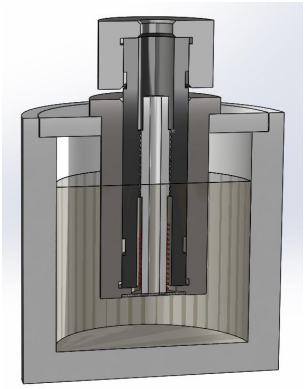

References

Slobozhanyuk, A., et al. (2020). *Magnetic resonance imaging machine*. U. S. Patent – No. 10. 732, 237. Issued August 4, 2020.

Godoy, J., et al. (2020). *Electron paramagnetic resonance (EPR) techniques and apparatus for performing EPR spectroscopy on a flowing fluid*. U. S. Patent – No. 10,564,308. Issued February 18, 2020.

Wang, H. (2018). *Parallel plate transmission line for broadband nuclear magnetic resonance imaging*. U. S. Patent No. 9,952,297. Issued April 24, 2018.

Hetherington, H. P., et al. (2016). *Transceiver apparatus, system and methodology for superior in-vivo imaging of human anatomy*. U. S. Patent No. 9,316,709. Issued April 19, 2016.

Yonamoto, T., et al. (2015). *Sample holder for electricity-detection electron spin resonance device*. U. S. Patent – No. 9,018,954. Issued April 28, 2015.

Neu, E., et al. (2014). *AFM-coupled microscale radiofrequency probe for magnetic resonance imaging and spectroscopy*. U. S. Patent No. 8,884,608. Issued November 11, 2014.

Tang, L., et al. (2014). *Waveguides configured with arrays of features for performing Raman spectroscopy*. U. S. Patent – No. 8,780,344. Issued July 15, 2014.

Trakic, A., et al. (2014). *MRI apparatus and method with moving field component*. U. S. Patent – No. 8,754,644. Issued June 17, 2014.

Wu, Y., et al. (2012). *Guided mode resonator based Raman enhancement apparatus*. U. S. Patent No. 8,330,952. Issued December 11, 2012.

Poponin, V. (2006). *Method and apparatus for enhanced nano-spectroscopic scanning*. U. S. Patent No. 7,151,598. Issued December 19, 2006.

Chandrakumar, N. (1998). *Device for excitation and detection of magnetic resonance using orthogonal transmitter probe coils*. U. S. Patent No. 5,719,499. Issued February 17, 1998.

Chapman, B., et al. (1997). *Gradient coils having increased performance and decreased power consumption for use in MR systems*. U. S. Patent – No. 5,663,648. Issued September 2, 1997.

Gentsch, M., et al. (1994). *Resonator for electron spin resonance spectroscopy*. U. S. Patent – No. 5, 293, 120. Issued March 8, 1994.

submitted 29.02.2026;
accepted for publication 13.03.2026;
published 30.04.2026

Contact: alexachapouski@gmail.com

The Austrian Journal of Technical and Natural Sciences, 2026 No 3–4
ISSN 2310-5607

PREMIER Publishing
ppublishing.org

DOI:10.29013/AJT-26-3.4-179-189

ARTIFICIAL INTELLIGENCE: NATURE AND PRINCIPLES OF IMPLEMENTATION (Artificial Intelligence: Characteristics and Applicability Indices in Modern Smart Automated Industry and in the Ecosystem and Infrastructure of Innovative Startups)

Aliaksandr Achapouski [1]

[1] Architect of AI-Based Security Systems, Specializing in Digital Identity Infrastructure and Real-Time Authentication Phoenix, Arizona

Cite: *Achapouski A. (2026). Artificial Intelligence: Nature and Principles of Implementation. (Artificial Intelligence: Characteristics and Applicability Indices in Modern Smart Automated Industry and in the Ecosystem and Infrastructure of Innovative Startups). Austrian Journal of Technical and Natural Sciences 2026, No 3–4.* https://doi.org/10.29013/AJT-26-3.4-179-189

Abstract

This article examines the rapid advancement of artificial intelligence and its transformative impact on professional activities across creative, technical, and administrative domains. It emphasizes that although AI systems are capable of performing tasks traditionally assigned to junior specialists, including code generation and data processing, the essential role of human professionals remains in defining system architecture, supervising AI-driven workflows, integrating functional components, and ensuring overall logical coherence of technological solutions. Particular attention is devoted to the analysis of fields demonstrating the highest applicability of artificial intelligence, including computer science, mathematics, analytical office functions, and marketing-related processes. The article also addresses the impact of AI on healthcare and environmental initiatives, including the use of multimodal models for accelerated medical diagnostics and personalized treatment. Separate consideration is given to recent advances in cross-model interoperability, including algorithms for universal output translation and semantic token alignment, which significantly enhance collaborative efficiency among AI systems. The article concludes that the future of artificial intelligence will be determined not only by increasing computational performance, but also by the advancement of systemic integration, scalable interoperability, and the comprehensive deployment of intelligent systems across industries and innovation ecosystems.

Keywords: *Artificial intelligence, Artificial neural networks, Application of modern artificial intelligence technologies, Application of artificial intelligence technologies across various professional domains, Applicability indices of artificial intelligence technologies, Scope of professional tasks that can be performed using artificial intelligence and artificial neural networks; Applicability indices of AI technologies to different professions, Level of AI integration into professional activity, List of office and administrative positions and professions in fields such as marketing, where tasks include analysis, provision, and transmission of information*

Artificial Intelligence Applicability Indices and Cross-Model Interoperability in Modern Industry and Startup Ecosystems

Figure 1. *Examples of robots incorporating elements of artificial intelligence and artificial neural networks used in automated production lines of automotive manufacturing companies, for example, Ford*

The comprehensive integration of artificial intelligence and artificial neural networks into innovative technical solutions, including the incorporation within supersystems of control and management of non-contact monitoring and measurement elements based on the principles of electromagnetic resonance spectroscopy, necessitates a reconsideration and modification of the provisions of the Theory of Inventive Problem Solving (TRIZ) and the Algorithm of Inventive Problem Solving (ARIZ). In particular, it requires a revision of the 40 inventive principles and the approaches aimed at achieving the Ideal Final Result.

TRIZ and ARIZ were originally conceived as a “precise science.” For a certain period, their laws and methods corresponded to the level of technological development and engineering capabilities of that time.

However, what do the Theory and Algorithm of Inventive Problem Solving represent today in practical terms?

How have modern high technologies and processor-based systems influenced their integrative capabilities?

These are not the only questions requiring clarification. An important contemporary phenomenon is the widespread search for analogues of future inventions within biological systems, particularly in the context of biomechanical research. How does this trend correlate with the laws, methods, and principles of TRIZ and ARIZ?

At present, many of the most effective and innovative inventions arise from discoveries in living nature, which inspire engineers to develop novel technical solutions capable of addressing complex problems through unconventional methods and techniques.

When analyzed and forecasted using TRIZ methodologies and analytical techniques, and through technological–dialectical synthesis, this phenomenon may provide practical pathways for effective application in innovation processes, especially in biotechnology and genetic engineering.

An undeniable strength of TRIZ lies in its attempt to apply dialectical approaches to inventive problem solving, particularly through the identification and resolution of contradictions. To this end, TRIZ introduced a specialized algorithm (ARIZ), consisting of a sequence of logical procedures designed to reformulate inventive problems in terms of contradictions and to provide structured recommendations for their resolution.

Additionally, TRIZ literature contains numerous illustrative examples and problems of significant educational and analytical value.

Today, largely due to the integration of artificial intelligence and artificial neural networks, the processes of solution selection and decision-making occur at a substantially accelerated pace. This acceleration, in turn, necessitates the rapid adoption of related and adjacent technical decisions within innovation-driven environments.

Decision-making speed no longer allows sufficient time or opportunity to perform a qualified assessment of the correctness and adequacy of decisions using traditional, well-established methodologies; therefore, specialized algorithms are required that incorporate new and non-obvious solutions, which collectively ensure the most comprehensive and rapid responses to errors in the development of innovative projects, particu-

larly those based on inventions aligned with current technological realities.

The present publication further provides examples of six algorithms which, in combination with elements of artificial intelligence and artificial neural networks, make it possible to evaluate and classify the stages and phases of innovative startup project development and to analyze the feasibility of achieving the ideal final result within the project under examination.

This solution becomes particularly critical for edge devices – such as smartphones, drones, and autonomous vehicles – that must rely on limited computational resources in the absence of an internet connection. In the case of autonomous vehicles, faster data processing can prevent catastrophic outcomes. The research marks a new stage in the development of collaborative AI, enabling developers to seamlessly combine the strengths of different models to create more efficient and accessible solutions for millions of users worldwide.

Figure 2. *Examples of the application of artificial intelligence and artificial neural networks in various digital technologies across different areas of industrial activity*

This solution becomes particularly critical for edge devices such as smartphones, drones, and autonomous vehicles, which must rely on limited computational resources in the absence of an internet connection. In the case of autonomous vehicles, faster data processing can prevent catastrophic outcomes. The research marks a new stage in the development of collaborative AI, enabling developers to combine the best features of different models to create more efficient and accessible solutions for millions of users worldwide.

Figure 3. *A robot whose control and monitoring systems incorporate artificial intelligence*

These algorithms, arranged sequentially along the course of the innovation process

The six algorithms presented enable continuous monitoring of the development of an innovative project, including those incorporating elements of artificial intelligence and artificial neural networks.

However, given the current state of affairs, a relevant question arises: if contradictions, in their classical interpretation, do not exist, then how can non-existent contradictions be resolved? How can innovative technologies be developed using the principles and methods of the Theory of Inventive Problem Solving (TRIZ) and its algorithmic framework, while simultaneously applying new, effective, and constructive approaches?

Even without this consideration, the Theory of Inventive Problem Solving has exhibited a number of significant limitations, which evidently led to stagnation in its development after the death of its founder, as well as to considerable difficulties in its practical application.

What were these limitations?

Within TRIZ, an attempt was made to formulate laws governing the development of technical systems, which were intended to

serve as the foundation both for the theory itself and for a general problem-solving methodology. However, the majority of these so-called "laws" cannot truly be classified as such.

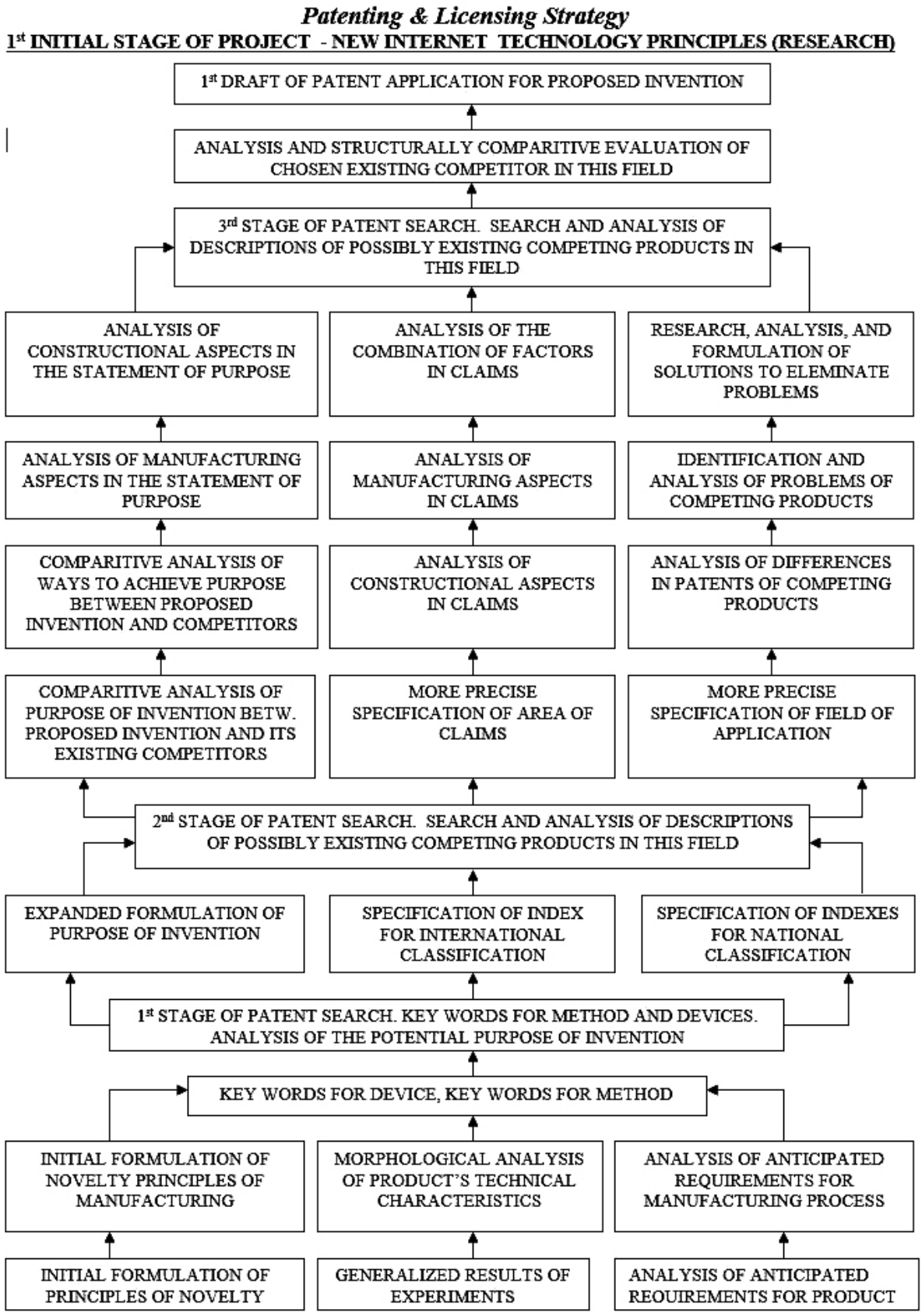

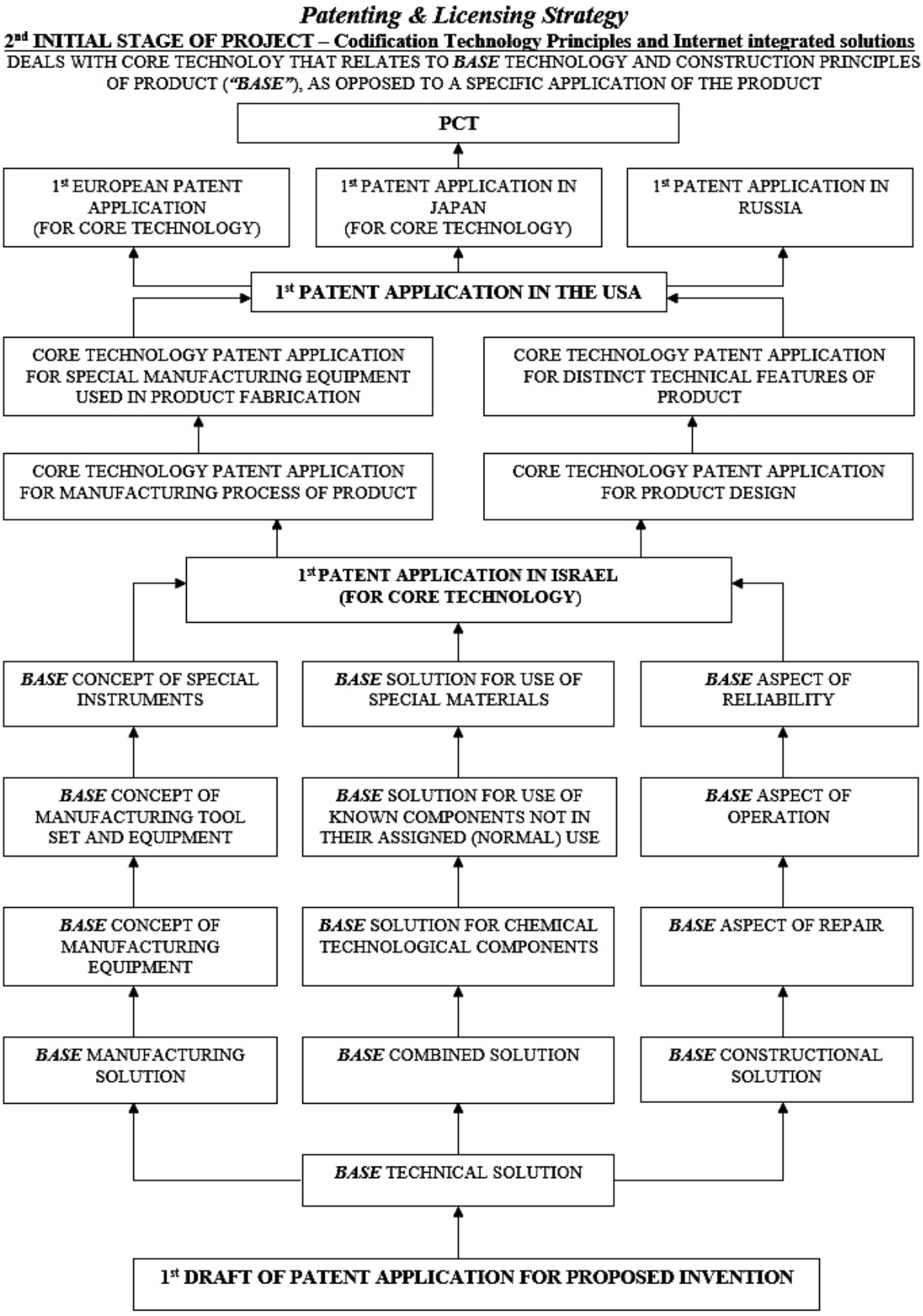
Patenting & Licensing Strategy
2nd INITIAL STAGE OF PROJECT – Codification Technology Principles and Internet integrated solutions
DEALS WITH CORE TECHNOLOY THAT RELATES TO BASE TECHNOLOGY AND CONSTRUCTION PRINCIPLES OF PRODUCT ("BASE"), AS OPPOSED TO A SPECIFIC APPLICATION OF THE PRODUCT
PCT
1st EUROPEAN PATENT APPLICATION (FOR CORE TECHNOLOGY)
1st PATENT APPLICATION IN JAPAN (FOR CORE TECHNOLOGY)
1st PATENT APPLICATION IN RUSSIA
1st PATENT APPLICATION IN THE USA
CORE TECHNOLOGY PATENT APPLICATION FOR SPECIAL MANUFACTURING EQUIPMENT USED IN PRODUCT FABRICATION
CORE TECHNOLOGY PATENT APPLICATION FOR DISTINCT TECHNICAL FEATURES OF PRODUCT
CORE TECHNOLOGY PATENT APPLICATION FOR MANUFACTURING PROCESS OF PRODUCT
CORE TECHNOLOGY PATENT APPLICATION FOR PRODUCT DESIGN
1st PATENT APPLICATION IN ISRAEL (FOR CORE TECHNOLOGY)
BASE CONCEPT OF SPECIAL INSTRUMENTS
BASE SOLUTION FOR USE OF SPECIAL MATERIALS
BASE ASPECT OF RELIABILITY
BASE CONCEPT OF MANUFACTURING TOOL SET AND EQUIPMENT
BASE SOLUTION FOR USE OF KNOWN COMPONENTS NOT IN THEIR ASSIGNED (NORMAL) USE
BASE ASPECT OF OPERATION
BASE CONCEPT OF MANUFACTURING EQUIPMENT
BASE SOLUTION FOR CHEMICAL TECHNOLOGICAL COMPONENTS
BASE ASPECT OF REPAIR
BASE MANUFACTURING SOLUTION
BASE COMBINED SOLUTION
BASE CONSTRUCTIONAL SOLUTION
BASE TECHNICAL SOLUTION
1st DRAFT OF PATENT APPLICATION FOR PROPOSED INVENTION

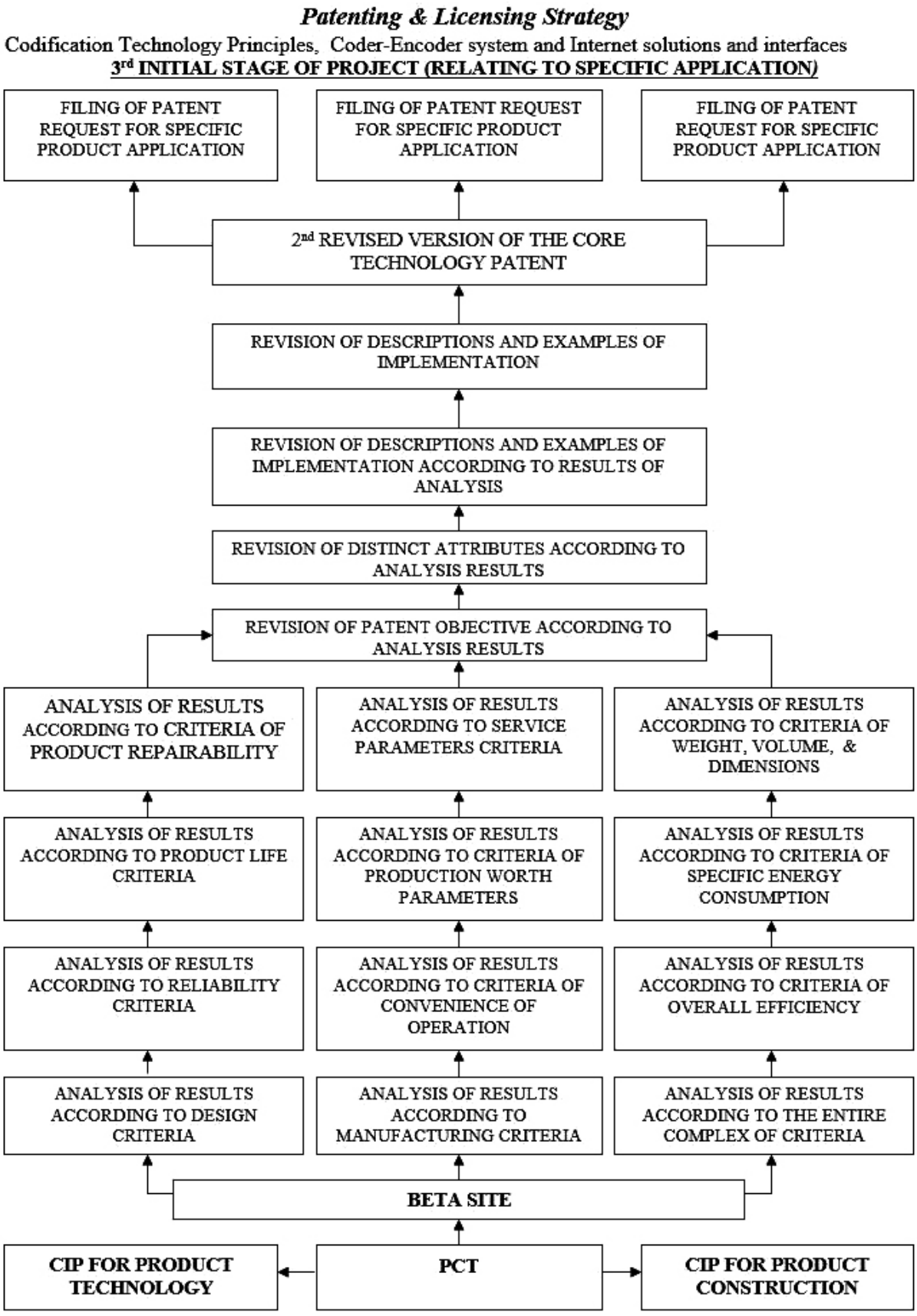
Patenting & Licensing Strategy
Codification Technology Principles, Coder-Encoder system and Internet solutions and interfaces
3rd INITIAL STAGE OF PROJECT (RELATING TO SPECIFIC APPLICATION)
FILING OF PATENT REQUEST FOR SPECIFIC PRODUCT APPLICATION
FILING OF PATENT REQUEST FOR SPECIFIC PRODUCT APPLICATION
FILING OF PATENT REQUEST FOR SPECIFIC PRODUCT APPLICATION
2nd REVISED VERSION OF THE CORE TECHNOLOGY PATENT
REVISION OF DESCRIPTIONS AND EXAMPLES OF IMPLEMENTATION
REVISION OF DESCRIPTIONS AND EXAMPLES OF IMPLEMENTATION ACCORDING TO RESULTS OF ANALYSIS
REVISION OF DISTINCT ATTRIBUTES ACCORDING TO ANALYSIS RESULTS
REVISION OF PATENT OBJECTIVE ACCORDING TO ANALYSIS RESULTS
ANALYSIS OF RESULTS ACCORDING TO CRITERIA OF PRODUCT REPAIRABILITY
ANALYSIS OF RESULTS ACCORDING TO SERVICE PARAMETERS CRITERIA
ANALYSIS OF RESULTS ACCORDING TO CRITERIA OF WEIGHT, VOLUME, & DIMENSIONS
ANALYSIS OF RESULTS ACCORDING TO PRODUCT LIFE CRITERIA
ANALYSIS OF RESULTS ACCORDING TO CRITERIA OF PRODUCTION WORTH PARAMETERS
ANALYSIS OF RESULTS ACCORDING TO CRITERIA OF SPECIFIC ENERGY CONSUMPTION
ANALYSIS OF RESULTS ACCORDING TO RELIABILITY CRITERIA
ANALYSIS OF RESULTS ACCORDING TO CRITERIA OF CONVENIENCE OF OPERATION
ANALYSIS OF RESULTS ACCORDING TO CRITERIA OF OVERALL EFFICIENCY
ANALYSIS OF RESULTS ACCORDING TO DESIGN CRITERIA
ANALYSIS OF RESULTS ACCORDING TO MANUFACTURING CRITERIA
ANALYSIS OF RESULTS ACCORDING TO THE ENTIRE COMPLEX OF CRITERIA
BETA SITE
CIP FOR PRODUCT TECHNOLOGY
PCT
CIP FOR PRODUCT CONSTRUCTION

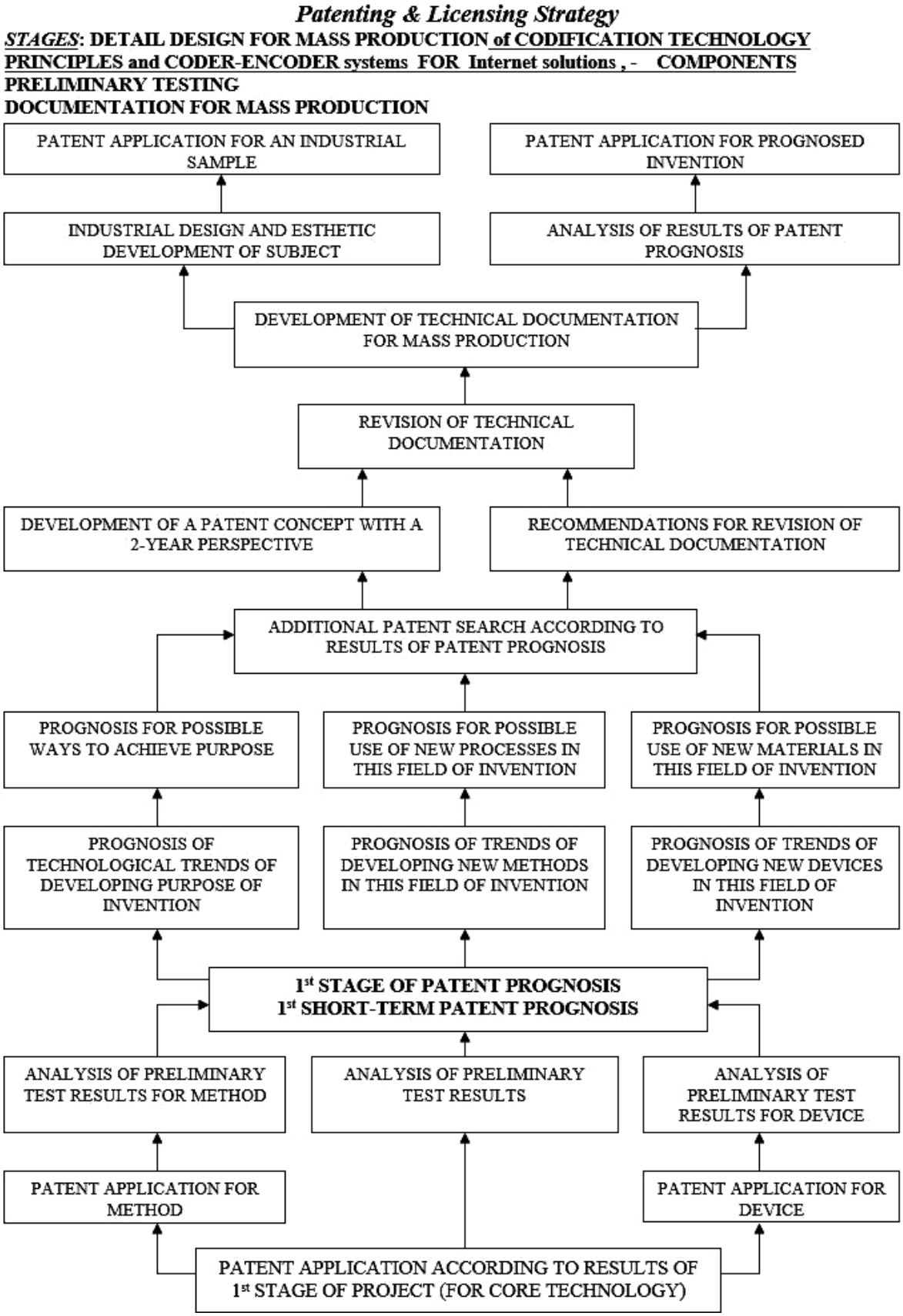
Patenting & Licensing Strategy
STAGES: DETAIL DESIGN FOR MASS PRODUCTION of CODIFICATION TECHNOLOGY
PRINCIPLES and CODER-ENCODER systems FOR Internet solutions , - COMPONENTS
PRELIMINARY TESTING
DOCUMENTATION FOR MASS PRODUCTION
PATENT APPLICATION FOR AN INDUSTRIAL SAMPLE
PATENT APPLICATION FOR PROGNOSED INVENTION
INDUSTRIAL DESIGN AND ESTHETIC DEVELOPMENT OF SUBJECT
ANALYSIS OF RESULTS OF PATENT PROGNOSIS
DEVELOPMENT OF TECHNICAL DOCUMENTATION FOR MASS PRODUCTION
REVISION OF TECHNICAL DOCUMENTATION
DEVELOPMENT OF A PATENT CONCEPT WITH A 2-YEAR PERSPECTIVE
RECOMMENDATIONS FOR REVISION OF TECHNICAL DOCUMENTATION
ADDITIONAL PATENT SEARCH ACCORDING TO RESULTS OF PATENT PROGNOSIS
PROGNOSIS FOR POSSIBLE WAYS TO ACHIEVE PURPOSE
PROGNOSIS FOR POSSIBLE USE OF NEW PROCESSES IN THIS FIELD OF INVENTION
PROGNOSIS FOR POSSIBLE USE OF NEW MATERIALS IN THIS FIELD OF INVENTION
PROGNOSIS OF TECHNOLOGICAL TRENDS OF DEVELOPING PURPOSE OF INVENTION
PROGNOSIS OF TRENDS OF DEVELOPING NEW METHODS IN THIS FIELD OF INVENTION
PROGNOSIS OF TRENDS OF DEVELOPING NEW DEVICES IN THIS FIELD OF INVENTION
1st STAGE OF PATENT PROGNOSIS
1st SHORT-TERM PATENT PROGNOSIS
ANALYSIS OF PRELIMINARY TEST RESULTS FOR METHOD
ANALYSIS OF PRELIMINARY TEST RESULTS
ANALYSIS OF PRELIMINARY TEST RESULTS FOR DEVICE
PATENT APPLICATION FOR METHOD
PATENT APPLICATION FOR DEVICE
PATENT APPLICATION ACCORDING TO RESULTS OF 1st STAGE OF PROJECT (FOR CORE TECHNOLOGY)

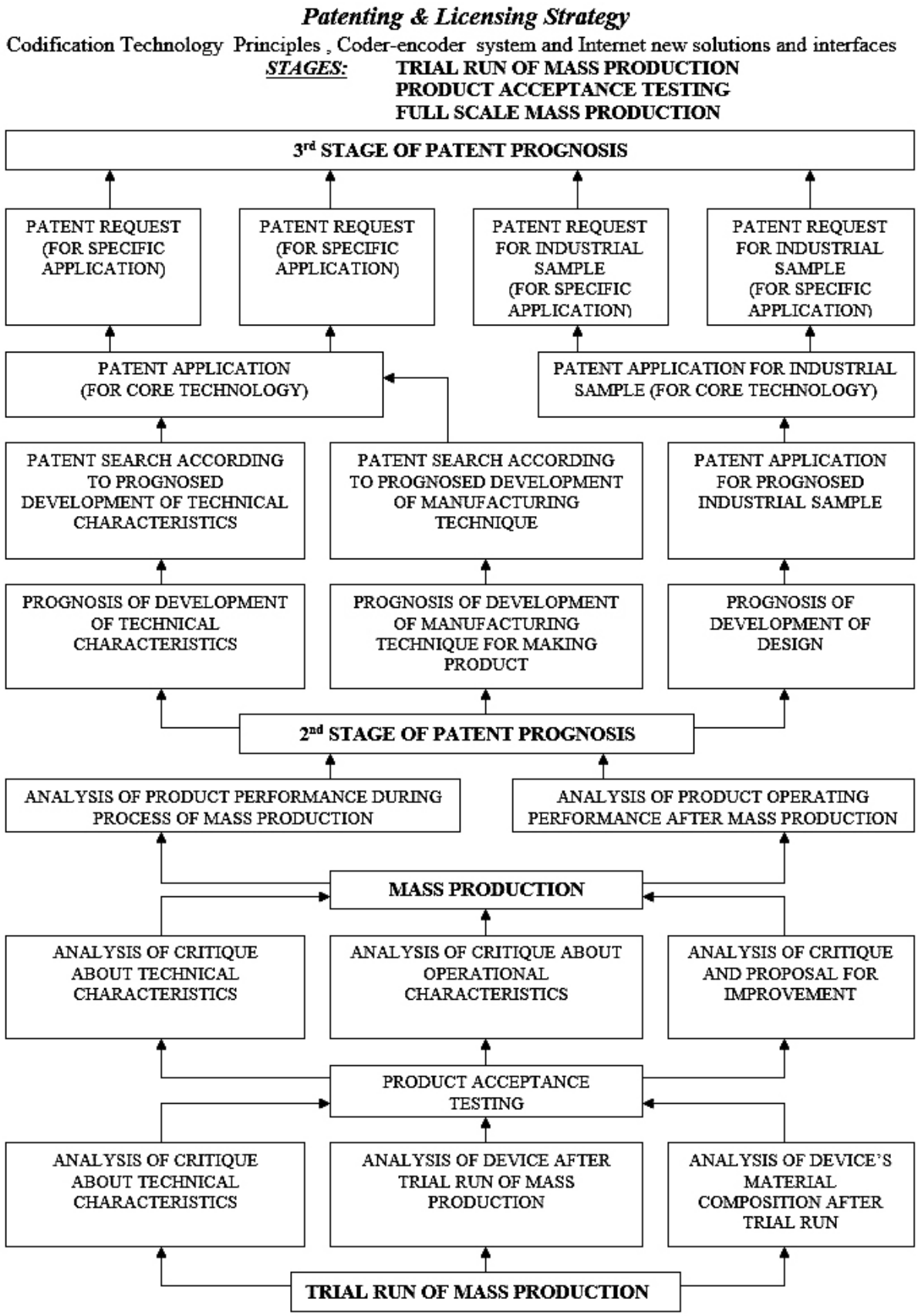
Patenting & Licensing Strategy
Codification Technology Principles , Coder-encoder system and Internet new solutions and interfaces
STAGES:
TRIAL RUN OF MASS PRODUCTION
PRODUCT ACCEPTANCE TESTING
FULL SCALE MASS PRODUCTION
3rd STAGE OF PATENT PROGNOSIS
PATENT REQUEST (FOR SPECIFIC APPLICATION)
PATENT REQUEST (FOR SPECIFIC APPLICATION)
PATENT REQUEST FOR INDUSTRIAL SAMPLE (FOR SPECIFIC APPLICATION)
PATENT REQUEST FOR INDUSTRIAL SAMPLE (FOR SPECIFIC APPLICATION)
PATENT APPLICATION (FOR CORE TECHNOLOGY)
PATENT APPLICATION FOR INDUSTRIAL SAMPLE (FOR CORE TECHNOLOGY)
PATENT SEARCH ACCORDING TO PROGNOSED DEVELOPMENT OF TECHNICAL CHARACTERISTICS
PATENT SEARCH ACCORDING TO PROGNOSED DEVELOPMENT OF MANUFACTURING TECHNIQUE
PATENT APPLICATION FOR PROGNOSED INDUSTRIAL SAMPLE
PROGNOSIS OF DEVELOPMENT OF TECHNICAL CHARACTERISTICS
PROGNOSIS OF DEVELOPMENT OF MANUFACTURING TECHNIQUE FOR MAKING PRODUCT
PROGNOSIS OF DEVELOPMENT OF DESIGN
2nd STAGE OF PATENT PROGNOSIS
ANALYSIS OF PRODUCT PERFORMANCE DURING PROCESS OF MASS PRODUCTION
ANALYSIS OF PRODUCT OPERATING PERFORMANCE AFTER MASS PRODUCTION
MASS PRODUCTION
ANALYSIS OF CRITIQUE ABOUT TECHNICAL CHARACTERISTICS
ANALYSIS OF CRITIQUE ABOUT OPERATIONAL CHARACTERISTICS
ANALYSIS OF CRITIQUE AND PROPOSAL FOR IMPROVEMENT
PRODUCT ACCEPTANCE TESTING
ANALYSIS OF CRITIQUE ABOUT TECHNICAL CHARACTERISTICS
ANALYSIS OF DEVICE AFTER TRIAL RUN OF MASS PRODUCTION
ANALYSIS OF DEVICE'S MATERIAL COMPOSITION AFTER TRIAL RUN
TRIAL RUN OF MASS PRODUCTION

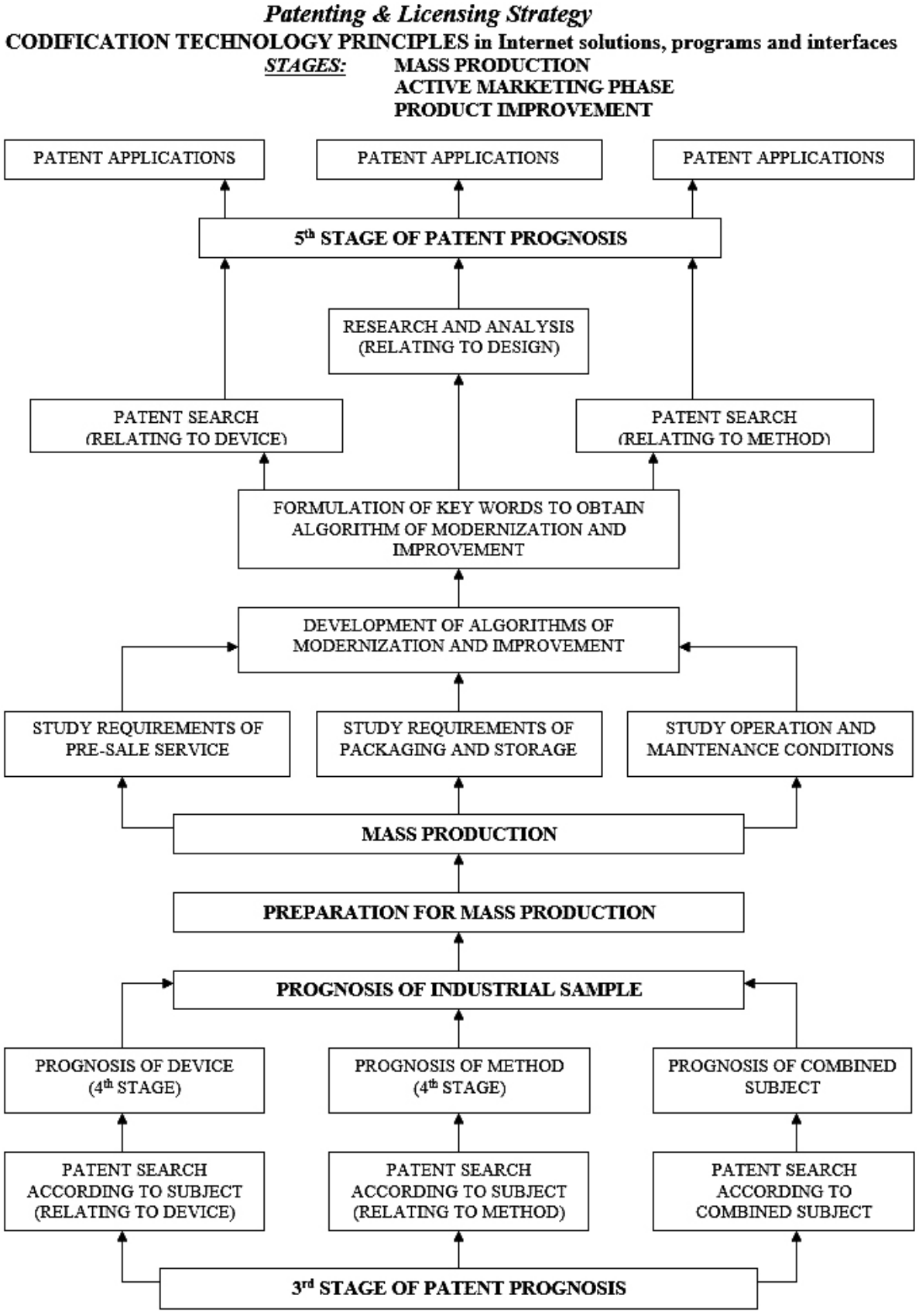

They would more accurately be described as partial patterns or tendencies in the evolution of technical systems, and even these are incomplete. As a result, a coherent and comprehensive problem-solving methodology based on universally applicable laws was never fully established.

The formulated "laws" were primarily used as methodological justifications for illustrative examples of inventions. At the same time, factors of commercial feasibility were largely excluded, and their influence on the application of evolving development patterns for modernization, optimization, and transformation of technical objects was not adequately considered. This omission significantly limited the ability to evolve an invention into a commercially viable and востребованный innovative product.

Recent patent disputes among the world's leading technology companies clearly demonstrate that the development laws proposed within TRIZ are insufficient to reflect the full diversity of tasks, functions, and characteristics of modern multifunctional systems. Given the emergence of new and continuously evolving factors that define innovative products, there is a need to reformulate these laws by integrating them with the principles governing the development of commercial structures and the commercialization of innovation.

The dialectical approach – based on the analysis of contradictions – which was embedded in the primary problem-solving tool, namely the Algorithm of Inventive Problem Solving (ARIZ), was significantly distorted through the introduction of new constructs such as "technical contradiction" and "physical contradiction." These constructs deviated from the essence of dialectical contradiction as defined in classical dialectical logic, resulting in difficulties in identifying contradictions when applying the algorithm to real-world inventive problems.

This raises a fundamental question that warrants special attention: what constitutes a real inventive problem? How can the correct or incorrect formulation of such a problem influence the commercialization potential of an invention? Furthermore, is it possible to reliably protect a newly developed technical solution from unauthorized replication?

The search for answers to these and many other questions has become an essential component of the modern dialectics of developing patenting and licensing strategies for inventions, particularly those involving elements of artificial intelligence and artificial neural networks.

References

US Patent 10,732,237
Slobozhanyuk, A., et al. *Magnetic Resonance Imaging Machine*.
United States Patent, August 4, 2020.
US Patent 10,564,308
Godoy, J., et al. *Electron Paramagnetic Resonance (EPR) Techniques and Apparatus for Performing EPR Spectroscopy on a Flowing Fluid*.
United States Patent, February 18, 2020.
US Patent 9,952,297
Wang, X. *Parallel Plate Transmission Line for Broadband Nuclear Magnetic Resonance Imaging*.
United States Patent, April 24, 2018.
US Patent 9,316,709
Hetherington, H., et al. *Transceiver Apparatus, System and Methodology for Superior In-Vivo Imaging of Human Anatomy*.
United States Patent, April 19, 2016.
US Patent 9,018,954
Yonamoto, T., et al. *Sample Holder for Electricity-Detection Electron Spin Resonance Device*.
United States Patent, April 28, 2015.
US Patent 8,884,608
Neu, E., et al. *AFM–Coupled Microscale Radiofrequency Probe for Magnetic Resonance Imaging and Spectroscopy*.
United States Patent, November 11, 2014.
US Patent 8,780,344

Tang, L., et al. *Waveguides Configured with Arrays of Features for Performing Raman Spectroscopy*.
United States Patent, July 15, 2014.

submitted 14.03.2026;
accepted for publication 28.03.2026;
published 30.04.2026

Contact: alexachapouski@gmail.com

The Austrian Journal of Technical and Natural Sciences, 2026 No 3–4
ISSN 2310-5607

PREMIER Publishing
ppublishing.org

DOI:10.29013/AJT-26-3.4-190-194

STRATEGIC PLANNING IN POWER GRID CONSTRUCTION PROJECTS

Yevhenii Bondar [1]

[1] Director of Vector Energy Group LLC

Cite: *Yevhenii Bondar. (2026). Strategic Planning in Power Grid Construction Projects. Austrian Journal of Technical and Natural Sciences 2026, No 3–4.* https://doi.org/10.29013/AJT-26-3.4-190-194

Abstract

Electricity transmission infrastructure projects in industrialized nations are consistently plagued by cost overruns and schedule delays, yet the role of strategic planning comprehensiveness as a determinant of project performance remains insufficiently examined at the project level. This study investigates how the depth and integration of strategic planning practices influence cost and schedule outcomes in power grid construction projects. The study draws on an adaptive construction management system integrating multi-dimensional risk assessment, machine learning-based failure prediction, and dynamic resource optimization, validated across 24 transmission line and substation projects in Europe and North America (2023–2025). Results demonstrate that comprehensively planned projects achieved average cost overruns of 5–12% and schedule delays of 5–15%, compared to 30–45% and 35–50%, respectively, for conventionally planned projects. Right-of-way acquisition, regulatory approvals, and design modifications jointly accounted for 55–65% of total documented delay time across the sample. Early stakeholder engagement, extended demand forecasting horizons of 15–20 years, cross-functional governance structures, and formal risk registers with active monitoring protocols are identified as the planning elements most strongly associated with superior performance. The study contributes empirical evidence linking planning comprehensiveness to measurable project outcomes and offers practical governance recommendations for utilities and regulators seeking to improve transmission infrastructure delivery.

Keywords: *transmission infrastructure, project planning, risk assessment, stakeholder management, cost overrun mitigation, grid modernization*

Introduction

Electricity transmission networks across industrialized nations confront an infrastructure crisis. The gap between infrastructure needs and deployment rates threatens energy transition objectives and system reliability. Recent analyses indicate that major power infrastructure initiatives frequently experience delays and budget overruns, with average cost escalations reaching significant proportions (Zhou et al., 2025). These failures impose substantial costs through con-

strained renewable energy deployment and persistent grid congestion.

Traditional project management approaches prove inadequate for contemporary transmission development. Grid construction involves not merely technical challenges but complex socio-political dynamics spanning property rights negotiations, environmental permitting, regulatory coordination across multiple jurisdictions, and community acceptance issues (Wang & Sharma, 2025).

Rather than treating projects as isolated technical undertakings, strategic frameworks integrate long-range capacity forecasting, systematic risk assessment, proactive stakeholder engagement, and adaptive management protocols (Al Nahyan et al., 2018). This research investigates how strategic planning methodologies influence project outcomes through analysis of recent transmission developments.

Methods

The empirical dataset comprises 24 transmission line and substation projects located in Europe and North America, initiated or completed between 2023 and 2025. Projects were selected based on three criteria: availability of complete budget and schedule documentation, documented planning processes covering at least initiation, survey and design, and implementation stages, and clear attribution of major delays and cost overruns in project reports.

The analytical framework draws upon lifecycle auditing concepts that encompass six critical stages: project initiation, survey and design, bidding and procurement, implementation, completion, and post-completion audit (Zhou et al., 2025). Projects were categorized based on strategic planning comprehensiveness using multiple dimensions: forecasting horizon length and scenario diversity, formal risk assessment presence, stakeholder engagement timing and depth, organizational integration, and adaptive management protocols. Projects were classified into three planning categories using explicit scoring rules. Group differences were assessed using one-way ANOVA (cost variance: $F(2, 21) = 14.7, p < 0.001$; schedule variance: $F(2, 21) = 11.3$, $p < 0.001$); pairwise comparisons employed Welch's t-test with Bonferroni correction, confirming significance at $\alpha = 0.05$ for all planning category pairs.

Performance analysis compared outcomes across planning categories using multiple metrics. Cost performance was assessed through percentage variance between final expenditure and initial approved budget. Schedule performance examined completion timeline versus original projections.

Results

On average, comprehensively planned projects experienced cost overruns of approximately 5–12 percent and schedule delays of 5–15 percent, compared to 15–30 percent and 20–35 percent respectively for moderate planning, and 30–45 percent and 35–50 percent for conventional planning. Right-of-way acquisition, design modifications, and regulatory approvals jointly accounted for around 55–65 percent of total documented delay time across the sample. Two contrasting patterns emerged from case analysis. Projects employing comprehensive strategic planning including extended demand forecasting, formal risk assessment protocols, and early stakeholder engagement achieved completion closer to budget and schedule despite encountering regulatory challenges. Conversely, projects using conventional planning approaches experienced severe cost escalation and delays primarily attributable to unanticipated stakeholder opposition and multiple route revisions necessitated by inadequate initial assessment. Across the sample, right-of-way issues accounted for roughly 20–25 percent of total delay time in conventional projects but only around 10–15 percent in comprehensively planned projects. Mean right-of-way acquisition duration was 8.3 months in comprehensive projects versus 19.7 months in conventional projects ($t(13) = 4.2$, $p = 0.001$).

Regulatory approval processes showed high variability across jurisdictions. Projects in jurisdictions with streamlined permitting procedures averaged approval periods shorter by approximately 30–40 percent than those in fragmented regulatory environments. Median permitting duration was 11.2 months in streamlined jurisdictions versus 17.8 months in fragmented regulatory environments.

Design modifications during construction generated substantial delays, particularly where geological surveys had been limited. In conventional projects, design changes contributed an estimated 15–20 percent of total delay time, while in comprehensively planned projects this share was closer to 5–10 percent, largely due to more extensive pre-construction investigations. Projects incorporating comprehensive geological surveys along entire routes before finalizing designs experienced fewer subsurface-related modifications compared to those conducting limited preliminary investigations (Kalogeropoulos et al., 2025).

Projects employing formal risk assessment frameworks incorporating quantitative evaluation methods demonstrated superior performance compared to initiatives using only qualitative risk identification. Effective risk management extends beyond initial assessment to include active monitoring systems. Organizations maintaining formal risk registers with regular updates and predefined escalation protocols responded more rapidly to emerging challenges. Projects with active risk registers resolved emerging schedule risks within a mean of 12 days, compared to 31 days in projects relying on periodic reviews ($t(15) = 3.8$, $p = 0.002$).

Projects initiating stakeholder engagement during route conceptualization experienced substantially fewer community-related delays compared to those beginning consultation after route selection. Early engagement enabled incorporation of local knowledge regarding environmental sensitivities, cultural resources, and land use constraints that might not appear in standard databases (Zuern & Harr, 2025). Engagement timing alone proved insufficient; consultation depth and responsiveness mattered substantially. Projects conducting multiple engagement rounds with demonstrated incorporation of feedback generated measurably better outcomes than single consultation events. Comprehensive stakeholder communication frameworks involving all parties in strategy formulation and decision-making processes proved essential for implementation success (Wang & Sharma, 2025).

Discussion

The empirical evidence demonstrates that strategic planning substantially improves transmission project performance through integration of multiple elements: extended forecasting horizons, formal risk assessment with active monitoring, meaningful stakeholder engagement, and organizational structures facilitating coordination. The performance differential between comprehensive and conventional planning approaches translates to substantial financial impacts that justify planning investments. This study makes three main contributions. First, it provides recent empirical evidence that the comprehensiveness of strategic planning strongly correlates with both cost and schedule performance in transmission projects. Second, it decomposes strategic planning into specific, observable dimensions and shows which combinations are associated with superior outcomes. Third, it links lifecycle auditing concepts and digital platforms to concrete governance mechanisms that can be applied in power-grid construction practice.

Right-of-way acquisition remains particularly challenging despite planning improvements, but the results indicate that treating land acquisition as a concurrent planning activity substantially reduces the risk of extreme delays. Early engagement and route flexibility do not remove right-of-way risks, yet they clearly separate high-performing projects from those that experienced multi-year schedule slippage. For example, a 380 kV transmission project in Central Europe initiated land acquisition 14 months before route approval and completed right-of-way negotiations within the design phase, avoiding an estimated 22-month delay experienced by a comparable project where negotiations began post-approval.

Taken together, the technical performance data and the stakeholder evidence point to the same conclusion. The costs of inadequate planning are not distributed evenly across the project lifecycle. They concentrate heavily in the implementation phase, where they are most disruptive and most expensive to resolve.

Several promising approaches to persistent planning challenges merit attention. Route corridor concepts with multiple spe-

cific alignment options preserve flexibility while enabling stakeholder input. Modular engineering approaches allow equipment procurement before finalizing detailed specifications. Regulatory pre-filing consultations clarify approval requirements and identify potential concerns before formal submissions. These practices require regulatory acceptance and organizational capabilities not yet universal (Kalogeropoulos et al., 2025).

The study has limitations that affect how broadly the findings can be applied. The sample of 24 projects was selected based on documentation availability, which introduces selection bias toward better-documented projects and may overrepresent organisations with stronger planning cultures. The geographic scope is limited to Europe and North America, and the relationship between planning quality and project outcomes may differ in contexts with weaker regulatory institutions or different land tenure systems. The observation window covers only the construction phase. Whether comprehensively planned projects deliver proportionately better operational performance over 30 to 40 year service lives remains an open empirical question.

Conclusion

Strategic planning significantly improves transmission project outcomes through synergistic integration of forecasting, risk assessment, stakeholder engagement, and organizational coordination. Despite clear performance advantages, comprehensive strategic planning remains inconsistently implemented across the utility sector. Organizational barriers include short-term budget pressures discouraging upfront planning investment, capability gaps limiting sophisticated analytical methods, and institutional inertia favoring established practices.

References

Al Nahyan, M. T., Hawas, Y. E., Aljassmi, H., & Maraqa, M. (2018). Capturing the stakeholders' managerial competency risks of mega infrastructure projects: A fuzzy logic modelling approach. International Journal of Project Organisation and Management, – 10(2). – P. 109–136. URL: https://doi.org/10.1504/IJPOM.2018.092087

Di Maddaloni, F., & Davies, A. (2017). The influence of local community stakeholders in megaprojects: Rethinking their inclusiveness to improve project performance. International Journal of Project Management, – 35(8). – P. 1537–1556. URL: https://doi.org/10.1016/j.ijproman.2017.08.011

Kalogeropoulos, T., Kirytopoulos, K., & Ventura, Z. (2025). Driving forces for multinational construction consortiums: The case of a Greek mega project. International Journal of Project Organisation and Management, – 17(1). – P. 47–76.

Li, Y., Zhang, H., & Chen, X. (2012). Study on the whole process risk management system of power grid construction projects. Asian Social Science, – 8(8). – P. 68–76. URL: https://doi.org/10.5539/ass.v8n8p68

Rouhanizadeh, B., & Sadeghi, N. (2023). Inter organisational governance in megaprojects: A systematic review and an agenda for future research. International Journal of Project Management, – 41(2). – P. 123–140. URL: https://doi.org/10.1016/j.ijproman.2023.01.004

Schipper, R. P. J., & Silvius, A. J. G. (2018). Towards a conceptual framework for sustainable project portfolio management. International Journal of Project Organisation and Management, – 10(3). – P. 191–221.

Siemiatycki, M. (2015). Cost overruns on infrastructure projects: Patterns, causes, and cures. IMFG Perspectives, – (11). – P. 1–16. Toronto: Institute on Municipal Finance and Governance, University of Toronto.

Wang, C. Q., & Sharma, M. (2025). Project management methods against failure factors in complex infrastructure projects: The Netherlands view. International Journal of Project Organisation and Management, – 17(1). – P. 77–104.

Zhou, M., Chen, Y., Zhou, L., Zhan, J., & Chong, H. Y. (2025). Strengthening power grid projects' governance and sustainability through lifecycle auditing. Scientific Reports, – 15. – 36442 p. URL: https://doi.org/10.1038/s41598-025-20389-9

submitted 14.03.2026;
accepted for publication 28.03.2026;
published 30.04.2026

Contact: bondaryevhenii13@gmail.com

The Austrian Journal of Technical and Natural Sciences, 2026 No 3–4
ISSN 2310-5607

PREMIER Publishing
ppublishing.org

DOI:10.29013/AJT-26-3.4-195-202

MODULAR SYSTEM ARCHITECTURE FOR REGENERATION AND RECIRCULATION OF PROCESS FLUIDS. (Modular system architecture for regeneration and recirculation of process fluids, including water and aqueous solutions)

Volodymyr Ikonnikov [1]

[1] Independent Researcher Odesa, Ukraine

Cite: *Ikonnikov V. (2026). Modular system architecture for regeneration and recirculation of process fluids. (Modular system architecture for regeneration and recirculation of process fluids, including water and aqueous solutions). Austrian Journal of Technical and Natural Sciences 2026, No 3–4.* https://doi.org/10.29013/AJT-26-3.4-195-202

Abstract

This article examines existing industrial methods for the treatment of water contaminated by technological processes and production waste, including chemical reagent-based treatment methods, non-reagent purification methods, and combined treatment technologies. Particular attention is devoted to the analysis of the limitations of current approaches and their inability to fully satisfy the growing technological, environmental, and economic requirements of modern industrial production. The article substantiates the necessity of implementing a comprehensive integrated approach to industrial wastewater treatment and presents an innovative integrated technology incorporating recent developments in the field. The proposed technology is structured as a sequence of functionally interconnected yet technologically independent treatment stages, each based on distinct physical and chemical principles. The study emphasizes that contemporary challenges in water treatment and water conditioning can no longer be effectively resolved through isolated or partially combined conventional methods. It is concluded that only a comprehensive multi-stage treatment approach can meet the increasingly stringent demands of modern industrial systems and ensure effective, scalable, and technologically adaptable wastewater treatment solutions.

Keywords: *Water treatment methods; Water and aqueous solutions; Chemical reagent-based treatment; Non-reagent treatment and purification; Combined treatment methods; Integrated technologies*

Introduction

In combination with recent innovative concepts proposed and published by leading specialists, particularly Vladyslav Drapii, the author introduces an integrated technological approach that can be implemented through a system of complete, autonomous, and standardized technological modules, configured as follows:

Figure 1. *Nine principal modular technological configurations encompassing all processing stages and operations required for the formation of a modular technological equipment complex intended for the purification, regeneration, and recirculation of process fluids, including water and aqueous solutions*

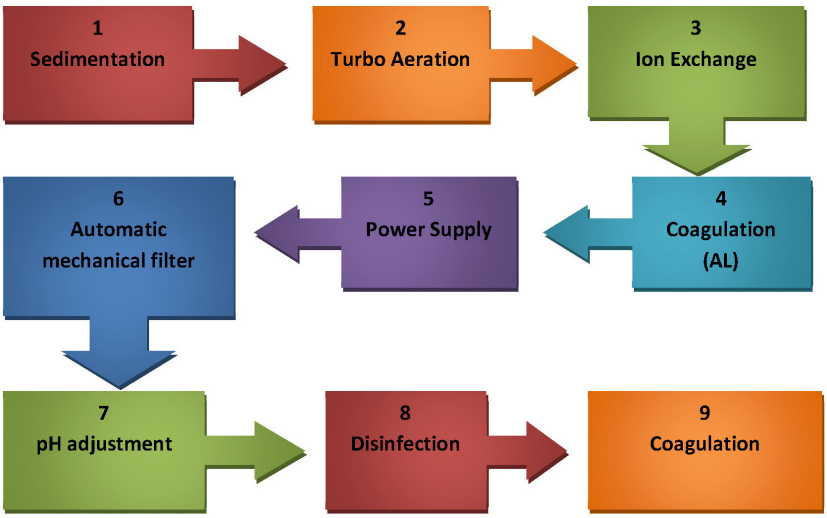

Among the presented modules, **Module 5 – the power supply unit** is relatively universal, whereas the remaining eight modules have more specialized application areas:

- **Module 1 – Sedimentation module**, which may be designed as a sedimentation column or as a sedimentation tank with a parallelepiped configuration;
- **Module 2 – Turbo-aeration module**, which may have at least two configurations: one utilizing foam generators and another employing a system for mixing and in-line homogenization;
- **Module 3 – Ion-exchange treatment module**, which may have multiple configurations, one of the most effective being based on ion-exchange columns equipped with capsules for ion-exchange resins made from carbon–carbon composite fabrics;
- **Module 4 – Coagulation module**, utilizing aluminum ions as a coagulant, generated in electrochemical reactors with aluminum anodes;
- **Module 6 – Automatic mechanical filtration module**, incorporating automated cleaning of filtration sections and in-line regeneration of filtering elements;
- **Module 7 – pH adjustment module**, intended for regulating acidity and alkalinity;
- **Module 8 – Electrochemical non-reagent disinfection module;**
- **Module 9 – Final electrochemical coagulation module.**

As shown in the diagram, the system inlet is equipped with a receiving tank incorporating several elements that enable preliminary treatment of process fluid that has completed its operating cycle. This initial treatment is performed using a membrane filter connected via a check valve to an inlet pump, which feeds the fluid to a primary sedimentation column. Depending on the flow rate, the sedimentation column may consist of one, two, or three sections.

After the first stage of sedimentation, the fluid is directed to electrochemical reactors for pH adjustment (acidity or alkalinity), which are controlled and powered by a multifunctional power supply unit.

Following pH adjustment, and in order to establish alkaline conditions optimal for efficient sedimentation, the fluid is transferred to a specialized sedimentation module with a specific geometry designed to facilitate the separation of formed sedimentation conglomerates within an upward flow.

Upon completion of the sedimentation process, the fluid, based on a level sensor signal, is delivered by a centrifugal pump to mechanical filtration modules, where residual conglomerate particles that were not captured within the sedimentation layer are removed.

Figure 2. *Example of a modular system configuration for the regeneration of process fluids, including water and aqueous solutions*

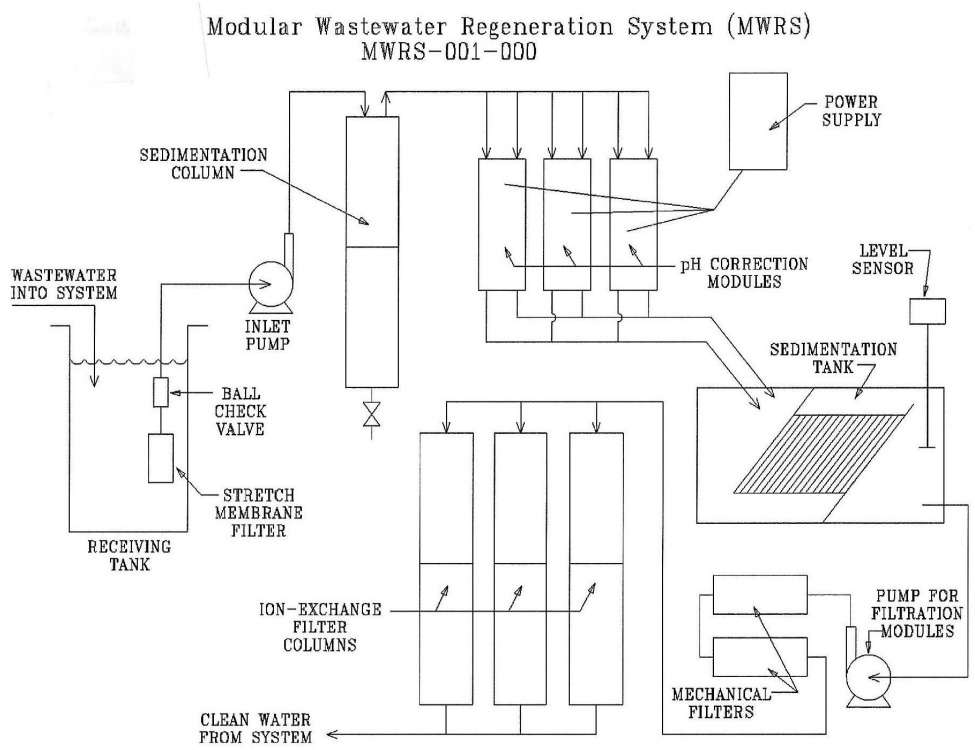

Since the mechanical filters operate in an in-line (continuous) mode, the pressure generated by the filtration pumps is sufficient to feed the fluid, after mechanical filtration, directly into the ion-exchange treatment columns.

Based on the findings and proposals presented in the publications and patent applications of Vladyslav Drapii, as well as his multifunctional forecast regarding the development of environmentally sustainable technological systems, the author of the present publication has significantly expanded the technical capabilities of ion-exchange treatment columns, which warrants further detailed consideration.

It is particularly important to note that, for ion-exchange treatment, not only synthetic ion-exchange resins should be used, but also natural materials, among which zeolite represents one of the most effective options.

Under the modular design concept for ion-exchange columns proposed by Vladyslav Drapii – where a column consists of at least two modular sections – it becomes possible to utilize multiple ion-exchange materials with different exchange capacities within a single column. For example, zeolite may be applied in the upper section, while synthetic ion-exchange resin may be used in the lower section.

The combination of these materials ensures optimal performance in purification, regeneration, and recirculation processes.

This modular system configuration is conceptually aligned with the inventions and developments of Vladyslav Drapii, a recognized innovator in the field of non-reagent, high-efficiency, real-time treatment of liquids, including water and aqueous solutions, in directed flow systems.

Practical implementation has demonstrated that the hierarchical system of specialized yet autonomous technological modules proposed by Vladyslav Drapii – each possessing a distinct technological function, an independent operational cycle, and requiring no chemical reagents or synthetic activating additives – enables the formation of higher-level modules from lower-level components within a fully efficient economic and technological framework.

Moreover, the absence of introduced chemical reagents allows for the immediate initiation of continuous (in-line) recirculation processes following the completion of regeneration operations, while maintaining a high level of quality of process fluids and solutions.

Figure 3. *A modular system with an intermediate module incorporating a pre-filter at the inlet and a series of mechanical filters at the outlet of the intermediate module, upstream of the electrochemical reactors for pH adjustment (acidity and alkalinity)*

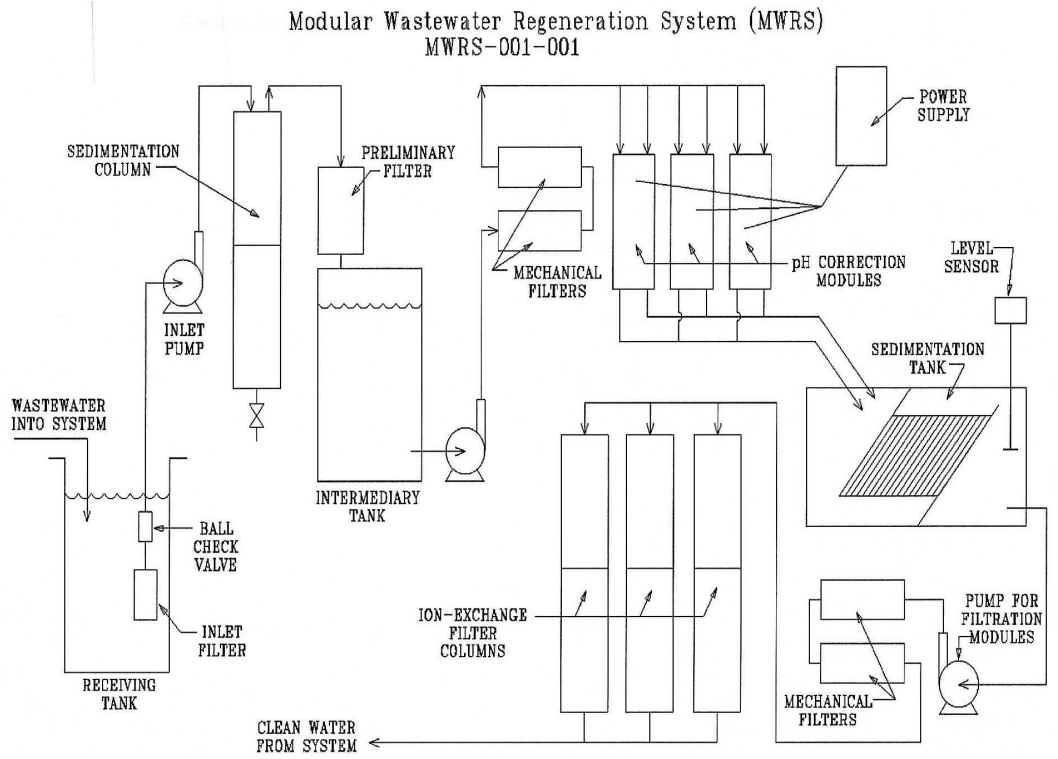

Figure 4. *The most compact modular system configuration without intermediate technological or structural elements*

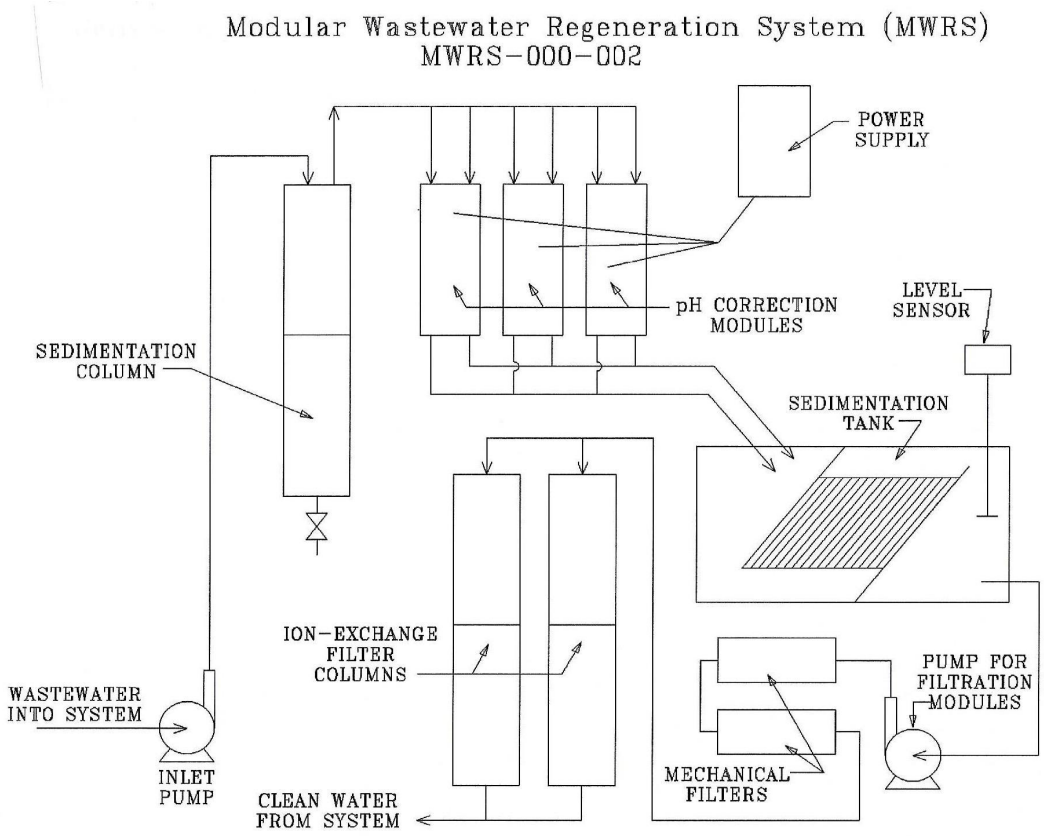

Thus, as demonstrated by the presented figures and diagrams, the hierarchical structure of vertically integrated modular systems enables the simultaneous resolution of technological and environmental challenges while meeting the needs of industrial operations of any type and level of waste contamination, ensuring full regeneration and subsequent recirculation of process fluids.

Furthermore, this approach contributes to addressing the transformation of industrial systems of varying scales and degrees of organizational flexibility into so-called smart manufacturing systems.

Figure 5. *Basic IP*

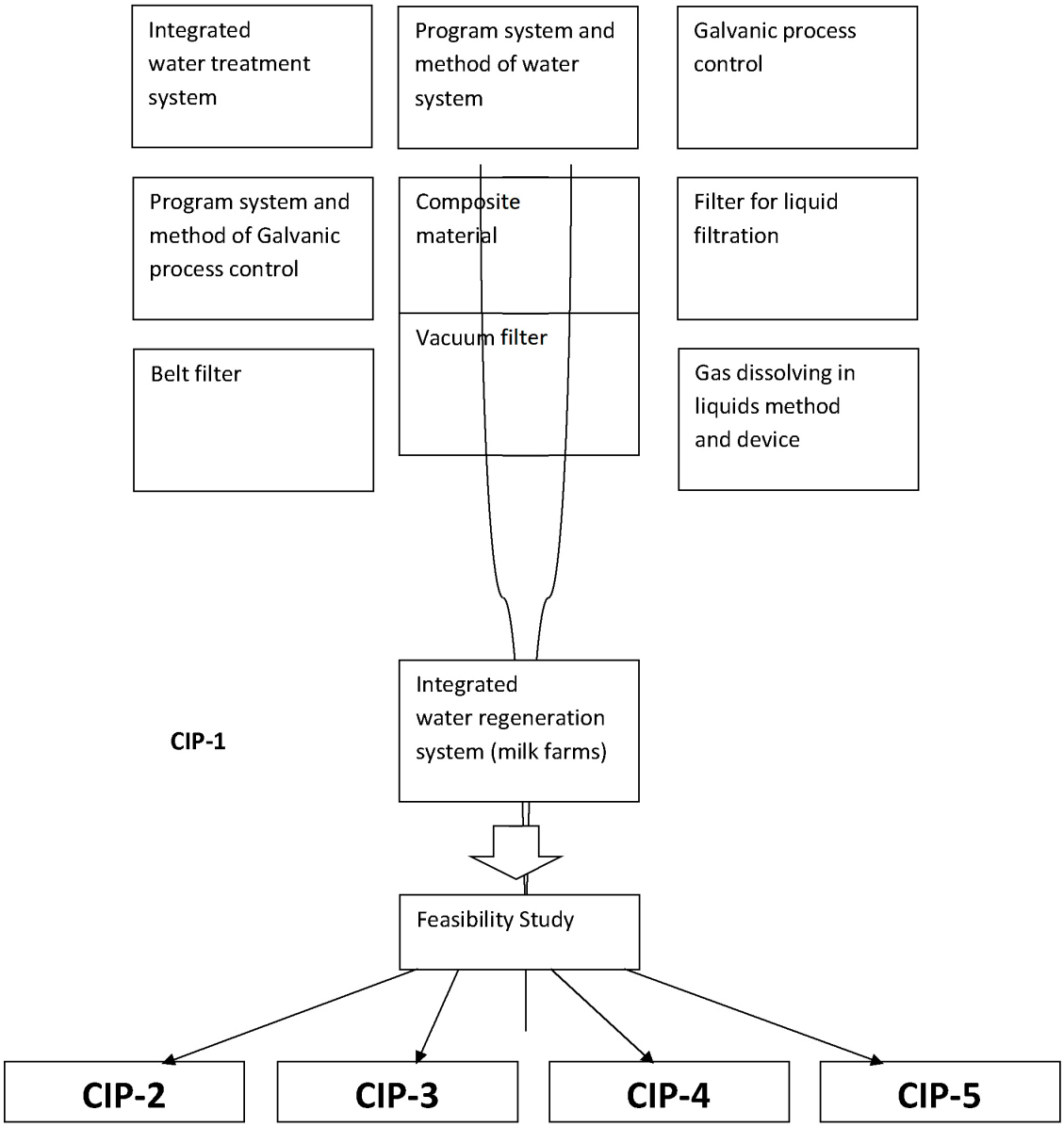

As shown in the presented algorithmic diagram, which is also developed based on innovative concepts and proposals derived from the inventions and publications of Vladyslav Drapii, a total of **14 objects** are identified and represented. Each of these objects constitutes a complex of modules composed of autonomous modules of a lower combinatorial level.

Each of the presented modules represents an independent subject of patent protection, and all possible combinations of these modules likewise constitute full subjects of patent protection and valid objects for further patent continuation (in accordance with applicable U.S. patent law).

As of today, users of water treatment technologies face a number of challenges that

prevent auxiliary water treatment operations from achieving the same level of efficiency as primary industrial processes. The key challenges include:

- continuous limitations in available water resources suitable for technological processes;
- ongoing deterioration in the quality of natural water resources;
- steadily increasing cost of water resources;
- increasingly stringent regulatory standards for wastewater discharge, leading to higher treatment costs;
- continuously rising requirements for the quality parameters of process water;
- the introduction of new synthetic and organic materials in modern production processes, requiring continuous modernization of water treatment systems or significantly expanded operational capabilities, resulting in increased capital and operational costs;
- the existence of numerous industrial facilities operating with outdated equipment that has reached the end of its service life, where replacement is either economically burdensome or technically unfeasible.

Figure 6. *Integrated water treatment technology*

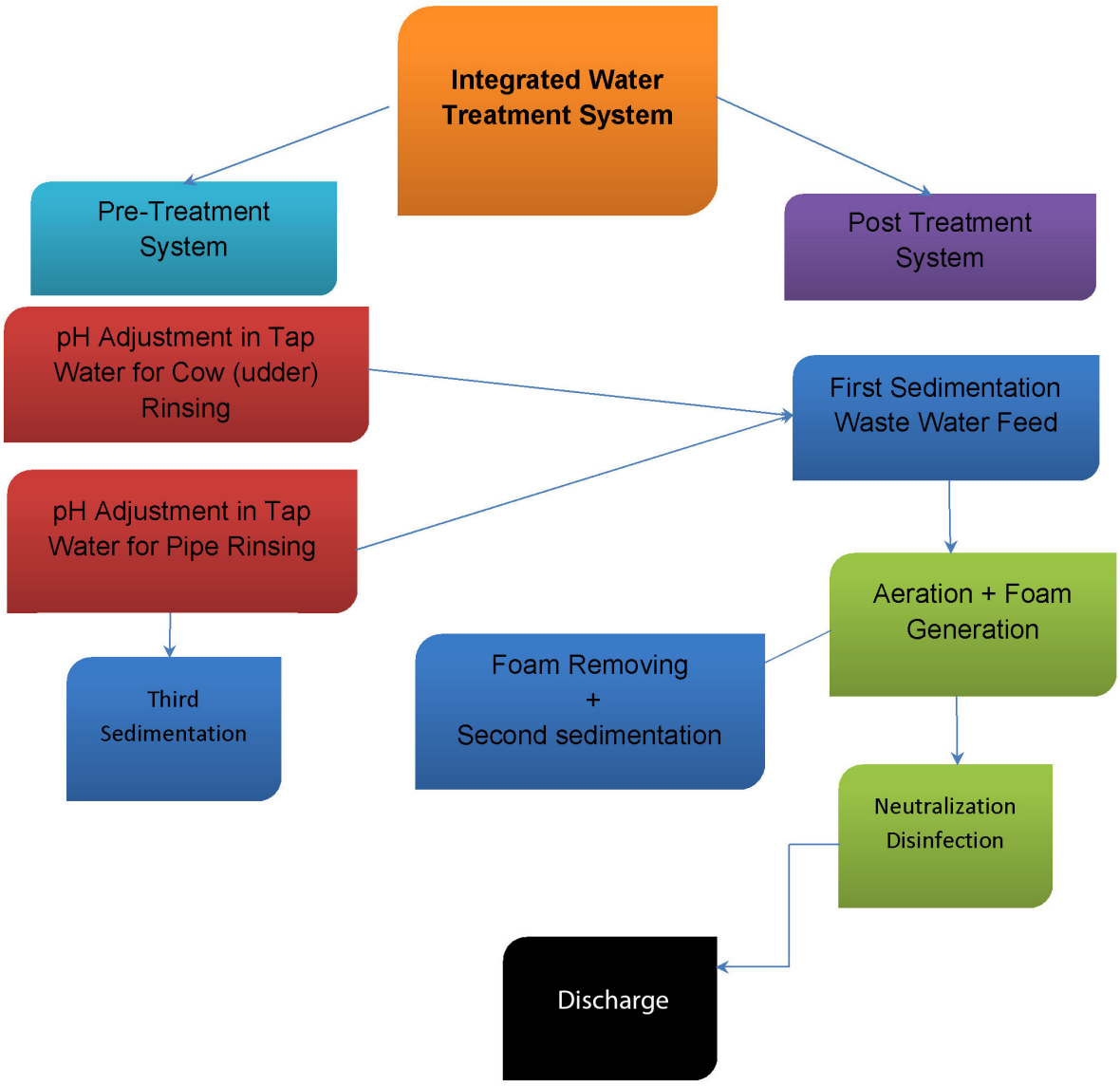

Patent and Licensing Landscape and Patentability of the Proposed Technologies

Based on preliminary analysis and patent searches related to the proposed water treatment methods, the following subject areas have been identified for patent applications:

- a комплекс of modules for advanced treatment of water and aqueous solutions, and an associated method of use;
- a comprehensive water treatment method and technological modules for its implementation;
- a method for electrolytic extraction of metals from water or aqueous solutions, and electrode cells for its implementation;
- a method for aerodynamic foaming of water in a continuously moving flow, and a foam generator for implementing the method;
- an integrated method of filtration combined with ion-exchange treatment and biosorption;
- an electrode cell for electrocoagulation with coaxial electrodes;
- an electrode cell for electrocoagulation with a continuously moving belt cathode;
- an electrode cell for pH adjustment (acidity/alkalinity) using blocks of polarizable soluble electrodes;
- an electrode cell for pH adjustment using volumetric porous electrodes;
- an electrode cell for pH adjustment using continuously moving belt electrodes;
- an electrode cell for electrochemical disinfection, and associated electrode systems for implementation.

For each patent application, prototypes and analogs have been identified based on the developments and inventions of Vladyslav Drapii, the author of the proposed methods. Based on the results of the preliminary patent search and structural analysis, the full patentability of the above technical solutions has been established.

Based on the foregoing, it becomes possible – through the integration of vertically structured modular systems – to develop a block diagram of an integrated technological complex in which the flexibility and selectivity of each process are addressed at the level of individual modules within the lowest tier of the hierarchical structure.

References

US Patent Application 20100224506
Process and Apparatus for Complex Treatment of Liquids.
United States Patent Application, September 9, 2010.

US Patent Application 20100224497
Device and Method for the Extraction of Metals from Liquids.
United States Patent Application, September 9, 2010.

US Patent Application 20110069579
Fluid Mixer with Internal Vortex.
United States Patent Application, March 24, 2011.

US Patent Application 20100193445
Foaming of Liquids.
United States Patent Application, August 5, 2010.

US Patent Application 20150130091
Foaming of Liquids.
United States Patent Application, May 14, 2015.
US Patent 6,139,714

Method and Apparatus for Adjusting the pH of a Liquid.
United States Patent, October 31, 2000.

US Patent 9,144,774
Fluid Mixer with Internal Vortex.
United States Patent, September 29, 2015.

submitted 15.04.2026;
accepted for publication 29.04.2026;
published 30.04.2026

Contact: v.drapii@legarithm.io

The Austrian Journal of Technical and Natural Sciences, 2026 No 3–4
ISSN 2310-5607

PREMIER Publishing
ppublishing.org

DOI:10.29013/AJT-26-3.4-203-209

APPLICATIONS OF COMPLEX DYNAMIC HOMOGENIZATION TECHNOLOGY. (Possible applications of complex dynamic homogenization technology for hydrocarbon fuel mixtures in internal combustion engines)

Mykhailo Korobko [1]

[1] Specialist in the field of engineering, technologies, and concepts of infrastructure and ecosystems of smart transport and intelligent garage complexes G Motion Collision center Los Angeles, CA, United States

Cite: *Korobko M. (2026). Applications of complex dynamic homogenization technology. (Possible applications of complex dynamic homogenization technology for hydrocarbon fuel mixtures in internal combustion engines). Austrian Journal of Technical and Natural Sciences 2026, No 3–4.* https://doi.org/10.29013/AJT-26-3.4-203-209

Abstract

The dynamic homogenization system is characterized by compact dimensions and an optimized geometric configuration, with fully standardized fuel inlet and outlet connections that enable seamless integration into internal combustion engines without requiring structural modifications. Modern engines equipped with high-pressure fuel pumps can incorporate the system without altering existing fuel supply architectures. The technology is applicable to both stationary engines and those used in transportation.

The system can be enhanced with an additional module designed to produce two types of fuel emulsions – compressible and incompressible – while enabling the efficient incorporation of up to eight supplementary components into the fuel composition. It also provides the capability to dissolve combustible gases into liquid hydrocarbon fuels in a continuous flow prior to injection into the combustion chamber, without requiring structural modifications.

The proposed technology demonstrates broad applicability across various fuel types, including liquid hydrocarbons, gasoline- and diesel-based mixtures, fuel oil, as well as liquid biofuels and complex biofuel compositions.

Keywords: *Homogenization; Dynamic homogenization; Complex dynamic homogenization; Applications of homogenization technology; Hydrocarbon fuel mixtures; Internal combustion engines; Liquid injection into the system; Discharge of homogenized liquid from the system; Stationary internal combustion engines; Internal combustion engines installed on vehicles; Minimal modification of the fuel system; Equipping with a dynamic homogenization system*

Types of internal combustion engines in which complex dynamic fuel homogenization technology and fuel mixture homogenization technology can be applied.

Figure 1. *Device for compressible emulsion*

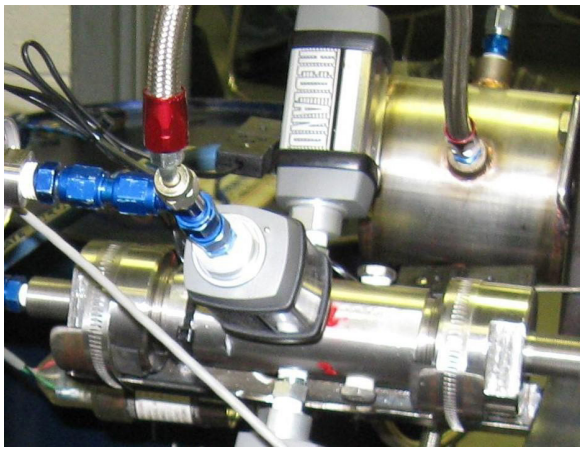

Figure 2. *Device for compressible emulsion*

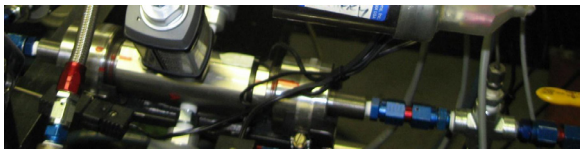

The dynamic homogenization system has minimal overall dimensions and an optimal geometric shape.

The liquid inlets into the system and outlets of the homogenized liquid from the system are completely standard, therefore the dynamic homogenization system for fuel mixtures can be installed on any internal combustion engine.

Modern engines that include a high-pressure pump can be equipped with a dynamic homogenization system for the fuel mixture without any modifications to the fuel system.

Equipping with a dynamic homogenization system can be carried out both on stationary internal combustion engines and on internal combustion engines installed in vehicles.

The dynamic homogenization system can be equipped with an additional system for forming two types of fuel emulsions: compressible emulsions and incompressible emulsions.

The dynamic homogenization system enables efficient emulsification of up to eight additional components in the emulsion.

Without modification, the dynamic homogenization system can effectively dissolve combustible gases in the flow of liquid hydrocarbon fuel prior to injection into the combustion chamber, both in stationary internal combustion engines and in internal combustion engines installed in vehicles.

Figure 3. *Device for compressible emulsion*

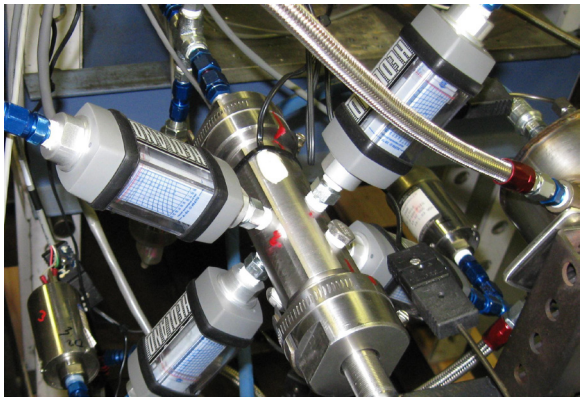

Types of liquid hydrocarbon fuels that can be subjected to dynamic homogenization.

Using dynamic homogenization technology, any types of liquid hydrocarbon fuels can be processed.

Using dynamic homogenization technology, any types of fuel mixtures based on gasoline, all types of diesel fuel, and fuel oil can be processed.

Using dynamic homogenization technology, any types of liquid biofuels can be processed.

Using dynamic homogenization technology, any types of biofuel compositions can be processed.

Dynamic Homogenization of Fuel Without Impurities

During storage of liquid hydrocarbon fuels, fuel agglomerations may form, which can later cause problems with injection and uniform combustion.

The higher the fuel viscosity, the higher the probability of formation of agglomerates and other types of fuel inhomogeneity.

The fuel dynamic homogenization system is installed in the engine fuel system on the fuel pipeline between the engine fuel pump and the high-pressure pump of the engine.

During fuel passage through the dynamic homogenization system, homogenization occurs in the flow under the level of turbulence, after which the high-pressure pump completes the dynamic homogenization process in volume and dimensional factors in a three-dimensional coordinate system.

The operation of the fuel dynamic homogenization system does not require any additional energy sources or additional structural elements.

The fuel dynamic homogenization system can also be used in processes and apparatus for homogenization in parallel with fuel recirculation in storage tanks during fuel production and during storage at fuel filling stations.

Dynamic Homogenization of Fuel Mixtures Based on Gasoline

Fuel mixtures based on gasoline, such as gasoline-ethanol blends and gasoline-methanol blends, during long-term storage may exhibit gravitational separation of water from the hydrocarbon part of the fuel mixture.

The dynamic homogenization system in gasoline engines using gasoline-ethanol or gasoline-methanol blends as fuel is installed between the fuel pump and the engine high-pressure pump.

During the passage of the fuel mixture in which water has separated from gasoline through the dynamic homogenization system, homogenization occurs in the flow under the level of turbulence, after which the high-pressure pump completes the dynamic homogenization process in volume and dimensional factors in a three-dimensional coordinate system.

During the homogenization process, water in the form of micro-droplets is uniformly distributed throughout the volume of the hydrocarbon fuel mixture, after which the mixture is transformed into a micro- or nano-emulsion.

Figure 4. *Device for compressible emulsion*

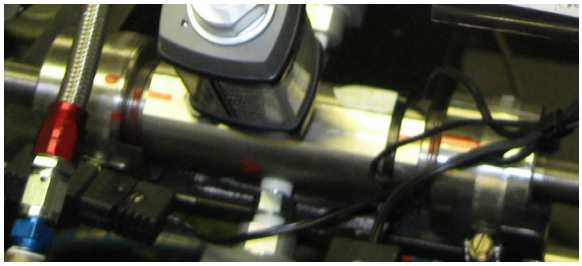

According to test results of the emulsion obtained using the dynamic homogenization system, soot concentration in exhaust gases is reduced by 97%, and the level and rate of heat release increase by at least 35%.

For installation of the dynamic homogenization system on a gasoline engine, no original additional components are required, and no structural modifications to the engine are necessary.

Figure 5. *Device for compressible emulsion*

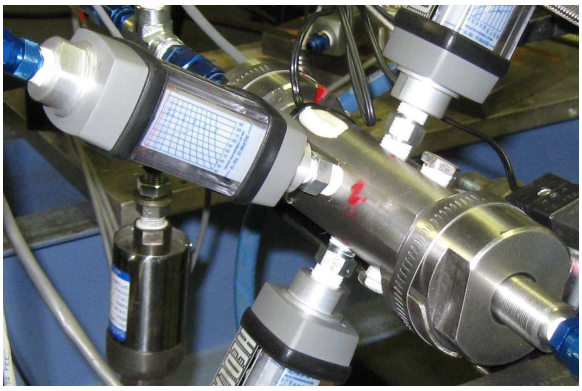

Dynamic Homogenization of Fuel Mixtures Based on Diesel Fuel

Preparation of fuel mixtures from diesel fuel and ethanol or methanol is extremely difficult due to the large difference in viscosity of these materials.

The dynamic homogenization system for fuel mixtures can produce a high-quality and homogeneous mixture of diesel fuel and ethanol or methanol within fractions of a second, directly in the pipeline and in any required proportion.

The dynamic homogenization system in diesel engines using a mixture of diesel fuel with ethanol or methanol as fuel is installed between the fuel pump and the high-pressure pump of the diesel engine.

During the passage of the fuel mixture in which water has separated from gasoline through the dynamic homogenization system, homogenization occurs in the flow under the level of turbulence, after which the high-pressure pump completes the dynamic homogenization process in volume and dimensional factors in a three-dimensional coordinate system.

During the homogenization process, water in the form of micro-droplets is uniformly distributed throughout the volume of the hydrocarbon fuel mixture, after which the mixture is transformed into a micro- or nano-emulsion.

According to test results of the emulsion obtained using the dynamic homogenization system, soot concentration in exhaust gases

is reduced by 97%, and the level and rate of heat release increase by at least 35%.

For installation of the dynamic homogenization system on a diesel engine, no original additional components are required, and no structural modifications to the engine are necessary.

Dynamic Homogenization of Fuel Mixtures Based on Heavy Diesel Fuel

Preparation of fuel mixtures from heavy diesel fuel and ethanol or methanol is extremely difficult due to the large difference in viscosity of these materials.

The dynamic homogenization system for fuel mixtures can produce a high-quality and homogeneous mixture of heavy diesel fuel and ethanol or methanol within fractions of a second, directly in the pipeline and in any required proportion.

The dynamic homogenization system in heavy diesel engines using a mixture of heavy diesel fuel with ethanol or methanol as fuel is installed between the fuel pump and the high-pressure pump of the engine (if present). If a high-pressure pump is not part of the engine, the dynamic homogenization system is installed on the fuel pipeline after the fuel pump.

During the passage of the fuel mixture in which either water has separated from heavy diesel fuel or agglomerates of heavy diesel fuel have formed through the dynamic homogenization system, homogenization occurs in the flow under the level of turbulence, after which the high-pressure pump or injectors complete the dynamic homogenization process in volume and dimensional factors in a three-dimensional coordinate system.

During the homogenization process, water in the form of micro-droplets is uniformly distributed throughout the volume of the hydrocarbon fuel mixture, after which the mixture is transformed into a micro- or nano-emulsion.

According to test results of the emulsion obtained using the dynamic homogenization system, soot concentration in exhaust gases is reduced by 97%, and the level and rate of heat release increase by at least 35%.

For installation of the dynamic homogenization system on an engine using heavy diesel fuel, no original additional components are required, and no structural modifications to the engine are necessary.

Dynamic Homogenization of Fuel Mixtures Based on Fuel Oil

Preparation of fuel mixtures from fuel oil and ethanol or methanol is extremely difficult due to the large difference in viscosity of these materials and due to the inhomogeneity of fuel oil.

The dynamic homogenization system for fuel mixtures can produce a high-quality and homogeneous mixture of fuel oil and ethanol or methanol within fractions of a second, directly in the pipeline and in any required proportion.

In cases of particularly high inhomogeneity of fuel oil, the structural simplicity of the system allows its staged use with the formation of a gradual (step-by-step) sequential scheme for preparing a fuel mixture based on fuel oil.

The dynamic homogenization system in large engines using a mixture of fuel oil with ethanol or methanol as fuel is installed between the fuel pump and the subsequent element of the engine fuel system.

During the passage of the fuel mixture in which water has separated from fuel oil or in which agglomerates and lumps have formed in the fuel oil flow through the dynamic homogenization system, homogenization occurs in the flow under the level of turbulence, after which the injector or nozzle completes the dynamic homogenization process in volume and dimensional factors in a three-dimensional coordinate system.

During the homogenization process, water in the form of micro-droplets is uniformly distributed throughout the volume of the hydrocarbon fuel mixture, after which the mixture is transformed into a micro- or nano-emulsion.

According to test results of the emulsion obtained using the dynamic homogenization system, soot concentration in exhaust gases is reduced by 97%, and the level and rate of heat release increase by at least 35%.

For installation of the dynamic homogenization system on the specified engine, no original additional components are required, and no structural modifications to the engine are necessary.

Preparation of Fuel Mixtures at Oil Refineries

At oil refineries, the system for dynamic homogenization of hydrocarbon liquids must include a high-pressure pump operating on the principle of a diesel engine high-pressure pump.

The specified integrated system can be used either as a pump for mixing components of the fuel mixture or as a system ensuring recirculation of the fuel mixture in storage tanks.

Installation of such systems can be carried out on existing equipment without its alteration or modernization; however, in this case, the system must include pumps for supplying mixture components into the system.

One of the applications of the dynamic homogenization system at oil refineries is the formation of a fuel mixture during the supply of its components into a transport tank. Since the time required to prepare the fuel mixture in the system amounts to fractions of a second, preparation during transfer into a transport tank eliminates the need for dedicated storage tanks for the fuel mixture at the facility.

Figure 6. *Device for compressible emulsion*

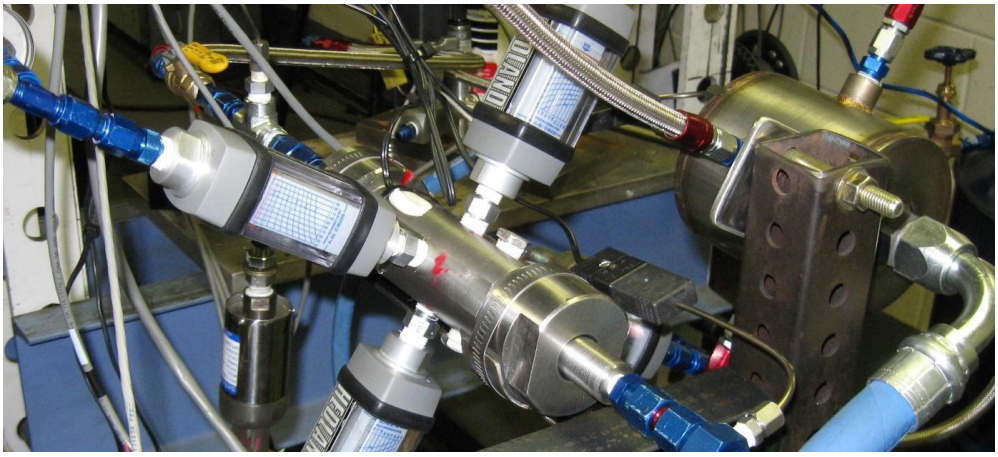

Figure 7. *Device for compressible emulsion*

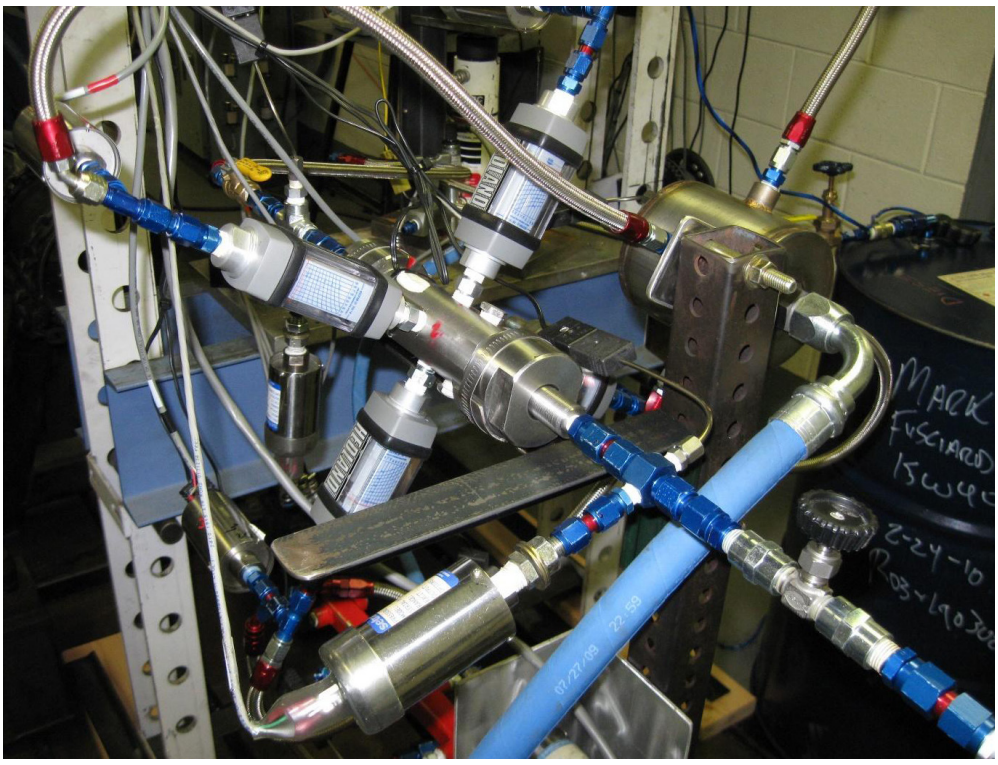

Preparation of Fuel Mixtures at Fuel Filling Stations

At fuel filling stations, the system for dynamic homogenization of hydrocarbon liquids must include a high-pressure pump operating on the principle of a diesel engine high-pressure pump.

The specified integrated system can be used either as a pump for mixing components of the fuel mixture or as a system ensuring recirculation of the fuel mixture in storage tanks.

Installation of such systems can be carried out on existing equipment without its alteration or modernization; however, in this case, the system must include pumps for supplying mixture components into the system.

One of the applications of the dynamic homogenization system at fuel filling stations is the formation of a fuel mixture during the direct supply of its components into the fuel tank of a car or other vehicle. Since the time required to prepare the fuel mixture in the system amounts to fractions of a second, preparation during filling into a vehicle tank eliminates the need for dedicated storage tanks for the fuel mixture at the facility.

Preparation of Fuel Mixtures Directly Within the Internal Combustion Engine

In cases where an additional tank for a second fuel component can be installed on a vehicle, fuel mixture preparation can be carried out by the dynamic homogenization system directly in the fuel pipeline.

The feasibility of this option was tested on a serial diesel engine, in which a water-in-oil fuel emulsion was produced, i.e., diesel fuel was emulsified with ordinary tap water.

As a result of using such an emulsion, soot concentration in exhaust gases was reduced by 97% (mixing ratio in the emulsion: 20% water to 80% diesel fuel).

Installation of the Dynamic Homogenization System on a Newly Manufactured Internal Combustion Engine

For installing the dynamic homogenization system on a newly manufactured internal combustion engine, no new elements are required in the engine design.

The system is introduced into the fuel pipeline after the fuel pump, and its outlet is connected to the inlet of the high-pressure pump, or, if it is absent, to the inlet of the structural component following the fuel pump.

Installation of the Dynamic Homogenization System on a Retro Internal Combustion Engine

For installing the dynamic homogenization system on a repaired or modified internal combustion engine, no new elements are required in the engine design.

The system is introduced into the fuel pipeline after the fuel pump, and its outlet is connected to the inlet of the high-pressure pump, or, if it is absent, to the inlet of the structural component following the fuel pump.

Installation of the Dynamic Homogenization System on Industrial Facilities For the Production of Fuel Mixtures

The system can be supplied by the manufacturer in a modular form.

The composition of the system and its functions can be modified at the manufacturing facility without additional design work.

The system has no limitations or elements that would prevent its installation on any industrial equipment.

Installation of the Dynamic Homogenization System on Tanks With Fuel Mixture at Fuel Filling Stations

The system can be supplied by the manufacturer in a modular form and can be produced at any required scale.

The composition of the system and its functions can be modified at the manufacturing facility without additional design work.

The system has no limitations or elements that would prevent its installation on any industrial equipment.

References

Oguni, T., et al. (2021). Secondary Battery and Manufacturing Method Thereof. *United States Patent Application* 20210104744 A1, April 8, 2021.
Oikawa, M. (2021). Battery Electrode and Method for Manufacturing the Same. *United States Patent Application* 20210104719 A1, April 8, 2021.
Shelton IV, F. E., et al. (2021). Modular Battery Powered Handheld Surgical Instrument and Methods Therefor. *United States Patent Application* 20210100579 A1, April 8, 2021.
Seki, H., et al. (2021). Secondary Battery, Battery Pack, Vehicle, and Stationary Power Supply. *United States Patent Application* 20210091416 A1, March 25, 2021.
Londarenko, Y. Y. (2021). Multi-Layer Battery Configurations. *United States Patent Application* 20210091402 A1, March 25, 2021.
Lane, R. C. (2021). High Voltage Battery Module Parallel Cell Fusing System. *United States Patent Application* 20210091363 A1, March 25, 2021.
Balaram, H., et al. (2021). Battery Pack with Attached System Module. *United States Patent Application* 20210091360 A1, March 25, 2021.
Dou, S., et al. (2021). Lithium-Ion Battery and Apparatus. *United States Patent Application* 20210075063 A1, March 11, 2021.
Nakayama, T. (2021). Non-Aqueous Electrolyte Secondary Battery. *United Sttes Patent Application* 20210075060 A1, March 11, 2021.
Lee, J., et al. (2021). Secondary Lithium Battery Anode and Secondary Lithium Battery Including Same. *United States Patent Application* 20210075015 A1, March 11, 2021.
Park, B. Y., et al. (2021). Prelithiated and Methods for Prelithiating an Energy Storage Device. *United States Patent Application* 20210075008 A1, March 11, 2021.
Kim, Y.-K., et al. (2021). Positive Electrode Active Material for Rechargeable Lithium Battery and Rechargeable Lithium Battery Including Same. *United States Patent Application* 20210066712 A1, March 4, 2021.
Lane, R. C. (2021). Method to Prevent or Minimize Thermal Runaway Events in Lithium Ion Batteries. *United States Patent Application* 20210066683 A1, March 4, 2021.

submitted 27.03.2026;
accepted for publication 11.04.2026;
published 30.04.2026

Contact: sedova.alina7810@gmail.com

The Austrian Journal of Technical and Natural Sciences, 2026 No 3–4
ISSN 2310-5607

PREMIER Publishing
ppublishing.org

DOI:10.29013/AJT-26-3.4-210-216

CONCEPT OF SMART HOME INFRASTRUCTURE. (Innovative smart home infrastructure components for energy supply, backup energy storage, water supply, and water treatment)

Alisa Lahunina [1]

[1] Architect Hanber-Trade Odesa, Ukraine

Cite: *Lahunina A. (2026). Concept of Smart Home Infrastructure. (Innovative smart home infrastructure components for energy supply, backup energy storage, water supply, and water treatment). Austrian Journal of Technical and Natural Sciences 2026, No 3–4.* https://doi.org/10.29013/AJT-26-3.4-210-216

Abstract

This article examines innovative smart home infrastructure components designed for energy supply, backup energy storage, water supply and purification, water regeneration and recirculation, clean air provision, air regeneration, and oxygen enrichment, as well as the issues of integrated real-time monitoring and control of these systems. The article emphasizes the importance of integrating advanced technical and software solutions corresponding to the global state of the art in technological and structural innovation in order to enable the implementation of artificial intelligence and artificial neural network elements in smart home design and operational processes. Particular attention is devoted to the logistics of generating innovative technical solutions within the framework of modern smart home, smart building, and smart house infrastructure, as well as to the methodological aspects of developing technical solutions possessing both inventive merit and commercial potential. The article substantiates the necessity of a systematic approach to the evaluation, structuring, and commercialization of new technologies with due consideration of market requirements, investment attractiveness, production constraints, and objective economic factors. It is concluded that the development of modern innovative solutions in the field of smart infrastructure requires a transition from autonomous standalone inventions to comprehensive integrated technological ecosystems capable of ensuring sustainable competitiveness and compliance with contemporary infrastructural, environmental, and social requirements.

Keywords: *Smart home infrastructure; smart home infrastructure components; innovative smart home infrastructure components; innovative smart home infrastructure components for energy supply; innovative smart home infrastructure components for backup energy storage; innovative smart home infrastructure components for water supply, water treatment, regeneration, and recirculation; innovative smart home infrastructure components for clean air supply, air regeneration, and oxygen saturation; comprehensive integrative issues of active real-time monitoring and control of these components and their interconnections.*

Characteristics of the Integrated Nature of the Proposed Technology

Analysis of the proposed technology with respect to the use of only known and repeatedly tested physical principles and laws embodied in a compact integral engineering or technological solution;

Analysis of the proposed technology and the device (method) for its implementation, allowing their application in real industrial systems without the slightest change or modification of their design or the slightest alteration of their operating principle;

Analysis of the proposed technology with respect to the use of only known and widely utilized components and combinations thereof;

Analysis of the proposed technology with respect to the possibility of integrated use, alongside widely known components, of new components in various combinations with known ones, which are formed within the proposed process due to the properties and characteristics of the device for implementation of the proposed technology;

Analysis of the proposed technology with respect to the level of universality and flexibility allowing flexible technological schemes to be applied within the same device or method for implementation of the technology;

Analysis of the composition of the proposed technology with respect to the possibility of use or presence of a system for control, monitoring, and regulation of parameters based on a minimum number of monitored and regulated process parameters having direct dependence upon and immediate influence on the efficiency level of both the process itself and the device during its operation, taking into account the achievement of required technological, energy, and environmental results;

Description of the process.

Possible components of the proposed technology and device.

Description of design variants of the device taking into account the possibility of integrated activation and increased efficiency of its principal operating principles.

Description of advantages for the process obtained during operation of the proposed device due to the properties and characteristics of the device itself.

Description of known tested technologies preceding the emergence of the proposed technology and of how they positively influenced this technology and its output parameters and characteristics.

Characteristics of the proposed technology.

Sequential description of the technological stages of the proposed process.

Principal schematic of devices and components included in the industrial system utilizing the proposed integrated technology.

Operating procedure of the proposed device based on the example of its implementation in a real industrial system.

Operational characteristics of the proposed technology at the initial stages of application.

Operational characteristics of the proposed technology at subsequent stages of its application.

Methods for regulating the principal operating characteristics of the proposed technology; possibility of remote control of the regulation process; principal regulated parameters; feedback during regulation.

Principal operating parameters of the proposed technology forming its advantages over known alternatives and technologies.

Description of the proposed process or of the comprehensive/integrative nature of the proposed technology; advantages arising from implementation of the proposed process or technology.

Estimated and calculated characteristics of the proposed process.

Technical and commercial advantages of application of the proposed technology; its possible integrated nature and the influence of this aspect.

Work with the block diagram of patent-licensing strategy.

After completion of the above analysis of the situation, a sufficient amount of information may be accumulated for preparation of patent-licensing strategy block diagrams.

Depending on the complexity of the technical solution, the block diagrams may differ substantially; however, such diagrams will certainly be more effective and reliable if, prior to their preparation, a forecast is made regarding the development of the field of technology to which the proposed technical solution or the subject matter of the future invention belongs.

At present, numerous informational tools exist for such forecasting, and their analysis in combination with understanding of the technical and commercial essence of the invented technology allows such forecasting to be carried out with sufficient accuracy.

Thereafter, the initial sections of the block diagram may be completed in accordance with the proposed template and the planned implementation may be carried out.

This article examines innovative smart home infrastructure components relating to water supply, water purification, water regeneration, and water recirculation.

There exists positive global experience in water treatment without the use of chemical materials and reagents.

The installation uses membrane filters in parallel with automatic self-cleaning mechanical filters, and three dual electrochemical reactors are integrated into the installation, which transforms the installation into a relatively large unit requiring significant space for installation and connection, thereby creating substantial difficulties for many residential properties, including those having smart home status.

Figure 1. *Shows such an innovative installation for treatment, purification, and regeneration of wastewater*

Therefore, during the formation of smart home infrastructure, this issue was taken into account from the earliest stages, and the concept of water treatment, operation, and recirculation for smart home needs was substantially redesigned.

Electrochemical Treatment of Industrial Wastewater for Purification from Heavy Metal Ions and for Enabling Repeated Reuse of Purified Water in Recirculation Mode

This problem arose long ago in the field of industrial wastewater treatment.

Purification of Industrial Wastewater From Heavy Metals

The principal problem in modern industrial production is the necessity of using water for technological processes and maintaining the required level of water quality throughout the technological process.

Because it is impossible to maintain the required water quality level for prolonged periods, water that has completed its service cycle is removed from the process and replaced with new water possessing the required properties and parameters.

Because the cost of water is constantly increasing, efforts are being made to identify methods for repeated reuse of water resources.

In addition, the requirements for water discharged from technological processes are continuously increasing, and such water must be brought to required standards before discharge into sewage systems.

Informational Materials on Global Industrial Production Associated With Generation of Waste In The Form of Aqueous Solutions Containing Metal Ions

The principal sources of wastewater contamination by metal ions include:

- rinse waters from electroplating facilities of all types;
- water used for cooling hot metal surfaces;
- water used for washing transport and process containers for chemical reagents and materials;
- water used in rinsing after metal pickling;
- water used in metallized paint and coating application processes;
- water used in mining operations.

In general, the volume of water requiring special treatment prior to disposal amounts to no less than 200–250 cubic meters per day for an average enterprise engaged in electroplating operations.

To illustrate the overall volumes of water requiring treatment and purification, annual water consumption for air-conditioning systems with water-cooled heat exchangers in Israel may be cited as an example, amounting to approximately 150,000,000 cubic meters per year.

General Classification of Wastewater; Place of Electrochemical Technologies Within This Classification

Industrial wastewater is classified as follows:

- water not containing metals in ionic form;
- water containing metals in ionic form in concentrations up to 1 gram per liter;
- water containing metals in concentrations up to 5 grams per liter;
- water containing metals in concentrations up to 10 grams per liter;
- water containing metals in concentrations exceeding 10 grams per liter.

In all such cases, metal ions may be present either in pure form or in the form of chemical complexes comprising metals and various non-metallic materials and compounds, including organic substances.

Electrochemical technologies are capable of exerting real influence on all types and classes of wastewater, including water not containing metals, specifically through acidity/alkalinity adjustment and turbo-flotation for separation of conductive and dielectric components of aqueous solutions.

Classification Of Technical Solutions For Wastewater Purification; Methods of Metal Removal From Wastewater

Approximately 16 different technological methods of purification of metal-containing wastewater are known.

The most widespread is purification using chemical reagents, whereby caustic soda is added to water to increase alkalinity until metal hydroxides precipitate.

Artificial coagulation and flocculation methods need not be considered due to their poor economic efficiency resulting from high cost.

The only method capable of competing with chemical reagent treatment in terms of cost and efficiency is electrocoagulation.

This method has recently gained popularity, especially in high-technology industries, but it cannot comprehensively resolve all existing problems.

Transition to electrocoagulation systems at enterprises currently using chemical reagent purification requires substantial capital expenditures while failing to solve all fundamental problems.

All known methods fail to solve the problem of water purification for repeated reuse and, consequently, the problem of reducing water consumption for technological needs.

Popularity of Existing Water Purification Technologies

As noted above, the most common technology remains purification of wastewater using chemical reagents.

Electrocoagulation technology has recently begun gaining popularity.

Market positioning and competitive landscape of the proposed technologies

These technologies are applied at virtually all enterprises using water for technological purposes.

There exists a vast number of local integrator companies which construct purification systems based on general purification principles and customer-specific requirements.

Large consumers such as Intel utilize major companies concentrating broad water purification technologies, but even these companies – such as Vivendi, France – use local integrators as subcontractors.

Thus, major corporations are technology rights holders granting smaller companies rights to use their technologies, while large customers rely upon guarantees of technology holders.

Free Market Niches and How New Smart-Home-Suitable Technology May Occupy Them

The majority of water treatment technologies currently used involve chemical reagent processes.

The niche of non-chemical reagent technologies is practically unoccupied.

Even less occupied is the niche of non-chemical technologies that do not generate difficult-to-dispose waste, which is critically important for smart home applications.

At present, such technologies are practically absent from the market, and seven technological modules derived from electrochemical process specialists' developments, together with all modifications and configurations, provide grounds for occupying market sectors related to comprehensive purification, regeneration, and repeated reuse of water resources, including smart home water infrastructure.

As of today, no technologies have been identified that enable regeneration and repeated reuse of industrial wastewater with minimal economically acceptable costs and near-complete absence of toxic waste.

Furthermore, electrochemical processing modules can be integrated into existing installations and lines utilizing chemical and other technologies.

In such cases, electrochemical processing modules solve local technological tasks while significantly increasing the technical level of existing technologies.

Entry into the smart home market for electrochemical technologies through this category is therefore substantially facilitated.

Current Main Competitors of Electrochemical Processing Technology

At present, technologies proposed on the basis of electrochemical methods are not used anywhere due to the substantial novelty of these technologies.

Once the principal base elements of the technology are implemented, the most likely competitors may become large companies such as Zenon (Canada) and Vivendi (France).

Particularly novel is the method proposed for smart home infrastructure involving aerodynamic foaming and resulting separation of conductive and non-conductive fractions in treated water or aqueous solutions.

This problem currently hinders broader implementation of electrochemical technologies.

This innovative method has been tested and demonstrated promising results.

Comparison of Electrochemical Processing With Similar Technologies

The most advanced currently used technologies for purification of metal-containing wastewater are electrocoagulation technologies.

Despite their advantages over older chemical methods, electrocoagulation does not resolve all critical issues of water purification and possesses substantial disadvantages eliminated by the integrated electrochemical processing technology.

The principal advantages of electrochemical processing technology include:

- absence of need for sedimentation processes;
- absence of toxic waste requiring complex and expensive disposal methods;
- absence of process sensitivity to acidity level of treated water and no need for acidity correction;
- universality of electrochemical reactor modules allowing inexpensive and simple customization for customer-specific conditions while preserving core technological and structural principles, including smart home water treatment principles;
- possibility of broad and deep standardization of electrochemical processing modules;

- possibility of integration into any technological line;
- possibility of preliminary separation of conductive and non-conductive components of aqueous solutions;
- possibility of combining electrochemical metal extraction with natural and biological ion-exchange materials.

Separate consideration should be given to the economic advantages of electrochemical processing technology.

References and Patent-Licensing Materials

United States Patent Application No. 20210094846 (A1).
Connor, Jr., Michael James, et al. *Hybrid Electrochemical and Membrane-Based Processes for Treating Water with High Silica Concentrations.*
April 1, 2021.

United States Patent Application No. 20210078887 (A1).
Yang, Qifeng, et al. *Treatment Process and Treatment System of Enhanced Up-Flow Multiphase Wastewater Oxidation.*
March 18, 2021.

United States Patent Application No. 20210060522 (A1).
El-Shall, M. Samy, et al. *Graphene-Based Materials for the Efficient Removal of Pollutants from Water.*
March 4, 2021.

United States Patent Application No. 20210029977 (A1).
Alcantar, Norma Arcelia, et al. *Compositions and Methods to Remove Ammonia in Freshwater and Saltwater Fish Storage Systems.*
February 4, 2021.

United States Patent Application No. 20210002151 (A1).
Hao, Xiaogang, et al. *Method and Device for Removing Chloride Ion in Desulfurized Wastewater by Electrochemical Coupling.*
January 7, 2021.

United States Patent Application No. 20210046431 (A1).
Awadh, Tawfik Abdo Saleh, et al. *Simultaneous Sorption of Dyes and Toxic Metals from Waters Using Titania-Incorporated Polyamide.*
February 18, 2021.

United States Patent Application No. 20200406194 (A1).
Demeter, Ethan. *Electrodialysis Process and Bipolar Membrane Electrodialysis Devices for Silica Removal.*
December 31, 2020.

United States Patent Application No. 20200399148 (A1).
Avraham, Eran, et al. *Method and Apparatus for Electrochemical pH Control.*
December 24, 2020.

United States Patent Application No. 20200381758 (A1).
Shiue, Lih-Ren, et al. *System for Generating Electricity Using Oxygen from Water*. December 3, 2020.
alfa1logistics@gmail.com

submitted 14.04.2026;
accepted for publication 28.04.2026;
published 30.04.2026

Contact: sedova.alina7810@gmail.com

The Austrian Journal of Technical and Natural Sciences, 2026 No 3–4
ISSN 2310-5607

PREMIER Publishing
ppublishing.org

DOI:10.29013/AJT-26-3.4-217-223

MONITORING THE QUALITY OF DRINKING WATER AND MILK. (Inventions in the field of non-contact monitoring of the quality of drinking water and cow's milk in real time)

Marakshyna Alina [1]

[1] Aesthetician LLC MYHOME NYC INC. Odessa, Ukraine

Cite: *Marakshyna A. (2026). Monitoring the quality of drinking water and milk.(Inventions in the field of non-contact monitoring of the quality of drinking water and cow's milk in real time). Austrian Journal of Technical and Natural Sciences 2026, No 3–4.* https://doi.org/10.29013/AJT-26-3.4-217-223

Abstract

This article examines issues related to quality control of drinking water and milk as critically important components affecting human health and technologically sensitive production processes. The primary objective of the study is to identify the limitations of existing monitoring technologies and to substantiate the need for more comprehensive and continuous quality control systems capable of ensuring reliable assessment of key safety and purity indicators. The research is based on an analytical evaluation of current monitoring technologies and applicable regulatory requirements, including a comparative analysis of major quality indicators such as water conductivity and the specific characteristics of milk as a high water-content product requiring enhanced quality control. The findings demonstrate that existing systems do not provide full control over critical quality parameters. The article concludes that the implementation of continuous, accurate, and mobile monitoring systems for water and milk is necessary, particularly in sectors requiring elevated levels of safety, reliability, and technological precision.

Keywords: *Drinking water, Cow's milk, Range of technical capabilities, New visions of regulatory quality requirements, Equivalent mobile, reliable and accurate control technology, Need for continuous monitoring, Device for selective identification in real time of the current value of the complex digital indicator of the dynamic state of drinking water quality, Complex Digital indicator of the dynamic state of cow's milk, Integral equivalent of the current value of the content and concentration of components in water*

Introduction:

Inventions in the field of non-contact monitoring of the quality of drinking water and cow's milk. The quality of drinking water practically determines the quality of life. In all methods of water quality control, it is accepted that the conductivity of water is a clear indicator of its purity.

The more impurities in water, the lower its electrical resistance, and the cleaner the water, the higher its electrical resistance.

This suited everyone for a long time, until international terrorism reached such a level of spread as it does now and until general environmental pollution reached such unprecedented scale and dimensions as it does now.

These are of course not all the factors that determine the urgent need for more complete control of water quality, but they are very important.

Almost all existing technologies, devices and equipment for water quality control have a very narrow range of technical capabilities and do not cover all the parameters that must be constantly monitored in order not to allow water to reach the user that, due to the above reasons, is contaminated to such an extent that it poses a danger to human life and health.

Milk is one of the most important products in a complete diet, and since a significant percentage of its composition is also water, it requires equivalent mobile, reliable and accurate control technology, adapted both to the increased quality requirements of milk and to new visions of regulatory requirements for quality.

When monitoring the quality of milk, adaptation to new technological conditions and processes of its industrial processing is also very important.

Based on this far from complete set of information, we can make a reasonable conclusion about the need for constant monitoring of the quality of milk and water before use.

Such technologies have been invented and below is a brief description of these technologies:

1. Device for monitoring the current value of drinking water quality in real time

The device is designed to monitor and evaluate in real time the current value of a complex digital indicator of the dynamic state of drinking water quality; The device can be adapted to process water quality control systems at the inlet to the process and to monitor the quality of wastewater before discharge into the sewer system or before returning to the process after regeneration

Complex Digital indicator of the dynamic state of water and aqueous solutions, this is an integral parameter, which, according to the criteria of frequency, amplitude, resistance, parameters of resonance phenomena, inductance and a complex of dynamic characteristics of the water flow, is an integral equivalent of the current value of the content and concentration of components in water and the relationship, including biological, between the specified components and parameters.

The device for selective identification in real time of the current value of a complex digital indicator of the dynamic state of drinking water quality is a compact device designed for operation as part of water supply pipeline systems, as part of water flow meters or in field conditions powered by solar batteries

The device has minimal energy consumption.

The device includes functionally interconnected systems for input, output, control and transformation of water flow, wherein the system for transformation of water flow includes an aerodynamic mechanism for removing gases from said flow.

The device can be designed for use in stationary conditions and designed for express analysis.

The device and the procedure for working with it do not require special training of the operator or user.

2. Device for monitoring the current value of cow's milk condition in real time

The device is designed to monitor and evaluate in real time the current value of a complex digital indicator of the dynamic state of cow's milk quality

Complex Digital indicator of the dynamic state of cow's milk is an integral parameter, which, according to the criteria of frequency, amplitude, resistance, inductance and a complex of dynamic characteristics of the milk flow, is an integral equivalent of the current value of the content and concentration of components in cow's milk and the relationship, including biological, between the specified components

The device for its selective identification in real time is a compact device designed for operation in dairy farm conditions or in the field, powered by solar batteries.

The device has minimal energy consumption.

The device includes functionally interconnected systems for input, output, control and transformation of milk flow, wherein the system for transformation of milk flow includes an aerodynamic mechanism for removing gases from the milk flow.

The device can be designed for use in stationary conditions and designed for express analysis.

3. Complex integral indicator of water and aqueous solutions quality and device for its identification in real time

A digital indicator of the dynamic state of drinking water quality, which, when comparing the pulse directed to the sensor according to the criteria of frequency, amplitude, resistance, inductance and the same parameters arising in the pipeline from resonance phenomena in the flow, in combination with a set of dynamic characteristics of the water flow, is an integral equivalent of the current value of the content and concentration of components in the water

The device for its selective identification in real time is a compact device designed for operation in urban or main water supply systems or in the field, powered by solar batteries.

The device has minimal energy consumption.

The device includes functionally interconnected systems for input, output, control and transformation of the water flow supplied for control, wherein the water flow transformation system includes an aerodynamic mechanism for removing gases from the flow.

The complex integral indicator of water quality also includes a complex integral indicator of the sensor, which for each type of sensor, its design parameters and parameters of the signal supplied to the sensor, is a constant value, which is confirmed by the results of a series of tests in more than 1000 cycles on 4 types of sensors.

The device can be designed for use in stationary conditions and designed for express analysis.

4. Comprehensive integral indicator of cow's milk quality and a device for its identification in real time

A digital indicator of the dynamic state of cow's milk, which, according to the criteria of frequency, amplitude, resistance, inductance and a complex of dynamic characteristics of the milk flow, is an integral equivalent of the current value of the content and concentration of components in cow's milk.

The device for its selective identification in real time is a compact device designed for operation in dairy farm conditions or in the field, powered by solar batteries.

The device has minimal energy consumption.

The device includes functionally interconnected systems for input, output, control and transformation of milk flow, wherein the system for transformation of milk flow includes an aerodynamic mechanism for removing gases from the milk flow.

The device can be designed for use in stationary conditions and designed for express analysis.

5. Dynamic indicator of the current value of the number of somatic cells in cow's milk and a device for its selective identification in real time

A digital indicator of the dynamic state of cow's milk, which, according to the criteria of frequency, amplitude, resistance, inductance and a complex of dynamic characteristics of the milk flow, is an integral equivalent of the current value of the content and concentration of somatic cells in cow's milk.

The device for its selective identification in real time is a compact device designed for operation in dairy farm conditions or in the field, powered by solar batteries.

The device has minimal energy consumption.

The device includes functionally interconnected systems for input, output, control and transformation of milk flow, wherein the system for transformation of milk flow includes an aerodynamic mechanism for removing gases from the milk flow.

The device can be designed for use in stationary conditions and designed for express analysis.

6. Dynamic complex indicator of the current value of fat concentration in cow's milk and a device for its selective identification in real time

A digital indicator of the dynamic state of cow's milk, which, according to the criteria of frequency, amplitude, resistance, inductance and a set of dynamic characteristics of the milk flow, is an integral equivalent of the current value of the content and concentration of fat or fatty acids in cow's milk

The device for its selective identification in real time is a compact device designed for operation in dairy farm conditions or in the field, powered by solar batteries.

The device has minimal energy consumption.

The device includes functionally interconnected systems for input, output, control and transformation of milk flow, wherein the system for transformation of milk flow includes an aerodynamic mechanism for removing gases from the milk flow.

The device can be designed for use in stationary conditions and designed for express analysis.

7. Dynamic complex indicator of the current value of lactose content in cow's milk and a device for its selective identification in real time

A digital indicator of the dynamic state of cow's milk, which, according to the criteria of frequency, amplitude, resistance, inductance and a complex of dynamic characteristics of the milk flow, is an integral equivalent of the current value of the lactose content in cow's milk.

The device for its selective identification in real time is a compact device designed for operation in dairy farm conditions or in the field, powered by solar batteries.

The device has minimal energy consumption.

The device includes functionally interconnected systems for input, output, control and transformation of milk flow, wherein the system for transformation of milk flow includes an aerodynamic mechanism for removing gases from the milk flow.

The device can be designed for use in stationary conditions and designed for express analysis.

8. A comprehensive integral indicator of mastitis in a cow and a device for its identification in real time

A digital indicator that, based on the criteria of frequency, amplitude, resistance and inductance, is an integral equivalent or indicator of the occurrence of mastitis in a cow

The device for its real-time identification is a compact device designed for operation in dairy farm conditions or in the field, powered by solar batteries.

The device has minimal energy consumption.

The device includes functionally interconnected systems for input, output, control and transformation of milk flow, wherein the system for transformation of milk flow includes an aerodynamic mechanism for removing gases from the milk flow.

The device can be designed for use in stationary conditions and designed for express analysis.

9. Device for selective identification in real time of cow's milk quality during its transportation to the collection tank after milking

A compact unit designed for use on a dairy farm or in the field, powered by solar panels.

The device has minimal energy consumption.

The device includes functionally interconnected systems for input, output, control and transformation of milk flow, wherein the system for transformation of milk flow includes an aerodynamic mechanism for removing gases from the milk flow.

10. Device for contactless monitoring of cow's milk condition parameters

The device includes systems for introducing milk for control, removing the milk flow from the control zone, a sensory electronic integrated control module with an interface

The device may include a signal identification system and a device for accelerated comparison of identified signals with a standard.

11. Device for simultaneous monitoring of several parameters of cow's milk condition during transportation

The device has two versions

The first version is intended for installation on tanks to control the quality of milk during transportation and when transferring milk for processing into dairy products.

The second version is designed for installation on flexible or rigid pipelines through which milk is directed to storage tanks; this version can additionally have real-time temperature measurement functions.

12. Device for express analysis of cow's milk quality

The device is a mobile compact device with an internal cavity into which milk (or any other liquid) is introduced for analysis.

Around the cavity there is a sensor, selectively tuned to a specific parameter of either milk or any other liquid.

The device does not require setup or calibration and has several levels of protection.

13. Device for selective express analysis of cow's milk quality parameters

The device is a mobile compact device with an internal cavity into which milk (or any other liquid) is introduced for analysis.

Around the cavity there is a sensor, selectively tuned to a specific parameter of either milk or any other liquid.

The device does not require setup or calibration and has several levels of protection.

14. Contactless sensors for milk level in containers

The device controls the level of milk (or any other liquid) in a special section of the pipeline connected to the tank in which the liquid level is controlled.

The device has several design options.

It can be located in a container with liquid, it can be located outside the container, it can have different sensor designs.

15. Device for complex control of milk level in containers with simultaneous assessment of integral milk quality indicator at this level

The device controls the level of milk (or any other liquid) in a special section of the pipeline connected to the tank in which the liquid level is controlled.

The specified section of the pipeline is both a resonant sensor, which is configured to monitor and evaluate the integral quality indicator of milk (and any other liquid), and a level sensor.

The device can also simultaneously monitor any physical characteristics of milk or liquid, such as conductivity, density, acidity level.

16. Device for complex control of milk level in containers with simultaneous assessment of the number of somatic cells in milk at this level

The device controls the level of milk (or any other liquid) in a special section of the pipeline connected to the tank in which the liquid level is controlled.

The specified section of the pipeline is both a resonant sensor, which is configured to monitor the number of somatic cells, and a level sensor.

The device can also simultaneously monitor any physical characteristics of milk or liquid, such as conductivity, density, acidity level.

17. Device for complex control of milk level in containers with simultaneous assessment of fat content in milk at this level

The device controls the level of milk (or any other liquid) in a special section of the pipeline connected to the tank in which the liquid level is controlled.

The specified section of the pipeline is both a resonant sensor, which is configured to monitor the concentration of fat, and a level sensor.

18. Device for complex control of milk level in containers with simultaneous assessment of lactose content in milk at this level

The device controls the level of milk (or any other liquid) in a special section of the pipeline connected to the tank in which the liquid level is controlled.

The specified section of the pipeline is both a resonant sensor, which is configured to monitor the concentration of lactose, and a level sensor.

19. Device for complex monitoring of milk level in containers with

simultaneous assessment of blood traces in milk at this level

The device controls the level of milk (or any other liquid) in a special section of the pipeline connected to the tank in which the liquid level is controlled.

The specified section of the pipeline is both a resonant sensor, which is configured to monitor the concentration of blood, and a level sensor.

20. Device for complex control of milk level in containers with simultaneous sequential assessment of the concentration of basic components in this milk at this level

The device controls the level of milk (or any other liquid) in a special section of the pipeline connected to the tank in which the liquid level is controlled.

The specified section of the pipeline is both a resonant sensor, which is configured to control parameters, and a level sensor.

21. Device for complex control of milk level in containers with simultaneous assessment of concentration of several basic components in this milk at this level

The device controls the level of milk (or any other liquid) in a special section of the pipeline connected to the tank in which the liquid level is controlled.

The specified section of the pipeline is simultaneously a resonant sensor that is configured to control the parameters and concentrations of components in milk or any other liquid and has several sensors, each configured to control one parameter, and each sensor is also a level sensor.

22. Device for changing the level of turbulence of milk flow

The device is designed to convert and dynamically transform the turbulent flow of milk with the formation of a local zone of laminar flow in it, in which milk is monitored using a resonant sensor.

In addition, when transforming the flow, the device releases air from the milk flow and stabilizes its hydrodynamic characteristics.

23. Device for preparing milk flow for real-time monitoring of condition parameters

The device is designed to convert and dynamically transform the milk flow with the formation of a local laminar flow zone, in which milk is monitored using a resonant sensor.

24. Device for monitoring the level of gas content in milk in real time

The device is a resonant sensor that records changes in a set of parameters in milk depending on the concentration of air or any other gas in it.

The device can simultaneously control the degree of filling of the pipeline in which the milk flow moves and the level of turbulence of the milk flow in the pipeline.

25. Milk aeration process control system with real-time air content monitoring in milk

Milk aeration process control system with air content level control in milk; the system has feedback with a resonant sensor and changes the parameters of compressed air depending on the air concentration in milk

The system includes a resonant sensor, an interface and a converter of signals from the sensor into control signals to the compressed air source, with the help of which the pressure and flow rate of compressed air are changed.

The system also includes an aerodynamic function for introducing air into the milk.

List of references, patent and license information

United States Patent No. 10,732,237, Slobozhanyuk et al., August 4, 2020. *Magnetic Resonance Imaging Machine.*

United States Patent No. 10,564,308, Godoy et al., February 18, 2020. *Electron Paramagnetic Resonance (EPR) Techniques and Apparatus for*

Performing EPR Spectroscopy on a Flowing Fluid.

United States Patent No. 9,952,297, Wang, April 24, 2018.
Parallel Plate Transmission Line for Broadband Nuclear Magnetic Resonance Imaging.

United States Patent No. 9,316,709, Hetherington et al., April 19, 2016.
Transceiver Apparatus, System and Methodology for Superior In-Vivo Imaging of Human Anatomy.

United States Patent No. 9,018,954, Yonamoto et al., April 28, 2015.
Sample Holder for Electricity-Detection Electron Spin Resonance Device.

United States Patent No. 8,884,608, Neu et al., November 11, 2014.
AFM–Coupled Microscale Radiofrequency Probe for Magnetic Resonance Imaging and Spectroscopy.

United States Patent No. 8,780,344, Tang et al., July 15, 2014.
Waveguides Configured with Arrays of Features for Performing Raman Spectroscopy.

submitted 12.04.2026;
accepted for publication 26.04.2026;
published 30.04.2026

Contact: 3338830@gmail.com

The Austrian Journal of Technical and Natural Sciences, 2026 No 3–4
ISSN 2310-5607

PREMIER Publishing
ppublishing.org

DOI:10.29013/AJT-26-3.4-224-233

INDEPENDENT SCIENTIFIC ANALYSIS. (Of the article "Electrochemical Treatment of Industrial Wastewater: A Comprehensive Analytical Review and Conceptual Evaluation")

Ihor Bereshko [1]

[1] Department of Ecology and Technogenic Safety, National Aerospace University "Kharkiv Aviation Institute"

Cite: *Bereshko I. (2026). Independent Scientific Analysis. (of the article "Electrochemical Treatment of Industrial Wastewater: A Comprehensive Analytical Review and Conceptual Evaluation"). Austrian Journal of Technical and Natural Sciences 2026, No 3–4.* https://doi.org/10.29013/AJT-26-3.4-224-233

Abstract

The article presents a novel electrochemical technology for wastewater treatment based on volumetric permeable electrodes operating in a flow-through regime. The proposed system enables controlled modification of water properties, including pH adjustment and microbial inactivation.

The study introduces a modular reactor design based on chemically stable materials and highlights the integration of non-contact monitoring systems using electromagnetic resonance spectroscopy. The approach is evaluated in the context of modern electrochemical water treatment methods, including advanced oxidation processes and hybrid systems (Brillas & Garcia-Segura, 2025; Ganiyu et al., 2020).

The technology is presented as a cost-effective and scalable alternative to existing electrochemical treatment methods.

Keywords: *electrochemical wastewater treatment; volumetric electrochemical reactors; permeable electrodes; flow-through systems; three-dimensional (3D) electrodes; advanced oxidation processes (EAOPs); electro-Fenton; reactive electrochemical membranes (REM); non-contact sensing; electromagnetic resonance spectroscopy; real-time monitoring; sustainable water treatment; decentralized water systems; modular reactor design*

Statement of Independence

I confirm that I am an independent expert in the relevant field and that I do not have any personal, financial, or professional relationships with the author of the reviewed work. This review is based solely on my professional knowledge, experience, and evaluation of the submitted article.

Structure of the Review

1. Abstract
2. Keywords
3. General information about the article
4. Relevance and Research Context
5. System Architecture and Operational Principles

3. General Information about the Article

The article by Vladyslav Meleshko, entitled "Electrochemical Treatment of Industrial Wastewater", is devoted to the development and analysis of an original electrochemical approach for water and wastewater treatment.

The work lies at the intersection of electrochemistry, environmental engineering, and water treatment technologies, addressing current challenges in sustainable water purification. The proposed system is based on the flow-through treatment of water passing through volumetric permeable electrodes made of chemically resistant non-metallic materials, enabling controlled modification of physicochemical parameters such as pH and microbiological activity.

The study demonstrates a strong applied orientation and proposes a versatile technological solution suitable for multiple sectors, including agriculture, medicine, and industrial processing.

4. Relevance and Research Context

The global demand for clean water continues to increase due to industrialization, population growth, and the emergence of persistent contaminants such as pharmaceuticals and micro-pollutants. Conventional water treatment technologies often fail to completely remove such contaminants or generate harmful by-products (Oturan & Aaron, 2014).

Electrochemical advanced oxidation processes (EAOPs) have emerged as promising solutions due to their ability to generate highly reactive species such as hydroxyl radicals (•OH), which enable effective degradation of organic pollutants (Ganiyu et al., 2020). However, existing systems, including boron-doped diamond (BDD) electrodes and reactive electrochemical membranes (REM), are often limited by high cost, operational complexity, and scalability challenges (Panizza & Cerisola, 2009; Du et al., 2025).

In this context, the article addresses a highly relevant research problem by proposing a simplified electrochemical system that maintains functional efficiency while reducing structural and economic complexity.

5. System Architecture and Operational Principles

The proposed technology is based on a flow-through electrochemical reactor in which water passes through the internal volume of permeable electrodes optionally separated or structurally organized without functional membrane dependence.

Figure 1. *Conceptual diagram of the volumetric flow-through electrochemical reactor*

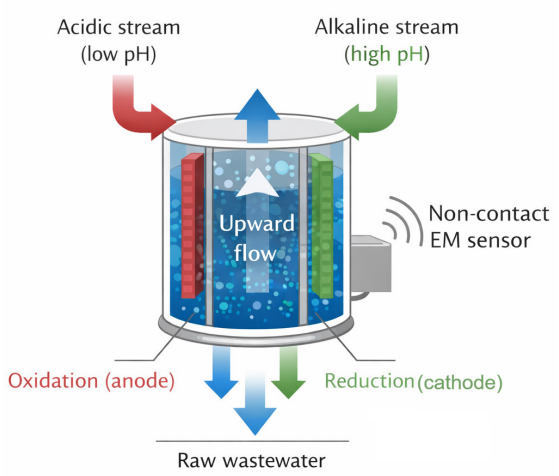

The system is characterized by:

- vertical electrode configuration;
- upward flow of liquid;
- controllable residence time;
- use of carbon-based materials;

- symmetric and asymmetric electrode designs for pH regulation.

The system allows for the generation of different types of treated water, including acidic, alkaline, and disinfected water, making it suitable for a wide range of applications.

The conceptual design and operating principles of the proposed electrochemical reactor are presented in Figure 1.

6. Scientific Novelty and Conceptual Contribution

The scientific novelty of the proposed approach lies in several key aspects.

- First, the use of volumetric permeable electrodes establishes a three-dimensional electrochemical reaction environment, directly aligning with emerging trends in reactor design aimed at enhancing surface area and mass transfer efficiency (Rodrigo et al., 2014);
- Second, the implementation of a flow-through regime enables continuous treatment with improved hydrodynamic control, resulting in enhanced mass transfer and overall process efficiency;
- Third, the system provides a simplified alternative to membrane-based technologies, such as reactive electrochemical membranes (REM), by eliminating membrane-associated limitations while preserving the advantages of flow-through operation (Du et al., 2025);
- Fourth, the integration of non-contact sensing based on electromagnetic resonance introduces real-time monitoring capabilities without direct interaction with the treated fluid, addressing a critical limitation of conventional electrochemical systems.

Finally, the development of a flexible and modular system architecture enables scalability and adaptability across a wide range of operational conditions and application domains.

7. Practical Significance and Technology Readiness

The proposed technology demonstrates clear practical relevance by combining low-cost materials, architectural simplicity, and operational flexibility. In contrast to many advanced electrochemical systems that depend on expensive electrodes or complex configurations, this approach relies on carbon-based and polymer components, enabling economically viable deployment across both decentralized and industrial scales.

A defining advantage is the reduction of operational complexity. The use of permeable electrodes and gravity-driven flow eliminates the need for sophisticated control systems and highly specialized personnel, thereby expanding applicability to low-resource and distributed treatment scenarios.

Scalability is inherently supported by a modular reactor design, allowing capacity adjustment without fundamental system redesign. The technology can be deployed as compact local units (50–250 L/h) or integrated into larger treatment infrastructures with minimal capital modification. Compatibility with existing systems further lowers barriers to adoption.

Beyond treatment efficiency, the system introduces functional versatility by generating chemically distinct output streams (acidic, alkaline, and disinfected water), enabling a single platform to perform multiple process roles that are typically separated across different technologies.

The integration of non-contact sensing provides real-time process visibility without exposure to aggressive media, addressing a key limitation of conventional systems lacking reliable monitoring. This capability supports process stability and enables future automation and data-driven control.

Taken together, these features position the technology as a cost-efficient, scalable, and multifunctional platform with strong potential across sectors including water treatment, agriculture, food processing, and high-purity industrial applications. Its capacity to integrate into existing infrastructure while expanding functional performance underscores its relevance for next-generation water treatment systems.

8. Experimental Basis and Theoretical Limitations

The article by Meleshko (2026) provides a conceptual and structural description of the

proposed reactor system, outlining its design principles and key operational parameters. However, it does not yet include a comprehensive quantitative characterization of the underlying electrochemical processes.

In contrast, contemporary research in electrochemical water treatment places strong emphasis on the mechanistic and kinetic understanding of system performance. This includes detailed analysis of:

- reactive species generation, particularly hydroxyl radical formation pathways;
- electrochemical reaction kinetics and rate-limiting steps;
- energy efficiency metrics (e.g., kWh/m³);
- and degradation pathways of target contaminants (Brillas & Garcia-Segura, 2025; Ganiyu et al., 2020).

The absence of such quantitative data in the study by Meleshko (2026) limits the ability to rigorously evaluate process efficiency, benchmark performance against existing technologies, and predict scaling behavior.

Nevertheless, the framework proposed by Meleshko (2026) establishes a solid foundation for further investigation. Future work should focus on integrating electrochemical diagnostics, kinetic modeling, and energy analysis, enabling a transition from qualitative description to quantitatively validated system performance.

9. Positioning within Modern Electrochemical Treatment Technologies

Electrochemical wastewater treatment has rapidly evolved toward highly efficient oxidation systems, including EAOPs, electro-Fenton processes, reactive electrochemical membranes (REM), and photoelectrochemical (PEC) platforms. These approaches achieve high removal efficiencies; however, they remain constrained by critical limitations, including electrode and membrane fouling, narrow operational pH windows, high material costs, and limited integration of real-time monitoring and adaptive control (Brillas & Garcia-Segura, 2025; Oturan & Aaron, 2014; Ganiyu et al., 2020).

The technology proposed in this article departs from conventional surface-based electrochemical paradigms by employing a volumetric, flow-through electrode architecture, enabling distributed reaction zones and tunable residence time. Coupled with non-contact sensing for in situ monitoring, this approach addresses key bottlenecks in process stability and scalability.

Rather than competing with established systems, the proposed configuration is best understood as a platform for integration, capable of interfacing with and enhancing existing electrochemical and photoelectrochemical processes.

9.1. Reactive Electrochemical Membranes (REM)

To establish a baseline for comparison, the analysis begins with reactive electrochemical membrane (REM) systems, which represent one of the most advanced implementations of flow-through electrochemical treatment.

Reactive electrochemical membranes (REM) represent one of the most rapidly developing directions in electrochemical water treatment, combining filtration and electrochemical oxidation within a single functional unit (Du et al., 2025; Zhu et al., 2023). These systems are characterized by flow-through operation, localized reaction zones, and high current densities, enabling efficient removal of micropollutants.

The proposed technology described in this work exhibits strong conceptual similarities with REM systems, particularly in terms of flow-through architecture and distributed reaction zones. However, a key distinction lies in the absence of functionally loaded membranes. Instead, the system employs permeable, chemically stable non-metallic electrodes, allowing the liquid to pass through the electrode volume.

This design eliminates one of the primary limitations of REM systems – membrane fouling, which significantly reduces operational efficiency and increases maintenance requirements (Du et al., 2025).

Potential synergy:

Hybridization of REM selectivity with the volumetric electrode concept proposed here could enable the development of highly efficient and fouling-resistant electrochemical reactors, particularly suitable for selective removal of persistent organic pollutants.

A conceptual comparison between reactive electrochemical membrane systems and the proposed volumetric reactor architecture is presented in Figure 2.

Figure 2. *Comparison of reactive electrochemical membrane systems and a volumetric flow-through electrochemical reactor*

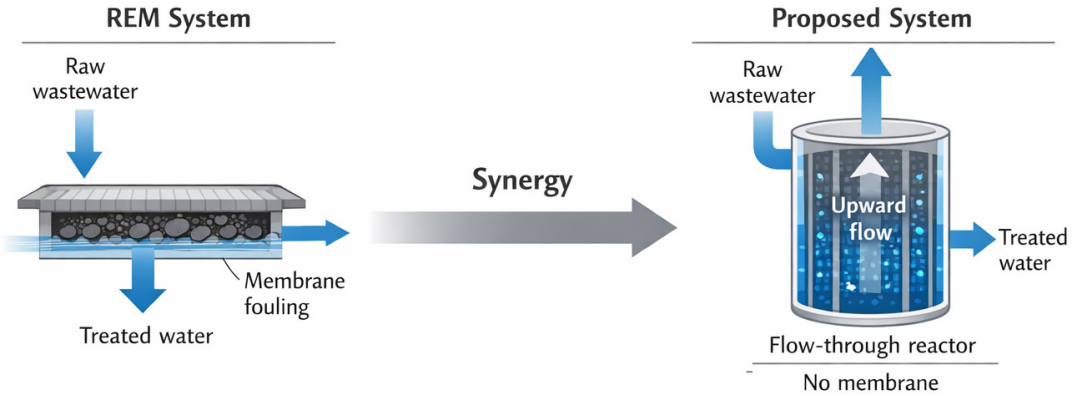

9.2. Electro-Fenton Processes

While REM systems emphasize reactor architecture and mass transfer, electro-Fenton processes provide a complementary perspective focused on the generation of highly reactive oxidative species.

Electro-Fenton processes are widely recognized as one of the most effective advanced oxidation methods due to their ability to generate hydroxyl radicals (•OH) in situ, enabling deep mineralization of organic contaminants (Oturan & Aaron, 2014; Heidari et al., 2023; Li et al., 2025).

The proposed system utilizes carbon-based permeable electrodes, which are highly suitable for electro-Fenton applications due to their ability to catalyze hydrogen peroxide generation at the cathode. Moreover, the volumetric configuration enhances:

- interfacial area;
- mass transfer;
- and residence time control.

A significant advantage of the proposed technology is its ability to dynamically regulate pH conditions through electrochemical separation, as described in Section 2. This capability addresses a major limitation of conventional electro-Fenton systems, which typically require strictly acidic conditions.

Potential synergy:

Integration of electro-Fenton mechanisms into the proposed reactor design could lead to the development of high-efficiency hybrid oxidation systems, operating under broader pH conditions and reduced energy demand.

Figure 3. *Conceptual integration of electro-Fenton processes with a volumetric electrochemical reactor*

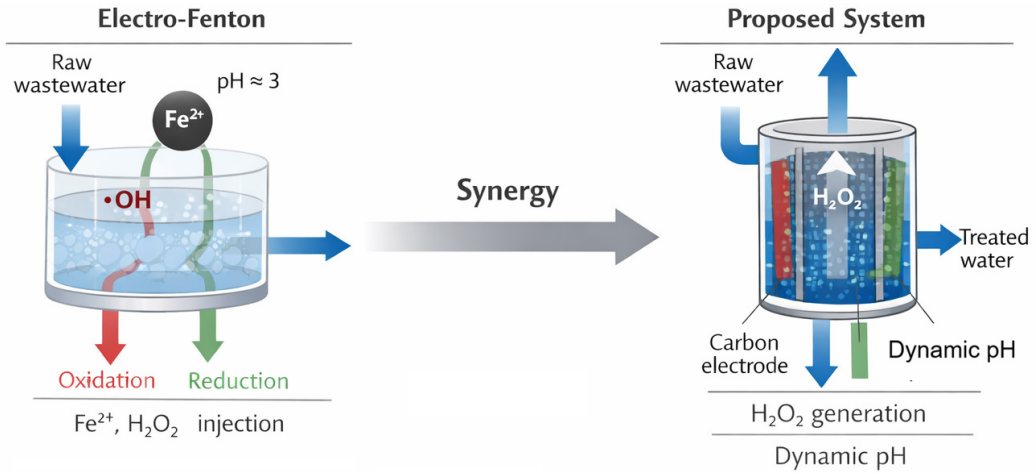

The integration of electro-Fenton mechanisms with the proposed volumetric electrochemical system is illustrated in Figure 3.

9.3. 3D Electrochemical Reactors

Beyond reaction pathways, reactor geometry plays a defining role, making it necessary to consider three-dimensional electrochemical reactors as a structural analogue to the proposed system.

Three-dimensional electrochemical reactors are known for their enhanced performance due to increased active surface area and improved mass transfer (Rodrigo et al., 2014; Ganiyu et al., 2020).

The technology presented in this study inherently corresponds to the concept of a 3D electrochemical reactor, as it involves fluid flow through a permeable electrode volume, rather than along electrode surfaces.

Distinctive features of the proposed approach include:

- gravity-driven upward flow, ensuring stable hydrodynamics;
- controllable residence time, directly influencing reaction kinetics;
- modular design, enabling scalability and flexible implementation.

Unlike conventional 3D systems, the proposed configuration also enables simultaneous generation of chemically distinct streams (acidic and alkaline fractions), which expands its functional applicability.

Potential synergy:

Further development could involve the incorporation of catalytic or porous media within the electrode structure to enhance reaction selectivity and efficiency.

A structural comparison between conventional 3D electrochemical reactors and the proposed system is shown in Figure 4.

Figure 4. *Comparison of conventional 3D electrochemical reactors and a volumetric flow-through system*

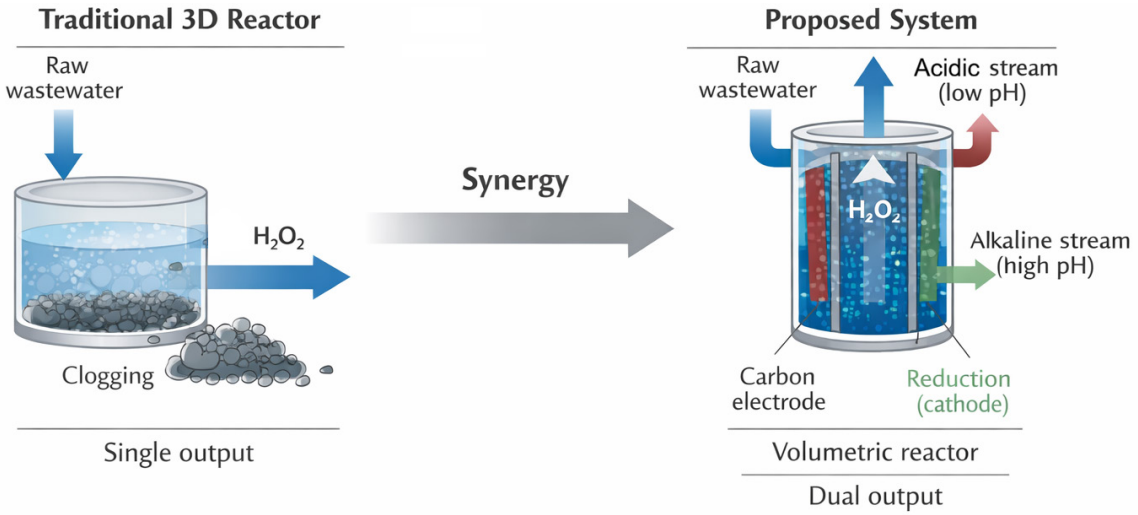

9.4. Photoelectrochemical Systems (PEC)

Although electrochemical systems dominate the field, photoelectrochemical approaches introduce additional functionality through light-driven processes and highlight challenges in system control and scalability.

Photoelectrochemical (PEC) systems are increasingly considered a promising approach for sustainable wastewater treatment, combining light-driven and electrochemical processes (Dong et al., 2025; Amaya Santos et al., 2025). However, their large-scale implementation remains limited by process instability and the lack of real-time monitoring.

A unique contribution of the proposed system is the integration of a non-contact resonant sensing technology, based on electromagnetic spectroscopy principles. This sensor:

- operates without direct contact with the liquid;
- provides high sensitivity (down to 10^{-6} mg/L);
- enables continuous, real-time monitoring of water composition.

Potential synergy:

Integration of this sensing approach into PEC systems could enable adaptive process control, significantly improving system stability and scalability – two of the major challenges identified in recent PEC research.

The potential enhancement of photoelectrochemical systems through integration of non-contact sensing is illustrated in Figure 5.

Figure 5. *Integration of non-contact sensing into photoelectrochemical systems*

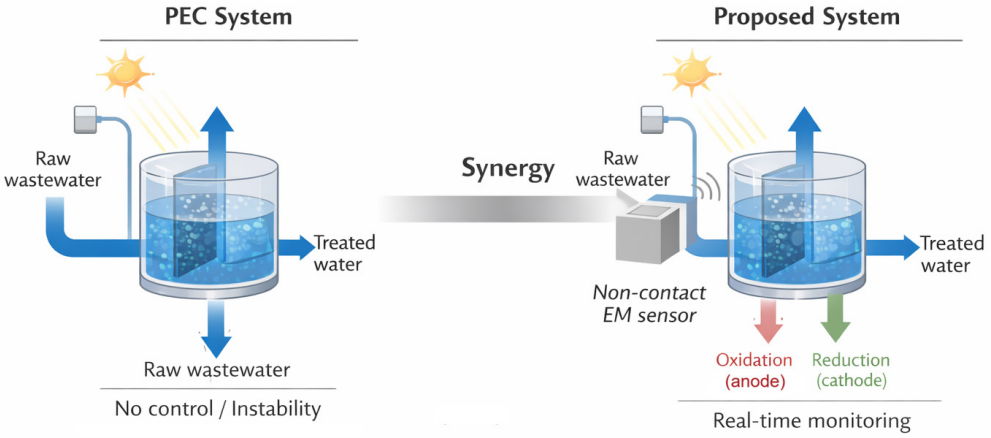

9.5. BDD-Based Systems (Boron-Doped Diamond Electrodes)

At the material level, these considerations naturally lead to a comparison with high-performance electrode systems, particularly those based on boron-doped diamond (BDD).

Boron-doped diamond (BDD) electrodes are considered among the most powerful materials for electrochemical oxidation due to their ability to generate highly reactive species and their exceptional stability (Panizza & Cerisola, 2009; Martínez-Huitle & Brillas, 2009).

Despite their advantages, BDD systems are limited by:

- high production costs;
- complex fabrication processes;
- limited scalability.

In contrast, the proposed system utilizes carbon-based composite electrodes, offering:

- significantly lower cost;
- chemical stability;
- ease of manufacturing and scaling.

While BDD systems maximize oxidation power at the electrode surface, the proposed technology emphasizes volumetric processing and hydrodynamic optimization, representing a fundamentally different approach.

Potential synergy:

Hybrid systems combining localized BDD electrodes with volumetric carbon-based reactors could provide an optimal balance between performance and cost.

Figure 6. *Comparison of boron-doped diamond electrode systems and a volumetric electrochemical reactor*

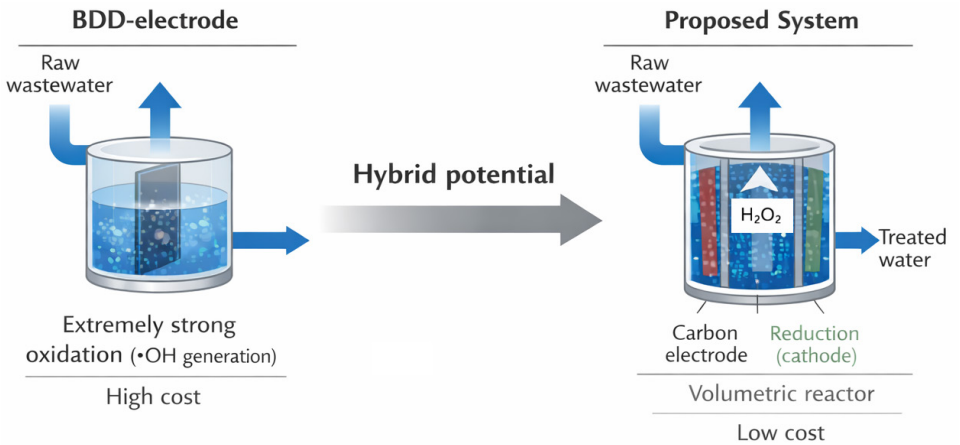

A comparison between BDD-based systems and the proposed reactor concept is presented in Figure 6.

Overall Positioning within EAOP Framework

Modern electrochemical advanced oxidation processes (EAOPs) are evolving toward systems that combine high oxidation efficiency, improved mass transfer, reduced energy consumption, and integrated monitoring capabilities (Brillas & Garcia-Segura, 2025; Ganiyu et al., 2020).

Within this framework, the proposed technology can be positioned as a multifunctional platform, integrating:

- volumetric electrochemical treatment (3D reactor concept);
- flexible control of physicochemical parameters (pH, residence time);
- cost-effective electrode materials;
- embedded real-time monitoring.

Rather than competing directly with existing technologies, the system demonstrates strong potential as a hybridization platform, capable of integrating:

- electro-Fenton processes;
- photoelectrochemical systems;
- membrane-based electrochemical reactors;
- anodic oxidation technologies.

Conclusion of Comparative Analysis

The proposed system should not be viewed as a direct alternative to existing electrochemical treatment technologies, but rather as an integrative architecture capable of combining multiple mechanisms within a single framework.

Its key advantage lies in the synergistic combination of:

- electrochemical reactivity;
- volumetric hydrodynamics;
- and advanced sensing capabilities.

This positions the technology as a promising candidate for next-generation water treatment systems, particularly in applications requiring adaptability, scalability, and cost-efficiency.

10. Limitations and Research Gaps

Despite the conceptual strength of the approach proposed by Meleshko (2026), several limitations remain that constrain its current scientific and practical validation.

A primary limitation is the lack of detailed mechanistic analysis. Modern electrochemical treatment research emphasizes the identification of dominant oxidation pathways, including hydroxyl radical (•OH) generation and alternative reactive species formation (Brillas & Garcia-Segura, 2025; Ganiyu et al., 2020). In the absence of such analysis, the fundamental reaction mechanisms governing the proposed system remain insufficiently characterized.

Closely related is the absence of quantitative kinetic data, including reaction rates, current efficiencies, and limiting steps. Without these parameters, it is not possible to establish a rigorous comparison with established electrochemical advanced oxidation processes (EAOPs) or to predict system behavior under varying operational conditions.

Another important gap concerns the formation and fate of by-products. Contemporary studies highlight that incomplete oxidation may lead to the generation of intermediate compounds, some of which can be more toxic than the parent pollutants (Oturan & Aaron, 2014). The lack of by-product analysis limits the assessment of the system's environmental safety and treatment completeness.

The limited discussion of energy consumption further constrains practical evaluation. Energy efficiency, typically expressed in kWh/m³, is a critical parameter in benchmarking electrochemical technologies (Brillas & Garcia-Segura, 2025). Without such data, the economic feasibility and scalability of the system cannot be fully assessed.

Taken together, these limitations do not diminish the conceptual contribution of the work but rather define a clear roadmap for future research, particularly in the direction of quantitative validation, mechanistic elucidation, and pilot-scale implementation.

11. Environmental Significance of the Technology

The technology proposed by Meleshko (2026) demonstrates notable potential in the context of sustainable and environmentally responsible water treatment.

A key advantage is the reduced reliance on chemical reagents, as the system is based on

electrochemical processes that generate reactive species in situ. This aligns with current trends in green water treatment technologies, where minimizing secondary chemical inputs is a major objective (Ganiyu et al., 2020).

The system also shows strong potential for decentralized and distributed applications, enabled by its modular design, operational simplicity, and relatively low infrastructure requirements. Such characteristics are particularly important for rural, remote, or resource-limited regions, where centralized treatment systems are often impractical.

From an environmental perspective, the use of carbon-based and polymer materials offers advantages in terms of reduced material toxicity and improved lifecycle sustainability compared to more resource-intensive alternatives such as boron-doped diamond electrodes. Additionally, the absence of membrane components eliminates issues related to membrane disposal and fouling-related waste streams.

The capability to generate functionally distinct water streams (acidic, alkaline, disinfected) further enhances resource efficiency by enabling targeted reuse of treated water across different applications, including sanitation, agriculture, and industrial processes.

Moreover, the integration of non-contact sensing technology supports real-time monitoring and process optimization, which is critical for minimizing energy consumption and preventing over-treatment. Such features are increasingly recognized as essential for the development of intelligent and adaptive water treatment systems (Dong et al., 2025).

In the broader context, technologies of this type contribute to achieving global sustainability objectives, including water reuse, pollution reduction, and resource efficiency, which are central to international environmental frameworks and water management strategies.

The technology is directly aligned with global sustainability frameworks, particularly UN Sustainable Development Goal 6 (Clean Water and Sanitation).

12. Conclusion and Future Outlook

The study presents an innovative and practically oriented approach to electrochemical water treatment. Its simplicity, flexibility, and integration with advanced monitoring technologies position it as a promising candidate for next-generation water treatment systems.

The proposed system should be viewed not as a single-process solution, but as a platform technology capable of integrating multiple electrochemical and hybrid treatment mechanisms. This positioning significantly expands its applicability and aligns it with current trends toward modular, adaptive, and decentralized water treatment systems.

Overall, the technology represents a transition toward more adaptable, scalable, and resource-efficient electrochemical treatment systems, with strong potential for both industrial and decentralized applications.The proposed technology represents a shift from surface-limited electrochemical systems toward volumetric, process-integrated architectures, offering a new direction for scalable and adaptive water treatment.

Its combination of low-cost materials, modular design, and integrated sensing positions it as a viable candidate for next-generation decentralized water treatment systems.

Based on the above analysis, the reviewed article represents a scientifically grounded and practically significant contribution to the field of electrochemical water treatment and demonstrates strong potential for further development and application.

References

Meleshko, V. (2026). Electrochemical Treatment of Industrial Wastewater. Published online at IntellectualArchive.com, March 4, 2026.

Brillas, E., & Garcia-Segura, S. (2025). Electrochemical advanced oxidation processes for real wastewater remediation: Systems, performance, and generated oxidants. ACS Electrochemistry, – 2(1). – 45–68. URL: URL: https://doi.org/10.1021/acselectrochem.5c00311.

Oturan, M. A., & Aaron, J.-J. (2014). Advanced oxidation processes in water/wastewater treatment: Principles and applications. A review. Critical Reviews in Environmental Sci-

ence and Technology, – 44(23). – P. 2577–2641. URL: https://doi.org/10.1080/10643389.2013.829765.
Heidari, Z., Pelalak, R., & Zhou, M. (2023). Recent progress in electro-Fenton process for wastewater treatment at near-neutral pH: A review. Chemical Engineering Journal, – 468. – 143600 p. URL: https://doi.org/10.1016/j.cej.2023.143600.
Li, X., Zhang, Y., Wang, H., & Chen, G. (2025). Advances in heterogeneous electro-Fenton processes for efficient water treatment. Journal of Hazardous Materials, – 465. – 133210 p. URL: https://doi.org/10.1016/j.jhazmat.2024.133210.
Du, M., Li, W., Zhang, D., & Chen, Z. (2025). Recent advances in electrochemical membrane reactors based on cathodic carbon membranes for water treatment. Journal of Membrane Science, – 712. – 121345 p. URL: https://doi.org/10.1016/j.memsci.2024.121345.
Zhu, Y., Wang, L., & Chen, Z. (2023). Electrochemical anodic oxidation-based membrane systems for micropollutant removal. ACS ES&T Engineering, – 3(4). – P. 1123–1137. URL: https://doi.org/10.1021/acsestengg.3c00179
Dong, T., Li, J., & Wang, S. (2025). Recent advances in oxidant-involved photoelectrochemical systems for sustainable wastewater treatment. Nature Reviews Clean Technology, – 1. – P. 45–67. URL: https://doi.org/10.1038/s44296-025-00084-6.
Amaya Santos, G., Martínez-Huitle, C. A., & Rodrigo, M. A. (2025). Scaling-up photoelectrochemical oxidation processes: From laboratory to industrial applications. Water Research, – 248. – 120715 p. URL: https://doi.org/10.1016/j.watres.2025.120715.
Martínez-Huitle, C. A., & Brillas, E. (2009). Decontamination of wastewaters containing synthetic organic dyes by electrochemical methods: A general review. Applied Catalysis B: Environmental, – 87(3–4). – P. 105–145. URL: https://doi.org/10.1016/j.apcatb.2008.09.017.
Panizza, M., & Cerisola, G. (2009). Direct and mediated anodic oxidation of organic pollutants. Chemical Reviews, – 109(12). – P. 6541–6569. URL: https://doi.org/10.1021/cr9001319.
Rodrigo, M. A., Oturan, N., & Oturan, M. A. (2014). Electrochemically assisted remediation of pesticides in soils and water: A review. Chemical Reviews, – 114(17). – P. 8720–8745. URL: https://doi.org/10.1021/cr5002059.
Ganiyu, S. O., Martínez-Huitle, C. A., & Oturan, M. A. (2020). Electrochemical advanced oxidation processes for wastewater treatment: Advances in formation and detection of reactive species and mechanisms. Current Opinion in Electrochemistry, – 22. – P. 57–64. URL: https://doi.org/10.1016/j.coelec.2020.04.002.

submitted 04.04.2026;
accepted for publication 19.04.2026;
published 30.04.2026

Contact: klevka@gmail.com

The Austrian Journal of Technical and Natural Sciences, 2026 No 3–4
ISSN 2310-5607

PREMIER Publishing
ppublishing.org

DOI:10.29013/AJT-26-3.4-234-238

MODULAR INTEGRATION SOLUTIONS FOR ELECTRONIC SYSTEMS. (Electronic system modules, including laser diode components, featuring an intensive cooling system utilizing diamond – copper composite materials)

Prykhodko Ostap Volodymyrovych [1]

[1] Director of LLC "Ukrainian Holding of Construction Projects" Kyiv, Ukraine

Cite: *Prykhodko O.V. (2026). Modular Integration Solutions for Electronic Systems. (Electronic system modules, including laser diode components, featuring an intensive cooling system utilizing diamond - copper composite materials). Austrian Journal of Technical and Natural Sciences 2026, No 3–4.* https://doi.org/10.29013/AJT-26-3.4-234-238

Abstract

This article examines one of the key engineering challenges of modern electronics – the provision of reliable and efficient thermal management in the development of complex electronic devices, particularly those incorporating laser diodes and high-intensity lighting components. The critical importance of effective heat dissipation for maintaining operational stability, extending service life, and preserving the performance characteristics of thermally sensitive electronic and optoelectronic systems is emphasized. Particular attention is devoted to the analysis and substantiation of integrative technical solutions aimed at improving cooling efficiency while minimizing energy losses and eliminating the need for additional structural cooling elements or separate energy-consuming thermal regulation systems. The article investigates modern approaches to passive and integrative heat dissipation, including structural and material-based solutions that ensure effective thermal conductivity and heat removal directly through the functional architecture of the device. It is demonstrated that the implementation of advanced integrative cooling solutions significantly improves thermal regulation efficiency, reduces structural system complexity, minimizes parasitic energy consumption, and enhances the overall energy efficiency of high-performance electronic and lighting devices. The article concludes that the development and integration of innovative thermal management architectures constitute a strategically important direction in the advancement of next-generation electronic and optoelectronic systems, particularly for applications requiring high power density, compact design, and enhanced energy efficiency.

Keywords: *Integrative modules, Electronic systems, Laser diodes, Optical power, Diamond spheres, Ductile material, Composite material, Pseudo-porous structure, Optical cable, Laser radiation, Flat-emitter lamp*

Introduction:

In order to eliminate energy losses and increase output efficiency, particularly in various lighting systems, there is an active search for integrative technical solutions that enable performance improvement without the use of additional structural elements or additional energy consumption for cooling.

In parallel, research and development efforts are focused on identifying and refining technical solutions that, through a concise and simplified design, allow for an increase in the output optical power of lighting devices while maintaining relatively low power input and, consequently, low energy consumption.

The author of this publication considers the most effective approach to be comprehensive integrative solutions, as presented in the scientific and technological publications and books of Oleksandr Sylyaiev, a recognized innovator in this field.

What fundamentally distinguishes Oleksandr Sylyaiev's proposals and developments from those of other authors is the extensive platform for experimental computer modeling, made possible by his broad and in-depth expertise in system-based and combinatorial modeling methods applied across related innovative processes, including at the intersections of fundamental scientific disciplines.

In analyzing the innovative technologies presented in his publications, Oleksandr Sylyaiev advances a critically important concept for addressing the problem: the combinatorial structure of each solution – that is, the harmonious integration and mutual complementarity between conventional technologies and materials and innovative technologies and materials, primarily composite-based.

Moreover, among Oleksandr Sylyaiev's contributions, particular importance is attributed to the principle of integration and comprehensive adaptation of new materials and technological approaches within the framework of existing, proven technologies and materials, which are prepared for transformation and enhancement at a new, innovative level.

The following image presents an axial cross-section of such a device, providing a more detailed and convenient view for analysis.

Figure 1.

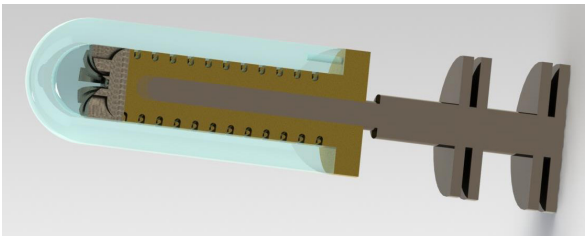

As can be seen from the design of the innovative lamp, the functions of several fundamental structural elements are integrated into a single system.

The lamp holder incorporates a vortex-type heat sink, the axis and discs of which are made of a diamond–copper composite, serving as a key component of the lamp's cooling system.

Each element of this system is multifunctional: in addition to heat transfer and heat accumulation, the structure of these components – formed from numerous composite micro-globules – also performs a critical function of dissipating thermal flows. This is achieved due to the pseudo-porous structure of the composite.

Let us consider the innovative structure of the diamond – copper composite (Appendix 1).

The original manufacturing process of the composite globules begins with the formation of diamond spheres from synthetic diamond, with a diameter of 5–7 microns (this size may vary depending on the geometry of the component and operating conditions).

Subsequently, these spheres are coated with copper using specialized equipment and an original innovative technology (Appendix 2).

The coating thickness is selected such that, during the molding of the lamp component, a sufficient amount of ductile material is present on the diamond spheres to ensure metal flow and complete filling of the interstitial spaces between the synthetic diamond spheres.

As a result, a pseudo-porous structure is formed, in which diamond spheres – characterized by exceptional thermal conductivity and complete electrical insulation – are uniformly distributed.

Such a structure enables instantaneous heat dissipation and uniform distribution across the cross-sectional area of the heat sink discs.

Optical fiber is placed within spiral grooves in the lamp housing, through which laser radiation from the laser module is transmitted. The optical fiber is coiled in a spiral and positioned within the grooves at a diameter that induces uniform emission along the entire cylindrical surface, which is significantly more efficient than emission from the fiber end.

In order to separate the laser radiation from the output light of the lamp, a phosphor layer is applied to the optical fiber, designed to produce a specific emission spectrum.

As a result, the final light output of the lamp is non-toxic, and due to the emission area being several orders of magnitude larger than that of the fiber end, a laser diode with a power of 1–2 W can achieve an equivalent output corresponding to a 60–75 W conventional lamp.

The presented models demonstrate that, based on the general principles of innovative design proposed by Oleksandr Sylyaiev, it is possible – within conventional forms and structures, such as ion-exchange filters – to achieve near-ideal results using natural and entirely safe materials, with unique performance characteristics:

– complete absence of chemical reagents in the process;
– utilization of natural ion-exchange properties;
– exceptionally high exchange capacity, including for the purification of liqui
– contaminated with radioactive substances.

Figure 2.

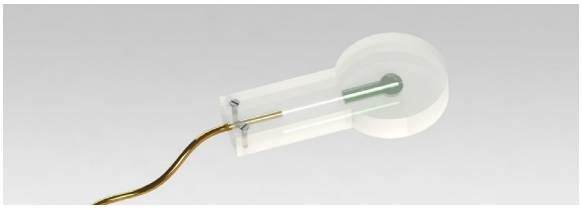

The following image shows a miniature lamp in which a phosphor mixture is applied to the end of an optical fiber according to a defined geometry in a three-dimensional coordinate system, enabling emission in the white spectral range.

The diameter of the optical fiber is only 120 microns, allowing for the creation of micro-miniature light sources suitable for use in highly compact optoelectronic systems.

Figure 3.

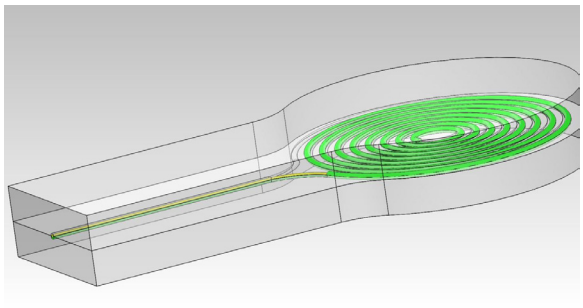

The following image shows a lamp with a flat emitter connected to a single optical fiber.

In addition to overall energy efficiency, such a system makes it possible to achieve the required level of illumination over a specified area with minimal cost and maximum design simplicity.

This configuration also allows the application of virtually any combination or mixture of phosphors onto the spiral (planar spiral) section at the end of the optical fiber, enabling the desired light emission parameters to be obtained.

Figure 4.

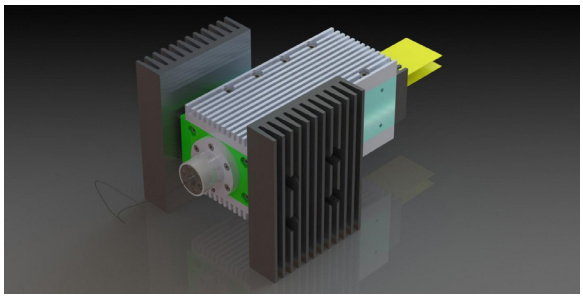

The following image shows a laser diode module designed based on the principles of active cooling utilizing a heat dissipation effect in components made of a pseudo-porous diamond–copper composite.

One of the key innovative integrative features of the presented design is the use of thermoelectric coolers in combination with heat-conducting and heat-dissipating structural elements of the module housing.

The thermoelectric coolers are positioned between the external heat sinks and the module housing. Heat-conducting elements of the structure transfer thermal flows from the printed circuit board to the housing walls, on which the thermoelectric coolers are mounted. In turn, the base surfaces of the heat sinks are pressed against the coolers, and additional components of the module requiring continuous cooling can be mounted on these heat sinks as needed.

Practical application has demonstrated that reliable cooling enables maximum stabilization of the output parameters of laser radiation. This, in turn, significantly expands the range of output configurations of the module and, when necessary, allows the laser radiation to be distributed among multiple optical fibers, each supplying a separate lighting device.

Figure 5.

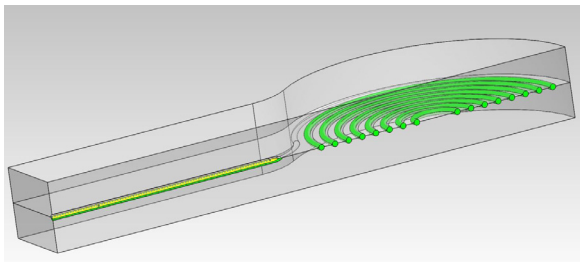

The image shows models of such devices.

Figure 6.

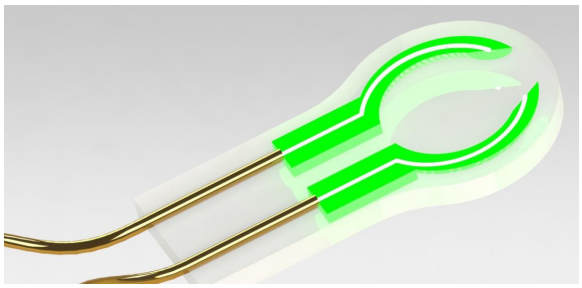

Figure 7.

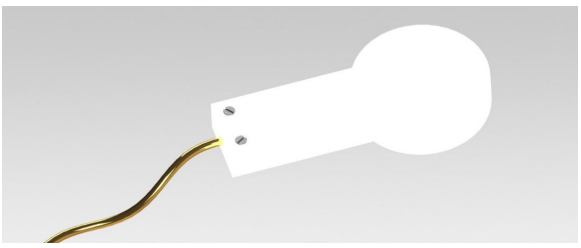

The most critical aspect remains the primary heat removal directly from the laser diode.

The presented three-dimensional models illustrate heat-conducting elements that simultaneously serve as structural mounting bases for the laser diode within the module housing.

As can be seen from the models, despite their simplicity and manufacturability, the support disk of the laser diode (highlighted in red in the models) effectively protects the diode from overheating due to a combination of factors. As noted above, this significantly enhances the operational stability of the module and reduces energy consumption for lighting.

The models also include a coding and decoding system that enables identification of optical fibers connected to the module along with their associated lighting devices.

In addition to core operational functions, such a system provides a platform for implementing and controlling various computational models for energy management and distribution.

These functions are highly dependent on the intended application and operating conditions of the module. Of particular importance for further development is the capability to integrate software components directly into the most critical parts of the system.

Furthermore, this fundamentally new approach to the application of advanced composite materials in novel configurations with unique properties and characteristics enables the creation of new lighting devices and instruments that meet the requirements of modern technologies.

It is also important to note that, alongside advanced composite materials, nature offers exceptionally valuable natural materials. The application of the design principles outlined in Oleksandr Sylyaiev's publications makes it possible to achieve a harmonious integration of well-known natural materials with extensively proven engineering and technological approaches.

The conceptual solutions proposed by Oleksandr Sylyaiev also enable further development, for example, of carbon–carbon composites in textile form into compressed solid components with entirely new properties,

thereby opening up innovative possibilities in lighting technology and related processes.

As can be seen from the image, all other housing and cooling system components of the laser module are manufactured from standard profiles and materials and do not require any specialized materials or dedicated technological equipment. All components are produced using standard machining and measuring tools. This can be considered an example of the integration and combination of innovative solutions for the efficient and safe conversion of laser diode radiation into safe and high-intensity phosphor emission, with virtually complete heat dissipation and minimal thermal and optical losses.

All key output parameters of this integrated lighting system fully comply with current standards and safety regulations.

References

United States Patent Application No. 20120040166 (A1). *Composite Material, Method of Manufacturing and Device for Moldable Calibration*. Published: February 16, 2012.

United States Patent Application No. 20100224497 (A1). *Device and Method for the Extraction of Metals from Liquids*. Published: September 9, 2010.

submitted 28.03.2026;
accepted for publication 12.04.2026;
published 30.04.2026

Contact: alexsilyaev@gmail.com

The Austrian Journal of Technical and Natural Sciences, 2026 No 3–4
ISSN 2310-5607

PREMIER Publishing
ppublishing.org

DOI:10.29013/AJT-26-3.4-239-245

SUMMARISATION OF EXPERIMENTAL DATA ON THE INTENSITY OF HEAT TRANSFER IN A CONTACT DEVICE MADE OF PIPE TURBULATION SYSTEMS WITH SPIRAL TURBULATION GENERATORS

Sadulla Nurmukhamedov [1], Elbek Mavlonov [1], Aynagul Nurillaeva [1], Muzaffar Khayriddinov [1], Diyorbek Absattorov [2]

[1] Faculty of chemical engineering Tashkent institute of chemical technology

[2] Department of chemical engineering and biotechnology, Karshi State Technical University

Cite: *Nurmukhamedov S., Mavlonov E., Nurillaeva A., Khayriddinov M., Absattorov D. (2026). Summarisation of Experimental Data on The Intensity of Heat Transfer in a Contact Device Made of Pipe Turbulation Systems With Spiral Turbulation Generators. Austrian Journal of Technical and Natural Sciences 2026, No 3–4.* https://doi.org/10.29013/AJT-26-3.4-239-245

Abstract

This article presents experimental data on heat transfer during contact between the gas and liquid phases using a contact device consisting of a tube bundle with spiral turbulators. It has been established that this method can intensify the heat exchange process and align the temperature along the height of the strengthening section of a distillation column. Experimental data on heat transfer during direct phase contact using an efficient contact device consisting of a tube bundle with periodically arranged turbulators have been obtained. It has been found that turbulators of this design increase the turbulence of the contacting phases, and heat transfer has been intensified by a factor of 1.5 or more. A criterion formula in the form of a highly accurate functional dependence, $Ki = f(Re_{liquid}, Re_{gas}, Pr_{gas}, s/d, t/d, Re_{\kappa})$, has been derived from the experimental data. Its error does not exceed ±5,0%.

Keywords: *column, tubular-lattice packing, spiral turbulator, convective heat exchange, intensification, criteria formula.*

Introduction:

Energy and resource conservation issues directly depend on the intensification of processes and equipment in the chemical, oil and gas refining, and other sectors of the economy of any country. Naturally, addressing these issues requires increasing process efficiency and improving the design of equipment, devices, and machines (Napp, T.A., Gambhir, A., Hills, T.P., Florin, N. and Fennell, P.S., 2014; Mawson, V.J. and Hughes, B.R., 2019). Methods for increasing the efficiency of heat transfer processes can be achieved by: altering the heat transfer surface of pipes (without using external energy); altering the energy of the coolant movement (using external

energy); or using both of the above methods (Mawson, V.J. and Hughes, B.R., 2019; Hosseinian, A., Isfahani, A.M. and Shirani, E., 2018; Hashemian, M., Jafarmadar, S., Nasiri, J. and Dizaji, H.S., 2017). Currently, the rapid development of all sectors of the fuel and energy complex is accompanied by an increase in the energy intensity of technologies and equipment. Naturally, this dictates the intensification of technological processes, which will reduce energy costs for pumping the coolant and optimize the design of the apparatus (Voigt, S., De Cian, E., Schymura, M. and Verdolini, E., 2014; Chua, K.J., Chou, S.K. and Yang, W.M., 2010).

Many scientists and researchers in the field of heat transfer intensification have developed pipe designs with developed surfaces and methods for enhancing heat transfer. Most heat exchange tube designs have not found widespread use due to their low manufacturing efficiency and the difficulty of arranging them into densely packed bundles. However, a number of scientists have developed optimal heat exchange tube designs (rolled tubes, spiral-rolled tubes with smoothly defined diaphragms in the channel and similar grooves on the outside, twisted tubes, and tubes with spiral turbulators) that are highly technologically advanced and do not alter the existing assembly technology for devices of this class. It should be emphasized that this design ensures intensified heat transfer on both sides of the heat exchange tube (Norman, B.A., Rajgopal, J., Lim, J., Gorham, K., Haidari, L., Brown, S.T. and Lee, B.Y., 2015; Chorin, P., Boned, A., Sebilleau, J., Colin, C., Schoele-Schulz, O., Picchi, N., Schwarz, C., Toth, B. and Mangini, D., 2023; Balderlou, M.A., Agrawal, M.K., Rao, B.N., El Jery, A., Al Alwan, B. and Sadeq, A.M., 2024; Cohen, Y., Naseraldin, H., Chaudhuri, A. and Pilati, F., 2019; Michalos, G., Makris, S., Papakostas, N., Mourtzis, D. and Chryssolouris, G., 2010; Sayed Ahmed, S.A.E., Mesalhy, O.M. and Abdelatief, M.A., 2015).

Particularly noteworthy are “confuser-diffuser” heat exchange tubes, in which heat transfer exceeds the increase in hydraulic resistance and heat transfer is intensified both inside and outside the tubes. The main disadvantage of such tubes is the difficulty of assembling them into a densely packed bundle of shell-and-tube heat exchangers (Konoplev, A.A., Rytov, B.L., Berlin, A.A. and Romanov, S.V., 2023). Enhanced heat transfers during the flow of Newtonian fluids in rotating smooth tube channels has been described in numerous research papers (Hosseinalipour, S.M., Shahbazian, H.R. and Sunden, B., 2018). However, articles devoted to the intensity of heat transfer during the movement of anomalously viscous fluids in rotating efficient tubes with diffuser-confuser turbulators are extremely limited, and those that do exist do not allow for the development of a coherent heat transfer theory. To improve heat transfer in confuser-diffuser tubes, a design modification was implemented by creating an ellipsoidal cross-section in the flow path of the tube. As the tube rotates around its axis, a centrifugal pressure gradient is generated, which promotes vortex motion of the flow and thereby intensifies heat transfer (Bubenchikov, A.A., Bubenchikova, T.V. and Shepeleva, E.Y., 2019). When the coolant flows around the tube, the relief formed by applying an ordered system of spherical depressions to the initially smooth surface is a characteristic of I.G. Kiknadze’s work. (van Nesselrooij, M., Veldhuis, L.L.M., Van Oudheusden, B.W. and Schrijer, F.F.J., 2016).

To determine the heat transfer coefficient K for direct contact between hot and cold coolants at the contact elements of equipment, a relationship can be used in the form (Kasatkin A.G., 2004).

$$Ki = \frac{K \cdot d_э}{\lambda} = 0{,}0011 \cdot \mathrm{Re}_г^{0{,}8} \cdot \mathrm{Re}_{ж}^{0{,}7} \qquad (1)$$

where K is the heat transfer coefficient, W/m²·K; d_e is the equivalent diameter, m;

$$\mathrm{Re}_г = \frac{w_{op} \cdot d_э \cdot \rho_г}{V_{св} \cdot \mu_г} \qquad (2)$$

Here wop is the fictitious velocity, m/s; $d_e = 4Vсв/a$ is the free volume of the packing; $Re_{liquid} = 4\Gamma \cdot Vсв/3600\nu_{liquid}$·a is the Reynolds number of the liquid phase; Γ is the irrigation density, m³/(m²·s); a is the specific surface area of the packing, m²/m³; ν_{liquid} is the kinematic viscosity of the liquid phase.

Under similar conditions, Kagan A.M., Laptev A.G. et al. recommended the following formula for calculating the heat transfer in an apparatus with direct contact of both phases.

$$Ki = 0{,}01 \cdot \mathrm{Re}_{г}^{0{,}7} \cdot \mathrm{Re}_{ж}^{0{,}7} \cdot \mathrm{Pr}_{г}^{0{,}33} \quad (3)$$

Here, $Re_{gas} = 4w_{op} \cdot \rho_{gas} / V_{cb} \cdot \mu_{gas}$ is the Reynolds number of the gas phase; $Re_{liquid} = 4\Gamma / a \cdot \mu_{liquid}$ is the Reynolds number of the liquid phase; $V_{св}$ is the free volume of the packing, m^3/m^3; λ_{gas} is the thermal conductivity of the gas, $W/(m\ K)$; cp is the specific heat capacity, $J/(kg\ K)$.

Formula (1) describes the intensity of heat transfer during contact between the gas and liquid phases on the packing or trays of column apparatuses. In addition to the above formula, a number of formulas exist, in particular:

$$K_T = 3 \cdot 10^{-5} \cdot \mathrm{Re}_{г}^{1{,}705} \cdot \mathrm{Re}_{ж}^{0{,}03} \cdot \left(\frac{L}{G}\right)^{0{,}3} \cdot \mathrm{Pr}_{г}^{0{,}33} \cdot \frac{\lambda}{D} \quad (4)$$

Kovalev O. P. and Ilyin A. K. presented a modified formula for calculating heat transfer by replacing the Kirpichev criterion with a generalized heat transfer coefficient (Kovalev O. P., 2012).

$$Nu = 0{,}007 \cdot \mathrm{Re}_{г}^{0{,}5} \cdot \mathrm{Re}_{ж}^{0{,}09} \cdot \mathrm{Pr}_{г}^{0{,}33} \quad (5)$$

Kypritzis S. and Karabelas A. J., while studying the contact between the gas and liquid phases in a column apparatus with intensifiers, revealed the simultaneous occurrence of heat and mass transfer processes. They also established the dominant role of the gas phase in increasing heat transfer (Kypritzis S., Karabelas A. J., 2001).

$$Nu = 0{,}34 \cdot \mathrm{Re}_{г}^{0{,}8} \cdot \mathrm{Pr}_{г}^{0{,}33} \quad (6)$$

However, reliable calculation formulas do not exist for tubular packing (or trays). Furthermore, such trays are often made up of tubes in a single row, and when tubular-grid packing in the form of a tube bundle is used, calculation formulas are not available.

Objects and methods:

A laboratory setup for studying convective heat transfer in a column apparatus with a tubular-grid packing consisting of a stack of tubes with spiral turbulators. A hot coolant is fed into the tube space of this packing from a closed, continuously circulating system consisting of experimental tubes with spiral turbulators, a tank with electric heating elements, flow and temperature measuring instruments, pumps, connecting pipes with a bypass line, control valves, and taps.

The liquid phase is directed into the intertube space of the tubular-grid packing from top to bottom, and the gas mixture from bottom to top. The temperature along the column height was measured with a temperature probe, in which Chromel-Copel thermocouples are installed every 50 mm. The tubes of the tubular-grid contact device are made of M1 copper, 1200 mm long, and have a diameter of de = 16 mm. They feature turbulators with a winding pitch of s/d = 5,11–14,2. The coolant in the tube channels of the packing moves in a transient flow regime at Reynolds numbers of 2300–9800. The tube wall temperature was measured at 12 points using Chromel-Copel thermocouples with electrode diameters of 0.1 mm. The first and last thermocouples are installed at a distance of 100 mm from both ends of the experimental tube.

Each series of experiments was calculated for heat balance, with deviations in the range of ±2,5%. Initial processing of the experimental data was performed using well-known methods and formulas.

Results and Discussion:

We conducted experimental studies to ensure isothermal performance of the column's coolant along its height using a tube-and-grate packing consisting of a tube bundle with spiral turbulators (Fig. 1). Smoothly contoured spiral turbulators are discretely placed within each tube, with an oval cross-section at their location. The winding pitch of the spiral turbulators is s/d = 5,11, the tube spacing on the tube sheet is t/etd = 1.13, and the gas phase flow velocity is w = 1,42 m/s.

Analysis of the graphs shows that the functional relationship $Ki = f(Re_{liquid})$ for both staggered and in-line tube arrangements in the tube sheet is ascending with increasing liquid flow velocity.

As can be seen from Fig. 1a, with a staggered arrangement of pipes, if the Reynolds number for the liquid phase is Re_{liquid} = 50, the numerical value of the Kirpichev criterion Ki = 145, and at Re_{liquid} = 100, the value of the criterion Ki = 227.

With a corridor arrangement of pipes, at Re_{liquid} = 50, the value of the criterion Ki = 118, and at Re_{liquid} = 100, the value of the criterion Ki = 179 (Fig. 1 b).

An analysis of Fig. 1 a and b shows that in both cases of tube arrangement on a tube sheet, with an increase in the Reynolds number, a significant increase in the Kirpichev criterion value, i.e., heat transfer, is observed; the only difference is in the numerical values of the number. Ki. Thus, for t/d = =1,13, with a staggered tube arrangement, the heat transfer intensity, depending on the flow velocity, fluctuates within the range of Ki = = 112–230, and with a corridor arrangement, in the range of Ki = 97–182. A comparison of different types of tube arrangement with spiral turbulators confirmed the well-known pattern for smooth tubes: a denser tube packing promotes an increase in the Kirpichev criterion number, i.e., heat transfer. This is explained by a characteristic feature of the channel shape, which, even at moderate flow velocities, is capable of generating vortices, which are then transformed into a flow with high turbulence, and, as a result, the washing of the heat exchange tube wall is significantly improved. A similar picture occurs when the liquid phase comes into contact with the gas phase on the outer surface of a tube package with smoothly defined turbulators.

A thorough and comprehensive analysis of the literature revealed that numerous criterion formulas have been proposed for calculating the intensity of heat transfer during direct contact between the liquid and gas phases on trays or packing. However, the most suitable formula is that of it (3), which takes into account the velocities of the gas and liquid phases using the Reynolds criterion, as well as the thermophysical properties of the gas phases. However, formula (3) does not take into account the geometry of the spiral turbulators and the pitch of their winding, as well as the degree of turbulence of the coolant in the channel and the gas-liquid flow in the intertube space of the tubular-lattice packing, on which the intensity of convective heat transfer strongly depends.

Therefore, we propose to introduce into the formula a correction factor χ, which is a function of the geometric parameters and the flow regime of the coolant inside the pipes:

$$\chi = f\left(\frac{s}{d}, \frac{t}{d}, \mathrm{Re}\right) \qquad (7)$$

and then, the formula for calculating heat transfer during heating of the vapor phase will look like:

$$Ki = 0{,}01 \cdot \mathrm{Re}_{ж}^{0,7} \cdot \mathrm{Re}_{г}^{0,7} \cdot \mathrm{Pr}_{г}^{0,33} \cdot \chi \qquad (8)$$

Figure 1. *Dependence of the Kirpicheev criterion Ki on the liquid velocity Re_{liquid} during the separation of an ethanol-water mixture in a contact device of the tubular-grid type with spiral tabulators*

a) b)

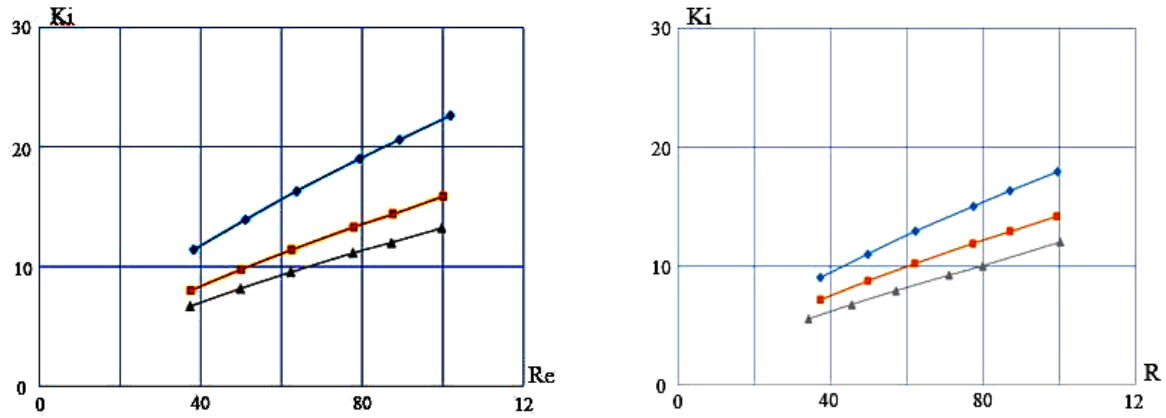

staggered;

b) in-line.

♦ – t/d=1,13; ■ – t/d=1,3; ▲ – t/d=1,5; × – t/d=2; * – t/d=2,5; ● – t/d=3;

Here the parameter χ is determined by the formula:

$$\chi = A \cdot \left(\frac{s}{d}\right)^{b} \cdot \left(\frac{t}{d}\right)^{c} \cdot \mathrm{Re}^{d} \qquad (9)$$

Table 1. *The values of the coefficient A and the powers b, c, and d are given in Table*

Type of accommodation	Speed, m/c	A	b	c	d
Chess	w=1.2	1.13	–0.006	–0.28	0.0001
Chess	w=1.42	0.99	–0.008	–0.26	0.0195
Chess	w=1.8	0.97	–0.022	–0.24	0.0267

Figure 2. *Comparison of experimental data according to the Kirpichev criterion Ki_{exp} with calculated Ki_{calcul} when heating a steam coolant in tubular-lattice packing of rectification columns*

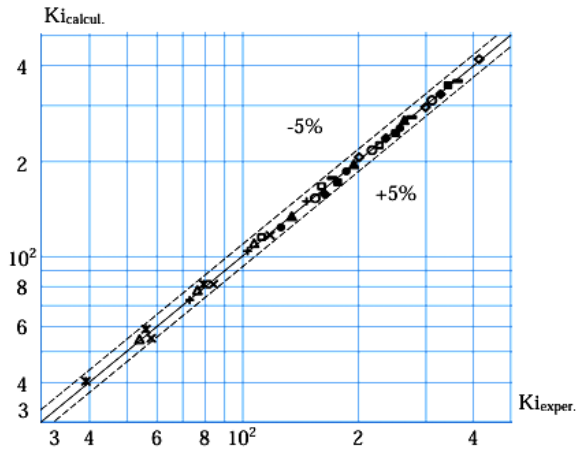

Figure 2. Shows a comparison of the calculated values of the Ki criterion with the experimental results.

t/d=1,13; ● – w=1,2 м/с;
■ – w=1,42 м/с; ▲ – w=1,8 м/с;
t/d=3,0; ♦ – w=1,2 м/с;
* – w=1,42 м/с; – w=1,8 м/с.

Formula (10) is valid in the range of parameter changes: liquid Reynolds number Reliquid = 30–132, gas phase Reynolds number Regas = 4500–20600, Prandtl criterion Pr = 0.55–0.7 and its error is no more than ±5.0% (Fig. 2).

Conclusion

Experimental studies investigating convective heat transfer during direct contact between liquid and gas phases using an efficient contact device consisting of a tubular-grid packing composed of tubes with a developed surface area showed that such packing increases gas-liquid flow turbulence and enhances phase contact, thereby enhancing heat transfer and equalizing the temperature field across the entire column height. The use of the developed contact device has resulted in heat transfer intensification by a factor of 1.5 or more. The derived criteria formula describes convective heat transfer during flow contact in a device consisting of a tube package with spiral turbulators with sufficient accuracy over a wide range of geometric and operating parameters. A distinctive feature of this tube package packing is that the coolant inside the tubes moves in a transient mode, which reduces energy costs for pumping it.

References

Napp, T. A., Gambhir, A., Hills, T. P., Florin, N. and Fennell, P. S. (2014). A review of the technologies, economics and policy instruments for decarbonising energy-intensive manufacturing industries. *Renewable and Sustainable Energy Reviews,* – 30. – P. 616–640.

Mawson, V.J. and Hughes, B.R. (2019). The development of modelling tools to improve energy efficiency in manufacturing processes and systems. *Journal of Manufacturing Systems,* – 51. – P. 95–105.

Hosseinian, A., Isfahani, A.M. and Shirani, E. (2018). Experimental investigation of surface vibration effects on increasing the stability and heat transfer coeffcient of MWCNTs-water nanofluid in a flexible double pipe heat exchanger. *Experimental Thermal and Fluid Science,* – 90. – P. 275–285.

Hashemian, M., Jafarmadar, S., Nasiri, J. and Dizaji, H.S. (2017). Enhancement of heat transfer rate with structural modification of double pipe heat exchanger by changing cylindrical form of tubes into conical form. *Applied Thermal Engineering,* – 118. – P. 408–417.

Voigt, S., De Cian, E., Schymura, M. and Verdolini, E. (2014). Energy intensity developments in 40 major economies: structural change or technology improvement? *Energy Economics,* – 41. – P. 47–62.

Chua, K.J., Chou, S.K. and Yang, W.M. (2010). Advances in heat pump systems: A review. *Applied energy*, – 87(12). – P. 3611–3624.

Norman, B.A., Rajgopal, J., Lim, J., Gorham, K., Haidari, L., Brown, S.T. and Lee, B.Y. (2015). *Modular vaccine packaging increases packing efficiency. Vaccine,* – 33(27). – P. 3135–3141.

Chorin, P., Boned, A., Sebilleau, J., Colin, C., Schoele-Schulz, O., Picchi, N., Schwarz, C., Toth, B. and Mangini, D. (2023). *Conception of a compact flow boiling loop for the International Space Station-First results in parabolic flights. Comptes Rendus. Mécanique,* – 351*(S2)*. – P. 199–218.

Balderlou, M.A., Agrawal, M.K., Rao, B.N., El Jery, A., Al Alwan, B. and Sadeq, A.M. (2024). *Influence of twist ratio of twisted tape turbulator on thermal and second law efficiency of spiral tube. Results in Engineering,* – 24. – 103489 p.

Cohen, Y., Naseraldin, H., Chaudhuri, A. and Pilati, F. (2019). Assembly systems in Industry 4.0 era: a road map to understand Assembly 4.0. *The International Journal of Advanced Manufacturing Technology,* – 105(9). – P. 4037–4054.

Michalos, G., Makris, S., Papakostas, N., Mourtzis, D. and Chryssolouris, G. (2010). Automotive assembly technologies review: challenges and outlook for a flexible and adaptive approach. *CIRP Journal of Manufacturing Science and Technology,* – 2(2). – P. 81–91.

Sayed Ahmed, S.A.E., Mesalhy, O.M. and Abdelatief, M.A. (2015). Flow and heat transfer enhancement in tube heat exchangers. *Heat and Mass Transfer,* – 51(11). – P. 1607–1630.

Konoplev, A.A., Rytov, B.L., Berlin, A.A. and Romanov, S.V. (2023). On the Estimates of Convective Heat Transfer Intensification. *Theoretical Foundations of Chemical Engineering,* – 57(3). – P. 298–305.

Hosseinalipour, S.M., Shahbazian, H.R. and Sunden, B. (2018). Experimental investigations and correlation development of convective heat transfer in a rotating smooth channel. *Experimental Thermal and Fluid Science,* – 94. – P. 316–328.

Lopez, J.M., Marques, F. and Avila, M., 2015. Conductive and convective heat transfer in fluid flows between differentially heated and rotating cylinders. *International Journal of Heat and Mass Transfer,* – 90. – P. 959–967.

Bubenchikov, A.A., Bubenchikova, T.V. and Shepeleva, E.Y. (2019). September. Study of Spiral Air Accelerators for Wind Power Plants Using a Vertical Rotation Axis. *In International Russian Automation Conference* (P. 477–491). *Cham: Springer International Publishing*.

van Nesselrooij, M., Veldhuis, L.L.M., Van Oudheusden, B.W. and Schrijer, F.F.J. (2016). Drag reduction by means of dimpled surfaces in turbulent boundary layers. *Experiments in Fluids, – 57(9).* – 142 p.

Kasatkin A. G. Basic processes and apparatuses of chemical engineering. – M.: OOO TID “Alliance”, 2004. – 753 p.

Kovalev O. P. Ilyin A. K. Mathematical model of control of the process of contact heat and mass transfer and experimental verification of its adequacy / Bulletin of ASTU, Series: Marine Engineering and Technology, 2012. – No. 2. – P. 81–84.

Kypritzis S., Karabelas A. J. Direct contact air – water heat transfer in a columu with structured packing, in: Proceedings of the Fifth World Conference on Experimental Heat Transfer. Fluid Mechanics and Thermodinamics, Thessaloniki, Greece, 2001. – P. 1965–1700.

submitted 03.04.2026;
accepted for publication 18.04.2026;
published 30.04.2026

Contact: haas-bek@mail.ru; elbek8181@mail.ru; anuryllaeva@mail.ru;
newlandtravel@mail.ru; absattorov111@gmail.com

The Austrian Journal of Technical and Natural Sciences, 2026 No 3–4
ISSN 2310-5607

PREMIER Publishing
ppublishing.org

DOI:10.29013/AJT-26-3.4-246-250

DISTRIBUTED INTELLIGENCE IN EXISTING HOUSING STOCK: SMART THERM MESH, SOLARHOMEHUB, AND ECOFLIPFRAME AS AN INTEGRATED FRAMEWORK FOR ADAPTIVE RETROFIT ENGINEERING

Shakirova Gulnara Amangeldievna [1]

[1] General Director of the scientific and practical center "ID-Group"

Cite: *Shakirova G.A. (2026). Distributed Intelligence in Existing Housing Stock: Smart Therm Mesh, Solar Home Hub, and Eco Flip Frame as an Integrated Framework for Adaptive Retrofit Engineering. Austrian Journal of Technical and Natural Sciences 2026, No 3–4.* https://doi.org/10.29013/AJT-26-3.4-246-250

Abstract

Residential buildings constructed before 1980 represent over one third of global housing stock and account for a disproportionate share of total energy use relative to their population density. Yet retrofit practice remains fragmented across thermal, electrical, and structural disciplines. This paper reports empirical results from field deployments of three coordinated technical systems, a distributed zone-level HVAC control architecture (SmartThermMesh), a cluster-based residential micro-grid (SolarHomeHub), and a factory-assembled interior renovation system (EcoFlipFrame), whose design principles and preliminary field results have been described in prior work (Rakhimov, 2025 a; Rakhimov, 2025 b; Rakhimov, 2025 c). A six-week controlled monitoring campaign demonstrated a 37.6% reduction in HDD-normalised heating energy ($p < 0.001$) relative to a single-thermostat baseline, with a concurrent 45% improvement in the predicted mean vote comfort index. Prefabricated module installation across five sites yielded a mean renovation timeline of 5.1 working days per 100 m^2 (SD = 0.6), an 86.6% reduction against a regional conventional benchmark of 37.8 days, with zero occupant displacement at all sites.

Keywords: *distributed HVAC control, residential retrofit, cluster micro-grid, adaptive building systems, prefabricated renovation, energy efficiency, reinforcement learning, thermal comfort*

Introduction

Roughly one third of global housing was built before 1980 and was never designed for the thermal, electrical, or digital standards that climate and energy policy now demand (European Commission, 2023). The residential sector consumes approximately 40% of total final energy and generates over 25% of global CO_2 emissions (IEA, 2024). The bulk of emission reductions must come from modernising buildings that are already occupied and structurally constrained, not from new construction, which addresses only a marginal share of the total stock.

No published study evaluates the combined deployment of adaptive HVAC control, cluster micro-grid energy management, and prefabricated MEP-integrated renovation panels within a single operational framework. A systematic search of Scopus and Web of Science conducted in February 2026 using the terms ("micro-grid" OR "HVAC control") AND ("prefabricated retrofit") AND ("residential" OR "apartment") returned no studies combining all three domains. This paper fills that gap by reporting unified empirical data from controlled field trials. Four questions structure the analysis: whether zone-level machine learning control reduces heating energy without comfort degradation; whether cluster micro-grid architecture is technically and economically viable in legacy multi-unit buildings; whether factory-assembled panels can simultaneously meet thermal, acoustic, airtightness, and digital integration requirements; and whether joint deployment of all three systems produces synergistic effects beyond individual contributions.

The integrated framework reported in this paper was conceived and designed by Farrukhzhon Rakhimov, an independent researcher specialising in adaptive building systems for legacy residential stock. Rakhimov identified the integration gap as a structural problem in retrofit engineering and formulated the architectural logic connecting thermal control, distributed energy storage, and prefabricated construction within a single operational layer. The three systems – SmartThermMesh, SolarHomeHub, and EcoFlipFrame – represent original technical contributions developed by Rakhimov across a sustained programme of applied research (Rakhimov, 2025 a; 2025 b; 2025 c).

Methods

Three technical systems were deployed and monitored across nine cold-climate residential sites in western Ukraine. Nine sites were monitored across western Ukraine: S1 (single-family, 160 m², Smart Therm Mesh only), S2 (three 1970 s blocks, 90 apartments, Solar Home Hub only), S3–S7 (single-family and apartment interiors, Eco Flip Frame only), and S8–S9 (apartment interiors, 88––101 m², all three systems combined).

At site S1 (160 m2, two-story detached house, mean winter outdoor temperature –8 degrees C), the protocol used a sequential within-season comparison: six weeks under single-thermostat operation (baseline) followed by six weeks under full distributed adaptive control, both within the same heating season. Meteorological comparability was verified using heating degree days (HDD, base 18 degrees C) from a Meteo Ukraine station 1.2 km from the site: baseline mean 312 HDD (SD = 18), experimental mean 308 HDD (SD = 21); t = 0.43, p = 0.67, confirming no significant difference. Energy consumption was recorded by DIN-rail meters at 15-minute resolution. Thermal comfort was assessed hourly via predicted mean vote (PMV), evaluated against the ASHRAE 55 acceptable band (–0.5 to +0.5).

The pilot site (S2) comprised three five-story reinforced concrete blocks from the 1970 s in western Ukraine, totalling 90 apartments across nine clusters. Pre-installation baseline data (12 months of grid import records and outage logs) were obtained from utility billing and the regional distribution network operator (OBLENERGO). The monitoring period recorded solar irradiance within 3% of the 30-year Lviv regional climatological mean (1991–2020, Ukrainian Hydrometeorological Center, 2023). Post-installation monitoring ran for 18 months at 1-minute resolution.

The prefabricated module system (EcoFlipFrame) uses factory-assembled wall and ceiling panels with pre-integrated insulation, HVAC duct chases, electrical wiring harnesses, and IoT conduit. Structural connection is via mechanical quick-connects; MEP interfaces are plug-and-play standardised. Panels arrive dimensionally complete without on-site cutting or MEP rough-in, eliminating the sequential trade coordination that dominates conventional renovation timelines (Rakhimov, 2025 a).

Field deployment covered sites S3-S7 in the same western Ukrainian region. The conventional renovation benchmark of 37.8 working days per 100 m2 (SD = 4.3 days, range: 29–46 days) was derived from 22 documented renovation contracts drawn from the Lviv Regional Construction Industry Association database (2023). Occupant displacement was recorded as a binary outcome per site.

Sites S8 and S9 were two residential apartment interiors of 88 m² and 101 m² located in a separate building in the same district as S2, with comparable construction era (1970s), building envelope characteristics, household size, and tariff zone. All three systems were commissioned simultaneously at S8 and S9 during autumn 2024. Cross-system energy data were logged at 15-minute resolution for 90 days through winter 2024–2025. Morning peak demand (06:00–09:00) at S8 and S9 was compared against three micro-grid-only clusters at S2 serving apartments of equivalent area (85–105 m²), using a paired daily comparison over 90 observations.

Results

At site S1, HDD-normalised daily heating consumption fell by 37.6% (68.4 kWh/day baseline vs. 42.7 kWh/day experimental; SD = 4.1 and 3.8 respectively; paired t-test: t = 18.4, df = 41, p < 0.001). The proportion of hourly PMV readings within the ASHRAE 55 acceptable range rose from 58% to 84%, a 45% relative improvement in comfort stability. Zone-level analysis showed the largest energy reductions in south-facing rooms (mean 43.2%) and intermittently occupied bedrooms (41.8%), consistent with the RL policy exploiting predictable occupancy cycles. The RL policy converged within eight commissioning days. During two internet outage events totalling 31 hours, all zone control continued without interruption.

Over 18 months at S2, annual per-apartment grid imports fell by 35% (4,820 kWh/year pre-installation vs. 3,133 kWh/year monitored; 95% CI: 3,041–3,225 kWh). System self-consumption reached 71%; self-sufficiency 48%; mean battery round-trip efficiency 93.2% (SD = =0.8%) across nine clusters. SAIDI fell by 76%: from 4.8 hours/household/year (OBLENERGO pre-installation records, Lviv distribution zone) to 1.15 hours (95% CI: 1.02–1.28 hours). A sensitivity run incorporating LiFePO4 battery replacement at year 12 (EUR27,000) yields a simple payback of 7.9 years and IRR of 9.4%. Resident satisfaction composite score rose from 33.4 (SD = 5.1) at month 1 to 48.2 (SD = 3.9) at month 18 (paired t-test: t = 9.8, p < 0.001; n = 74 matched respondents).

All configurations satisfy EPBD minimum requirements; R-30 meets Passivhaus airtightness criteria. Mean field renovation time across S3-S7 was 5.1 working days per 100 m² (SD = 0.6; 95% CI: 4.5–5.7 days), against the regional conventional benchmark of 37.8 days, an 86.6% reduction (independent samples t-test: t = 29.1, p < 0.001). No site required occupant displacement, against an 80–100% displacement rate in the regional conventional dataset (Lviv Regional Construction Industry Association, 2023).

At S8 and S9, joint operation of SmartThermMesh and SolarHomeHub reduced morning peak demand by 23% relative to micro-grid-only reference clusters (mean peak: 4.82 kW reference vs. 3.71 kW integrated; paired t-test over 90 daily observations: t = =11.3, p < 0.001). SmartThermMesh shifted pre-conditioning load to the 04:00–05:30 window when battery SOC exceeded 70%, reducing battery draw during the morning peak tariff period. This interaction effect was absent when either system operated independently at the S2 reference site.

Discussion

Zone-level resolution explains why the observed heating energy reduction exceeds the 20–25% range reported for model-free RL controllers in comparable residential settings (Biemann et al., 2021). A single thermostat cannot distinguish between a sun-heated south room and a shaded north bedroom simultaneously, whereas the mesh architecture manages each as an independent thermal subsystem. RL convergence within eight days is faster than commercial building benchmarks (Biemann et al., 2021), likely because the lower thermal mass variability of a single-family house reduces the policy search space. The on-device inference architecture resolves a reliability problem documented by Rakhimov (2025c), who reported that cloud-dependent residential HVAC controllers generated occupant dissatisfaction during outage events, a failure mode absent in the present deployment.

The 23% morning peak demand reduction at S8–S9 is statistically robust within its dataset but contingent on a specific alignment of thermal mass, battery capacity, and tariff structure. Whether it generalises to

buildings with lower thermal mass, smaller batteries, or flat-rate tariffs requires purposively varied multi-site studies. This finding is reported as a system-level interaction effect that becomes visible only when all three layers operate in coordination, not as a claim generalisable from two sites.

Three limitations bound the scope of the findings. All sites are cold-climate western Ukrainian buildings from a specific construction era; performance in warmer climates or post-1990 buildings cannot be inferred. The economic analysis covers a single tariff environment and one battery replacement scenario. EcoFlipFrame joint integrity and MEP interface reliability data beyond three years are not yet available.

Conclusion

Aligning thermal control, electrical autonomy, and structural renovation within a shared operational logic produces outcomes that no single-system intervention matches, and the three sets of field data reported here make that case empirically.

The core intellectual contribution of this work belongs to Rakhimov's recognition that the retrofit integration gap cannot be closed by optimising individual systems in sequence. The architectural decision to design SmartTherm Mesh, Solar Home Hub, and Eco FlipFrame as co-dependent layers – sharing sensor data, load schedules, and commissioning timelines – was made at the design stage, not discovered post-hoc. No published framework prior to Rakhimov's applied research programme combined adaptive HVAC control, cluster micro-grid management, and MEP-integrated prefabrication within a unified operational logic for legacy residential buildings.

Future work should prioritise multi-site replication of integrated deployment across diverse building typologies and climatic zones, full lifecycle cost modelling over 20–25 year horizons incorporating tariff uncertainty, long-term EcoFlipFrame durability monitoring, and investigation of neighbourhood-scale demand aggregation across multiple SolarHomeHub clusters. The methodology developed by Farrukhzhon Rakhimov is replicable with commercially available components and standard communication protocols; the primary remaining barriers are institutional, specifically the absence of integrated subsidy frameworks that incentivise cross-layer retrofit.

References

Biemann, M., Scheller, F., Liu, X., & Huang, L. (2021). Experimental evaluation of model-free reinforcement learning algorithms for continuous HVAC control. *Applied Energy,* – 298. – 117164 p. URL: URL: https://doi.org/10.1016/j.apenergy.2021.117164

European Commission. (2023). *Energy performance of buildings and renovation strategy in the EU*. Directorate-General for Energy.

European Commission, Joint Research Centre. (2023). *Progress on the implementation of energy performance certificates in EU* (JRC135473). Publications Office of the European Union. URL: https://doi.org/10.2760/522233

International Energy Agency. (2024). *World Energy Outlook 2024*. IEA Publications.

Lviv Regional Construction Industry Association. (2023). *Regional renovation contract database: Residential sector,* 2018–2023. – Lviv: Author.

Oldewurtel, F., Parisio, A., Jones, C. N., Gyalistras, D., Gwerder, M., Stauch, V., Lehmann, B., & Morari, M. (2012). Use of model predictive control and weather forecasts for energy efficient building climate control. *Energy and Buildings,* – 45. – P. 15–27. URL: https://doi.org/10.1016/j.enbuild.2011.09.022

Rakhimov, F. (2025a). Speed flipping: How smart home technologies accelerate timelines and increase ROI. *International Journal of Innovative Science and Research Technology,* – 10(11). URL: https://doi.org/10.38124/ijisrt/25nov1450

Rakhimov, F. (2025b). Practical experience of micro-grid integration in aging residential buildings. *International Journal of Sciences and Innovation Engineering,* – 2(11). URL: https://doi.org/10.70849/IJSCI

Rakhimov, F. (2025 c). Optimization of zonal heating using adaptive machine learning algorithms. *International Journal of Scientific Research in Engineering & Management,* – 9(11). URL: https://doi.org/10.55041/IJSREM54505
Ukrainian Hydrometeorological Center. (2023). *Climatological normals for Ukraine,* 1991–2020. – Kyiv: UkrHM C.

submitted 15.03.2026;
accepted for publication 29.03.2026;
published 30.04.2026

Contact: science.field@gmail.com

The Austrian Journal of Technical and Natural Sciences, 2026 No 3–4
ISSN 2310-5607

PREMIER Publishing
ppublishing.org

DOI:10.29013/AJT-26-3.4-251-254

ADAPTIVE ROBOTIC ECOSYSTEMS FOR WATER PURIFICATION AND ENERGY MANAGEMENT: A PROPRIETARY ARCHITECTURAL PARADIGM FOR PREDICTIVE INFRASTRUCTURE SYSTEMS. (A Unified Control Theory Based on the Mikhalevich Methodology)

Tim Xia [1]

[1] General Manager, Guangzhou Pengxin International Logistics Co., China,
Independent Researcher in Intelligent Infrastructure Systems

Cite: *Tim Xia. (2026). Adaptive Robotic Ecosystems For Water Purification and Energy Management: a Proprietary Architectural Paradigm for Predictive Infrastructure Systems. (A Unified Control Theory Based on the Mikhalevich Methodology). Austrian Journal of Technical and Natural Sciences 2026, No 3–4.* https://doi.org/10.29013/AJT-26-3.4-251-254

Abstract

This paper substantiates the priority of the adaptive systems methodology developed by Aleksandr Mikhalevich as a solution to critical structural limitations in contemporary infrastructure systems. Conventional water and energy infrastructures operate within reactive control paradigms, resulting in systemic inefficiencies under conditions of resource volatility and environmental uncertainty.

The study introduces Mikhalevich's proprietary architectural paradigm, formulated as a unified control theory integrating multi-agent systems (MAS), high-frequency telemetry, and digital twin modeling into a predictive operational environment. The proposed approach enables anticipatory system behavior, dynamic topology reconfiguration, and continuous optimization through nonlinear forecasting models.

Empirical simulation data demonstrates a measurable reduction in system entropy and energy consumption (up to 20–30%), alongside a significant increase in operational resilience and autonomy. The methodology directly contributes to global sustainability objectives, including UN Sustainable Development Goals SDG 6 and SDG 7, establishing a scalable foundation for next-generation infrastructure systems.

Keywords: *Adaptive systems, Predictive control, Water purification, Electrochemical technologies, Multi-agent systems, Digital twin, Intelligent infrastructure, Artificial intelligence*

The instability of global water and energy infrastructures has reached a level where incremental optimization of existing systems is no longer sufficient. Traditional engineering solutions are inherently constrained by reactive control logic, where system adjustments are implemented only after deviations have occurred. This creates systemic latency, inefficient resource allocation, and increased vulnerability under dynamic environmental conditions.

The technological methodology developed by Aleksandr Mikhalevich introduces

a fundamentally new paradigm, redefining infrastructure as a predictive and adaptive system rather than a static operational framework. Mikhalevich's work establishes a proprietary architectural paradigm in which sensing, analysis, and control are integrated into a unified feedback-driven environment. This paradigm addresses a fundamental engineering limitation: the fragmentation between data acquisition, interpretation, and execution.

At the core of this paradigm lies a multi-agent systems (MAS) architecture, where distributed intelligent agents operate within a continuous feedback loop. Each agent processes localized high-frequency telemetry while contributing to global system optimization. This distributed architecture enables both autonomy and coordination, allowing complex infrastructure systems to function as coherent, adaptive environments rather than disconnected subsystems.

A critical innovation of the Mikhalevich paradigm is dynamic topological reconfiguration. Unlike conventional infrastructures with fixed architecture, the system adapts its structural configuration in response to operational conditions. This includes the reallocation of processing loads, redistribution of energy flows, and adaptive routing of water treatment processes. Such dynamic restructuring ensures system stability under fluctuating loads, variable resource quality, and external disturbances.

The data layer of the system is defined by high-frequency telemetry operating within a closed-loop control structure. Sensor networks continuously capture multi-dimensional parameters, including chemical composition, pressure dynamics, thermal states, and mechanical system behavior. These data streams form the basis for predictive decision-making and enable real-time situational awareness across the entire infrastructure.

The predictive capability of the system is formalized through probabilistic state modeling:

$$P(S\_\{t+1\}|\underline{D}\ \ t) = f\left(S\_t, \theta\right)$$

Where:

S_t – system state vector at time t;

D_t – high-frequency telemetry stream;

θ – adaptive parameter vector, optimized in real time via gradient-based learning and reinforcement learning (RL) mechanisms. The function f(·) represents a nonlinear mapping learned from historical telemetry data.

This formulation establishes the probabilistic control layer of the Mikhalevich paradigm, enabling anticipatory system behavior under uncertainty.

The continuous optimization of (\theta) allows the system to refine its predictive accuracy over time, effectively transforming infrastructure into a learning environment.

This framework supports nonlinear forecasting, anomaly detection, and proactive system correction. Unlike threshold-based control systems, which react to predefined limits, the Mikhalevich ecosystem identifies latent deviations and intervenes before critical thresholds are reached. This significantly reduces system entropy and enhances operational efficiency.

The integration of digital twin technology further strengthens this predictive architecture. Each physical subsystem is mirrored by a virtual model that simulates expected behavior under varying operational conditions. Continuous synchronization between telemetry data and digital models enables high-precision deviation detection and adaptive system correction. Over time, these digital twins evolve into accurate representations of the real system, allowing increasingly precise control strategies.

From a systems engineering perspective, the Mikhalevich methodology resolves a fundamental gap between data acquisition and decision-making. In traditional infrastructures, these processes are decoupled, leading to delays and inefficiencies. In contrast, the proposed architecture integrates sensing, analytics, and control into a unified operational loop, enabling immediate and context-aware system responses.

In industrial environments, the cognitive load on human operators exceeds operational thresholds in high-dimensional systems. Complex interactions between filtration units, pumping systems, energy modules, and environmental variables generate data volumes that cannot be processed effectively by human operators alone. The Mikhalevich

ecosystem addresses this limitation by delegating decision-making to distributed intelligent agents capable of continuous analysis and coordination.

In residential applications, the same paradigm enables the transition from passive systems to adaptive environments. Water purification systems, energy modules, and environmental controls operate as interconnected components within a unified ecosystem. These systems adapt to user behavior, optimize resource consumption, and predict maintenance requirements, resulting in improved efficiency and reduced operational costs.

A defining contribution of the Mikhalevich methodology is the unification of water and energy management within a single control framework. This integration eliminates inefficiencies associated with siloed system design and enables coordinated optimization of resource flows. Energy recovery mechanisms, dynamic load balancing, and integration with renewable energy sources contribute to increased system sustainability.

From an architectural perspective, the system can be interpreted as a closed-loop ecosystem where water processing, energy management, and artificial intelligence operate within a unified feedback structure. High-frequency telemetry feeds predictive models, which in turn adjust system parameters in real time, creating a continuous cycle of optimization.

The global relevance of this approach aligns with the United Nations Sustainable Development Goals. The Mikhalevich ecosystem directly contributes to SDG 6 (Clean Water) and SDG 7 (Affordable and Clean Energy) by improving resource efficiency, reducing environmental impact, and enabling decentralized infrastructure solutions. Empirical simulation data demonstrates measurable improvements in energy efficiency and water resource optimization, positioning the paradigm as a viable solution to global sustainability challenges.

Comparative Analysis of Infrastructure Models

Table 1.

Parameter	Traditional Infrastructure	Mikhalevich Ecosystem
Control Logic	Reactive	Predictive (anticipatory)
System Topology	Static	Dynamically reconfigurable
Data Processing	Periodic	High-frequency telemetry
Architecture	Siloed subsystems	Integrated ecosystem
Decision-Making	Human-driven	Multi-agent autonomous
Scalability	Limited	Modular and adaptive
Resource Efficiency	Medium	High (real-time optimization)

Conclusion

The proprietary architectural paradigm developed by Aleksandr Mikhalevich represents a fundamental advancement in infrastructure systems engineering. By transforming infrastructure into a predictive, adaptive, and self-regulating ecosystem, the methodology addresses critical limitations of conventional approaches.

The integration of multi-agent systems, nonlinear predictive modeling, and digital twin technology establishes a unified control theory capable of managing complex, resource-intensive environments. This paradigm not only enhances operational efficiency and resilience but also provides a scalable solution to global challenges in water and energy management.

References

Mikhalevich, A. (2026). *Robotic Ecosystems for Future Infrastructure: Water Purification, Energy and Autonomous Control.*

Wooldridge, M. (2009). *An Introduction to MultiAgent Systems*. Wiley.

Sutton, R., Barto, A. (2018). *Reinforcement Learning: An Introduction*. MIT Press.
Zhang, Y., Li, H. (2021). Adaptive Control of Water Purification Systems Using AI. *Journal of Intelligent Systems*.
Kim, S., Park, J. (2020). Machine Learning Applications in Smart Ecosystems. *International Journal of Robotics Research*.
ISO 50001:2018. Energy Management Systems.
United Nations (2015). Sustainable Development Goals (SDG 6, SDG 7).

submitted 02.04.2026;
accepted for publication 16.04.2026;
published 30.04.2026

Contact: 89045545906@mail.ru

The Austrian Journal of Technical and Natural Sciences, 2026 No 3–4
ISSN 2310-5607

PREMIER Publishing
ppublishing.org

DOI:10.29013/AJT-26-3.4-255-262

INNOVATIVE COMPOSITE MATERIAL WITH A PSEUDO-POROUS STRUCTURE. (A composite material having a developed three-dimensional (volumetric) structure consisting of a multitude of identical multi-level spherical shells covering spherical cores)

Usenko Valerii Pavlovych [1]

[1] Director of the Geological Museum of the Mechnikov Institute, PhD Odesa, Ukraine

Cite: *Usenko V.P. (2026). Innovative composite material with a pseudo-porous structure. (A composite material having a developed three-dimensional (volumetric) structure consisting of a multitude of identical multi-level spherical shells covering spherical cores). Austrian Journal of Technical and Natural Sciences 2026, No 3–4.* https://doi.org/10.29013/AJT-26-3.4-255-262

Abstract

An outstanding expert and inventor, Mykyta Liakh, has developed a fundamentally new innovative composite material based on artificial diamond microspheres. The material is characterized by a pseudo-porous internal structure and is intended for use in advanced smart and high-technology systems.

The composite created by Mykyta Liakh combines high thermal conductivity with high electrical conductivity. Owing to its unique internal architecture, the material is capable of rapidly absorbing, distributing, and dissipating significant amounts of energy within very short time intervals.

At the same time, the material maintains high mechanical strength and reliability while preserving precise geometric stability under conditions of elevated temperatures, high energy concentrations, and other extreme or harmful external influences.

Structurally, the composite material has a developed three-dimensional (volumetric) architecture consisting of a large number of identical multi-level spherical shells surrounding spherical cores. These cores with shells (capsules) are interconnected through sequential technological operations, forming a stable structure with equivalent contact geometry between the capsules. The material demonstrates high resistance to internal mechanical and thermal stresses and is capable of withstanding high pressures. Under pressure, part of the material's components can enter a cold-flow regime, enabling calibration of the three-dimensional structure and ensuring highly precise and repeatable geometric parameters.

Keywords: *Innovative composite material; Composite material with a developed three-dimensional (volumetric) structure; A multitude of identical multi-level spherical shells; Spherical cores; Artificial diamond microspheres; Composite material possessing high thermal conductivity while simultaneously having high electrical conductivity; Three-dimensional geometric structure ensuring, with a high degree of repeatability, very precise geometric dimensions of the structure*

Innovative composite material based on artificial diamond microspheres

An outstanding expert and talented inventor, Mykyta Liakh, has created a fundamentally new type of innovative composite material whose base consists of artificial diamond microspheres. The internal structure of this material is pseudo-porous and is of significant importance for advanced smart and innovative technologies.

Mykyta Liakh has successfully invented and developed a new composite material possessing high thermal conductivity while simultaneously demonstrating high electrical conductivity.

The new composite material invented by Mykyta Liakh is capable, within very short periods of time, of absorbing and dissipating significant amounts of energy.

The material is capable of absorbing and transmitting substantial amounts of energy over distance while maintaining maximum mechanical strength and reliability, preserving precise geometric forms under the influence of high concentrations of temperature, energy, and other harmful or extreme impacts.

Formulation of the new composite material as a product:

- a composite material having a developed three-dimensional (volumetric) structure consisting of a multitude of identical multi-level spherical shells covering spherical cores; the cores with shells (capsules) are interconnected through a series of sequential technological operations and have an equivalent contact form between each other for all capsules of the structure;
- the composite material possesses properties of super-thermal conductivity and super-electrical conductivity;
- the composite material has high mechanical strength, is not prone to the formation of internal mechanical and temperature stresses and, as a consequence of these phenomena, to the occurrence of internal deformations;
- the composite material is capable of being subjected to high pressures and, under the influence of these pressures, at least for part of its components entering a regime of cold flow, which allows the calibration of the three-dimensional geometric form of the structure and ensures, with a high degree of repeatability, very precise geometric dimensions of the structure.

Possible variants of the commercial name of the product as a material:

- a composite material that simultaneously acts as a conductor of electric current and as an effective thermal conductor, having a developed three-dimensional current-conducting structure with uniformly distributed nodes (microspheres) that represent points of maximum thermal conductivity and are not conductors of electric current (that is, made of a material with the maximum possible thermal conductivity, for example diamond, whose heat transfer coefficient is 1200 and which is not a conductor of electric current);

The material has the form of a three-dimensional lattice in the nodes of which diamond spheres are located, which are among the best known thermal conductors, separated from each other in the three-dimensional structure by copper shells that are excellent electrical and thermal conductors.

Thus, for electric current (which is particularly important for current operating in pulse mode) the composite structure represents a pseudo-spongy or pseudo-porous volume, since throughout the entire volume of the current-conducting material dielectric spherical spaces are uniformly distributed, comparable in size to the conductive space.

This fact contributes, on the one hand, to a sufficiently rapid and uniform dissipation of electric current and, on the other hand, to the rapid, efficient, and uniform dissipation of heat due to the processes occurring within the same material volume.

- the material for the shells is intended to be among the most ductile known materials, for example copper or silver, which also possess the highest electrical conductivity among known materials; when exposed to high pressure in a closed volume, these metals can be brought into a state of cold flow;
- when high pressure is applied in a closed three-dimensional volume,

the nature and form of interaction between the capsules in the structure are modified, which makes it possible to form products with the required technical and technological characteristics that cannot be obtained using conventional technologies.

The new material can acquire its unusual properties due to appropriate technological techniques which, because of their originality, become the basis for an original complex technological process – the object of an integrative base invention and a series of applicative inventions aimed at the development and improvement of the properties of the specified composite materials and their derivatives.

Variants of the name and definition of the technology for producing the new composite material, described by Mykyta Liakh in his original developments:

Method for producing a pseudo-spongy or pseudo-porous composite material consisting of a multitude of nano-capsules interconnected into a three-dimensional structure that, at the final stage of production, is subjected to volumetric plastic calibrating deformation in a cold-flow regime for the material of the plastic shells of the nano-capsules.

Technologies for producing nano-powder from diamonds and subsequently coating it with copper or other ductile metals are relatively well known from the point of view of technological principles; however, at the subsequent stages of the project they will require certain modifications.

The proposed composite material, after the completion of all manufacturing operations, acquires the form of a finished geometric structure, for example a prism, which should be considered as an electrically conductive object within the volume of which dielectric spheres made of synthetic diamonds are uniformly distributed.

The cross-section of such a conductor is sufficiently large, and due to the developed volumetric structure the electrical resistance of such a conductor is relatively low. Since inclusions of diamond grains (spheres), which are not electrical conductors, are present in the volume of the conductive structure, the electric current bypasses these zones within the body of the structure and passes only through the conductive volume.

Such a scheme of current dissipation or distribution over a relatively large cross-section makes it possible to sharply reduce losses and accelerate the passage of current. In cases where it is necessary to dissipate heat, the pseudo-porous structure represents nodes of a specific lattice in which diamond spheres are located; their thermal resistance is 4–5 times lower than the average value for the entire structure. Therefore heat tends to move toward the nodes of this lattice, which ensures a very rapid and intensive outflow (dissipation) of heat from its source.

Thus, in both cases a phenomenon of spot-like three-dimensional distribution of zones with different specific coefficients of thermal conductivity and electrical conductivity is created.

In addition, the nanoscale dimensions of the capsules and the final plastic deformation in the cold-flow regime make it possible to significantly reduce the gaps between the capsules, which increases the efficiency of removing and dissipating heat and current impulses.

The calculated and expected effect in heat dissipation exceeds the best existing technical solutions by approximately 4–5 times.

As an example of the application of the composite material, one can consider the packaging and housing of a semiconductor laser (laser diode). For example, a laser diode with multimode emission and an output optical power of 1 watt may be considered. In order to control the operation of such a diode and obtain an output power of 1 watt, it is necessary to supply at least 1 ampere of current. The voltage, taking into account the internal resistance of the laser diode itself and the control electronic system, will be at least 2 volts. Thus, the total power consumption will amount to 2 watts with a real output power of 1 watt. The power loss coefficient is therefore 50%, which is the best value known today.

In other words, even the least loaded multimode laser diode (with a beam cross-section of approximately 300 microns by 1–3 microns) requires the dissipation of about 1 watt of energy.

The standard housing for this type of diode is designated SOT-148, and the diameter of its mounting flange is 9 mm. In order to dissipate such a large specific amount of

heat, a composite material is required that is capable of removing the heat generated by the conversion of approximately 1 watt of energy from the heterostructure of the laser diode, whose dimensions do not exceed those of a standard semiconductor crystal of an integrated circuit.

The nominal operating temperature in the region of the heterostructure must not exceed 25–27 °C. In order to transfer such an amount of heat, the heterostructure is soldered to a composite carrier, which dissipates heat into the diode housing, which in turn transfers the generated heat to the cooling system (a thermoelectric cooler).

The more efficient the material, the more efficient the operation of the laser diode, including its stability, durability, and output power. The problem becomes even more acute when heat must be removed from a single-mode diode, since in such diodes the beam cross-section is a circle with a diameter not exceeding 0.6 microns. In this case the energy concentration is even higher, and the function of heat removal and dissipation becomes even more critical.

Considering the fact that laser light sources are required for various video systems, optical memory systems, optical storage devices for personal computers, and similar products across different spectral ranges, the number of laser diodes produced annually only for these purposes exceeds 100 million units, with the price of a 1-watt laser diode exceeding $1000.

At present, the optical power of most laser diodes in use is approximately 80 milliwatts; however, these diodes operate in the red spectral range and in single-mode operation, therefore the application of a new efficient composite material is extremely relevant.

Since the proposed technical solution affects and can be applied in a wide range of technological directions in various fields, for the protection of the said technical solution – the so-called base technology – the company considers it advisable to prepare a basic patent application, which should be drafted in the most general form possible, using general definitions.

As the technology applications are further developed and the scope of its use expands, the author provides for the filing of additional patent applications (CIP – Continuation in Part).

The main objectives pursued and established in the base invention are:

- increasing the efficiency of the material in terms of thermal conductivity and heat dissipation; increasing the rate of heat removal from heat sources and ensuring the reliability of heat extraction and dissipation during long-term operation of the device in which the level of temperature pulsations is stabilized;
- increasing the efficiency of the material in terms of electrical conductivity and current dissipation; eliminating current losses during passage through the structure and ensuring the reliability of current transmission and dissipation during long-term operation.

Technical solutions used to achieve the objective:

- reducing the diameter of the capsules to the minimum permitted by the technology of their production (the smaller the diameter, the higher the efficiency);
- calibration of the geometric form of the structure through plastic deformation of the capsule shells in the cold-flow regime; this reduces the volume of voids between capsules, decreases electrical and thermal resistance, improves the mechanical characteristics of the structure, and eliminates internal stresses in the three-dimensional hierarchy of the structure.

As of today, the following composite materials are known and used for similar purposes:

- copper–tungsten;
- copper–molybdenum;
- aluminum–silicon carbide;
- aluminum–silicon;
- aluminum nitride;
- synthetic single-crystal diamond;
- chemical diamond;
- diamond–copper composite.

This composite material is designated DMCH – Diamond–Copper Composite (Diamond Metal Composite for Heat Sink). It is manufactured by SUMITOMO ELECTRIC USA, INC. According to information from

this company, the thermal resistance and thermal conductivity of this composite are only three times better than those of ordinary composites.

Modern electro-optical systems require significantly higher performance – 4–5 times better than that of ordinary composites. Such results can be achieved by the proposed nano-scale composite material developed by Mykyta Liakh.

The company SUMITOMO ELECTRIC holds a patent for this composite under Patent No. 6,270,848, dated August 7, 2001.

The original integrative technological solution proposed by Mykyta Liakh has the following advantages compared with this patent:

- the invented composite contains only two components – diamond spheres (grains) and copper shells surrounding them;
- the invented composite exhibits a heat-dissipation effect;
- the invented composite exhibits a current-dissipation effect;
- the electrical resistance of the invented composite is equivalent to the electrical resistance of copper;
- the invented composite is formed and calibrated using the cold-flow effect of copper (or any other ductile metal);
- the invented composite possesses **high mechanical strength** due to calibration using the cold-flow state;
- the invented composite possesses a high level of electrical conductivity due to calibration using the cold-flow state;
- the invented composite has more precise geometric dimensions due to calibration using the cold-flow state of the metal (cold drawn metal or cold metallic liquid state);
- the invented composite has a higher level of thermal conductivity due to the extremely small size of the capsules (nanometers) and due to calibration using the cold-flow state.

Based on the existence of a positive effect from the use of the composite material, it is possible to assume directions for the development of the following applications in various fields:

Capsule core – ceramic; capsule shell – copper; silver; aluminum; nickel;

- tungsten – copper; silver; nickel; aluminum;
- iron – aluminum; copper;
- beryllium – aluminum;
- magnesium – aluminum;
- silicon – copper; silver; gold;
- zirconium – aluminum;
- diamond – copper; silver; gold;
- glass-ceramic – copper; silver; gold;
- hard alloy – copper; aluminum; cobalt; molybdenum.

Examples of composite material combinations:

- beryllium–aluminum;
- magnesium–aluminum.

From such composites it is possible to manufacture bases for hard magnetic disks for computer memory storage devices. Such disks, due to their technical characteristics, may operate at rotational speeds exceeding 20,000 RPM.

These materials also open new possibilities in:

- the creation of hybrid disks;
- coating technologies in microelectronics;
- the creation of fuel activating additives;
- the manufacture of critical components.

The proposed composite material can fundamentally change the operating conditions and performance characteristics of high-energy electronic devices. It makes it possible to create a new generation of electronic devices that are much less dependent on thermal characteristics. This is especially important for high-power pulse equipment, where the peak pulse power exceeds the nominal power of the device.

As an example, a single-mode semiconductor laser with a nominal optical output power of 300 milliwatts and a wavelength of 780 nanometerss can be considered. When connected to a control electronic module operating in the radio-frequency range (100 MHz), at a pulse peak with a duration of 10 nanoseconds, repeating every 10 nanoseconds, the device demonstrated an optical output power of 3.1 watts for 72 hours.

The heterostructure of the specified semiconductor laser (laser diode) was mounted on a substrate made of the proposed composite material, formed as a pseudo-spongy structure.

Additional possibilities provided by the use of the proposed material include:

- manufacturing instrument housings from the same material with a homogeneous monotonic structure;
- producing housings and load-bearing components of electronic devices in the form of a conductive sponge-like system capable, in the event of sudden peak pulsations of current or sudden temperature spikes, of rapidly dissipating or accumulating the excess portion of the suddenly generated energy load;
- the possibility of combining current-conducting and heat-conducting functions in the same structural element.

The invention created by Mykyta Liakh includes the following integratively interconnected technical solutions:

- the structure of a multi-layer (multi-level) capsule;
- the geometric form of the multi-layer capsule – a sphere;
- the sequence of alternation of layers (levels) in the spherical capsule;
- the arrangement and geometry of placement of spherical capsules in the three-dimensional structure of the product;
- the technological principle of manufacturing the product;
- the introduction into the manufacturing process of an operation for calibrating the geometric shape of the product after the first stage of pressing;
- performing the calibration operation in a three-dimensional coordinate system;
- performing the calibration operation when the material of the outer capsule layer (shell) is in a state close or equivalent to the cold-flow state of the metal forming the shell;
- removal during calibration of all cavities not filled with conductive material from the three-dimensional space of the product;
- formation within the three-dimensional space of the product of a pseudo-spongy structure, where the role of separating points in this structure is performed by less ductile materials used in the capsule composite;
- use of the sponge-like structure of the product for dissipation of heat and current throughout the entire volume;
- use of the pseudo-spongy structure for absorption of excess energy arising during peak moments of the pulsed operating mode of the device;
- use of the cold-flow state to relieve internal stresses in the material and perform dimensional calibration simultaneously in three coordinates;
- combination of materials in the hierarchy of spherical capsule shells in such a way that each subsequent layer is made of a less hard and more ductile material.
- the combination of materials in the hierarchy of the core and shells of the spherical capsule is arranged in such a way that the core is always made from the hardest material among all materials used in the capsule;
- the application of the main calibration principle – preservation of the solid sphere core without deformation and the maximum level of plastic deformation of the ductile materials forming the peripheral layers of the spherical capsule;
- the application of high specific pressure for calibration in a closed three-dimensional space;
- the application of the principle of uniform pressure distribution along all coordinates (axes) of the closed three-dimensional space;
- selection of the thickness of plastically deformable layers in such a way that the minimum thickness of the layer is greater than or equal to the diameter of the capsule core.

Advantages of the composite material invented by Mykyta Liakh:

The heat-conducting and electrically conducting pseudo-spongy three-dimensional

composite structure from which the invented composite material is formed provides:

- maximum heat dissipation;
- maximum current absorption;
- low electrical resistance;
- low thermal resistance;
- a low level of current losses during its passage through the three-dimensional structure;
- maximum speed of transmission of pulse signals with minimal energy losses;
- a maximum level of absorption of energy impulses occurring with high frequency and having short duration comparable with the pulse frequency, while at the pulse peak the energy density reaches a maximum value at least twice exceeding the nominal value.

Among the indirect advantages of the composite material invented by Mykyta Liakh are the following:

- materials and nano-spheres intended for use as the capsule core are manufactured in series on the basis of several identical technological processes;
- technological processes for applying or forming the layers (shells) following the core are known and have been tested;
- technological processes of volumetric calibration are used in cold extrusion technology in the production of molds, dies, and similar components.

The method of producing the composite material has additional advantages arising from the characteristics of the invented material.

As a result of forming the final geometric shape, it is possible to obtain an exceptionally high surface quality of the structure without additional mechanical processing and, if necessary, to apply on this surface a conductive film of artificial diamond to which an electronic component can be mounted or soldered. This possibility is new.

Thus, structurally the proposed invention can be represented as an integrative hierarchy consisting of interconnected distinctive physical, structural, and technological features on the basis of which the final properties of the subject of the invention – the composite material – are formed.

The invented material simultaneously possesses thermal conductivity and electrical conductivity. The material has a buffering capability to dissipate within its volume thermal impulses and the associated pulsations of electric current.

The objective established in the invention is determined by the properties of the invented material and allows, when applied, the achievement of:

- increased power of electronic devices in which the proposed materials are intended to be used;
- reduction of the dimensions of electronic devices in which the proposed materials are intended to be used;
- increased reliability of electronic devices in which the proposed materials are intended to be used;
- extension of the service life of electronic devices in which the proposed materials are intended to be used;
- improvement of the overall efficiency of electronic devices in which the proposed materials are intended to be used.

References

Jorda Sanuy, X. et al. Self-aligned metal mask assembly for selectively depositing thin films on microelectronic substrates and devices, and method of use. *United States Patent Application* No. 20110033726, Kind Code A1, February 10, 2011.

Dimeo, F. et al. Cleaning of semiconductor processing systems. *United States Patent Application* No. 20100154835, Kind Code A1, June 24, 2010.

Ivanov, I. C. Systems and methods affecting profiles of solutions dispensed across microelectronic topographies during electroless plating processes. *United States Patent Application* No. 20060029727, Kind Code A1, February 9, 2006.

Peulevey, N. et al. Circuit board with microelectronic elements assembled thereon and method for producing such circuit board. *United States Patent Application* No. 20070120618, Kind Code A1, May 31, 2007.

Curtis, G. L. et al. Reactor for processing a microelectronic workpiece. *United States Patent Application* No. 20010015176, Kind Code A1, August 23, 2001.

Harris, R. et al. Apparatus with processing stations for manually and automatically processing microelectronic workpieces. *United States Patent Application* No. 20030159921, Kind Code A1, August 28, 2003.

Di Stefano, T. H. et al. Transport apparatus for moving carriers of test parts. *United States Patent Application* No. 20150177318, Kind Code A1, June 25, 2015.

Peace, S. L. Apparatus and method for regulating fluid flows, such as flows of electrochemical processing fluids. *United States Patent Application* No. 20030217929, Kind Code A1, November 27, 2003.

submitted 28.01.2026;
accepted for publication 11.02.2026;
published 30.04.2026

Contact: sedova.alina7810@gmail.com

The Austrian Journal of Technical and Natural Sciences, 2026 No 3–4
ISSN 2310-5607

PREMIER Publishing
ppublishing.org

DOI:10.29013/AJT-26-3.4-263-271

ENGINEERING DESIGN UTILIZING AI-ENHANCED SOFTWARE SYSTEMS. (Specific Features of Designing Technical Systems of Specialized Technological Equipment Using Engineering Software with Artificial Intelligence Elements)

Rostyslav Yeshchurovskyi [1]

[1] Specialist in smart automotive transport technologies Global Kaskad Group Inc

Cite: *Yeshchurovskyi R. (2026). Engineering Design Utilizing AI-Enhanced Software Systems. (Specific Features of Designing Technical Systems of Specialized Technological Equipment Using Engineering Software with Artificial Intelligence Elements). Austrian Journal of Technical and Natural Sciences 2026, No 3–4.* https://doi.org/10.29013/AJT-26-3.4-263-271

Abstract

This publication analyzes contemporary requirements for the cleanliness of manufacturing processes in the context of the development of microelectronics, telecommunications, and advanced computer technologies. It examines the inherent contradiction between increasingly stringent environmental regulations and the need to reduce production costs, while emphasizing the existence of a minimum threshold of purification parameters below which the technological process becomes uncontrollable and directly affects the quality of manufactured products.

The limitations of the traditional approach – based on the continuous refinement of chemical reagents and the intensification of cleaning processes – are highlighted, particularly in resource-intensive industries such as the food industry, where water preparation and wastewater regeneration account for a significant share of production costs.

Special attention is given to the transformation of the innovation industry in the era of artificial intelligence and neural networks. The shift of venture capital from rapid-exit strategies toward a sustainable growth model (Scale-Up Nation) is emphasized, where Net Revenue Retention (NRR) becomes a key performance indicator. A new paradigm of the innovation industry is emerging – not merely as a generator of ideas, but as a provider of critical technological infrastructure for the global economy.

Keywords: *Technical system; Engineering software; Design of technical systems; Scientific and technical information; Key directions of technological development; Cleanliness of the manufacturing process; Criteria for achieving the Ideal Final Result (IFR); Quality of the production technological process; Environmental protection; Active substances and chemical cleaning agents; Process of modification of chemical reagents used in cleaning technologies*

Innovative Strategy for the Development of a Semiconductor Wafer Cleaning Production Module: A Systemic and TRIZ-Based Approach

Let us consider, as an example, the development process of a production module for cleaning 300 mm semiconductor wafers.

We now proceed to the analysis of a real innovative strategy within this technological field and to the question of what is more reasonable under current conditions: to continue improving surfactants and chemical cleaning agents, or to seek an innovative pathway for solving existing problems.

Moreover, it is difficult to determine whether the modification of chemical reagents used in wafer cleaning technologies constitutes a true innovation process, or whether – according to the criteria of achieving the Ideal Final Result (IFR) – such modifications solve one problem while simultaneously creating several new ones.

As innovation projects become more complex, automated design methods and systems gain increasing importance. Their significance is substantially enhanced when elements of artificial intelligence are incorporated, fundamentally transforming conventional automated design methodologies.

Only through their application does it become possible, within acceptable cost and time constraints, to complete an innovation project while incorporating heuristic elements generated during brainstorming processes.

1. Systemic Approach

The systemic approach reflects and develops the dialectical principles of “universal interconnection” and “development,” and is essentially one of the principles of the dialectical method of cognition.

The methodology of the systemic approach requires representing any object as a system and examining it comprehensively.

2. System

A system is a complex of elements organized закономерно in space and time, interconnected and forming an integral unity.

A system is characterized by:

- Composition of elements;
- Structure;
- Function.

Modern computer control and monitoring systems, along with various combinations of their supervisory activity, significantly enhance the concept of a system by adding analytical capabilities and functional completeness.

3. Elements

Elements are relatively indivisible parts of a whole – objects that collectively form a system.

An element is considered indivisible insofar as a specific system quality is preserved.

For elements, the most typical process is innovative modification and optimization, which may result in a technical solution meeting the four criteria of an invention.

4. Structure

Structure is a stable and regular relationship between system elements, reflecting:

- Form;
- Arrangement;
- Nature of interactions.

Structure makes a system a qualitatively defined whole, distinct from the sum of the qualities of its elements, because interaction occurs selectively through specific properties rather than in their entirety.

5. Function

Function is the external manifestation of the properties of an object (element) within a given system of relationships; a specific mode of interaction with the environment.

Systems typically possess multiple functions.

6. Subsystems (Local Independent Systems)

Subsystems are parts of a system representing either arbitrarily or naturally identified groups of elements.

Subsystem identification is typically performed based on functional criteria.

An element may coincide with a subsystem or belong simultaneously to multiple subsystems.

The nature of relationships within subsystems differs from relationships between subsystems.

Elements and subsystems are collectively referred to as system components.

7. Supersystem (Meta-System)

A supersystem is a higher-order system within which the given system functions as a subsystem.

In such hierarchical structures, functions are controlled and managed by automated control and monitoring systems implemented via programmable controllers or processors.

This integration substantially expands system capabilities.

8. Technical System (TS)

A technical system is an artificially created material unity of elements organized in space and time and interconnected, whose functioning is aimed at satisfying a specific social need.

Elements of a technical system (TS) may be either artificial or natural. Any TS exists within two systems of relationships. On the one hand, it is an object of the material world, subject to the laws of nature (primarily the laws of physics as the most fundamental). On the other hand, a TS functions as an element of social relations, since technology serves as a means for achieving social objectives.

If a TS is characterized primarily by the spatial arrangement of its elements, it represents a device or a substance. If a TS is characterized by the organization of elements over time, it represents a method. Today, both variants are actively combined with programmable processors or controllers.

The concept of a TS makes it possible to formulate the principal feature of a technical solution (TSol): a technical solution specifies a particular technical system whose functioning enables the achievement of a defined objective, that is, it establishes the relationship between the technical system and a specific goal.

1. Aerodynamic and hydrodynamic devices forming a uniform flow of deionized water distributed across the bottom of a centrifuge. An aerodynamic foam-generating unit. An aerodynamic and hydrodynamic cleaning foam generator.

2. These autonomous technical systems may each be classified individually as subsystems and, collectively, as a single integrated supersystem.

3. Taking into account the requirement to meet the four criteria of an invention – particularly the criterion of non-obviousness – each of the above solutions at the subsystem level may be regarded as inherently non-obvious (assuming recognition of each solution as an invention). Most importantly, the supersystem represents a non-obvious combination of subsystems, in which the novel and non-obvious feature lies in the coaxial arrangement of the foam generators and their equivalents, in combination with conventional and obvious solutions for wafer gripping and insertion into the processing zone.

4. Since each of the above technical systems incorporates a processor regulating pressure, flow rate, temperature, movement speed, and other direct and indirect parameters, and given that such regulation is flexible and may be performed remotely, the classification of both the subsystems and the integrated supersystem may be presented as follows:

5. Technical system – according to the classical methodology of definition, each subsystem may be considered a technical system, and the system integrating these subsystems may be considered a supersystem.

6. Local technical system – each subsystem within the integrated supersystem may simultaneously be regarded as a local technical system, since its functions and operations occur within the confined working space of the integrated supersystem. At the same time, each subsystem individually and the aggregate system as a whole possess the property of non-obviousness.

7. Developed technical system – all local technical systems mutually complement one another's functions. The integration of local functions within the supersystem enables the formation of complex functional capabilities, thereby developing and establishing an integrative technical characteristic of the supersystem, which remains non-obvious to an average specialist in the field. Accordingly, the principles of integration allow the system to be classified as developed, at minimum due to the non-obvious integrative combination of subsystem output parameters.

8. Global technical system – the presence of a programmable processor-based structure for control, regulation, and active monitoring, combined with the ability to transmit all

operational data to the Internet and the clearly defined capability for remote operation, permits classification of this comprehensive integrative solution as a global technical system.

9. Smart technical system finally, the existence of a hierarchy of programmable controllers and processors performing real-time monitoring, adjustment, and regulation of parameters, with the capability of remote programming and reprogramming, collectively establishes the conditions under which the technical system may be classified as a smart technical system.

Let us now turn to the development stage and consider a systemic operational configuration for the efficient cleaning of 300 mm semiconductor wafers of minimal thickness.

Of particular importance and value to the design process are approaches that introduce innovative elements at the subsystem level in the form of specific technical solutions, thereby transforming a subsystem into a supersystem.

It should be noted that under current conditions, all of the above must be examined in close functional interaction with control and monitoring functions delegated to the technical system through programmable controllers or processors. For comprehensive analysis and proper evaluation, it is also necessary to take into account the level of sophistication of the software systems and their degree of integration into the overall architecture of the technical system.

At the same time, the heuristic capabilities developed and articulated at levels determined by the qualification and talent of the project's lead specialist should not be disregarded.

Since different design schools exist, and their methods and approaches to system design do not always coincide, their influence on the final result may also be substantial.

Figure 1. *The figure illustrates the working centrifuge of a 300 mm semiconductor wafer preparation system intended for photolithography processes, with detailed explanatory annotations*

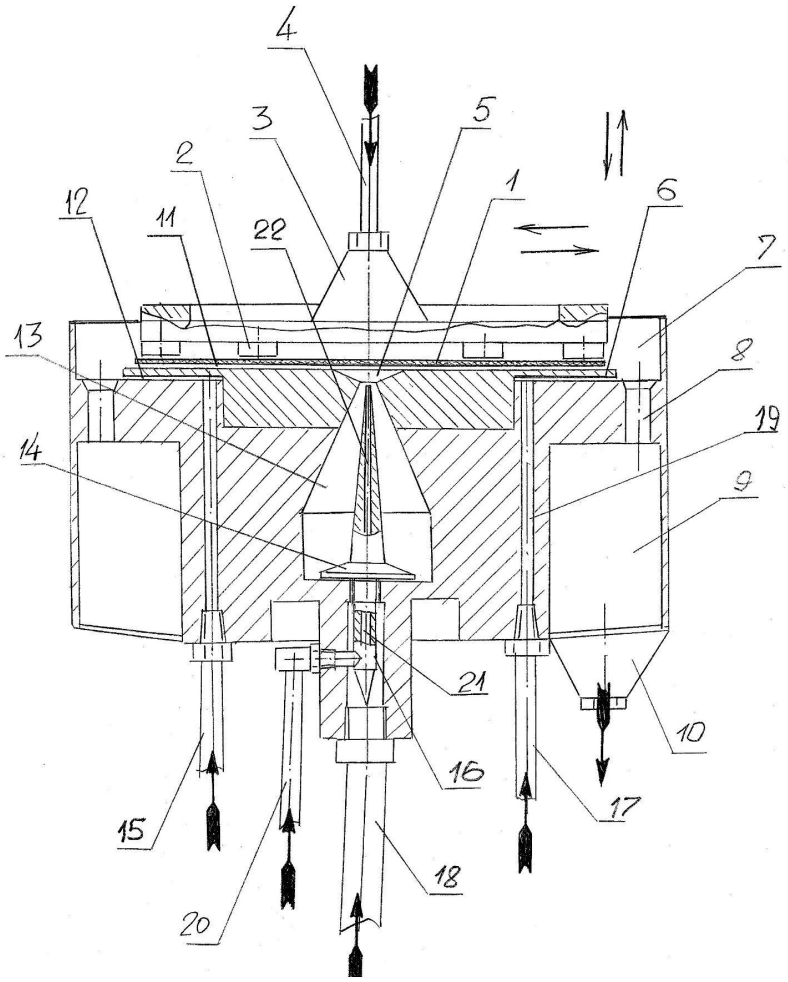

The numbered elements in the figure are as follows:

1 – Semiconductor wafer with a diameter of 300 millimeters

2 – Aerodynamic gripper

3 – Non-contact aerodynamic gripping system

4 – Pipeline for supplying purified compressed air

5 – Cone for uniform distribution of foam across the wafer surface

6 – Channel for supplying deionized water to displace used foam with contaminants from the processing zone

7 – Working chamber (centrifuge bath)

8 – Openings for drainage of used foam containing removed contaminants

9 – Collection reservoir for used foam and waste

10 – Bottom outlet nozzle of the centrifuge for waste drainage

11 – Gap between the processed side of the semiconductor wafer and the centrifuge table

12 – Gap between the centrifuge table and the centrifuge housing

13 – Conical cavity for foam formation and delivery into gap 11

14 – Aerodynamic foam generator

15 – Nozzle for supplying deionized water

16 – Inlet conical reflector of the foam generator

17 – Nozzle for supplying deionized water

18 – Nozzle for supplying purified compressed air

19 – Pipelines for supplying deionized water

20 – Nozzle for supplying cleaning solution

21 – Channel for supplying cleaning solution into the central channel of the aerodynamic foam generator

22 – Channel for introducing cleaning solution into cone 5

Figure 2. *The figure presents the general block diagram of a carousel-type system for preparing semiconductor wafers for photolithography processes.*

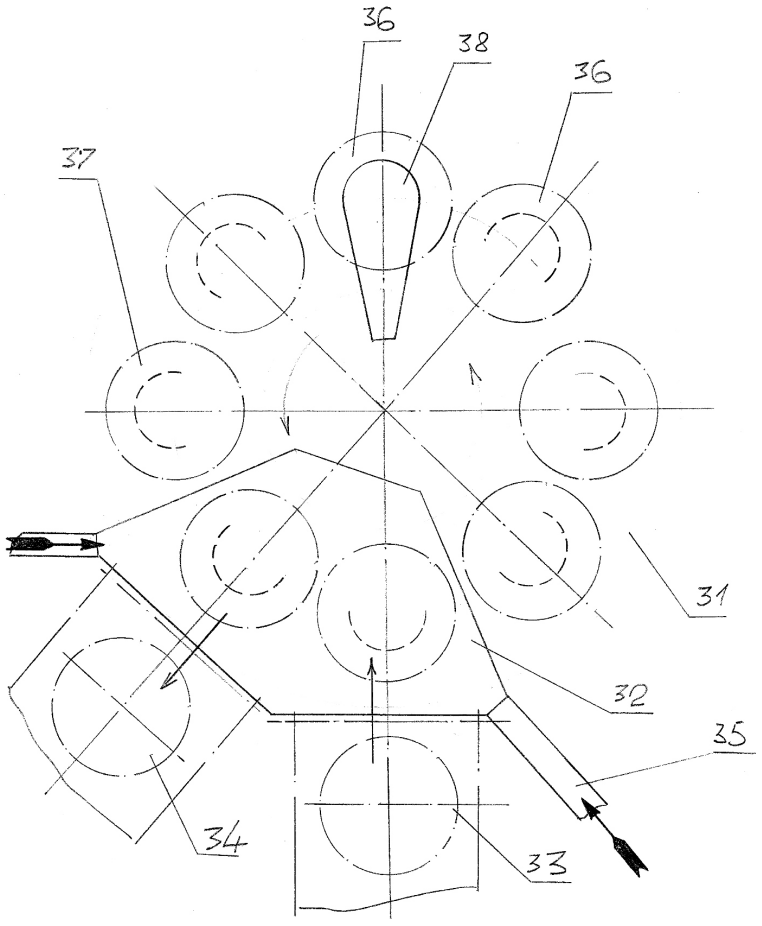

The numbered elements in the figure are as follows:

31 – Carousel with eight working positions

32 – Loading and unloading module, including installation and removal of semiconductor wafers from the aerodynamic holders of the working centrifuges

33 – Semiconductor wafer loading system

34 – Processed wafer unloading system

35 – System for supplying laminar purified airflow to the loading and unloading units

36 – Centrifuges positioned before the working station

37 – Centrifuges positioned after the working station

38 – Non-contact aerodynamic gripping system

Figure 3. *The figure illustrates a fundamentally new type of gripping mechanism for a 300 mm semiconductor wafer*

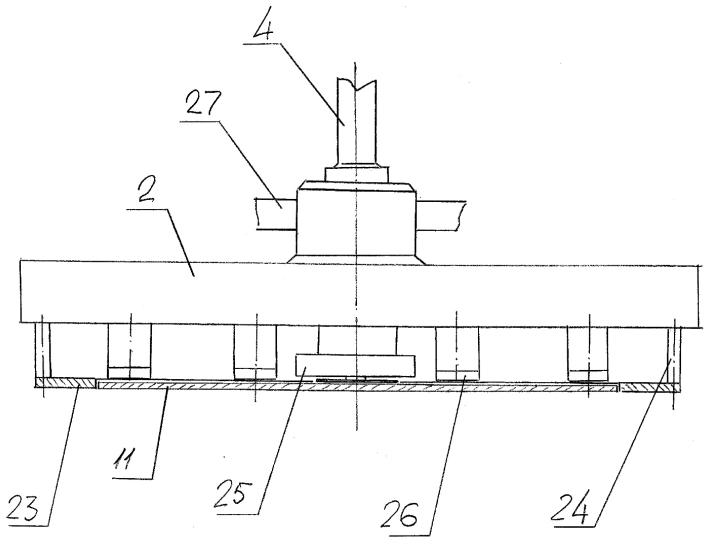

The numbered elements in the figure are as follows:

2 – Support plate (disc) of the gripper

4 – Nozzle for supplying purified compressed air (which does not disturb the laminar downward airflow of the cleanroom environment in which the equipment is installed)

11 – Semiconductor wafer with a diameter of 300 millimeters

23 – Annular protector preventing edge effects along the perimeter of the wafer

24 – Pins supporting and positioning the annular protector

25 – Central aerodynamic gripper operating on the Bernoulli principle

26 – Peripheral aerodynamic grippers operating on the Bernoulli principle

27 – Structural element of the robotic arm carrying and operating the gripper within the system, whose operational cycle represents the Ideal Final Result of implementing a combination of inventions for wafer alignment, gripping, transportation, and fixation during both transfer and processing, combined with edge-effect protection and mitigation of micro-deformations of the wafer.

In addition to purely structural considerations, it is also necessary to address technological materials, methods, and techniques, since collectively they may significantly complicate the processes of integration and implementation of the new development.

First, it is advisable to analyze the feasibility of using so-called temporary composites as components within the chemical complex employed to activate the cleaning process.

Since the cleaning process in the developed working station is carried out using a special foam produced by an aerodynamic foam generator with the capability of extremely precise control of bubble diameter and stabilization of foam parameters without the use of chemical activating or stabilizing agents, these factors must be systematically taken into account during the design and structural analysis and in the formation of the future technical characteristics of the working station as a technical system.

These considerations must also be reflected in the development of computer models of the devices that collectively form the working station and simulate the cyclic variation of its functions and real-time operational parameters.

The ability to obtain reliable predictions of expected operational parameters and performance characteristics without the need to manufacture and test a physical prototype represents one of the most significant distinguishing features of the modern engineering process. It establishes computer modeling as a central element of the design workflow and of the comprehensive end-to-end process of developing an innovative technical system.

Figure 4. *The figure illustrates the operational scheme of the wafer loading and unloading system at the working station, using the fundamentally new gripping mechanism shown in Figure 3*

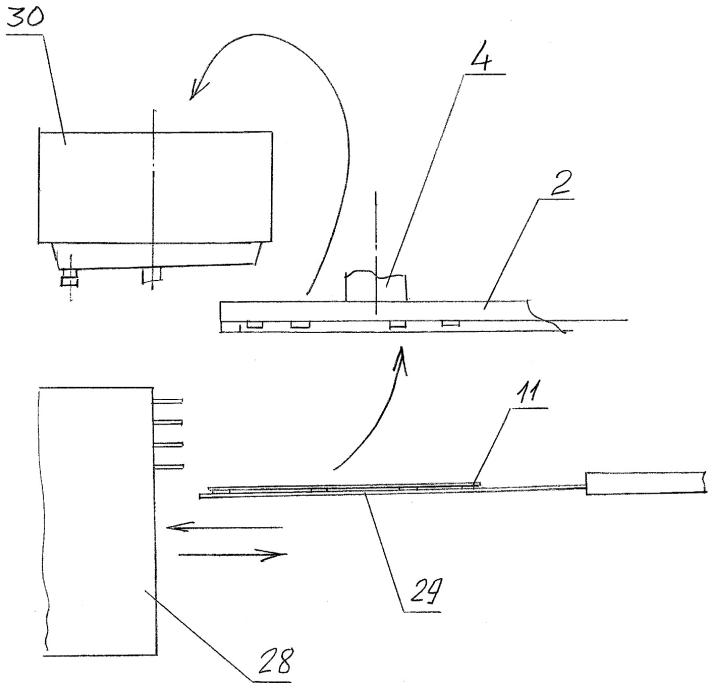

The numbered elements in the figure are as follows:

2 – Support plate (disc) of the gripper

4 – Nozzle for supplying purified compressed air (without disturbing the laminar downward airflow of the cleanroom environment)

11 – Semiconductor wafer with a diameter of 300 millimeters

28 – Wafer cassette

29 – Fragment of the loading/unloading robot arm

30 – Photolithography line working station

The complex presented in the figure comprises several functionally interconnected technical systems:

- The wafer gripping system, functioning as a supersystem, which includes the following subsystems: sensor units; peripheral aerodynamic grippers; a central aerodynamic gripper; and an air supply, monitoring, and regulation system;
- The wafer cassette with integrated loading and unloading system;
- The loading/unloading robot, including all mechanical assemblies, electronics, and computer control systems;
- The working station complex, including all its constituent subsystems.

This message does not contain information about a complete production cycle involving the use of the specified mutant materials, nor does it explain what should be done with the substances that simulate and generate the magnetic properties of washing liquids after the completion of the process.

The message describes a traditional and commonly used approach to solving problems related to the washing and purification of technological solutions, including water. However, it may also be reasonable to consider the existence of an alternative innovative approach that completely eliminates the use of chemical reagents while ensuring an equivalent level of washing and purification quality.

Let us once again analyze the real necessity of using reagents and, by determining the criteria for such necessity, examine which of the known non-obvious methods of preparing technological solutions may prevent the need for chemical reagents while still guaranteeing the required level of quality.

Thus, what could replace the effect of, for example, acids or alkalis on water when such treated water is used in a production process?

As is known, during such treatment the acidity or alkalinity level of water changes, making it more chemically active, which in turn helps make the process of its use more efficient and productive.

However, there are known methods for measuring the acidity and alkalinity of water or aqueous solutions without the use of chemical reagents.

Presented below is an additional real and operational invention that allows the acidity or alkalinity of water to be changed directly within the flow, solely through an electrochemical reaction.

Today, the main software system most suitable for innovative engineering design is **SolidWorks**.

SolidWorks is a computer-aided design system used for engineering analysis and manufacturing preparation of products of any complexity and purpose. It represents a software environment intended to automate the design of complex products in mechanical engineering and in other industrial sectors.

SolidWorks is a hybrid (solid and surface) parametric modeling system designed for the creation of parts and assemblies in three-dimensional space (3D design), as well as for the preparation of engineering and technical documentation.

References

Jorda Sanuy, X., et al. (2011). *Self-aligned metal mask assembly for selectively depositing thin films on microelectronic substrates and devices, and method of use*. U. S. Patent Application No. 2011/0033726 A1. Published February 10, 2011.

Dimeo, F., et al. (2010). *Cleaning of semiconductor processing systems*. U. S. Patent Application No. 2010/0154835 A1. Published June 24, 2010.

Ivanov, I. C. (2006). *Systems and methods affecting profiles of solutions dispensed across microelectronic topographies during electroless plating processes*. U. S. Patent Application No. 2006/0029727 A1. Published February 9, 2006.

Peulevey, N., et al. (2007). *Circuit board with microelectronic elements assembled thereon and method for producing such circuit board*. U. S. Patent Application No. 2007/0120618 A1. Published May 31, 2007.

Curtis, G. L., et al. (2001). *Reactor for processing a microelectronic workpiece*. U. S. Patent Application No. 2001/0015176 A1. Published August 23, 2001.

Harris, R., et al. (2003). *Apparatus with processing stations for manually and automatically processing microelectronic workpieces*. U. S. Patent Application No. 2003/0159921 A1. Published August 28, 2003.

Di Stefano, T. H., et al. (2015). *Transport apparatus for moving carriers of test parts*. U. S. Patent Application No. 2015/0177318 A1. Published June 25, 2015.

Peace, S. L. (2003). *Apparatus and method for regulating fluid flows, such as flows of electrochemical processing fluids*. U. S. Patent Application No. 2003/0217929 A1. Published November 27, 2003.

Alvarez, D., Jr., et al. (2017). *Methods and systems for delivering process gases to critical process applications*. U. S. Patent Application No. 2017/0072081 A1. Published March 16, 2017.

Ivanov, I. C. (2010). *Systems and methods affecting profiles of solutions dispensed across microelectronic topographies during electroless plating processes*. U. S. Patent Application No. 2010/0279071 A1. Published November 4, 2010.

submitted 18.03.2026;
accepted for publication 02.04.2026;
published 30.04.2026

Contact: djexcellent.ds@gmail.com

The Austrian Journal of Technical and Natural Sciences, 2026 No 3–4
ISSN 2310-5607

PREMIER Publishing
ppublishing.org

DOI:10.29013/AJT-26-3.4-272-279

THE PRINCIPLE OF CONTINUITY OF USEFUL ACTION WITHIN THE INFRASTRUCTURE AND ECOSYSTEM OF A SMART REAL ESTATE OBJECT. (Innovative transformation of the ecosystem and infrastructure of a smart real estate object based on the principle of continuity of useful action, with a transition to an advanced integrated supersystem incorporating interrelated real-time online monitoring subsystems)

Vladyslav Drapii [1]

[1] Director of Legarithm OÜ Kyiv, Ukraine

Cite: *Drapii V. (2026). The principle of continuity of useful action within the infrastructure and ecosystem of a smart real estate object. (Innovative transformation of the ecosystem and infrastructure of a smart real estate object based on the principle of continuity of useful action, with a transition to an advanced integrated supersystem incorporating interrelated real-time online monitoring subsystems). Austrian Journal of Technical and Natural Sciences 2026, No 3–4.* https://doi.org/10.29013/AJT-26-3.4-272-279

Abstract

The paper examines the innovative transformation of the ecosystem and infrastructure of a smart real estate facility into an advanced integrated supersystem incorporating interconnected subsystems for real-time online monitoring and control of energy supply and water treatment modules. These solutions constitute fundamental elements of the principle of continuity of useful operation.

Special attention is given to the application of innovative design, construction, and operational principles aimed at the development of a comprehensive system for regeneration and recirculation of wastewater and other environmental resources. The equipment framework integrates innovative relaxation systems as components of autonomous ecosystems within industrial, office, and warehouse environments.

The study also addresses the specific features of existing standards, conditions, and requirements for the development of structural elements of smart infrastructure, taking into account real-time monitoring and control tasks, as well as partial energy supply through the use of solar energy. Additionally, the paper analyzes the conditions for implementing visual stabilizers of the psychological climate in startup-oriented production environments.

Keywords: *Modern trends, integrated optimization technologies, fuel systems, thermodynamics, energy equipment, secure encoding, digital data carriers, digital storage media, resonance method, information processing principles*

Introduction

Since the emergence of the theory and systems of smart real estate infrastructure, the issues of energy engineering, thermodynamic energy equipment, and energy supply with minimal costs and minimal environmental impact have become extremely acute.

As these issues are highly comprehensive, in order to determine the strategy and the most effective trends in the development of this field, the author offers the reader introductory information on this topic.

Modern Trends in the Development of Technologies for Comprehensive Optimization of Fuel Systems of Thermodynamic Energy Equipment

In recent years, specialists and industrial practitioners have carried out significant work in the search for and selection of the most practical and efficient technical solutions aimed at the comprehensive optimization of the processes of preparation and supply of fuel mixtures into the combustion chambers of thermodynamic equipment.

Experimental installations have been carried out on diesel engines, boilers, diesel generators, gas turbines, and other thermodynamic equipment.

At the same time, within the framework of systematic research, investigators and designers have mainly focused on technical solutions related to the modification of fuel preparation systems and the associated systems for supplying fuel into the combustion chambers of thermodynamic equipment.

It should be noted that at the same time, new developments have appeared in this technological field in the so-called practical aspect, when an integrative synthesis of the level of efficiency of technical ideas occurred in combination with the capabilities and interests of investment partners.

In such studies, the conclusions, recommendations, and characteristics of multidisciplinary specialists, who equally possess both technological and design approaches as well as the specifics of investment support at all stages of project implementation, are of particular interest to innovation-oriented developers.

In this regard, developments, publications, inventions, and investment strategies created comprehensively by well-known specialists with the participation of the author of this publication are of exceptional importance for the integrated practice of design and its implementation.

In these original and, to a certain extent, unique developments, a clear logical relationship is observed between the investment strategy and the stages and phases of project development corresponding to its requirements and constraints.

From the author's perspective, in whose developments the coordination of investment criteria and design parameters is linked by a specific algorithm, the professional fundamental knowledge and experience of developers of smart technologies, both in the field of technology and in the field of targeted financing of innovative projects, play an exceptionally important role, and their proper and harmonious combination is a guarantee of the commercial success of the project.

Principle of Continuity of Useful Operation

Work should be carried out continuously (all parts of the system must operate at full load at all times);

Work should be carried out continuously (all parts of the system must operate at full load and with controlled dynamics).

For a full understanding of the importance of this principle, it should be noted the subtleties of modern process-based control, in which a pause in the operational cycle of any system is also an object of control.

That is, continuity of operation includes all parts of the working cycle, including pauses.

This principle explains the necessity and possibility of incorporating algorithms into modern inventions.

In addition, switching the direction of actions and movements, as well as changes in pulsation dynamics, require program-controlled switching of the direction of movement of control elements and tools, among which the most effective have proven to be non-contact electromagnetic resonance instruments, which, when using a flat coil, exhibit extremely high response speed.

Furthermore, the use of a multilayer flat coil makes it possible to significantly increase the accuracy and penetration depth of the

signal impulse and to significantly reduce the dependence of measurement accuracy on electronic noise.

The principle of continuity of useful operation in so-called smart developments, which are most relevant today, may be represented by the following innovative development based on two technological directions: the principles of electromagnetic resonance spectroscopy applied for high-speed and accurate measurement and reading of the thickness of a coding layer.

Cybersecurity System

At present, cybersecurity systems based on innovative methods and approaches are of particular importance.

One of the key technologies used for this purpose is comprehensive encoding and decoding technology.

Protective Encoding of Optical Discs and Digital External Storage Media

General Information

All projects in this group of technical solutions are based on a single method of encoding and subsequent identification of the recording of a coding element.

The essence of the principle consists in applying a coding coating or its technological equivalent to the protected object and subsequently measuring the thickness of this coating, which determines whether the measurement results correspond to the code.

If the obtained result coincides with the established code, positive identification of the coding element occurs; if it does not coincide, negative identification occurs, resulting in stopping or blocking the operational cycle of the equipment or the information consumer, for example, a computer.

Additional Technological Features

Technologically, the issues of applying special coatings have been resolved, and this technology has been repeatedly tested in similar tasks related to the control of film thickness on solar panel surfaces and in traditional semiconductor manufacturing.

In connection with the emergence of new formats for recording and reading data on optical media using blue lasers, as well as the beginning of production of multilayer optical discs based on the same technology, the proposed principles and technical solutions for protective encoding have become even more significant.

This is due to the increasing amount of information stored on each disc, and the absence of protection leads to increasing losses of confidential or classified data.

Additionally, it is necessary to indicate the capability of encoding each layer in multilayer discs, whereby each recording layer is encoded. This represents a significant improvement in the three-dimensional structuring of optical storage media and enables localized selective encoding of information within a single disc for highly sensitive or classified data.

Organization of Corporate Protection Systems

The proposed technology, when applied to the organization of information flow protection within a corporation, ensures protection at multiple system levels, including real-time monitoring of the status and location of each disc within the organization.

When applied to mobile external storage media, the same advantages are expected as in the case of optical media.

Resonance Method (Brief Description)

The method involves the creation of an alternating electromagnetic field in the space where the test sample is located. This field acts as an intermediary between the resonant circuit and the sample.

The resonant circuit acts both as an emitter of this field and as a receiver of changes introduced by the sample.

Under the influence of the external alternating electromagnetic field, various electrical phenomena may be induced in the sample, including conduction currents, displacement currents, and ionic currents.

According to the principle of superposition, these phenomena distort the electromagnetic field, and these distortions are detected by the resonant sensor.

The system measures the resulting impedance, which reflects the properties of the sample.

Changes in impedance affect the frequency characteristics of the resonant circuit, including resonance frequency and amplitude.

Data Processing Principle

The use of multiple sensors operating at different frequencies enables the identification of material composition based on frequency-dependent impedance behavior.

This phenomenon is widely studied in electromagnetic resonance spectroscopy, commonly referred to as Electrochemical Impedance Spectroscopy (EIS).

By solving systems of linear equations based on sensor data, it becomes possible to determine the concentration of components within a sample.

Application Example: Drip Irrigation Systems

As an example, the author proposes technical solutions for drip irrigation systems, which can be adapted for pipeline systems in agricultural facilities.

The system includes a nozzle (injector) in which water is mixed with air droplets within a vortex tube.

The structure consists of capsules with a compressed air core and a water оболочка, forming a compressible flow.

Figure 1.

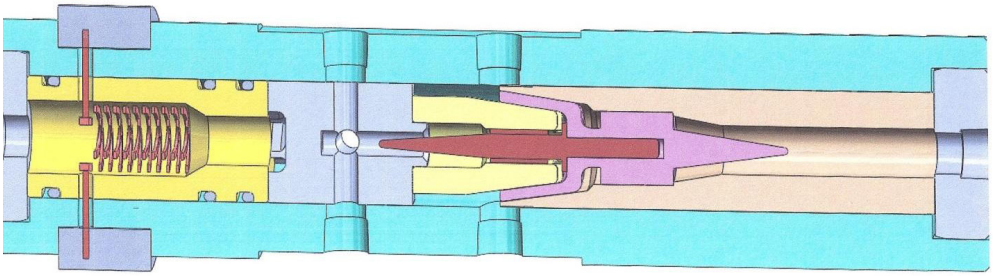

The device shown in this figure presents a design in which the hydrodynamic function is combined with a coaxially arranged non-contact monitoring system based on electromagnetic resonance spectroscopy.

This enables real-time online monitoring of the parameters of the compressible fluid exiting the device.

Figure 2.

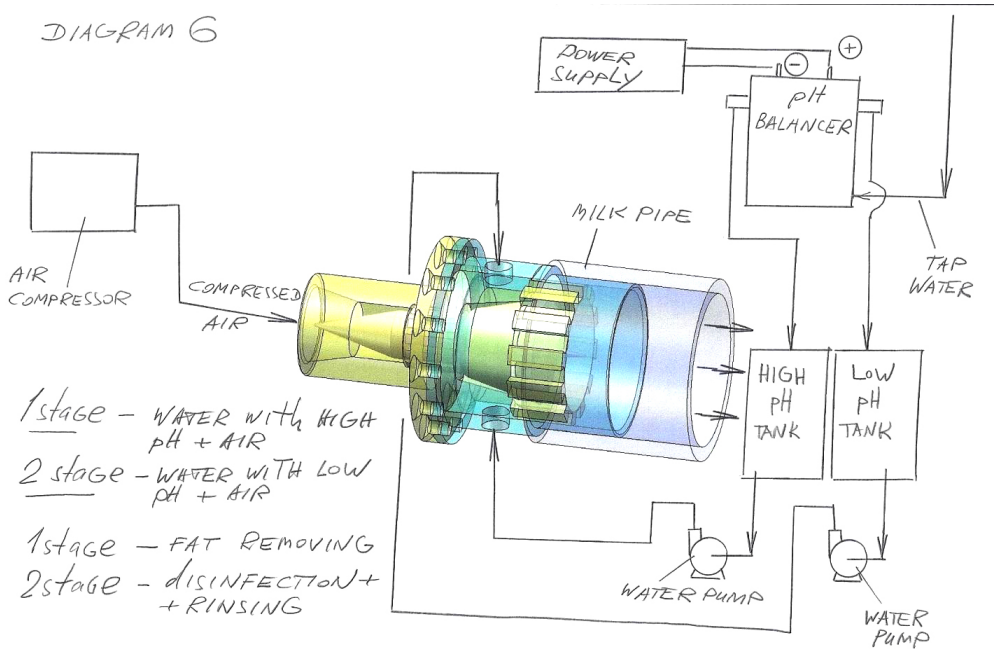

Figure 3.

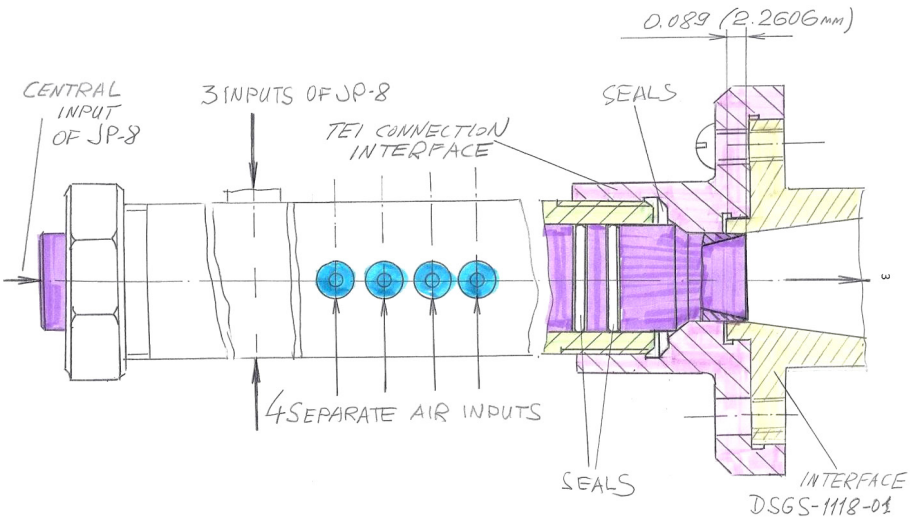

Figure 4.

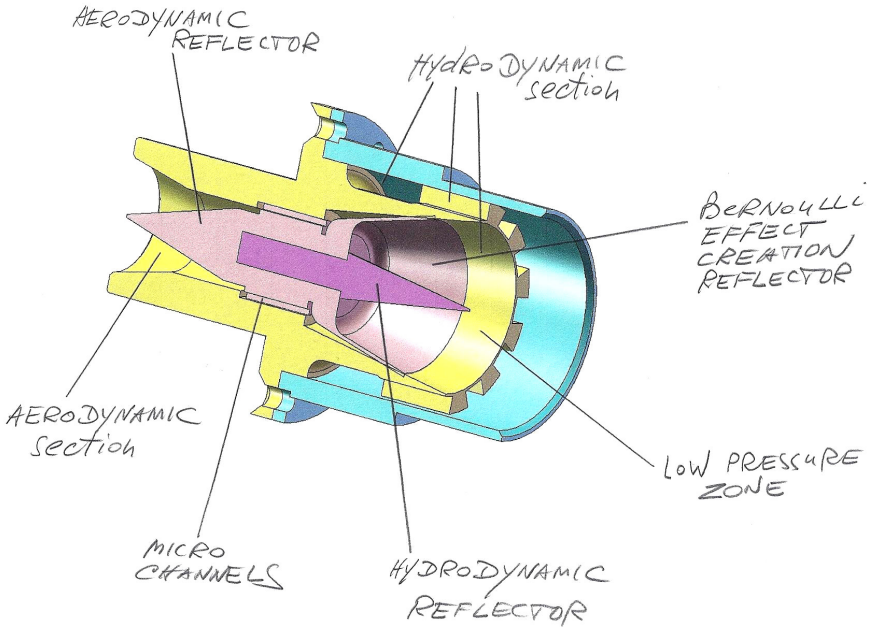

Figure 5.

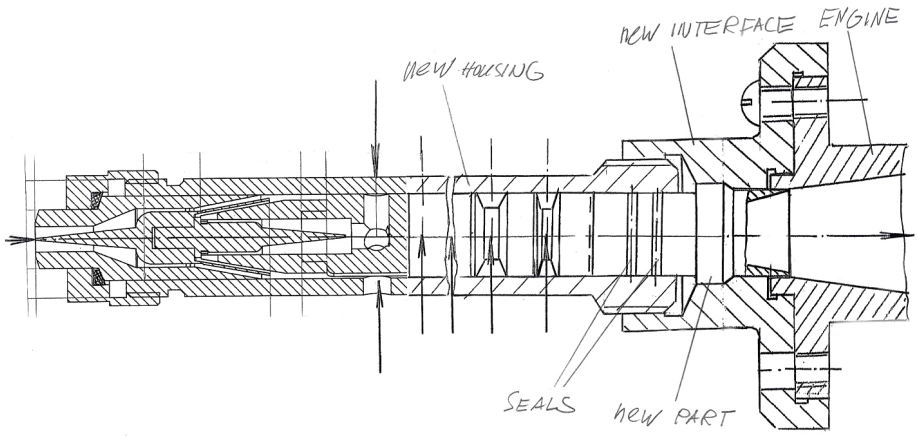

Figure 6.

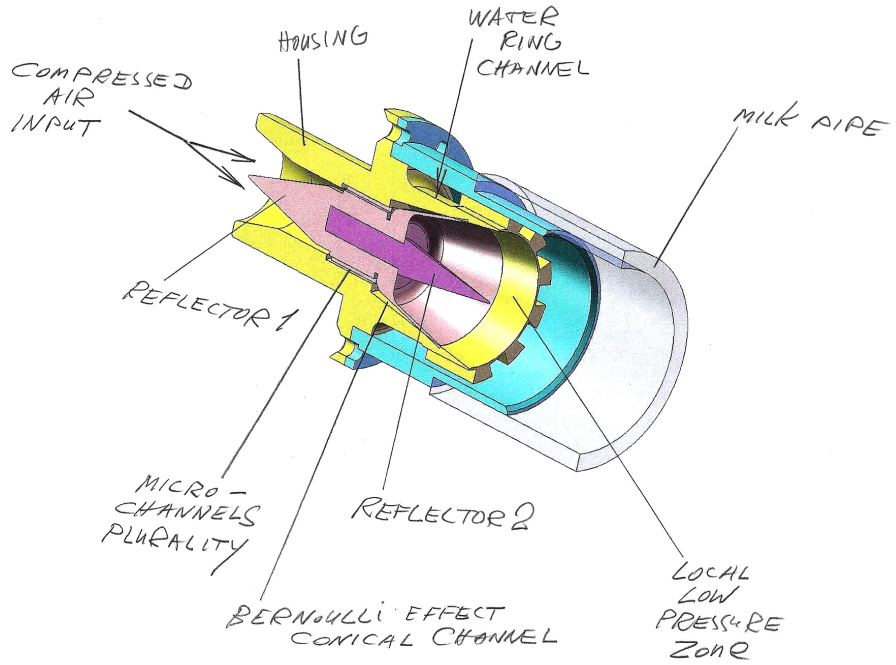

Figure 7.

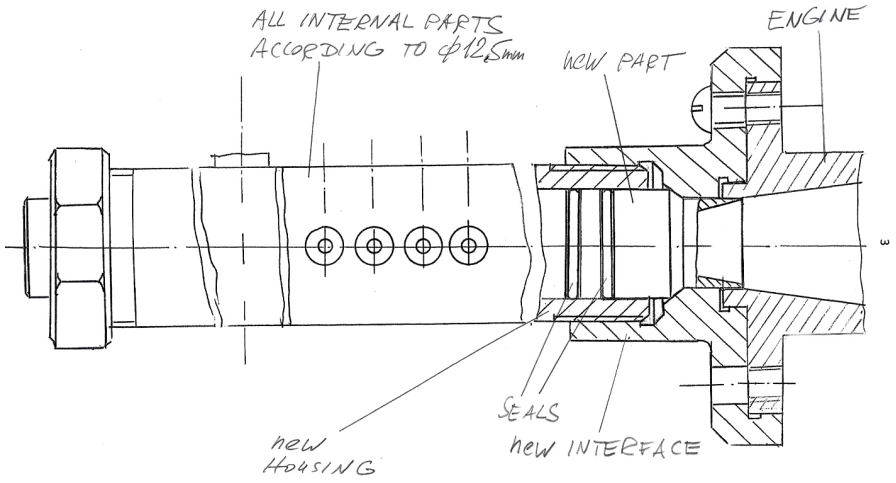

Figure 8.

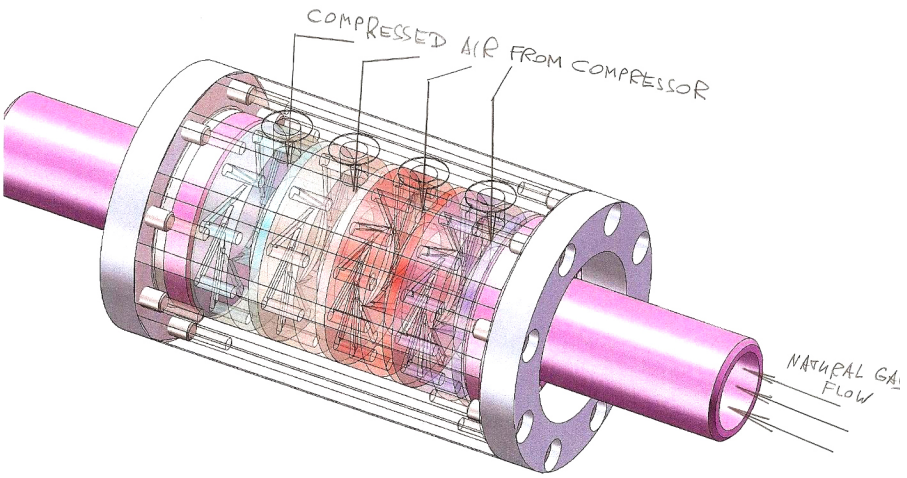

Figure 9.

The figures present three-dimensional models of the system components with labels and annotations.

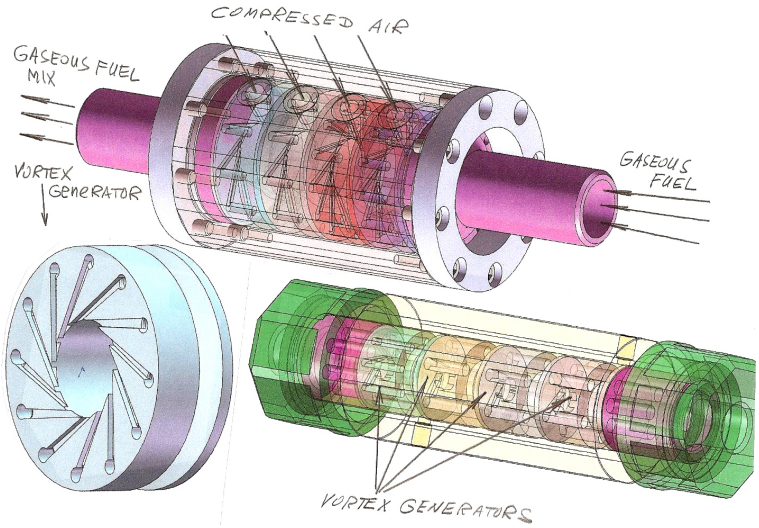

Figure 10.

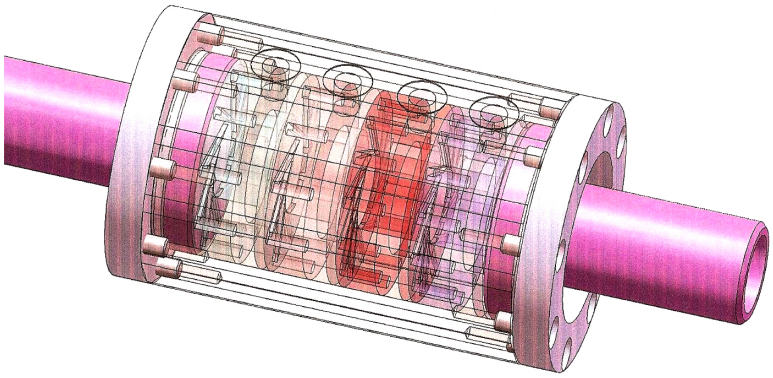

Figure 11.

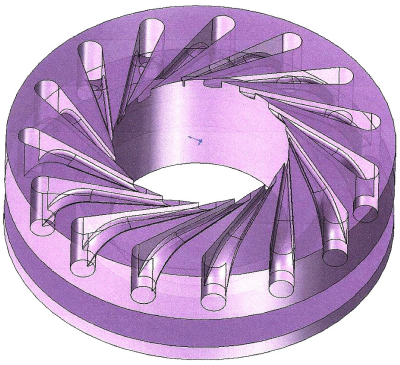

Figure 12.

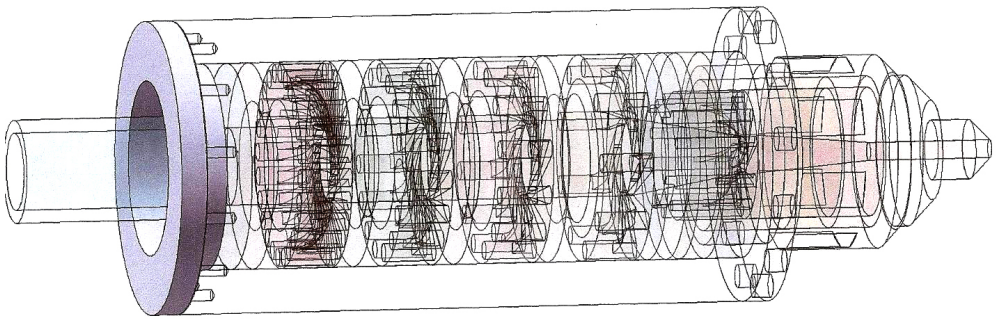

The figures present three-dimensional models of the system components with labels and annotations.

References

United States Patent Application No. 20100193445, Kind Code A1, August 5, 2010. *Foaming of Liquids*.

United States Patent Application No. 20100224497, Kind Code A1, September 9, 2010. *Device and Method for the Extraction of Metals from Liquids*.

United States Patent Application No. 20100224506, Kind Code A1, September 9, 2010. *Process and Apparatus for Complex Treatment of Liquids*.

United States Patent Application No. 20110069579, Kind Code A1, March 24, 2011. *Fluid Mixer with Internal Vortex*.

United States Patent Application No. 20120102736, Kind Code A1, May 3, 2012. *Micro-Injector and Method of Assembly and Mounting Thereof*.

submitted 06.04.2026;
accepted for publication 20.04.2026;
published 30.04.2026

Contact: vladislavdrapii@gmail.com

The Austrian Journal of Technical and Natural Sciences, 2026 No 3–4
ISSN 2310-5607

PREMIER Publishing
ppublishing.org

DOI:10.29013/AJT-26-3.4-280-285

HOMOGENIZATION IN FUEL SYSTEMS OF THERMODYNAMIC EQUIPMENT. (Homogenization of flows of various liquids in pipelines in real time; potential applications of dynamic homogenization technology in fuel systems of thermodynamic equipment)

Konstantin Lobodenko [1]

[1] Technical Specialisti Car

Cite: *Lobodenko K. (2026). Homogenization in Fuel Systems of Thermodynamic Equipment. (Homogenization of flows of various liquids in pipelines in real time; potential applications of dynamic homogenization technology in fuel systems of thermodynamic equipment). Austrian Journal of Technical and Natural Sciences 2026, No 3–4.* https://doi.org/10.29013/AJT-26-3.4-280-285

Abstract

This paper provides a comprehensive explanation of all key aspects of the technology and the device through which it is implemented. In addition, it analyzes the critically important practical experience of transport industry executive and leading specialist Dmytro Lysenko, comparing it with the results obtained from specialized testing and experimental validation.

Dynamic reagent-free homogenization is considered as a fundamental process enabling increased accuracy of non-contact monitoring of fluid conditions in pipelines, including systems monitored via aerial imaging or unmanned aerial vehicles. For the successful commercialization of this integrated technology, it is essential to identify all viable implementation points, specifically those where the technology demonstrates clear practical demand.

General conditions are examined in relation to the properties of the proposed technology. In liquid hydrocarbon fuels, the formation of clots during storage may occur, potentially leading to issues with injection and uniform combustion. The higher the fuel viscosity, the greater the probability of clot formation and other forms of inhomogeneity. Therefore, the implementation of proposed non-contact real-time monitoring technologies requires precise consideration of the required level of homogenization.

Keywords: *homogenization; homogenized fuel; liquid flow homogenization; fuel systems of thermodynamic equipment; dynamic mixing operations; dynamic homogenization system; engine fuel pump; high-pressure fuel pump; in-flow homogenization based on turbulence level; dimensional factor in a three-dimensional coordinate system*

Introduction

This paper provides a brief characterization of technological components that determine the applicability of the technology across various technical and commercial contexts. These components are based

on significant operational results obtained under the leadership of Dmytro Lysenko during targeted and systematic intensive operation of various transport systems.

In all cases, the discussion refers to a unified type of device designed to perform dynamic mixing operations along with simultaneous dynamic homogenization of liquid and gaseous physical media.

The paper further elaborates on dynamic reagent-free homogenization as a core process for improving the accuracy of non-contact monitoring of fluids in pipelines, including those monitored through aerial surveillance or UAV-based systems. For effective commercialization, it is necessary to identify application areas where the technology is unequivocally required.

The general operating conditions are considered based on the properties of the technology, with particular emphasis on its development contributions by Dmytro Lysenko. As previously noted, hydrocarbon fuels during storage may develop clots, leading to complications in injection systems and combustion uniformity. Increased fuel viscosity significantly raises the likelihood of such inhomogeneities, requiring precise evaluation of homogenization requirements for the implementation of monitoring technologies.

General Requirements and Conditions

As an example, consider a diesel engine as part of a diesel generator power system. A dynamic fuel homogenization system may be installed within the engine's fuel system, specifically in the fuel pipeline between the engine fuel pump and the high-pressure fuel pump.

As fuel passes through the dynamic homogenization system, in-flow homogenization occurs based on turbulence levels. Subsequently, the high-pressure pump completes the homogenization process to the maximum achievable extent and within the appropriate dimensional parameters in a three-dimensional coordinate system.

The operation of the dynamic fuel homogenization system does not require any additional energy sources or supplementary structural elements.

The system may also be applied in processes and equipment for homogenization in parallel with fuel recirculation within storage tanks during fuel production and storage at refueling stations.

The integrated dynamic fuel homogenization technology can be applied to various types of internal combustion engines. Due to its compact dimensions and optimized geometric configuration, the system can be installed on virtually any internal combustion engine without structural modifications.

Figure 1. *Illustrates a device for dynamic real-time homogenization in pipelines with a flow rate of up to 100 liters per hour at operating pressures ranging from 3 to 15 bar*

Extensive testing has demonstrated that the homogenization process does not result in any pressure drop within the pipelines. At the same time, pulsations and fluctuations are significantly smoothed without any additional energy consumption. As shown in the figure, the device is highly compact, with an outer diameter of 40 millimeters, an internal working diameter of 30 millimeters, and a total length of 220 millimeters

Figure 2. *Shows online dynamic homogenization systems with operating diameters of 200 mm and 250 mm, designed for flow rates of 10,000 liters per hour and 15,000 liters per hour, respectively*

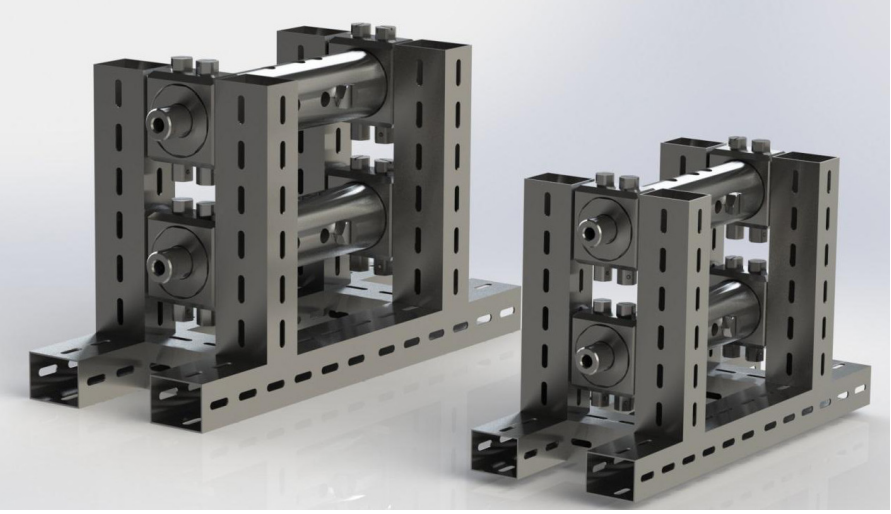

In installations of this type, the role of the homogenizing system is multifunctional. In addition to stabilizing and unifying the hydrodynamic parameters of fuel flows, such systems simultaneously address other critical challenges, primarily those related to improving the efficiency of this equipment, as formulated by Dmytro Lysenko

For comparison, it is appropriate to consider industrial systems capable of operating within fuel pipelines of large-scale power installations, such as gas turbine power units with capacities of 20 to 25 megawatts.

In recent years, the issue of forming fuel mixtures within fuel pipelines of energy equipment using biofuels, ethanol, and especially methanol has become particularly relevant, as such mixtures do not generate toxic waste and also reduce the specific cost of fuel.

For such fuels, when mixtures are formed, for example, with diesel fuel, homogenization plays a crucial role not only as a stabilizing factor but also as a factor preventing, for instance, water contained in the mixture from causing micro-explosions during evaporation and disrupting the burner flame.

When a fuel mixture is homogenized, microcapsules are formed in which, for example, a methanol core is surrounded by a diesel fuel shell. Upon injection, this core evaporates first, breaking the shell into microparticles with sizes not exceeding 0.5–0.8 microns. This significantly enhances combustion efficiency and completeness.

Most importantly, with such a structure of the fuel mixture, the energy of evaporation is preserved, providing an additional fuel saving of 1.5–2.5%. At consumption levels of 10,000 liters per hour, this can result in annual savings exceeding 100,000 USD per unit.

Modern engines equipped with high-pressure pumps can be fitted with a dynamic fuel homogenization system without any modifications to the fuel system.

The installation of dynamic homogenization systems can be implemented both on stationary internal combustion engines and on engines installed in vehicles.

The dynamic homogenization system may also be equipped with an additional system for forming two types of fuel emulsions – compressible and incompressible emulsions – in accordance with the developments of Dmytro Lysenko.

The system enables efficient emulsification of up to eight additional components within the fuel.

Without requiring any modifications, the dynamic homogenization system can effectively dissolve combustible gases in the flow of liquid hydrocarbon fuel prior to injection into the combustion chamber, both in stationary engines and in engines used in vehicles.

Dynamic homogenization is a highly versatile process that can be applied, with minimal adaptation, to a wide range of equipment and to virtually all types of liquid fuels.

Using dynamic homogenization technology, all types of liquid hydrocarbon fuels can be processed, including nearly all types of biofuels.

This technology is also applicable to all gasoline-based fuel mixtures, including blends with ethanol, methanol, and various activating additives.

Diesel fuel exists in multiple variations, with properties that differ significantly depending on climatic conditions. For example, when comparing base diesel fuel types in the United States, lighter diesel fuel No. 2 and heavier, more viscous diesel fuel No. 6 both require homogenization prior to injection, particularly in winter conditions.

When considering various grades of fuel oil, especially those with high sulfur content, it can be observed that homogenization alone, even without blending with lighter fuels, can reduce fuel consumption by up to 10% due to the advantages provided by the homogenization process.

Recently, new types of regenerated fuels have emerged based on various forms of diesel fuel and fuel oil blended with biofuels and other products of hydrocarbon processing or regeneration. The initial technical requirements for their use have been developed by Dmytro Lysenko.

Examples include fuel types such as JP-8 and JP-10 used in the United States, which also require homogenization and can serve as a basis for homogenized fuel mixtures when processed using this technology.

Dynamic homogenization technology can be applied to all types of liquid biofuels as well as to all types of biofuel compositions.

Despite gasoline being the most homogeneous type of liquid fuel, due to its widespread use in blends with ethanol – where ethanol content typically составляет at least 10–15% – he homogenization of gasoline and its blends has also become increasingly relevant.

Gasoline-based fuel mixtures, such as gasoline-ethanol and gasoline-methanol blends, may exhibit gravitational separation of water from the hydrocarbon phase during prolonged storage.

In gasoline engines using such mixtures, the dynamic homogenization system is installed between the fuel pump and the engine's high-pressure pump.

As the fuel mixture – where water has separated from gasoline – passes through the dynamic homogenization system, homogenization occurs within the flow based on turbulence levels. Subsequently, the high-pressure pump completes the homogenization process volumetrically and at the micron scale within a three-dimensional coordinate system.

During homogenization, water in the form of microdroplets is uniformly distributed throughout the hydrocarbon fuel mixture, transforming it into a micro- or nano-emulsion.

According to test results, the use of emulsions produced by the dynamic homogenization system reduces soot concentration in exhaust gases by up to 97%, while the intensity and rate of heat release increase by at least 35%.

The installation of a dynamic homogenization system on gasoline engines does not require any additional specialized components, nor does it require any structural modifications to the engine itself.

Figure 3. *Shows a device for online homogenization of gasoline and gasoline-based fuel mixtures for engines with a flow rate of 45 liters per hour and an operating diameter of 25 mm*

The figure presents the device in a disassembled configuration

As can be clearly seen from the figure, the device is highly engineered. This is primarily due to the fact that all internal components and the housing form a system of coaxial cylindrical and conical surfaces. The housing itself also functions as a precision gauge, determining the

position of each component and ensuring the accuracy of all working channels of the device. This is achieved, among other factors, through dimensional configurations that enable the so-called double Bernoulli effect and ensure the required level of cavitation-induced ruptures within the flow of homogenized fuel or other process and working fluids.

For significantly more viscous diesel fuels and fuel compositions, the necessity of homogenization becomes even more evident. This applies both to pure diesel fuel and to mixtures based on diesel fuel and methanol, as well as to diesel–water emulsions of both types: water-in-oil emulsions, where the water content does not exceed 20%, and oil-in-water emulsions, where the water content reaches up to 50%.

The preparation of fuel mixtures based on diesel fuel and ethanol or methanol is extremely difficult due to the significant difference in viscosity between these components.

The dynamic homogenization system enables the production of a high-quality and homogeneous mixture of diesel fuel with ethanol or methanol within fractions of a second, directly within the pipeline and in any required proportion.

In diesel engines using fuel mixtures of diesel fuel with ethanol or methanol, the dynamic homogenization system is installed between the fuel pump and the high-pressure pump of the engine.

As the fuel mixture – where phase separation may occur – passes through the dynamic homogenization system, homogenization takes place within the flow based on turbulence intensity. Subsequently, the high-pressure pump completes the homogenization process volumetrically and at the micron scale within a three-dimensional coordinate system.

During homogenization, water in the form of microdroplets is uniformly distributed throughout the hydrocarbon fuel mixture, after which the mixture is transformed into a micro- or nano-emulsion.

According to test results, the use of emulsions produced by the dynamic homogenization system reduces soot concentration in exhaust gases by up to 97%, while the intensity and rate of heat release increase by at least 35%.

The installation of a dynamic homogenization system on a diesel engine does not require any additional specialized components, nor does it require any structural modifications to the engine itself.

Figure 4. *Shows the internal components of the device*

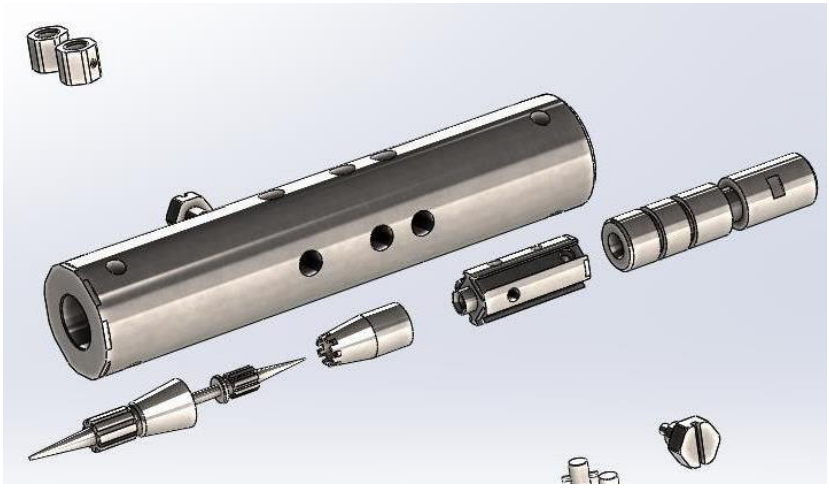

All working surfaces are coaxial, and the design contains no moving parts. Due to this mutual coaxiality, it is possible to achieve the precision of all working channels at the level of 25 microns, with a maximum tolerance of 1 micron

To summarize the implementation of fuel mixtures, the author recommends referring to the innovative integrated developments of Dmytro Lysenko, which reflect the most advanced requirements for so-called smart technologies within the infrastructure and ecosystem of intelligent transport systems. These technologies, to varying degrees, incorporate elements of artificial intelligence and artificial neural networks into control

and monitoring systems, in combination with measurement techniques based on electromagnetic resonance spectroscopy.

References

US Patent Application 20180162377. Colavincenzo, D. D. *Hybrid Commercial Vehicle Thermal Management Using Dynamic Heat Generator*. United States Patent Application, Kind Code A1, June 14, 2018.

US Patent Application 20180163649. Glugla, C. P., et al. *Method and System for Pre-Ignition Control*. United States Patent Application, Kind Code A1, June 14, 2018.

US Patent Application 20180171890. Kamei, W. *Dual Fumigation Homogeneous Charge Compression Ignition (DF-HCCI) Engine*. United States Patent Application, Kind Code A1, June 21, 2018.

US Patent Application 20180171925. Pavlov, K. J. *Secondary Fuel Injection System and Method for Diesel Engines*. United States Patent Application, Kind Code A1, June 21, 2018.

US Patent Application 20180179975. Merlino, G., et al. *Engine Control System Including Feed-Forward Neural Network Controller*. United States Patent Application, Kind Code A1, June 28, 2018.

submitted 03.04.2026;
accepted for publication 17.04.2026;
published 30.04.2026

Contact: lysenko.dmytrous@gmail.com

Contents

Section 6. Medical science

Section 7. Technical sciences in general